Selection among Replicators and Protocell Chemotaxis

Robert J. H. Scanes



A thesis presented in partial fulfilment of the requirements for the award of

Doctor of Philosophy
of the
University of Oxford

Supervisor: Prof. Stephen P. Fletcher

Department of Chemistry

Trinity Term 2019

Declaration

This thesis describes work conducted under the supervision of Professor Stephen Fletcher in the Chemistry Research Laboratory, Oxford, between June 2016 and August 2019. The thesis is entirely my own work except where otherwise indicated and acknowledged. It has not been submitted for any other degree at this university or at any other institution.

Robert J. H. Scanes

Abstract

This thesis describes a series of projects which have autocatalysis as the overarching theme.

Chapter 1 is a general introduction to the construction of chemical models of biological systems. There is a discussion of what mechanisms are used to achieve autocatalysis. The biomimetic work of chapters 3 and 4 use lipid replicators, so there is particular focus on the physical autocatalysis of lipid aggregates and their use in prebiotic models. The roles that lipids play in life are used as an illustration of the promise they offer to systems chemists. A brief history of biological homochirality is given.

Two designs for novel asymmetric autocatalytic reactions are described in chapter 2, both based on hydrogen bonding catalysis. Though neither system showed the desired amplification of chirality, this work led to the study of positive nonlinear effects within thiourea catalysis.

Projects which attempt to couple lipid replication with protocell behaviour are presented in chapter 3. In this chapter oil droplets are used as simple model protocells. Interestingly, feedback between the motion of droplets and a lipid forming reaction are observed, with the system showing striking chemotaxis. In the second part of this chapter other systems are used to explore the relationship between lipid formation and compartment division.

Chapter 4 describes observations relating to transient lipid replicators which can be fuelled to be maintained out of equilibrium. An initial finding shows that fuelling can result in dramatic oscillations, as well as stable concentrations. When lipids compete for resources, they typically show a succession through time, an interesting protocell model. Which replicating species dominates results from a multitude of combined effects which cannot be predicted simply using rates of formation of each lipid in isolation.

Finally, chapter 5 outlines the conclusions that can be drawn from these results and what future work remains.

Acknowledgements

I must firstly thank my family, particularly my parents Nigel and Julie, who have always been very supportive of me in all my endeavours and in myself. Their patience in the face of my constant discussions of all things literary and historical, and the associated profusion of books and antiques, is something I will never be able to show enough gratitude for. Felan has been a great love in my life, generously building with me something noble and helping me no end. He and his family have welcomed me into their lives in a way I didn't know was possible.

I would like to thank those teachers, mentors and models who have played a role in getting me to Oxford. Those who showed extraordinary belief in me, to whom I am indebted include Mr. Morley, John Sutton, Warren Galloway, David Spring and Richard Dorrell. Among those who truly inspired me to pursue science I have to rank Ron Laskey, John Gurdon, David Summers, Lewis Wolpert, William Bateson and Thomas Hunt-Morgan.

Thanks must go to all those behind the things that have really stimulated me in my time here, without which I surely would not have been able to complete this work. The works of Melville, Sedaris, Pym, Hardy, Woolf, Wodehouse and Waugh stand out. And thanks to the libraries of Oxford and their staff for providing me with the most exquisite balance of intellectual fulfilment, space and distraction.

Oxford has taught me many lessons, I suppose that of one of the most important is best surmised by the words of Kaveh Akbar, "there are no good kings. Only beautiful palaces." Coming up, coming out and coming down have oftentimes lacked Brideshead's gaiety and levity. *Et in Arcadia ego*. When I experienced homophobia I needed help from people here, I'm very glad I found Jonathan Burton, Robin Darwall-Smith and Andrew during that hardest of times. It is testament to their characters.

Without my friends I certainly would not have made it through this. Paddy and Arron, Sarah, Josh, and Sam have been monumentally supportive, as have been my school friends, and those here in Oxford. Of course, Nada has a very special place in my heart, I cannot imagine this time without you, you are a purest joy.

I thank the research group for training and help, science is a team sport played by individuals. Reece, this has been quite the journey, thanks for being there all the way. Thank you Wieland and Alex, you have been very kind to me, I will remember the good laughs we have had for many years to come. Sedef and Chus you were always superb people to work with, outstandingly good to be around as well. I enjoyed a great deal the times I had travelling, and not, with Elias, certainly would have been a lot worse without you. I couldn't forget the catharsis of sharing asymmetric autocatalysis horror stories with Elena, I really wish that had come along earlier in my time.

Those who I worked directly must get particular mention. Andrew was as sharp as a tac and showed extreme confidence in me, which in hindsight helped a great deal. Lily you were a star, I think I have never laughed so much in my life. Josh, we had a fun and intense year, you're a good and understanding friend. I never did find out how many fires it was in the end. Michael, you worked hard to move things forward, I think it has yielded good things. Thanks to my collaborators at the University of Twente from the Katsonis Group. You were a pleasure to work with and welcoming to me on my visits.

I would like to thank Steve for what he did for my projects and what support he gave when chemistry wasn't on my side. I certainly would not have been able to come up with it all on my own.

Abbreviations

app	apparent
aq.	aqueous
Ar	aryl
br	broad
Bu	butyl or *n*-butyl
c	concentration
CAC	critical aggregation concentration
CMC	critical micelle concentration
CPC	critical propulsion concentration
CSTR	continuous stirred-tank reactor
CVC	critical vesicle concentration
d	doublet
d	deuterated
D	configuration relative to dextrorotatory glyceraldehyde
DAG	diacylglycerols
DEP	diethyl phthalate
DFT	density functional theory
DLS	dynamic light scattering
DMAP	4-dimethylaminopyridine
DMSO	dimethyl sulfoxide
dod	dodecane
EDC	1-ethyl-3-(3-dimethylaminopropyl)carbodiimide
ee	enantiomeric excess
eq. or equiv.	equivalents
ES	electrospray ionisation
Et	ethyl
g	grams
Gly	glycine
h	hours
HDA	2-hexyldecanoic acid
HEPES	4-(2-hydroxyethyl)-1-piperazineethanesulfonic acid
hept	heptet
HPLC	high performance liquid chromatography
HRMS	high resolution mass spectrometry

Hz	hertz
i	*ipso* or *iso*
IR	infrared
iSCAT	interferometric scattering microscopy
J	joules
J	coupling constant
L	litre
L	configuration relative to levorotatory glyceraldehyde
Leu	leucine
LRMS	low resolution mass spectrometry
Lys	lysine
M	molar concentration
m	metre
m	*meta*
maj	major
Me	methyl
MES	2-morpholinoethanesulfonic acid
min	minute or minor
mol	mole
mp	melting point
MPC	2-methacryloyloxyethyl phosphorylcholine
N	no, absence of compound in reaction
Nu	nucleophile
ND	not determined
o	*ortho*
oct	octan-1-ol
oct a	1-octanoic acid
p	*para*
PDMS	polydimethylsiloxane
pent	pentan-1-ol
Ph	phenyl
pH	decimal logarithm of the reciprocal of the hydrogen ion activity
Piv	pivaloyl
pKa	decimal logarithm of the acid dissociation constant
Pr	propyl

PTFE	polytetrafluoroethylene
q	quartet
quat	quaternary
R	chemical moiety
rpm	revolutions per minute
SFC	supercritical fluid chromatography
SYBR Green I	N',N'-dimethyl-N-[4-[(*E*)-(3-methyl-1,3-benzothiazol-2-ylidene)methyl]-1-phenylquinolin-1-ium-2-yl]-N-propylpropane-1,3-diamine
t	triplet
t	*tert*, tertiary
TBS	*tert*-butyldimethylsilyl
TC	thiophene-2-carboxylate
TFA	trifluoroacetic acid
THF	tetrahydrofuran
TLC	thin layer chromatography
t_R	retention time
TRIS	tris(hydroxymethyl)aminomethane
TTAB	tetradecyltrimethylammonium chloride
UPLC	ultra high performance chromatography
UV	ultraviolet
v	volume
Y	yes, presence of compound in reaction
δ	chemical shift
λ	wavelength
ν_{max}	maximum absorbance
°C	degree Celsius

Contents

Declaration v

Abstract vii

Acknowledgements ix

Abbreviations xi

1. General introduction 1

1. 1 Building chemical models of living systems 3

1. 2 Autocatalysis 6

1. 3 Biological homochirality 15

1. 4 The role of lipids in life and application to systems chemistry 16

1. 5 References 19

2. Designs for asymmetric autocatalysis via organocatalysis 27

2. 1 Introduction 29

2. 2 Attempts towards asymmetric autocatalysis using aziridine thioureas and ureas 36

2. 3 Designs for an asymmetric autocatalysis with atropoisomerism 42

2. 4 Nonlinear effects in thiourea organocatalysis 46

2. 5 Conclusions and outlook 50

2. 6 Experimental 53

2. 7 References 139

3. Replicating lipids and protocell behaviour 147

3. 1 Introduction 149

3. 2 Self-propelling protocells and lipid replicators 163

3. 3 Behaviour of large drop protocells 171

3. 4 Conclusions and future work 189

3. 5 Experimental 191

3. 6 References 207

4. Self-replication and selection away-from-equilibrium 213

4. 1 Introduction 215

4. 2 System optimisation and mechanistic understanding 235

4. 3 Reaction kinetics and competition between replicators 252

4. 4 Other thiol-disulfide exchange systems 282

4. 5 Conclusions and future work 288

4. 6 Experimental 291

4. 7 References 383

5. Conclusions and future work 389

5.1 Asymmetric autocatalysis 391

5.2 Lipids and protocell behaviour 392

5.3 Self-replication and selection 394

5.4 Final remarks 396

5.5 References 401

Description of Electronic Supporting Information 403

Chapter 1.

General introduction

Chapter 1

General introduction

1. 1 Building chemical models of living systems

Biology has been and remains a huge source of inspiration for those working in the physical sciences.[1,2] We are now positioned as synthetic chemists to build highly complex functional systems, due to the advances in molecular motors, improved analysis of mixtures and advances in theoretical understanding of non-equilibrium systems. The design and study of the sum properties of chemical mixtures has been heralded by some as "systems chemistry", although the term lacks universal acceptance.[3–5] I believe the ultimate aim of this field is emergence in the Aristotelian sense, that is to build systems which are in some sense greater than the sum of their parts.

Life evades definition, having a "I know it when I see it" nature rather than anything that can easily be uniquely distinguished from the non-living.[6–9] Perhaps this is why a recent study was able to compare 123 distinct definitions taken from the scientific literature.[10] Probably the most commonly used is NASA's so-called working definition, which states that life is a "self-sustaining chemical system capable of Darwinian evolution."[6]

Darwin informs so much of how biology is viewed in the contemporary world and what it means to be alive. Though oft seen as a singular genius today, his work built extensively on theories and experimental findings of a great many others. The closing words of the Origin of Species hint at the enormous philosophical impact of the theory of evolution by means of natural selection and the implications for early life on Earth:

"There is grandeur in this view of life [natural selection], with its several powers, having been originally breathed into a few forms or into one; and that, whilst this planet has gone cycling on according to the fixed law of gravity, from so simple a beginning endless forms most beautiful and most wonderful have been, and are being, evolved."[11]

Understanding abiogenesis, that is the transition from a non-living to a living environment, will require casting the conceptual net wider than Darwin. Darwin's world is essentially a Malthusian one, where it pays to be selfish and reproduce quickly. However in a prebiotic environment without highly evolved biomolecules, it seems very likely that specificity of chemical interactions would be significantly lower than in life.[12,13] This would mean effects of selection are unlikely to efficiently act on the individual "species", but rather act more broadly on the level of populations of interacting groups of chemicals.[14–16] In such an environment, we can imagine cooperative aspects to fitness, mutually beneficial interactions and emergent properties of mixtures more significant than today, with success not merely being the product of mutation rate, the ability to survive, and reproduction rate.[17]

Living matter is distinguished by essentially three broad properties; reproduction, metabolism driven by constant consumption of energy, and homeostasis, all of which are hard to emulate in synthetic systems. In life, all these processes are closely interrelated, but provide us with a platform to think about the design of functional systems. Together, these properties combine to allow higher function, enabling development, adaptability and ultimately evolution, endowing all sorts of biological advantages.

Reproduction in molecular systems can be achieved through autocatalysis and there has been great development over the past 30 years in the field of molecular replication. Though largely been studied out of fundamental interest rather than practical function,

autocatalytic processes can be used to accelerate drug release[18,19] and select for particular polymorphs of active pharmaceutical ingredients in crystallisation.[20,21]

Metabolism allows maintenance of dynamic high energy states in living systems, adapting to need and external stimuli. Making chemical systems tied to a constant consumption of energy is of great current interest for the ability to sustain function away from equilibrium and rapidly switch between states.[22,23] Recently the Fletcher group reported a system whereby fuelling sustains a population of replicating lipid which is otherwise unstable to its environment.[24]

Homeostasis is the maintenance of stable chemical and physical states needed for efficient function. Strict regulation is needed for homeostasis, through feedback between components.[25,26] How physical and chemical processes can be coupled will be essential to the development of self-healing dynamic materials.[27] Designing interactions between parts of complex functional materials is very challenging at the molecular level, it is on the border of what is possible by chemical intuition, and progress is likely to arise by a using holistic approach like systems chemistry.[28]

Construction of life-like systems is one of the key challenges of science today, with diverse interdisciplinary areas from soft robotics to artificial cells.[29,30] Despite extensive efforts, scientists are a long way from *de novo* life formation.[31] Without a generally accepted definition of life, what constitutes "coming to life" could be if anything more contentious.[32] Although I am not sure what will satisfy the scientific community, it will surely involve the development of complex structures displaying these three properties of reproduction, homeostasis and consumption of free energy.

Long overlooked in the field of materials, lipid forming reactions show great promise in the synthesis of functional systems. Within this thesis I explore a design concept for

building life-like systems which starts with coupling of physical autocatalysis to some function. From here, the nonlinear kinetics of autocatalysis opens up many possibilities for feedback between components, as well as oscillations.

1. 2 Autocatalysis

In an autocatalytic reaction a product or products act as a catalyst for the reaction.[33,34] Autocatalytic reactions typically show two characteristics, firstly, a sigmoidal relationship between product concentration and time. Secondly, initial reaction rate is increased by presence of added product. Definitions similar to this are common to chemistry,[35] and exclude certain behaviours sometimes referred to autocatalysis in biochemistry, such as self-splicing or "autocatalytic" RNAs.[36,37] Here, particular RNA sequences can adopt conformations which allow, through sequential intramolecular reactions, cleavage of the RNA strand. In a sense they are acting on themselves, hence "auto" and this type of reaction usually requires enzymes or other catalysts, hence "catalysis". They would however fall outside of my definition, as the product does not catalyse the reaction and reactions do not show sigmoidal kinetics. The substrates are considered unstable molecules rather than autocatalysts.

Among the oldest reported autocatalytic reactions in organic chemistry are the acidic bromination of acetone and the formose reaction. Whilst the first may be familiar to the undergraduate, it highlights that autocatalytic reactions can be unspecific, simply forming HBr throughout. There have been many reviews of autocatalytic reactions and molecular replication.[33,38–40] Broadly autocatalytic reactions can be divided into three categories, depending on mechanism (Figure 1. 2. 1a-c). Firstly there is network autocatalysis, which occurs in a network of chemical steps which consumes product for some steps, but overall produces more of a product than is consumed, for example $HBrO_2$ in the Belousov–

Zhabotinski reaction (Figure 1. 2. 1a).[41] These reactions are sometimes referred to as autoinductive, though the distinction is subjective and outside my scope.[35] Network autocatalysis is an area often ignored in systems chemistry due to the difficulty in designing networks with the required properties. An exception to this is chemical sensing, where the decomposition of self-immolative chemical probes allows for exponential amplification of a signal. This has been applied to fluoride detection in nerve agent detection models (Figure 1. 2. 2).[42,43]

A second type of autocatalysis is template replication, drawing inspiration from nucleotide replication of life, which is achieved through binding two or more starting materials onto a molecule of product (Figure 1. 2. 1b).[39,44] This typically functions by bringing the precursors together through template binding and so raising the effective concentration of two reagents, allowing them to react at a faster rate than they would by a bimolecular pathway. The first example of non-enzymatic template replication was reported in 1986 by von Kiedrowski (Figure 1. 2. 3).[45,46] Templating can control of orientation of the substrates, allowing for diastereoselectivity in which products are formed.[47] Whilst this can lead to highly specific interactions, often poor catalysis is shown due to the product remaining bound to the template that created it, so-called product inhibition.

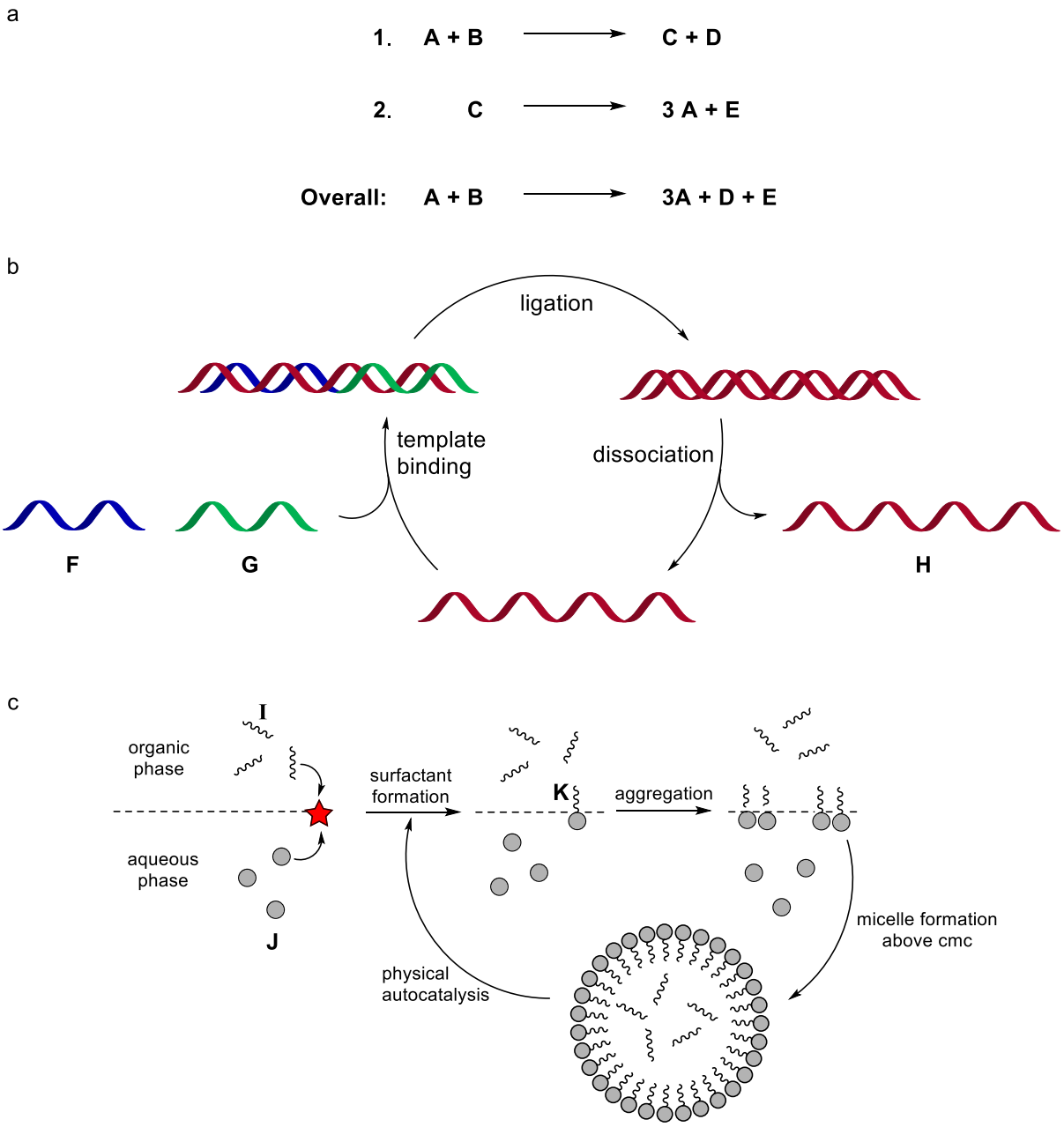


*Figure 1. 2. 1. Three general categories of autocatalytic reactions by mechanism. a – Network autocatalysis. In a series of chemical steps, some consume a compound (**A**), some downstream steps also produce the same compound (**A**), with overall a net production of the autocatalyst. b – Template replication. Typically, two reactants (**F** and **G**) are brought into close proximity by a template (**H**), which undergo ligation and dissociation to form two molecules of template. c – Physical autocatalysis. Reactions are characterised by being catalysed by some aggregate of product. In this example, two phase separated reagents (**I** and **J**) react to form an amphiphilic surfactant product **K**. **K** aggregates to form micelles, which increase the rate of formation of **K**.*

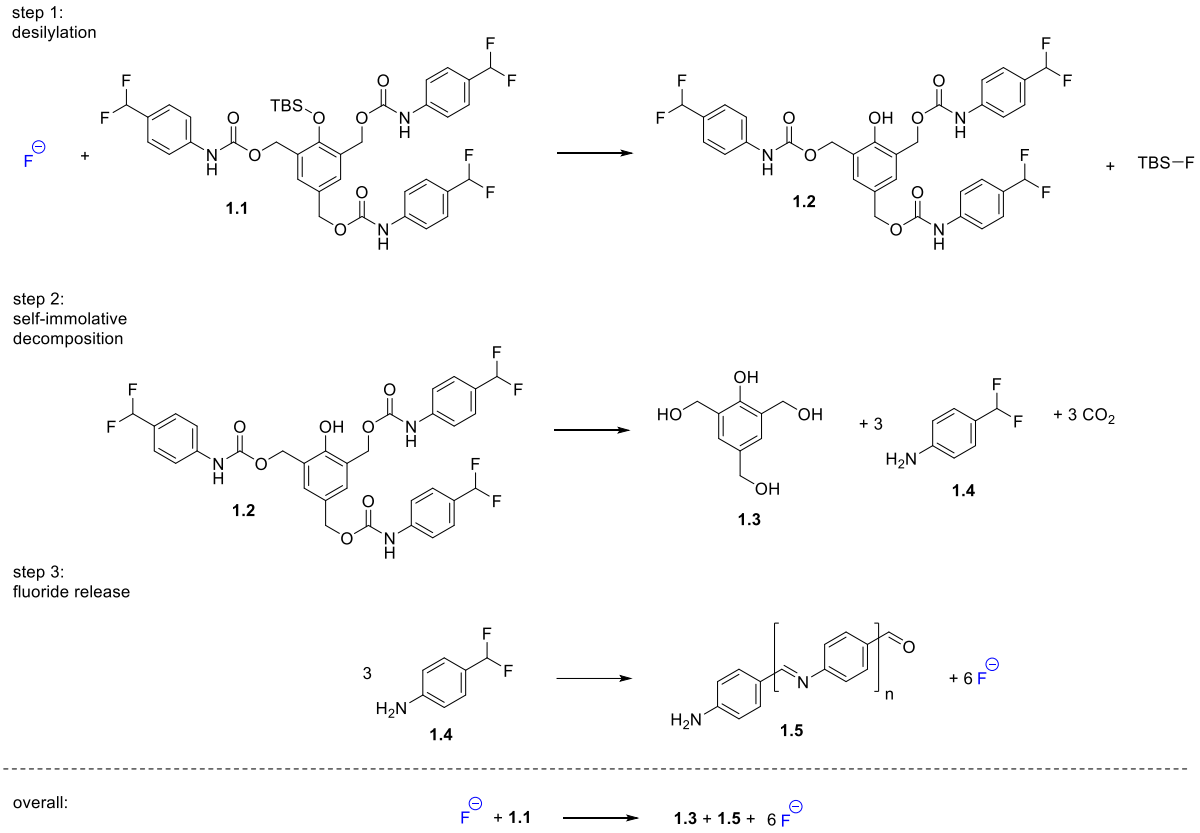


Figure 1. 2. 2. Example of an autoinductive network for the amplification of fluoride used in a model for sensing nerve agents. In the first step, ***1.1*** *reacts in an equimolar ratio with fluoride to give* ***1.2****. Secondly,* ***1.2*** *decomposes via a series of quinone methide intermediates to give* ***1.3****, carbon dioxide and three equivalents of* ***1.4****. Finally, there is the fluoride amplifying step, where* ***1.4*** *decomposes to oligomers of* ***1.5*** *and fluoride. Note that equivalents of water and base (pyridine) have been excluded for clarity, both of which are in large excess. Multiple chemical steps have been grouped together for clarity.*[43]

A third group of autocatalytic reactions involve the formation of assemblages such as fibres or lipid aggregates (Figure 1. 2. 1c).[48–52] These systems operate under heterogeneous conditions, promising for the development of complex systems. As these reactions involve formation of supramolecular aggregates and material transfer between phases, this mechanism of action is sometimes called physical autocatalysis and is the subject of much of this thesis. The specificity of interactions varies in these systems with the nature of the aggregates formed.

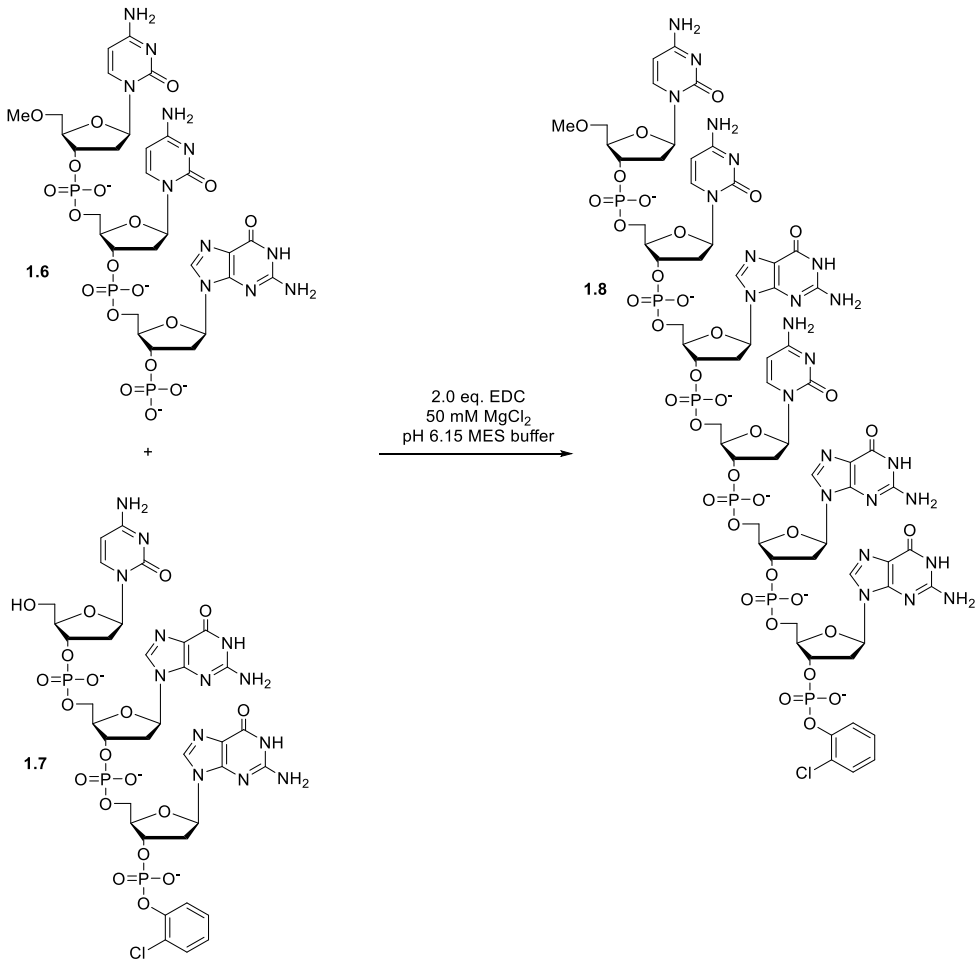


Figure 1. 2. 3. A self-replicating hexadeoxynucleotide reported by von Kiedrowski.[45] *Here **1.6** and **1.7** are ligated in the presence of a carbodiimide coupling agent, with the product, **1.8**, acting as a template for the reaction. EDC = 1-Ethyl-3-(3-dimethylaminopropyl)carbodiimide.*

The first examples of autocatalysis involving micelles were described by Luisi and coworkers in a series of publications beginning in 1990 (Figure 1. 2. 4).[53–56] Here alcohol oxidation or ester hydrolysis give octanoate salts as products which aggregate as either micelles or inverse micelles depending on the reaction conditions. The work of Luisi is of prime relevance to synthetic biology and abiogenesis, showing the formation of catalytically active surfactant product which through aggregation forms discrete compartments *de novo*.[57,58] Since the initial discovery, other autocatalytic micelle forming systems have been reported where the products are ethylene glycols,[59]

phosphocholines,[60,61] N-oxide[62] and sugar-based surfactants,[63] showing that there is some generality to this means of lipid replication.

Luisi's self-reproducing micelles are a minimal synthetic model for autopoiesis, the modern concept of which was introduced by Maturana and Varela in the 1970s.[64,65] An autopoietic unity (be it a cell, factory or other entity) is a delimited network of processes continuously producing all its components including the boundary. For such systems to grow and increase in total population they require a constant supply of energy and material from the outside. In models of such systems, each individual step may be, but are not necessarily, autocatalytic, but the whole system can be considered autocatalytic. As defined, autopoietic unity does not necessarily grow or reproduce, but may have the capacity to do so.

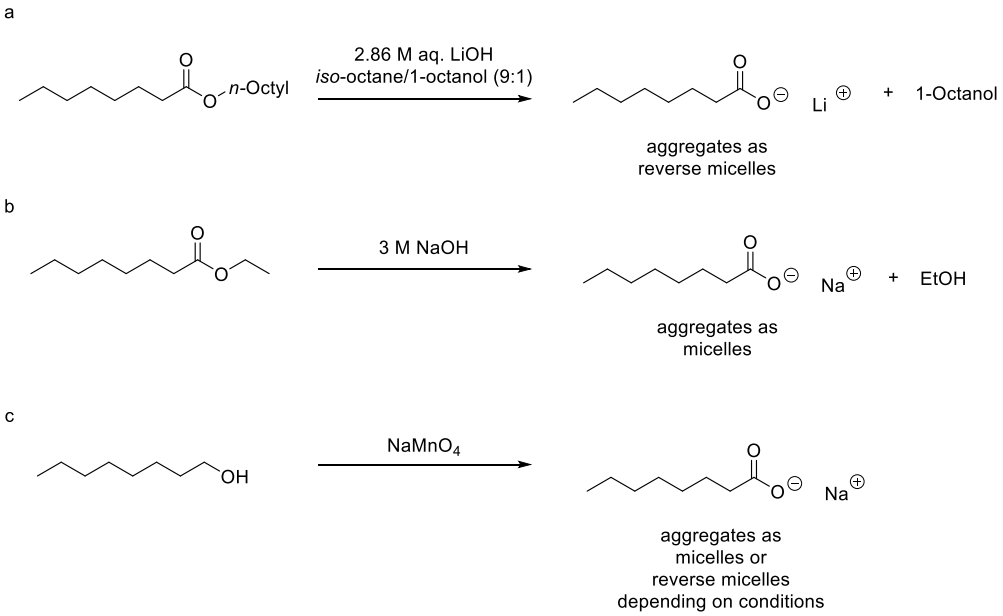


Figure 1. 2. 4. A series of autocatalytic systems based on the aggregation of octanoate salts developed by Luisi and coworkers a – Hydrolysis of octyl octanoate by LiOH, where the product forms reverse micelles.[53] *b – hydrolysis of ethyl octanoate by NaOH, where the product aggregates as micelles. Acidifying this mixture by HCl addition or CO_2 bubbling gave vesicles.*[56] *c – Oxidation of 1-octanol where the product aggregates either as micelles or reverse micelles, showing autocatalytic kinetics in both cases.*[55]

The mechanism of how autocatalysis occurs in these systems is disputed. Luisi and Mavelli favour a micellar catalysis model,[66,67] with the surfactant forming reaction occurring at the micelle surface. Buhse favours a phase transfer model,[68,69] whereby the hydrophobic component is released into the bulk aqueous phase to react. Also, contributions from the changing nature of the organic-aqueous interface, such as reducing surface tension, cannot be excluded. It seems likely that system specific combinations of contributions lead to the observed autocatalysis, and possibly different factors are more or less significant at different time points of the reaction. My work in physical autocatalysis focuses on gross behaviours of populations of replicating molecules, the precise mechanism by which autocatalysis arises was not investigated at length.

Hardy et al. reported a self-reproducing vesicle system based on copper-catalysed azide-alkyne cycloaddition chemistry (Figure 1. 2. 5).[70] In this work the authors describe a method of autocatalytic production of a membrane bound Cu(I)-ligand complex, which also acts as the catalyst for the formation of the vesicle forming triazole phospholipid. With the addition of precursor molecules, the authors make a population of vesicles which can recover back to an initial concentration through a series of repeated dilutions.

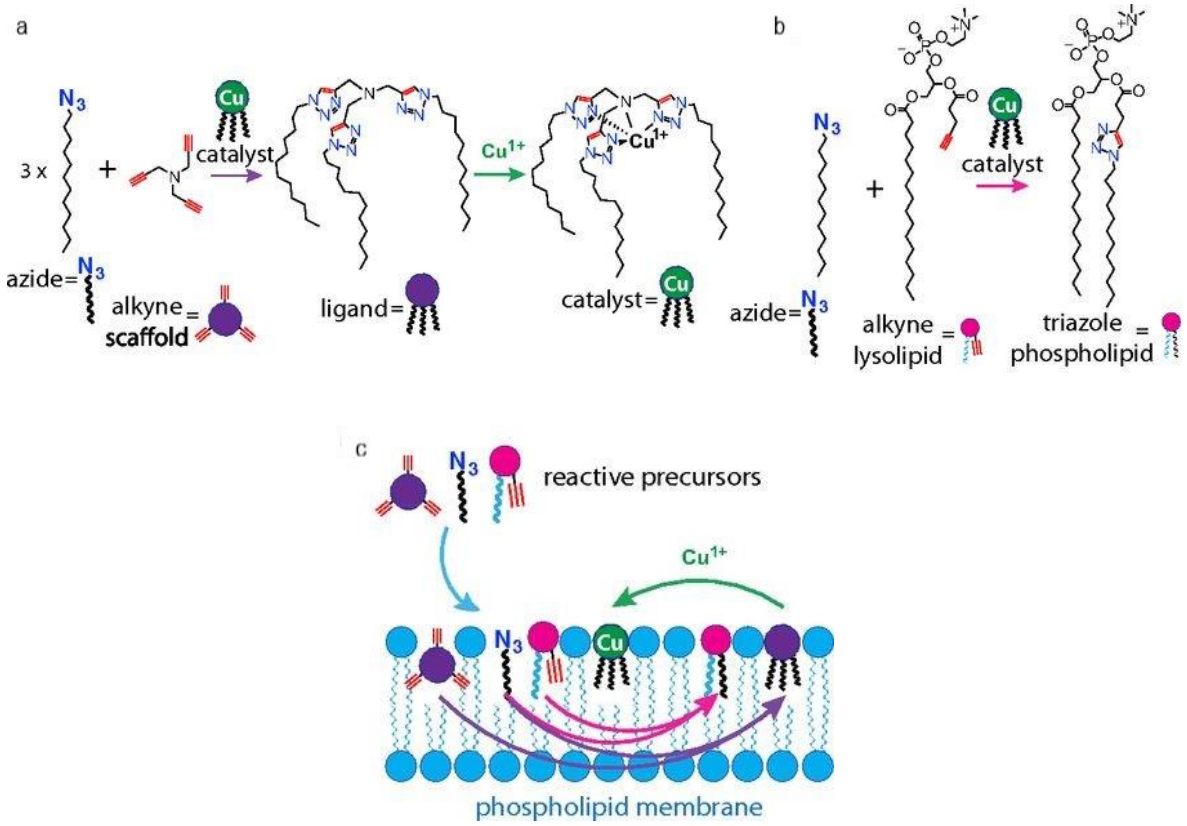


Figure 1. 2. 5. Self-reproducing vesicles reported by Hardy et al. a – reaction scheme for the autocatalytic synthesis of a Cu(I)-ligand complex. b – reaction scheme for the synthesis of a triazole phospholipid catalysed by the Cu(I)-ligand complex in a. c – The production of membrane forming products drive growth and division of vesicles. Adapted with permission.[70]

One difficulty of achieving autopoiesis in a synthetic cell is that a greater number of functional components requires a greater level of regulation, which will inevitably require the coupling of physical and chemical processes.[71] A striking example of the possibilities that can arise from the interplay of chemical and physical effects comes from a protocell model of Sugawara (Figure 1. 2. 6). Vesicles grow by incorporating **1.11**, produced from precursor **1.9**, a process catalysed by **1.10** in the vesicle membrane. In this work, the division of self-reproducing vesicles was coupled to DNA replication, leading to vesicles with more DNA dividing faster.[72–74] This bears close conceptual relation to the hypothetical "core and shell" replication system proposed by Szotak, Bartel and Luisi,[75]

however the system does not show autopoiesis as the catalysts of lipid formation and oligonucleotide reproduction are not replicated, instead becoming diluted through time.

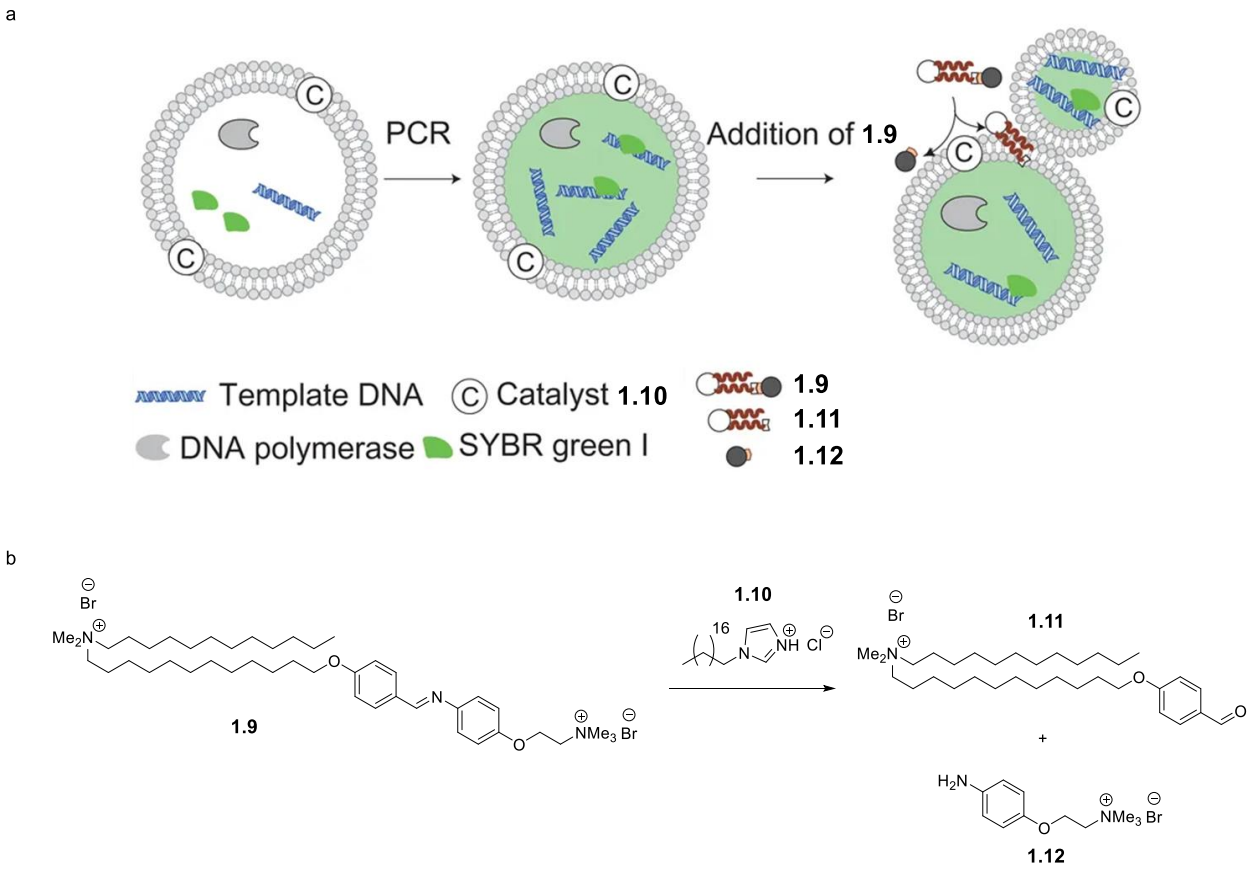


*Figure 1. 2. 6. DNA replication within self-reproducing vesicles. a – conceptual diagram showing DNA replication occurs in the vesicle lumen, and surfactant formation occurs at the membrane. b – reaction scheme for the production of **1.11** from surfactant precursor **1.9** in the presence of nucleophilic catalyst **1.10**. **1.12** is produced as a biproduct. PCR = polymerase chain reaction. Adapted with permission.*[73]

Though it is now possible to observe competition within groups of synthetic replicators, no chemical model has yet shown unconstrained chemical evolution, which for many would be a requirement for the genesis of artificial life.[76,77] It is difficult to predict what will be needed to create a chemical system that can truly evolve. I believe that evolution demands the ability of a system to gain a wide range of functions and this will only be

met by a system which can show high structural diversity. To me, this points towards replicating systems in which many different supramolecular interactions are found.

1. 3 Biological homochirality

The origin of biological homochirality remains one of science's great mysteries. Whilst the possible advantages of homochirality to proto-biopolymers such as fidelity in replication and function are clear, it is unknown whether homochiral building blocks were a prerequisite for life on Earth or came about as a result of it.[12,78–81] Asymmetric autocatalysis has long been proposed as a possible means by which small enantiomeric excesses (ee) could be amplified to larger ones, though experimental realisation has been notoriously challenging.[82–84] There remains a single well established reaction which shows an increase in ee through asymmetric autocatalysis, the alkylation of pyrimidine aldehydes by diisopropylzinc, the Soai reaction.[85,86] My attempts to find a novel reaction in which enantioselectivity increases in time using organocatalysis are described in chapter 2.

Knowledge of homochirality in the molecules of life began with Pasteur over a century and a half ago.[87,88] In a time after the Wöhler urea synthesis, the optical activity of many biologically derived compounds can be seen as biochemistry's last remaining bastion of Vitalism, that is the belief that there is a fundamental difference between synthetic and biological matter.[89,90] Pasteur resolved the problem of why certain molecules when derived from nature (now known to be enantiomerically pure or enriched) showed optical activity, but seemingly identical compounds prepared by chemical synthesis (now known to be racemates) had none. This was done with the now famous manual separation of enantiomers of tartrate salts, whereby mirror-image crystal forms were distinguished by eye, then could be dissolved to give solutions of equal and opposite optical activity.[87,91]

This established the principle of stereoisomerism and showed that optically active compounds did not have to derive from life. It is now known that the biopolymers of life are with rare exceptions constructed exclusively from L-amino acids and D-sugars, a picture that was forming around the turn of the twentieth century led by the work of Fischer.[92–94]

Pleasing, more than a century after Pasteur's work tartrate played another key role in the story, the first determination of absolute configuration of an organic molecule was for tartrate in the X-ray crystallography studies of Bijvoet et al, which could be extrapolated to the sugars and amino acids.[95,96]

1. 4 The role of lipids in life and application to systems chemistry

Biochemical lipids are derived from either condensation of ketoacyl groups (such as fatty acids) or from isoprene units (such as sterols). Lipids have a wide variety of critical functions to the cell, far beyond mere energy storage.

One key role is cellular compartmentalisation. Cells use membrane bound organelles for specialised functions, enabling sets of reactions which would ordinarily be incompatible to occur simultaneously within a cell.[97] Compartmentalisation allows the isolation of metabolites from enzymes which would catalyse their destruction, so without this control, futile cycles would abound, with energy dissipated rather than utilised. Higher effective concentrations of substrates and catalysts are made possible by compartmentalisation, achieved through protein targeting and vesicle trafficking, further increasing overall metabolic efficiency.

Covalent attachment of lipids to proteins acts as a method of spatial control in catalysis. Lipidation of proteins, for example prenylation and fatty acylation, is a common class of

post-translational modification, targeting peptides to bilayers. These processes are reversible, allowing for dynamic and responsive "switching" of peptide localisation.

In bacteria, control of membrane properties is achieved through altering lipid composition, which may be required in response to stress. This is achieved by both *de novo* lipid synthesis, but also chemical modification of existing lipids, for example by altering chain length, and in unsaturated lipids cyclopropanation and *cis* to *trans* isomerisation.[98] Lipids also have a catalysis role in metabolism, lipoic acid is a cofactor for two enzymes of the citric acid cycle, acting as a redox-catalyst, interconverting between its disulfide and dithiol forms.[99]

Lipids are important to cell-signalling, being both common activators of G-protein coupled receptors and also second messengers, for example diacylglycerols, DAG. They also function as extracellular signals, as highlighted by prostaglandins involvement in vasodilation and the inflammation response.[100] Lipids also used as the sensors in signalling pathways. One of the most familiar of these is retinal, the light sensitive component of rhodopsin used in mammalian vision. When light is absorbed by the protonated Schiff base of 11-*cis*-retinal on Lysine-296 the retinal undergoes an isomerisation to all-*trans* retinal. This induces a large conformational change in the rhodopsin protein to the metarhodopsin II form, which in turn activates transducin, the first step in the signal transduction pathway.[101,102]

We believe that lipids are highly promising materials for nanotechnology, currently underused. In synthetic systems, they can adopt different morphologies such as micelles and vesicles, but also more "structural" extended phases like the hexagonal phase and bilayers more generally.[103] The structures lipids adopt can be changed through chemical modification or in response to environmental change. We believe that it is currently possible to draw inspiration from the diverse roles of lipids in life to build functional and

adaptive systems. This offers a different approach to much of traditional supramolecular chemistry, which has privileged structural specificity (highly ordered structures) over diversity of constituent parts, and what may be achieved by having differing and dynamic components. In the same way that building dissipative systems has required a change in the designer's thought processes away from stable, long shelf-life products, we believe that the study of emergence within chemical systems requires a move towards systems that can generate a multiplicity of forms.

Lipid mixtures provide a candidate for our philosophy, with monomers showing the ability to replicate, to aggregate into defined or diverse structures and influence their physical environment through dissolution of hydrophobic material and altering surface tension properties.[104] Though this may seem vague, I hope the results are not. In this thesis, I explore a series of systems which use some of the properties of lipids to show higher function that would otherwise be challenging to achieve. First among these is described in chapter 3, whereby formation of a lipid replicator drives the motion of a protocell through surface tension effects. Through chemotaxis, there is a mutualistic coupling between the physical and chemical processes, with lipid formation causing motion and motion accelerating lipid formation.

Complex behaviour of lipid mixtures is discussed in chapter 4, where a system of competing transient replicators is studied. Here, we see that the dominant surfactant monomer can change through time, allowing succession of replicating lipids, a simple model of chemical evolution built from wholly synthetic parts. In addition to chemical succession, these systems show an increase in structural complexity, with the spontaneous formation of compartments as vesicles.

1. 5 References

1. Benyus, J. M. *Biomimicry : innovation inspired by nature*. (Quill, 1998).
2. Vincent, J. F. V. Biomimetics - A review. *Proceedings of the Institution of Mechanical Engineers, Part H: Journal of Engineering in Medicine* **223**, 919–939 (2009).
3. Kindermann, M., Stahl, I., Reimold, M., Pankau, W. M. & Von Kiedrowski, G. Systems chemistry: Kinetic and computational analysis of a nearly exponential organic replicator. *Angew. Chemie - Int. Ed.* **44**, 6750–6755 (2005).
4. Grzybowski, B., Otto, S. & Philp, D. Systems chemistry: A web themed issue. *Chem. Commun.* **50**, 14924–14925 (2014).
5. Kiedrowski, G. Von, Otto, S. & Herdewijn, P. Welcome home, systems chemists. *J. Syst. Chem.* **1**, 1 (2010).
6. Benner, S. A. Defining life. *Astrobiology* **10**, 1021–30 (2010).
7. Vitas, M. & Dobovišek, A. Towards a General Definition of Life. *Orig. Life Evol. Biosph.* **49**, 77–88 (2019).
8. Tsokolov, S. A. Why is the definition of life so elusive? Epistemological considerations. *Astrobiology* **9**, 401–412 (2009).
9. Rutherford, A. *Creation*. (Viking, 2013).
10. Trifonov, E. N. Vocabulary of definitions of life suggests a definition. *J. Biomol. Struct. Dyn.* **29**, 259–266 (2011).
11. Darwin, C. *On the origin of species by means of natural selection, or the preservation of favoured races in the struggle for life.* (John Murray, 1859).
12. Levy, M. & Ellington, A. D. The descent of polymerization. *Nat. Struct. Biol.* **8**, 580–582 (2001).
13. Rose, S. P. R. (Steven P. R. & Bullock, S.) *The chemistry of life.* (Penguin, 1991).
14. Smith, J. M. Hypercycles and the origin of life. *Nature* **280**, 445–446 (1979).
15. Vaidya, N. *et al.* Spontaneous network formation among cooperative RNA replicators. *Nature* **491**, 72–77 (2012).
16. Kauffman, S. A. *The origins of order : self-organization and selection in evolution*. (Oxford University Press, 1993).
17. Yeates, J. A. M., Hilbe, C., Zwick, M., Nowak, M. A. & Lehman, N. Dynamics of prebiotic RNA reproduction illuminated by chemical game theory. *Proc. Natl. Acad. Sci. U. S. A.* **113**, 5030–5035 (2016).
18. Siepmann, J., Elkharraz, K., Siepmann, F. & Klose, D. How autocatalysis accelerates drug release from PLGA-based microparticles: A quantitative treatment. *Biomacromolecules* **6**, 2312–2319 (2005).
19. Ford Versypt, A. N., Pack, D. W. & Braatz, R. D. Mathematical modeling of drug delivery from autocatalytically degradable PLGA microspheres - A review. *J. Control. Release* **165**, 29–37 (2013).

20. Cabri, W., Ghetti, P., Pozzi, G. & Alpegiani, M. Polymorphisms and patent, market, and legal battles: Cefdinir case study. *Org. Process Res. Dev.* **11**, 64–72 (2007).

21. Bond, A. D., Boese, R. & Desiraju, G. R. On the polymorphism of aspirin: Crystalline aspirin as intergrowths of two 'polymorphic' domains. *Angew. Chemie - Int. Ed.* **46**, 618–622 (2007).

22. Van Rossum, S. A. P., Tena-Solsona, M., Van Esch, J. H., Eelkema, R. & Boekhoven, J. Dissipative out-of-equilibrium assembly of man-made supramolecular materials. *Chem. Soc. Rev.* **46**, 5519–5535 (2017).

23. De, S. & Klajn, R. Dissipative Self-Assembly Driven by the Consumption of Chemical Fuels. *Adv. Mater.* **30**, 1706750 (2018).

24. Morrow, S. M., Colomer, I. & Fletcher, S. P. A chemically fuelled self-replicator. *Nat. Commun.* **10**, 1011 (2019).

25. Aoki, S. K. *et al.* A universal biomolecular integral feedback controller for robust perfect adaptation. *Nature* **570**, 533–537 (2019).

26. Nghe, P. *et al.* Prebiotic network evolution: Six key parameters. *Mol. Biosyst.* **11**, 3206–3217 (2015).

27. Balazs, A. C., Fischer, P. & Sen, A. Intelligent Nano/Micromotors: Using Free Energy To Fabricate Organized Systems Driven Far from Equilibrium. *Acc. Chem. Res.* **51**, 2979–2979 (2018).

28. There's plenty of room at the top. *Nat. Nanotechnol.* **14**, 729–729 (2019).

29. Lancia, F., Ryabchun, A. & Katsonis, N. Life-like motion driven by artificial molecular machines. *Nat. Rev. Chem.* **3**, 536–551 (2019).

30. Whitesides, G. M. Soft Robotics. *Angew. Chemie - Int. Ed.* **57**, 4258–4273 (2018).

31. Schwille, P. How Simple Could Life Be? *Angew. Chemie - Int. Ed.* **56**, 10998–11002 (2017).

32. Cronin, L. *et al.* The imitation game - A computational chemical approach to recognizing life. *Nat. Biotechnol.* **24**, 1203–1206 (2006).

33. Bissette, A. J. & Fletcher, S. P. Mechanisms of Autocatalysis. *Angew. Chemie - Int. Ed.* **52**, 12800–12826 (2013).

34. Le Vay, K., Weise, L. I., Libicher, K., Mascarenhas, J. & Mutschler, H. Templated Self-Replication in Biomimetic Systems. *Advanced Biosystems* **3**, 1800313 (2019).

35. Blackmond, D. G. An examination of the role of autocatalytic cycles in the chemistry of proposed primordial reactions. *Angew. Chemie - Int. Ed.* **48**, 386–390 (2009).

36. Quijano, M. R. *et al.* Distinct Autocatalytic α- N-Methylating Precursors Expand the Borosin RiPP Family of Peptide Natural Products. *J. Am. Chem. Soc.* **141**, 9637–9644 (2019).

37. Teixeira, A. *et al.* Autocatalytic RNA cleavage in the human β-globin pre-mRNA promotes transcription termination. *Nature* **432**, 526–530 (2004).

38. Clixby, G. & Twyman, L. Self-replicating systems. *Org. Biomol. Chem.* **14**, 4170–4184 (2016).

39. Patzke, V. & Kiedrowski, G. von. Self replicating systems. *Arkivoc* **2007**, 293–310 (2007).

40. Kosikova, T. & Philp, D. Exploring the emergence of complexity using synthetic replicators. *Chemical Society Reviews* **46**, 7274–7305 (2017).

41. Hudson, J. L. & Mankin, J. C. Chaos in the Belousov–Zhabotinskii reaction. *J. Chem. Phys.* **74**, 6171–6177 (1981).

42. Sun, X., Dahlhauser, S. D. & Anslyn, E. V. New Autoinductive Cascade for the Optical Sensing of Fluoride: Application in the Detection of Phosphoryl Fluoride Nerve Agents. *J. Am. Chem. Soc.* **139**, 4635–4638 (2017).

43. Sun, X., Reuther, J. F., Phillips, S. T. & Anslyn, E. V. Coupling Activity-Based Detection, Target Amplification, Colorimetric and Fluorometric Signal Amplification, for Quantitative Chemosensing of Fluoride Generated from Nerve Agents. *Chem. - A Eur. J.* **23**, 3903–3909 (2017).

44. Wintner, E. A., Conn, M. M. & Rebek, J. Studies in Molecular Replication. *Acc. Chem. Res.* **27**, 198–203 (1994).

45. von Kiedrowski, G. A Self-Replicating Hexadeoxynucleotide. *Angew. Chemie - Int. Ed. Eng.* **25**, 932–935 (1986).

46. Inoue, T. & Orgel, L. E. A nonenzymatic RNA polymerase model. *Science* **219**, 859–862 (1983).

47. Kosikova, T. & Philp, D. A Critical Cross-Catalytic Relationship Determines the Outcome of Competition in a Replicator Network. *J. Am. Chem. Soc.* **139**, 12579–12590 (2017).

48. Carnall, J. M. A. *et al.* Mechanosensitive self-replication driven by self-organization. *Science* **327**, 1502–1506 (2010).

49. Giuseppone, N. Toward self-constructing materials: A systems chemistry approach. *Acc. Chem. Res.* **45**, 2178–2188 (2012).

50. Hardy, M. D. *et al.* Self-reproducing catalyst drives repeated phospholipid synthesis and membrane growth. *Proc. Natl. Acad. Sci. U. S. A.* **112**, 8187–8192 (2015).

51. Rubinov, B., Wagner, N., Rapaport, H. & Ashkenasy, G. Self-replicating amphiphilic β-sheet peptides. *Angew. Chemie - Int. Ed.* **48**, 6683–6686 (2009).

52. Ikeda, K. & Nakano, M. Self-reproduction of nanoparticles through synergistic self-assembly. *Langmuir* **31**, 17–21 (2015).

53. Angelica Bachmann, P., Walde, P., Luigi Luisi, P. & Lang, J. Self-Replicating Reverse Micelles and Chemical Autopoiesis. *J. Am. Chem. Soc.* **112**, 8200–8201 (1990).

54. Angelica Bachmann, P., Luisi, P. L. & Lang, J. Self-Replicating Reverse Micelles. *Chim. Int. J. Chem.* **45**, 266–268 (1991).

55. Bachmann, P. A., Walde, P., Luisi, P. L. & Lang, J. Self-Replicating Micelles: Aqueous Micelles and Enzymatically Driven Reactions in Reverse Micelles. *J. Am. Chem. Soc.* **113**, 8204–8209 (1991).

56. Bachmann, P. A., Luisi, P. L. & Lang, J. Autocatalytic self-replicating micelles as models for prebiotic structures. *Nature* **357**, 57–59 (1992).

57. Billingham, J. & Coveney, P. V. Kinetics of self-replicating micelles. *J. Chem. Soc. Faraday Trans.* **90**, 1953 (1994).

58. Ruiz-Mirazo, K., Briones, C. & de la Escosura, A. Prebiotic Systems Chemistry: New Perspectives for the Origins of Life. *Chem. Rev.* **114**, 285–366 (2014).

59. Nguyen, R., Allouche, L., Buhler, E. & Giuseppone, N. Dynamic combinatorial evolution within self-replicating supramolecular assemblies. *Angew. Chemie - Int. Ed.* **48**, 1093–1096 (2009).

60. Bissette, A. J., Odell, B. & Fletcher, S. P. Physical autocatalysis driven by a bond-forming thiol–ene reaction. *Nat. Commun.* **5**, 4607 (2014).

61. Ortega-Arroyo, J., Bissette, A. J., Kukura, P. & Fletcher, S. P. Visualization of the spontaneous emergence of a complex, dynamic, and autocatalytic system. *Proc. Natl. Acad. Sci. U. S. A.* **113**, 11122–11126 (2016).

62. Kust, P. R. & Rathman, J. F. Synthesis of Surfactants by Micellar Autocatalysis: N,N-Dimethyldodecylamine N-Oxide. *Langmuir* **11**, 3007–3012 (1995).

63. Post, E. A. J. & Fletcher, S. P. Controlling the Kinetics of Self-Reproducing Micelles by Catalyst Compartmentalization in a Biphasic System. *J. Org. Chem.* **84**, 2741–2755 (2019).

64. Maturana, H. R. & Varela, F. J. *Autopoiesis and cognition: the realization of the living*. (D. Reidel Pub. Co, 1980).

65. Razeto-Barry, P. Autopoiesis 40 years Later. A Review and a Reformulation. *Orig. Life Evol. Biosph.* **42**, 543–567 (2012).

66. Luisi, P. L. & Varela, F. J. Self-replicating micelles - A chemical version of a minimal autopoietic system. *Orig. Life Evol. Biosph.* **19**, 633–643 (1989).

67. Chizmadzhew, Y. A., Maestro, M. & Mavelli, F. A simplified kinetic model for an autopoietic synthesis of micelles. *Chem. Phys. Lett.* **226**, 56–62 (1994).

68. Buhse, T., Nagarajan, R., Lavabre, D. & Micheau, J. C. Phase-transfer model for the dynamics of 'micellar autocatalysis'. *J. Phys. Chem. A* **101**, 3910–3917 (1997).

69. Buhse, T., Lavabre, D., Nagarajan, R. & Micheau, J. C. Origin of autocatalysis in the biphasic alkaline hydrolysis of C-4 to C-8 ethyl alkanoates. *J. Phys. Chem. A* **102**, 10552–10559 (1998).

70. Hardy, M. D. *et al.* Self-reproducing catalyst drives repeated phospholipid synthesis and membrane growth. *Proc. Natl. Acad. Sci. U. S. A.* **112**, 8187–8192 (2015).

71. Suzuki, K. & Ikegami, T. Shapes and self-movement in protocell systems. *Artif. Life* **15**, 59–70 (2009).

72. Kurihara, K. *et al.* A recursive vesicle-based model protocell with a primitive model cell cycle. *Nat. Commun.* **6**, 8352 (2015).

73. Kurihara, K. *et al.* Self-reproduction of supramolecular giant vesicles combined with the amplification of encapsulated DNA. *Nat. Chem.* **3**, 775–781 (2011).

74. Luisi, P. L. & Stano, P. Synthetic biology: Minimal cell mimicry. *Nat. Chem.* **3**, 755–756 (2011).

75. Szostak, J. W., Bartel, D. P. & Luisi, P. L. Synthesizing life. *Nature* **409**, 387–390 (2001).

76. Duim, H. & Otto, S. Towards open-ended evolution in self-replicating molecular systems. *Beilstein Journal of Organic Chemistry* **13**, 1189–1203 (2017).

77. Mason, S. F. (Stephen F.) *Chemical evolution : origin of the elements, molecules, and living systems*. (Clarendon Press, 1991).

78. Coveney, P. V., Swadling, J. B., Wattis, J. A. D. & Greenwell, H. C. Theory, modelling and simulation in origins of life studies. *Chemical Society Reviews* **41**, 5430–5446 (2012).

79. Saghatellan, A., Yokobayashi, Y., Soltani, K. & Ghadiri, M. R. A chiroselective peptide replicator. *Nature* **409**, 797–801 (2001).

80. Pizzarello, S., Huang, Y. & Alexandre, M. R. Molecular asymmetry in extraterrestrial chemistry: Insights from a pristine meteorite. *Proc. Natl. Acad. Sci. U. S. A.* **105**, 3700–3704 (2008).

81. Wu, M., Walker, S. I. & Higgs, P. G. Autocatalytic replication and homochirality in biopolymers: Is homochirality a requirement of life or a result of it? *Astrobiology* **12**, 818–829 (2012).

82. Frank, F. C. On spontaneous asymmetric synthesis. *Biochim. Biophys. Acta* **11**, 459–463 (1953).

83. Wynberg, H. Asymmetric autocatalysis: Facts and fancy. *J. Macromol. Sci. Part A - Chem.* **26**, 1033–1041 (1989).

84. (Palyi, G., Kurdi, R. & Zucchi, C.) *Advances in Asymmetric Autocatalysis and Related Topics* (ELSEVIER ACADEMIC Press, 2017).

85. Soai, K., Niwa, S. & Hori, H. Asymmetric self-catalytic reaction. Self-production of chiral 1-(3-pyridyl)alkanols as chiral self-catalysts in the enantioselective addition of dialkylzinc reagents to pyridine-3-carbaldehyde. *J. Chem. Soc. Chem. Commun.* **14**, 982–983 (1990).

86. Soai, K., Shibata, T., Morioka, H. & Choji, K. Asymmetric autocatalysis and amplification of enantiomeric excess of a chiral molecule. *Nature* **378**, 767–768 (1995).

87. Pasteur, L. Relation qui peut exister entre la forme crystalline et la compostion chimique, et sur las cause de la polarization rotatoire. *Ann Chim Phys* **26**, 535–538 (1848).

88. Blackmond, D. G. The origin of biological homochirality. *Cold Spring Harb. Perspect. Biol.* **2**, a002147 (2010).

89. Ramberg, P. J. The Death of Vitalism and The Birth of Organic Chemistry: Wohler's Urea Synthesis and the Disciplinary Identity of Organic Chemistry. *Ambix* **47**, 170–195 (2000).

90. Schummer, J. The notion of nature in chemistry. *Stud. Hist. Philos. Sci. Part A* **34**, 705–736 (2003).

91. Vander Hook, S. *Louis Pasteur : groundbreaking chemist & biologist*. (ABDO Pub. Company, 2011).

92. Kunz, H. Emil Fischer - Unequalled classicist, master of organic chemistry research, and inspired trailblazer of biological chemistry. *Angew. Chemie - Int. Ed.* **41**, 4439–4451 (2002).

93. Creighton, T. E. *Proteins : structures and molecular properties*. (W.H. Freeman, 1993).

94. Pisarewicz, K., Mora, D., Pflueger, F. C., Fields, G. B. & Mari, F. Polypeptide chains containing D-γ-hydroxyvaline. *J. Am. Chem. Soc.* **127**, 6207–6215 (2005).

95. Bijvoet, J. M., Peerdeman, A. F. & Van Bommel, A. J. Determination of the absolute configuration of optically active compounds by means of X-rays. *Nature* **168**, 271–272 (1951).

96. Cahn, R. S., Ingold, C. K. & Prelog, V. The specification of asymmetric configuration in organic chemistry. *Experientia* **12**, 81–94 (1956).

97. Chen, A. H. & Silver, P. A. Designing biological compartmentalization. *Trends in Cell Biology* **22**, 662–670 (2012).

98. Zhang, Y. M. & Rock, C. O. Membrane lipid homeostasis in bacteria. *Nat. Rev. Microbiol.* **6**, 222–233 (2008).

99. Raddatz, G. & Bisswanger, H. Receptor site and stereospecifity of dihydrolipoamide dehydrogenase for R- and S-lipoamide: A molecular modeling study. *J. Biotechnol.* **58**, 89–100 (1997).

100. Ricciotti, E. & Fitzgerald, G. A. Prostaglandins and inflammation. *Arterioscler. Thromb. Vasc. Biol.* **31**, 986–1000 (2011).

101. Polard, T. D., Earnshaw, W. C., Lippincott-Schwartz, J. & Johnson, G. T. *Cell Biology*. (Elsevier, 2017).

102. Spudich, J. L., Yang, C.-S., Jung, K.-H. & Spudich, E. N. Retinylidene Proteins: Structures and Functions from Archaea to Humans. *Annu. Rev. Cell Dev. Biol.* **16**, 365–392 (2000).

103. Hamley, I. W. *Introduction to soft matter : synthetic and biological self-assembling materials*. (John Wiley & Sons, 2007).

104. Budin, I. & Szostak, J. W. Physical effects underlying the transition from primitive to modern cell membranes. *Proc. Natl. Acad. Sci. U. S. A.* **108**, 5249–5254 (2011).

Chapter 2

Designs for asymmetric autocatalysis via organocatalysis

Chapter 2

Designs for asymmetric autocatalysis via organocatalysis

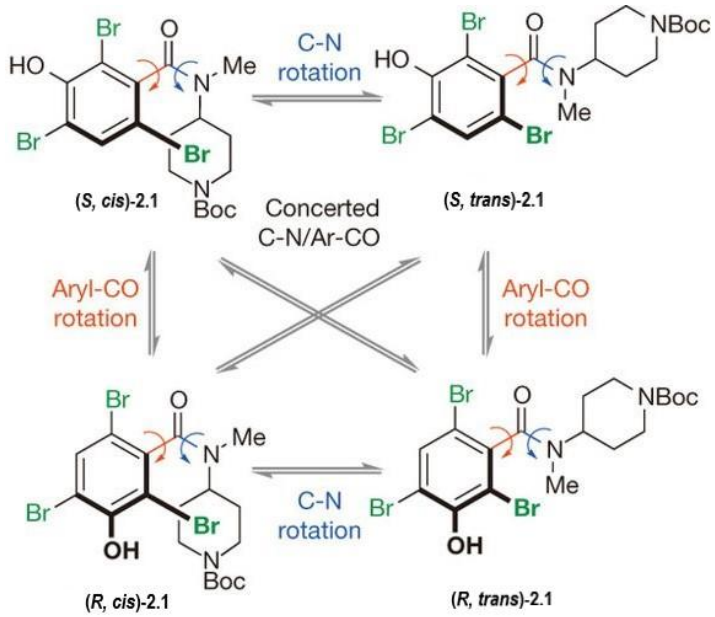
2. 1 Introduction

2. 1. 1 The origins of homochirality and asymmetric autocatalysis

Despite biological homochirality being known since the late nineteenth century, its historic origin remains a mystery. Spontaneous increase in enantiomeric excess of one compound within a homogenous environment is thermodynamically unfavourable, reducing entropy. So to achieve this the process must be coupled to another, thermodynamically favourable process. In simple kinetic resolutions, a chiral catalyst is used to selectively react with one enantiomer of starting material over the other, leading to an increase in ee of the starting material. Recently a catalytic deracemization was reported by the Bach group, whereby energy absorbed from light drives the deracemization of allenes through the action of a chiral triplet sensitiser catalyst.[1] Methods such as this do not solve the origin of molecular asymmetry however, as they require enantiopure catalyst.

Without a chiral catalyst, a spontaneous increase in ee may seem impossible within a homogeneous system, however this is not the case, as demonstrated by Miller's group.[2] They report that a diasteromeric mixture of an atropisomeric aryl amide **2.1** undergoes enantiomeric enrichment spontaneously coupled to the enantiomeric depletion of another diastereomer (Figure 2. 1. 1. 1). Diasteromers interconvert through bond rotation toward equilibrium, (*trans*)-**2.1** increases in ee through time with a concomitant decrease in ee of (*cis*)-**2.1**.

a



b

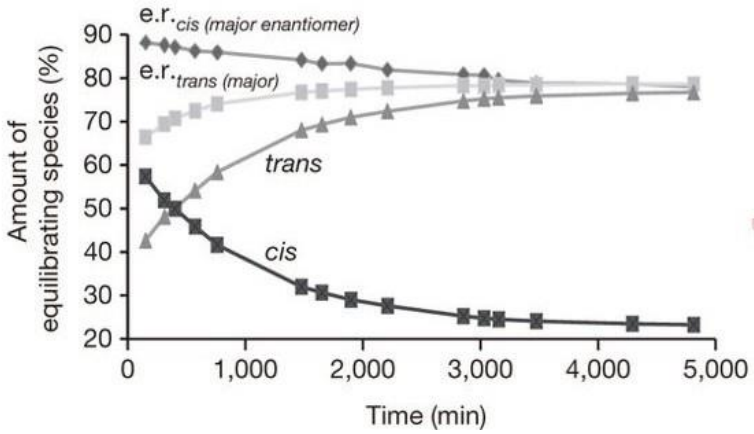


*Figure 2. 1. 1. 1. a – the four stereoisomers of **2.1** and the possible interconversions between them via bond rotations. DFT studies suggest that interconversion primarily occurs through rotation about the C-N bonds. b – Plot of the composition of a solution of **2.1** through time. Adapted with permission.*[2]

Asymmetric autocatalysis has been proposed as a possible mechanism of amplifying the small ees found in abiotic environments, like meteorites, to the levels found in life.[3,4]

As originally described in the Frank model, an asymmetric autocatalytic reaction requires high enantioselectivity and mutual antagonism between enantiomers of product to increase in ee through time.[5] Antagonism between enantiomers, or cross-inhibition, is a way to "silence" the minor enantiomer reducing its catalytic effects. Antagonism of this type was later discovered, described by Kagan as positive nonlinear effects.[6] Without

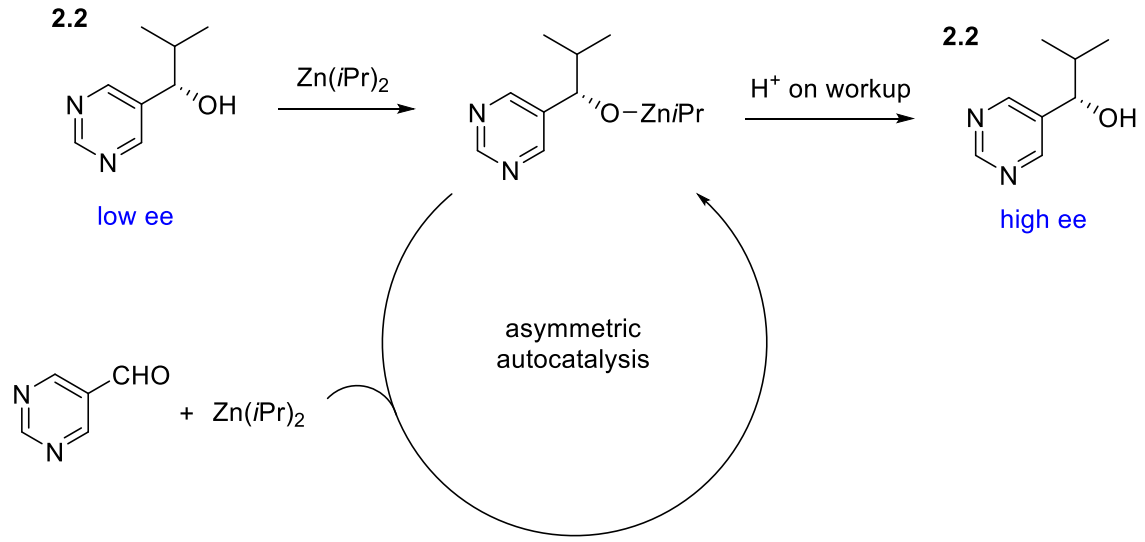
positive nonlinear effects, any reaction which was not completely enantioselective would produce some of the minor enantiomer, which would go on to produce more product with the opposite selectivity to the major enantiomer, leading towards a racemic product composition. Achieving both requirements of autocatalysis and positive nonlinear effects is highly challenging.

The only well studied example of this phenomenon is the alkylation of pyrimidine aldehydes by diisopropylzinc in the Soai reaction (figure 2. 1. 1. 2).[7–10] In their seminal report, the authors were able to increase the enantiomeric enrichment of the pyrimidine alcohol product **2.2** from 5% ee to 89% ee in just four successive iterations of the reaction.[8] The reaction is extraordinarily sensitive to the addition of chiral additives, with chiral mineral faces and even small molecules chiral only by isotopic substitution leading to reliable induction of absolute chirality.[11–13] The reaction has a narrow substrate scope for enantiomeric enrichment to occur, with diisopropylzinc being the only alkylating agent and a small range of substitutions on the 2-position of the pyrimidine being tolerated.

The specificity of reagents required for the reaction to proceed with increasing enantioenrichment is testament to the complexity of the mechanism. Blackmond et al. studied the reaction by calorimetry, which showed racemic and enantiopure product both catalyse the reaction albeit at differing rates, a finding that precludes purely "reservoir model" type behaviour in the reaction.[14] The authors found their results to be consistent with a catalytically active dimer model. Further studies, based on calorimetry and DFT calculations have suggested the importance of tetrameric structures.[9,15,16] In terms of outlook, studies into the mechanism are still ongoing, currently being investigated by the groups of Scott Denmark and Oliver Trapp.[17] Doubtless a great many aggregated species

are present, the precise roles of which are yet to be seen. Providing a definitive mechanism is still very much an open area of research.

a



b

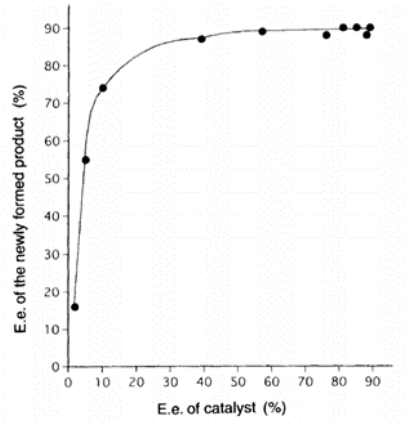


*Figure 2. 1. 1. 2. The Soai reaction. a – reaction scheme where an initially low ee of **2.2** can be amplified to higher ee using asymmetric autocatalysis. b – relationship between the ee of added **2.2** and isolated **2.2** after reaction. The major enantiomer is S-**2.2**. Here the catalyst loading is 0.20 eq., and the reaction is performed at 0 °C in toluene for 96 h. Adapted with permission.*[8]

Unsuccessful attempts toward asymmetric autocatalysis are unlikely to be reported in the literature, and therefore it is very hard to establish what designs have been attempted and what progress has been made in other reactions. One interesting related study was reported by Stork and Trapp, inspired by prior work where one enantiomer of a low activity racemic catalyst can be activated by the addition of a single enantiomer of chiral ligand to form highly active and enantioselective catalyst.[18,19] The authors designed a

flexible phosphoramidite containing an amide motif known to have an unusually strong non-covalent interaction with another amide (Figure 2. 1. 1. 3).[20] The product of their hydrogenation reaction is the second amide, which they expected to bind to the ligand *in situ* and rigidify it. In this work, the chiral catalyst becomes more enantioselective upon binding the product, thus leading to an increase in enantioselectivity through time. The reaction does not show chiral symmetry breaking as the Soai reaction does, as the catalyst is chiral and binding both enantiomers of product endow enantioselectivity towards the same absolute chirality of product (*S*).

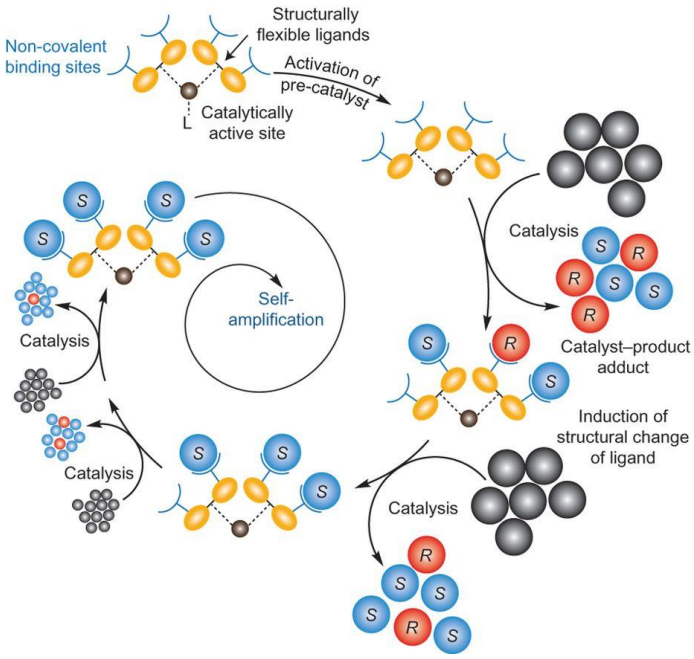


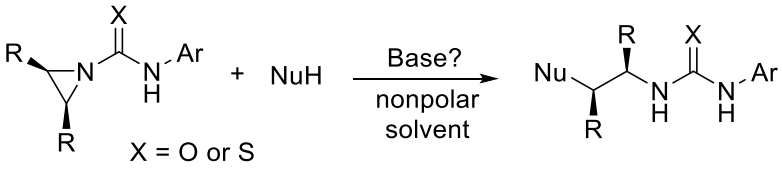
Figure 2. 1. 1. 3. Autoinductive hydrogenation, showing increase in enantioselectivity through time. Reproduced with permission.[18]

We believe that the development of an organocatalytic asymmetric autocatalytic reaction could show greater prebiotic relevance than the otherwise exceptional Soai reaction. Typically organocatalytic reactions are much less sensitive to air and moisture than those involving organometallics. Self-replication of chiral molecules using template replication has been investigated, though no examples of asymmetric autocatalysis have been yet reported, probably due to low selectivities.[21,22]

2. 1. 2 Design for asymmetric autocatalysis using organocatalysis

We designed a reaction based on either urea or thioureas (Figure 2. 1. 2. 1). Here the addition of a nucleophile to a *meso*-aziridine forms a chiral urea or thiourea, which may activate starting material through hydrogen bonding. Nonlinear effects may arise from aggregation of the autocatalyst. There was great progress in the development of thiourea and urea organocatalysis in the early years of the new millennium.[23–25] Whilst thioureas are typically stronger H bond donors, ureas can be more effective in certain transformations.[26,27] The use of ureas has been somewhat limited by their greater propensity for aggregation,[26,28] which in our design may actually be advantageous as a possible source of nonlinear effects.

a



b

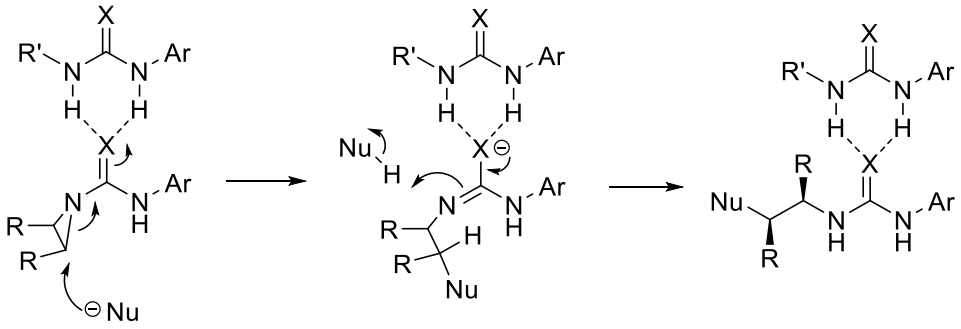


Figure 2. 1. 2. 1. Design for an asymmetric autocatalytic reaction. a – an addition reaction between a nucleophile and a meso-aziridine to form a thiourea or urea catalyst, b – the envisaged activation mode, where the product catalyst activates the starting material through hydrogen bonding.

Numerous desymmetrisations of aziridines have been reported and the topic has been reviewed extensively.[29–31] Typically chiral Lewis acids (Cr(III),[32] Y(III),[33] Gd(III)[34] and others) or Brønsted acids are used, though there are a few examples using chiral counterions.[35,36] There has been a single report of using thioureas or ureas in these

desymmetrisations, whereby Mita and Jacobsen show a bifunctional thiourea **2.3** catalyses the addition of HCl to *meso*-aziridines (Figure 2. 1. 2. 2).[37] We hoped that despite the ubiquity of acidic activation in prior aziridine desymmetrisations we would be able to find conditions or substrates where hydrogen bonding catalysis is sufficient.

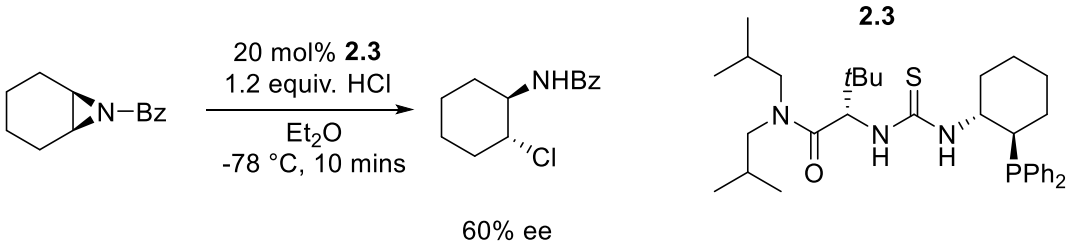


Figure 2. 1. 2. 2. Thiourea catalysed desymmetrisation of aziridines by addition of HCl. Adapted with permission.[37]

The Frank model provides us with a way to approach the daunting challenge of asymmetric autocatalysis. Firstly, we needed to establish that a reaction of our design showed autocatalysis, that is small molecule thioureas or ureas can function as replicators. There is a single example of a thiourea replicator, however the thiourea moiety is not believed to play an active role in autocatalysis.[38] Secondly, we needed to show that nonlinear effects can be found in thiourea or urea catalysis (see section 2. 4). Thirdly, we would need to couple these two things together, combining nonlinear effects and autocatalysis in a single reaction.

Finding nonlinear effects in our system design seemed likely due to the close structural similarity with a series of compounds studied in the Feringa group.[39,40] They found nonlinear effects in the gelation of a series of bis-ureas (Figure 2. 1. 2. 3). For compound **2.4**, the racemate forms a gel, whilst enantiopure compound does not. Bizarrely, for **2.5** the trend is reversed, with enantiopure compound being a gelator and racemate being crystalline.

Since our study, the Meijer group has reported investigations into *trans*-1,2-bis(amido)cyclohexanes substituted with other functional groups, amides and thioamides, also showing similar differences in the properties between racemic and enantiopure compounds.[41] Perhaps most interestingly, in their system the effects in gelator molecules is well correlated to crystalline analogues. This opens the possibility for screening and design of desired self-sorting and chiral discrimination properties in the solid state, aided with crystal structures to determine the importance of particular interactions, and then be able to translate this to supramolecular assembly in a gelator.

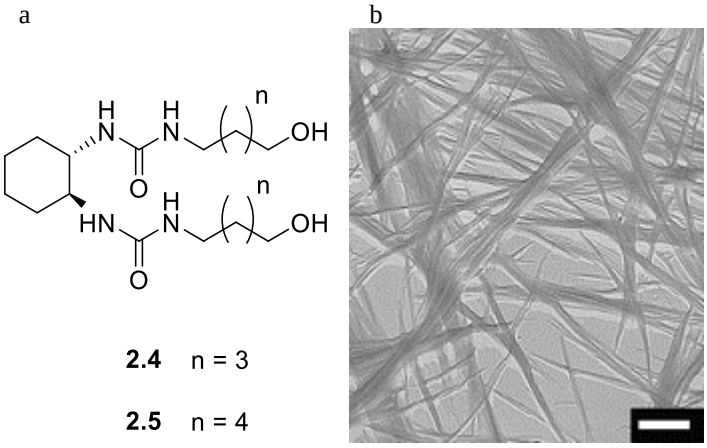


Figure 2. 1. 2. 3. a – Structures of bis-urea compounds studied for their aggregation effects. b – Transmission electron micrograph of hydrogel formed with racemic ***2.5****. Scale bar = 1 µm. Reproduced with permission.*[40]

2. 2 Attempts towards asymmetric autocatalysis using aziridine thioureas and ureas

2. 2. 1 Synthesis of substrates

Aziridine **2.6** was synthesised according to the method of Nambutemi (Figure 2. 2. 1. 1).[42] Several literature methods for formation of **2.7** were tried,[43–45] with only the method of Krasnova being successful, but with low, poorly-reproducible yields.[46]

Contrary to their report, the reaction commonly stalled at intermediate **2.8** which was found to form **2.7** upon treatment with acetic acid in chloroform.

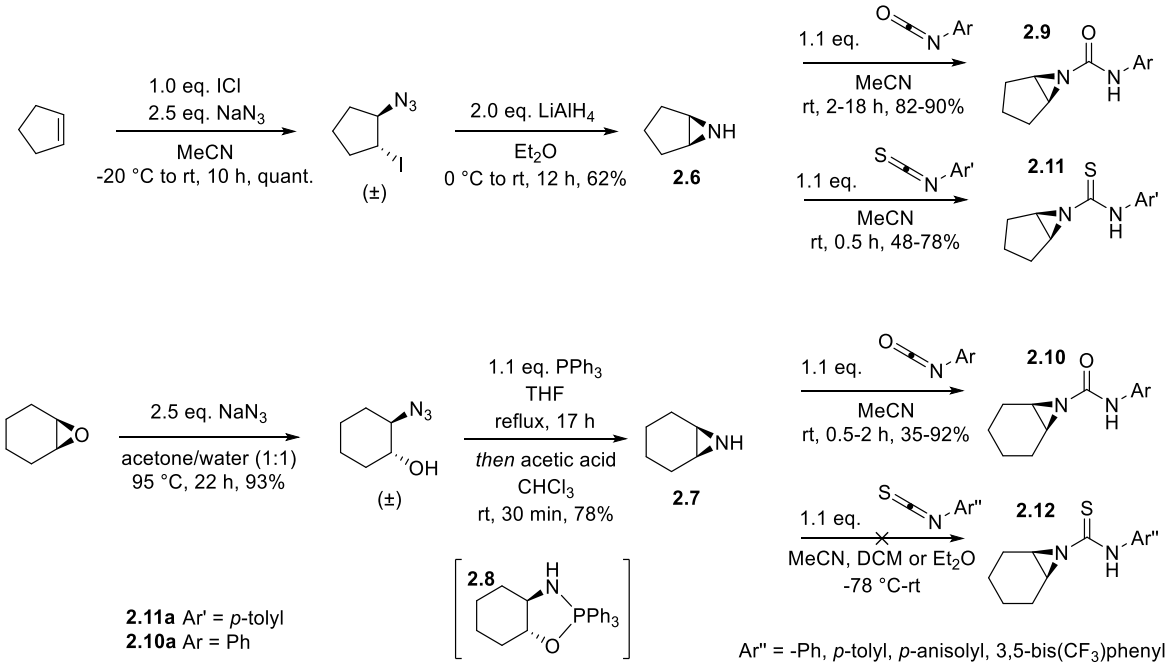


Figure 2. 2. 1. 1. Synthesis of meso-aziridine substrates.

Both aziridines **2.6** and **2.7** reacted with isocyanates to give the desired substrates **2.9** and **2.10** respectively. The thioureas **2.11** and **2.12** behave surprising differently to their urea counterparts. Reactions to form **2.11** were not tolerant of electron deficient isothiocyanates. Although **2.12** appeared to be formed at -78 °C by TLC, the reactions required up to 72 h to go to completion. However, **2.12** was unstable at temperatures above -40 °C, decomposing to a polymeric mixture for all aryl substitution patterns tried.

2. 2. 2 Reactivity of substrates with nucleophiles

A wide range of nucleophiles were screened for reaction with substrates **2.9**, **2.10** and **2.11** in nonpolar solvents (Tables 2. 6. 2. 1-3). Reactions were performed both in the presence and absence of a product mimic (e.g. **2.13**), with the aim of observing a difference in reactivity suggestive of potential autocatalysis (Figure 2. 2. 2. 1a). Hard nucleophiles were found to be unreactive, due to deprotonation of the substrates. The vast

majority of soft nucleophiles were unreactive with all substrates, even when refluxed in toluene for 18 h. Substrate **2.11a** was found to unproductively react with morpholine and DMAP at the thiocarbonyl. Substrate **2.10a** was found exclusively to react with aryl thiols to give the urea products, the sole example of desired reactivity. Disappointingly the only case where a difference in reactivity on addition of the product mimic was observed was a decomposition (Table 2. 6. 2. 1, entry 12).

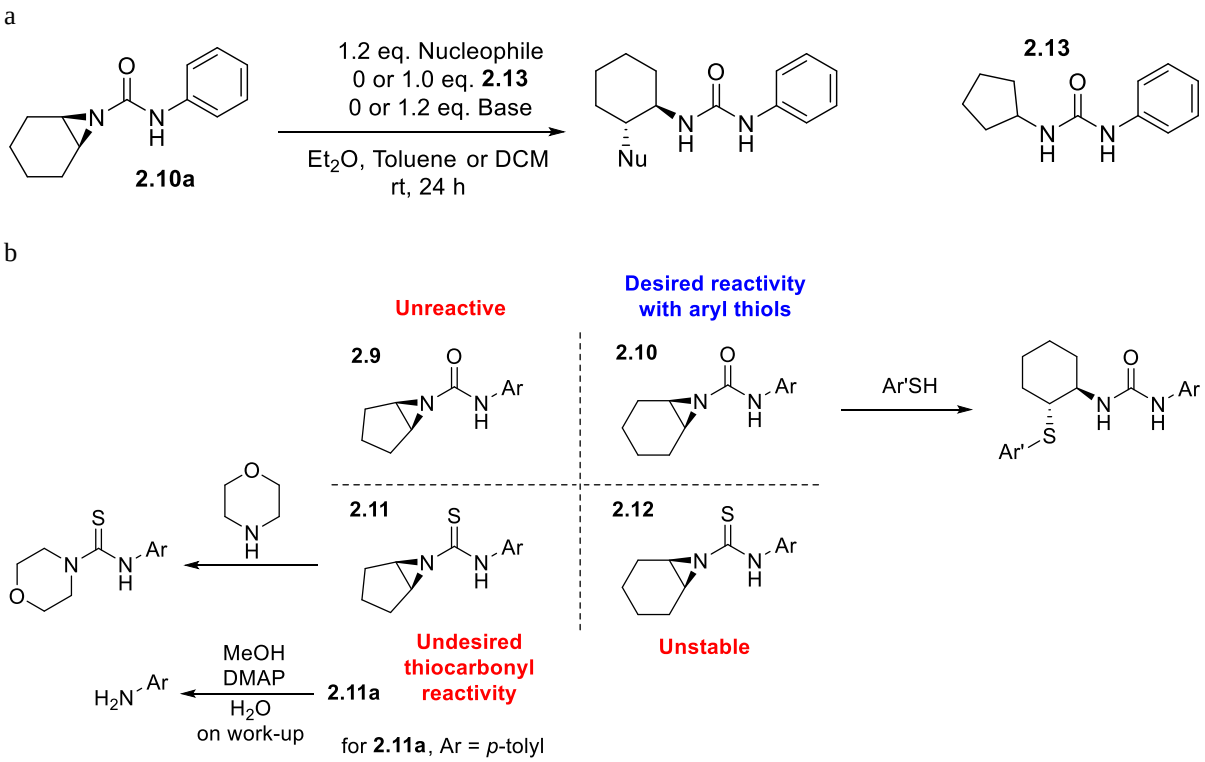


*Figure 2. 2. 2. 1. a – Typical nucleophile screening conditions, b – Summary of the observed reactivities of the substrates **2.9**, **2.10** and **2.11**.*

Substrates **2.14**, **2.9a** and **2.15** were designed in order to try to make more reactive urea substrates (Figure 2. 2. 2. 2). **2.14** and **2.9a** were developed to test if the lack of reactivity was due to intramolecular aryl CH-carbonyl interaction blocking hydrogen bonding to the carbonyl (see **2.9b**, figure 2. 2. 2. 2), however both substrates were found to be unreactive (Table 2. 6. 2. 4).[47] Urea **2.15** was inspired by the observed rate enhancements of S_N2 reactions at benzylic carbons, but this substrate was unreactive to a series of conditions

(Table 2. 6. 2. 4).[48] As urea substrates of structure **2.9** were less reactive than those of **2.10**, thiourea **2.16** was synthesised to see if the lack of desired reactivity was specific to the [3.1.0] bicycle motif in **2.11**, however this substrate was also unreactive (Table 2. 6. 2. 5).

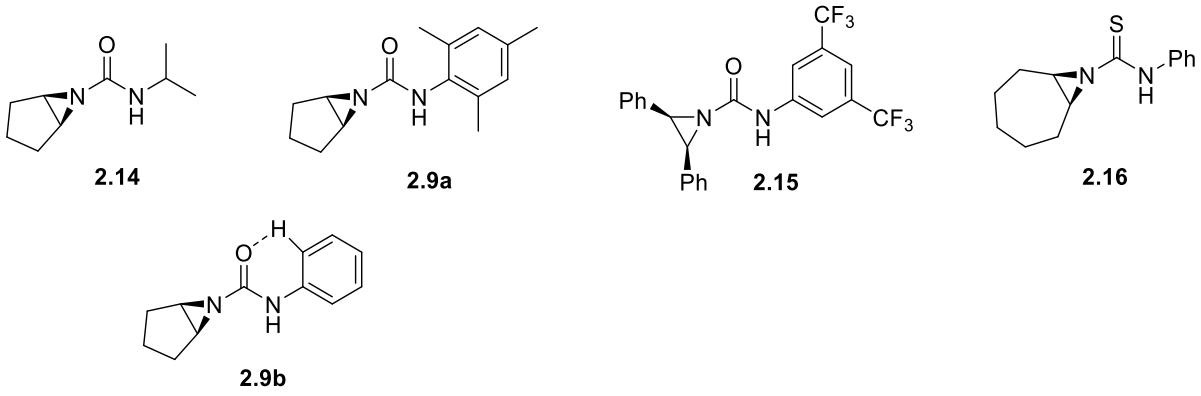
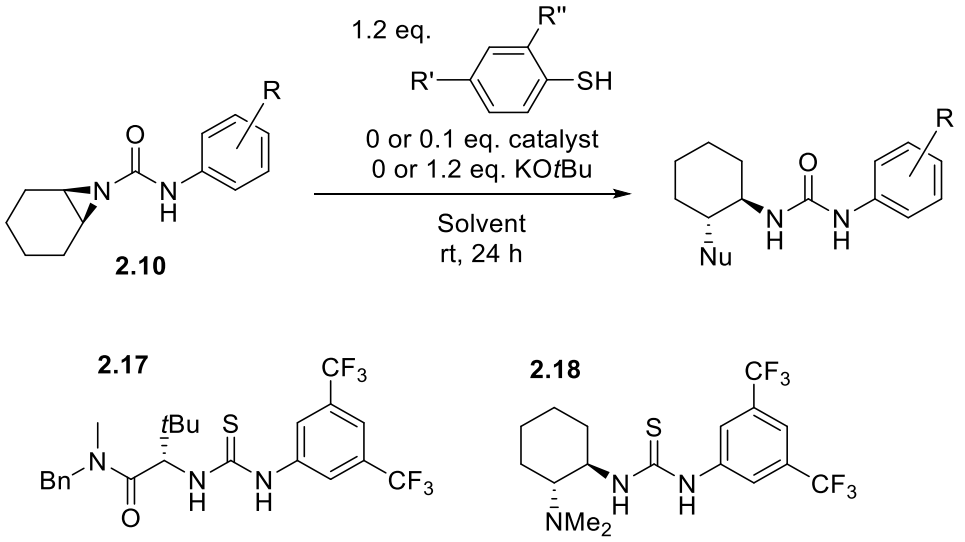


Figure 2. 2. 2. 2. Other urea and thiourea substrates tested, none of which showed desired reactivity.

2. 2. 3 Enantioselectivity using thiourea catalysts and reaction kinetics

Thiourea catalysts known to promote enantioselective reactions were added to the reaction (Table 2. 2. 3. 1) to test whether enantioselectivity could be imparted by a chiral hydrogen bond donor.[49,50] If so, the structures of the reagents and conditions found could influence the design of asymmetric autocatalytic versions of the reaction. A range of conditions were tried for reaction between phenyl urea substrate **2.10a** and 4-methylbenzenethiol, with negligible ees being observed in all cases (Table 2. 2. 3. 1 entries 1-2 and tables 2. 6. 3. 1 and 2. 6. 3. 2). Concerned that autocatalysis may be counteracting the selectivity of the thiourea, the substrate **2.10** was modified to bear electron donating or withdrawing substituents on the aryl ring. It was hoped that this would alter the catalytic efficiency of the product, so selectivity arising solely from the chiral thiourea could be observed. Very low ees resulted in all cases (Table 2. 2. 3. 1 entries 3-6 and tables 2. 6. 3. 3-5). In an attempt to restrict degrees of freedom in the

transition states, more sterically demanding aryl thiols were used but low selectivities still resulted (Table 2. 2. 3. 1 entries 7-8 and table 2. 6. 3. 6). Under some conditions a strong catalytic effect is observed, all with very low selectivity (e.g. compare table 2. 2. 3. 1 entries 5 and 6, 7 and 8).

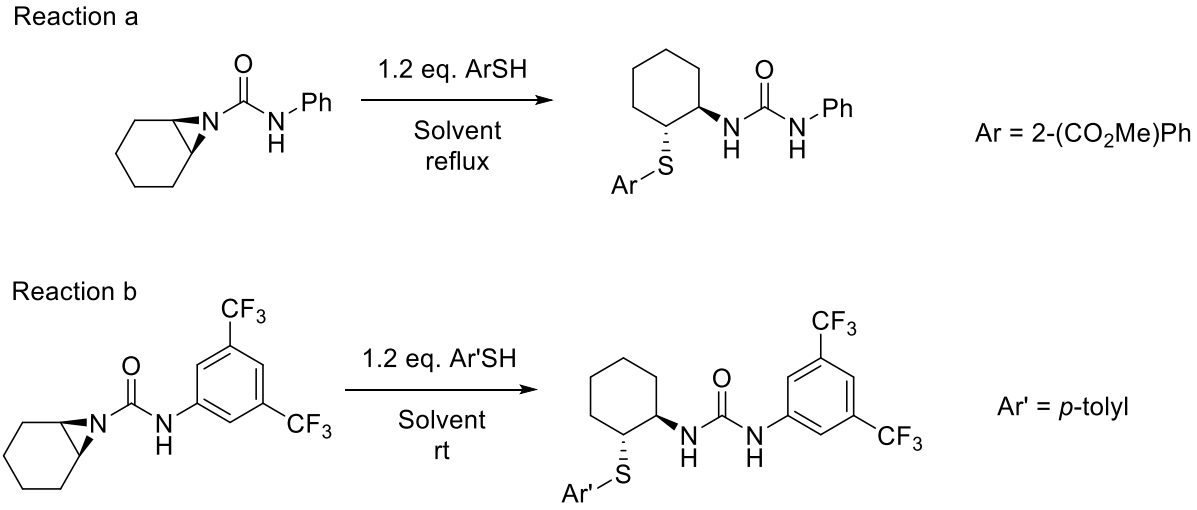


Entry	R	R’	R’’	Solvent	Base (eq.)	Catalyst	Conversion (%)[a]	ee (%)
1	H	Me	H	Toluene	0	-	15	ND
2	H	Me	H	Toluene	0	**2.17**	100	2.2
3	4-OMe	Me	H	Et_2O	1.2	-	100	ND
4	4-OMe	Me	H	Et_2O	1.2	**2.17**	100	7.1
5	3,5-bis(CF_3)	Me	H	Toluene	1.2	-	6	ND
6	3,5-bis(CF_3)	Me	H	Toluene	1.2	**2.18**	100	3.0
7	H	H	CO_2Me	Et_2O	0	-	8	ND
8	H	H	CO_2Me	Et_2O	0	**2.17**	93	2.6

Table 2. 2. 3. 1. Selected results from enantioselectivity screening of the addition of aryl thiols to meso-aziridines in the presence of chiral thiourea catalysts. ND denotes not determined. a – Conversion was calculated from crude reaction mixtures by ^1H NMR spectroscopy. n = 1.

Kinetic analysis of these reactions though ^1H NMR spectroscopy proved challenging, as inhomogeneity lead to irregular sampling. For a few selected examples, we tested if the reactions were autocatalytic by comparing conversion of the reaction with and without the

addition of product at the start (Table 2. 2. 3. 2). Some reactions showed variation in rate, making monitoring these kinetics challenging (Table 2. 2. 3. 2 entries 1 and 2). None showed any significant rate enhancement on addition of product, thus no autocatalysis was detectable under the conditions used.



Entry	Reaction	Additive	Reaction time (h)	Solvent	Conversion (%)[a]
1	a	-	18	Toluene	64
2	a	-	6	Toluene	100
3	a	0.2 eq. product	6	Toluene	100
4	a	-	18	DCM	2
5	a	0.2 eq. product	18	DCM	2
6	b	-	20	Et_2O	5
7	b	0.1 eq. product	20	Et_2O	5
8	b	-	20	Toluene	1
9	b	0.1 eq. product	20	Toluene	6

Table 2. 2. 3. 2. Attempts to detect autocatalysis in ring openings, showing variability in reaction rate and no detectable autocatalysis. a – Conversion was calculated from crude reaction mixtures by ^1H NMR spectroscopy. n = 1.

2. 2. 4 Conclusions

From our initial design, only one substrate showed the desired reactivity and did so only with one class of nucleophiles, aryl thiols. As this reaction did not show any apparent autocatalysis, nor was it possible to induce enantioselectity by the addition of chiral thiourea catalysts, the reaction was judged to be not promising to develop further.

2. 3 Designs for an asymmetric autocatalysis with atropoisomerism

2. 3. 1 Biaryl thiourea design

Figure 2. 3. 1. 1 illustrates the design for a dynamic kinetic asymmetric transformation which may show autocatalysis, inspired by the structure of Wang's Morita–Baylis–Hillman thiourea catalyst, **2.19**.[51] We propose there may exist suitable R groups such that **2.20** can invert due to the restricted rotation about the aryl-aryl C–C bond arising from the seven-membered ring, however the product **2.21** is atropisomeric. This idea is based heavily on the so called "lactone concept" of Bringmann.[52,53] This method of desymmetrisation has been used to create a unidirectional chemically fuelled motor.[54]

The cyclic nature of these starting materials creates conformational restriction on the thiourea. In the product however there is no such restriction, with many conformations possible. As thioureas typically catalyse reactions in what is called the (*syn*,*syn*) conformation, through the "clamp-like" binding mode, we imagined the starting material would not be catalytically active, but the product would.

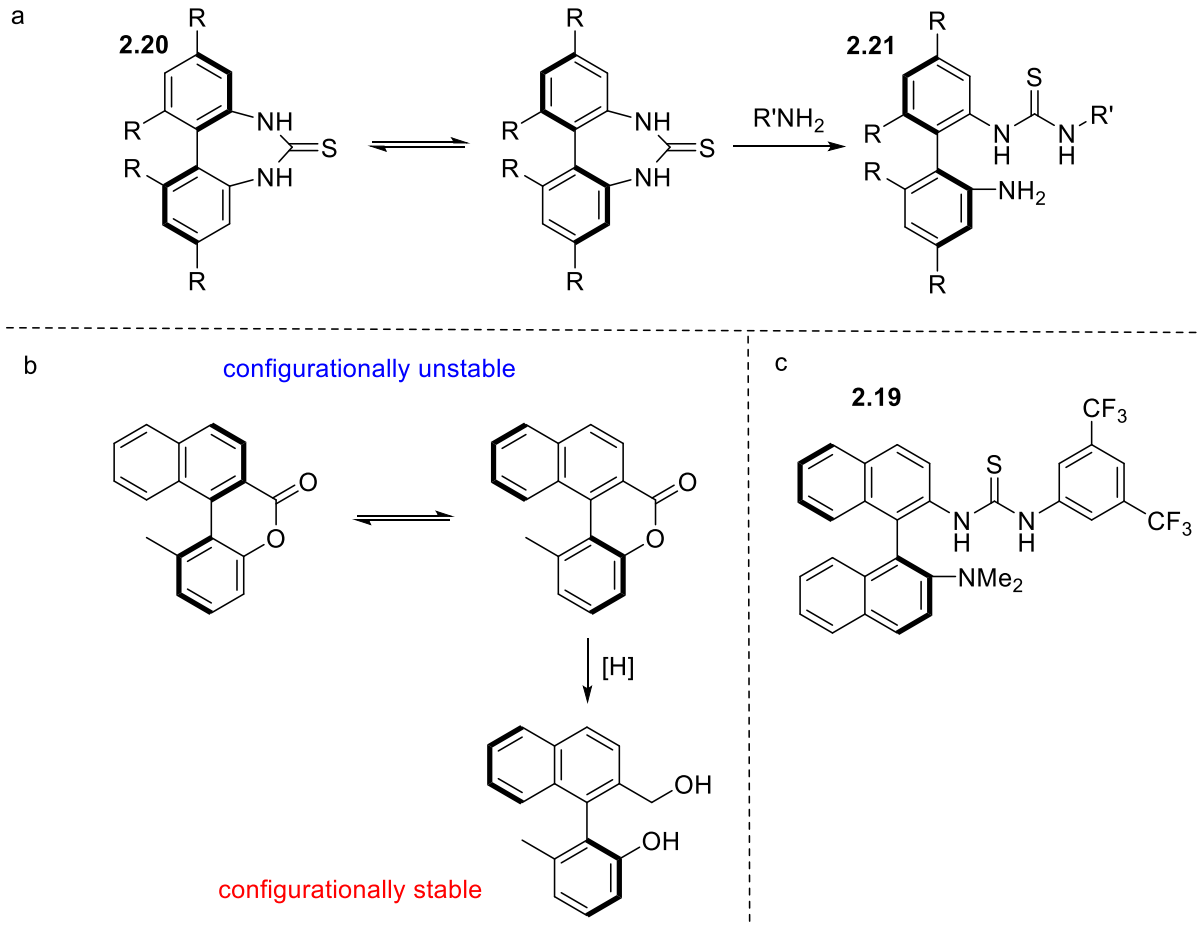


Figure 2. 3. 1. 1. a – Reaction design for an asymmetric autocatalytic desymmetrisation of a cyclic thiourea, ***2.20****. b – the "lactone concept" of Bringmann, whereby dynamic kinetic resolutions can be achieved on cyclic systems to form atropisomeric products. c – Wang's thiourea catalyst for Morita–Baylis–Hillman reactions.*

Despite the pioneering work of Bringmann, dynamic kinetic resolutions (DKRs) of atropisomeric compounds are rare, let alone autocatalytic ones.[55] During our study a DKR of naphthamides was reported by Fugard et al. (Figure 2. 3. 1. 2) using phase transfer catalyst **2.22**.[56] Here, internal hydrogen bonding between the naphthyl OH and amide nitrogen stabilises the transition state of racemisation significantly (estimated to be 40 kJ mol^{-1} by DFT), leading to a stereodynamic starting material. On alkylation this hydrogen bond is lost and the product is of fixed stereochemistry.

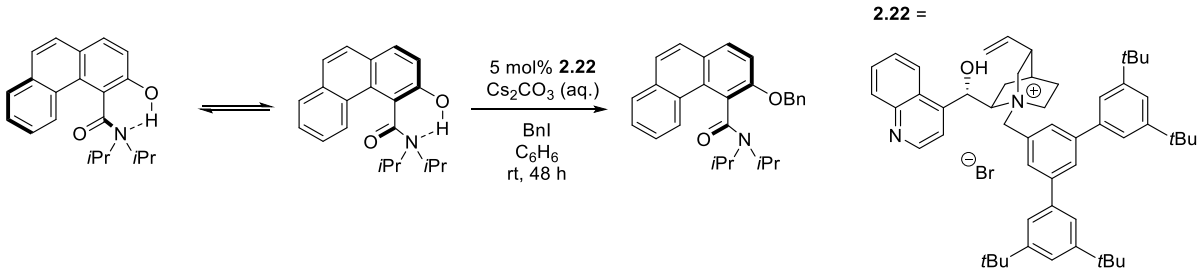


Figure 2. 3. 1. 2. Dynamic kinetic resolution of naphthamides. Adapted with permission.[56]

2. 3. 2 Biaryl thiourea reactivity and stereochemistry

The reactivity of cyclic thiourea towards nitrogen nucleophiles was investigated in a range of apolar solvents (Figure 2. 3. 2. 1). Unfortunately, in no case were desired acyclic thiourea products observed, even on heating to reflux overnight. Seeking more reactive nucleophiles to affect the same transformation, organometallic reagents were employed (Figure 2. 3. 2. 2). In all cases no nucleophilic addition was observed, with a colour change indicative of substrate deprotonation being observed in several cases. All reactions in figures 2. 3. 2. 1 and 2. 3. 2. 2 were also performed on the urea analogue **2.24**, and in all cases no productive reaction was observed (Figure 2. 3. 2. 3).

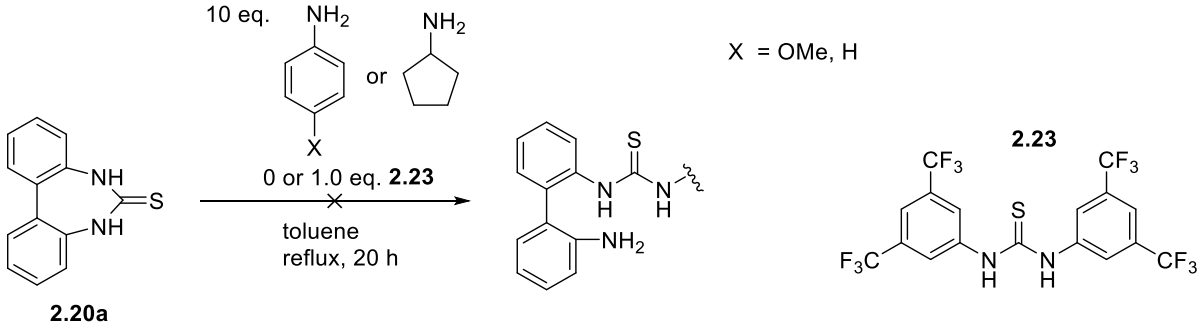


*Figure 2. 3. 2. 1. Screening reactivity of cyclic thiourea **2.20a**. Reactions were performed in the presence and absence of Schreiner's thiourea **2.23** as a product mimic. All reactions were also repeated in diethyl ether and dichloromethane as a solvent, at room temperature overnight. In all cases no reaction was observed.*

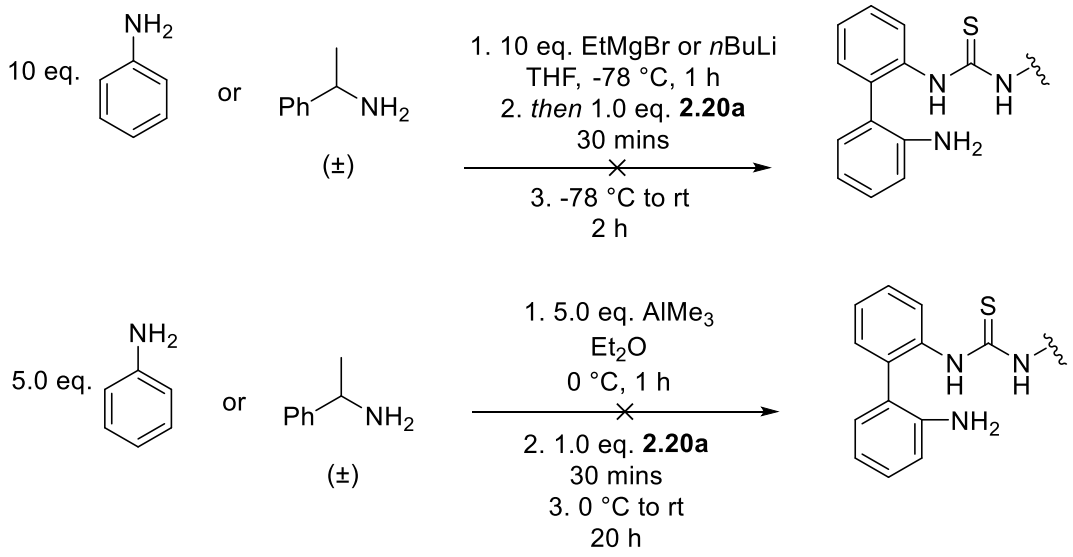


*Figure 2. 3. 2. 2. Reactivity of cyclic thiourea **2.20a** toward organometallics. In all cases no reaction was observed.*

2.24

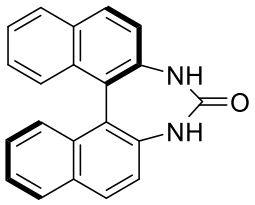


*Figure 2. 3. 2. 3. Cyclic urea **2.24** which alongside cyclic thiourea **2.20a** showed no reactivity towards nitrogen nucleophiles.*

2.20a (Figure 2. 3. 2. 4) was inferred to racemise rapidly at room temperature, as it gave a single absorbance peak by HPLC and UPLC, using several chiral columns (Chiralpak IA-IG) with a range of solvent gradients. Cyclic thioureas **2.20b** and **2.20c** were resolved using semi-preparative HPLC. This allowed the measurement of the racemisation barriers, however this could only be given as a range as these substrates decomposed faster than inverting, as did **2.25**. This suggested that the bridging thiocarbonyl rather than lowering the barrier to inversion in fact fixes the conformation, although the barriers for the corresponding diamines were not measured. Since our study, compounds of structure

2.20 have been reported to interconvert above 50 °C with higher cyclic oligomers, a possible route for the decomposition we observe.[57]

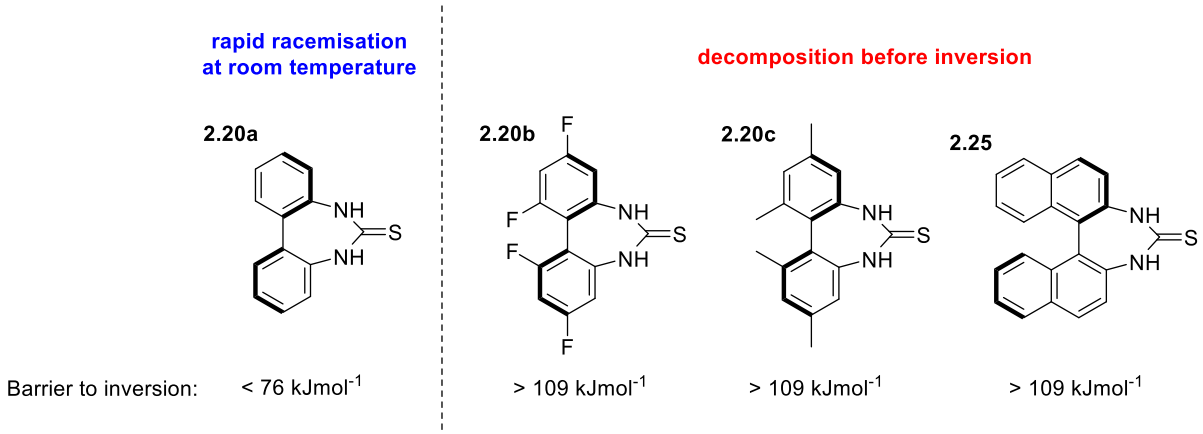


*Figure 2. 3. 2. 4. Inversion barriers for cyclic thioureas, as measured in toluene. The absolute configuration of **2.20b-c** used is unknown. n = 1.*

2. 4 Nonlinear effects in thiourea organocatalysis

2. 4. 1 Prior work

As previously discussed, for autocatalysis with asymmetric amplification to be possible with thioureas, strong nonlinear effects would be required. To the best of our knowledge only one prior observation of nonlinear effects in asymmetric urea or thiourea catalysis has been reported (Figure 2. 4. 1. 1).[58] Here, a biphasic nitroaldol reaction is catalysed by a guanidium-thiourea surfactant catalyst **2.26**. The strength of the nonlinear effect here is relatively small and it is hard to tell if this effect was specific to these conditions, or could also be found in homogenous thiourea catalysis.

To investigate potential nonlinear effects are possible in thiourea catalysis, we chose to investigate Ricci's thiourea, **2.27** (Figure 2. 4. 1. 2a).[59,60] It was selected on the basis that it contained multiple hydrogen bonding motifs (the thiourea and hydroxyl moieties) and catalysed a number of different asymmetric reactions, many with high

enantioselectivities.[59,61–66] Promisingly, nonlinear effects (similar to those discussed in section 2. 1. 2) have been reported with **2.28**[67], which shows good gelation properties in many solvents, with only the enantiopure (and not racemic) urea gelating (Figure 2. 4. 1. 2b).

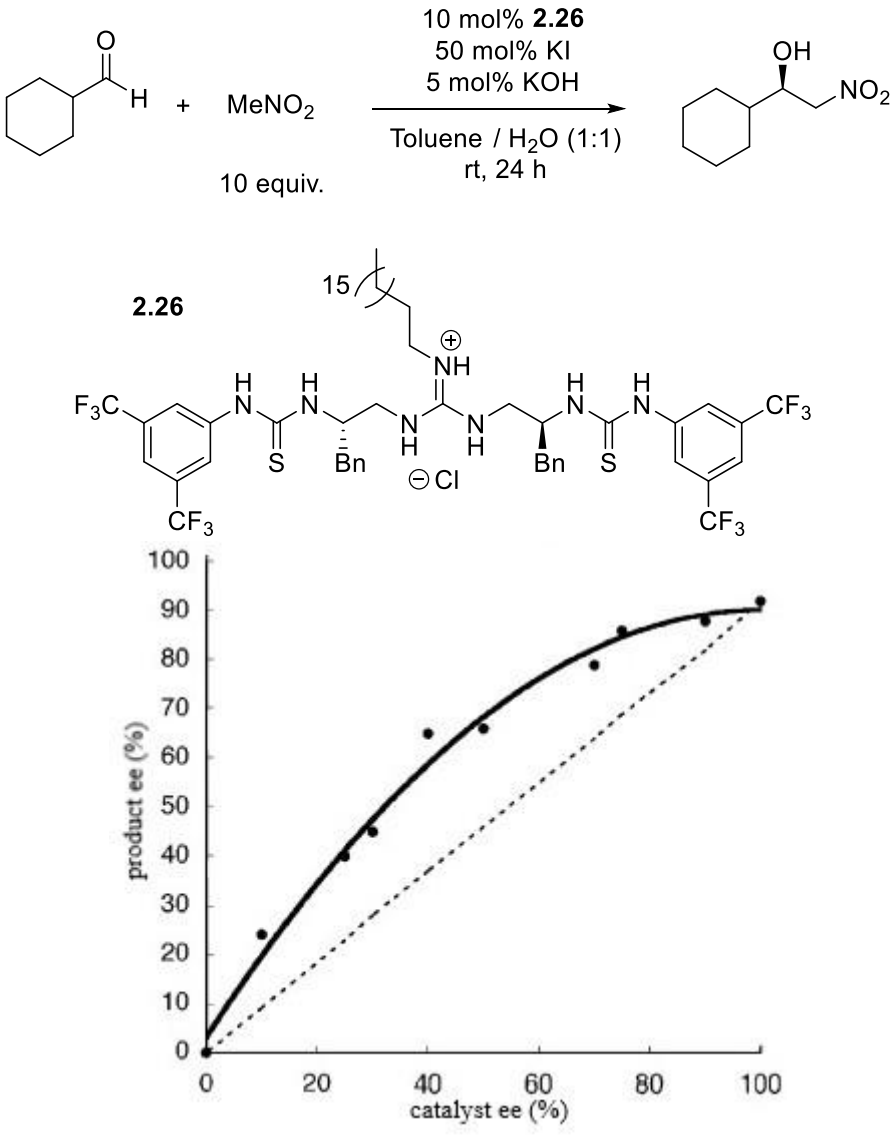
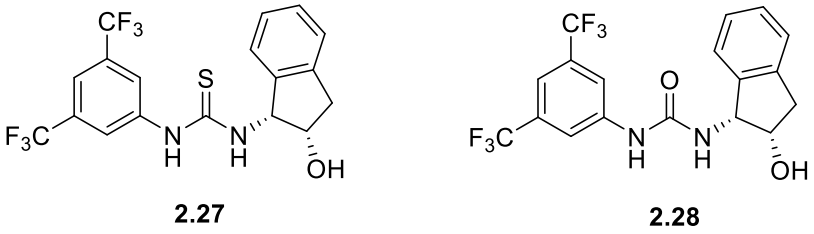


Figure 2. 4. 1. 1. Nitroaldol reaction showing weak nonlinear effects in the presence of guanidium-thiourea catalyst, ***2.26****. Adapted with permission.*[58]

a



2.27 **2.28**

b

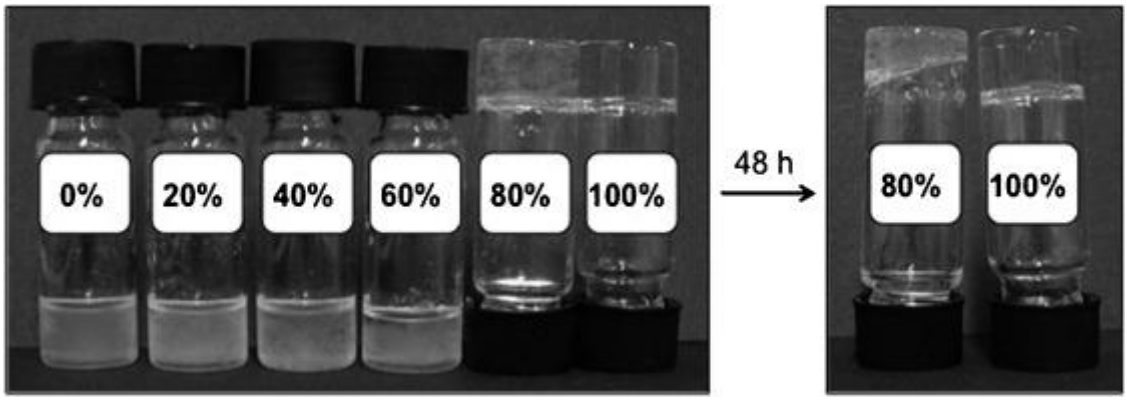
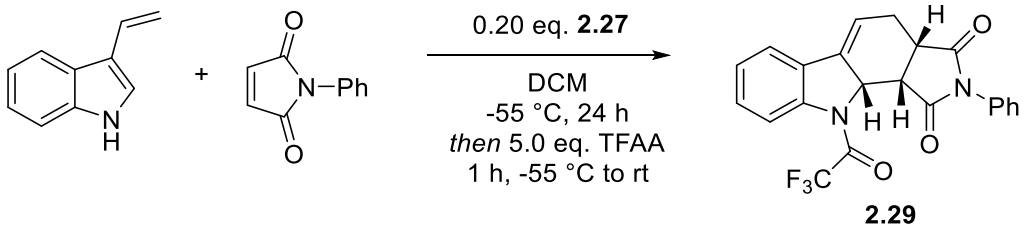


*Figure 2. 4. 1. 2. a – Ricci's thiourea **2.27**, originally reported as a catalyst in a Friedel–Crafts reaction and has subsequently been used in many transformations. Its urea variant, **2.28**, which shows nonlinear effects in gelation.*[59] *b – Nonlinear gelation effects of **2.28** in toluene. Racemic and low ee scalemic mixtures of **2.28** do not form gels, 80% ee **2.28** forms a weak gel, and enantiopure **2.28** forms a true gel. The percentages on the vials represent the ee of **2.28** contained. Adapted with permission.*[67]

2. 4. 2 Results

Using the reported conditions for a Diels–Alder reaction to form **2.29** we observed a linear relationship between catalyst and product ee in both toluene and dichloromethane.[61] Decreasing the temperature from –25 °C to –55 °C resulted in the expected increased enantioselectivities and in the case of dichloromethane a strong positive nonlinear effect was observed (Figure 2. 4. 2. 1). At these temperatures, precipitation of racemic catalyst was observed in dichloromethane. This suggests the effect arises from lower solubility of the racemate than the enantiopure catalyst, so the solution phase ee is higher than the overall ee of catalyst in the reaction. This is analogous to the reservoir effect proposed by Kagan in the ML2 model and similar racemate precipitation leading to nonlinear effects

has been observed in phosphoric acid catalysis.[6,68,69] Deviation from the curve at high catalyst ee can be attributed to eutectic behaviour.[70]



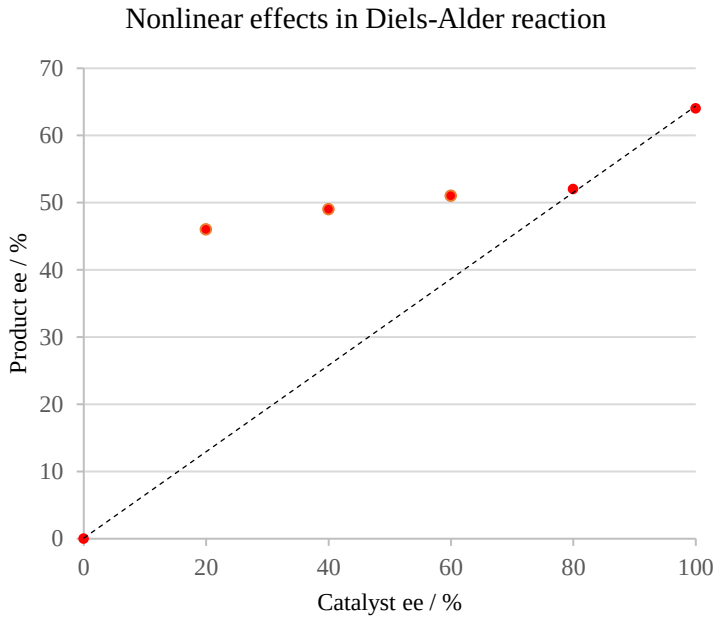
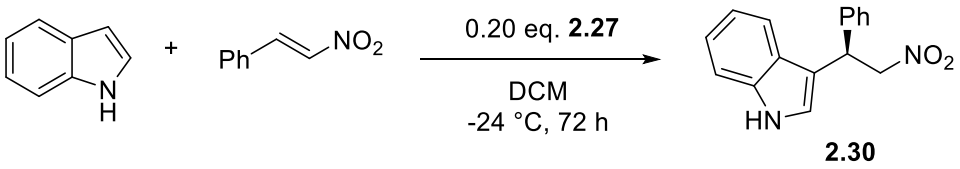


Figure 2. 4. 2. 1. Nonlinear effects in Diels–Alder reaction between 3-vinylindole and N-phenylmaleimide to form ***2.29****. n = 1.*

A second reaction was also investigated, a Friedel–Crafts reaction between indole and nitroolefins to form **2.30**.[59] Here the reported conditions are 15 times more concentrated with respect to catalyst than the Diels–Alder reaction and so no detectable eutectic behaviour is observed. This reaction was difficult to study due to large thermal effects during setup and associated errors. The best results are shown in figure 2. 4. 2. 2. Substrates with greater steric bulk **2.31** and **2.32** were synthesised, in the hopes of increasing enantioselectivity, which would allow the study this reaction at room temperature (Figure 2. 4. 2. 3). However, these substrates show very low reactivity. **2.33** was initially more promising, with 65% ee in a room temperature reaction, however the

relationship between catalyst ee and product ee could not be reliably determined. This was apparently due to heterogenous reaction mixtures which changed through time, partially gelated and partially crystalline, and low conversions even after 72 h.



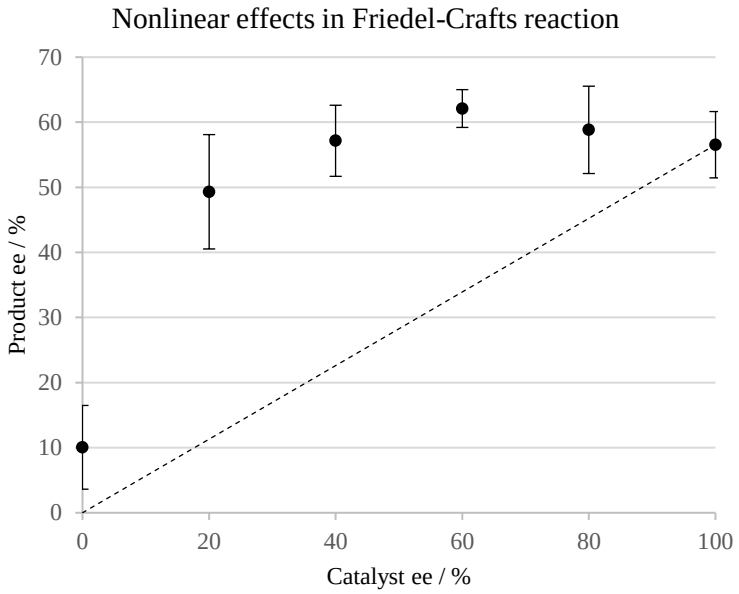


Figure 2. 4. 2. 2. Nonlinear effects in Friedel–Crafts reaction between indole and trans-β-nitrostyrene. n = 3, error bars show one standard deviation and are typically too small to be visible.

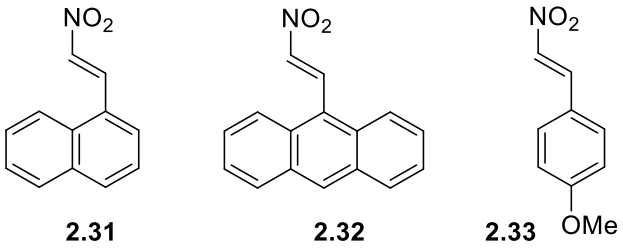


*Figure 2. 4. 2. 3. Sterically bulky nitroolefins, **2.31** and **2.32** prepared for nonlinear effects studies. They unfortunately showed low reactivity. **2.33** showed unreliable effects.*

2. 5 Conclusions and outlook

The work in section 2. 2 was ultimately unsuccessful due to the lack of desired reactivity of the aziridine substrates, which for most nucleophiles did not react or decomposed. For

the one reaction that showed the desired regioselectivity, the substrate scope was highly limited and induction of any significant enantioselectivity into this reaction using known hydrogen bonding catalysts proved unsuccessful. Lacking conditions for induction of asymmetry, this reaction also did not show significant autocatalysis kinetics under the conditions studied. The cyclic thiourea/urea design in section 2.3 had neither the desired conformational properties nor reactivity for asymmetric autocatalysis.

Fortunately, we were able to demonstrate that it is possible for strong positive nonlinear effects to be present in thiourea catalysis, a key criterion for building an asymmetric autocatalytic reaction according to the Frank model. In section 2. 4 we show that one catalyst displays nonlinear effects in both a Friedel–Crafts reaction and a Diels–Alder reaction. Although there were no obvious designs for an autocatalytic formation of this particular catalyst, these results suggest an unconventional way of designing asymmetric autocatalytic reactions, whereby catalysts are screened for nonlinear effects in known reactions. Structures showing strong positive nonlinear effects could then be identified and autocatalytic reactions to make them designed.

The designs for the work of this chapter have largely been based on homogeneous reactions. It seems likely to me that future asymmetric autocatalytic reactions will exploit heterogenous environments as a means of achieving nonlinear effects, for example through conglomerates. Phase change in crystallisation can also give rise to autocatalysis. A related process is Viedma ripening which can occur when a solid is in equilibrium with a solution phase of the chiral compound is able to racemise.[71] If the solid crystallises as conglomerates, a racemic solid may undergo a deracemisation to a single enantiomer, by mechanical agitation.

2. 6 Experimental

2. 6. 1 General synthetic experimental information

Materials and reaction setup: All reagents, obtained from Acros, Alfa, Fluorochem, Manchester Organics, Sigma-Aldrich and TCI, were used directly as supplied unless otherwise noted. Anhydrous chloroform, dichloromethane, tetrahydrofuran, diethyl ether, toluene, benzene, hexanes, dimethyl formamide and acetonitrile were obtained from an MBRAUN SPS-800 solvent purification system, using activated alumina columns under nitrogen. Anhydrous methanol was purchased from Sigma-Aldrich. All reactions were performed in flame-dried glassware under an atmosphere of argon by balloon or Schlenk technique, unless otherwise stated in the text.

Chromatography: Thin layer chromatography (TLC) was used to monitor reaction progress. TLC analysis was performed on pre-coated aluminum based plates (0.2 mm Merck Kieselgel 60 with F_{254}) and plates were developed under UV irradiation (254 nm) and/or with potassium permanganate, Dragendorff reagent, iodine or phosphomolybdic acid staining and subsequent heating. Column chromatography was performed with silica gel (Macherey-Nagel Kieselgel 60 M, 0.040–0.063 mm). Petroleum ether used had a boiling point range of 40-60 °C.

Nuclear magnetic resonance spectroscopy: ^{1}H Nuclear magnetic resonance (NMR) spectra were recorded at ambient probe temperatures on the following instruments: Bruker AVII500 with ^{13}C cryoprobe (500 MHz) or Bruker AVIII400HD (400 MHz). Spectra were referenced to residual protons in $CDCl_3$ (δ 7.26), CD_3OD (δ 3.31), acetone-d_6 (δ 2.05), D_2O (δ 4.79) or DMSO-d_6 (δ 2.50). Chemical shifts (δ) are reported as parts per million (ppm). Coupling constants (J) are given in Hz to an accuracy of 0.5 Hz. Assignment of ^{1}H resonances were determined on the basis of unambiguous

chemical shift, coupling patterns, by analysis of 2D NMR (COSY, HSQC and/or HMBC) and/or by analogy to fully interpreted spectra of closely structurally related compounds. ^{13}C NMR spectra (^{1}H decoupled) were recorded at ambient probe temperatures on the instruments mentioned above (126 MHz and 101 MHz respectively), referenced to the solvents $CDCl_3$ (δ 77.16), CD_3OD (δ 49.15), acetone-d_6 (δ 29.84) or DMSO-d_6 (δ 39.52). ^{19}F NMR spectra were recorded at ambient probe temperatures on Bruker AVIII400HD (377 MHz) instruments and referenced to $CFCl_3$ in $CDCl_3$ (δ 0.00). ^{31}P NMR spectra were recorded at ambient probe temperatures on Bruker AVIII400HD (162 MHz) instruments and referenced to phosphoric acid (δ 0.00).

Mass spectrometry: Low resolution mass spectra were recorded on an Agilent 6120 Quadrupole mass spectrometer with an Agilent pump and a CTC autosampler, using positive electrospray ionization (ES+), and are reported for known compounds of molecular mass over 100 Daltons where possible, otherwise high resolution is given. High resolution mass spectra (HRMS) were recorded by the Departmental Mass Spectrometry Service, Department of Chemistry, University of Oxford. Data were obtained on a Thermo Scientific Exactive mass spectrometer with a Waters Acquity autosampler and pump (ES+), or on an Agilent 7200 Accurate Mass QTOF GCMS using a SIM Direct Insertion Probe or a Waters GCT mass spectrometer using a Temperature Programmed Solids Probe (electron impact, EI+, or field ionization, FI+) in positive mode. The parent ion $[M]^+$ or adduct ($[M+H]^+$, $[M+Na]^+$, $[M–H]^–$) etc. are calculated to four decimal places. All values are within an error of 5 ppm.

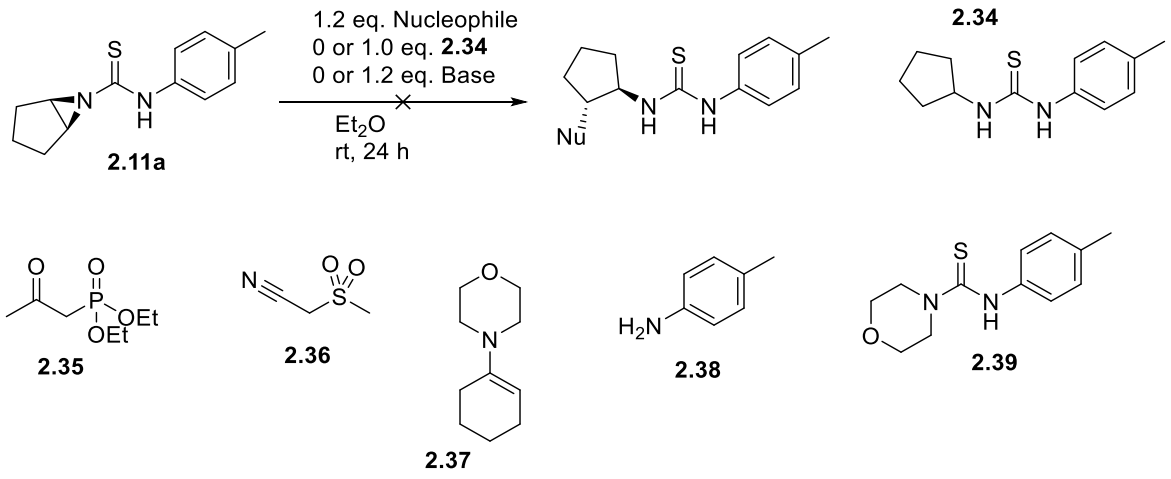
Infrared spectroscopy: All IR spectra were recorded as pure material (solids or oils) or thin films made by solvent evaporation on a Bruker Tensor 27 FTIR instrument with a Pike Miracle ATR ZnSe module. Wavelengths of maximum absorbance (ν_{max}) are reported in wavenumbers (cm^{-1}). A selection of characteristic resonances are reported.

Melting points: Melting points were obtained using a Leica Galen III hot stage microscope and are uncorrected. They are recorded for all solids formed by recrystallisation or precipitation, from the solvent specified in the text.

Enantiomeric excesses: Enantiomeric excesses were measured using either an Agilent 1260 Infinity series HPLC unit with Chiralpak® columns (250×4.6 mm) and HP Chemstation software, or using a Waters Acquity UPC2 SFC system with Chiralpak® columns (150 × 3 mm) and Empower software. Solvents, including carbon dioxide cylinder (provided by Boc), were of HPLC grade. For HPLC the samples and columns were at ambient temperatures, for SFC the sample temperature was 10 °C and the column temperature was 30 °C. Eluent systems are specified in the text.

Optical rotations: Optical rotations ($[\alpha]^{T}_{D}$) were recorded from a Perkin Elmer 241 Polarimeter at 25 °C and are reported in units of degree ml (g dm)$^{-1}$. Sample concentrations (*c*) are measured in mg ml^{-1}.

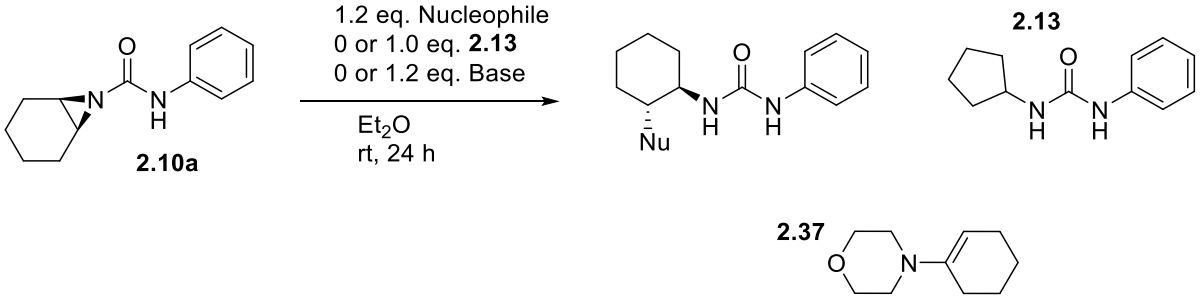
2. 6. 2 Additional tables for meso-aziridine reactivity studies



Entry	Nucleophile	Base (eq.)	Conversion (%)
1	MeOH	0	0
2	MeOH[a]	0	65 of **2.38**[e]
3	phenol	0	0

4	phenol	1.2[b]	0
5	potassium acetate	0	0
6	cyclopentylamine[c]	0	0
7	methyl hydrazine[c]	0	0
8	pyridine	0	0
9	morpholine	0	57 of **2.39**
10	pyrazole	0	0
11	imidazole	0	0
12	sodium azide	0	0[f]
13	4-methylbenzenethiol[c]	0	0
14	2-chlorobenzenethiol	0	0
15	butanethiol[c]	0	0
16	benzyl thiol	0	0
17	thioacetic acid	1.2[b]	0
18	**2.35**	1.2[d]	0
19	**2.36**	1.2[b]	0
20	**2.37**	0	trace **2.39**
21	indole[c]	0	0
22	dimethylmalonate	1.2[b]	0
23	nitromethane[c]	1.2[b]	0

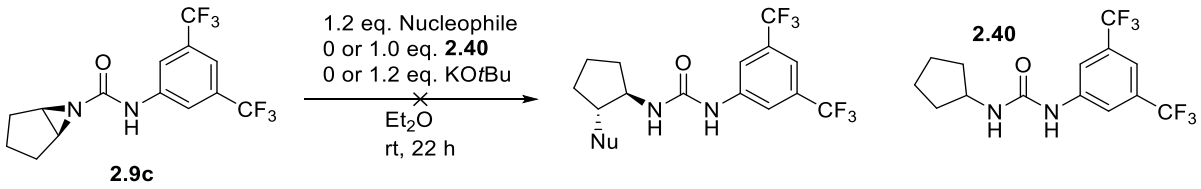
*Table 2. 6. 2. 1. Nucleophile screening for reaction with aziridine thiourea **2.11a**. All reactions were performed both in the absence and presence product mimic **2.34**, which gave identical results in all cases except for sodium azide. a – In the presence of 0.2 eq. DMAP, b – base was potassium tert-butoxide, c – reactions were repeated in dichloromethane and toluene, heated to reflux for 18 h, giving the same result, d – base was sodium hydride, e – isolated yield in the absence of **2.34** is given, with the similar result of 57% being obtained in the presence of **2.34**, f – complete decomposition of the substrate was observed in the case of additive **2.34**, no reaction was observed in the absence of **2.34**.*



Entry	Nucleophile	Base (eq.)	Conversion (%)
1	MeOH	0	0
2	MeOH[a]	0	0
3	MeOH	1.2[b]	0

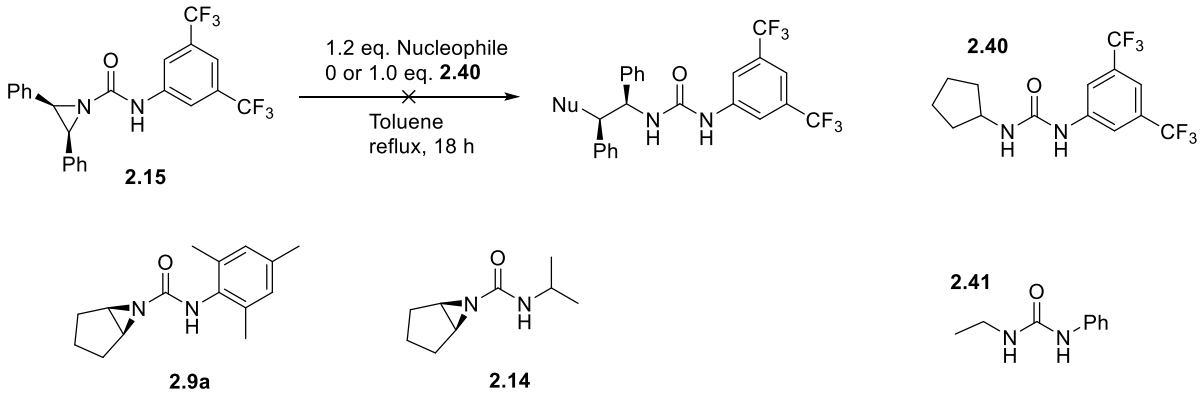
4	phenol	0	0
5	thioacetic acid	1.2[b]	0
6	sodium acetate	0	0
7	cyclopentylamine	0	0
8	methyl hydrazine	0	0
9	pyrrolidine	0	0
10	dimethylamine	0	0
11	sodium azide	0	0
12	4-methylbenzenethiol	0	67[c]
13	butanethiol	0	0
14	**2.37**	0	0
15	indole	0	0
16	dimethylmalonate	1.2[b]	0
17	nitromethane	1.2[b]	0
18	ethylmagnesium bromide	0	0
19	trimethylaluminium	0	0

*Table 2. 6. 2. 2. Nucleophile screening for reaction with aziridine urea **2.10a**. All reactions were performed both in the absence and presence product mimic **2.13**, which gave identical results in all cases. a – in the presence of 20% DMAP, b – base was potassium tert-butoxide, c – isolated yield in the absence of **2.13** is given, with the similar result of 62% being obtained in the presence of **2.13**.*



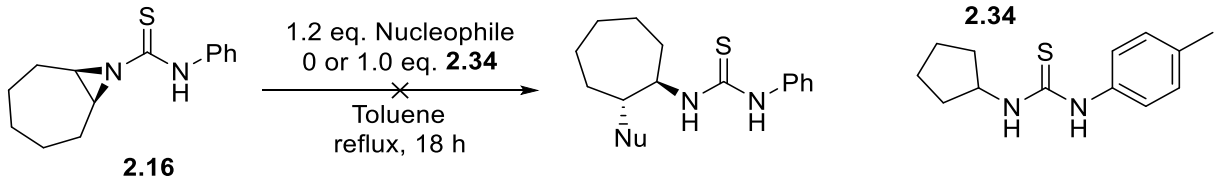
Entry	Nucleophile	Base (eq.)	Conversion (%)
1	phenol[a]	0	0
2	4-methylbenzenethiol[a]	0	0
3	4-methylbenzenethiol	1.2	0
4	2-chlorobenzenethiol[a]	0	0
5	2-chlorobenzenethiol	1.2	0
6	1-pentanethiol[a]	0	0
7	1-pentanethiol	1.2	0
8	cyclopentylamine[a]	0	0
9	methyl hydrazine[a]	0	0
10	sodium azide[a]	0	0

*Table 2. 6. 2. 3. Nucleophile screening for reaction with aziridine urea **2.9c**. All reactions were performed both in the absence and presence product mimic **2.40**, which gave identical results in all cases. a – Reactions were repeated in toluene and dichloromethane, heated to reflux for 18 h, with the same results.*



Entry	Nucleophile	Conversion (%)
1	phenol[a]	0
2	4-methylbenzenethiol[a,b]	0
3	2-chlorobenzenethiol[a]	0
4	1-pentanethiol[a,b]	0
5	cyclopentylamine[a,b]	0
6	methyl hydrazine[a,b]	0
7	sodium azide[a,b]	0

*Table 2. 6. 2. 4. Nucleophile screening for reaction with aziridine urea **2.15**. All reactions were performed both in the absence and presence product mimic **2.40**, which gave identical results in all cases. a – Reactions were repeated in diethyl ether and dichloromethane at room temperature for 22 h, with the same results, b – Reactions were also performed with **2.9a** as the electrophile and **2.41** as the product mimic, and **2.14** as the electrophile and **2.41** as the product mimic, all with the same results.*

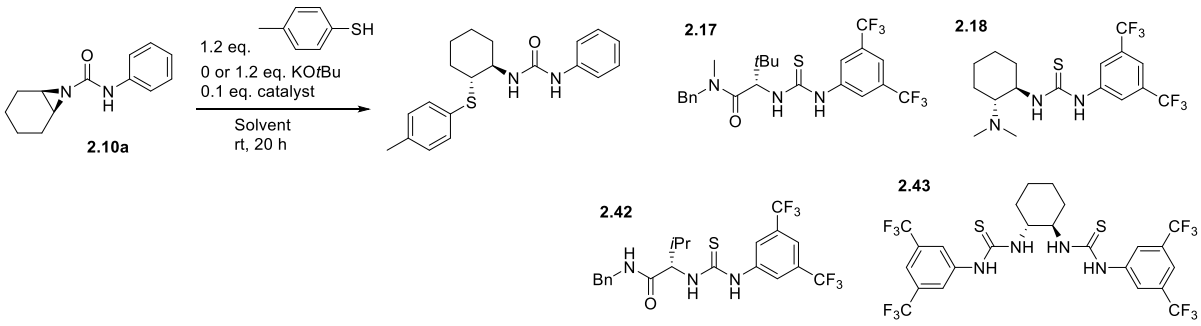


Entry	Nucleophile	Conversion (%)
1	4-methylbenzenethiol	0
2	1-butanethiol	0
3	cyclopentylamine	0
4	methyl hydrazine	0
5	sodium azide	0

*Table 2. 6. 2. 5. Nucleophile screening for reaction with aziridine urea **2.16**. All reactions were performed both in the absence and presence product mimic **2.34**, which gave identical results in all cases. All*

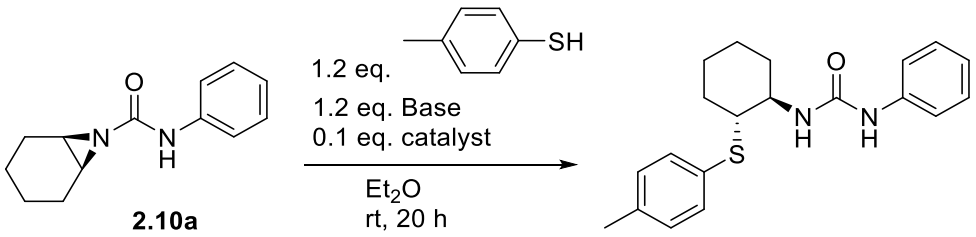
reactions were also performed in diethyl ether and dichloromethane at room temperature for 20 h, with the same results.

2. 6. 3 Additional tables for meso-aziridine enantioselectivy screening



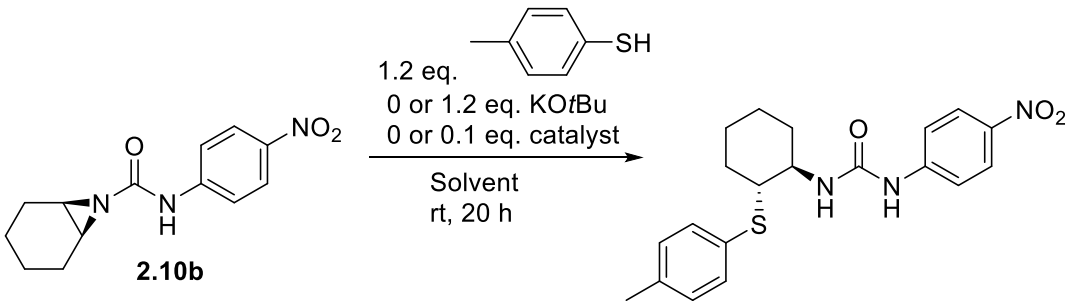
Entry	Catalyst	Base (eq.)	Solvent	Conversion (%)	ee (%)
1	**2.17**	0	Et_2O	65	0.8
2	**2.18**	0	Et_2O	100	2.6
3	**2.42**	0	Et_2O	12	-3.6
4	**2.43**	0	Et_2O	31	-2.0
5	**2.17**	1.2	Et_2O	55	1.3
6	**2.18**	1.2	Et_2O	69	3.0
7	**2.42**	1.2	Et_2O	15	5.4
8	**2.43**	1.2	Et_2O	22	5.2
9	**2.17**	0	toluene	100	2.2
10	**2.18**	0	toluene	43	2.0
11	**2.42**	0	toluene	19	0.9
12	**2.43**	0	toluene	20	1.4
13	**2.17**	1.2	toluene	36	7.8
14	**2.18**	1.2	toluene	24	1.2
15	**2.42**	1.2	toluene	12	5.6
16	**2.43**	1.2	toluene	19	10.1
17	**2.17**	0	DCM	35	-1.6
18	**2.18**	0	DCM	100	0.8
19	**2.17**	1.2	DCM	trace	ND
20	**2.18**	1.2	DCM	13	-1.2

Table 2. 6. 3. 1. Enantioselective reaction screen between 4-methylbenzenethiol and phenyl substrate, ***2.10a****.*



Entry	Catalyst	Base	Conversion (%)	ee (%)
1	**2.17**	Et_3N	0	ND
2	**2.18**	Et_3N	68	-1.7
3	**2.17**	NH_3	0	ND
4	**2.18**	NH_3	43	1.0
5	**2.17**	2,6-lutidine	0	ND
6	**2.18**	2,6-lutidine	46	0.9
7	**2.17**	NaO*t*Bu	51	2.0
8	**2.18**	NaO*t*Bu	32	2.4
9	**2.17**	LiOMe	100	0.1
10	**2.18**	LiOMe	100	0.5

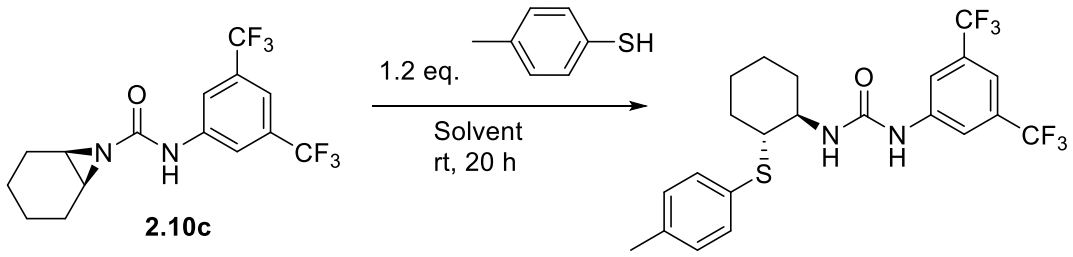
Table 2. 6. 3. 2. Base screen for the enantioselective reaction between 4-methylbenzenethiol and phenyl substrate, ***2.10a.***



Entry	Catalyst	Base (eq.)	Solvent	Conversion (%)	ee (%)
1	-	0	Et_2O	0	ND
2	-	0	toluene	0	ND
3	-	1.2	Et_2O	49	ND
4	-	1.2	toluene	13	ND
5	**2.17**	0	Et_2O	0	ND
6	**2.17**	0	toluene	0	ND
7	**2.17**	1.2	Et_2O	30	1.9
8	**2.17**	1.2	toluene	35	5.0
9	**2.18**	0	Et_2O	44	1.2
10	**2.18**	0	toluene	0	ND

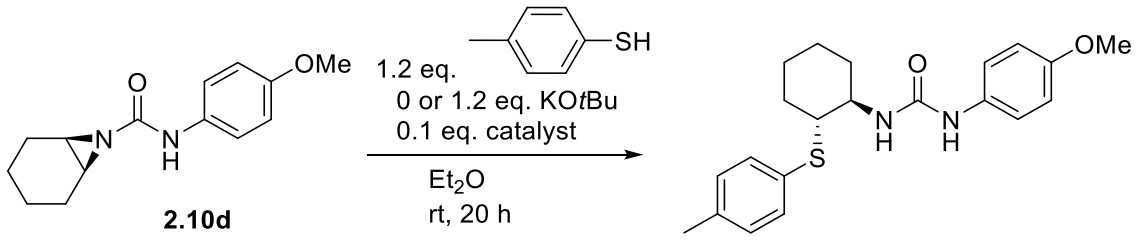
11	**2.18**	1.2	Et_2O	54	2.2
12	**2.18**	1.2	toluene	trace	ND

*Table 2. 6. 3. 3. Enantioselective reaction screen between 4-methylbenzenethiol and 4-nitrophenyl substrate, **2.10b**.*



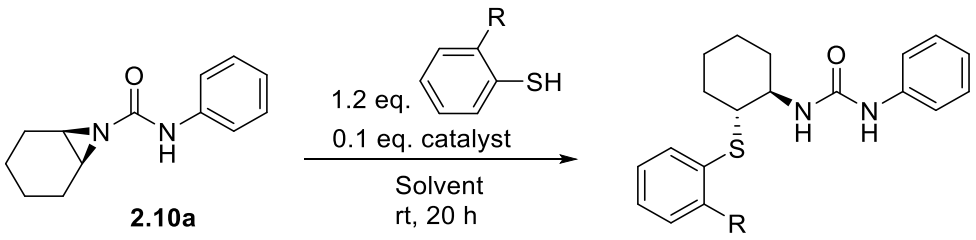
Entry	Catalyst	Base (eq.)	Solvent	Conversion (%)	ee (%)
1	-	0	Et_2O	4	ND
2	-	0	toluene	trace	ND
3	-	1.2	Et_2O	33	0.6
4	-	1.2	toluene	6	ND
5	**2.17**	0	Et_2O	0	ND
6	**2.17**	0	toluene	0	ND
7	**2.17**	1.2	Et_2O	84	2.3
8	**2.17**	1.2	toluene	42	3.0
9	**2.18**	0	Et_2O	75	0.1
10	**2.18**	0	toluene	26	2.2
11	**2.18**	1.2	Et_2O	6	-0.2
12	**2.18**	1.2	toluene	44	0.6

*Table 2. 6. 3. 4. Enantioselective reaction screen between 4-methylbenzenethiol and 3,5-bis(trifluoromethyl)phenyl substrate, **2.10c**.*



Entry	Catalyst	Base (eq.)	Conversion (%)	ee (%)
1	**2.17**	0	100	0.6
2	**2.18**	0	100	-0.7
3	**2.17**	1.2	100	7.1
4	**2.18**	1.2	100	-1.6

*Table 2. 6. 3. 5. Enantioselective reaction screen between 4-methylbenzenethiol and 4-methoxyphenyl substrate, **2.10d**.*



Entry	Catalyst	R	Solvent	Conversion (%)	ee (%)
1	-	Me	Et_2O	trace	ND
2	-	Me	toluene	0	ND
3	-	CO_2Me	Et_2O	8	ND
4	-	CO_2Me	toluene	35	ND
5	**2.17**	Me	Et_2O	trace	ND
6	**2.17**	Me	toluene	0	ND
7	**2.17**	CO_2Me	Et_2O	84	-1.9
8	**2.17**	CO_2Me	toluene	40	-1.3
9	**2.18**	Me	Et_2O	20	1.1
10	**2.18**	Me	toluene	trace	ND
11	**2.18**	CO_2Me	Et_2O	93	1.1
12	**2.18**	CO_2Me	toluene	52	1.9

Table 2. 6. 3. 6. Enantioselective reaction between ortho-substituted benzenethiols and phenyl substrate, ***2.10a****.*

2. 6. 4 Setup of reactions for nonlinear effect studies

Reactions were setup in SAMCO 1.75 mL Trident vials with Fisherbrand cylindrical 10 x 6 mm PTFE stir bars. Preliminary results found no effect of exposure to air or atmospheric moisture and thus all further reactions were performed under air with no attempt to exclude water.

Diels–Alder reaction: Stock solutions of each enantiomer of catalyst **2.29** (0.4 M in reaction solvent, typically dichloromethane) were prepared. These stock solutions were added to stirred vials in an isopropanol cooling bath in amounts to give the desired catalyst ee, of a total volume of 0.75 mL (0.2 equiv.), with (1*R*,2*S*)-**2.29** as the major enantiomer. To these vials were then added N-phenylmaleimide (0.15 mmol, 1.0 equiv.)

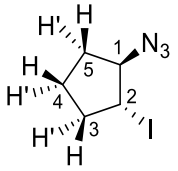
and stirred for 15 minutes. A stock solution of 3-vinyl indole (2.4 M in reaction solvent, 0.75 mL, 1.2 equiv.) was then added and the vials capped. Freshly prepared 3-vinyl indole solutions were used for each reaction series, as it was observed to readily oxidise. Reactions were performed as a series with catalyst ee between 0-100% in 20% intervals, with all reactions in a series being performed in parallel on the same day.

Friedel–Crafts reaction: Stock solutions of each enantiomer of catalyst **2.29** (6.0 M in dichloromethane) were prepared. These stock solutions were added to stirred vials containing the nitrostyrene (0.10 mmol) in an isopropanol cooling bath in amounts to give the desired catalyst ee, of a total volume of 100 µL (0.2 equiv.), with (1*R*,2*S*)-**2.29** as the major enantiomer stirred for 5 minutes. To these vials were then added indole (0.15 mmol, 1.5 equiv.). After around 30 minutes the reactions were transferred to a –24 °C freezer for the remainder of the reaction time. Reactions were performed as a series with catalyst ee between 0-100% in 20% intervals, with all reactions in a series being performed in parallel on the same day.

2. 6. 5 Synthesis and characterization of compounds

2. 6. 5. 1 Synthesis of aziridines

(±)-*trans*-1-Azido-2-iodocyclopentane, 2.34

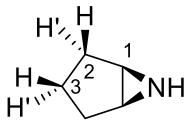


To a stirred suspension of sodium azide (8.20 g, 125.5 mmol, 2.5 equiv.) in acetonitrile (50 mL) was added dropwise iodine monochloride solution (56.5 mL, 56.5 mmol, 1.0 equiv., 1.0 M in dichloromethane) at -20 °C for 20 minutes. To this was added cyclopentene (5.05 mL, 56.5 mmol, 1.0 equiv.) and allowed to warm to room temperature and stirred for 10 h. The reaction mixture was then poured onto water (125 mL), the layers separated and the aqueous extracted with diethyl ether (3 × 125 mL). The combined organics were washed with 5% aqueous solution of sodium thiosulphate (150 mL), brine (2 × 150 mL), dried ($MgSO_4$) and solvent removed *in vacuo*. (±)-*trans*-1-Azido-2-iodocyclopentane (13.41 g, 56.5 mmol, 100%) was obtained as a yellow oil without further purification.

IR (film, ν_{max} / cm^{-1}) 2968, 2874, 2094, 1727, 1439, 1347, 1328, 1246, 1208, 1169, 1118, 1033; **^{1}H NMR** (400 MHz, $CHCl_3$) δ 4.15 (dt, *J* = 7.0, 4.5 Hz, 1H, CHN_3), 4.10 (q, *J* = 5.5 Hz, 1H, CHI), 2.35 – 2.26 (m, 1H, C5H or C5H'), 2.23 – 2.03 (m, 2H,C5H or C5H' + C4H or C4H'), 1.92 – 1.74 (m, 2H, C4H or C4H' + C3H or C3H'), 1.72 – 1.61 (m, 1H, C3H or C3H'); **^{13}C NMR** (101 MHz, $CHCl_3$) δ 71.6 (C1), 36.7 (C5), 29.3 (C2), 28.7 (C3), 22.5 (C4); **LRMS** (ES+) calc. for $C_5H_9IN_3$ $[M+H]^+$ 237.0, found 235.0.

Data consistent with literature values.[42]

6-Azabicyclo[3.1.0]hexane, 2.6

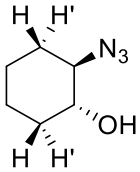


To a stirred solution of (±)-*trans*-1-azido-2-iodocyclopentane, **2.34** (13.51g, 56.5 mmol, 1.0 equiv.) in diethyl ether (250 mL) was added dropwise lithium aluminium hydride solution in diethyl ether (4.0 M, 28.25 mL, 2.0 equiv.) at 0 °C, and stirred for 1 h. The mixture was allowed to warm to room temperature and stirred for 12 h. 20% sodium hydroxide solution (20 mL) was added slowly and stirred vigorously for 1 h. The white aluminium salts were filtered and washed thoroughly with diethyl ether. The filtrate was dried ($MgSO_4$) and concentrated under reduced pressure in a water/ice bath to yield 6-azabicyclo[3.1.0]hexane (3.00 g, 34.8 mmol, 62%) as a colourless oil.

IR (thin film, ν_{max} / cm^{-1}) 3231, 3029, 2955, 2859, 2362, 2127, 1675, 1444, 1349, 1321, 1294, 1164, 1055; **^{1}H NMR** (400 MHz, $CDCl_3$) δ 2.25 (s, 2H, C1H), 1.68 (dd, *J* = 12.5, 7.5 Hz, 2H, C2H or C2H'), 1.50 – 1.32 (m, 3H, C2H or C2H' + C3H or C3H'), 1.17 – 1.05 (m, 1H, C3H or C3H'), 0.45 (s, 1H, NH); **^{13}C NMR** (101 MHz, $CDCl_3$) δ 35.4 (C1), 27.1 (C2), 18.0 (C3).

Data consistent with literature values.[42]

(±)-*trans*-2-Azidocyclohexan-1-ol, 2.35



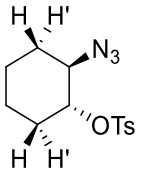
Cyclohexene oxide (10.0 mL, 98.8 mmol, 1.0 equiv.) and sodium azide (16.06 g, 247.0 mmol, 2.5 equiv.) in water/ acetone (1:1, 120 mL) was heated to reflux for 17 h.

The acetone was removed *in vacuo* and the residue extracted with diethyl ether (3 × 50 mL). The combined extracted were washed with water (2 × 40 mL), brine (30 mL) and dried ($MgSO_4$). The solvent was removed *in vacuo* to yield (±)-*trans*-2-azidocyclohexan-1-ol (12.93 g, 91.6 mmol, 93%) as a yellow oil without further purification.

IR (thin film, ν_{max} / cm^{-1}) 3366, 2935, 2862, 2090, 1451, 1257, 1119, 1068; **^{1}H NMR** (400 MHz, $CDCl_3$) δ 3.40 – 3.33 (m, 1H, C*H*OH), 3.20 – 3.13 (m, 1H, CHN_3), 2.40 (s, 1H, OH), 2.08 – 1.97 (m, 2H, C3H or C3H' + C6H or C6H'), 1.80 – 1.67 (m, 2H, C3H or C3H' + C6H or C6H'), 1.38 – 1.16 (m, 4H, $C4H_2$ + $C5H_2$); **^{13}C NMR** (101 MHz, $CDCl_3$) δ 73.7 (C1), 67.2 (C2), 33.1 (C6), 29.9 (C3), 24.3 (C4 or C5), 23.9 (C4 or C5); **LRMS** (ES+) calc. for $C_6H_{11}ON_3Na$ $[M+Na]^+$ 164.1, found 164.2.

Data consistent with literature values.[46]

(±)-*trans*-2-Azidocyclohexyl 4-methylbenzenesulfonate, 2.36

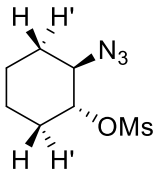


Tosyl chloride (1.35 g, 7.06 mmol, 2.0 equiv.) was added to a stirred solution of (±)-*trans*-2-azidocyclohexan-1-ol, **2.35** (0.500 g, 3.53 mmol, 1.0 equiv.) in pyridine (3.5 mL) at room temperature. After 16 h, the reaction mixture was poured onto water (10 mL) and extracted with ethyl acetate (3 x 10 mL). The combined organics were washed with 1 M hydrochloric acid until they were acidic, dried ($MgSO_4$) and the solvent was removed *in vacuo.* The residue purified by column chromatography (ethyl acetate/ petroleum ether (1:9)) to give (±)-*trans*-2-azidocyclohexyl 4-methylbenzenesulfonate as a white solid (599.4 mg, 2.03 mmol, 58%).

IR (solid, ν_{max} / cm^{-1}) 2935, 2878, 1685, 1640, 1618, 1548, 1360, 1251, 1204, 1165, 1141, 1120, 1065; **^{1}H NMR** (400 MHz, $CDCl_3$) δ 7.88 – 7.82 (m, 2H, CHCS), 7.38 – 7.31 (m, 2H, C*H*CHCS), 4.26 (ddd, *J* = 10.5, 9.0, 4.5 Hz, 1H, C*H*OTs), 3.40 – 3.29 (m, 1H, CHN_3), 2.45 (s, 3H, CH_3), 2.21 – 2.14 (m, 1H, C3H'), 2.05 – 1.99 (m, 1H, C6H), 1.78 – 1.62 (m, 1H, C3H), 1.59 – 1.47 (m, 1H, C6H'), 1.39 – 1.18 (m, 4H, $C4H_2$ + $C5H_2$); **^{13}C NMR** (101 MHz, $CDCl_3$) δ 146.3 (CS), 141.0 (*quat* C), 130.7 (SCCH*C*H), 128.9 (SC*C*HCH), 77.4 (C1), 68.1 (C2), 34.2 (C6), 26.5 (C3), 24.2 (C4 or C5), 23.7 (C4 or C5), 21.0 (CH_3); **LRMS** (ES+) calc. for $C_{13}H_{18}O_3N_3{}^{32}S$ $[M+H]^+$ 296.1, found 296.3.

Data consistent with literature values.[72]

(±)-*trans*-2-Azidocyclohexyl methylsulfonate, 2.37



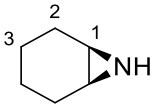
Mesyl chloride (410 μL, 5.30 mmol, 1.5 equiv.) was added to a solution of (±)-*trans*-2-azidocyclohexan-1-ol (0.500 g, 3.53 mmol, 1.0 equiv.) in pyridine (15 mL) at 0 °C and stirred for 30 minutes beforing being allowed to warm to room temperature. After 18 h, the solvent was removed *in vacuo* and the residue purified by column chromatography (ethyl acetate/ petroleum ether (1:9)) to give (±)-*trans*-2-azidocyclohexyl methylsulfonate as a colourless oil (703 mg, 3.21 mmol, 91%).

IR (oil, ν_{max} / cm^{-1}) 2984, 2870, 1443, 1417, 1350, 1221, 1163, 1144, 1076; **^{1}H NMR** (400 MHz, $CDCl_3$) δ 4.35 (ddd, *J* = 11.0, 9.5, 5.0 Hz, 1H, C*H*OMs), 3.46 (ddd, *J* = 11.0, 9.5, 5.0 Hz, 1H, CHN_3), 3.11 (s, 3H, CH_3), 2.33 – 2.24 (m, 1H, C3H'), 2.18 – 2.09 (m, 1H, C6H), 1.84 – 1.71 (m, 1H, C3H), 1.66 – 1.52 (m, 1H, C6H'), 1.46 – 1.21 (m, 4H, $C4H_2$ + $C5H_2$); **^{13}C NMR** (101 MHz, $CDCl_3$) δ 78.1 (C1), 66.8 (C2), 37.7 (CS), 33.5

(C6), 26.3 (C3), 24.4 (C4 or C5), 23.6 (C4 or C5); **LRMS** (ES+) calc. for $C_7H_{13}O_3N_3Na$ $[M+Na]^+$ 242.1, found 242.2.

Data consistent with literature values.[72]

(1*R*,6*S*)-7-Azabicyclo[4.1.0]heptane, 2.7

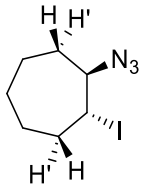


To a solution of (±)-*trans*-2-azidocyclohexan-1-ol, **2.35** (12.00 g, 85.0 mmol, 1.0 equiv.) in tetrahydrofuran (90 mL) was added triphenylphosphine (24.52 g, 93.5 mmol, 1.1 equiv.) was heated to reflux for 17 h. The reaction mixture was then allowed to cool to room temperature, and the solvent removed *in vacuo*. The residue was dissolved in chloroform (50 mL), acetic acid (2 mL) added and stirred at room temperature for 30 min. The reaction mixture was extracted with 2M hydrochloric acid (2 × 30 mL), the aqueous neutralized with 2M sodium hydroxide solution and extracted with dichloromethane (3 × 50 mL). The combined organic extracts were dried ($MgSO_4$) and the solvent removed in vacuo. This yielded (1*R*,6*S*)-7-azabicyclo[4.1.0]heptane (6.44 g, 66.3 mmol, 78%) as a yellow oil without further purification.

IR (thin film, ν_{max} / cm^{-1}) 3267, 2997, 2930, 2855, 1649, 1440, 1417, 1358, 1251, 1215, 1167, 1143, 1120, 1071, 1027; **^{1}H NMR** (400 MHz, $CDCl_3$) δ 2.08 (t, *J* = 1.5 Hz, 2H, C*H*NH), 1.77 – 1.68 (m, 4H, CH_2CHNH), 1.33 – 1.22 (m, 2H, CH_2), 1.19 – 1.07 (m, 2H, CH_2), 0.84 (s, 1H, NH); **^{13}C NMR** (101 MHz, $CDCl_3$) δ 28.3 (C1), 23.9 (C2), 19.3 (C3).

Data consistent with literature values.[46]

(±)-*trans*-1-Azido-2-iodocycloheptane, 2.38



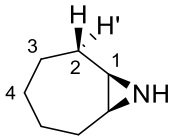
To a stirred suspension of sodium azide (6.24 g, 96.0 mmol, 2.5 equiv.) in acetonitrile (40 mL) was added dropwise iodine monochloride solution (38.4 mL, 1.0 M in dichloromethane, 38.4 mmol, 1.0 equiv.) at -20 °C for 10 minutes. To this was added cycloheptene (4.48 mL, 38.4 mmol, 1.0 equiv.) and allowed to warm to room temperature and stirred for 2 h. The reaction mixture was then poured onto water (125 mL), the layers separated and the aqueous extracted with diethyl ether (3 × 125 mL). The combined organics were washed with 5% aqueous solution of sodium thiosulphate (150 mL), brine (2 × 150 mL), dried ($MgSO_4$) and solvent removed *in vacuo*.

(±)-*trans*-1-Azido-2-iodocyclopentane (10.12 g, 38.2 mmol, 99%) was obtained as a yellow oil without further purification.

IR (film, ν_{max} / cm^{-1}) 2929, 2858, 2353, 2345, 2088, 145, 1349, 1255, 1196, 1255, 1196, 1178, 1118, 1040, 1010; **^{1}H NMR** (400 MHz, $CDCl_3$) δ 4.17 (td, *J* = 8.5, 3.5 Hz, 1H, C2H), 3.86 (td, *J* = 8.5, 3.0 Hz, 1H, C1H), 2.27 (dddd, *J* = 14.5, 8.5, 3.5, 2.0 Hz, 1H, C3H or C3H'), 2.20 – 2.08 (m, 1H, C3H or C3H'), 2.05 – 1.94 (m, 1H, C7H or C7H'), 1.81 – 1.46 (m, 7H, C7H or C7H' + $C4H_2$ + $C5H_2$ + $C6H_2$); **^{13}C NMR** (101 MHz, $CHCl_3$) δ 72.1 (C2), 37.4 (C1), 37.1 (C3), 31.5 (C7), 27.2 (CH_2), 26.7 (CH_2), 22.9 (CH_2); **LRMS** (ES+) calc. for $C_7H_{12}IN_3Na$ $[M+Na]^+$ 288.0, found 288.5.

Data consistent with literature values.[73]

8-Azabicyclo[5.1.0]octane, 2.39



To a stirred solution of (±)-*trans*-1-Azido-2-iodocyclopentane, **2.38** (5.00 g, 18.9 mmol, 1.0 equiv.) in diethyl ether (50 mL) was added dropwise lithium aluminium hydride solution (9.40 mL, 37.8 mmol, 2.0 equiv., 4.0 M in diethyl ether) at 0 °C over the course of 20 minutes, allowed to warm to room temperature and stirred for 1 h. 20% sodium hydroxide solution (15 mL) was added slowly and stirred vigorously for 1 h. The white aluminium salts were filtered and washed thoroughly with diethyl ether. The filtrate was dried ($MgSO_4$) and concentrated under reduced pressure in a water/ice bath to yield 8-azabicyclo[5.1.0]octane (1.96 g, 17.6 mmol, 93%) as a colourless oil.

IR (thin film, ν_{max} / cm^{-1}) 3246, 2985, 2917, 2848, 2345, 1579, 1454, 1352, 1281, 1190, 1070, 1009; **^{1}H NMR** (400 MHz, $CDCl_3$) δ 2.09 – 1.97 (m, 2H, C1H), 1.64 – 1.50 (m, 2H, C2H or C2H'), 1.40 – 1.16 (m, 8H, C2H or C2H' + $C3H_2$ + $C4H_2$), 0.74 (s, 1H, NH); **^{13}C NMR** (101 MHz, $CDCl_3$) δ 34.3 (C1), 32.1 (C2=3 or C4), 30.7 (C2), 26.6 (C3 or C4); **LRMS** (ES+) calc. for $C_7H_{14}N$ $[M+H]^+$ 112.1, found 112.2.

Data consistent with literature values.[73]

***cis*-2,3-Diphenyloxirane, 2.40**



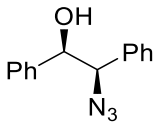
To a stirred solution of *cis*-stilbene (1.00 mL, 5.61 mmol, 1.0 equiv.) in dichloromethane (30 mL) was added 3-chloroperbenzoic acid (1.51 g, 6.73 mmol, 1.2 equiv.) at 0 °C, allowed to warm to room temperature and stirred for 24 h. The reaction mixture was

diluted with dichloromethane (30 mL), washed with saturated aqueous solution of sodium thiosulphate (40 mL), water (40 mL) and then brine (40 mL), dried ($MgSO_4$). The solvent removed *in vacuo* to yield. (*cis*)-2,3-diphenyloxirane **3** as a white solid (1.090 g, 5.55 mmol, 98%).

IR (thin film, ν_{max} / cm^{-1}) 2877, 2656, 2547, 1690, 1573, 1415, 1301, 1261; **^{1}H NMR** (400 MHz, $CDCl_3$) δ 7.26 – 7.09 (m, 10H, ArH), 4.38 (s, 2H, ArCH); **^{13}C NMR** (101 MHz, $CDCl_3$) δ 133.9 (*i*Ph), 130.3 (*o*Ph), 129.9 (*m*Ph), 128.3 (*p*Ph), 59.0 (Ar*C*H). **LRMS** (ES+) calc. for $C_{14}H_{12}ONa$ $[M+Na]^+$ 219.1, found 219.2.

Data consistent with literature values.[44]

(±)-(1*R*,2*R*)-2-Azido-1,2-diphenylethan-1-ol, 2.41



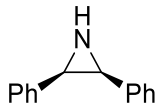
(*cis*)-2,3-Diphenyloxirane, **2.40** (947.7 mg, 4.83 mmol, 1.0 equiv.) and sodium azide (785.0 mg, 12.08 mmol, 2.5 equiv.) in water/acetone (1:1, 25 mL) was heated to reflux for 48 h. The acetone was removed in vacuo and the residue extracted with diethyl ether (3 × 15 mL). The combined extracted were washed with water (2 × 10 mL), brine (7.5 mL) and dried ($MgSO_4$). The solvent was removed in vacuo to yield (±)-(1*R*,2*R*)-2-azido-1,2-diphenylethan-1-ol (917.8 mg, 3.84 mmol, 66%) as a yellow oil without further purification.

IR (thin film, ν_{max} / cm^{-1}) 2916, 2849, 2657, 2549, 1690, 1574, 1416, 1302, 1262; **^{1}H NMR** (400 MHz, $CDCl_3$) δ 7.37 – 7.33 (m, 3H, ArH), 7.33 – 7.28 (m, 3H, ArH), 7.17 – 7.09 (m, 4H, ArH), 4.85 (d, *J* = 8.0 Hz, 1H, C*H*OH), 4.72 (d, *J* = 8.0 Hz, 1H, CHN_3), 2.85 (s, 1H, OH); **^{13}C NMR** (100 MHz, $CDCl_3$) δ 139.1 (*i*Ph), 135.8 (*i*Ph), 128.7 (PhH),

128.2 (PhH), 128.1 (PhH), 128.1 (PhH), 127.7 (PhH), 127.0 (PhH), 78.0 (CO), 72.7 (CN); **LRMS** (ES+) calc. for $C_{14}H_{14}N_3O$ $[M+H]^+$ 240.1 found 239.2.

Data consistent with literature values.[44]

(2*R*,3*S*)-2,3-Diphenylaziridine, 2.42



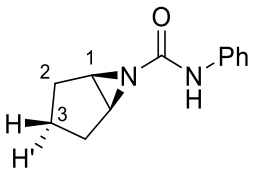
To a stirred solution of (±)-2-azido-1,2-diphenylethan-1-ol, **2.41** (917.8 mg, 3.84 mmol, 1.0 equiv.) in acetonitrile (4 mL) was added triphenylphosphine (892 mg, 3.84 mmol, 1.0 equiv.) and stirred at room temperature for 1 h. The solvent was removed *in vacuo* and the residue dissolved in dichloromethane (6 mL), acetic acid (12 μL) added, and stirred for 30 min at room temperature. The solvent was removed *in vacuo* and the residue purified by column chromatography (EtOAc/ petroleum ether (1:4)) to give (2*R*,3*S*)-2,3-diphenylaziridine as a white solid (366.7 mg, 1.88 mmol, 50%).

IR (thin film, ν_{max} / cm^{-1}) 3312, 3061, 3028, 2360, 2341, 1683, 1604, 1496, 1453, 1411, 1317, 1192, 1073, 1027; **^{1}H NMR** (400 MHz, $CDCl_3$) δ 7.19 – 7.05 (m, 10H, ArH), 3.60 (s, 2H, C*H*NH), 1.57 (s, 1H, NH); **^{13}C NMR** (101 MHz, $CDCl_3$) δ 136.7 (*i*Ph), 128.1 (ArH), 127.8 (ArH), 126.7 (ArH), 40.0 (CHNH); **LRMS** (ES+) calc. for $C_{14}H_{14}N$ $[M+H]^+$ 196.1, found 196.0.

Data consistent with literature values.[44]

2. 6. 5. 2 Synthesis of ureas

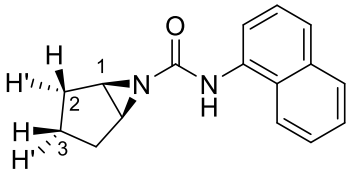
(1*R*,5*S*)-N-Phenyl-6-azabicyclo[3.1.0]hexane-6-carboxamide, 2.9b



To a stirred solution of 6-azabicyclo[3.1.0]hexane, **2.6** (90.0 mg, 1.083 mmol, 1.0 equiv.) in acetonitrile (5 mL) was added phenyl isocyanate (118 μL, 1.083 mmol, 1.0 equiv.) and stirred for 2 h. The solvent was removed *in vacuo* and the residue purified by column chromatography (EtOAc/ petroleum ether (1:4)) to give (1*R*,5*S*)-N-phenyl-6-azabicyclo[3.1.0]hexane-6-carboxamide as a white solid (191.2 mg, 0.872 mmol, 87%).

IR (solid, ν_{max} / cm^{-1}) 3284, 2956, 2857, 1655, 1597, 1533, 1498, 1439, 1375, 1318, 1262, 1247, 1227, 1177, 1089, 1028, 1000; **^{1}H NMR** (400 MHz, $CDCl_3$) δ 7.44 (d, *J* = 8.0 Hz, 2H, *o*Ph), 7.34 – 7.27 (m, *J* = 7.5 Hz, 2H, *m*Ph), 7.11 – 7.02 (m, 2H, *p*Ph + NH), 2.75 (s, 2H, C1H), 1.97 – 1.77 (m, $C2H_2$), 1.50 – 1.38 (m, 1H, C3H or C3H'), 1.33 – 1.21 (m, 1H, C3H or C3H'); **^{13}C NMR** (101 MHz, $CDCl_3$) δ 164.2 (C=O), 138.4 (*i*Ph), 129.1 (*m*Ph), 123.7 (*p*Ph), 119.1 (*o*Ph), 38.3 (C1), 24.1 (C2), 20.1 (C3); **HRMS** (ES+) calc. for $C_{12}H_{15}ON_2$ $[M+H]^+$ 203.1179, found 203.1179.

(1*R*,5*S*)-N-(Naphthalen-1-yl)-6-azabicyclo[3.1.0]hexane-6-carboxamide, 2.9d

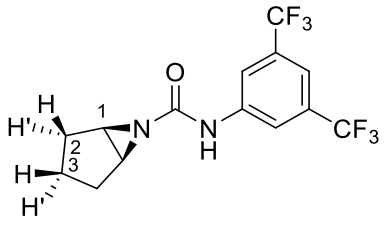


To a stirred solution of 6-azabicyclo[3.1.0]hexane, **2.6** (90.0 mg, 1.083 mmol, 1.0 equiv.) in acetonitrile (5 mL) was added 1-naphthyl isocyanate (118 μL, 1.083 mmol, 1.0 equiv.)

and stirred for 2 h. The solvent was removed in vacuo and the residue purified by column chromatography (EtOAc/ petroleum ether (1:4 to 1:3)) to give (1*R*,5*S*)-N-(naphthalen-1-yl)-6-azabicyclo[3.1.0]hexane-6-carboxamide as a white crystalline solid (246.0 mg, 0.975 mmol, 90%).

IR (thin film, ν_{max} / cm^{-1}) 3250, 3049, 2956, 2856, 1653, 1597, 1529, 1498, 1437, 1376, 1344, 1305, 1260, 1227, 1184, 1171, 1103, 1072, 1016; **^{1}H NMR** (400 MHz, DMSO-d_6) δ 9.51 (s, 1H, NH), 8.07 – 8.02 (m, 1H, Nap5H or Nap8H), 7.95 – 7.88 (m, 1H, Nap5H or Nap8H), 7.74 (d, *J* = 8.0 Hz, 1H, Nap4H), 7.59 – 7.44 (m, 4H, Nap2H + Nap3H + Nap6H + Nap7H), 3.06 (s, 2H, C1H), 2.07 – 1.89 (m, 2H, C2H or C2H'), 1.64 – 1.50 (m, 3H, C2H or C2H' + C3H or C3H'), 1.29 – 1.10 (m, 1H, C3H or C3H'); **^{13}C NMR** (101 MHz, DMSO-d_6) δ 162.6 (C=O), 134.1 (*quat* C), 133.7 (*quat* C), 128.3 (*quat* C), 128.0 (Nap5 or Nap8), 126.0 (ArH), 125.7 (ArH), 125.6 (ArH), 124.9 (Nap4), 123.1 (Nap5 or Nap8), 122.1 (ArH), 42.9 (C1), 26.7 (C2), 19.5 (C3); **HRMS** (ES+) calc. for $C_{16}H_{17}ON_2$ $[M+H]^+$ 253.1335, found 253.1332.

(1*R*,5*S*)-N-(3,5-Bis(trifluoromethyl)phenyl)-6-azabicyclo[3.1.0]hexane-6-carboxamide, 2.9c

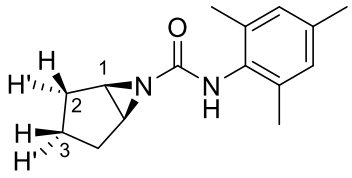


To a stirred solution of 6-azabicyclo[3.1.0]hexane, **2.6** (90.0 mg, 1.083 mmol, 1.0 equiv.) in acetonitrile (5 mL) was added 3,5-bistrifluoromethylphenyl isocyanate (186.8 μL, 1.083 mmol, 1.0 equiv.) and stirred for 2 h. The solvent was removed in vacuo and the residue purified by column chromatography (EtOAc/ petroleum ether (3:17)) to give

(1*R*,5*S*)-N-(3,5-bis(trifluoromethyl)phenyl)-6-azabicyclo[3.1.0]hexane-6-carboxamide as a white solid (278.5 mg, 0.823 mmol, 82%).

IR (thin film, ν_{max} / cm^{-1}) 3273, 2959, 1665, 1624, 1564, 1474, 1441, 1375, 1339, 1311, 1278, 1260, 1175, 1130, 1003; **^{1}H NMR** (400 MHz, $CDCl_3$) δ 7.95 (d, *J* = 1.5 Hz, 2H, CHNH), 7.55 (s, 1H), 7.30 (s, 1H, CCF_3CHCCF_3), 3.16 (dd, *J* = 1.5, 1.0 Hz, 2H, C1H), 2.10 – 2.00 (m, 2H, C2H or C2H'), 1.73 – 1.61 (m, 3H, C2H or C2H' + C3H or C3H'), 1.42 – 1.23 (m, 1H, C3H or C3H'); **^{13}C NMR** (101 MHz, $CDCl_3$) δ 162.2 (C=O), 139.9 (ArN), 132.5 (q, *J* = 33.5 Hz, *C*CF_3), 123.3 (q, *J* = 273.0 Hz, CF_3), 118.7 (NC*C*HCCF_3), 116.8 (CCF_3*C*HCCF_3), 45.1 (C1), 27.2 (C2), 19.8 (C3); **^{19}F NMR** (377 MHz, $CDCl_3$) δ -63.08; **HRMS** (ES+) calc. for $C_{14}H_{13}ON_2F_6$ $[M+H]^+$ 339.0927, found 339.0926.

(1*R*,5*S*)-N-Mesityl-6-azabicyclo[3.1.0]hexane-6-carboxamide, 2.9a

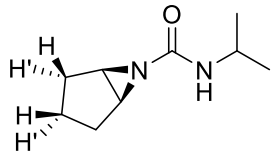


To a stirred solution of 6-azabicyclo[3.1.0]hexane, **2.6** (90.0 mg, 1.083 mmol, 1.0 equiv.) in acetonitrile (5 mL) was added 2,4,6-trimethylphenyl isocyanate (174.6 mg, 1.083 mmol, 1.0 equiv.) and stirred for 18 h. The solvent was removed in vacuo and the residue purified by column chromatography (EtOAc/ petroleum ether (1:3)) to give (1*R*,5*S*)-N-mesityl-6-azabicyclo[3.1.0]hexane-6-carboxamide as a white solid (231.8 mg, 0.949 mmol, 88%).

IR (thin film, ν_{max} / cm^{-1}) 3726, 3238, 2959, 2920, 2856, 2360, 2341, 1655, 1609, 1516, 1438, 1378, 1333, 1308, 1269, 1230, 1184, 1082, 1037; **^{1}H NMR** (400 MHz, DMSO-d_6) δ 8.69 (s, 1H, NH), 6.84 (s, 2H, ArH), 2.96 (s, 2H, C1H), 2.27 – 2.17 (m, 4H, C3H or C3H' + CHCC*H*$_3$CH), 2.10 (s, 6H, CH_3CN), 2.03 – 1.94 (m, 2H, C2H or C2H'), 1.63 –

1.51 (m, 3H, C2H or C2H' + C3H or C3H'); **^{13}C NMR** (101 MHz, DMSO-d_6) δ 162.2 (C=O), 135.3 (*quat* C), 135.1 (*quat* C), 132.6 (*quat* C), 128.3 (ArH), 42.6 (C1), 26.8 (C2), 20.5 (CHC*C*H$_3$CH), 19.6 (C1), 18.1 (C*C*H$_3$CN); **HRMS** (ES+) calc. for $C_{15}H_{21}N_2O$ $[M+H]^+$ 245.1648, found 245.1647.

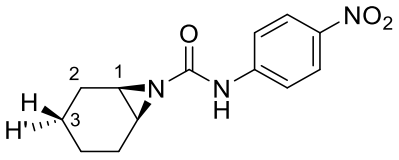
(1*R*,5*S*)-N-Isopropyl-6-azabicyclo[3.1.0]hexane-6-carboxamide, 2.14



To a stirred solution of 6-azabicyclo[3.1.0]hexane, **2.6** (90.0 mg, 1.083 mmol, 1.0 equiv.) in acetonitrile (5 mL) was added isopropyl isocyanate (107.0 μL, 1.083 mmol, 1.0 equiv.) and stirred for 48 h. The solvent was removed in vacuo and the residue purified by column chromatography (EtOAc/ petroleum ether (2:3)) to give (1*R*,5*S*)-N-isopropyl-6-azabicyclo[3.1.0]hexane-6-carboxamide as a white solid (158.8 mg, 0.944 mmol, 87%).

IR (thin film, ν_{max} / cm^{-1}) 3257, 2967, 2950, 1659, 1640, 1545, 1453, 1381, 1363, 1343, 1305, 1267, 1229, 1195, 1081; **^{1}H NMR** (400 MHz, $CDCl_3$) δ 5.01 (br s, 1H, NH), 3.87 (dhept, *J* = 8.0, 6.5 Hz, 1H, CH$_3$C*H*CH$_3$), 2.92 (s, 2H, C1H), 2.02 – 1.92 (m, 2H, C2H or C2H'), 1.66 – 1.48 (m, 3H, C2H or C2H' + C3H or C3H'), 1.36 – 1.22 (m, 1H, C3H or C3H'), 1.12 (d, *J* = 6.5 Hz, 6H, CH$_3$); **^{13}C NMR** (101 MHz, $CDCl_3$) δ 164.1 (C=O), 43.9 (N*C*H(CH$_3$)$_2$), 42.6 (C1), 27.2 (C2), 23.0 (C3), 20.0 (CH$_3$); **HRMS** (ES+) calc. for $C_9H_{17}ON_2$ $[M+H]^+$ 169.1335, found 169.1336.

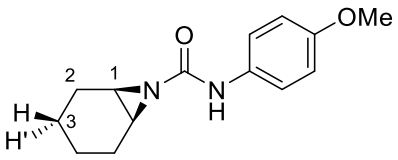
(1*R*,6*S*)-N-(4-Nitrophenyl)-7-azabicyclo[4.1.0]heptane-7-carboxamide, 2.10b



To a stirred solution of (1*R*,6*S*)-7-azabicyclo[4.1.0]heptane, **2.7** (50 mg, 0.515 mmol, 1.0 equiv.) in acetonitrile (2.5 mL) was added 4-nitrophenyl isocyanate (101.4 mg, 0.618 mmol, 1.2 equiv.) and stirred for 30 min. The solvent was removed *in vacuo* and the residue purified by column chromatography (acetone/ petroleum ether (1:9)) to give (1*R*,6*S*)-N-(4-nitrophenyl)-7-azabicyclo[4.1.0]heptane-7-carboxamide as a white solid (100.0 mg, 0.383 mmol, 74%).

IR (thin film, ν_{max} / cm^{-1}) 3292, 2936, 2858, 1672, 1611, 1597, 1546, 1506, 1440, 1409, 1330, 1303, 1248, 1213, 1177, 1111, 1081; **^{1}H NMR** (500 MHz, $CDCl_3$) δ 8.22 – 8.17 (m, 2H, $CHNO_2$), 7.65 – 7.59 (m, 2H, CHNH), 7.37 (s, 1H, NH), 2.84 – 2.80 (m, 2H, C1H), 1.97 – 1.83 (m, 4H, $C2H_2$), 1.50 – 1.40 (m, 2H, C3H or C3H'), 1.35 – 1.23 (m, 2H, C3H or C3H'); **^{13}C NMR (**126 MHz, $CDCl_3$) δ 163.1 (C=O), 144.3 (ArN), 143.1 (ArN), 125.3 (*C*HCNH), 118.3 (*C*HCNO_2), 39.0 (C1), 24.0 (C2), 20.0 (C3); **HRMS** (ES+) calc. for $C_{13}H_{16}N_3O_3$ $[M+H]^+$ 262.1186, found 262.1188.

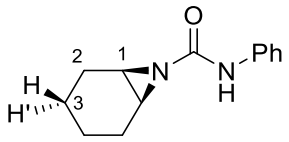
(1*R*,6*S*)-N-(4-Methoxyphenyl)-7-azabicyclo[4.1.0]heptane-7-carboxamide, 2.10d



To a stirred solution of (1*R*,6*S*)-7-azabicyclo[4.1.0]heptane, **2.7** (50 mg, 0.515 mmol, 1.0 equiv.) in acetonitrile (2.5 mL) was added 4-methoxyphenyl isocyanate (80.2 μL, 0.618 mmol, 1.2 equiv.) and stirred for 30 min. The solvent was removed *in vacuo* and the residue purified by column chromatography (acetone/ petroleum ether (1:9)) to give (1*R*,6*S*)-N-(4-methoxyphenyl)-7-azabicyclo[4.1.0]heptane-7-carboxamide as a white solid (109.2 mg, 0.474 mmol, 92%).

IR (thin film, ν_{max} / cm^{-1}) 3283, 2935, 1657, 1601, 1511, 1440, 1411, 1313, 1299, 1241, 1178, 1078, 1035; **^{1}H NMR** (500 MHz, $CDCl_3$) δ 7.37 - 7.31 (m, 2H, C*H*NH), 7.07 (s, 1H, NH), 6.87–6.81 (m, 2H, C*H*$COCH_3$), 3.78 (s, 3H, OCH_3), 2.73 (br s, 2H, C1H), 2.08–1.74 (m, 4H, $C2H_2$), 1.42 (br s, 2H, C3H or C3H'), 1.26 (br s, 2H, C3H or C3H'); **^{13}C NMR** (126 MHz, $CDCl_3$) δ 163.6 (C=O), 156.0 (ArO), 131.6 (ArN), 121.0 (*C*HCN), 114.3 (*C*H$COCH_3$), 55.6 (CH_3), 38.2 (C1), 24.1 (C2), 20.1 (C3); **HRMS** (ES+) calc. for $C_{14}H_{19}O_2N_2$ $[M+H]^+$ 247.1441, found 247.1439.

(1*R*,6*S*)-N-Phenyl-7-azabicyclo[4.1.0]heptane-7-carboxamide, 2.10a

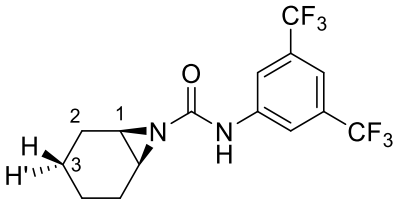


To a stirred solution of (1*R*,6*S*)-7-azabicyclo[4.1.0]heptane, **2.7** (500 mg, 5.15 mmol, 1.0 equiv.) in acetonitrile (25 mL) was added phenyl isocyanate (738 μL, 6.18 mmol, 1.2 equiv.) and stirred for 2 h. The solvent was removed *in vacuo* and the residue purified by column chromatography (acetone/ petroleum ether (1:9)) to give (1*R*,6*S*)-N-phenyl-7-azabicyclo[4.1.0]heptane-7-carboxamide as a white solid (927.8 mg, 4.63 mmol, 90%).

IR (thin film, ν_{max} / cm^{-1}) 3296, 2935, 2860, 1658, 1599, 1532, 1499, 1438, 1407, 1315, 1262, 1245, 1217; **^{1}H NMR** (400 MHz, $CDCl_3$) δ 7.45 (d, *J* = 8.0 Hz, 2H, *o*Ph), 7.31 – 7.24 (m, 3H, NH + *m*Ph), 7.06 (t, *J* = 7.5 Hz, 1H, *p*Ph), 2.80 – 2.68 (m, 2H, C1H), 1.99 – 1.74 (m, 4H, $C2H_2$), 1.49 – 1.35 (m, 2H, C3H or C3H'), 1.34 – 1.17 (m, 2H, C3H or C3H'); **^{13}C NMR** (101 MHz, $CDCl_3$) δ 163.5 (C=O), 138.4 (ArN), 129.1 (*m*Ph), 123.6 (*p*Ph), 119.1 (*o*Ph), 38.2 (C1), 24.0 (C2), 20.0 (C3); **LRMS** (ES+) calc. for $C_{13}H_{17}ON_2$ $[M+H]^+$ 217.1, found 217.2.

Data consistent with literature values.[74]

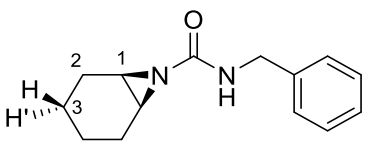
(1*R*,6*S*)-N-(3,5-Bis(trifluoromethyl)phenyl)-7-azabicyclo[4.1.0]heptane-7-carboxamide, 2.10c



To a stirred solution of (1*R*,6*S*)-7-azabicyclo[4.1.0]heptane, **2.7** (250 mg, 2.57 mmol, 1.0 equiv.) in acetonitrile (12.5 mL) was added 3,5-bis(trifluoromethyl)phenyl isocyanate (532 μL, 3.09 mmol, 1.2 equiv.) and stirred for 1 h. The solvent was removed *in vacuo* and the residue purified by column chromatography (acetone/ petroleum ether (1:9)) to give (1*R*,6*S*)-N-(3,5-bis(trifluoromethyl)phenyl)-7-azabicyclo[4.1.0]heptane-7-carboxamide as a white solid (314.6 mg, 0.893 mmol, 35%).

IR (thin film, ν_{max} / cm^{-1}) 2942, 1671, 1561, 1473, 1440, 1384, 1325, 1277, 1214, 1175, 1131; **^{1}H NMR** (400 MHz, $CDCl_3$) δ 7.98 – 7.95 (m, 2H, C*H*NH), 7.56 – 7.53 (m, 1H, CCF_3CHCCF_3), 7.32 (s, 1H, ArNH), 2.81 (dq, *J* = 2.0, 1.0 Hz, 2H, C1H), 1.98 – 1.81 (m, 4H, $C2H_2$), 1.52 – 1.38 (m, 2H, C3H or C3H'), 1.35 – 1.23 (m, 2H, C3H or C3H'); **^{13}C NMR** (101 MHz, $CDCl_3$) δ 163.3 (C=O), 139.9 (ArN), 132.5 (q, *J* = 33.5 Hz, *C*CF_3), 123.3 (q, *J* = 273.0 Hz, CF_3), 118.7 (NC*C*HCCF_3), 117.3 – 116.5 (m, CCF_3*C*HCCF_3), 39.0 (C1), 24.0 (C2), 20.0 (C3); **^{19}F NMR** (377 MHz, $CDCl_3$) δ -63.05; **HRMS** (ES+) calc. for $C_{15}H_{14}ON_2F_6$ $[M+H]^+$ 353.1083, found 353.1084.

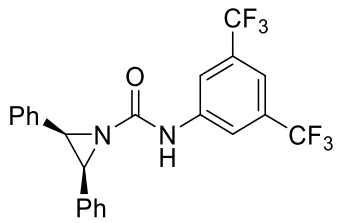
(1*R*,6*S*)-N-Benzyl-7-azabicyclo[4.1.0]heptane-7-carboxamide, 2.43



To a stirred solution of (1*R*,6*S*)-7-azabicyclo[4.1.0]heptane, **2.7** (50 mg, 0.515 mmol, 1.0 equiv.) in acetonitrile (2.5 mL) was added benzyl isocyanate (76.3 μL, 0.618 mmol, 1.2 equiv.) and stirred for 30 min. The solvent was removed *in vacuo* and the residue purified by column chromatography (acetone/ petroleum ether (1:9)) to give (1*R*,6*S*)-N-benzyl-7-azabicyclo[4.1.0]heptane-7-carboxamide as a white solid (94.1 mg, 0.409 mmol, 79%).

IR (thin film, ν_{max} / cm^{-1}) 3292, 3030, 2933, 2857, 1650, 1531, 1454, 1439, 1415, 1363, 1342, 1282, 1231, 1124, 1081, 1028; **^{1}H NMR** (400 MHz, $CDCl_3$) δ 7.33 – 7.21 (m, 5H, ArH), 5.56 (s, 1H, NH), 4.34 (d, *J* = 6.0 Hz, 2H, C*H*NH), 2.65 – 2.54 (m, 2H, CH_2Ph), 1.87 – 1.70 (m, 4H, C2H_2), 1.41 – 1.29 (m, 2H, C3H or C3H'), 1.25 – 1.13 (m, 2H, C3H or C3H'). **^{13}C NMR** (101 MHz, $CDCl_3$) δ 166.0, 138.7, 128.7, 127.8, 127.5, 44.9, 37.6, 24.1, 20.1; **HRMS** (ES+) calc. for $C_{14}H_{19}ON_2$ $[M+H]^+$ 231.1492, found 231.1492.

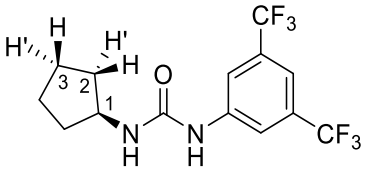
(2*R*,3*S*)-N-(3,5-Bis(trifluoromethyl)phenyl)-2,3-diphenylaziridine-1-carboxamide, 2.15



To a stirred solution of (2*R*,3*S*)-2,3-diphenylaziridine, **2.42** (88.6 mg, 0.454 mmol, 1.0 equiv.) in acetonitrile (2.5 mL) was added 3,5-bis(trifluoromethyl)phenyl isocyanate (86.1 μL, 0.499 mmol, 1.1 equiv.) and stirred for 22 h. The solvent was removed *in vacuo* and the residue purified by column chromatography (acetone/ petroleum ether (3:97 to 4:96)) to give (2*R*,3*S*)-N-(3,5-bis(trifluoromethyl)phenyl)-2,3-diphenylaziridine-1-carboxamide as a white solid (173.4 mg, 0.385 mmol, 85%).

IR (thin film, ν_{max} / cm^{-1}) 3286, 3080, 2924, 2360, 1665, 1625, 1571, 1476, 1445, 1410, 1382, 1331, 1318, 1303, 1275, 1263, 1229, 1166, 1131, 1111, 1066, 1028; **^{1}H NMR** (400 MHz, $CDCl_3$) δ 8.02 (s, 2H, CHNH), 7.59 (s, 1H, CCF_3CHCCF_3), 7.48 (s, 1H, NH), 7.24 – 7.14 (m, 10H, PhH), 4.10 (s, 2H, ArCH); **^{13}C NMR** (126 MHz, $CDCl_3$) δ 162.0 (C=O), 139.6 (*i*Ph), 133.5 (ArN), 132.6 (q, *J* = 33.5 Hz, *C*CF_3), 128.2 (*m*Ph), 127.9 (*o*Ph + *p*Ph), 123.2 (q, *J* = 273.0 Hz, CF_3), 118.9 (NC*C*HCCF_3), 117.3 (CCF_3*C*HCCF_3), 47.6 (Ar*C*H); **^{19}F NMR** (377 MHz, $CDCl_3$) δ -63.03; **HRMS** (ES+) calc. for $C_{23}H_{17}ON_2F_6$ [M+H]+ 451.1240, found 451.1241.

1-(3,5-Bis(trifluoromethyl)phenyl)-3-cyclopentylurea, 2.40

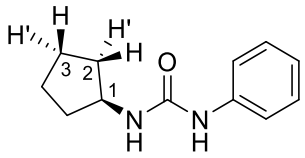


To a stirred solution of cyclopentylamine (106.9 μL, 1.083 mmol, 1.0 equiv.) in acetonitrile (5 mL) was added 3,5-bistrifluoromethylphenyl isocyanate (186.8 μL, 1.083 mmol, 1.0 equiv.) and stirred for 2 h. The solvent was removed *in vacuo* and the residue purified by column chromatography (EtOAc/ petroleum ether (1:9 to 3:17)) to give 1-(3,5-bis(trifluoromethyl)phenyl)-3-cyclopentylurea as a white solid (310.5 mg, 0.913 mmol, 84%).

IR (thin film, ν_{max} / cm^{-1}) 3293, 2963, 2874, 2495, 2408, 1634, 1566, 1480, 1443, 1399, 1377, 1276, 1171, 1128, 1109, 1014; **^{1}H NMR** (400 MHz, CD_3OD) δ 7.98 (s, 2H, $NCCHCCF_3$), 7.46 (s, 1H, $CF_3CCHCCF_3$), 4.05 (p, J = 6.5 Hz, 1H, C1H), 2.03 – 1.91 (m, 2H, C3H or C3H'), 1.78 – 1.57 (m, 4H, $C2H_2$), 1.53 – 1.42 (m, 2H, C3H or C3H'); **^{13}C NMR** (101 MHz, CD_3OD) δ 157.2 (C=O), 143.6 (ArN), 133.3 (q, *J* = 33.0 Hz, *C*CF_3), 125.0 (q, *J* = 272.0 Hz, CF_3), 119.0 (CCF_3*C*HCN), 115.5 (CCF_3*C*HCCF_3), 53.1

(C1), 34.2 (C2), 24.7 (C3); **^{19}F NMR** (377 MHz, CD_3OD) δ -63.07; **HRMS** (ES+) calc. for $C_{14}H_{15}ON_2F_6$ $[M+H]^+$ 341.1083, found 341.1084.

1-Cyclopentyl-3-phenylurea, 2.13

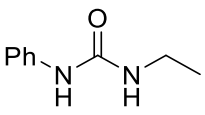


To a stirred solution of cyclopentylamine (356 μL, 3.61 mmol, 1.0 equiv.) in acetonitrile (18 mL) was added phenyl isocyanate (517 μL, 4.33 mmol, 1.2 equiv.) and stirred for 1 h. The precipitate was washed with cold hexanes, yielding 1-cyclopentyl-3-phenylurea (813.4 mg, 2.77 mmol, 77%) as a white crystalline solid without further purification.

IR (thin film, ν_{max} / cm^{-1}) 3317, 2923, 2853, 2359, 1638, 1595, 1545, 1497, 1539, 1314, 1248, 1230, 1154, 1127, 1081, 1043; **^{1}H NMR** (400 MHz, DMSO-d_6) δ 8.27 (s, 1H, NHAr), 7.36 (d, *J* = 8.5 Hz, 2H, *o*Ph),), 7.20 (t, *J* = 8.0 Hz, 2H, *m*Ph), 6.87 (d, J = 8.0 Hz, 2H, *p*Ph), 6.05 (d, *J* = 7.5 Hz, 1H, C1NH), 3.51 – 3.40 (m, 1H, C1H), 1.84 – 1.76 (m, 2H, C2H'), 1.70 – 1.61 (m, 2H, C3H or C3H'), 1.36 – 1.24 (m, 2H, C3H or C3H'), 1.21 – 1.10 (m, 2H, C2H), **^{13}C NMR** (101 MHz, DMSO-d_6) δ 154.4 (C=O), 140.6 (*i*Ph), 128.6 (*m*Ph), 120.9 (*o*Ph), 117.4 (*p*Ph), 47.6 (C1), 33.0 (C2), 24.4 (C3); **LRMS** (ES+) calc. for $C_{12}H_{17}ON_2$ $[M+H]^+$ 205.1, found 205.0; **mp** (acetonitrile) 211.3 °C.

Data consistent with literature values.[75]

1-Ethyl-3-phenylurea, 2.41



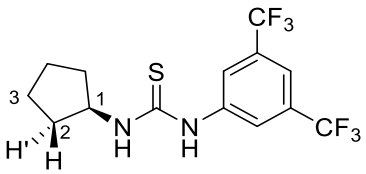
To a stirred solution of aniline (1.27 mL, 13.89 mmol, 1.1 equiv.) in acetonitrile (15 mL) was added ethyl isocyanate (1.00 mL, 12.63 mmol, 1.0 equiv.) and stirred for 6 h. The solvent was removed *in vacuo* and the residue purified by recrystallisation from acetonitrile to give 1-ethyl-3-phenylurea as a white crystalline solid (1.634 g, 9.95 mmol, 79%).

IR (thin film, ν_{max} / cm^{-1}) 3318, 2972, 2931, 1643, 1594, 1551, 1497, 1440, 1379, 1310, 1235, 1175, 1154, 1076, 1030; **^{1}H NMR** (400 MHz, $CDCl_3$) δ 7.93 (s, 1H, ArNH), 7.29 – 7.22 (m, 2H, *o*Ph), 7.21 – 7.15 (m, 2H, *m*Ph), 6.99 – 6.91 (m, 1H, *p*Ph), 5.99 (t, *J* = 5.5 Hz, 1H, CH_2NH), 3.15 (qd, *J* = 7.0, 5.5 Hz, 2H, CH_2CH_3), 1.02 (t, *J* = 7.0 Hz, 3H, CH_3); **^{13}C NMR** (101 MHz, $CDCl_3$) δ 157.0 (C=O), 139.3 (*i*Ph), 129.0 (*m*Ph), 122.9 (*p*Ph), 120.1 (*o*Ph), 34.9 (CH_2), 15.4 (CH_3); **LRMS** (ES+) calc. for $C_9H_{13}N_2O$ $[M+H]^+$ 165.1, found 165.0, **mp** (acetonitrile) 99.6 °C.

Data consistent with literature values.[76]

2. 6. 5. 3 Synthesis of thioureas

1-(3,5-Bis(trifluoromethyl)phenyl)-3-cyclopentylthiourea, 2.44

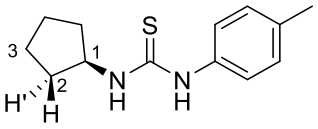


To a stirred solution of cyclopentylamine (106.9 μL, 1.083 mmol, 1.0 equiv.) in acetonitrile (5 mL) was added 3,5-bistrifluoromethylphenyl isothiocyanate (197.1 μL, 1.083 mmol, 1.0 equiv.) and stirred for 2 h. The solvent was removed *in vacuo* and the residue purified by column chromatography (EtOAc/ petroleum ether (1:9)) to give

1-(3,5-bis(trifluoromethyl)phenyl)-3-cyclopentylthiourea as a white solid (351.3 mg, 0.986 mmol, 91%).

IR (thin film, ν_{max} / cm^{-1}) 3255, 2964, 2349, 1624, 1564, 1531, 1469, 1383, 1343, 1269, 1176, 1129, 1106, 1044; **^{1}H NMR** (400 MHz, DMSO-d_6) δ 9.83 (s, 1H, ArNH), 8.42 – 8.14 (m, 3H, C*H*NH + C1NH), 7.70 (s, 1H, C1HN*H*), 4.51 (s, 1H, C1H), 2.08 – 1.86 (m, 2H, C2H or C2H'), 1.78 – 1.41 (m, 6H, $C3H_2$ + C2H or C2H'); **^{13}C NMR** (101 MHz, DMSO-d_6) δ 180.3 (C=S), 142.5 (ArN), 130.1 (d, *J* = 32.5 Hz, *C*CF_3), 123.3 (q, *J* = 273.0 Hz, CF_3), 121.6 (NC*C*HCCF_3), 115.8 (CCF_3*C*HCCF_3), 55.8 (C1), 32.3 (C2), 23.8 (C3); **^{19}F NMR** (377 MHz, DMSO-d_6) δ -61.68; **HRMS** (ES+) calc. for $C_{14}H_{15}N_2F_6{}^{32}S$ $[M+H]^+$ 357.0855, found 357.0857.

1-Cyclopentyl-3-(*p*-tolyl)thiourea, 2.34



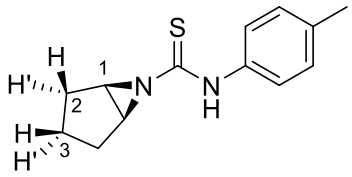
To a stirred solution of cyclopentylamine (400.0 μL, 4.03 mmol, 1.0 equiv.) in acetonitrile (18 mL) was added *p*-tolyl isothiocyanate (629.7 mg, 4.22 mmol, 1.05 equiv.) and stirred for 1 h. The solvent was removed in vacuo and the residue purified by column chromatography (acetone/ petroleum ether (1:4)) to give 1-cyclopentyl-3-(*p*-tolyl)thiourea as a white solid (866.4 mg, 3.70 mmol, 92%).

IR (solid, ν_{max} / cm^{-1}) 3217, 3042, 2956, 2865, 1537, 1447, 1413, 1315, 1112, 1017; **^{1}H NMR** (400 MHz, CDCl3) δ 7.94 (s, 1H, ArNH), 7.19 (d, *J* = 8.0 Hz, 2H, C*H*CH_3), 7.06 (d, *J* = 8.0 Hz, 2H, C*H*NH), 5.92 (s, 1H, C1HN*H*), 4.64 (q, *J* = 7.5 Hz, 1H, C1H), 2.34 (s, 3H, CH_3), 2.14 – 1.98 (m, 2H, C2H or C2H'), 1.66 – 1.53 (m, 4H, $C3H_2$), 1.35

(m, 2H, C2H or C2H'); **^{13}C NMR** (101 MHz, DMSO-d_6) δ 179.9 (C=S), 137.0 (ArN), 133.1 (*C*CH_3), 128.9 (CHNH), 123.2 (*C*HCCH_3), 55.2 (C1), 32.1 (C2), 23.4 (C3); **LRMS** (ES–) calc. for $C_{13}H_{17}N_2{}^{32}S$ $[M–H]^-$ 233.1, found 233.1.

Data consistent with literature values.[77]

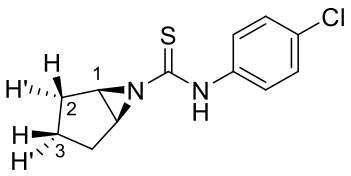
(1*R*,5*S*)-N-(*p*-Tolyl)-6-azabicyclo[3.1.0]hexane-6-carbothioamide, 2.11a



To a stirred solution of 6-azabicyclo[3.1.0]hexane, **2.6** (454.0 mg, 4.99 mmol, 1.0 equiv.) in acetonitrile (5 mL) was added *p*-tolyl isothiocyanate (969.8 mg, 6.50 mmol, 1.2 equiv.) and stirred for 30 min. The solvent was removed *in vacuo* and the residue purified by column chromatography (acetone/ petroleum ether (1:19)) to give (1*R*,5*S*)-N-(*p*-tolyl)-6-azabicyclo[3.1.0]hexane-6-carbothioamide as a white solid (899.9-mg, 3.87 mmol, 78%).

IR (thin film, ν_{max} / cm^{-1}) 3170, 2958, 2857, 1588, 1515, 1370, 1313, 1301, 1230, 1203, 1156, 1134, 1081, 1021; **^{1}H NMR** (400 MHz, $CDCl_3$) δ 7.20 – 7.14 (m, 4H, ArH), 3.12 (s, 1H, NH), 2.34 (s, 1H, C1H), 1.94 – 1.77 (m, 1H, C3H or C3H'), 1.66 – 1.51 (m, 2H, C2H or C2H'), 1.49 – 1.38 (m, 2H, C2H or C2H'), 1.34 – 1.22 (m, 1H, C3H or C3H'); **^{13}C NMR** (101 MHz, $CDCl_3$) δ 193.8 (C=S), 136.2 (ArN), 129.8 (*C*HCCH_3), 123.7 (*C*HCNH), 121.8 (*C*CH_3), 49.5 (C1), 27.1 (C2), 21.1 (C3); **HRMS** (ES+) calc. for $C_{13}H_{17}N_2{}^{32}S$ $[M+H]^+$ 233.1107, found 233.1107.

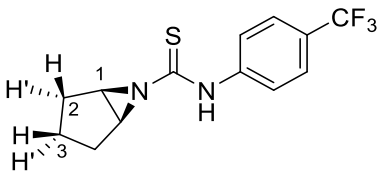
(1*R*,5*S*)-N-(4-Chlorophenyl)-6-azabicyclo[3.1.0]hexane-6-carbothioamide, 2.11b



To a stirred solution of 6-azabicyclo[3.1.0]hexane, **2.6** (71.2 mg, 0.858 mmol, 1.0 equiv.) in acetonitrile (5 mL) was added 4-chlorophenyl isothiocyanate (174.5 mg, 1.029 mmol, 1.2 equiv.) and stirred for 30 min. The solvent was removed in vacuo and the residue purified by column chromatography (acetone/ petroleum ether (1:19)) to give (1*R*,5*S*)-N-(4-chlorophenyl)-6-azabicyclo[3.1.0]hexane-6-carbothioamide as a white solid (103.3 mg, 0.409 mmol, 48%).

IR (thin film, ν_{max} / cm^{-1}) 3187, 2960, 2360, 1579, 1521, 1490, 1369, 1395, 1280, 1229, 1203, 1156, 1089, 1012; **^{1}H NMR** (400 MHz, $CDCl_3$) δ 8.93 (s, 1H, NH), 7.44 – 7.22 (m, 4H, ArH), 3.17 (s, 2H, C1H), 2.08 – 1.80 (m, 2H, C2H or C2H'), 1.74 – 1.44 (m, 3H, C2H or C2H' + C3H or C3H'), 1.39 – 1.19 (m, 1H, C3H or C3H'); **^{13}C NMR** (101 MHz, $CDCl_3$) δ 193.7 (C=S), 131.4 (ArN), 129.2 (*C*HCCl), 128.7 (CCl), 124.6 (CHNH), 49.5 (C1), 27.0 (C2), 19.9 (C3); **HRMS** (ES+) calc. for $C_{12}H_{14}N_2{}^{35}Cl^{32}S$ $[M+H]^+$ 253.0561, found 253.0559.

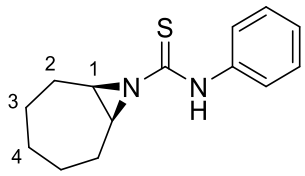
(1*R*,5*S*)-N-(4-(Trifluoromethyl)phenyl)-6-azabicyclo[3.1.0]hexane-6-carbothioamide, 2.11c



To a stirred solution of 6-azabicyclo[3.1.0]hexane, **2.6** (225.8 mg, 2.71 mmol, 1.0 equiv.) in acetonitrile (13.5 mL) was added 4-(triflouromethyl)phenyl isothiocyanate (605.7 mg, 2.98 mmol, 1.1 equiv.) and stirred for 30 min. The solvent was removed *in vacuo* and the residue purified by column chromatography (acetone/ petroleum ether (1:19)) to give (1*R*,5*S*)-N-(4-(trifluoromethyl)phenyl)-6-azabicyclo[3.1.0]hexane-6-carbothioamide as a white solid (899.9 mg, 3.87 mmol, 78%).

IR (thin film, ν_{max} / cm^{-1}) 2958, 1580, 1524, 1319, 1242, 1205, 1158, 1113, 1065; **^{1}H NMR** (400 MHz, $CDCl_3$) δ 9.19 (s, 1H, NH), 7.60 (d, *J* = 8.5 Hz, 2H, C*H*NH), 7.53 – 7.45 (m, 2H, $CHCCF_3$), 3.26 – 3.18 (m, 1H, C1H), 1.99 (dd, *J* = 13.5, 7.5 Hz, 2H, C2H or C2H'), 1.66 (dt, *J* = 12.0, 8.0 Hz, 1H, C3H or C3H'), 1.60 – 1.49 (m, 2H, C2H or C2H'), 1.39 – 1.22 (m, 1H, C3H or C3H'); **^{13}C NMR** (101 MHz, $CDCl_3$) δ 193.6 (C=S), 141.0 (ArN), 127.6 (d, *J* = 33.0 Hz, *C*CF_3), 126.7 (q, *J* = 274.0 Hz, CF_3),126.4 (q, *J* = 4.0 Hz, *C*HCCF_3), 122.6 (*C*HCNH), 49.8 (C1), 27.1 (C2), 20.0 (C3); **^{19}F NMR** (377 MHz, $CDCl_3$) δ -62.27; **HRMS** (ES+) calc. for $C_{13}H_{14}N_2F_3{}^{32}S$ $[M+H]^+$ 287.0824, found 287.0826.

(1*R*,7*S*)-N-Phenyl-8-azabicyclo[5.1.0]octane-8-carbothioamide, 2.16



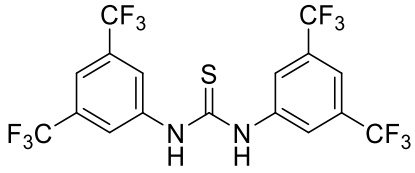
To a stirred solution of 8-azabicyclo[5.1.0]octane, **2.39** (50.0 mg, 0.450 mmol, 1.0 equiv.) in acetonitrile (2.5 mL) was added phenyl isothiocyanate (57.3 μL, 0.480 mmol, 1.2 equiv.) and stirred for 1 h. The solvent was removed *in vacuo* and the residue purified

by column chromatography (acetone/ petroleum ether (1:9)) to give (1*R*,7*S*)-N-phenyl-8-azabicyclo[5.1.0]octane-8-carbothioamide as a yellow solid (47.0 mg, 0.191 mmol, 42%).

IR (thin film, ν_{max} / cm^{-1}) 3164, 2922, 2848, 2353, 1592, 1523, 1496, 1444, 1426, 1380, 1314, 1291, 1270, 1234, 1215, 1166, 1108, 1088, 1045; **^{1}H NMR** (400 MHz, $CDCl_3$) δ 8.93 (s, 1H, NH), 7.39 – 7.20 (m, 5H, ArH), 2.65 (s, 2H, C1H), 1.68 – 1.16 (m, 10H, $C2H_2$ + $C3H_2$ + $C4H_2$); **^{13}C NMR** (101 MHz, $CDCl_3$) δ 197.6 (C=S), 138.6 (ArN), 129.2 (ArH), 127.0 (ArH), 125.4 (ArH), 48.3 (C1), 31.4 (C2), 28.9 (C3), 25.8 (C4); **LRMS** (ES–) calc. for $C_{14}H_{17}N_2{}^{32}S$ $[M–H]^-$ 245.1, found 245.0.

Data consistent with literature values.[78]

1,3-Bis(3,5-bis(trifluoromethyl)phenyl)thiourea, 2.23



A solution of 3,5-bis(trifluoromethyl)aniline (100.0 μL, 0.640 mmol, 1.0 equiv.) and 3,5-bis(trifluoromethyl)phenyl isothiocyanate (140 μL, 0.768 mmol, 1.2 equiv.) in dichloromethane (6 mL) was heated to reflux for 18 h. The solvent was removed *in vacuo* and the residue purified by recrystallisation (ethyl acetate/ petroleum ether (1:49)) to give 1,3-bis(3,5-bis(trifluoromethyl)phenyl)thiourea as a white crystalline solid (303.7 mg, 0.607 mmol, 95%).

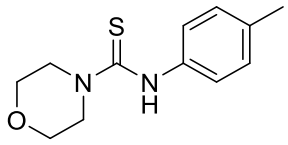
IR (thin film, ν_{max} / cm^{-1}) 3048, 1551, 1465, 1372, 1325, 1273, 1170, 1122, 1107, 1004; **^{1}H NMR** (400 MHz, DMSO-d_6) δ 10.66 (s, 1H, NH), 8.21 (s, 2H, CHCN), 7.83 (s, 1H, CCF_3CHCCF_3); **^{13}C NMR** (101 MHz, DMSO-d_6) δ 180.6 (C=S), 141.2 (CN), 130.4

(q, *J* = 33.0 Hz, *C*CF_3), 124.47 – 123.87 (m, *C*HCN), 123.2 (q, *J* = 272.0 Hz, CF_3), 118.04 – 117.13 (m, CCF_3*C*HCCF_3); **^{19}F NMR** (377 MHz, DMSO-d_6) δ -61.72, **LRMS** (ES–) calc. for $C_{17}H_8F_{12}N_2{}^{32}S$ $[M–H]^-$ 499.0, found 499.0; **mp** (ethyl acetate/ petroleum ether) 197.1 °C.

Data consistent with literature values.[79]

2. 6. 5. 4 Synthesis of undesired products of aziridine thiourea reactions

N-(*p*-Tolyl)morpholine-4-carbothioamide, 2.45

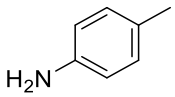


A solution of (1*R*,5*S*)-N-(*p*-tolyl)-6-azabicyclo[3.1.0]hexane-6-carbothioamide, **2.11a** (50.0 mg, 0.215 mmol, 1.0 equiv.) in toluene (20 mL) was added morpholine (188 μL, 2.15 mmol, 10.0 equiv.) and stirred for 18 h. The solvent was removed *in vacuo* and the residue purified by column chromatography (acetone/ petroleum ether (1:3)) to give N-(*p*-tolyl)morpholine-4-carbothioamide as a white solid (29.1 mg, 0.123 mmol, 57%).

IR (thin film, ν_{max} / cm^{-1})3235, 2963, 2919, 2853, 2349, 1590, 1518, 1458, 1415, 1327, 1305, 1270, 1227, 1207, 1156, 1110, 1065, 1027; **^{1}H NMR** (400 MHz,$CDCl_3$) δ 7.56 (s, 1H, NH), 7.09 (d, *J* = 8.0 Hz, 2H, C*H*NH), 6.99 (d, *J* = 8.0 Hz, 2H, C*H*CH_3), 3.72 (dd, *J* = 6.0, 3.5 Hz, 4H, CH_2N), 3.63 (dd, *J* = 6.0, 3.5 Hz, 4H, CH_2O), 2.29 (s, 3H, CH_3); **^{13}C NMR** (101 MHz, $CDCl_3$) δ 183.2 (C=S), 137.2 (C*C*NH), 135.3 (*C*CH_3), 129.6 (*C*CCH_3), 124.0 (*C*CNH), 66.1 (CO), 49.3 (CH_2N), 21.0 (CH_3); **LRMS** (ES–) calc. for $C_{12}H_{15}N_2{}^{32}SO$ $[M–H]^-$ 235.1, found 235.1.

Data consistent with literature values.[80]

***p*-Toluidine, 2.46**



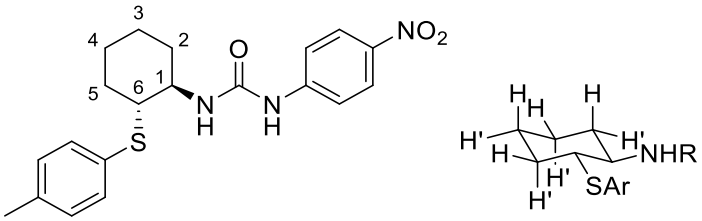
To a stirred solution of (1*R*,5*S*)-N-(*p*-tolyl)-6-azabicyclo[3.1.0]hexane-6-carbothioamide, **2.11a** (20.0 mg, 86.1 μmol, 1.0 equiv.) in dichloromethane (0.8 mL) was added methanol (35 μL, 0.861 mmol, 10 equiv.) followed by 4-dimethylaminopyridine (2.1 mg, 0.2 mmol, 0.2 equiv.) then and stirred for 18 h. Water (0.8 mL) was added, resulting in vigorous bubbling. Once the bubbling had ceased, the mixture was diluted with dichloromethane (5 mL) and water (3 mL), the phases separated and the aqueous extracted with dichloromethane (3 × 5 mL). The combined organics were washed with brine (5 mL), dried ($MgSO_4$) and the solvent removed *in vacuo.* The residue purified by column chromatography (acetone/ petroleum ether (1:4)) to give *p*-toluidine as a white solid (6.0 mg, 56 μmol, 65%).

IR (thin film, ν_{max} / cm^{-1}) 3348, 3013, 2920, 2862, 2351, 1620, 1514, 1455, 1267, 1178, 1123, 1040; **^{1}H NMR** (400 MHz, $CDCl_3$) δ 6.98 (d, *J* = 8.0 Hz, 2H, C*H*CH_3), 6.62 (d, *J* = 8.0 Hz, 2H, C*H*CNH_2), 3.52 (br s, 2H, NH_2), 2.25 (s, 3H, CH_3); **^{13}C NMR** (101 MHz, $CDCl_3$) δ 143.7 (CN), 129.4 (*C*CN), 127.2 (*C*CH_3), 114.9 (*C*CCH_3), 20.1 (CH_3); **LRMS** (ES+) calc. for $C_7H_{10}N$ $[M+H]^+$ 108.1, found 108.2.

Data consistent with literature values.[81]

2. 6. 5. 5 Synthesis of thiol opened ureas

(±)-1-(4-Nitrophenyl)-3-((1*R*,2*R*)-2-(*p*-tolylthio)cyclohexyl)urea, 2.47

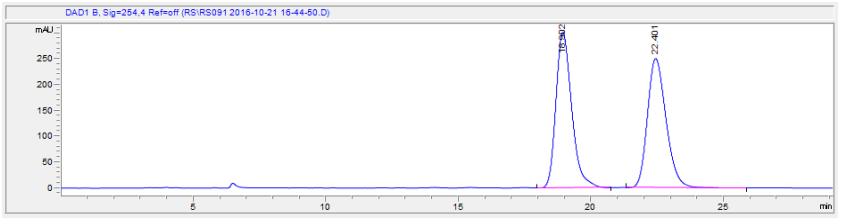


(1*R*,6*S*)-N-(4-Nitrophenyl)-7-azabicyclo[4.1.0]heptane-7-carboxamide, **2.10b** (20.0 mg, 76.5 μmol, 1.0 equiv.), 4-methylbenzenethiol (11.4 mg, 91.8 μmol, 1.2 equiv.) and potassium *tert*-butoxide (10.3 mg, 91.8 μmol, 1.2 equiv.) were stirred in diethyl ether (0.4 mL) at room temperature for 18 h. The reaction mixture was diluted with diethyl ether (5 mL), and worked up with water (5 mL), the phases separated and the aqueous extracted with diethyl ether (3 × 3 mL). The combined organics were washed with brine (5 mL), dried ($MgSO_4$) and the solvent removed *in vacuo*. The residue was purified by column chromatography (acetone/ petroleum ether (1:4)) to give (±)-1-(4-nitrophenyl)-3-((1*R*,2*R*)-2-(*p*-tolylthio)cyclohexyl)urea as an off-white solid (13.7 mg, 35.5 μmol, 46%).

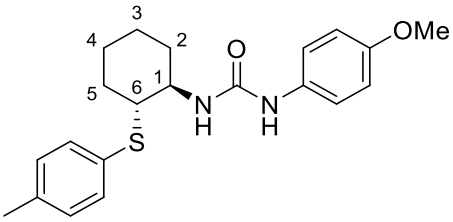
IR (thin film, ν_{max} / cm^{-1}) 3658, 2979, 2888, 1461, 1382, 1252, 1152, 1072; **^{1}H NMR** (500 MHz, $CDCl_3$) δ 8.13 (d, *J* = 8.5 Hz, 2H, C*H*CNH), 7.51 (d, *J* = 8.5 Hz, 2H, $CHCNO_2$), 7.34 (s, 1H, ArNH), 7.30 (d, *J* = 8.0 Hz, 2H, C*H*CCH_3), 7.07 (d, *J* = 8.0 Hz, 2H, C*H*CS), 5.36 (d, *J* = 7.5 Hz, 1H, C1NH), 3.59 (tdd, *J* = 10.5, 7.5, 4.0 Hz, 1H, C1H), 2.84 (td, *J* = 11.0, 4.0 Hz, 1H, C6H), 2.30 (s, 3H, CH_3), 2.28 – 2.22 (m, 1H, C2H'), 2.11 – 2.01 (m, 1H, C5H), 1.74 – 1.61 (m, 5H, C3H + C4H'), 1.44 – 1.34 (m, 1H, C5H'), 1.32 – 1.15 (m, 4H, C2H + C3H' + C4H); **^{13}C NMR** (126 MHz, $CDCl_3$) δ 154.1 (C=O), 145.8 (ArNH), 142.2 (CNO_2), 138.0 ($ArCH_3$), 133.8 (*C*HCCH_3), 129.9 (*C*HCS), 129.5 (ArS), 125.4 (*C*HCNH), 117.9 (*C*HCNO_2), 54.0 (C1), 52.6 (C6), 34.3 (C2), 33.2 (C5), 25.9 (C4),

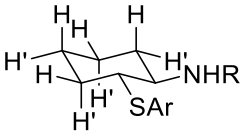
24.7 (C3), 21.3 (CH_3); **HRMS** (ES+) calc. for $C_{20}H_{23}N_3O_3S$ $[M+H]^+$ 386.1533, found 386.1532.

The enantiomeric excess was determined by HPLC [Chiralpak® IC; hexane:*i*PrOH 80:20; 1.0 ml min^{-1}, λ= 254 nm, t_R (min)= 18.90 min, t_R (maj)= 22.40 min.



(±)-1-(4-Methoxyphenyl)-3-((1*R*,2*R*)-2-(*p*-tolylthio)cyclohexyl)urea, 2.48

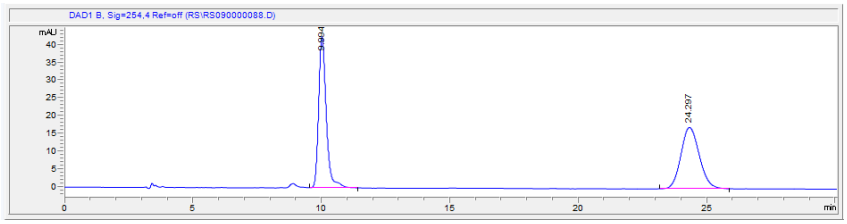




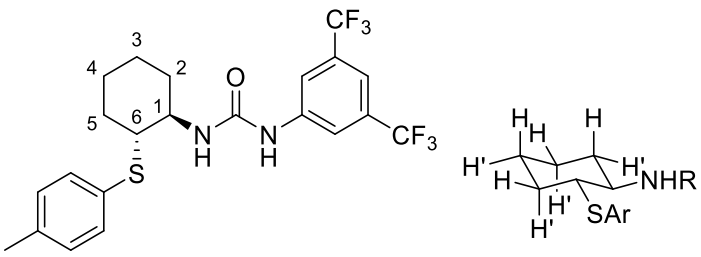
(1*R*,6*S*)-N-(4-Methoxyphenyl)-7-azabicyclo[4.1.0]heptane-7-carboxamide, **2.10d** (20.0 mg, 81.2 μmol, 1.0 equiv.), 4-methylbenzenethiol (12.1 mg, 97.4 μmol, 1.2 equiv.) and potassium *tert*-butoxide (10.9 mg, 97.4 μmol, 1.2 equiv.) were stirred in diethyl ether (0.4 mL) at room temperature for 18 h. The reaction mixture was diluted with diethyl ether (5 mL), and worked up with water (5 mL), the phases separated and the aqueous extracted with diethyl ether (3 × 3 mL). The combined organics were washed with brine (5 mL), dried ($MgSO_4$) and the solvent removed *in vacuo*. The residue was purified by column chromatography (acetone/ petroleum ether (1:4)) to give (±)-1-(4-methoxyphenyl)-3-((1*R*,2*R*)-2-(*p*-tolylthio)cyclohexyl)urea as a white solid (11.8 mg, 31.8 μmol, 39%).

IR (thin film, ν_{max} / cm^{-1}) 3316, 2928, 2854, 2360, 2160, 2020, 1972, 1640, 1600, 1559, 1510, 1463, 1411, 1317, 1298, 1243, 1179, 1105, 1038; **^{1}H NMR** (500 MHz, DMSO-d_6) δ 8.26 (s, 1H, ArN*H*), 7.36 – 7.25 (m, 4H, HC=CS + HC=CN), 7.18 – 7.09 (m, 2H, C*H*CCH$_3$), 6.86 – 6.77 (m, 2H, C*H*COCH$_3$), 6.22 (d, *J* = 8.5 Hz, 1H, C1N*H*), 3.69 (s, 3H, OCH$_3$), 3.50 (m, 1H, C1H), 3.07 (td, *J* = 9.5, 3.5 Hz, 1H, C6H), 2.00 – 1.89 (m, 2H, C2H' + C5H), 1.65 – 1.54 (m, 2H, C3H + C4H'), 1.36 – 1.19 (m, 4H, C2H + C3H' + C4H + C5H'); **^{13}C NMR** (126 MHz, DMSO-d_6) δ 155.2 (*C*OCH$_3$), 153.8 (C=O), 136.4 (*C*CH$_3$), 133.7 (*C*=CS), 132.2 (ArS), 130.3 (ArN), 129.6 (*C*HCH$_3$), 119.2 (*C*=CN), 113.9 (*C*HCOCH$_3$), 79.7 (OCH$_3$), 55.1 (C1), 50.8 (C6), 32.7 (C2 or C5), 32.0 (C2 or C5), 24.4 (C3 or C4), 23.8 (C3 or C4), 20.6 (*C*CH$_3$); **HRMS** (ES+) calc. for $C_{21}H_{27}N_2O_2S$ $[M+H]^+$ 371.1788, found 371.1787.

The enantiomeric excess was determined by HPLC [Chiralpak® IC; hexane:*i*PrOH 80:20; 1.0 ml min^{-1}, λ= 275 nm, t_R (min)= 9.99 min, t_R (maj)= 24.30 min.



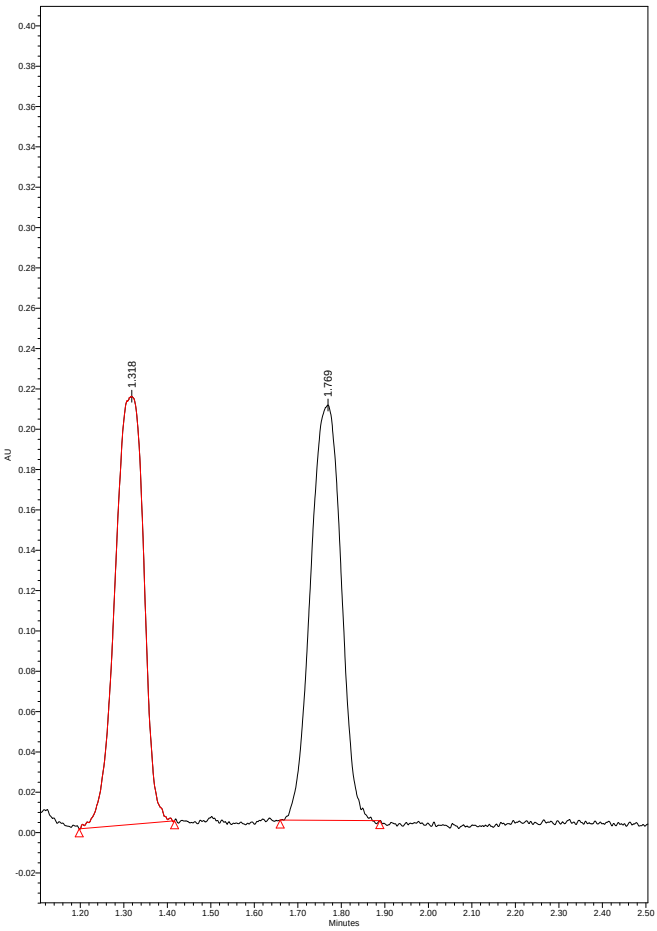
(±)-1-(3,5-Bis(trifluoromethyl)phenyl)-3-((1*R*,2*R*)-2-(*p*-tolylthio)cyclohexyl)urea, 2.49



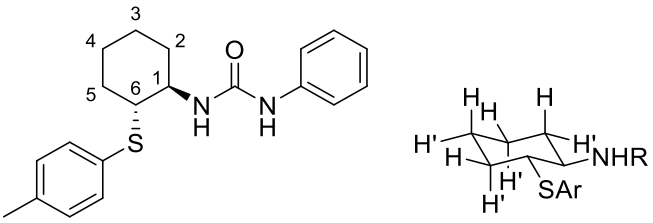
(1*R*,6*S*)-N-(3,5-Bis(trifluoromethyl)phenyl)-7-azabicyclo[4.1.0]heptane-7-carboxamide, **2.10c** (15.0 mg, 42.6 μmol, 1.0 equiv.) and 4-methylbenzenethiol (26.5 mg, 0.213 mmol, 5.0 equiv.) were heated to reflux in toluene (5 mL) for 18 h. The reaction mixture was diluted with diethyl ether (5 mL), and worked up with water (5 mL), the phases separated and the aqueous extracted with diethyl ether (3 × 3 mL). The combined organics were washed with brine (5 mL), dried ($MgSO_4$) and the solvent removed *in vacuo*. The residue was purified by column chromatography (acetone/ petroleum ether (1:4)) to give (±)-1-(3,5-bis(trifluoromethyl)phenyl)-3-((1*R*,2*R*)-2-(*p*-tolylthio)cyclohexyl)urea as a white solid (10.2 mg, 21.4 μmol, 50%).

IR (thin film, ν_{max} / cm^{-1}) 3334, 3300, 2935, 2859, 1653, 1565, 1492, 1473, 1441, 1386, 1276, 1254, 1229, 1217, 1176, 1131; **^{1}H NMR** (400 MHz, $CDCl_3$) δ 7.81 (s, 2H, $NCCHCCF_3$), 7.47 (s, 1H, CCF_3CHCCF_3), 7.33 – 7.28 (m, 2H, HC=CS), 7.08 (d, *J* = 8.0 Hz, 2H, C*H*CCH_3), 6.89 (s, 1H, ArNH), 5.10 (d, *J* = 7.0 Hz, 1H, C1NH), 3.58 (tdd, *J* = 10.5, 7.0, 4.0 Hz, 1H, C1H), 2.87 (td, *J* = 11.0, 4.0 Hz, 1H, C6H), 2.32 – 2.23 (m, 4H, CH_3 + C2H'), 2.11 – 2.04 (m, 1H, C5H), 1.69 (m, 2H, C3H + C4H'), 1.48 – 1.14 (m, 4H, C2H + C3H' + C4H + C5H'); **^{13}C NMR** (101 MHz, $CDCl_3$) δ 154.2 (C=O), 140.7 (ArN), 138.0 (ArS), 133.7 (H*C*=CS), 132.3 (q, *J* = 33.5 Hz, *C*CF_3), 130.0 (*C*HCCH_3), 129.55 (*C*CH_3), 123.3 (q, *J* = 273.0 Hz, CF_3), 118.7 (CCF_3*C*HCCF_3), 116.0 (NC*C*HCCF_3), 54.4 (C1), 52.6 (C6), 34.3 (C2), 33.2 (C5), 26.0 (C3 or C4), 24.7 (C3 or C4), 21.2 (CH_3); **^{19}F NMR** (377 MHz, $CDCl_3$) δ -63.04; **HRMS** (ES+) calc. for $C_{22}H_{23}N_2OF_6{}^{32}S$ $[M+H]^+$ 477.1430, found 477.1429.

The enantiomeric excess was determined by analytical chiral SFC [Chiralpak® IB, 90:10 CO_2 : MeOH 1.5 mL min^{-1}, t_R(maj) = 1.32 min, t_R (min) = 1.77 min]



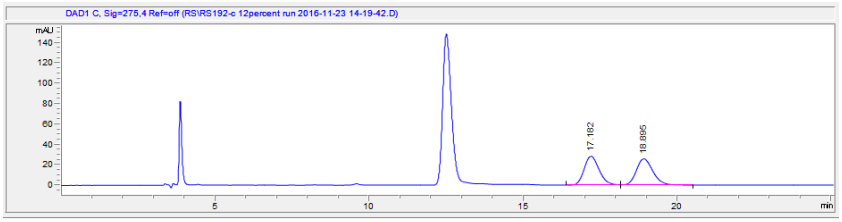
(±)-1-Phenyl-3-((1*R*,2*R*)-2-(*p*-tolylthio)cyclohexyl)urea, 2.50



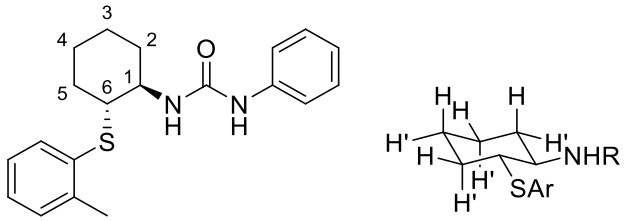
(1*R*,6*S*)-N-Phenyl-7-azabicyclo[4.1.0]heptane-7-carboxamide, **2.10a** (50.0 mg, 0.249 mmol, 1.0 equiv.) and 4-methylbenzenethiol (62.0 mg, 0.500 mmol, 2.0 equiv.) were heated to reflux in toluene (20 mL) for 17 h. The solvent removed *in vacuo* and the residue purified by column chromatography (acetone/ petroleum ether (1:4)) to give (±)-1-phenyl-3-((1*R*,2*R*)-2-(*p*-tolylthio)cyclohexyl)urea as a white solid (61.8 mg, 0.182 mmol, 73%).

IR (thin film, ν_{max} / cm^{-1}) 3313, 2929, 2854, 1626, 1566, 1497, 1443, 1316, 1295, 1253, 1232; **^{1}H NMR** (400 MHz, DMSO-d_6) δ 8.43 (s, 1H, ArNH), 7.42 – 7.37 (m, 2H, *o*Ph), 7.35 – 7.29 (m, 2H, C*H*CCH$_3$), 7.26 – 7.19 (m, 2H, *m*Ph), 7.17 – 7.10 (m, 2H, HC=CS), 6.88 (tt, *J* = 7.5, 1.0 Hz, 1H, *p*Ph), 6.29 (d, *J* = 8.5 Hz, 1H, C1HN*H*), 3.51 (qd, *J* = 9.0, 4.0 Hz, 1H, C1H), 3.08 (td, *J* = 9.5, 4.0 Hz, 1H, C6H), 2.27 (s, 3H, CH$_3$), 2.02 – 1.89 (m, 2H, C2H' + C5H), 1.65 – 1.53 (m, 2H, C3H + C4H'), 1.36 – 1.18 (m, 4H, C2H' + C3H + C4H' + C5H'); **^{13}C NMR** (101 MHz, DMSO-d_6) δ 154.5 (C=O), 140.5 (ArN), 136.5 (*C*CH$_3$), 132.4 (*C*HCCH$_3$), 130.2 (ArS), 129.7 (*C*=CS), 128.7 (*m*Ph), 121.0 (*p*Ph), 117.6 (*o*Ph), 50.9 (C1), 50.8 (C6), 32.8 (C2 or C5), 32.1 (C2 or C5), 24.5 (C3 or C4), 23.9 (C3 or C4), 20.7 (CH$_3$); **HRMS** (ES+) calc. for $C_{20}H_{25}N_2O^{32}S$ $[M+H]^+$ 341.1683, found 341.1682.

The enantiomeric excess was determined by HPLC [Chiralpak® IC; hexane:*i*PrOH 88:12; 1.0 ml min^{-1}, λ= 275 nm, t_R (maj)= 17.18 min, t_R (min)= 18.90 min.



1-Phenyl-3-((1*R*,2*R*)-2-(*o*-tolylthio)cyclohexyl)urea, 2.51

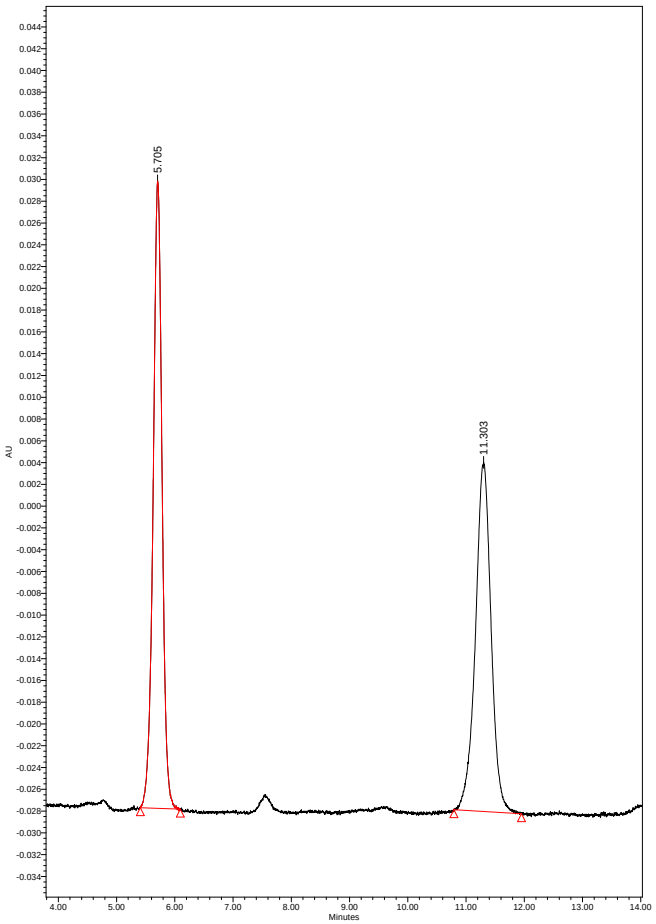


(1*R*,6*S*)-N-Phenyl-7-azabicyclo[4.1.0]heptane-7-carboxamide, **2.10a** (50.0 mg, 0.250 mmol, 1.0 equiv.) and 4-methylbenzenethiol (62.0 mg, 0.500 mmol, 2.0 equiv.) were

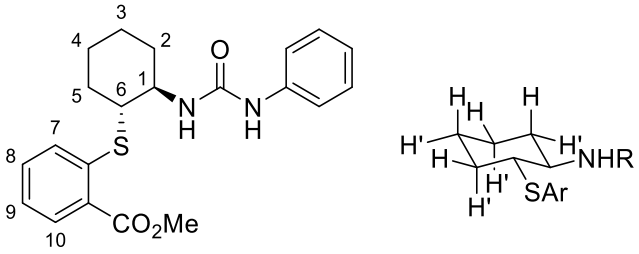
heated to reflux in toluene (5 mL) for 18 h. The solvent removed *in vacuo* and the residue purified by column chromatography (acetone/ petroleum ether (1:4)) to give (±)-1-phenyl-3-((1*R*,2*R*)-2-(*o*-tolylthio)cyclohexyl)urea as a colourless oil (63.7 mg, 0.188 mmol, 75%).

IR (thin film, ν_{max} / cm^{-1}) 3323, 3059, 2933, 2855, 1643, 1596, 1555, 1498, 1469, 1441, 1317, 1230; **^{1}H NMR** (400 MHz, $CDCl_3$) δ 7.41 – 7.36 (m, 1H, C*H*CCH_3), 7.30 – 7.26 (m, 2H, ArH), 7.25 – 7.20 (m, 2H, *m*Ph), 7.18 – 7.13 (m, 1H, ArH), 7.12 – 7.09 (m, 2H, ArH), 7.07 (s, 1H, ArNH), 7.04 – 6.98 (m, 1H, *p*Ph), 5.44 (d, *J* = 8.0 Hz, 1H, C1NH), 3.76 (tdd, *J* = 10.0, 8.0, 4.0 Hz, 1H, C1H), 2.95 (td, *J* = 10.5, 4.0 Hz, 1H, C6H), 2.37 (s, 3H, CH_3), 2.25 – 2.15 (m, 1H, C2H'), 2.04 – 1.94 (m, 1H, C5H), 1.69 – 1.57 (m, 2H, C3H + C4H'), 1.41 (dtd, *J* = 14.0, 11.0, 3.5 Hz, 1H, C5H'), 1.35 – 1.09 (m, 3H, C2H + C3H' + C4H); **^{13}C NMR** (101 MHz, $CDCl_3$) δ 155.6 (C=O), 140.3 (ArN), 138.9 (ArS), 134.1 (*C*CH_3), 132.5 (*C*HCCH_3), 130.4 (ArH), 129.3 (ArH), 127.1 (ArH), 126.5 (ArH), 123.5 (*p*Ph), 120.9 (*o*Ph), 53.4 (C1), 51.9 (C6), 34.0 (C2), 32.8 (C5), 25.5 (C3 or C4), 24.5 (C3 or C4), 21.1 (CH_3); **HRMS** (ES+) calc. for $C_{20}H_{25}N_2O^{32}S$ $[M+H]^+$ 341.1682, found 341.1686.

The enantiomeric excess was determined by analytical chiral SFC [Chiralpak® IB, 90:10 CO_2 : MeOH 1.5 mL min^{-1}, t_R(maj) = 5.71 min, t_R (min) = 11.30 min]



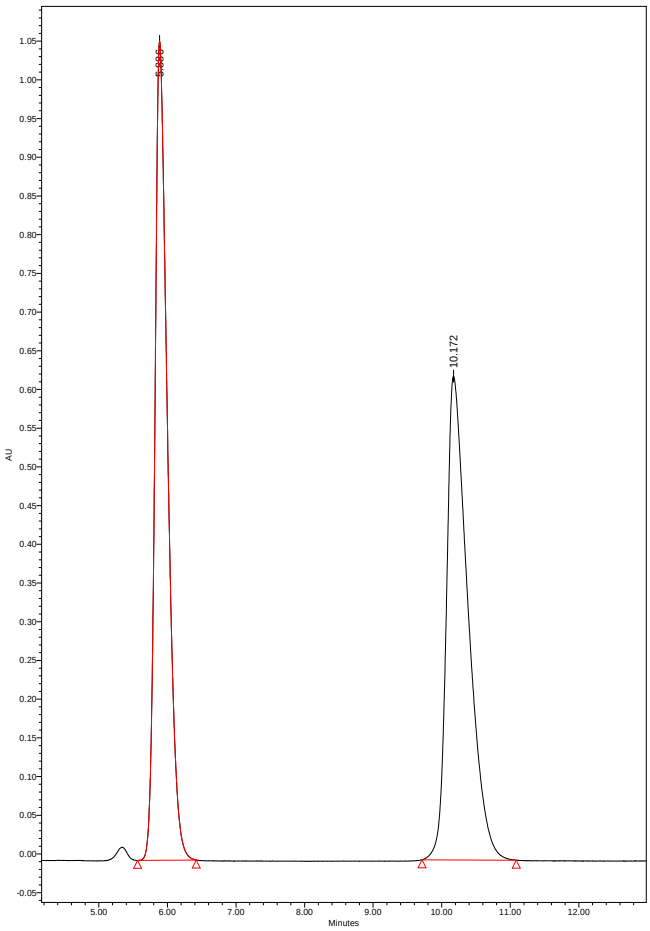
(±)-Methyl 2-(((1*R*,2*R*)-2-(3-phenylureido)cyclohexyl)thio)benzoate, 2.52



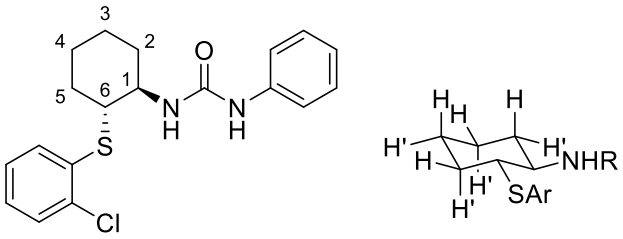
(1*R*,6*S*)-N-Phenyl-7-azabicyclo[4.1.0]heptane-7-carboxamide, **2.10a** (50.0 mg, 0.250 mmol, 1.0 equiv.) and 4-methylthiosalicylate (68.8 mg, 0.500 mmol, 2.0 equiv.) were heated to reflux in toluene (5 mL) for 20 h. The solvent removed *in vacuo* and the residue purified by column chromatography (acetone/ petroleum ether (1:4)) to give (±)-methyl 2-(((1*R*,2*R*)-2-(3-phenylureido)cyclohexyl)thio)benzoate as a white foam (63.6 mg, 0.165 mmol, 66%).

IR (thin film, ν_{max} / cm^{-1}) 3322, 2930, 2853, 2353, 2344, 1643, 1596, 1555, 1499, 1441, 1317, 1249, 1228, 1154, 1125, 1043; **^{1}H NMR** (400 MHz, $CDCl_3$) δ 7.77 (dd, *J* = 8.0, 1.5 Hz, 1H, C7H), 7.62 (dd, *J* = 8.0, 1.0 Hz, 1H, C10H), 7.45 – 7.39 (m, 1H, C9H), 7.33 – 7.23 (m, 6H, *o*Ph + *m*Ph + *p*Ph), 7.05 – 6.99 (m, 1H, C8H), 6.53 (s, 1H), 5.50 (d, *J* = 6.5 Hz, 1H, C1NH), 3.89 (s, 3H, CH_3), 3.63 (qd, *J* = 10.0, 5.5 Hz, 1H, C2H'), 3.15 (td, *J* = 10.5, 4.0 Hz, 1H, C5H), 2.42 – 2.29 (m, 1H), 2.23 – 2.12 (m, 1H), 1.77 – 1.53 (m, 3H), 1.47 – 1.18 (m, 3H); ^{13}C NMR (101 MHz, $CDCl_3$) δ 168.3 (CO_2CH_3), 155.3 (NC=O), 139.0 (ArN), 136.8 (ArS), 132.9 (CCO_2CH_3) 132.9 (C10), 132.0 (C9), 130.5 (C7), 129.2 (PhH), 126.6 (PhH), 123.3 (C8), 120.4 (PhH), 53.7 (C1), 52.6 (CH_3), 52.0 (C6), 33.7 (C2), 33.3 (C5), 25.6 (C3 or C4), 24.3 (C3 or C4); **HRMS** (ES+) calc. for $C_{21}H_{25}N_2O_3{}^{32}S$ $[M+H]^+$ 385.1580, found 385.1581.

The enantiomeric excess was determined by analytical chiral SFC [Chiralpak® IB, 90:10 CO_2 : MeOH 1.5 mL min^{-1}, t_R(maj) = 5.88 min, t_R (min) = 10.17 min]



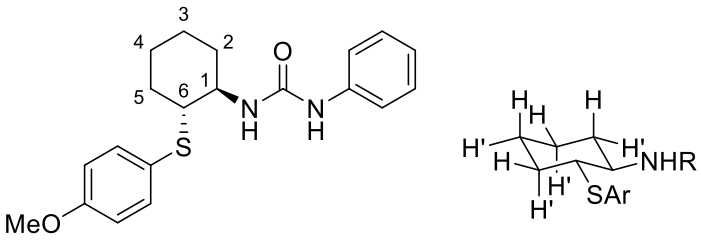
(±)-1-((1*R*,2*R*)-2-((2-Chlorophenyl)thio)cyclohexyl)-3-phenylurea, 2.53



(1*R*,6*S*)-N-Phenyl-7-azabicyclo[4.1.0]heptane-7-carboxamide, **2.10a** (100.0 mg, 0.499 mmol, 1.0 equiv.) and 2-chlorothiophenol (67.9 µL, 0.599 mmol, 1.2 equiv.) were stirred in diethyl ether (2.5 mL) for 16 h. The solvent removed *in vacuo* and the residue purified by column chromatography (acetone/ petroleum ether (1:9)) to give (±)-1-((1*R*,2*R*)-2-((2-chlorophenyl)thio)cyclohexyl)-3-phenylurea as a white solid (140.4 mg, 0.389 mmol, 78%).

IR (thin film, ν_{max} / cm^{-1}) 3323, 2921, 2851, 1644, 1596, 1555, 1498, 1442, 1317, 1249, 1229, 1035; **^{1}H NMR** (500 MHz, $CDCl_3$) δ 7.57 – 7.53 (m, 1H, CHCCl), 7.41 – 7.36 (m, 1H, HC=CS), 7.31 – 7.28 (m, 3H, *o*Ph + *p*Ph), 7.21 – 7.15 (m, 2H, *m*Ph + CHC=CS), 7.10 – 7.05 (m, 1H, C*H*CHCCl), 6.48 (s, 1H, ArNH), 5.08 (d, *J* = 7.5 Hz, 1H, C1NH), 3.75 (tdd, *J* = 10.0, 7.5, 4.0 Hz, 1H, C1H), 3.12 (td, *J* = 10.5, 4.0 Hz, 1H, C6H), 2.28 (ddt, *J* = 13.0, 5.5, 3.5 Hz, 1H, C2H'), 2.07 – 1.95 (m, 1H, C5H), 1.76 – 1.59 (m, 2H, C3H + C4H'), 1.54 – 1.46 (m, 1H, C5H'), 1.44 – 1.35 (m, 1H, C4H), 1.32 – 1.15 (m, 2H, C2H + C3H'); **^{13}C NMR** (126 MHz,$CDCl_3$) δ 155.3 (C=O), 138.5 (ArN or ArS), 137.1 (ArN or ArS), 134.5 (ArCl), 133.6 (*C*HCCl), 130.1 (*C*=CS), 129.5 (*p*Ph), 128.6 (*m*Ph or *C*HC=CS), 127.3 (*m*Ph or *C*HC=CS), 124.1 (*C*HCHCCl), 121.7 (*o*Ph), 53.5 (C1), 51.2 (C6), 33.8 (C2), 32.8 (C5), 25.5 (C3), 24.5 (C4); **HRMS** (ES+) calc. for $C_{19}H_{22}N_2OSCl$ $[M+H]^+$ 361.1136, found 361.1137.

(±)-1-((1*R*,2*R*)-2-((4-Methoxyphenyl)thio)cyclohexyl)-3-phenylurea, 2.54

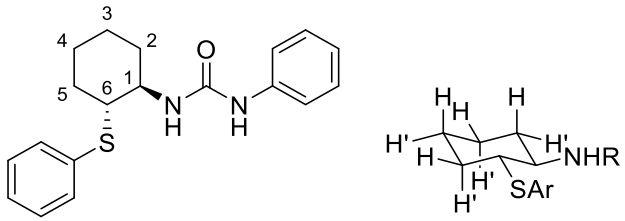


(1*R*,6*S*)-N-Phenyl-7-azabicyclo[4.1.0]heptane-7-carboxamide, **2.10a** (100.0 mg, 0.499 mmol, 1.0 equiv.) and 4-methoxythiophenol (73.7 μL, 0.599 mmol, 1.2 equiv.) were stirred in diethyl ether (2.5 mL) for 16 h. The solvent removed *in vacuo* and the residue purified by column chromatography (acetone/ petroleum ether (1:9)) to give (±)-1-((1*R*,2*R*)-2-((4-methoxyphenyl)thio)cyclohexyl)-3-phenylurea as a white oil (96.6 mg, 0.271 mmol, 54%).

IR (thin film, ν_{max} / cm^{-1}) 3324, 2932, 2855, 1642, 1594, 1553, 1494, 1440, 1317, 1284, 1245, 1202, 1173, 1137, 1102, 1032; **^{1}H NMR** (400 MHz, $CDCl_3$) δ 7.70 – 7.65 (m, 1H, ArNH), 7.31 – 7.26 (m, 2H, C*H*$COCH_3$), 7.25 – 7.18 (m, 2H, *o*Ph), 7.16 – 7.04 (m, 2H, *m*Ph), 6.89 – 6.82 (m, 1H, *p*Ph), 6.70 – 6.64 (m, 1H, HC=CS), 5.84 (d, *J* = 8.0 Hz, 1H, C1NH), 3.64 – 3.51 (m, 3.4H, CH_3 + C1H), 3.50 – 3.41 (m, 0.6H, C1H), 2.72 (td, *J* = 10.5, 4.0 Hz, 0.4H, C6H), 2.47 (td, *J* = 11.0, 4.0 Hz, 0.6H, C6H), 2.09 – 1.97 (m, 1H, C2H), 1.93 – 1.76 (m, 1H, C5H'), 1.53 – 1.38 (m, 2H, C3H' + C4H), 1.30 – 0.89 (m, 4H, C2H' + C3H + C4H' + C5H); **^{13}C NMR** (101 MHz, $CDCl_3$) δ 159.7 (C–O), 156.1 (C=O), 139.3 (ArN), 139.2 (ArN), 136.6 (*C*$COCH_3$), 134.1 (ArS), 133.1 (*C*$COCH_3$), 129.1 (*m*Ph), 129.1 (*m*Ph), 128.9 (Ar), 127.2 (Ar), 123.3 (Ar), 123.0 (*p*Ph), 120.4 (*o*Ph), 114.4 (*C*=CS), 55.3 (CH_3), 52.8 (C6), 52.6 (C1), 52.2 (C6), 34.1 (C2), 33.9 (C2), 33.0 (C5), 29.8 (CH_2), 25.6 (CH_2), 25.4 (CH_2), 24.5 (CH_2), 24.5 (CH_2); **HRMS** (ES+) calc. for $C_{20}H_{25}N_2O_2{}^{32}S$ $[M+H]^+$ 357.1631, found 357.1627.

Some peak duplication in ^{1}H and ^{13}C NMR spectra arose from the presence of rotamers.

(±)-1-Phenyl-3-((1*R*,2*R*)-2-(phenylthio)cyclohexyl)urea, 2.55



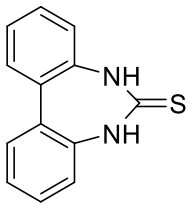
(1*R*,6*S*)-N-Phenyl-7-azabicyclo[4.1.0]heptane-7-carboxamide, **2.10a** (10.0 mg, 50 μmol, 1.0 equiv.) and thiophenol (6.2 μL, 60 μmol, 1.2 equiv.) were stirred in toluene (0.5 mL) at 90 °C for 18 h. The solvent removed *in vacuo* and the residue purified by column chromatography (acetone/ petroleum ether (1:4)) to give (±)-1-phenyl-3-((1*R*,2*R*)-2-(phenylthio)cyclohexyl)urea as a white solid (9.8 mg, 30 μmol, 65%).

IR (thin film, ν_{max} / cm^{-1}) 3322, 3057, 2933, 2855, 1643, 1596, 1554, 1498, 1477, 1440, 1317, 1249, 1229, 1083, 1024; **^{1}H NMR** (400 MHz, $CDCl_3$) δ 7.52 – 7.48 (m, 1H, *p*Ph), 7.45 – 7.40 (m, 2H, *o*Ph), 7.33 – 7.20 (m, 9H, ArH), 7.05 (tt, *J* = 7.0, 2.0 Hz, 1H, *p*Ph), 6.79 (s, 1H, ArNH), 5.23 (d, *J* = 8.0 Hz, 1H, C1NH), 3.66 (tdd, *J* = 10.0, 7.5, 4.0 Hz, 1H, C1H), 2.89 (td, *J* = 10.5, 4.0 Hz, 1H, C6H), 2.29 – 2.19 (m, 1H, C2H'), 2.11 – 2.01 (m, 1H, C5H), 1.86 (s, 1H, C3H or C4H'), 1.73 – 1.58 (m, 2H, C3H or C4H' + C2H), 1.48 – 1.38 (m, 1H, C5H'), 1.35 – 1.12 (m, 2H, C3H' + C4H); **^{13}C NMR** (101 MHz, $CDCl_3$) δ 155.4 (C=O), 138.8 (ArN), 134.0 (ArS), 133.1 (*o*Ph), 129.4 (ArH), 129.2 (*quat* C), 129.2 (*quat* C), 129.0 (ArH), 128.4 (*quat* C), 127.6 (ArH), 127.4 (*p*Ph), 127.3 (ArH), 125.4 (*quat* C), 123.7 (*p*Ph), 121.1 (ArH), 53.3 (C1), 52.4 (C6), 34.2 (C2), 33.2 (C5), 25.8 (C3 or C4), 24.6 (C3 or C4); **HRMS** (ES+) calc. for $C_{19}H_{23}N_2O^{32}S$ $[M+H]^+$ 327.1526, found 327.1526.

Some peak duplication in ^{1}H and ^{13}C NMR spectra arose from the presence of rotamers.

2. 6. 5. 6 Synthesis of biaryl thioureas and ureas

5,7-Dihydro-6H-dibenzo[d,f][1,3]diazepine-6-thione, 2.20a



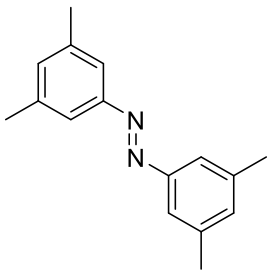
To a stirred solution of 2,2′-biphenyldiamine (515.0 mg, 2.80 mmol, 1.0 equiv.) in tetrahydrofuran (10 mL) was added triethylamine (781 μL, 5.60 mmol, 2.0 equiv.) then thiophosgene (215 μL, 2.80 mmol, 1.0 equiv.) at room temperature for 3 h. The reaction mixture was diluted with diethyl ether (30 mL), poured onto water (25 mL) and the

phases separated. The aqueous was extracted with diethyl ether (3 × 25 mL), the combined organics washed with brine (30 mL), dried ($MgSO_4$) and the solvent was removed *in vacuo.* The residue was purified column chromatography (ethyl acetate/ petroleum ether (1:9 to 1:4)) to give 5,7-dihydro-6H-dibenzo[d,f][1,3]diazepine-6-thione as a white solid (556.7 mg, 2.46 mmol, 88%).

IR (thin film, ν_{max} / cm^{-1}) 3225, 2360, 2339, 2274, 2211, 2119, 2082, 2051, 1658, 1581, 1570, 1506, 1477, 1387, 1330, 1281, 1230, 1201, 1173, 1146, 1050; **^{1}H NMR** (400 MHz, DMSO-d_6) δ 7.41 (dd, *J* = 8.0, 1.5 Hz, 1H, C*H*CHCHCHN), 7.30 (td, *J* = 7.5, 1.5 Hz, 1H, C*H*CHCN), 7.20 (td, *J* = 7.5, 1.5 Hz, 1H, C*H*CHCHN), 7.10 (dd, *J* = 8.0, 1.5 Hz, 1H, C*H*CN), 3.37 (s, 1H, NH); **^{13}C NMR** (101 MHz, DMSO-d_6) δ 193.8 (C=S), 141.0 (C(*C*–N)C), 130.0 (C(*C*–C)C), 129.2 (*C*HCHCHCHN), 128.8 (*C*HCHCN), 125.6 (*C*HCHCHN), 121.5 (*C*HCN); **LRMS** (ES–) calc. for $C_{13}H_9N_2S$ $[M–H]^–$ 225.0, found 225.1.

Data consistent with literature values.[82]

(*E*)-1,2-Bis(3,5-dimethylphenyl)diazene, 2.56



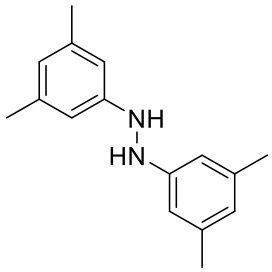
3,5-Dimethylaniline (10.0 mL, 80.8 mmol, 1.0 equiv.) was added dropwise to a solution of (diacetoxyiodo)benzene (26.0 g, 80.8 mmol, 1.0 equiv.) in dichloromethane (320 mL) and stirred at room temperature for 1 h. Solvent was removed *in vacuo* and the residue

was purified by column chromatography (ethyl acetate/ petroleum ether (1:99 to 1:39)) to give (*E*)-1,2-bis(3,5-dimethylphenyl)diazene as a red solid (2.28 g, 9.58 mmol, 24%).

IR (thin film, ν_{max} / cm^{-1}) 3008, 2917, 2857, 2353, 2345, 1608, 1462, 1292, 1259, 1129, 1039; **^{1}H NMR** (400 MHz, $CDCl_3$) δ 7.53 (s, 4H, CHCN), 7.12 (s, 2H, $CH_3C\mathit{H}CH_3$), 2.42 (s, 12H, CH_3); **^{13}C NMR** (126 MHz, $CDCl_3$) δ 152.9 (CN), 138.8 ($\mathit{C}CH_3$), 132.5 ($CCH_3\mathit{C}HCCH_3$), 120.6 (CHCN), 21.3 (CH_3); **LRMS** (ES+) calc. for $C_{16}H_{18}N_2Na$ $[M+Na]^+$ 261.1, found 261.1.

Data consistent with literature values.[83]

1,2-Bis(3,5-dimethylphenyl)hydrazine, 2.57

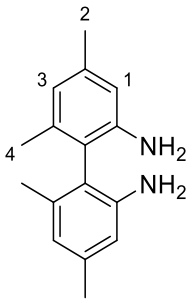


(*E*)-1,2-Bis(3,5-dimethylphenyl)diazene, **2.56** (540 mg, 2.27 mmol, 1.0 equiv.) was added to a biphasic mixture of sodium dithionate (7.31 g, 42.0 mmol, 18 equiv.), methanol (40 mL), water (40 mL) and dichloromethane (12 mL) and heated to reflux overnight then allowed to cool to room temperature. The reaction mixture was extracted with dichloromethane (3 × 30 mL), the combined organics washed with brine (40 mL) and dried ($MgSO_4$). The solvent was removed *in vacuo* and the residue was purified by column chromatography (ethyl acetate/ petroleum ether (1:19)) to give 1,2-bis(3,5-dimethylphenyl)hydrazine as an off-white solid (472.0 mg, 1.96 mmol, 86%).

IR (thin film, ν_{max} / cm^{-1}) 3342, 3010, 2915, 2858, 2349, 1770, 1745, 1607, 1596, 1463, 1374, 1317, 1293, 1257, 1165, 1129, 1038; **^{1}H NMR** (400 MHz, $CDCl_3$) δ 7.14 (s, 4H, CHCN), 5.46 (s, 2H, $CH_3C\mathit{H}CH_3$), 2.27 (s, 12H, CH_3); **^{13}C NMR** (101 MHz, $CDCl_3$) δ 139.3 (CN), 121.9 (*C*HCN), 120.7 ($CH_3\mathit{C}HCH_3$), 110.2 ($\mathit{C}CH_3$), 21.6 (CH_3); **LRMS** (ES+) calc. for $C_{16}H_{20}N_2Na$ $[M+Na]^+$ 263.2, found 263.1.

Data consistent with literature values.[84]

(±)-4,4',6,6'-Tetramethyl-[1,1'-biphenyl]-2,2'-diamine, 2.58



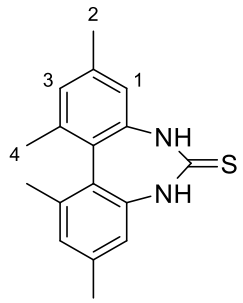
A mixture of concentrated sulfuric acid (6.5 mL) and water (3.5 mL) was heated to 90 °C and 1,2-bis(3,5-dimethylphenyl)hydrazine, **2.57** (300.0 mg, 1.248 mmol, 1.0 equiv.) added. After 5 minutes the reaction mixture was neutralized with 2 M sodium hydroxide solution, allowed to further cool to room temperature and extracted with diethyl ether (4 × 200 mL). The combined organics were washed with brine (150 mL), dried ($MgSO_4$) and the solvent removed *in vacuo*. The residue was purified by column chromatography (ethyl acetate/ petroleum ether (1:19 to 1:4)) to give (±)-4,4',6,6'-tetramethyl-[1,1'-biphenyl]-2,2'-diamine as a white solid (21.5 mg, 0.089 mmol, 7%). The product was found to be highly unstable and so was quickly further reacted.

IR (thin film, ν_{max} / cm^{-1}) 3449, 3354, 3021, 2917, 2360, 2341, 1611, 1570, 1478, 1441, 1329, 1292, 1206, 1102, 1000; **^{1}H NMR** (400 MHz, $CDCl_3$) δ 6.55 (s, 2H, C1H), 6.48 (s,

2H, C3H), 3.41 (s, 4H, NH_2), 2.27 (s, 6H, C4H_3), 1.93 (s, 6H, C2H_3); **^{13}C NMR** (126 MHz, $CDCl_3$) δ 144.4 (ArN), 138.1 (*C*CH_3), 138.0 (*C*CH_3), 121.3 (C3), 119.6 (NC*C*CH_3), 113.6 (C1), 21.4 (C2), 19.7 (C4); **LRMS** (ES+) calc. for $C_{16}H_{21}N_2$ $[M+H]^+$ 241.2, found 241.2.

Data consistent with literature values.[85]

(±)-1,3,9,11-Tetramethyl-5,7-dihydro-6H-dibenzo[d,f][1,3]diazepine-6-thione, 2.20c



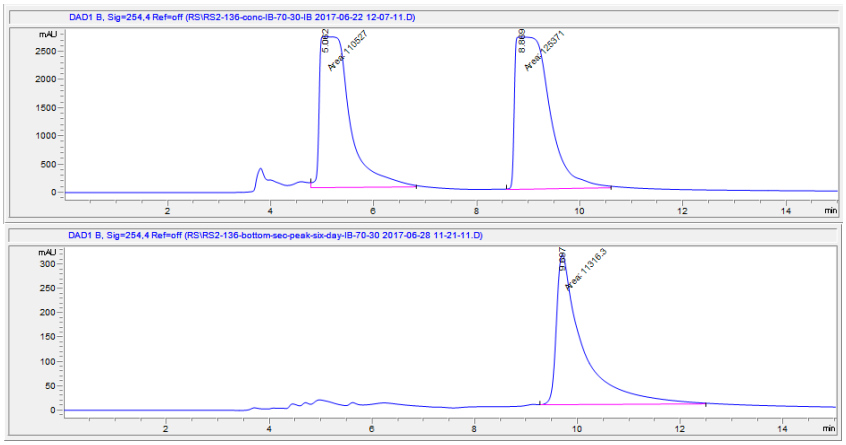
To a stirred solution of 4,4',6,6'-tetramethyl-[1,1'-biphenyl]-2,2'-diamine, **2.58** (18.0 mg, 0.075 mmol, 1.0 equiv.) in tetrahydrofuran (5 mL) was added triethylamine (20.9 μL, 0.150 mmol, 2.0 equiv.) then thiophosgene (5.8 μL, 0.075 mmol, 1.0 equiv.) at room temperature for 18 h. The reaction mixture was diluted with diethyl ether (20 mL), poured onto water (25 mL) and the phases separated. The aqueous was extracted with diethyl ether (3 × 25 mL), the combined organics washed with brine (30 mL), dried ($MgSO_4$) and the solvent was removed *in vacuo.* The residue was purified column chromatography (ethyl acetate/ petroleum ether (0:100 to 1:9)) to give (±)-1,3,9,11-tetramethyl-5,7-dihydro-6H-dibenzo[d,f][1,3]diazepine-6-thione as a white solid (10.4 mg, 0.037 mmol, 49%).

IR (thin film, ν_{max} / cm^{-1}) 3203, 2918, 2849, 2360, 2349, 1618, 1546, 1493, 1408, 1387, 1172, 1143; **^{1}H NMR** (400 MHz, $CDCl_3$) δ 7.53 (s, 2H, NH), 6.95 (s, 1H, C1H), 6.61 (s,

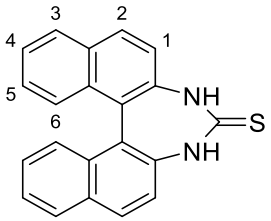
1H, C3H), 2.32 (s, 6H, C4H_3), 2.12 (s, 6H, C2H_3); **^{13}C NMR** (126 MHz, $CDCl_3$) δ 196.7 (C=S), 142.6 (ArN), 138.5 (*C*CH_3), 138.0(*C*CH_3), 128.9 (C1), 126.2 (NC*C*CCH_3), 118.9 (C3), 21.0 (C2), 19.8 (C4); **HRMS** (ES+) calc. for $C_{17}H_{19}N_2{}^{32}S$ $[M+H]^+$ 283.1264, found 263.1264.

The enantiomeric excess was determined by HPLC [Chiralpak® IB; hexane:*i*PrOH 70:30; 1.0 ml min^{-1}, λ= 254 nm, t_1 = 5.08 min, t_2 = 8.87 min.

Method used for separation of enantiomers was similar to that reported by Mistry and Fletcher.[86]



(±)-3,5-Dihydro-4H-dinaphtho[2,1-d:1',2'-f][1,3]diazepine-4-thione, 2.25



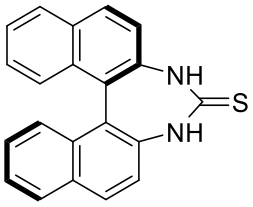
To a stirred solution of (*R*)-(+)-1,1′-binaphthyl-2,2′-diamine (25.0 mg, 0.088 mmol, 0.5 equiv.) and (*S*)-(−)-1,1′-binaphthyl-2,2′-diamine (25.0 mg, 0.088 mmol, 0.5 equiv.) in tetrahydrofuran (10 mL) was added triethylamine (49 µL, 0.352 mmol, 2.0 equiv.) then

thiophosgene (6.74 μL, 0.088 mmol, 0.5 equiv.) at room temperature for 17 h. The reaction mixture was diluted with diethyl ether (25 mL), poured onto water (25 mL) and the phases separated. The aqueous was extracted with diethyl ether (3 × 25 mL), the combined organics washed with brine (30 mL), dried ($MgSO_4$) and the solvent was removed *in vacuo.* The residue was purified column chromatography (ethyl acetate/ petroleum ether (1:9)) to give (±)-3,5-dihydro-4H-dinaphtho[2,1-d:1',2'-f][1,3]diazepine-4-thione as a white solid (52.9 mg, 0.162 mmol, 92%).

IR (thin film, ν_{max} / cm^{-1}) 3225, 2982, 2162, 1997, 1626, 1580, 1535, 1470, 1426, 1387, 1317, 1274, 1208, 1156, 1141, 1028; **^{1}H NMR** (400 MHz, DMSO-d_6) δ 10.39 (s, 2H, NH), 8.05 – 7.92 (m, 4H, C2H + C3H), 7.49 – 7.39 (m, 4H, C1H + C4H), 7.23 (ddd, *J* = 8.5, 7.0, 1.5 Hz, 2H, C5H), 6.90 (dd, *J* = 8.5, 1.0 Hz, 2H, C6H); **^{13}C NMR** (101 MHz, DMSO-d_6) δ 197.3 (C=S), 142.8 (CN), 132.2 (*quat* C), 131.6 (*quat* C), 129.9 (C2), 128.9 (C3), 127.0 (C5), 126.7 (C6), 125.8 (C4), 124.2 (*quat* C), 122.6 (C1); **LRMS** (ES+) calc. for $C_{21}H_{15}N_2S$ $[M+H]^+$ 327.1, found 327.0.

Data consistent with literature values.[87]

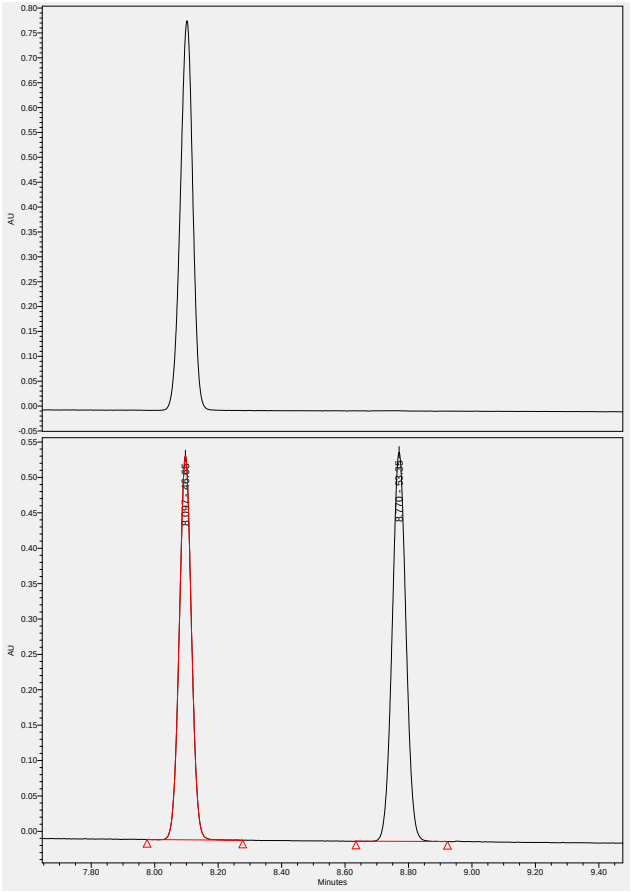
(*R*)-3,5-dihydro-4H-dinaphtho[2,1-d:1',2'-f][1,3]diazepine-4-thione, 2.25



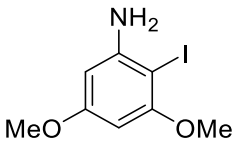
Analogously to the racemate, (*R*)-3,5-dihydro-4H-dinaphtho[2,1-d:1',2'-f][1,3]diazepine-4-thione was prepared using (*R*)-(+)-1,1′-binaphthyl-2,2′-diamine (250.0 mg, 0.879 mmol, 1.0 equiv.) as a white solid (280.9 mg, 0.861 mmol, 98%).

[α]D (*c* = 1.0, $CHCl_3$): -244.8 °. All other physical properties were found to be as those of the racemate.

The enantiomeric excess was determined by analytical chiral SFC [Chiralpak® IA, 99:1 – 90:10 CO_2 : MeOH over 5 min, 90:10 thereafter, 1.5 ml/min, t_R(R) = 8.10 min, t_R(S) = 8.77 min]



2-Iodo-3,5-dimethoxyaniline, 2.59



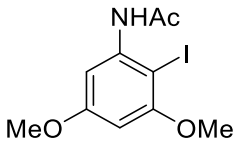
To a solution of iodine monochloride (858.5 mg, 5.28 mmol, 1.2 equiv.) in diethyl ether (50 mL) was added 3,5-dimethoxyaniline (674.0 mg, 4.40 mmol, 1.0 equiv.) then saturated aqueous sodium carbonate (50 mL) and stirred vigorously for 30 minutes. After this the layers were separated, the aqueous extracted with diethyl ether (3 × 25 mL), the combined organics washed with brine (50 mL), dried ($MgSO_4$) and the solvent removed *in vacuo.* The residue was purified by column chromatography (ethyl acetate/ cyclohexane (1:9)) to give 2-iodo-3,5-dimethoxyaniline as a light sensitive white solid (2.28 g, 9.58 mmol, 24%). The compound was handled and stored in the dark.

Note: Iodine monochloride is commonly available in dichloromethane, which is unsuitable for this transformation. The presence of dichloromethane in this reaction leads to undesired *para* selectivity.

IR (thin film, ν_{max} / cm^{-1}) 2847, 2811, 1684, 1603, 1559, 1432, 1364, 1331, 1254, 1184, 1046; **^{1}H NMR** (400 MHz, $CDCl_3$) δ 6.02 (d, *J* = 2.5 Hz, 1H, ArH), 5.90 (d, *J* = 2.5 Hz, 1H, ArH), 4.23 (s, 2H, NH_2), 3.82 (s, 3H, OCH_3), 3.76 (s, 3H, OCH_3); **^{13}C NMR** (101 MHz, $CDCl_3$) δ 161.1 (ArO), 159.4 (ArO), 148.9 (ArN), 94.8 (ArH), 92.0 (ArH), 63.6 (CI), 55.9 (OCH_3), 54.6 (OCH_3); **HRMS** (ES+) calc. for $C_8H_{10}O_2NINa$ $[M+Na]^+$ 301.9648, found 301.9654.

Data consistent with literature values.[88]

N-(2-Iodo-3,5-dimethoxyphenyl)acetamide, 2.60

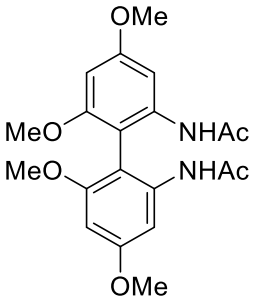


To a stirred solution of 2-iodo-3,5-dimethoxyaniline, **2.59** (400.0 mg, 1.43 mmol, 1.0 equiv.) in dichloromethane (14 mL) was added triethylamine (437 μL, 3.15 mmol, 2.2 equiv.) followed by acetic anhydride (163 μL, 1.72 mmol, 1.2 equiv.) at 0 °C, then allowed to warm to room temperature. After 4 h, water (10 mL) was added, the layers were separated and the aqueous extracted with dichloromethane (2 × 25 mL). the combined organics washed with brine (50 mL), dried ($MgSO_4$) and the solvent removed *in vacuo*. The residue was purified by column chromatography (ethyl acetate/ petroleum ether (1:5)) to give N-(2-iodo-3,5-dimethoxyphenyl)acetamide as a white solid (367.3 mg, 1.14 mmol, 80%).

IR (solid, ν_{max} / cm^{-1}) 2960, 1649, 1611, 1539, 1464, 1423, 1360, 1335, 1248, 1116, 1081; **^{1}H NMR** (400 MHz, $CDCl_3$) δ 7.69 (br d, *J* = 18.0 Hz, 1H, ArH), 6.25 (d, *J* = 2.5 Hz, 1H, ArH), 3.85 (s, 3H, OCH_3), 3.83 (s, 3H, OCH_3), 2.24 (s, 3H, C=OCH_3); **^{13}C NMR** (101 MHz, $CDCl_3$) δ 168.7 (C=O), 160.8 (ArO), 157.5 (ArO), 150.3 (ArN), 100.4 (ArH), 97.3 (ArH), 69.5 (CI), 55.9 (OCH_3), 55.4 (OCH_3), 24.6 (CH_3C=O); **LRMS** (ES+) calc. for $C_{10}H_{13}O_3NNa$ $[M+Na]^+$ 344.1, found 344.2.

Data consistent with literature values.[89]

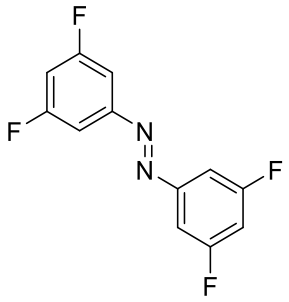
(±)-N,N'-(4,4',6,6'-Tetramethoxy-[1,1'-biphenyl]-2,2'-diyl)diacetamide, 2.61



To a solution of N-(2-iodo-3,5-dimethoxyphenyl)acetamide, **2.60** (105.0 mg, 0.327 mmol, 1.0 equiv.) in N-methyl-2-pyrrolidone (2 mL) was added copper(I) thiophene-2-carboxylate (155.9 mg, 0.818 mmol, 2.5 equiv.) and stirred at room temperature for 16 h. The reaction mixture was diluted with ethyl acetate (10 mL) and passed through a silica plug, washing with ethyl acetate. Solvent was removed *in vacuo* and the residue was purified by column chromatography (ethyl acetate/ petroleum ether (2:3)) to give (±)-N,N'-(4,4',6,6'-tetramethoxy-[1,1'-biphenyl]-2,2'-diyl)diacetamide as a white solid (57.1 mg, 0.147 mmol, 90%).

IR (thin film, ν_{max} / cm^{-1}) 3404, 2937, 2360, 1663, 1605, 1505, 1453, 1421, 1370, 1331, 1300, 1263, 1223, 1200, 1155, 1100, 1068; **^{1}H NMR** (400 MHz, $CDCl_3$) δ 7.58 (s, 2H, ArH), 6.90 (s, 2H, ArH), 6.38 (d, *J* = 2.5 Hz, 2H, NH), 3.87 (s, 6H, OCH_3), 3.70 (s, 6H, OCH_3), 1.95 (s, 6H, C=OCH_3); **^{13}C NMR** (126 MHz, $CDCl_3$) δ 168.9 (C=O), 161.3 (ArO), 158.3 (ArO), 138.6 (ArN), 104.3 (*quat* C), 98.9 (ArH), 95.8 (ArH), 56.1 (OCH_3), 55.6 (OCH_3), 24.9 (CH_3C=O); **HRMS** (ES+) calc. for $C_{20}H_{25}O_6N_2Na$ $[M+Na]^+$ 411.1527, found 411.1526.

(*E*)-1,2-Bis(3,5-difluorophenyl)diazene, 2.62

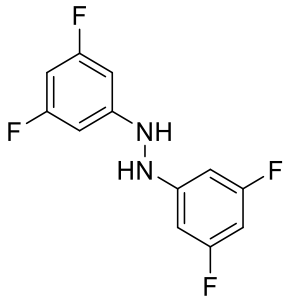


(Diacetoxyiodo)benzene (7.48 g, 23.2 mmol, 1.0 equiv.) was added slowly in portions to a solution of 3,5-difluoroaniline (3.00 g, 23.2 mmol, 1.0 equiv.) in dichloromethane (160 mL) and stirred at room temperature for 2 h. Solvent was removed *in vacuo* and the residue was purified by column chromatography (pure petroleum ether) to give (*E*)-1,2-bis(3,5-difluorophenyl)diazene as a orange solid (2.15 g, 8.45 mmol, 72%).

IR (thin film, ν_{max} / cm^{-1}) 3106, 2360, 2341, 1598, 1461, 1443, 1333, 1305, 1208, 1160, 1120; **^{1}H NMR** (400 MHz, $CDCl_3$) δ 7.48 – 7.41 (m, 4H, CHCN), 6.96 (tt, *J* = 8.5, 2.5 Hz, 2H, CFCHCF); **^{13}C NMR** (101 MHz, $CDCl_3$) δ 160.3 (dd, *J* = 248.0, 15.0 Hz, CF), 150.7 (t, *J* = 13.5 Hz, CN), 104.2 – 103.5 (m, *C*CN), 104.2 (t, *J* = 27.0 Hz, CF*C*CF); **^{19}F NMR** (377 MHz, $CDCl_3$) δ -104.79 (s); **HRMS** (ES-) calc. for $C_{12}H_6N_2F_4$ $[M]^{-\cdot}$ 254.0473, found 254.0473.

Though previously reported, no characterization data has been reported in the literature.[90]

1,2-Bis(3,5-difluorophenyl)hydrazine, 2.63

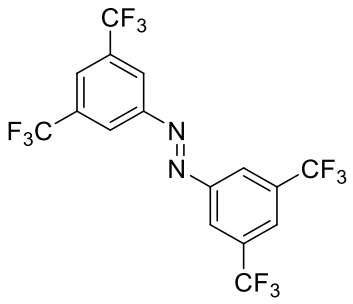


(*E*)-1,2-Bis(3,5-difluorophenyl)diazene, **2.62** (1.50 g, 5.90 mmol, 1.0 equiv.) was added to a biphasic mixture of sodium dithionate (10.27 g, 59.0 mmol, 10.0 equiv.), methanol (50 mL), water (50 mL) and dichloromethane (15 mL) and heated to reflux for 3.5 hours, then allowed to cool to room temperature. The reaction mixture was extracted with dichloromethane (3 × 30 mL), the combined organics washed with brine (50 mL) and dried ($MgSO_4$). The solvent was removed *in vacuo* and the residue was purified by column chromatography (ethyl acetate/ petroleum ether (1:9)) to give 1,2-bis(3,5-difluorophenyl)hydrazine as a white solid (1.36 g, 5.31 mmol, 90%).

IR (thin film, ν_{max} / cm^{-1}) 3319, 2980, 2360, 2341, 1640, 1601, 1524, 1477, 1424, 1146, 1110, 1013, 1001; **^{1}H NMR** (400 MHz, $CDCl_3$) δ 6.39 – 6.32 (m, 4H, CHCN), 6.30 (tt, *J* = 8.5, 2.5 Hz, 2H, CFCHCF), 5.81 (s, 2H, NH); **^{13}C NMR** (101 MHz, $CDCl_3$) δ 164.2 (dd, *J* = 246.0, 15.5 Hz, CF), 150.6 (t, *J* = 12.5 Hz, CN), 95.9 – 94.9 (m, *C*CN + CF*C*CF); **^{19}F NMR** (377 MHz, $CDCl_3$) δ -108.81 (s); **HRMS** (ES-) calc. for $C_{12}H_7N_2F_4$ $[M-H]^-$ 255.0551, found 255.0550.

Data consistent with literature values.[91]

(*E*)-1,2-Bis(3,5-bis(trifluoromethyl)phenyl)diazene, 2.64

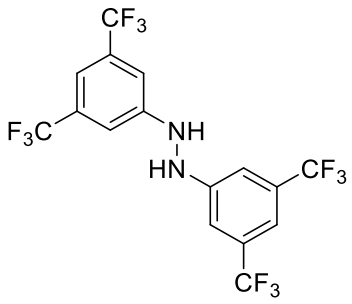


(Diacetoxyiodo)benzene (6.18 g, 19.2 mmol, 1.0 equiv.) was added slowly in portions to a solution of 3,5-bis(trifluoromethyl)aniline (3.00 mL, 19.2 mmol, 1.0 equiv.) in dichloromethane (160 mL) and stirred at room temperature for 2 h. Solvent was removed *in vacuo* and the residue was purified by column chromatography (pure petroleum ether) to give (*E*)-1,2-bis(3,5-difluorophenyl)diazene as a red solid (5.15 g, 11.4 mmol, 60%).

IR (thin film, ν_{max} / cm^{-1}) 2980, 2359, 1373, 1373, 1280, 1263, 1167, 1130; **^{1}H NMR** (400 MHz, $CDCl_3$) δ 8.46 (s, 4H, CHCN), 8.07 (s, 2H, CCF_3CHCCF_3); **^{13}C NMR** (101 MHz, $CDCl_3$) δ 152.1 (CN), 133.1 (q, *J* = 34.0 Hz, *C*CF_3), 125.2 (h, *J* = 4.0 Hz, $CF_3C\mathit{C}HCCF_3$), 123.4 (q, *J* = 4.0 Hz, $NC\mathit{C}HCCF_3$), 123.0 (q, *J* = 273.0 Hz, CF_3); **^{19}F NMR** (377 MHz, $CDCl_3$) δ -63.06; **HRMS** (ES-) calc. for $C_{16}H_6N_2F_{12}$ $[M]^{-\cdot}$ 454.0345, found 454.0348.

Data consistent with literature values.[92]

1,2-Bis(3,5-bis(trifluoromethyl)phenyl)hydrazine, 2.65

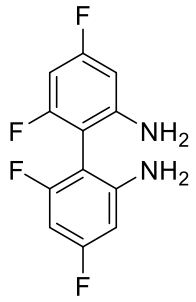


(*E*)-1,2-Bis(3,5-bis(trifluoromethyl)phenyl)diazene, **2.64** (3.00 g, 6.60 mmol, 1.0 equiv.) was added to a biphasic mixture of sodium dithionate (11.50 g, 66.0 mmol, 10.0 equiv.), methanol (50 mL), water (50 mL) and dichloromethane (15 mL) and heated to reflux for 2 hours, then allowed to cool to room temperature. The reaction mixture was extracted with dichloromethane (3 × 30 mL), the combined organics washed with brine (50 mL) and dried ($MgSO_4$). The solvent was removed *in vacuo* and the residue was purified by column chromatography (ethyl acetate/ petroleum ether (1:9)) to give 1,2-bis(3,5-bis(trifluoromethyl)phenyl)hydrazine as an off-white solid (2.32 g, 5.31 mmol, 77%).

IR (thin film, ν_{max} / cm^{-1}) 2923, 2361, 1614, 1472, 1423, 1375, 1277, 1165, 1120; **^{1}H NMR** (400 MHz, $CDCl_3$) δ 7.40 (s, 4H, CHCN), 7.29 (s, 2H, CCF_3CHCCF_3), 6.13 (s, 2H, NH); **^{13}C NMR** (101 MHz, $CDCl_3$) δ 148.8 (CN), 133.0 (q, *J* = 33.0 Hz, *C*CF_3), 123.3 (q, *J* = 274.0 Hz, CF_3), 114.1 (hept, *J* = 4.0 Hz, CF_3C*C*$HCCF_3$), 111.9 (q, *J* = 4.0 Hz, NC*C*$HCCF_3$); **^{19}F NMR** (377 MHz, $CDCl_3$) δ -63.21; **HRMS** (ES-) calc. for $C_{16}H_7N_2F_{12}$ $[M-H]^-$ 455.0423, found 455.0420.

Data consistent with literature values.[93]

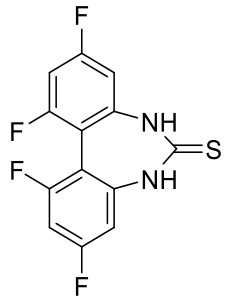
4,4',6,6'-Tetrafluoro-[1,1'-biphenyl]-2,2'-diamine, 2.66



A mixture of concentrated sulfuric acid (6.5 mL) and water (3.5 mL) was heated to 90 °C and 1,2-bis(3,5-difluorophenyl)hydrazine, **2.63** (200.0 mg, 0.781 mmol, 1.0 equiv.) added. After 5 minutes the reaction mixture was neutralized with 2 M sodium hydroxide solution, allowed to further cool to room temperature and extracted with diethyl ether (3 × 200 mL). The combined organics were washed with brine (150 mL), dried ($MgSO_4$) and the solvent removed *in vacuo*. The residue was purified by column chromatography (ethyl acetate/ petroleum ether (1:4 to 3:7)) to give 4,4',6,6'-tetrafluoro-[1,1'-biphenyl]-2,2'-diamine as a colourless oil (56.1 mg, 0.219 mmol, 28%).

IR (thin film, ν_{max} / cm^{-1}) 3635, 3220, 2339, 2312, 1657, 1620, 1555, 1511, 1442, 1381, 1336, 1280, 1182, 1110; **^{1}H NMR** (400 MHz, $CDCl_3$) δ 6.37 – 6.29 (m, 4H, ArH), 6.96 (s, 4H, NH); **^{13}C NMR** (101 MHz, $CDCl_3$) δ 164.4 (dd, *J* = 234.0, 15.5 Hz, CF), 161.2 (dd, *J* = 246.5, 15.5 Hz, CF), 147.6 – 147.3 (m, CN), 100.0 – 99.7 (m, *quat* C), 97.9 (dd, *J* = 25.0, 2.5 Hz, CN*C*HCF), 93.9 (t, *J* = 26.5 Hz, CF*C*HCF); **^{19}F NMR** (377 MHz, $CDCl_3$) δ -108.96 – -109.01 (m, *quat* CCF), -109.77 (q, *J* = 9.0 Hz, CNCHCF); **HRMS** (ES-) calc. for $C_{12}H_7N_2F_4$ $[M-H]^-$ 255.0551, found 255.0550.

(±)-1,3,9,11-Tetrafluoro-5,7-dihydro-6H-dibenzo[d,f][1,3]diazepine-6-thione, 2.20b

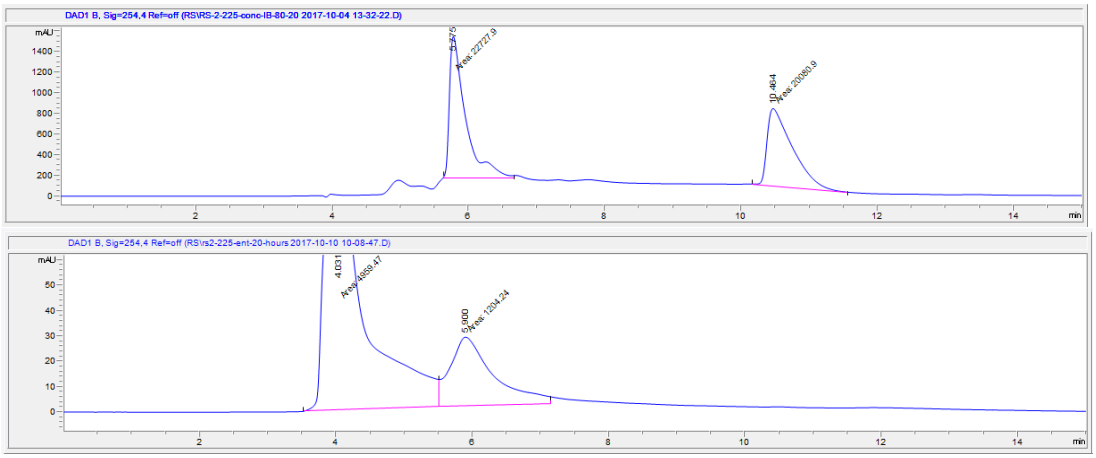


To a stirred solution of 4,4',6,6'-tetrafluoro-[1,1'-biphenyl]-2,2'-diamine, **2.66** (9.3 mg, 0.036 mmol, 1.0 equiv.) in tetrahydrofuran (5 mL) was added triethylamine (12.6 μL, 0.091 mmol, 2.5 equiv.), then thiophosgene (2.8 μL, 0.036 mmol, 1.0 equiv.) then 4-dimethylaminopyridine (0.9 mg, 0.007 mmol, 0.2 equiv.) at room temperature for 4 h. The reaction mixture was diluted with diethyl ether (20 mL), poured onto water (25 mL) and the phases separated. The aqueous was extracted with diethyl ether (3 × 25 mL), the combined organics washed with brine (30 mL), dried ($MgSO_4$) and the solvent was removed *in vacuo.* The residue was purified column chromatography (ethyl acetate/ petroleum ether (1:9)) to give (±)-1,3,9,11-tetrafluoro-5,7-dihydro-6H-dibenzo[d,f][1,3]diazepine-6-thione as a colourless oil (4.7 mg, 0.016 mmol, 44%).

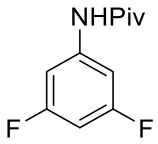
IR (thin film, ν_{max} / cm^{-1}) 3272, 3628, 3211, 2921, 2360, 2341, 1616, 1556, 1508, 1459, 1421, 1384, 1334, 1293, 1187, 1161, 1127; **^{1}H NMR** (400 MHz, $CDCl_3$) δ 7.81 (s, 1H), 6.81 (dtd, *J* = 8.5, 5.0, 2.5 Hz, 1H), 6.59 (dd, *J* = 8.5, 2.5 Hz, 1H); **^{13}C NMR** (101 MHz, $CDCl_3$) δ 179.1 (C=S), 164.6 (dd, *J* = 236.5, 15.5 Hz, CF), 160.9 (dd, *J* = 244.0, 15.5 Hz, CF), 147.5 – 147.3 (m, CN), 103.2 – 102.5 (m, *quat* C), 98.7 (dd, *J* = 25.5, 2.5 Hz, CN*C*HCF), 94.1 (t, *J* = 26.5 Hz, CF*C*HCF); **^{19}F NMR** (377 MHz, $CDCl_3$) δ -103.67 (p, *J* = 5.0 Hz), -107.42 (ddd, *J* = 13.5, 8.5, 5.0 Hz), **HRMS** (ES-) calc. for $C_{13}H_5N_2F_4{}^{32}S$ $[M-H]^-$ 297.0115, found 297.0113.

The enantiomeric excess was determined by HPLC [Chiralpak® IB; hexane:*i*PrOH 80:20; 1.0 ml min^{-1}, λ= 254 nm, t_1 = 5.78 min, t_2 = 10.46 min.

Method used for separation of enantiomers was similar to that reported by Mistry and Fletcher.[86]



N-(3,5-Difluorophenyl)pivalamide, 2.67

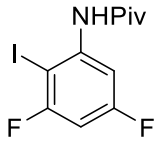


To a stirred solution of 3,5-fluoroaniline (1.00 g, 7.75 mmol, 1.0 equiv.) in dichloromethane (25 mL) was added triethylamine (1.62 mL, 11.63 mmol, 1.5 equiv.) then trimethylacetyl chloride (1.43 mL, 11.63 mmol, 1.5 equiv.), followed by 4-dimethylaminopyridine (189.3 mg, 1.55 mmol, 0.2 equiv.). After 4 h, water (20 mL) was added, the phases separated, the aqueous extracted with dichloromethane (2 × 15 mL), the combined organics washed with brine (20 mL), dried ($MgSO_4$) and the solvent removed *in vacuo.* The residue was purified column chromatography (ethyl acetate/ petroleum ether (1:19)) to give N-(3,5-difluorophenyl)pivalamide as a white solid (1.376 g, 6.41 mmol, 83%).

IR (thin film, ν_{max} / cm^{-1}) 3308, 2966, 1660, 1607, 1539, 1476, 1447, 1419, 1368, 1308, 1279, 1214, 1184, 1119, 1030; **^{1}H NMR** (400 MHz, $CDCl_3$) δ 7.43 (s, 1H, NH), 7.20 – 7.12 (m, 2H, CHCN), 6.53 (tt, *J* = 9.0, 2.0 Hz, 1H, CFCHCF), 1.30 (s, 9H, CH_3); **^{13}C NMR** (101 MHz, $CDCl_3$) δ 177.0 (C=O), 163.2 (dd, *J* = 246.5, 14.5 Hz, CF), 140.3 (t, *J* = 13.5 Hz, CN), 103.4 – 102.6 (m, *C*CN), 99.5 (t, *J* = 25.5 Hz, CF*C*CF), 39.9 (*C*CH_3), 27.6 (CH_3); **^{19}F NMR** (377 MHz, $CDCl_3$) δ -109.08 (t, *J* = 8.5 Hz); **LRMS** (ES+) calc. for $C_{11}H_{12}F_2NO$ $[M–H]^-$ 212.1, found 212.1.

Data consistent with literature values.[94]

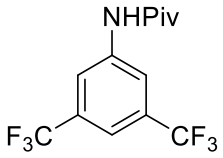
N-(3,5-Difluoro-2-iodophenyl)pivalamide, 2.68



To a stirred solution of N-(3,5-difluorophenyl)pivalamide, **2.67** (500.0 mg, 2.35 mmol, 1.0 equiv.) in tetrahydrofuran (8 mL) was added *n*-butyllithium solution (2.94 mL, 1.6 M in hexanes, 4.70 mmol, 2.0 equiv.) at -78 °C. After 30 minutes, iodine (2.98 g, 11.75 mmol, 5.0 equiv.) was added, and stirred for a further 15 minutes, then allowed to warm to room temperature. The reaction mixture was diluted with diethyl ether (25 mL), and worked up with water (20 mL), the phases separated and the aqueous extracted with diethyl ether (3 × 10 mL). The combined organics were washed with brine (15 mL), dried ($MgSO_4$) and the solvent removed *in vacuo*. The residue was purified column chromatography (ethyl acetate / petroleum ether (1:49)) to give N-(3,5-difluoro-2-iodophenyl)pivalamide as a light sensitive white solid (267.6 mg, 0.789 mmol, 34%). The compound was handled and stored in the dark.

IR (thin film, ν_{max} / cm^{-1}) 3395, 3111, 2964, 2353, 2345, 1693, 1592, 1521, 1479, 1436, 1414, 1396, 1367, 1348, 1285, 1192, 1158, 1121, 1037; **^{1}H NMR** (400 MHz, $CDCl_3$) δ 8.13 (d, *J* = 11.2 Hz, 1H, C6H), 8.05 (s, 1H, NH), 6.68 – 6.58 (m, 1H, C4H), 1.37 (s, 9H, CH_3); **^{13}C NMR** (101 MHz, $CDCl_3$) δ 177.1 (C=O), 164.5 (d, *J* = 247.0 Hz, C3), 162.7 (t, *J* = 3.5 Hz, C1), 161.7 (d, J = 246.5 Hz, C5), 104.3 (dd, *J* = 28.5, 3.0 Hz, C6), 99.4 (t, *J* = 27.5 Hz, C4), 70.9 (d, *J* = 28.5 Hz, C2), 40.63 (*C*CH_3), 27.73 (CH_3); **^{19}F NMR** (377 MHz, $CDCl_3$) δ -86.84 (t, *J* = 8.5 Hz, C3F), -108.25 (q, *J* = 8.5 Hz, C5F); **HRMS** (ES+) calc. for $C_{11}H_{13}NOF_2{}^{127}I$ $[M+H]^+$ 340.0004, found 340.0005.

N-(3,5-Bis(trifluoromethyl)phenyl)pivalamide, 2.69



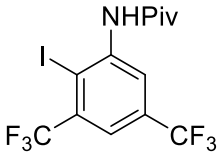
To a stirred solution of 3,5-bis(trifluoromethyl)aniline (1.21 mL, 7.75 mmol, 1.0 equiv.) in dichloromethane (25 mL) was added triethylamine (1.62 mL, 11.63 mmol, 1.5 equiv.) then trimethylacetyl chloride (1.43 mL, 11.63 mmol, 1.5 equiv.), followed by 4-dimethylaminopyridine (189.3 mg, 1.55 mmol, 0.2 equiv.). After 4 h water (20 mL) was added, the phases separated, the aqueous extracted with dichloromethane (2 × 15 mL), the combined organics washed with brine (20 mL), dried ($MgSO_4$) and the solvent removed *in vacuo.* The residue was purified column chromatography (ethyl acetate/ petroleum ether (1:19)) to give N-(3,5-bis(trifluoromethyl)phenyl)pivalamide as a white solid (2.253 g, 7.19 mmol, 93%).

IR (thin film, ν_{max} / cm^{-1}) 2353, 2254, 1693, 1535, 1472, 1431, 1380, 1278, 1183, 1142; **^{1}H NMR** (400 MHz, $CDCl_3$) δ 8.04 (s, 2H, CHCN), 7.73 (s, 1H, NH), 7.57 (s, 1H, CCF_3CHCCF_3)), 1.34 (s, 9H, CH_3); **^{13}C NMR** (101 MHz, $CDCl_3$) δ 177.5 (C=O), 139.6 –

139.5 (m, CN), 132.4 (q, J = 33.5 Hz, CCF$_3$), 123.2 (q, J = 273.0 Hz, CF$_3$), 120.2 – 119.6 (m, CHCN), 117.6 (hept, J = 4.0 Hz, CCF$_3$$C$HCCF$_3$), 40.0 ($CCH_3$), 27.6 (CH$_3$); **^{19}F NMR** (377 MHz, CDCl$_3$) δ -63.08; **LRMS** (ES+) calc. for $C_{13}H_{12}F_6NO$ $[M–H]^-$ 312.1, found 312.0.

Data consistent with literature values.[95]

N-(2-Iodo-3,5-bis(trifluoromethyl)phenyl)pivalamide, 2.70

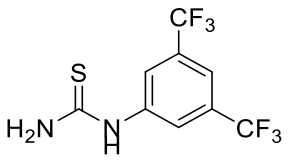


To a stirred solution of N-(3,5-bis(trifluoromethyl)phenyl)pivalamide, **2.69** (500.0 mg, 1.60 mmol, 1.0 equiv.) in tetrahydrofuran (8 mL) was added *n*-butyllithium solution (1.00 mL, 1.6 M in hexanes, 1.00 mmol, 1.0 equiv.) at -78 °C, followed by *t*-butyllithium solution (0.94 mL, 1.7 M in pentane, 1.00 mmol, 1.0 equiv.). After 45 minutes, iodine (2.03g, 8.0 mmol, 5.0 equiv.) was added, and stirred for a further 15 minutes, then allowed to warm to room temperature. The reaction mixture was diluted with diethyl ether (25 mL), and worked up with water (20 mL), the phases separated and the aqueous extracted with diethyl ether (3 × 10 mL). The combined organics were washed with brine (15 mL), dried ($MgSO_4$) and the solvent removed *in vacuo*. The residue was purified column chromatography (ethyl acetate/ petroleum ether (1:19)) to give N-(2-iodo-3,5-bis(trifluoromethyl)phenyl)pivalamide as a light sensitive white solid (590.1 mg, 1.34 mmol, 84%). The compound was handled and stored in the dark.

IR (thin film, ν_{max} / cm^{-1}) 3390, 2969, 1690, 1610, 1584, 1517, 1435, 1415, 1365, 1288, 1255, 1128, 1107, 1013; **^{1}H NMR** (400 MHz, CDCl$_3$) δ 8.86 (s, 1H, C4H), 8.30 (s, 1H,

NH), 7.63 (s, 1H, C6H), 1.40 (s, 9H, CH_3); **^{13}C NMR** (126 MHz, $CDCl_3$) δ 177.3 (C=O), 141.3 (C1), 135.4 (q, *J* = 31.5 Hz, C3*C*F_3), 132.0 (q, *J* = 34.0 Hz, C5*C*F_3), 123.1 (q, *J* = 273.5 Hz, C5), 122.3 (q, *J* = 275.0 Hz, C3), 121.3 - 121.0 (m, C6), 119.6 – 119.3 (m, C4), 92.0 (C2), 40.70 (*C*CH_3), 27.7 (CH_3); **^{19}F NMR** (377 MHz, $CDCl_3$) δ -62.91, -63.29; **HRMS** (ES+) calc. for $C_{13}H_{13}NOF_6{}^{127}I$ $[M+H]^+$ 439.9941, found 439.9941.

1-(3,5-Bis(trifluoromethyl)phenyl)thiourea, 2.71

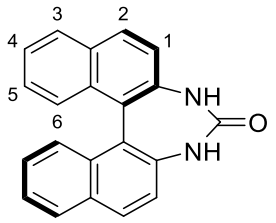


To a stirred solution of 3,5-bis(trifluoromethyl)phenyl isothiocyanate (1.5 mL, 8.21 mmol, 1.0 equiv.) in methanol (2 mL) was added aqueous ammonia solution (1.3 mL, 7 M in methanol, 9.04 mmol, 1.1 equiv.) at room temperature. After 3 hours the solvent removed *in vacuo*. The residue was purified column chromatography (methanol/ dichloromethane (0:100 to 1:49)) to give 1-(3,5-bis(trifluoromethyl)phenyl)thiourea as a white solid (994.0 mg, 3.45 mmol, 42%).

IR (thin film, ν_{max} / cm^{-1}) 3327, 3059, 1699, 1654, 1579, 1523, 1440, 1352, 1280, 1253, 1154; **^{1}H NMR** (400 MHz, $CO(CD_3)_2$) δ 9.67 (s, 1H, NH), 8.41 (s, 2H, NH_2), 7.77 (s, 1H, CF_3CHCF_3), 7.38 (s, 2H, CF_3CHCN); **^{13}C NMR** (101 MHz, $CO(CD_3)_2$) δ 184.1 (C=S), 137.9 – 139.8 (m, CN), 134.1 – 133.4 (m, *C*HCN), 131.7 (q, *J* = 33.5 Hz, *C*CF_3), 124.1 (q, *J* = 273.5 Hz, CF_3), 118.5 (hept, *J* = 4.0 Hz, CCF_3CHCCF_3); **^{19}F NMR** (377 MHz, $CO(CD_3)_2$) δ -65.71; **LRMS** (ES+) calc. for $C_9H_7N_2{}^{32}SF_6$ $[M+H]^+$ 289.0, found 289.0.

Data consistent with literature values.[96]

(*R*)-3,5-dihydro-4H-dinaphtho[2,1-d:1',2'-f][1,3]diazepin-4-one, 2.24



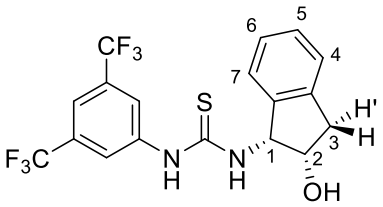
(*R*)-(+)-1,1′-Binaphthyl-2,2′-diamine (1.15 g, 4.04 mmol, 1.0 equiv.) and urea (486.1 mg, 8.08 mmol, 2.0 equiv.) in acetic acid (50 mL) were stirred and heated to 120 °C for 16 h. The reaction mixture was then allowed to cool to room temperature, poured onto saturated aqueous sodium carbonate (300 mL) and extracted with diethyl ether (3 × 100 mL). The combined organics were dried ($MgSO_4$) and the solvent was removed *in vacuo*. The residue was purified column chromatography (ethyl acetate/ petroleum ether (1:4)) to give (*R*)-3,5-dihydro-4H-dinaphtho[2,1-d:1',2'-f][1,3]diazepin-4-one as a white solid (160.0 mg, 0.516 mmol, 13%).

IR (thin film, ν_{max} / cm^{-1}) 3222, 2985, 2138, 1684, 1620, 1584, 1531, 1475, 1462, 1328, 1212, 1157, 1129, 1064, 1001; **^{1}H NMR** (400 MHz, $CDCl_3$) δ 9.24 (d, *J* = 8.5 Hz, 2H, C6H), 8.71 (s, 2H, NH), 8.05 (dd, *J* = 8.0, 1.5 Hz, 2H, C3H), 7.87 (d, *J* = 8.5 Hz, 2H, C2H), 7.71 (ddd, *J* = 8.5, 7.0, 1.5 Hz, 2H, C4H or C5H), 7.64 (d, *J* = 8.5 Hz, 2H, C1H), 7.54 (ddd, *J* = 8.0, 7.0, 1.0 Hz, 2H, C4H or C5H); **^{13}C NMR** (101 MHz, $CDCl_3$) δ 153.3 (C=O), 140.7 (CN), 133.7 (*quat* C), 128.4 (C2), 128.1 (C3), 127.3 (*quat* C), 126.2 (C4 or C5), 125.3 (C6), 122.5 (C4 or C5), 118.6 (C1), 117.2 (*quat* C); **HRMS** (ES-) calc. for $C_{21}H_{13}N_2O$ $[M-H]^-$ 309.1033, found 309.1035; **$[\alpha]_D$** (*c* = 1.0, $CHCl_3$): -238.1 °.

This compound has been previously reported, however without characterization.[97]

2. 6. 5. 7 Synthesis of starting materials, catalyst and products of nonlinear effects studies

1-(3,5-Bis(trifluoromethyl)phenyl)-3-((1*R*,2*S*)-2-hydroxy-2,3-dihydro-1H-inden-1-yl)thiourea, 2.27



3,5-Bis(trifluoromethyl)phenyl isothiocyanate (1.22 mL, 6.70 mmol, 1.0 equiv.) was added dropwise to (1*R*, 2*S*)-*cis*-1-amino-2-indanol (1.00 g, 6.70 mmol, 1.0 equiv.) in dichloromethane (15 mL) at room temperature for 16 h. Solvent was removed *in vacuo* and the residue was purified by recrystallization (acetone/ hexanes) to give 1-(3,5-bis(trifluoromethyl)phenyl)-3-((1*R*,2*S*)-2-hydroxy-2,3-dihydro-1H-inden-1-yl)thiourea as a white crystalline solid (1.47 g, 4.71 mmol, 70%).

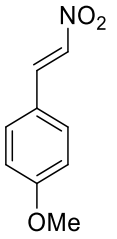
IR (thin film, ν_{max} / cm^{-1}) 3285, 2362, 2158, 2018, 1529, 1470, 1382, 1277, 1176, 1131, 1045; **^{1}H NMR** (400 MHz, DMSO-d_6) δ 10.59 (s, 1H, ArNH), 8.44 (s, 2H, C(CF_3)C*H*NH), 8.30 (d, *J* = 8.5 Hz, 1H, C1HN*H*), 7.75 (s, 1H, CCF_3CHCCF_3), 7.33 (d, *J* = 7.0 Hz, 1H, C7H), 7.30 – 7.15 (m, 3H, C4H + C5H + C6H), 5.85 (dd, *J* = 8.5, 5.0 Hz, 1H, C1H), 5.51 (d, *J* = 4.0 Hz, 1H, OH), 4.58 (q, *J* = 4.0 Hz, 1H, C2H), 3.14 (dd, *J* = 16.5, 4.5 Hz, 1H, C3H), 2.86 (d, *J* = 16.5 Hz, 1H, C3H'); **^{13}C NMR** (101 MHz, DMSO-d_6) δ 180.6 (C=S), 142.0 (*quat* C), 141.6 (*quat* C), 140.6 (*quat* C), 130.2 (q, *J* = 32.5 Hz, *C*CF_3), 127.5 (C4, C5 or C6), 126.3 (C4, C5 or C6), 125.1 (C4, C5 or C6), 124.3 (C7), 123.3 (q, *J* = 272.5 Hz, CF_3), 121.6 (CCF_3*C*HCN), 116.1 (CCF_3*C*HCCF_3), 71.9 (C2), 61.4 (C1), 40.0 (C3); **^{19}F NMR** (377 MHz, DMSO-d_6) δ -61.65; **LRMS** (ES+) calc.

for $C_{18}H_{15}F_6N_2OS$ $[M+H]^+$ 421.1, found 421.0; **mp** (acetone/ hexanes)172.6 °C;

[α]D (*c* = 1.0, $CHCl_3$): 17.2 °.

Data consistent with literature values.[59]

(*E*)-1-Methoxy-4-(2-nitrovinyl)benzene, 2.33

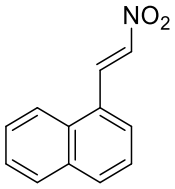


A mixture of *p*-anisaldehyde (1.20 mL, 7.88 mmol, 1.0 equiv.), nitromethane (4.27 mL, 78.8 mmol, 10.0 equiv.) and ammonium acetate (6.07 g, 78.8 mmol, 10.0 equiv.) in acetic acid (25 mL) was heated to 80 °C for 15 minutes and allowed to cool to room temperature. The reaction mixture was neutralized with 1 M sodium hydroxide solution and extracted with ethyl acetate (3 × 100 mL). The combined organics washed with brine (75 mL) and dried ($MgSO_4$). The solvent was removed *in vacuo* and the residue was purified by column chromatography (ethyl acetate/ petroleum ether (1:9 to 1:4)) to give (*E*)-1-methoxy-4-(2-nitrovinyl)benzene as a yellow solid (1.045 g, 5.83 mmol, 74%).

IR (thin film, ν_{max} / cm^{-1}) 3107.3, 2839, 2360, 1600, 1511, 1495, 1337, 1308, 1252, 1172, 1160, 1027; **^{1}H NMR** (400 MHz, $CDCl_3$) δ 7.84 (d, *J* = 12.5 Hz, 1H, ArC*H*), 7.47 – 7.39 (m, 3H, C*H*$COCH_3$ + C*H*NO_2), 6.89 – 6.85 (m, 2H, C*H*$CHCOCH_3$), 3.77 (s, 3H, OCH_3); **^{13}C NMR** (126 MHz, $CDCl_3$) δ 162.6 (*C*OCH_3), 138.7 (Ar*C*H), 134.6 (*C*HNO_2), 130.9 (*C*$HCOCH_3$), 122.1 (C*C*(=C)C), 114.5 (*C*HCHCO), 55.1 (CH_3); **LRMS** (ES+) calc. for $C_9H_9NO_3Na$ $[M+Na]^+$ 202.0, found 202.2.

Data consistent with literature values.[98]

(*E*)-1-(2-Nitrovinyl)naphthalene, 2.31

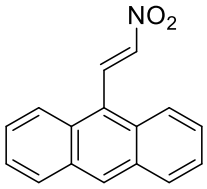


A mixture of 1-naphthaldehyde (1.93 mL, 14.2 mmol, 1.0 equiv.), nitromethane (5.31 mL, 98.0 mmol, 6.9 equiv.) and ammonium acetate (2.63 g, 34.1 mmol, 2.4 equiv.) in acetic acid (25 mL) was heated to 100 °C for 6 h and allowed to cool to room temperature. The reaction mixture was neutralized with 1 M sodium hydroxide solution and extracted with ethyl acetate (3 × 100 mL). The combined organics washed with brine (75 mL) and dried ($MgSO_4$). The solvent was removed *in vacuo* and the residue was purified by column chromatography (ethyl acetate/ petroleum ether (1:19)) to give (*E*)-1-(2-nitrovinyl)naphthalene as a red solid (1.472 g, 7.39 mmol, 52%).

IR (thin film, ν_{max} / cm^{-1}) 3107, 3051, 2345, 1631, 1572, 1503, 1396, 1333, 1271, 1243, 1208, 1173, 1143, 1090; **^{1}H NMR** (400 MHz, $CDCl_3$) δ 8.85 (d, *J* = 13.5 Hz, 1H, $CHNO_2$), 8.15 (d, *J* = 8.5 Hz, 1H, ArH), 8.01 (d, *J* = 8.5 Hz, 1H, ArH), 7.93 (d, *J* = 8.5 Hz, 1H, ArH), 7.77 (d, *J* = 7.0 Hz, 1H, ArH), 7.69 – 7.63 (m, 2H, $CHNO_2$ + ArH), 7.62 – 7.58 (m, 1H, ArH, 7.53 (t, *J* = 8.0 Hz, 1H, ArH); **^{13}C NMR** (101 MHz, $CDCl_3$) δ 138.7 (ArH), 136.3 ($CHNO_2$), 133.9 (*quat* C), 132.7 (ArH), 131.7 (*quat* C), 129.2 (ArH), 127.9 (*C*HCHNO$_2$), 127.1 (*quat* C), 127.0 (ArH), 126.5 (ArH), 125.6 (ArH), 123.1 (ArH); **LRMS** (ES+) calc. for $C_{12}H_9NO_2Na$ $[M+Na]^+$ 222.1, found 222.2.

Data consistent with literature values.[99]

(*E*)-9-(2-Nitrovinyl)anthracene, 2.32

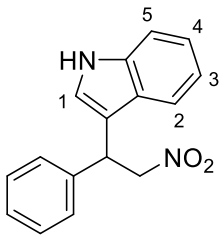


A mixture of 9-anthracenecarboxaldehyde (2.93 g, 14.2 mmol, 1.0 equiv.), nitromethane (5.31 mL, 98.0 mmol, 6.9 equiv.) and ammonium acetate (2.63 g, 34.1 mmol, 2.4 equiv.) in acetic acid (25 mL) was heated to 100 °C for 22 h and allowed to cool to room temperature. The reaction mixture was neutralized with 1 M sodium hydroxide solution and extracted with ethyl acetate (3 × 100 mL). The combined organics washed with brine (75 mL) and dried ($MgSO_4$). The solvent was removed *in vacuo* and the residue was purified by column chromatography (ethyl acetate/ petroleum ether (1:19 to 1:4)) to (*E*)-9-(2-nitrovinyl)anthracene as a red solid (2.408 g, 9.66 mmol, 68%).

IR (thin film, ν_{max} / cm^{-1}) 3450, 3051, 2851, 2295, 1668, 1624, 153, 1503, 1442, 1329, 1279, 1250, 1177, 1156, 1071, 1048, 1021; **^{1}H NMR** (400 MHz, $CDCl_3$) δ 8.71 (dq, *J* = 9.0, 1.0 Hz, 2H, ArH), 8.65 (d, *J* = 14.0 Hz, 1H, ArCH), 7.88 (dq, *J* = 9.0, 1.0 Hz, 2H, ArH), 7.80 – 7.73 (m, 2H), 7.44 (ddd, *J* = 9.0, 6.5, 1.5 Hz, 2H), 7.38 – 7.27 (m, 2H, $CHNO_2$ + ArH); **^{13}C NMR** (101 MHz, $CDCl_3$) δ 142.5 ($CHNO_2$), 135.6 (Ar*C*H), 135.1 (*quat* C), 130.4 (*quat* C), 129.2 (ArH), 129.1 (*quat* C), 127.5 (ArH), 125.6 (ArH), 124.2 (ArH), 123.5 (ArH); **LRMS** (ES+) calc. for $C_{16}H_{11}NO_2Na$ $[M+Na]^+$ 272.1, found 272.1.

Data consistent with literature values.[100]

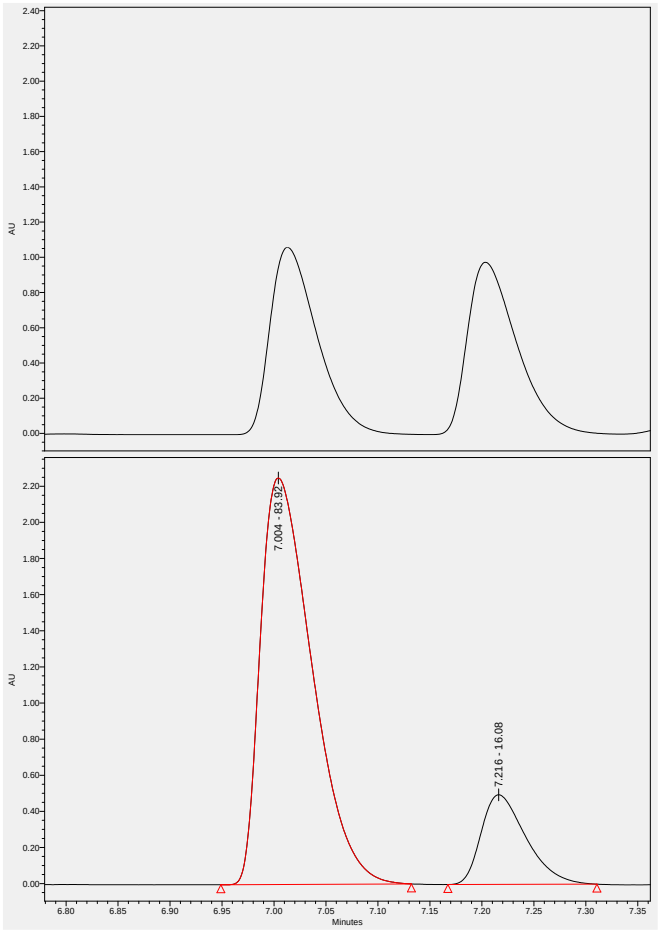
(±)-3-(2-Nitro-1-phenylethyl)-1H-indole, 2.30



Zinc acetate (11.0 mg, 0.05 mmol, 0.05 equiv.) was added to a solution of trans-β-nitrostyrene (149.2 mg, 1.0 mmol, 1.0 equiv.) and indole (117.2 mg, 1.0 mmol, 1.0 equiv.) in ethanol (4 mL) and stirred at room temperature for 2 h. Solvent was removed *in vacuo*, the residue diluted with water (25 mL), extracted with ethyl acetate (3 × 20 mL). The combined organics were dried ($MgSO_4$), the solvent removed *in vacuo* and the residue purified by column chromatography (ethyl acetate/ petroleum ether (3:17)) to give (±)-3-(2-nitro-1-phenylethyl)-1H-indole as a light yellow solid (115.7 mg, 0.434 mmol, 43%).

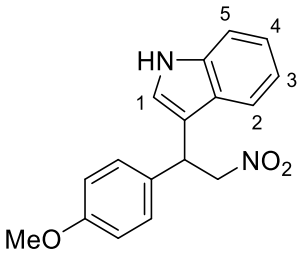
IR (thin film, ν_{max} / cm^{-1}) 3419, 3060, 2917, 1694, 1619, 1547, 1518, 1493, 1456, 1421, 1377, 1340, 1277, 1223, 1177, 1132, 1101, 1010; **^{1}H NMR** (400 MHz, $CDCl_3$) δ 7.99 (s, 1H, NH), 7.39 (dq, *J* = 8.0, 1.0 Hz, 1H, C2H), 7.27 – 7.17 (m, 6H, C5H + *o*Ph + *m*Ph + *p*Ph), 7.17 – 7.10 (m, 1H, C3H or C4H), 7.02 (ddd, *J* = 8.0, 7.0, 1.0 Hz, 1H, C3H or C4H), 6.86 (d, *J* = 2.5 Hz, 1H, C1H), 5.16 – 5.09 (t, *J* = 8.0 Hz, 1H, ArCH), 4.96 (ddd, *J* = 12.5, 7.5, 1.5 Hz, 1H, CH_2NO_2), 4.85 (dd, *J* = 12.5, 8.4 Hz, 1H, CH_2NO_2); **^{13}C NMR** (101 MHz, $CDCl_3$) δ 139.3 (*quat* C), 136.5 (*quat* C), 129.0 (ArH), 127.8 (ArH), 127.6 (ArH), 126.1 (*quat* C), 122.7 (ArH), 121.7 (C3 or C4), 120.0 (C3 or C4), 118.9 (C2), 114.3 (*quat* C), 111.5 (ArH), 79.6 (CH_2NO_2), 41.6 (Ar*C*H); **LRMS** (ES–) calc. for $C_{16}H_{15}N_2O_2$ $[M–H]^–$ 265.1, found 265.0; **[α]$_D$** (*c* = 3.0, ee = 68%, $CHCl_3$): 4.9 °.

The enantiomeric excess was determined by analytical chiral SFC [Chiralpak® IA, 99:1 – 90:10 CO_2 : MeOH over 5 min, 90:10 thereafter, 1.5 $mLmin^{-1}$, t_R(maj) = 7.00 min, t_R (min) = 7.22 min].



Data consistent with literature values.[59]

(±)-3-(1-(4-Methoxyphenyl)-2-nitroethyl)-1H-indole, 2.72

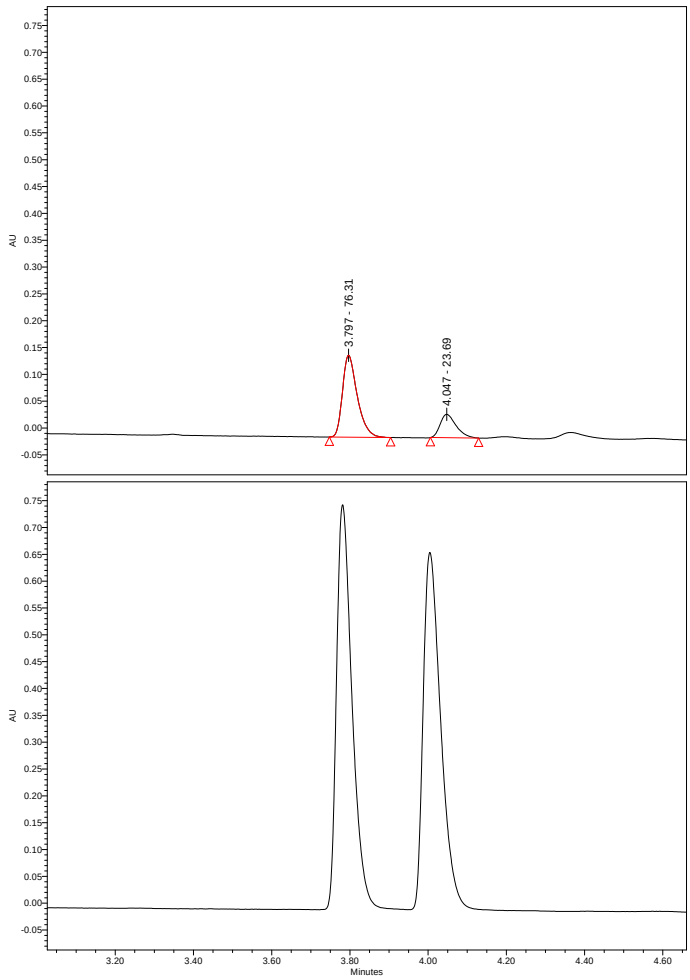


Indole (147.0 mg, 1.256 mmol, 1.5 equiv.) was added to a stirred solution of (*E*)-1-methoxy-4-(2-nitrovinyl)benzene, **2.33** (150.0 mg, 0.837 mmol, 1.0 equiv.) in

dichloromethane (5 mL), followed by 1,3-bis(3,5-bis(trifluoromethyl)phenyl)thiourea (83.7 mg, 0.167 mmol, 0.2 equiv.) and heated to reflux for 7 h. The solvent removed *in vacuo* and the residue purified by column chromatography (ethyl acetate/ petroleum ether (1:9) to (1:4)) to give (±)-3-(1-(4-methoxyphenyl)-2-nitroethyl)-1H-indole as a yellow oil (183.6 mg, 0.620 mmol, 74%).

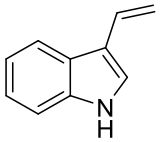
IR (thin film, ν_{max} / cm^{-1}) 3417, 2916, 2360, 1610, 1548, 1510, 1457, 1422, 1378, 1339, 1303, 1247, 1178, 1101, 1031; **^{1}H NMR** (400 MHz, $CDCl_3$) δ 8.08 (s, 1H, NH), 7.44 (dq, *J* = 8.0, 1.0 Hz, 1H, C2H), 7.36 (dt, *J* = 8.0, 1.0 Hz, 1H, C5H), 7.28 – 7.23 (m, 2H, C*H*CHCOCH$_3$), 7.20 (ddd, *J* = 8.0, 7.0, 1.0 Hz, 1H, C4H), 7.08 (ddd, *J* = 8.0, 7.0, 1.0 Hz, 1H, C3H), 7.02 (dt, *J* = 3.0, 1.5 Hz, 1H, C1H), 6.89 – 6.83 (m, 2H, C*H*COCH$_3$), 5.14 (t, *J* = 8.0 Hz, 1H, ArCH), 5.05 (dd, *J* = 12.5, 7.5 Hz, 1H, CH_2NO_2), 4.90 (dd, *J* = 12.5, 8.5 Hz, 1H, CH_2NO_2), 3.78 (s, 3H, CH_3); **^{13}C NMR** (101 MHz, $CDCl_3$) δ 159.0 (*C*OCH$_3$), 136.6 (*quat* C), 131.3 (*quat* C), 129.7 (*quat* C), 129.0 (*C*HCHCOCH$_3$), 122.8 (C4), 121.6 (C1), 120.1 (C3), 119.1 (C2), 114.9 (*quat* C), 114.4 (*C*HCOCH$_3$), 111.5 (C5), 79.9 (CH_2NO_2), 55.4 (CH_3), 40.9 (Ar*C*H); **LRMS** (ES–) calc. for $C_{17}H_{15}N_2O_3$ $[M–H]^–$ 295.1, found 295.1.

The enantiomeric excess was determined by analytical chiral SFC [Chiralpak® IA, 99:1 – 50:50 CO_2 : MeOH over 5 min, 1.5 $mLmin^{-1}$, t_R(maj) = 3.80 min, t_R (min) = 4.05 min.]



Data consistent with literature values.[101]

3-Vinyl-indole, 2.73



To a suspension of methyltriphenylphosphonium bromide (8.21 g, 23.0 mmol, 1.15 equiv.) in tetrahydrofuran (60 mL) was added n-butyllithium solution (12.5 mL, 20.0 mmol, 1.0 equiv., 1.6 M in hexanes) dropwise at -50 °C, and allowed to warm to 0 °C over 45 minutes. This was then cooled to -30 °C, and a premixed solution of 3-formyl indole (2.90 g, 20.0 mmol, 1.0 equiv.) and lithium bis(trimethylsilyl)amide solution (20.0 mL, 20.0 mmol, 1.0 equiv., 1.0 M in hexanes) added dropwise. The

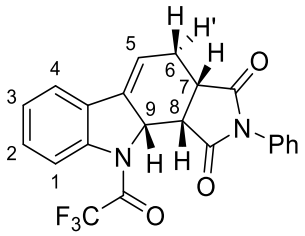
reaction mixture was allowed to warm to room temperature and stirred for an hour. The reaction mixture was then poured onto water (50 mL) and extracted with ethyl acetate (3 × 50 mL). The combined organics were washed with brine (30 mL), dried ($NaSO_4$) and the solvent removed *in vacuo*. The residue was purified by column chromatography (diethyl ether / petroleum ether (3:7)) to give 3-vinyl-indole as an off-white solid (2.42 g, 16.92 mmol, 85%).

IR (thin film, ν_{max} / cm^{-1}) 3395, 3100, 3054, 2978, 2353, 1631, 1569, 1528 1456, 1426, 1414, 1351, 1332, 1301, 1248, 1233, 1157, 1098; **^{1}H NMR** (400 MHz, DMSO-d_6) δ 7.84 (dd, *J* = 8.0, 1.0 Hz, 1H, C7H), 7.51 (d, *J* = 2.5 Hz, 1H, C2H), 7.44 (dt, *J* = 8.0, 1.0 Hz, 1H, C4H), 7.16 (ddd, *J* = 8.0, 7.0, 1.5 Hz, 1H, C5H), 7.09 (ddd, *J* = 8.0, 7.0, 1.0 Hz, 1H, C6H), 6.89 (dd, *J* = 18.0, 11.5 Hz, 1H, C*H*CH_2), 5.66 (dd, *J* = 18.0, 1.5 Hz, 1H, *cis*-ArCHCH_2), 5.07 (dd, *J* = 11.5, 1.5 Hz, 1H, *trans*-ArCHCH_2), 3.48 (s, 1H, NH); **^{13}C NMR** (126 MHz, DMSO-d_6) δ 137.6 (C8a), 130.9 (C6), 126.2 (C3a), 125.9 (C2), 122.3 (C5), 120.3 (C6 or C7), 120.2 (C6 or C7), 114.5 (C3), 112.5 (C4), 109.7 (CH_2); **LRMS** (ES+) calc. for $C_{10}H_{10}N$ $[M+H]^+$ 144.1, found 144.2.

cis and *trans* stereo descriptors are given relative to the indole moiety.

Data consistent with literature values.[61]

(±)-(3a*S*,10a*R*,10b*S*)-2-Phenyl-10-(2,2,2-trifluoroacetyl)-4,5,5a,10,10a,10b-hexahydropyrrolo[3,4-a]carbazole-1,3(2H,3aH)-dione, 2.29

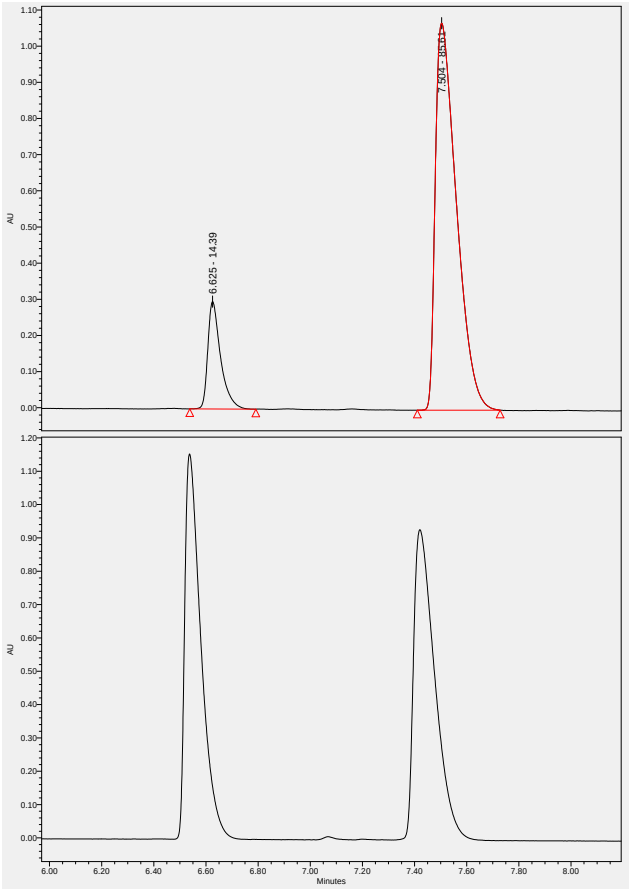


3-Vinyl-indole (200.0 mg, 1.40 mmol, 1.0 equiv.) and N-phenylmaleimide (242.4 mg, 1.40 mmol, 1.0 equiv.) were dissolved in dichloromethane (10 mL) and heated to reflux for 2 h. The reaction mixture was allowed to cool to room temperature, followed by addition of trifluoroacetic anhydride (1.47 mL, 7.00 mmol, 5.0 equiv.) added dropwise, and stirred for 30 minutes. This was then poured onto water (20 mL), the phases separated and the aqueous extracted with dichloromethane (3 × 10 mL). The combined organics were dried ($MgSO_4$) and solvent removed *in vacuo.* The residue was purified by column chromatography (ethyl acetate/ petroleum ether (1:4 to 1:3)) to give (±)-(3a*S*,10a*R*,10b*S*)-2-phenyl-10-(2,2,2-trifluoroacetyl)-4,5,5a,10,10a,10b-hexahydropyrrolo[3,4-a]carbazole-1,3(2H,3aH)-dione as a tan oil (300.2 mg, 0.724 mmol, 52%).

IR (thin film, ν_{max} / cm^{-1}) 2349, 2254, 1707, 1648, 1498, 1463, 1384, 1225, 1209, 1186, 1169, 1150, 1107; **^{1}H NMR** (400 MHz, $CDCl_3$) δ 8.38 (d, *J* = 8.0 Hz, 0.5H), 7.49 (t, *J* = 7.5 Hz, 1H, ArH), 7.36 – 7.25 (m, 4.5H, ArH), 7.22 – 7.12 (m, 1H, ArH), 6.93 (dd, *J* = 15.5, 7.5 Hz, 2H), 6.34 – 6.29 (m, 1H, C5H), 5.13 – 5.09 (m, 0.5H, C9H), 5.04 – 5.01 (m, 0.5H, C9H), 4.49 (t, *J* = 8.0 Hz, 0.5H, C8H), 4.00 (t, *J* = 8.0 Hz, 0.5H, C8H), 3.39 (t, *J* = 8.0 Hz, 1H, C7H), 3.17 (dd, *J* = 15.5, 8.0 Hz, 1H, C6H), 2.39 – 2.30 (m, 1H, C6H'); **^{13}C NMR** (101 MHz, $CDCl_3$) δ 178.0 (C7C=O or C8C=O), 177.5 (C7C=O or C8C=O), 173.8 (C7C=O or C8C=O), 173.0 (C7C=O or C8C=O), 154.6 (q, *J* = 38.5 Hz, *C*CF_3), 154.3(q, *J* = 40.5 Hz, *C*CF_3), 145.0 (*quat* C), 141.0 (*quat* C), 137.3 (*quat* C), 135.6 (*quat* C), 131.5 (*quat* C), 131.4 (*quat* C), 130.6 (*quat* C), 130.4 (ArH), 129.1 (ArH), 128.8, 126.3 (ArH), 126.2 (ArH), 125.6 (*quat* C), 121.3 (ArH), 120.2 (ArH), 119.3 (ArH), 115.3 (ArH), 114.1 (C5), 113.7 (C5), 61.6 (C9), 59.9 (C9), 42.2 (C8), 39.3 (C8), 38.4 (C7), 38.1 (C7), 25.5 (C6); **^{19}F NMR** (377 MHz, $CDCl_3$) δ -70.46, -71.42; **LRMS** (ES+)

calc. for $C_{22}H_{15}F_3N_2O_3Na$ $[M+Na]^+$ 435.1, found 435.0. **[α]D** (*c* = 0.28, ee = 63%, $CHCl_3$): 6.3 °.

The enantiomeric excess was determined by analytical chiral SFC [Chiralpak® IB, 99:1 – 90:10 CO_2 : MeOH over 5 min, 90:10 thereafter, 1.5 $mLmin^{-1}$, t_R(maj) = 7.50 min, t_R (min) = 6.63 min.]



As previously reported, some peak duplication in the ^1H and ^{13}C NMR spectra arose from the presence of rotamers. Data consistent with literature values.[61]

2. 7 References

1. Hölzl-Hobmeier, A. *et al.* Catalytic deracemization of chiral allenes by sensitized excitation with visible light. *Nature* **564**, 240–243 (2018).
2. Barrett, K. T., Metrano, A. J., Rablen, P. R. & Miller, S. J. Spontaneous transfer of chirality in an atropisomerically enriched two-axis system. *Nature* **508**, 71–75 (2014).
3. Feringa, B. L. & van Delden, R. A. Absolute Asymmetric Synthesis: The Origin, Control, and Amplification of Chirality. *Angew. Chemie - Int. Ed.* **38**, 3418–3438 (1999).
4. Blackmond, D. G. The origin of biological homochirality. *Cold Spring Harb. Perspect. Biol.***2**, a002147 (2010).
5. Frank, F. C. On spontaneous asymmetric synthesis. *Biochim. Biophys. Acta* **11**, 459–463 (1953).
6. Girard, C. & Kagan, H. B. Nonlinear Effects in Asymmetric Synthesis and Stereoselective Reactions: Ten Years of Investigation. *Angew. Chemie - Int. Ed.* **37**, 2922–2959 (1998).
7. Soai, K., Niwa, S. & Hori, H. Asymmetric self-catalytic reaction. Self-production of chiral 1-(3-pyridyl)alkanols as chiral self-catalysts in the enantioselective addition of dialkylzinc reagents to pyridine-3-carbaldehyde. *J. Chem. Soc. Chem. Commun.* **14**, 982–983 (1990).
8. Soai, K., Shibata, T., Morioka, H. & Choji, K. Asymmetric autocatalysis and amplification of enantiomeric excess of a chiral molecule. *Nature* **378**, 767–768 (1995).
9. Ercolani, G. & Schiaffino, L. Putting the mechanism of the Soai reaction to the test: DFT study of the role of aldehyde and dialkylzinc structure. *J. Org. Chem.***76**, 2619–2626 (2011).
10. (Palyi, G., Kurdi, R. & Zucchi, C.) *Advances in Asymmetric Autocatalysis and Related Topics* (ELSEVIER ACADEMIC Press, 2017).
11. Kawasaki, T. *et al.* Asymmetric autocatalysis: Triggered by chiral isotopomer arising from oxygen isotope substitution. *Angew. Chemie - Int. Ed.* **50**, 8131–8133 (2011).
12. Kawasaki, T. *et al.* Asymmetric autocatalysis triggered by carbon isotope (^{13}C/ ^{12}C) chirality. *Science* **324**, 492–495 (2009).
13. Hawbaker, N. A. & Blackmond, D. G. Rationalization of Asymmetric Amplification via Autocatalysis Triggered by Isotopically Chiral Molecules. *ACS Cent. Sci.***4**, 776–780 (2018).
14. Blackmond, D. G., McMillan, C. R., Ramdeehul, S., Schorm, A. & Brown, J. M. Origins of asymmetric amplification in autocatalytic alkylzinc additions *J. Am. Chem. Soc.* **123**, 10103–10104 (2001).
15. Buono, F. G. & Blackmond, D. G. Kinetic evidence for a tetrameric transition state in the asymmetric autocatalytic alkylation of pyrimidyl aldehydes. *J. Am. Chem. Soc.* **125**, 8978–8979 (2003).

16. Schiaffino, L. & Ercolani, G. Amplification of chirality and enantioselectivity in the asymmetric autocatalytic Soai reaction. *ChemPhysChem* **10**, 2508–2515 (2009).

17. Athavale, S., Simon, A., Houk, K. N. & Denmark, S. Demystifying the Soai Reaction. *ChemRxiv* (2019). doi:10.26434/chemrxiv.8979845.v1

18. Storch, G. & Trapp, O. By-design enantioselective self-amplification based on non-covalent product-catalyst interactions. *Nat. Chem.* **9**, 179–187 (2017).

19. Mikami, K. & Matsukawa, S. Asymmetric synthesis by enantiomer-selective activation of racemic catalysts. *Nature* **385**, 613–615 (1997).

20. Pirkle, W. H., Murray, P. G., Rausch, D. J. & McKenna, S. T. Intermolecular 1 H− 1 H Two-Dimensional Nuclear Overhauser Enhancements in the Characterization of a Rationally Designed Chiral Recognition System. *J. Org. Chem.* **61**, 4769–4774 (1996).

21. Wang, B. & Sutherland, I. O. Self-replication in a Diels–Alder reaction. *Chem. Commun.* 1495–1496 (1997).

22. Kindermann, M., Stahl, I., Reimold, M., Pankau, W. M. & Von Kiedrowski, G. Systems chemistry: Kinetic and computational analysis of a nearly exponential organic replicator. *Angew. Chemie - Int. Ed.* **44**, 6750–6755 (2005).

23. Doyle, A. G. & Jacobsen, E. N. Small-molecule H-bond donors in asymmetric catalysis. *Chem. Rev.* **107**, 5713–5743 (2007).

24. Pihko, P. M. *Hydrogen bonding in organic synthesis*. (WILEY-VCH, 2009).

25. Takemoto, Y. Recognition and activation by ureas and thioureas: Stereoselective reactions using ureas and thioureas as hydrogen-bonding donors. *Org. Biomol. Chem.* **3**, 4299–4306 (2005).

26. Berkessel, A., Cleemann, F., Mukherjee, S., Müller, T. N. & Lex, J. Highly efficient dynamic kinetic resolution of azlactones by urea-based bifunctional organocatalysts. *Angew. Chemie - Int. Ed.* **44**, 807–811 (2005).

27. Sun, L., Wu, X., Xiong, D. C. & Ye, X. S. Stereoselective Koenigs–Knorr Glycosylation Catalyzed by Urea. *Angew. Chemie - Int. Ed.* **55**, 8041–8044 (2016).

28. Sonsona, I. G., Marqués-López, E., Häring, M., Díaz, D. D. & Herrera, R. P. Urea activation by an external brønsted acid: Breaking self-association and tuning catalytic performance. *Catalysts* **8**, 305 (2018).

29. Borissov, A. *et al.* Organocatalytic enantioselective desymmetrisation. *Chemical Society Reviews* **45**, 5474–5540 (2016).

30. Wang, P. A. Organocatalyzed enantioselective desymmetrization of aziridines and epoxides. *Beilstein J. Org. Chem.* **9**, 1677–1695 (2013).

31. Schneider, C. Catalytic, enantioselective ring opening of aziridines. *Angew. Chemie - Int. Ed.* **48**, 2082–2084 (2009).

32. Li, Z., Fernández, M. & Jacobsen, E. N. Enantioselective ring opening of meso aziridines catalyzed by tridentate Schiff base chromium(III) complexes. *Org. Lett.* **1**, 1611–1613 (1999).

33. Wu, B., Gallucci, J. C., Parquette, J. R. & RajanBabu, T. V. Enantioselective desymmetrization of meso-aziridines with TMSN3 or TMSCN catalyzed by discrete yttrium complexes. *Angew. Chemie - Int. Ed.* **48**, 1126–1129 (2009).

34. Mita, T. *et al.* Catalytic enantioselective desymmetrization of meso-N-acylaziridines with TMSCN. *J. Am. Chem. Soc.* **127**, 11252–11253 (2005).

35. Cao, Y. M., Zhang, F. T., Shen, F. F. & Wang, R. Catalytic enantioselective ring-opening reaction of meso-aziridines with α-isothiocyanato imides. *Chem. - A Eur. J.* **19**, 9476–9480 (2013).

36. Zhang, J., Cao, D., Wang, H., Zhao, G. & Shang, Y. Enantioselective desymmetrization of meso-aziridines with aromatic thiols catalyzed by chiral bifunctional quaternary phosphonium salts derived from α-amino acids. *Tetrahedron* **71**, 1785–1791 (2015).

37. Mita, T. & Jacobsen, E. N. Bifunctional asymmetric catalysis with hydrogen chloride: Enantioselective ring opening of aziridines catalyzed by a phosphinothiourea. *Synlett* **2009**, 1680–1684 (2009).

38. Kamioka, S., Ajami, D. & Rebek, J. Synthetic autocatalysts show organocatalysis of other reactions. *Chem. Commun.* **47**, 7324–7326 (2009).

39. Zweep, N. *et al.* Balancing hydrogen bonding and van der waals interactions in cyclohexane-based bisamide and bisurea organogelators. *Langmuir* **25**, 8802–8809 (2009).

40. De Loos, M., Friggeri, A., Van Esch, J., Kellogg, R. M. & Feringa, B. L. Cyclohexane bis-urea compounds for the gelation of water and aqueous solutions. *Org. Biomol. Chem.* **3**, 1631–1639 (2005).

41. Kulkarni, C., Berrocal, J. A., Lutz, M., Palmans, A. R. A. & Meijer, E. W. Directing the Solid-State Organization of Racemates via Structural Mutation and Solution-State Assembly Processes. *J. Am. Chem. Soc.* **141**, 6302–6309 (2019).

42. Namutebi, M., McGarrigle, E. M. & Aggarwal, V. K. Ring-Opening of NH-Aziridines with Thiols in Ionic Liquids: Application to the Synthesis of Aminosulfide Catalysts for Asymmetric Epoxidation of Aldehydes. *Phosphorus. Sulfur. Silicon Relat. Elem.* **185**, 1250–1272 (2010).

43. Cheng, C.-Y., Lu, H.-Y., Lee, F.-M. & William Tam, S. Synthesis of (1′, 2′-trans)-3-phenyl-1-[2′-(N-pyrrolidinyl)cyclohexyl]-pyrrolid-2-ones as κ-selective opiates. *J. Pharm. Sci.* **79**, 758–762 (1990).

44. Monaco, M. R. *et al.* Activation of Carboxylic Acids in Asymmetric Organocatalysis. *Angew. Chemie - Int. Ed.* **53**, 7063–7067 (2014).

45. Row, R. D., Shih, H.-W., Alexander, A. T., Mehl, R. A. & Prescher, J. A. Cyclopropenones for Metabolic Targeting and Sequential Bioorthogonal Labeling. *J. Am. Chem. Soc.* **139**, 7370–7375 (2017).

46. Krasnova, L. B. & Yudin, A. K. Novel nitrogen containing chelating ligands from aziridines — Preparation, coordination studies, and catalytic application in the cyclopropanation of styrene. *Can. J. Chem.* **83**, 1025–1032 (2005).

47. Wittkopp, A. & Schreiner, P. R. Metal-Free, Noncovalent Catalysis of Diels–Alder Reactions by Neutral Hydrogen Bond Donors in Organic Solvents and in Water. *Chem. - A Eur. J.* **9**, 407–414 (2003).

48. Carey, F. A. & Sundberg, R. J. *Advanced organic chemistry*. (Springer, 2007).

49. Okino, T., Hoashi, Y., Furukawa, T., Xu, X. & Takemoto, Y. Enantio- and diastereoselective michael reaction of 1,3-dicarbonyl compounds to nitroolefins catalyzed by a bifunctional thiourea. *J. Am. Chem. Soc.* **127**, 119–125 (2005).

50. Sigman, M. S., Vachal, P. & Jacobsen, E. N. A General Catalyst for the Asymmetric Strecker Reaction. *Angew. Chemie - Int. Ed.* **39**, 1279–1281 (2000).

51. Wang, J., Li, H., Yu, X., Zu, L. & Wang, W. Chiral Binaphthyl-Derived Amine-Thiourea Organocatalyst-Promoted Asymmetric Morita−Baylis−Hillman Reaction. *Org. Lett.* **7**, 4293–4296 (2005).

52. Bringmann, G., Breuning, M. & Tasler, S. The lactone concept. *Synthesis* **1999**, 525–558 (1999).

53. Bringmann, G. *et al.* The lactone concept - A novel approach to the metal-assisted atroposelective construction of axially chiral biaryl systems. *J. Organomet. Chem.* **661**, 31–47 (2002).

54. Fletcher, S. P., Dumur, F., Pollard, M. M. & Feringa, B. L. Chemistry: A reversible, unidirectional molecular rotary motor driven by chemical energy. *Science* **310**, 80–82 (2005).

55. Ma, G., Deng, C., Deng, J. & Sibi, M. P. Dynamic kinetic resolution of biaryl atropisomers by chiral dialkylaminopyridine catalysts. *Org. Biomol. Chem.***16**, 3121–3126 (2018).

56. Fugard, A. J. *et al.* Hydrogen-Bond-Enabled Dynamic Kinetic Resolution of Axially Chiral Amides Mediated by a Chiral Counterion. *Angew. Chemie - Int. Ed.* **58**, 2795–2798 (2019).

57. Alajarin, M. *et al.* Exploring the Conversion of Macrocyclic 2,2′-Biaryl Bis(thioureas) into Cyclic Monothioureas: An Experimental and Computational Investigation. *J. Org. Chem.* **83**, 14022–14035 (2018).

58. Sohtome, Y. *et al.* Organocatalytic asymmetric nitroaldol reaction: Cooperative effects of guanidine and thiourea functional groups. *Chem. - An Asian J.* **2**, 1150–1160 (2007).

59. Herrera, R. P., Sgarzani, V., Bernardi, L. & Ricci, A. Catalytic enantioselective Friedel-Crafts alkylation of indoles with nitroalkenes by using a simple thiourea organocatalyst. *Angew. Chemie - Int. Ed.* **44**, 6576–6579 (2005).

60. Gimeno, M. C. & Herrera, R. P. Hydrogen Bonding Networks in Chiral Thiourea Organocatalysts: Evidence on the Importance of the Aminoindanol Moiety. *Cryst. Growth Des.* **16**, 5091–5099 (2016).

61. Gioia, C., Hauville, A., Bernardi, L., Fini, F. & Ricci, A. Organocatalytic asymmetric Diels-Alder reactions of 3-vinylindoles. *Angew. Chemie - Int. Ed.* **47**, 9236–9239 (2008).

62. Vallavoju, N. *et al.* Evaluating Thiourea Architecture for Intramolecular [2+2] Photocycloaddition of 4-Alkenylcoumarins. *Adv. Synth. Catal.* **356**, 2763–2768 (2014).

63. Sibi, M. P. & Itoh, K. Organocatalysis in conjugate amine additions. Synthesis of β-amino acid derivatives. *J. Am. Chem. Soc.* **129**, 8064–8065 (2007).

64. Lattanzi, A. Asymmetric Morita-Baylis-Hillman reaction catalyzed by simple amino alcohol derived thioureas. *Synlett* **2007**, 2106–2110 (2007).

65. Alcaine, A., Marqués-López, E., Merino, P., Tejero, T. & Herrera, R. P. Thiourea catalyzed organocatalytic enantioselective Michael addition of diphenyl phosphite to nitroalkenes. *Org. Biomol. Chem.* **9**, 2777–2783 (2011).

66. Sonsona, I. G., Marqués-López, E. & Herrera, R. P. The aminoindanol core as a key scaffold in bifunctional organocatalysts. *Beilstein Journal of Organic Chemistry* **12**, 505–523 (2016).

67. Schön, E. M., Marqués-Lõpez, E., Herrera, R. P., Alemán, C. & Díaz, D. D. Exploiting molecular self-assembly: From urea-based organocatalysts to multifunctional supramolecular gels. *Chem. - A Eur. J.* **20**, 10720–10731 (2014).

68. Blackmond, D. G. Kinetic aspects of nonlinear effects in asymmetric catalysis. *Acc. Chem. Res.* **33**, 402–411 (2000).

69. Li, N. *et al.* Asymmetric amplification in phosphoric acid catalyzed reactions. *Angew. Chemie - Int. Ed.* **49**, 6378–6381 (2010).

70. Klussmann, M. *et al.* Thermodynamic control of asymmetric amplification in amino acid catalysis. *Nature* **441**, 621–623 (2006).

71. Viedma, C. Chiral symmetry breaking during crystallization: Complete chiral purity induced by nonlinear autocatalysis and recycling. *Phys. Rev. Lett.* **94**, 065504 (2005).

72. Swift, G. & Swern, D. Chemistry of Epoxy Compounds. XX. Stereospecific Syntheses of Cis and Trans-1, 2-Diaminocyclohexanes and Aliphatic Vicinal Diamines. *J. Org. Chem.***32**, 511–517 (1967).

73. Wu, B., Gallucci, J. C., Parquette, J. R. & RajanBabu, T. V. Enantioselective Desymmetrization of *meso* -Aziridines with TMSN $_3$ or TMSCN Catalyzed by Discrete Yttrium Complexes. *Angew. Chemie - Int. Ed.* **48**, 1126–1129 (2009).

74. Subbaraj, A., Rao, O. S. & Lwowski, W. Functionalization of olefins by alkoximidoylnitrenes. *J. Org. Chem.* **54**, 3945–3952 (1989).

75. Izdebski, J. & Pawlak, D. No Title. *Synthesis* **1989**, 423–425 (1989).

76. Zhang , M. *et al.* Efficient Copper(II)-Catalyzed Transamidation of Non-Activated Primary Carboxamides and Ureas with Amines. *Angew. Chemie - Int. Ed.* **51**, 3905–3909 (2012).

77. Nagar, S., Singh, H. H., Sinha, J. N. & Parmar, S. S. Anticonvulsant and cardiovascular effects of substituted thiazolidones. *J. Med. Chem.* **16**, 178–180 (1973).

78. Hassner, A., Matthews, G. J. & Fowler, F. W. Stereochemistry. XLI. Reduction of .beta.-iodo azides. Stereospecific synthesis of aziridines. *J. Am. Chem. Soc.* **91**, 5046–5054 (1969).

79. Schreiner, P. R. & Wittkopp, A. H-bonding additives act like lewis acid catalysts. *Org. Lett.* **4**, 217–220 (2002).

80. Joyce, L. L. & Batey, R. A. Heterocycle Formation via Palladium-Catalyzed Intramolecular Oxidative C−H Bond Functionalization: An Efficient Strategy for the Synthesis of 2-Aminobenzothiazoles. *Org. Lett.* **11**, 2792–2795 (2009).

81. Chinnappan, A. *et al.* Transition metal based ionic liquid (bulk and nanofiber composites) used as catalyst for reduction of aromatic nitro compounds under mild conditions. *RSC Adv.* **3**, 3399 (2013).

82. Kreighbaum, W. E. & Scarborough, H. C. 6-Amino Derivatives of 5H-Dibenzo[d,f][1,3]diazepine. *J. Med. Chem.* **7**, 310–312 (1964).

83. Hu, Z. *et al.* Simple copper/TEMPO catalyzed aerobic dehydrogenation of benzylic amines and anilines. *Org. Biomol. Chem.* **10**, 1618 (2012).

84. Sydnes, L., Elmi, S., Heggen, P., Holmelid, B. & Malthe-Sørensen, D. Conversion of Azobenzenes into *N*,*N* ′-Diarylhydrazines by Sodium Dithionite. *Synlett* **2007**, 1695–1698 (2007).

85. Schmid, R., Cereghetti, M., Heiser, B., Schönholzer, P. & Hansen, H.-J. Axially Dissymmetric Bis(triaryl)phosphines in the Biphenyl series: Synthesis of (6,6′-dimethylbiphenyl-2,2′-diyl)bis(diphenylphosphine) ('BIPHEMP') and analogues, and their use in Rh(I)-catalyzed asymmetric isomerizations of *N*,*N* -diethylnerylamine. *Helv. Chim. Acta* **71**, 897–929 (1988).

86. Mistry, N. & Fletcher, S. P. Phosphoramidite Ligands Based on Simple 1,2-Diols: Synthesis, Use in Copper-Catalyzed Asymmetric Additions, and Achirotopic Stereogenic Phosphorus Centres. *Adv. Synth. Catal.* **358**, 2489–2496 (2016).

87. Atzrodt, J., Beckert, R. & Darsen, A. Synthesis of new axial chiral diisothiocyanates. *Tetrahedron Asymmetry* **8**, 2257–2260 (1997).

88. Batail, N. *et al.* First heterogeneous ligand- and salt-free Larock indole Synthesis. *Adv. Synth. Catal.* **351**, 2055–2062 (2009).

89. Zhu, D. *et al.* Enantioselective Intramolecular C−H Insertion of Donor and Donor/Donor Carbenes by a Nondiazo Approach. *Angew. Chemie - Int. Ed.* **55**, 8452–8456 (2016).

90. Goulet-Hanssens, A. *et al.* Electrocatalytic *Z* → *E* Isomerization of Azobenzenes. *J. Am. Chem. Soc.* **139**, 335–341 (2017).

91. Carlin, R. B. & Allen Heininger, S. The Benzidine Rearrangement. VI. The Rearrangement of 3,3′,5,5′-Tetrafluorohydrazobenzene in 2:1 Sulfuric Acid. *J. Am. Chem. Soc.***77**, 2272–2277 (1955).

92. Takeda, Y., Okumura, S. & Minakata, S. Oxidative dimerization of aromatic amines using *t*BuOI: Entry to unsymmetric aromatic azo compounds. *Angew. Chemie - Int. Ed.***51**, 7804–7808 (2012).

93. Levin, J. R., Cheisson, T., Carroll, P. J. & Schelter, E. J. Accessing relatively electron poor cerium(iv) hydrazido complexes by lithium cation promoted ligand reduction. *Dalt. Trans.* **45**, 15249–15258 (2016).

94. Florvall, L., Fagervall, I., Larsson, L.-G. & Ross, S. B. Prodrugs of neuron-selective monoamine oxidase inhibitors: amino acid derivatives of 1-(4-aminophenyl)-2-aminopropanes. *Eur. J. Med. Chem.* **34**, 137–151 (1999).

95. Reavill, D. R. & Richardson, S. K. Synthesis of Polysubstituted Aromatic Acids Using an Intramolecular Benzyne Cyclisation. *Synth. Commun.* **20**, 1423–1436 (1990).

96. Del Pozo, S., Vera, S., Oiarbide, M. & Palomo, C. Catalytic Asymmetric Synthesis of Quaternary Barbituric Acids. *J. Am. Chem. Soc.* **139**, 15308–15311 (2017).

97. Gottarelli, G. *et al.* Induction of the cholesteric mesophase in nematic liquid crystals: mechanism and application to the determination of bridged biaryl configurations. *J. Am. Chem. Soc.* **105**, 7318–7321 (1983).

98. Zhao, A. *et al.* $K_2S_2O_8$ -mediated nitration of alkenes with $NaNO_2$ and 2,2,6,6-tetramethylpiperidine-1-oxyl: stereoselective synthesis of (*E*)-nitroalkenes. *Tetrahedron Lett.* **57**, 80–84 (2016).

99. Roshandel, S., Gurung, L., Mathew, T. & Prakash, G. K. S. Chloro/bromotrimethylsilane-$Cu(NO_3)_2 \cdot 3H_2O$: Safe and efficient reagent system for the decarboxylative ipso-nitration and dibromination of cinnamic acids. *Tetrahedron Lett.* **58**, 2842–2845 (2017).

100. Yang, L. *et al.* A thiourea-functionalized metal–organic macrocycle for the catalysis of Michael additions and prominent size-selective effect. *Dalt. Trans.* **46**, 4086–4092 (2017).

101. An, L. T., Zou, J. P., Zhang, L. L. & Zhang, Y. Sulfamic acid-catalyzed Michael addition of indoles and pyrrole to electron-deficient nitroolefins under solvent-free condition. *Tetrahedron Lett.* **48**, 4297–4300 (2007).

Chapter 3

Replicating lipids and protocell behaviour

Chapter 3

Replicating lipids and protocell behaviour

Work in this chapter was in part undertaken in collaboration with Dhanya Babu (DB) and Dr. Rémi Plamont (RP), members of Nathalie Katsonis's group at University of Twente. All the experiments in section 3.2 were designed and performed jointly with DB and RP. ^{1}H NMR kinetics described in section 3. 5. 4 were designed and performed by RP. Chemicals in section 3.2 were synthesised by RJHS.

3. 1 Introduction

3. 1. 1 The role of directed motion in biology

Arguably the most widely used directed movement in life, chemotaxis is the movement towards or away from a chemical signal.[1] It is found at almost all length scales of biology and its usefulness is attested by the diverse mechanisms by which it is achieved. Chemotaxis enables prokaryotes to overcome diffusion in how they search for resources and avoid poisons.[2] For multicellular eukaryotes chemotactic cellular movements are key from the beginning of life, guiding sperm to egg and also controlling many processes of developmental biology.[3,4] It retains a central role in later life too, essential to wound healing and aiding inflammatory cells toward pathogens during infection.[5] Recent studies show that chemotaxis can even cause enzymes to travel toward higher concentrations of substrates, increasing metabolic efficiency through the colocalization of enzymes into metabalons.[6]

One powerful way chemotaxis is used is in spatial organisation, allowing through-space interaction between cells. The movement of cells in response to a chemical signal emitted by cells of the same type is known as autochemotaxis. At its simplest, positive or negative autochemotaxis enables microorganisms organise into functional structures beneficial to survival without hierarchical management or an overall blue-print, a phenomenon known as quorum sensing.[7,8] However, when multiple signals are combined, far more complex behaviour can be achieved, notably through the formation of Turing patterns.[9] In animals this allows in development initially uniform groups of cells to differentiate into separate cell lineages, forming complex tissues. Use of autochemotaxis as a dynamic and responsive self-assembly will surely be inspiration to supramolecular chemists for many years to come.

The methods by which chemotaxis is achieved depends on the length scale being operated in. At the cellular level chemotaxis is achieved generally through either the use of specific and highly complex organelles such flagella and cilia, or deformation and concomitant change of surface adhesion properties of the cell boundary, which is typically characterised by pseudopod formation.[7] Across the domains of bacteria and archaea the extremely high degree of conservation in certain genes required for assembly of flagella, levels usually only associated with transcriptional machinery, further attest to the evolutionary importance of directed motion.[10]

The challenge of powering and controlling motion at small length scales is hinted at in Richard Feynman's endearing lecture "There's Plenty of Room at the Bottom", now seen as a call to arms for nanoscientists.[11] In it he imagined a variant of a von Neumann machine, a device able to create copies of itself at one quarter scale. At some point, the materials must fail, be it because of viscous forces or materials sticking together due to van de Waals interactions. The difficulty for engineering motion on small length scales is

exemplified by being in a low Reynolds number regime, put simply viscous effects dominate over inertia.[12] This means propulsion much be achieved through deformations which are "non-reciprocal" in time, such as the turning of a corkscrew rather than the flapping of rigid fins. This is sometimes referred to as Scallop theorem.[13]

Though the role of movement in prebiotic systems is largely unexplored, the Mann group reported a system of protocells which showed chemotaxis in 2018.[14] The protocells had a semi-porous outer layer formed from clay and a central cavity containing two antagonistic enzymes (catalase and glucose oxidase) and DNA. In conditions containing high concentration of hydrogen peroxide, there is a net production of molecular oxygen within the protocell, reducing its density causing the protocell to arise in the water column. However, in conditions of low peroxide concentration and high glucose concentration, there is a net consumption of oxygen, leading to increased density and the protocells sink. In this manner, protocells were made to oscillate up and down over a centimetre length scale. Though impressive, this is proved a limited means of locomotion; other protocell architectures such as proteinosomes, coacervates and lipid vesicles were not suitable due to inelasticity or small size.

Building artificial systems with the properties of life, such as artificial cells, is a grand challenge within the natural sciences receiving increasing attention.[15,16] Though inspiration can be drawn from biology, how information can be transferred across lengths scales to elucidate function, all in a controlled manner, is daunting. It is not obvious how to make chemical processes which can translate or transfer into the physical processes needed to make viable artificial cells.[17] Coupling autocatalysis to other chemical, physical and biologically relevant processes is required for development of prebiotic models and artificial cells, which needs the chemistry to occur within complex mixtures.

3. 1. 2 Self-propelled systems

Knowledge of self-propelled objects on surface of water has a surprisingly long history, being familiar in Edo period Japan (1603-1868) in the form of the "floating doll" toy and the so-called camphor boat has been known in Europe since at least the 17th Century.[18–20] An amusing early report of self-propelled motion is conveyed to us in the letters of Benjamin Franklin,[21] where "an ingenious pupil" of a Yorkshire schoolmaster told him of "an odd appearance which had lately occurred to him":

"[He] threw upon the water [a pond] some flies that had been drowned in oil. These flies presently began to move, and turned round on the water very rapidly, as if they were vigorously alive, though on examination they were not so."

Fortunately Franklin was able to *"show that it was not any effect of life recovered in the flies, I imitated it by … paper cut in the form of a comma, of the size of a common fly; oil issuing from the point made the comma turn round"*[21]

Over the past 30 years a great profusion of self-propelled micro- and nano-scale objects have been made and studied.[22–24] These have typically been studied for fundamental interest rather than function, although the goal of using them as vectors for drug delivery has achieved much attention.[23,25,26] Also models for self-propelled objects which can clear up after oil spills have been developed.[27] Magnetic helical nanorods, based on their tumbling rate, can be used to measure local viscosity within heterogeneous environments at micrometer resolution.[28]

The most common mechanism of propulsion is probably the platinum-catalysed decomposition of hydrogen peroxide to oxygen and water.[29–31] Typically objects, be they rods, Janus spheres or even "micro-gears"[32] are constructed to be asymmetric, part made from gold and part from platinum. Motion is generally attributed to bubble generation,

however there are other contributing factors such as diffusiophoresis and self-electrophoresis which depend on scale.[33]

Other self-propulsion mechanisms of Janus particles include the ruthenium-catalysed polymerisation of a norbornene fuel,[34] asymmetric photo-decomposition of silver chloride[35] and local demixing of a solvent mixture close to criticality.[36] The motion of "artificial flagella" made of magnetic colloidal particles attached to red blood cells is controlled through oscillating magnetic field.[37]

Main research areas within the field include making systems which respond to their environment, and studying collective motion to mimic biology. So far, microswimmers have been studied which show directed motion in response to many stimuli, among which are light,[35,38] thermal gradients,[39] concentration gradients of chemicals,[40,41] electric fields[42] and magnetic fields.[37]

Collective motion has been extensively modelled and there are a number of experimental realisations.[43–45] Many microswimmers can show phase behaviour, transitioning between solid-like aggregates, liquid-like clustering which have a higher degree of motion and a gas-like phase with little or no mutual interaction.[46] Highly asymmetric particles can induce more complex collective behaviours, such as the formation of radiate structures known as asters, various clustering patterns and collective oscillations.[47,48]

3. 1. 3 Marangoni microswimmers

One of the simplest designs for a self-propelled objects are droplets of a hydrophobic oil, typically 10-1000 μm in diameter within an aqueous phase containing surfactant, so called Marangoni microswimmers (see figure 3. 1. 3. 1).[49] The mechanism by which motion occurs is discussed in detail in section 3. 2. 2. 1, but essentially involves asymmetric distribution of surfactant on the droplet surface causing surface tension

gradients which give rise to bulk fluid flows and motion. Droplets are attractive protocell models owing to their remarkable simplicity and generality, they may be formed from almost any two immiscible fluids under gentle agitation.[50,51]

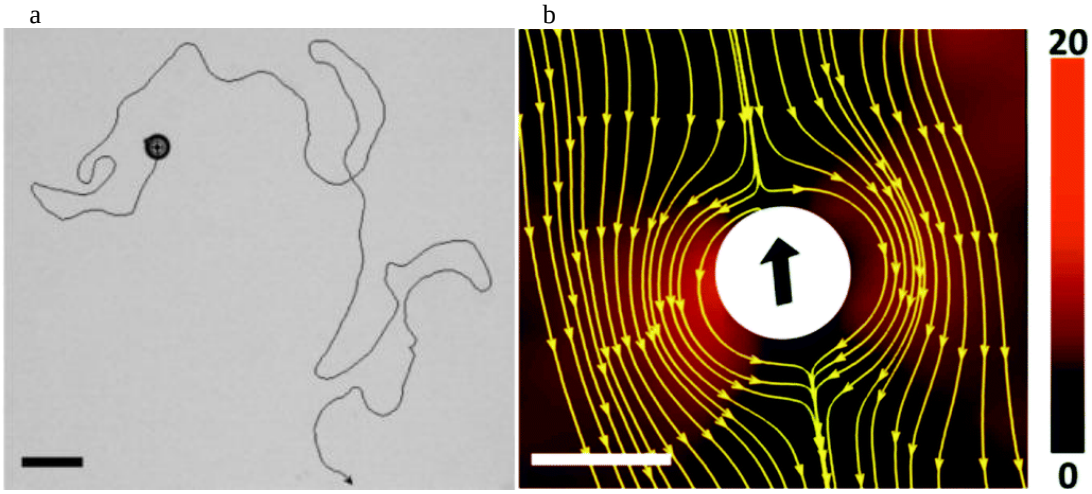


Figure 3. 1. 3. 1. Marangoni microswimmers – droplets as self-propelled objects. a – Path of a Marangoni microswimmer droplet made of squalene propelling in an aqueous medium containing 50 mM oleate surfactant. Scale bar = 300 µm. Reproduced with permission.[52] *b – Velocity field of the aqueous medium surrounding a Marangoni microswimmer droplet, relative to the reference frame of the droplet, obtained using a particle image velocimetry technique. Black arrow denotes the direction of motion of the droplet, and the yellow arrows the motion of the aqueous phase. Speed of the aqueous motion is indicated by the colour of the background, with a scale to the right in units of* μms^{-1}*. Scale bar = 100 µm. Reproduced with permission.*[53]

Despite their apparent simplicity Marangoni microswimmers can show complex function, such as collective behaviour. A well characterised example of this is negative autochemotaxis, droplets avoid each other's paths as there is a region depleted of micelles in the trail of a droplet, demonstrated by Jin et al. (Figure 3. 1. 3. 2).[40] Experiments in a microfluidic device with symmetric bifurcating channels were used to quantify the effect. They found a strong anticorrelation between the paths of sequential droplets, up to 90% at short times. This anticorrelation decays exponentially with time over a period of minutes. In this study they were also able to demonstrate maze-solving ability of these droplets,

moving up a concentration gradient of surfactant. Other types of collective behaviour such as clustering have been shown to be controllable through means as simple as the shape and dimensions of their environment.[54]

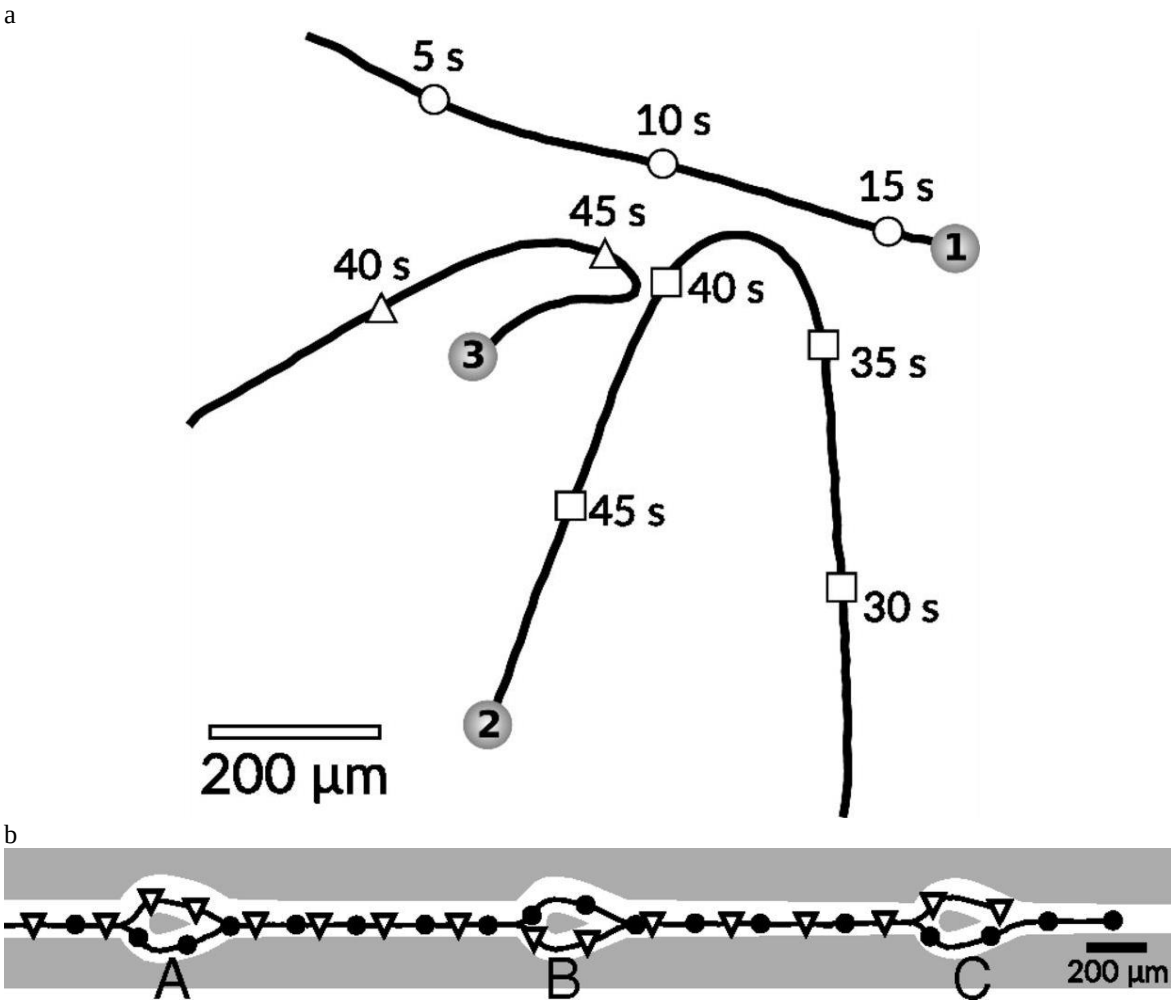


Figure 3. 1. 3. 2. Autochemotaxic effects within microswimmers. a – paths of three Marangoni swimmers (labelled 1, 2 and 3) within a field of surfactant containing aqueous. Time points along these paths are shown in seconds and marked with circles, squares and triangles for swimmers 1, 2 and 3 respectively. Swimmers avoid crossing the paths of others. b – paths of two sequential Marangoni swimmers through a PDMS microfluidic device, one marked with circles and the other triangles. Path avoidance leads to sequential swimmers alternating path within gates with equivalent trajectories. Reproduced with permission.[40]

Coupling the motion of these microswimmers to a chemical reaction offers a way to provide control and possibly develop complexity. In 2007 the group of Sugawara reported

a system of chemically driven self-propelled droplets (Figure 3. 1. 3. 3).[55] There is striking resemblance to the work Luisi, however the kinetics of Sugawara's system are not well established.[56] Here 0.2 µL oil drops of oleic anhydride in nitrobenzene were placed into an aqueous phase containing 10 mM oleate micelles. These drops were observed to self-propel and vesicles of oleate form in the aqueous, presumably due to reduced pH. Nature of the propulsion is complex, they report a series of stages, starting from spherically symmetric drops, gradually small structures form within the oil which show oscillatory motions. These motions subsequently synchronise and motion of the droplet begins. Whilst the work is pioneering in the field, there remain a number of open questions surrounding this study. Monitoring fluorescence of fluorescein added to the aqueous phase, they inferred a lowered pH in the trail of the droplets consistent with a self-generated pH gradient. They propose this is due to expulsion of oleic acid from the rear of the drops, but do not establish if the assumption of homogeneous fluorescein concentration is valid. The mechanism of movement and extent to which chemistry is coupled to this remains largely ambiguous.

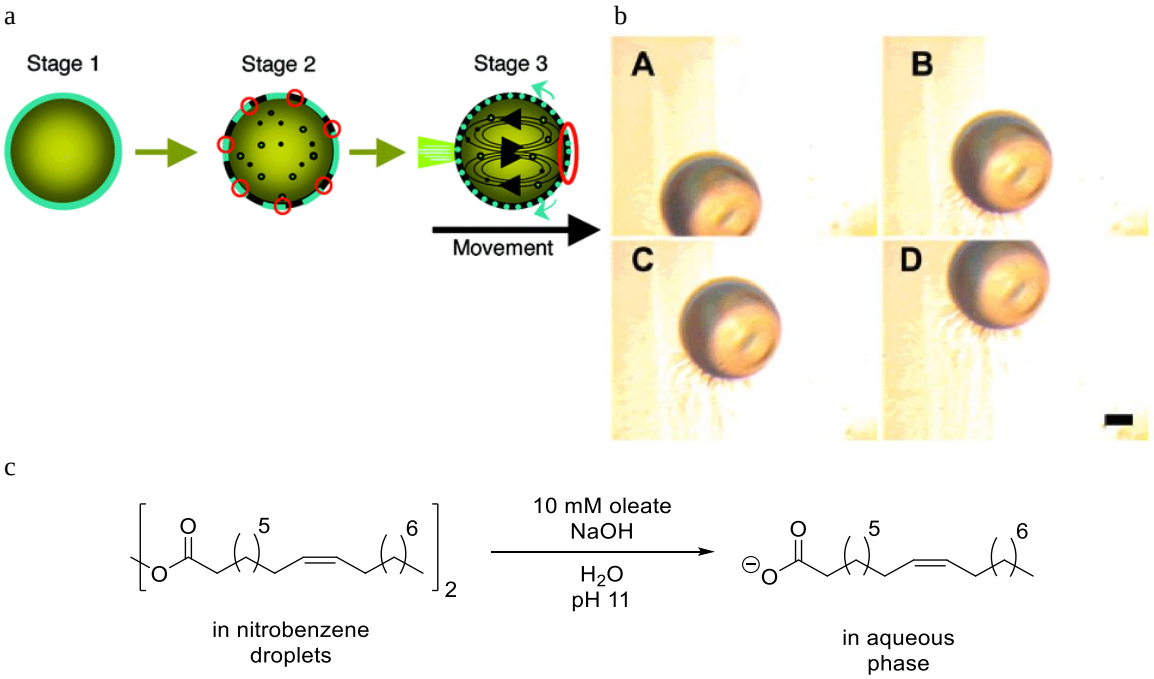


Figure 3. 1. 3. 3. Chemically driven droplets reported by Hanczyc et al.[55] *a – schematic diagram of the onset of motion in this system based on visual appearance. The authors divide this into stages: Stage 1, droplets are spherically symmetric and transparent; stage 2, the droplets begin to look turbid and internal structures form, supposed hydrolysis sites are circled in red; stage 3, spontaneous symmetry breaking occurs followed by motion. Motion of surfactant is shown by the blue arrows, and internal convection [sic] by the black arrows, b – a series of microscope images, A-D, taken at 2 s intervals showing the motion of a droplet. A "tail" of surfactant material can be seen at the rear of the moving droplet. Scale bar = 100 μm. c – chemical reaction proposed to cause the motion, hydrolysis of oleic anhydride contained within the droplets to oleate. Reproduced with permission.*[55]

A second system of fuel consuming self-propelled droplets was reported in 2009 based on distinct chemistry.[57] Here an imine amphiphile undergoes hydrolysis in the presence of 4-octylaniline droplets containing a fluorescent imidazole catalyst (Figure 3. 1. 3. 4). The location of reaction, extent of catalyst leaching and background hydrolysis rate are not investigated. Background hydrolysis rate is likely to be high as at t = 0 min only 80% of the precursor imine is available. It was observed that motion did not require the reaction, with motion also occurring in the presence of inert TTAB.

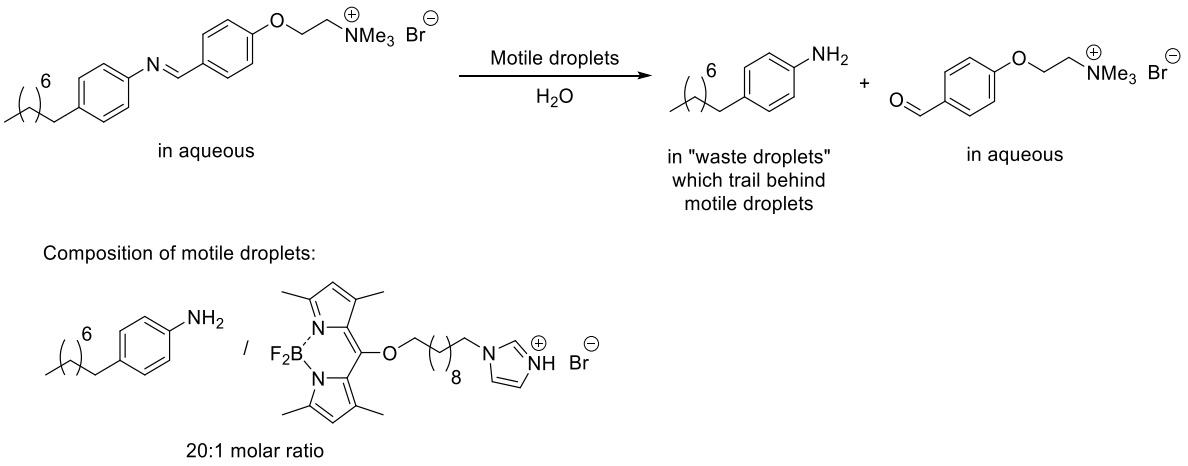


Figure 3. 1. 3. 4. Fuel consuming droplets of Toyota et al.[57] *An imine undergoes hydrolysis in the presence of an imidazole containing catalyst.*

Control is often poor in these systems; to the best of my knowledge only a single example of reversible change to the surfactant has been reported. Here negative phototaxis is induced upon UV irradiation of droplets in a medium containing a surfactant which has an azobenzene motif which undergoes a *cis-trans* isomerism.[58]

Light has also been used in irreversible processes to drive droplet motion (Figure 3. 1. 3. 5). 2-Nitrobenzyl oleate droplets stabilised with oleic acid of roughly 100 μm in diameter were prepared in pH 9.2 buffer. On exposure to UV light directional motion towards the light source (positive phototaxis) was observed. Motion was dependant on light, turning the lamp on and off resulted in starting and stopping droplet movement, which could be repeated several times. The effect can be explained by removal of the photoactive 2-nitrobenzyl protective group from oleate occurring faster in brighter light, leading to a larger surface concentration of oleate on the illuminated side and thus Marangoni stresses.[59] There have been a handful of further reports of reaction driven self-propelled droplets, either were a surfactant is formed[60,61] or chemically altered.[62,63]

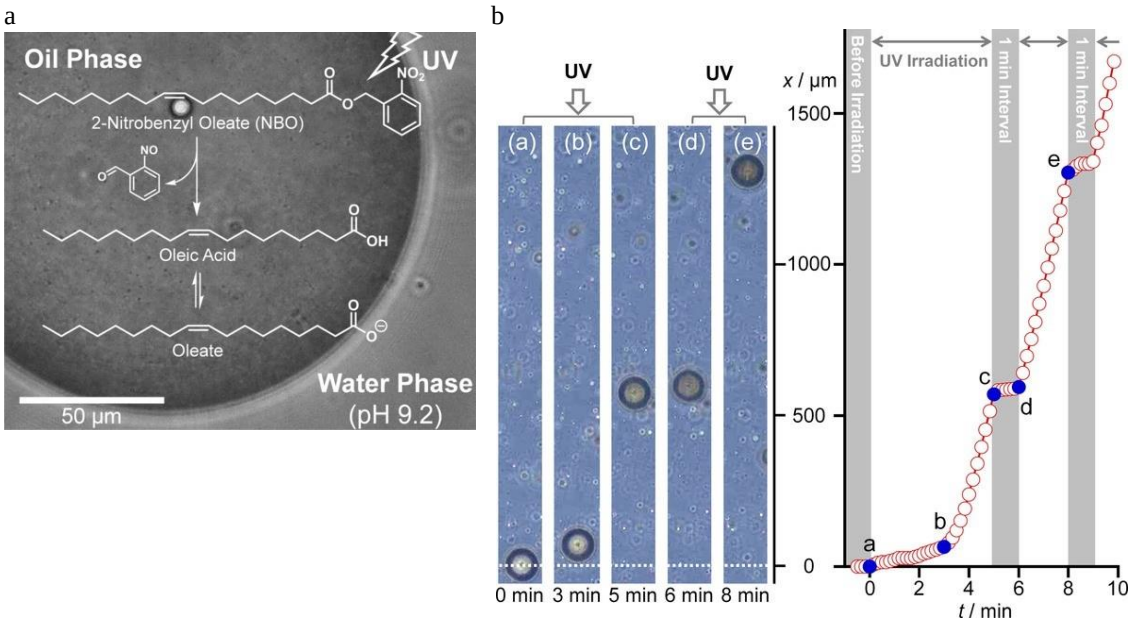


Figure 3. 1. 3. 5. A Marangoni microswimmer which moves towards UV light source. a – Diagram of the system design, showing 2-nitrobenzyl oleate which forms the oil phase of the drops undergoing photodecomposition to oleic acid and 2-nitrosobenzaldehyde. Oleate drives motion of the droplets through the Marangoni effect. b – A series of microscope images, (a)-(e), showing the motion of a droplet towards a light source. Time since beginning of the first irradiation is shown below. The graph to the right shows the displacement of the droplet with respect to time, showing that the droplet moves significantly faster when irradiated with UV light than not. Adapted with permission.[40]

It is worth noting that many motile droplet systems gain their function through interaction with an interface, such as a solid-liquid interface of the bottom of a container, or the liquid-air interface.[64–67] The work described in section 3.2 concerns the Marangoni swimmer type droplets and section 3.3 concerns droplets at an interface. Typically "surface drops" are propelled by some combination of: 1) the same factors effecting Marangoni swimmers and 2) interface specific effects such as stresses induced from asymmetric contact angles. The mechanism of propulsion in these systems is often poorly understood, with the droplets moving much faster than Marangoni swimmers.[64,68] Whilst Marangoni swimmers are typically spherical to minimise interfacial surface tension, surface drops are typically deformed, flattened out in the plane of the surface they interact with.[69]

A fascinating example of moving surface drops involves the maze solving droplets developed by Lagzi and coworkers (Figure 3. 1. 3. 6).[70] Here 1 µL droplets of mineral oil or DCM doped with between 20-60% (v/v) of 2-hexyldecanoic acid (HDA) were observed to move towards areas of low pH. Mazes were constructed in PDMS, then filled with pH 12.0-12.3 KOH solutions. A pH 1.2 HCl soaked agarose gel was placed at the exit and was left for 30-40 s. The droplets generally "solved" the 1.5 x 1.5 cm mazes in 1-3 minutes. Due to the high velocities of the droplets, up to around 10 mms^{-1}, compared to the observed Marangoni flows (around 0.1 mms^{-1}) another explanation of motion was required. They propose the droplet slowly leaches HDA into the aqueous, and the surface tension of the water-air interface around the drop is asymmetric, as the side nearer the acid source has a larger ratio of protonated to deprotonated HDA than the rear. Whilst mineral oil based droplets moved slower than DCM based ones, they were more likely to take the shortest path. Similar systems have been shown to respond to salt concentration, with chemotaxis towards higher NaCl concentrations being observed.[41] This was attributed to the salt lowering surface tension in decanoate solutions.

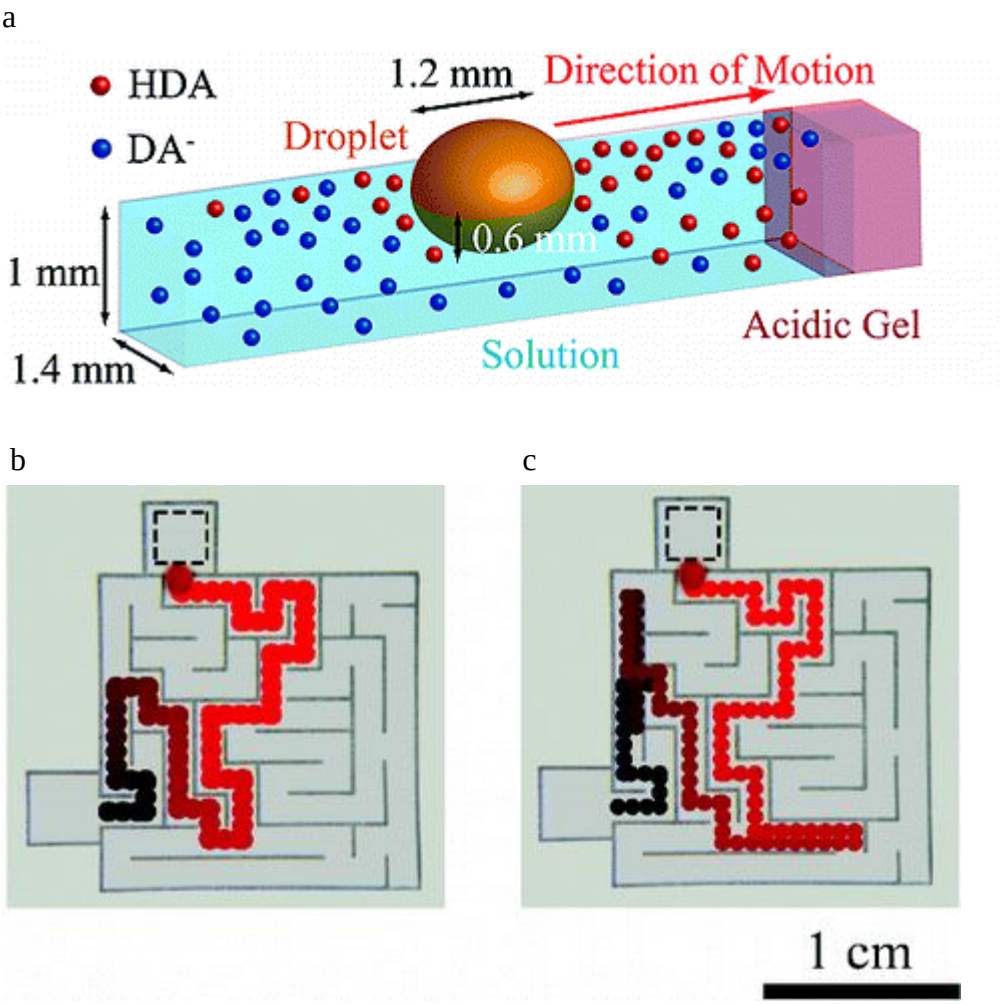


Figure 3. 1. 3. 6. Maze solving surface droplets which show directional motion towards regions of low pH. a – Schematic diagram of a droplet within the maze track. HDA – 2-hexyldecanoic acid, DA^- – 2-hexyldecanoate. b and c – Paths of two 20% (v/v) HDA in DCM droplets, both of which solve the maze. The lighter the shade of red of the position markers the later the time. Adapted with permission.[70]

3. 1. 4 Aims and design

Due to the prior literature we believed that inducing motion in droplets using self-replicating lipids would be achievable (Figure 3. 1. 4. 1). We were also interested to see if other functions could be induced, such as the division of droplet protocells. In autocatalytic lipid forming reactions physical effects such as the container shape and stirring rate have enormous effect reaction rate, see section 4. 2. 2 for an extreme example. The effect of motion or other droplet behaviour on the lipid forming reaction were unknown, although it seemed likely that the two processes may be interrelated. We

expected mechanism of motion in the protocells to be similar to that of known Marangoni microswimmers (Figure 3. 1. 4. 2).

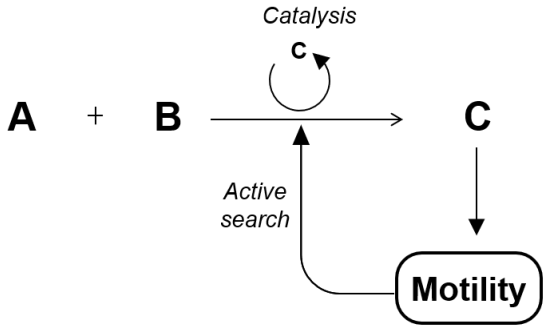


*Figure 3. 1. 3. 1. Conceptual image of the interaction between a reaction forming a self-replicating lipid, **C**, and the movement of protocells.*

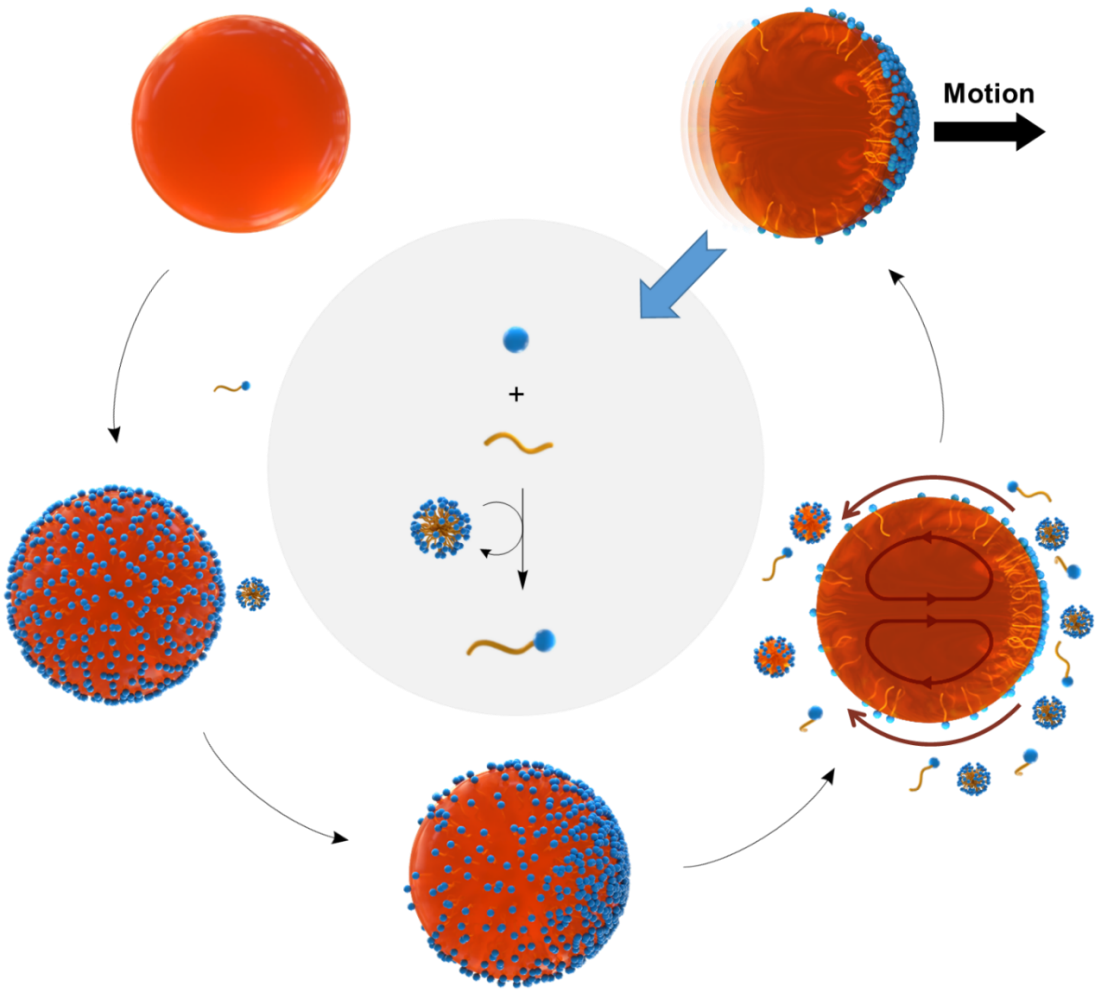


Figure 3. 1. 3. 2. System design. Lipid forming chemistry is highlighted in grey. A hydrophobic component (yellow line) and hydrophilic component (blue circle) react to form a lipid (yellow line attached to blue

circle). This process is catalysed by supramolecular aggregates of product. Interaction with droplet protocells is shown outside the grey circle. Initially droplets would become associated with lipid molecules through diffusion. Then a spontaneous symmetry breaking event leads to a polarisation in lipid coverage on the surface of the droplet. This polarisation leads to surface flows and flows of the bulk fluids. These flows lead to motion of the droplet. Interaction between motion and lipid synthesis is indicated by the blue arrow.

3. 2 Self-propelling protocells and lipid replicators

3. 2. 1 Initial findings

Droplets of a number of oils were prepared by microfluidic techniques, see section 3. 5. 1. We initially tested aqueous solutions of lipids **3.1** and **3.2** for droplet behaviour (Figure 3. 2. 1. 1). Mineral oil, silicone oil and hydrocarbons resulted in no behaviour, however octanol resulted in visible effects. In solutions of **3.2**, after some time there was the appearance of "whirling droplets" (Figure 3. 2. 1. 2). Here, small aqueous droplets are enveloped within the octanol droplets, and these small droplets rapidly move around, presumably driven by surface flows around the exterior octanol-aqueous interface (see also ESI video 1). In solutions of **3.1**, the droplets displayed rapid and sustained self-propulsion, moving many times their length over a period of seconds. As motion also required surface flows, we hypothesised these were two related behaviours, choosing to follow up on what could be achieved with **3.1**.

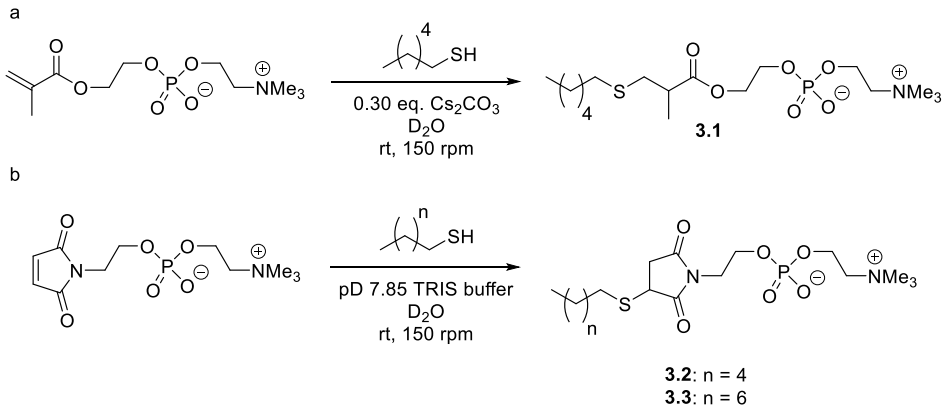


*Figure 3. 2. 1. 1. Lipids **3.1** and **3.2** tested for ability to induce droplet behaviour. Autocatalysis forming **3.1** and **3.3** has previously been studied by the Fletcher group under the conditions shown.*[71,72]

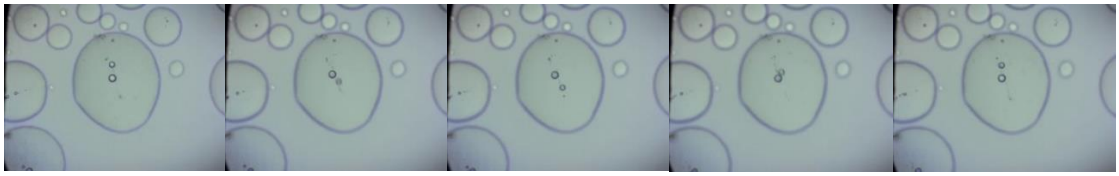


Figure 3. 2. 1. 2. Sequential snapshots of a video of "whirling droplets". Here, small aqueous droplets can be seen within large organic phase droplets, themselves within a bulk aqueous phase. The large droplets remain stationary, whilst the internal droplets move rapidly under an advective flow.

3. 2. 2 Optimised system

Finding that lipid **3.1** gave rise to motion, we were quickly able to find conditions to form it *in situ* which also resulted in droplet movement, based on the initial report of autocatalysis.[71] The setup is described in section 3. 5. 3. 1, and consists of forming a solution of MPC and Cs_2CO_3 in water, dispersing 1-hexanethiol as an emulsion within this and adding the droplets. See ESI video 2 for motion of these droplets under these reaction conditions.

Varying the concentration of **3.1**, at low concentrations, no propulsion was observed. Above a critical propulsion concentration (CPC) of 28 mM the average droplet speed was found to increase linearly with concentration up to around 120 mM, where speed plateaus at around 55 μms^{-1} (Figure 3. 2. 2. 1B). This maximum velocity is likely caused by lipid

transfer from micelles to the droplet surface becoming rate limiting.[52] Larger droplets move faster up until a diameter of around 120 µm (Figure 3. 2. 2. 1C). This has been proposed to be because larger droplets maintain a larger surfactant coverage gradient between leading and trailing edge.[73] As the droplets move octanol dissolves into the aqueous phase, as a result the propelling droplets decreasing in diameter by about 15% during the period of motion.

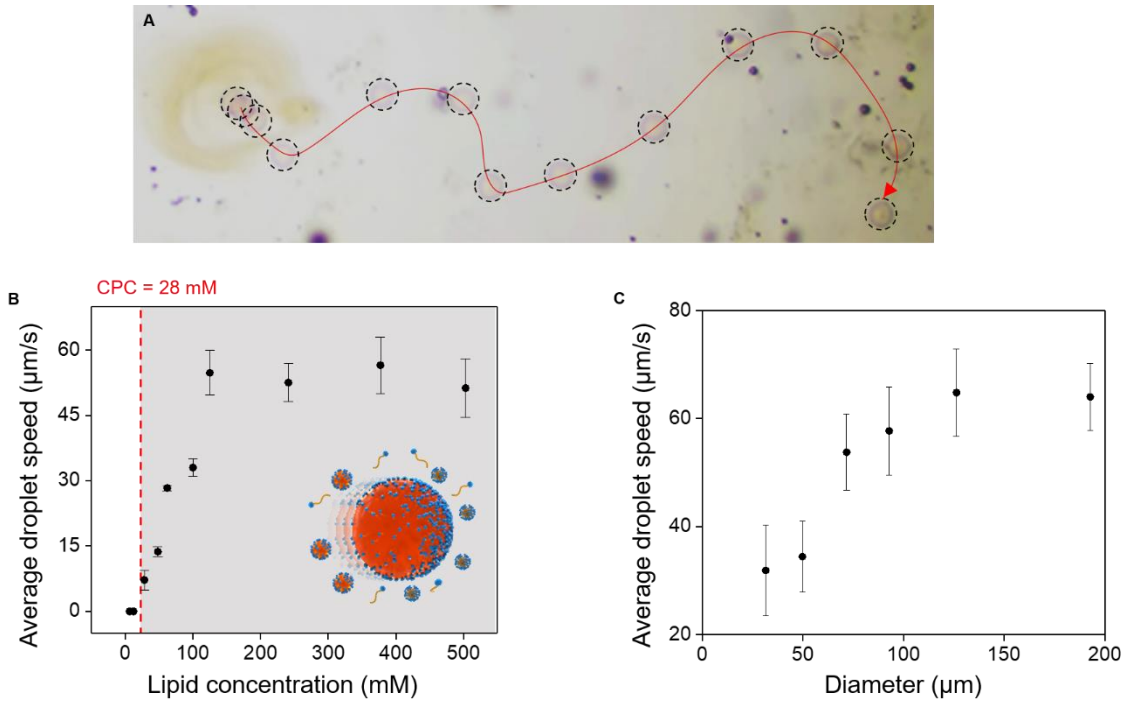


Figure 3. 2. 2. 1. Nature of motion of droplet protocells within optimised system. See ESI video 3. A – Path of one droplet tracked over a period of 80 seconds from the onset of motion, B – Mean droplet speed for 50 µm droplets at different lipid concentrations. Each point is the average of 5 droplets, error bars show one standard deviation. Below the critical propulsion concentration (dashed red line) no motion was observed. C – Mean speed of droplets of differing diameters, from ***3.1*** *formed in situ. Each point is the average of 5 droplets, error bars show one standard deviation.*

The speed profiles of individual droplets show fast changes in speed though rapid accelerations (Figure 3. 2. 2. 2A). This is due to stochasticity in micelle binding events to the leading edge of the droplet (see section 3. 2. 2. 1 for a discussion of mechanism). The complexity of droplet motion can be seen visually. Firstly there is a slow growth of a

corona of large aggregates around the droplet, which must contain octanol dissolved from the droplet due to its colour (Figure 3. 2. 2. 2B). After a long time, typically 10 to 25 minutes, the corona begins to expand away, forming a parachute shape. Shortly after the droplet begins to move, accelerating quickly to its average velocity. The lag phase is defined to be the period of time between mixing the lipid precursors and when a particular droplet begins moving. The lag phase is between 10 and 25 minutes and increases linearly with droplet diameter (Figure 3. 2. 2. 2D). We propose that for larger droplets a larger surfactant coverage difference is required to create the critical surface tension gradient needed to begin advective flows, and hence they have higher CPCs.

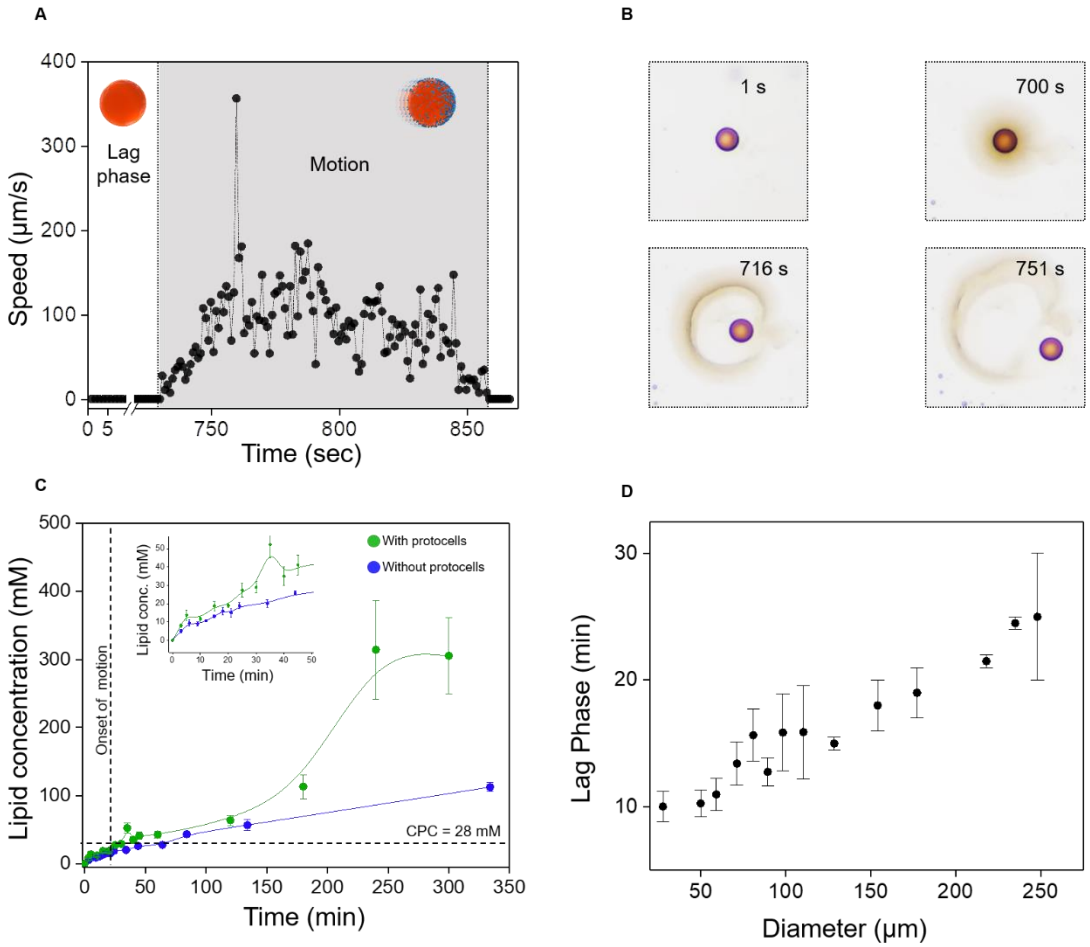


Figure 3. 2. 2. 2. Mutualism between lipid forming reaction and droplet motion. A – Speed of a single 100 μm octanol droplet over time. B – Snapshot images of the 100 μm octanol droplet shown in A and its aqueous environment at different time points. C – Kinetics of formation of surfactant ***3.1****. This was recorded*

in the presence (green) and absence (blue) of 150 µm octanol droplets. Experiments were performed in triplicate, error bars show one standard deviation. D – Relationship between lag phase and droplet diameter. Each point is the average of 5 droplets, error bars show one standard deviation.

Reaction kinetics of the system was studied by ^{1}H NMR spectroscopy, using 150 µm droplets (Figure 3. 2. 2. 2C). The lag phase for these droplets is 25 minutes, after which time the concentration of **3.1** formed is 25-30 mM, consistent with the CPC of 28 mM previously measured (Figure 3. 2. 2. 1B). Interestingly, not only does the lipid forming reaction cause motion of the droplets, motion accelerates the chemical reaction, a mutualistic effect. Whilst the droplets are stationary, the rate profiles of lipid formation are similar (before 25 mins). After the onset of motion, the rate of formation of lipid is higher in the presence of droplets than without (after 25 mins). The cause of the rate enhancement is thought to be chemotaxis of the droplets.

To demonstrate protocell chemotaxis experiments were designed where thiol was localised in bulk regions rather than dispersed through the aqueous (see section 3. 5. 3. 1 for details). Droplets were observed to move highly selectively towards the thiol reservoir, with all droplets moving in this direction (Figure 3. 2. 2. 3A). Motion is driven by lipid **3.1**, therefore the droplets actively move towards regions of higher concentration. Octanol droplets accelerate as they approach regions of thiol (Figure 3. 2. 2. 3B). Droplets of differing oil compositions, and therefore physical properties, were raced to compare their abilities to move (Figure 3. 2. 2. 3C). Octanol droplets moved significantly faster than those made of decanol, moving an average of 6 times the distance in the same time period. In an environment where motion was connected to some advantage, be it feeding or avoiding negative influences, there is an obvious analogy to fitness.

The Péclet number of a system quantifies the ratio of transport rates due to advection and diffusion. Marangoni microswimmers move in a high Péclet number regime (typically

100-1000), meaning advective, ie. bulk, flows of material outcompete diffusion.[74] This allows the mixing induced by motion to accelerate the reaction. Chemotaxis causes mixing (and therefore rate enhancement) within both the setup seen in figure 3. 2. 2. 3 where thiol is present in large droplets and also when thiol is dispersed through the aqueous as an emulsion. Here there are thiol-rich and thiol-poor regions through partial phase separation and in some droplet videos these can be seen by a hazy appearance.

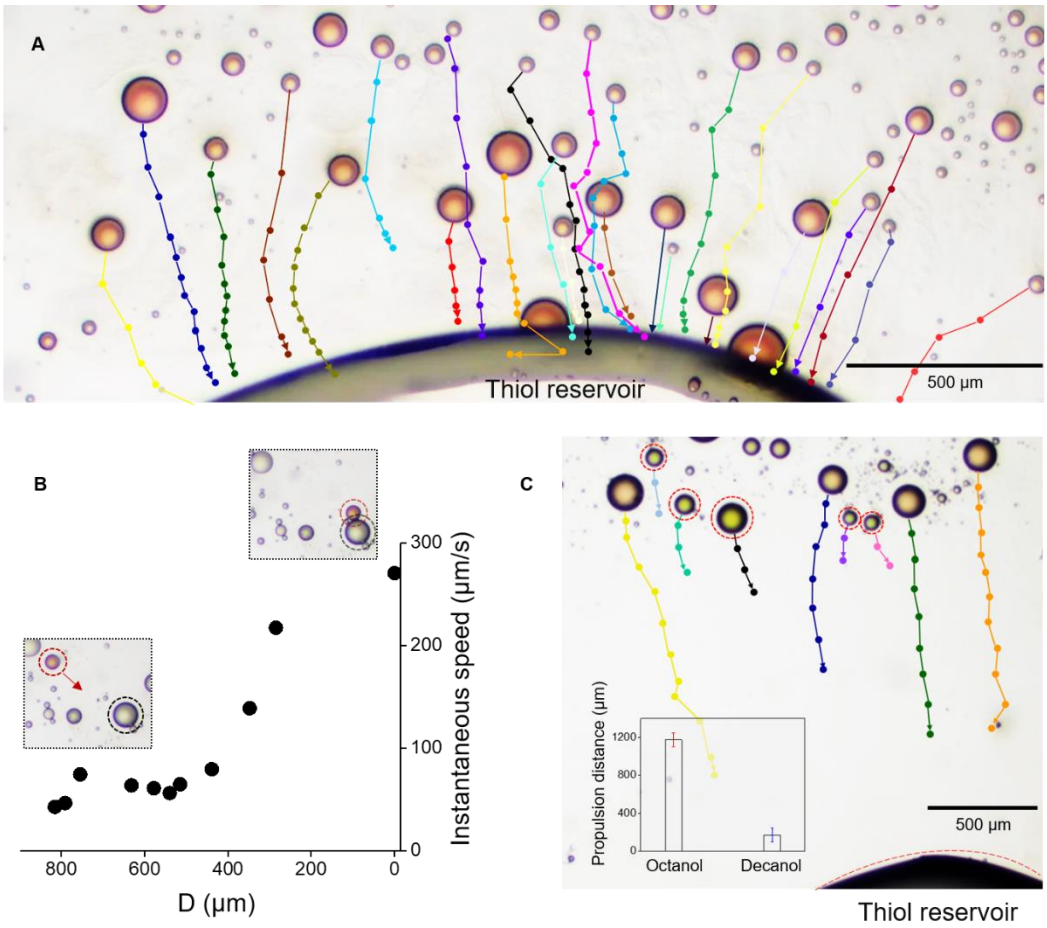


Figure 3. 2. 2. 3. Chemotaxis in droplet protocells. A – Motion of octanol droplets (dyed red) towards a 1-hexanethiol reservoir. Paths of individual droplets are tracked in different colours. See ESI video 4. B – Speed of a single 50 µm octanol droplet (circled red, inset) as it approaches a 1-hexanethiol droplet (circled blue, inset). D is the distance between the nearest edges of the thiol and octanol droplets. C – Competition experiment between octanol (dyed red, uncircled) and decanol (dyed yellow, circled red) droplets. Octanol droplets move an average of 6 times faster. n = 5, error bars show one standard deviation. See ESI video 5.

3. 2. 2. 1 Mechanism of motion

The mechanism of motion in our system appears to be similar those of previously reported Marangoni microswimmers.[53,75,76] The Marangoni effect is familiar on the macroscopic scale from its role in the "tears of wine", and is used to describe how surface tension gradients result in surface flows. Self-propelled droplets can have contributions from Marangoni effect, surfactant dissolution effects from the front of the droplet, phase transitions and separation of material from the back of the droplet. Generally the first is dominant, and in our case there is likely little or no contribution from surfactant dissolution as we are in a low surfactant regime for the beginnings of motion. Though some splitting is seen to the rear of the particle and there is shrinkage, this is assumed also to be negligible contributor to motion.

In homogeneous conditions, onset of motion requires spontaneous symmetry breaking, with the droplet being initially being spherically symmetric and becoming polarised in surface density of surfactant. The process of micelles coming to the surface arises from diffusion. Micelles diffuse in the aqueous phase, adsorb to the droplet surface when they come into contact. Aggregated surfactant is required for motion, the CPC (28 mM for 50 µm droplets) is greater than or equal to the CMC (20.8 mM), as unaggregated surfactant cannot generate large enough radial flows to initiate motion.[53] Increased local coverage of surfactant is the spontaneous symmetry breaking event.

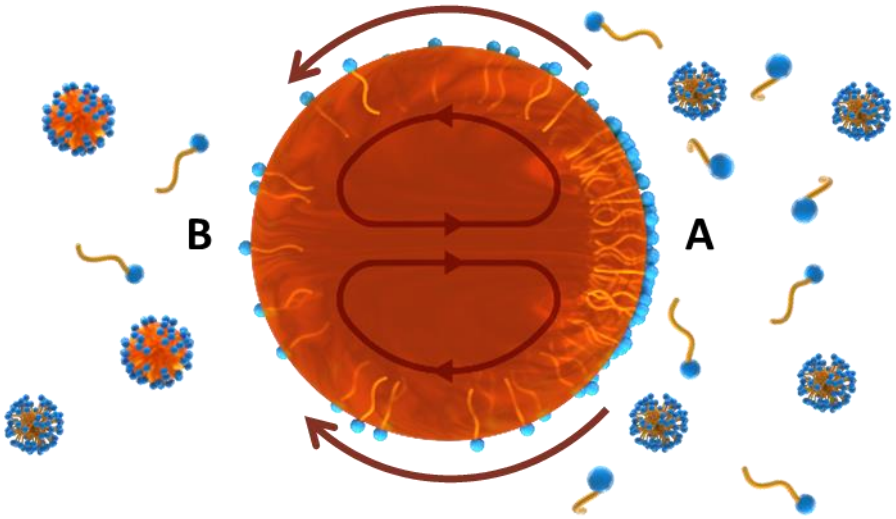


Figure 3. 2. 2. 1. 1. Diagram of bulk flows in Marangoni swimmers. Figure adapted with permission.[77]

Motion in Marangoni swimmers occurs when surfactant is asymmetrically distributed on the surface of the drop, away from the equilibrium distribution. Imagine a droplet where side A has stochastically more surfactant bound than side B (Figure 3. 2. 2. 1. 1). Presence of surfactant at the oil-water interface reduces local surface tension, γ, thus there will be lower surface tension on side A. The gradient of γ leads to a Stokes flow around the edge of the droplet from A to B, propelling the droplet in the direction B to A. Movement of the droplet induces a gradient of surfactant in the surrounding aqueous phase, as there is a surfactant depleted zone behind the droplet.[74] Thus more surfactant binds to side A leading to a reinforcement of the surfactant distribution, maintaining a steady state. At sufficiently high micelle concentration, the rate of micelle adsorption to the front surface is greater than the rate of advection of surfactant to back of droplet, sustaining motion.

As previously stated, the droplets move in the high Péclet number regime, the droplets move faster than surfactant diffuses around it into the surfactant depleted region trailing behind the droplet.[74] At long times, where the droplet has adsorbed an equilibrium coverage and distribution of surfactant, the motion stops.

Chemotaxis in this system arises from lipid gradients within the aqueous phase. Lipid **3.1** is produced near the thiol droplets as an interfacial reaction between 1-hexanethiol and MPC. This creates a gradient of **3.1**, decreasing with distance from the thiol reservoir. Rather than symmetry breaking on the droplet surface being stochastic, in this case the face closest the thiol has a higher surrounding concentration of **3.1**, micelle binding is more likely and moving up the concentration gradient sustains directed motion.

The nomenclature surrounding the type of motion present in Marangoni swimmers is somewhat confusing. The motion is described as diffusiophoresis,[39] as it is due to a concentration gradient of a chemical, in this case a surfactant. Where the droplets are active in homogeneous environments this is described as self-diffusiophoresis, as they induce the surfactant gradient as they move.[78] However in the presence of an external gradient, such as under chemotaxis conditions, then this is described as diffusiophoresis with contributions from self-diffusiophoresis.

3. 3 Behaviour of large drop protocells

3. 3. 1 Prior work

Gutierrez et al. reported in 2014 a robotic platform built for the automated evolution of oil mixtures, where diverse behaviours were observed.[79] To a Petri dish containing a basic surfactant-containing aqueous phase (20 mM TTAB, 5 M NaOH) was added 4 x 5 µL droplets of oil. The oils used were mixtures of 1-pentanol, 1-octanol, diethyl phthalate and either dodecane or 1-octanoic acid. The behaviour of the drops was recorded by a camera mounted above the dish and analysed using image tracking software. The authors observe many complex behaviours, each dependant on droplet composition (Figure 3. 3. 1. 1). Using this as a starting point, we wished to take one of the surfactant-forming autocatalytic reactions developed in the group and apply this to the

coupling of autocatalysis and physical processes. Ideally this would lead to changes that could be observed on a macroscopic scale.

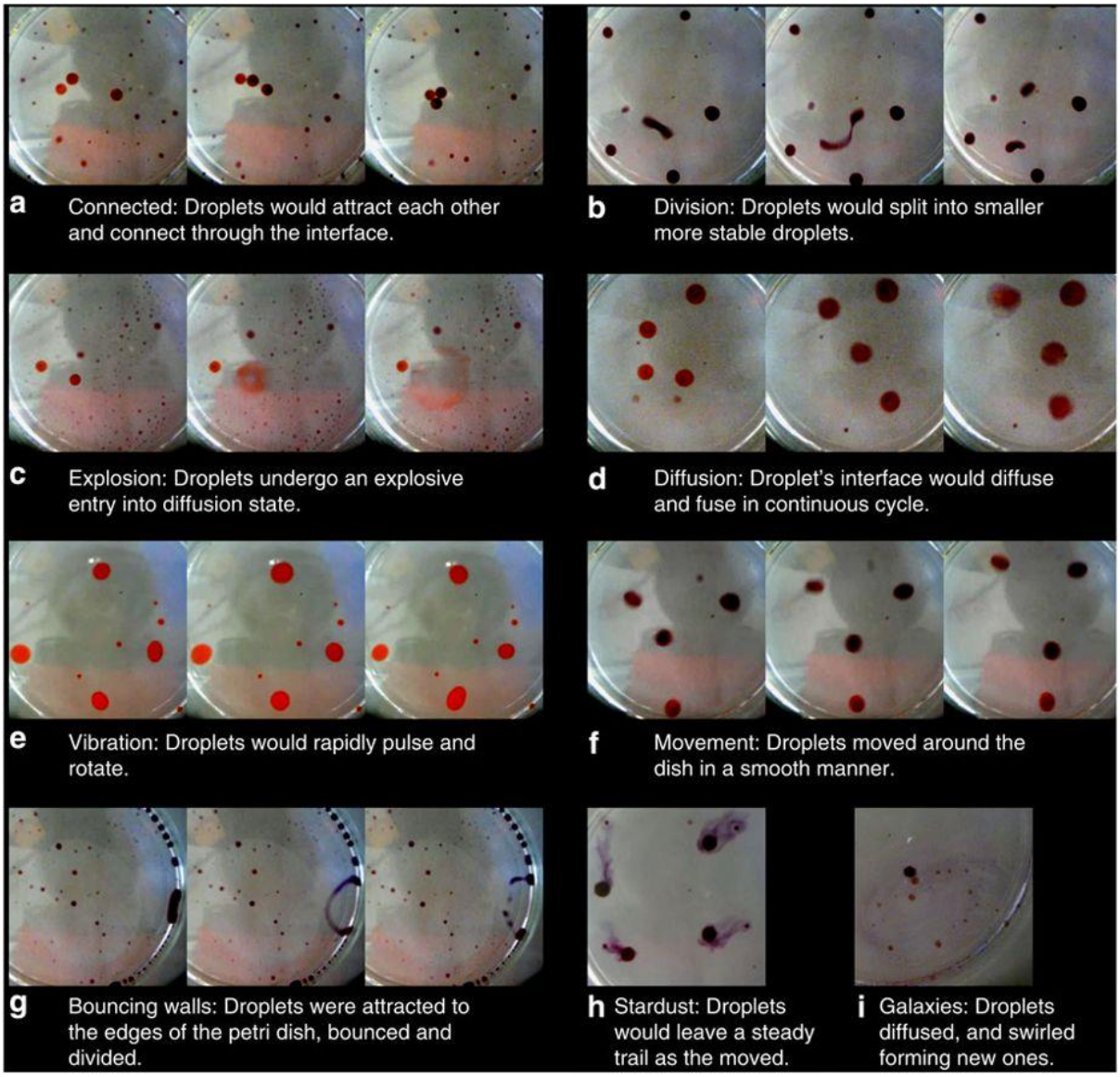


Figure 3. 3. 1. 1. The nine distinct behaviours identified by Gutierrez et al. by eye in oil drops. Each oil composition has differing proportions of dodecane, 1-pentanol, 1-octanol and diethyl phthalate. The aqueous phase was the same in all cases. Oils were dyed with Sudan III dye. Where a letter has multiple images, each is a snapshot in time, proceeding left to right. Reproduced with permission.[79]

The report drew our attention for a number of reasons. Firstly, with a relatively small diversity of oil composition a great number of behaviours or "phenotypes" were observed. Secondly, these behaviours were general enough that many arbitrary starting compositions showed behaviour that in a few (typically up to 21) rounds of evolution

could be optimised by a fitness parameter to a level where the behaviour was visually impressive and distinct.

The authors propose that the principle physical and chemical phenomena which lead to instability of the drops and cause motion are: deprotonation of the oil (likely only appreciable for octanoic acid), dissolution of the oil into the aqueous media, and dynamics arising from surface tension effects which group together as the Marangoni effect. When mixtures of the oils are used, complex behaviour likely arises from the different solubilities of the components leading to composition changes in time.

Initial aims of our study were to identify if certain oils in the mixtures imparted certain properties, or if behaviours arose as a result of the composition as a whole. Secondly the composition of aqueous phase is not discussed and may well not be optimal for our purposes, so we wished to investigate its role. Coupling self-replication with compartment division was the long-term aim for the project.[80] Figure 3. 3. 1. 2 shows three autocatalytic lipid forming reactions developed by the Fletcher group which seemed plausible candidates for this goal. In this study we envisaged that the alkyl thiol component would be present in the hydrophobic droplets and undergo reaction with the hydrophilic component dissolved in the aqueous phase.

The choice of oils used in the Gutierrez et al. study were octanol, pentanol, diethyl phthalate and octanoic acid or dodecane and it is unclear how arbitrary a choice that was. Except for a study by Nagai et al. where the division and motion of pentane droplets was found to be driven by a combination of Marangoni flows and evaporation, little is known about the effect of these oils on droplet behaviour.[81]

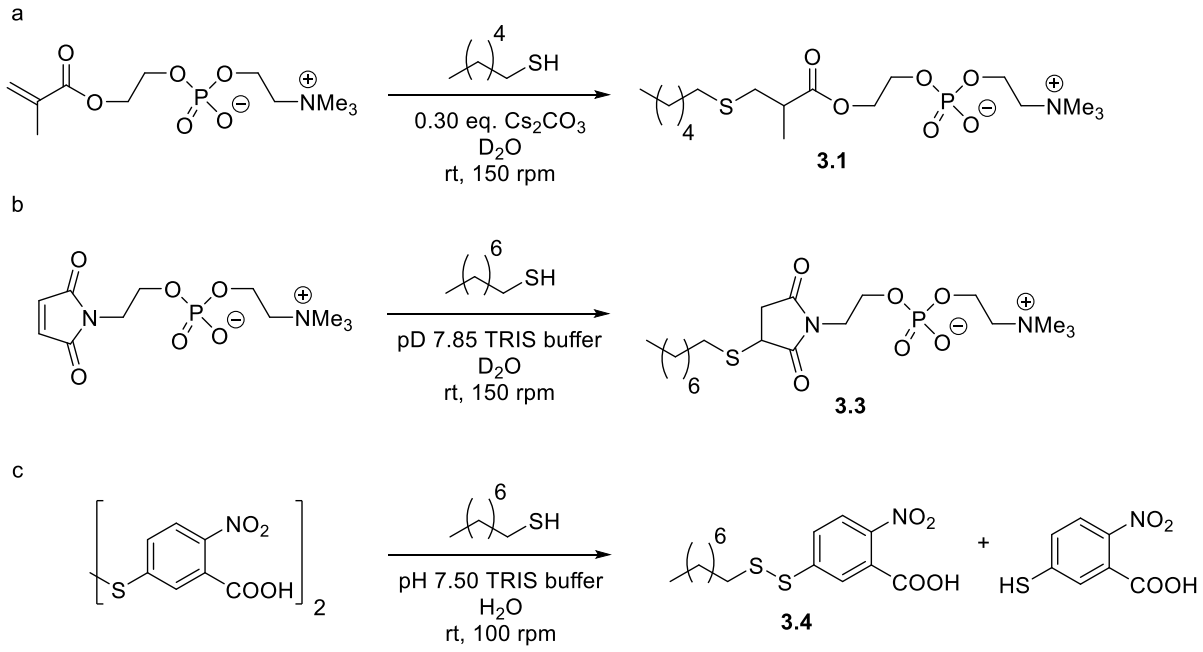


*Figure 3. 3. 1. 2. Candidate autocatalytic surfactant forming reactions for inducing droplet behaviour. The conditions given are the previously reported conditions where autocatalysis is observed. a – Thio-Michael reaction between 1-hexanethiol and MPC to form **3.1**,*[71] *b – Thio-Michael reaction between 1-octanethiol and a substituted maleimide to form **3.3**,*[71] *c – Thiol-disulfide exchange between 1-octanethiol and DTNB to form **3.4**.*[72]

3. 3. 2 Our study

We began by investigating whether diethyl phthalate used by Gutierrez et al. for its chemical or physical properties. It is present as a major component in all oil compositions showing division in the original study.[79] We hypothesised this may be due to effects resulting from alkaline hydrolysis. Under the reported conditions no hydrolysis was observed by ^{1}H NMR spectroscopy after 24 h.

Initial results showed that base in these systems was needed for droplet integrity, as when no base was used the oils formed thin films or slicks. The use of a buffer (such as TRIS or HEPES) also resulted in loss of integrity, meaning the conditions of the thiol-disulphide exchange or maleimide thio-Michael reactions in figure 3. 3. 1. 2b-c would need to be

adapted to be used here. Another early finding was that droplets in this setup regardless of oil and aqueous composition showed behaviour that appeared to be a combination of motion, vibration, and division (see figure 3. 3. 2. 1). Other “phenotypes” were very rare. This allowed us to assess something as nebulous as droplet behaviour in a defined manner.

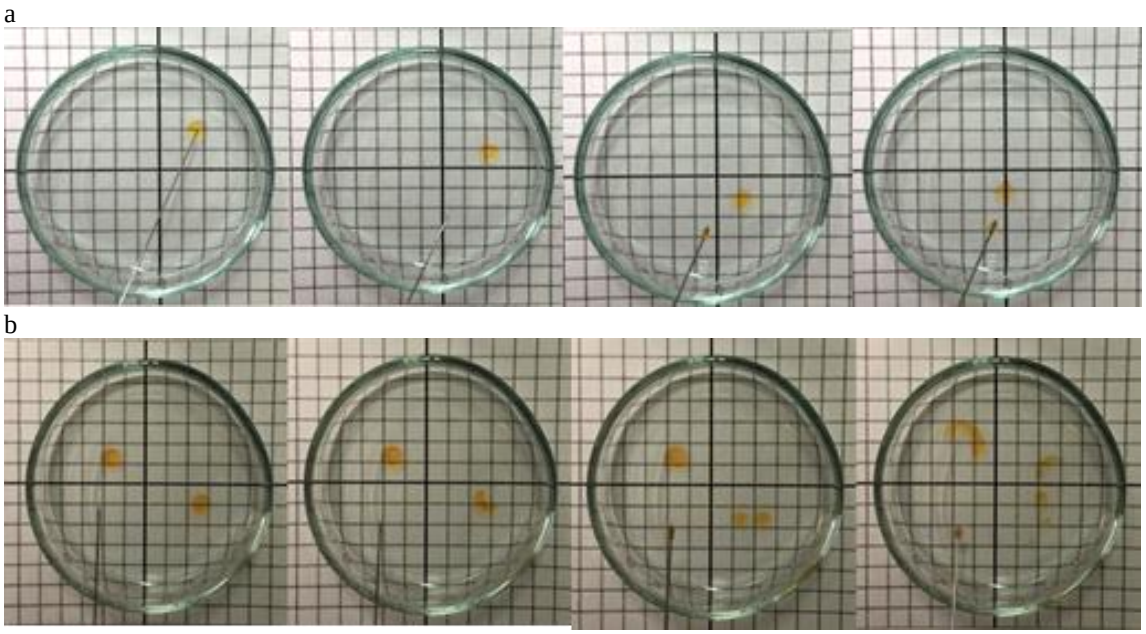


Figure 3. 3. 2. 1. Examples of droplet behaviours, as a series of pictures from a video. There is a 1 s interval between images in both series. The aqueous phase is 0.2 M NaOH with 20 mM CTAB in both cases. a – Movement. Droplets are dyed octanol. This example corresponds to table 3. 3. 2. 1. 2 entry 1. b – Division. Droplets are dyed pentanol. This example corresponds to table 3. 3. 2. 1. 2 entry 7.

3. 3. 2. 1 Optimisation of oil and aqueous compositions

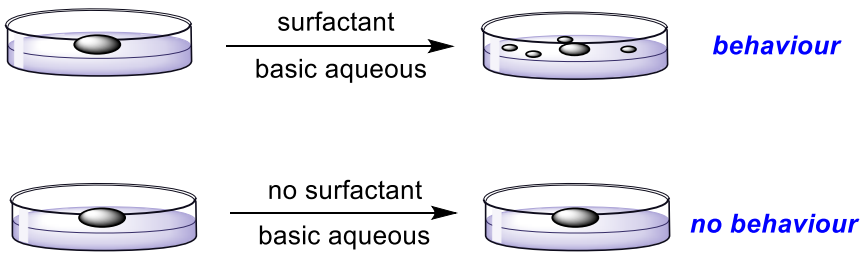


Figure 3. 3. 2. 1. 1. Diagram of the desired properties of a combination of an aqueous and oil composition, whereby behaviour is observed in the presence of a surfactant and no behaviour is observed in the absence of surfactant.

Firstly, we sought to identify a system in which oil droplets were stable and stationary in the absence of surfactant, but showed behaviour in the presence of a surfactant (Figure 3. 3. 2. 1. 1). In these cases, behaviour would be surfactant dependant. Hopefully, this behaviour would later be displayed when the droplet was doped with alkyl thiol and surfactant produced *in situ*. Table 3. 3. 2. 1. 1 shows some results which highlight a couple of unexpected points. Firstly, despite the report of Gutierrez et al. using 5 M sodium hydroxide throughout,[79] more behaviours and a higher degree of each behaviour was observed at lower concentrations (compare entry 1 with entries 2-4). Secondly, surfactant was not required for droplet behaviour in these systems (compare entries 3 with 6 and 4 with 7).

Entry	Droplet compos-ition	[NaOH] / M	[Surfactant][a] / mM	Droplet behaviour			
				Droplet definition	Motion	Vibration	Division
1	Oct	5.0	20	Good	Yes	No	No
2	Oct	1.0	20	Good	Yes	Yes	No
3	Oct	0.2	20	Good	Yes	Yes	No
4	Oct	0.04	20	Good	Yes	Yes	No
5	Oct	0	20	Poor	-	-	-
6	Oct	0.2	0	Good	Yes	Yes	Yes
7	Oct	0.04	0	Good	Yes	Yes	Yes

Table 3. 3. 2. 1. 1. Droplet behaviour observed in pure octanol droplets on an aqueous phase containing sodium hydroxide and surfactant. Similar results were observed for several other oil compositions. a – Surfactant used was CTAB, with similar results being obtained with SDS. n = 1.

At this point we clearly had to reconsider our system design in order to have the surfactant cause droplet behaviour. We found that in some cases a low concentration of surfactant could be used to achieve the desired property of stable, stationary droplets. This meant that if behaviour was to be coupled to autocatalysis, a small amount of a

stabilising surfactant would have to be present in the aqueous from the beginning of the reaction.

Some droplet behaviour was observed in the presence of 2 mM CTAB or SDS, however in the presence of 0.5 mM of either surfactant no behaviour was observed for many oil compositions. Oils were screened for behaviour in low and high CTAB concentrations (Tables 3. 3. 2. 2 and 3. 5. 6. 1). Of these, only three oils had the desired properties in 0.2 M sodium hydroxide. Pure octanol and a 2:1 octanol/pentanol mixture both showed motion and vibration in 20 mM CTAB, but no behaviour in 0.5 mM CTAB. 2:1 Octanol/pentanol droplets even showed division in 20 mM CTAB. The other oil composition, taken from the report of Gutierrez et al. was not very promising to maintain these properties when doped with thiol, as relatively small variations in composition resulted in undesired behaviour, compare table 3. 3. 2. 1. 2 entries 9-10 with entries 11-16. Table 3. 5. 6. 1 shows the results for similar screening in 5.0 M sodium hydroxide, which identified the same oil compositions as having behaviour in 20 mM CTAB and no behaviour in 0.5 mM CTAB.

Entry	Droplet composition	[CTAB] / mM	Droplet behaviour			
			Droplet definition	Motion	Vibration	Division
1	Oct	20	Good	Yes	Yes	No
2	Oct	0.5	Good	No	No	No
3	2:1 Oct/pent	20	Good	Yes	Yes	Yes
4	2:1 Oct/pent	0.5	Good	No	No	No
5	1:2 Oct/pent	20	Good	Yes	Yes	Yes
6	1:2 Oct/pent	0.5	Good	No	Yes	No
7	Pent	20	Good	Yes	Yes	Yes
8	Pent	0.5	Poor	-	-	-
9	4:36:18:42 oct a/oct/pent/DEP	20	Good	Yes	Yes	Yes

10	4:36:18:42 oct a/oct/pent/DEP	0.5	Good	No	No	No
11	40:20:40 oct/pent/DEP	20	Good	Yes	Yes	Yes
12	40:20:40 oct/pent/DEP	0.5	Good	Yes	No	No
13	5:20:15:60 oct a/oct/pent/DEP	20	Good	Yes	Yes	Yes
14	5:20:15:60 oct a/oct/pent/DEP	0.5	Good	No	No	Yes
15	5:60:15:20 oct a/oct/pent/DEP	20	Good	Yes	Yes	Yes
16	5:60:15:20 oct a/oct/pent/DEP	0.5	Good	No	No	Yes

Table 3. 3. 2. 1. 2. Behaviour observed in droplets of various oil compositions on an aqueous phase containing 0.2 M NaOH and surfactant. Composition used in entries 9 and 10 is taken from Gutierrez et al. where it is optimised for division under their conditions.[79] *oct a – octanoic acid, oct – octanol, pent – pentanol, DEP – diethyl phthalate. Pairs of entries which show the desired combination behaviours in high and low surfactant concentration are shown in green. See also ESI videos 6 and 7. n = 1.*

Further oils were screened, the results of a selection are shown in table 3. 3. 2. 1. 3. Many more compositions, all of which contained dodecane, were found to be suitable than in table 3. 3. 2. 1. 2. All these (Table 3. 3. 2. 1. 3) droplet compositions showed little or no behaviour under the more basic conditions of 5.0 M sodium hydroxide. Table 3. 3. 2. 1. 4 summarises all the oil compositions which were found to show some kind of droplet behaviour in 0.2 M NaOH solution containing 20 mM CTAB, but no behaviour in 0.2 M NaOH solution containing 0.5 mM CTAB.

Entry	Droplet composition	[CTAB] / mM	Droplet behaviour			
			Droplet definition	Motion	Vibration	Division
1	Dod	20	Poor	-	-	-
2	Dod	0.5	Poor	-	-	-

3	2:1 Dod/oct	20	Good	Yes	Yes	No
4	2:1 Dod/oct	0.5	Good	No	No	No
5	1:2 Dod /pent	20	Good	Yes	Yes	Yes[a]
6	1:2 Dod/pent	0.5	Good	No	No	No
7	1:2:2 oct/dod/DEP	20	Good	Yes	Yes	Yes
8	1:2:2 oct/dod/DEP	0.5	Good	No	No	No
9	1:1:4:4 oct/pent/dod/DEP	20	Good	No	Yes	Yes
10	1:1:4:4 oct/pent/dod/DEP	0.5	Good	No	No	No

Table 3. 3. 2. 1. 3. Further screening of behaviour observed in droplets of various oil compositions on an aqueous phase containing 0.2 M NaOH and surfactant. oct – octanol, pent – pentanol, dod – dodecane, DEP – diethyl phthalate. Pairs of entries which show the desired combination behaviours in high and low surfactant concentration are shown in green. a – a small degree of division was observed. n = 1.

Composition letter	Physical composition
a	Oct
b	2:1 Oct/pent
c	4:36:18:42 oct a/oct/pent/DEP
d	2:1 Dod/oct
e	1:2 Dod/pent
f	1:2:2 oct/dod/DEP
g	1:1:4:4 oct/pent/dod/DEP

Table 3. 3. 2. 1. 4. Summary of oil compositions which showed the desired properties in 0.2 M NaOH solutions containing 0.5 mM and 20 mM CTAB. n = 1.

Promising compositions were doped with 10% 1-hexanethiol and the resulting oils tested for behaviour on the surface of aqueous phases containing high and low concentrations of CTAB (Table 3. 3. 2. 1. 5). Disappointingly there is some loss of behaviour in many cases when thiol is introduced into the droplet compositions, compare for example table 3. 3. 2. 1. 2 entry 1 with table 3. 3. 2. 1. 5 entry 1, and table 3. 3. 2. 1. 2 entry 3 with

table 3. 3. 2. 1. 5 entry 3. How such small changes in composition like the addition of 10% alkyl thiol leads to such strong reduction in overall behaviour is unknown. Two thiol containing droplet compositions appeared promising to introduce into environments where lipids are being formed. These two compositions (1:9 1-hexanethiol/**b** and 1:9 1-hexanethiol/**e**) are discussed in the next section 3. 3. 2. 2 with the hopes of coupling macroscopic droplet behaviour with biphasic lipid forming reactions.

Entry	Droplet composition	[CTAB] / mM	Droplet behaviour			
			Droplet definition	Motion	Vibration	Division
1	1:9 1-hexanethiol/**a**	20	Good	No	No	No
2	1:9 1-hexanethiol/**a**	0.5	Good	No	No	No
3	1:9 1-hexanethiol/**b**	20	Good	Yes	No	No
4	1:9 1-hexanethiol/**b**	0.5	Good	No	No	No
5	1:9 1-hexanethiol/**c**	20	Good	No	No	No
6	1:9 1-hexanethiol/**c**	0.5	Good	No	No	No
7	1:9 1-hexanethiol/**d**	20	Good	Yes	No	No
8	1:9 1-hexanethiol/**d**	0.5	Good	No	No	No
9	1:9 1-hexanethiol/**e**	20	Good	Yes	No	Yes
10	1:9 1-hexanethiol/**e**	0.5	Good	No	No	No
11	1:9 1-hexanethiol/**f**	20	Good	Yes	No	No
12	1:9 1-hexanethiol/**f**	0.5	Poor	-	-	-
13	1:9 1-hexanethiol/**g**	20	Good	Yes	No	No
14	1:9 1-hexanethiol/**g**	0.5	Poor	-	-	-

*Table 3. 3. 2. 1. 5. Behaviour of 1-hexanethiol doped droplets. Though all the compositions **a-g** displayed the desired behaviour in 20 mM CTAB and lack of behaviour in 0.5 mM CTAB, only a small minority do when doped with 10% thiol. All droplet compositions were also tested in 0.2 M NaOH with no CTAB, all of which showed poor droplet definition. Here the most promising results are coloured green, although entries 7-8 also showed the desired combination of properties, but were excluded due to the relatively slow motion. See also ESI videos 8 and 9. n = 1.*

3. 3. 2. 2 Lipid forming reactions and droplet behaviour

In attempts to form lipid via thiol-disulfide exchange chemistry (Figure 3. 3. 2. 2. 1a), **3.5** was added to the aqueous to form **3.6**. However, in 0.2 M NaOH, we found that complete hydrolysis of **3.5** was observed, and **3.7** was observed by UPLC (Figure 3. 3. 2. 2. 1b). Interested in physical effects which could cause gradients of **3.5** and therefore resulting surfactant, **3.5** formation from **3.7** by addition of hydrogen peroxide was attempted. Addition of bulk hydrogen peroxide solutions to **3.7** did not result in any droplet behaviour (Figure 3. 3. 2. 2. 1c). Visually, the addition of hydrogen peroxide resulted in the rapid formation of a dark purple precipitate. ^{1}H NMR spectroscopy samples were taken immediately after hydrogen peroxide addition and 24 h later. In these samples, **3.6** was observed within a complex mixture of over-oxidation products, with no **3.5** was observed. These results are contrary to what may be expected from the results of chapter 4 and a prior report,[72] where a clean oxidation from **3.7** to **3.5** occurs at significantly lower addition rates of hydrogen peroxide and at lower pH.

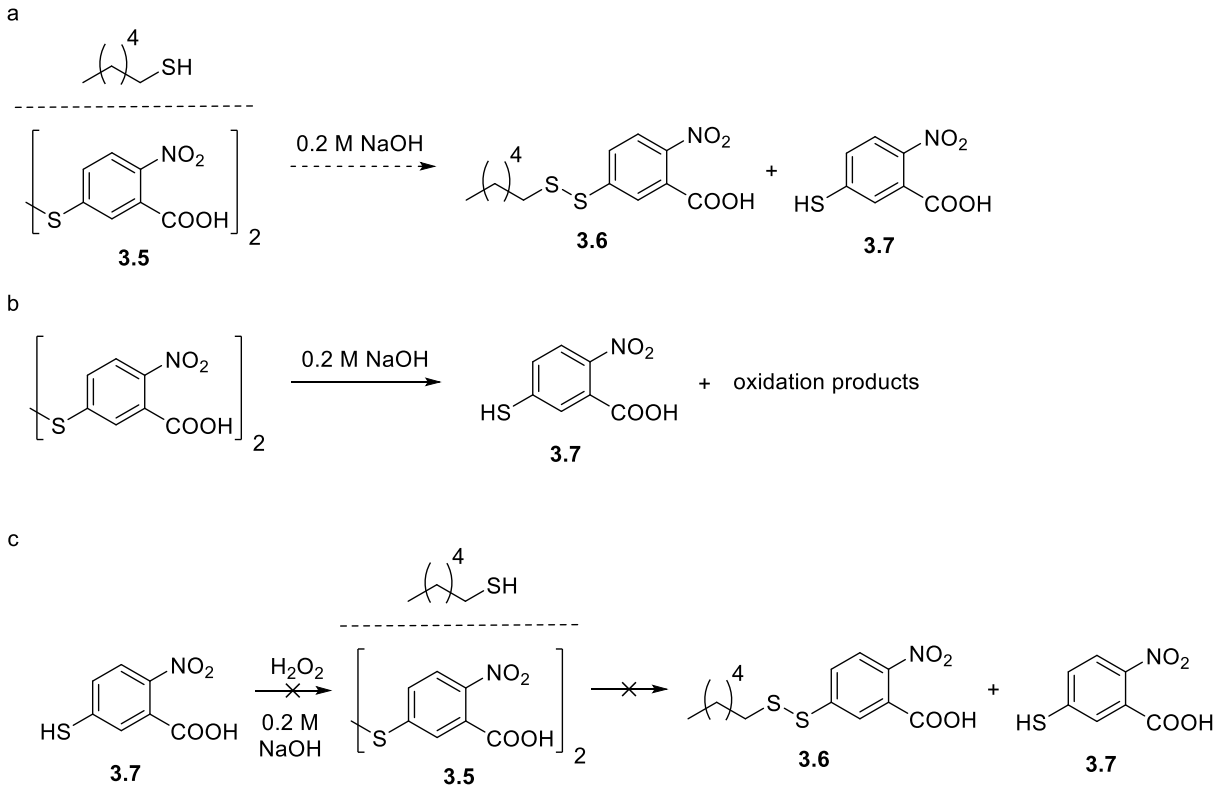


*Figure 3. 3. 2. 2. 1. a – Desired thiol-disulfide exchange reaction between 1-hexanethiol and **3.5** to form **3.6**. b –Observed reactivity of **3.5** in 0.2 M sodium hydroxide solution, a disulfide disproportionation resulting from alkaline hydrolysis. c – Desired means of forming lipid **3.6**, by in situ oxidation of **3.7** to **3.5** with H_2O_2, followed by thiol-disulfide exchange.*

Droplets of 1:9 1-hexanethiol/**b** and 1:9 1-hexanethiol/**e** were added to the surface of an aqueous phase containing **3.8**, MPC (Figure 3. 3. 2. 2. 2), in the hope of observing **3.1** induced droplet behaviour. No difference in behaviour was observed with MPC in the presence and absence of thiol, with a small amount of droplet division occurring in both cases over the course of one hour. Analysis of the aqueous by ^{1}H NMR spectroscopy indicated none of the desired product **3.1** after 8 h. Oils were prepared containing shorter chain length thiols (ethanethiol and 1-butanethiol) as their less hydrophobic nature may increase the rate of reaction. In all cases no droplet behaviour beyond a small amount of division was observed.

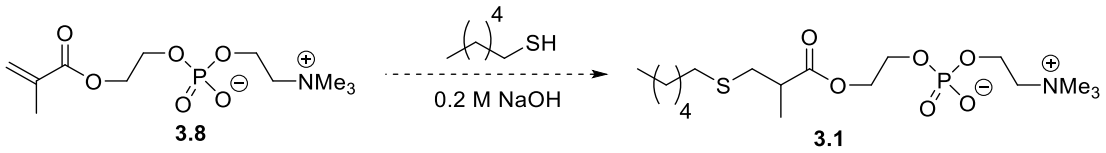


*Figure 3. 3. 2. 2. 2. Desired thio-Michael reaction between 1-hexanethiol and **3.8** to form **3.1**, where **3.1** may induce droplet behaviour. No **3.1** was observed by ^{1}H NMR spectroscopy.*

The nature of the Michael acceptor leads to a large difference in the rates of thiol addition and therefore the reported conditions under which autocatalysis was studied.[71] The α,β-unsaturated ester of MPC undergoes relatively slow addition, with the maleimide moiety of **3.9** being far faster (Figure 3. 3. 2. 2. 3). Using conditions close to the original report, 0.5 M TRIS buffer of pH 7.50 and pH 8.00 droplet definition was very poor for a range of oils, giving an oil-slick appearance.

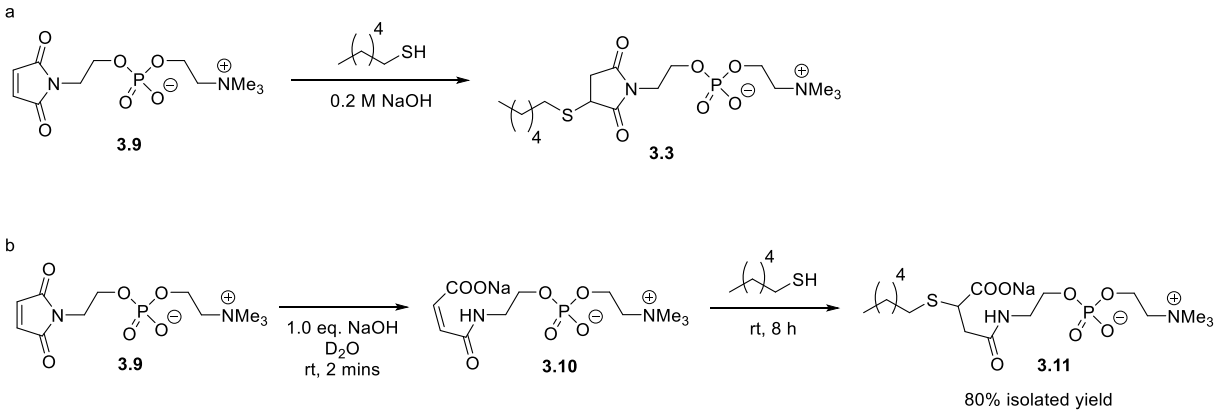


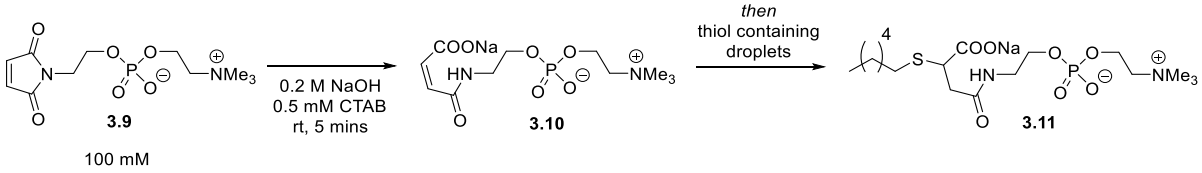
*Figure 3. 3. 2. 2. 3. a – Desired reactivity of **3.9** and 1-hexanethiol, to form **3.3**. b – Reaction scheme for the observed behaviour of maleimide **3.9** in the presence of sodium hydroxide and 1-hexanethiol. Initially there is a rapid hydrolysis to **3.10**, which undergoes Michael reaction with 1-hexanethiol to give **3.11**. This was observed in the presence of bulk thiol and thiol doped drops.*

Upon addition of maleimide **3.7** to NaOH solution a colour change was observed from a light pink to a burgundy purple, a process which was complete in approximately 2 minutes (Figure 3. 3. 2. 2. 3b). This was likely caused by formation of **3.10** which was observed by ^{1}H NMR spectroscopy, arising from maleimide ring hydrolysis. When **3.10**

is exposed to 1-hexanethiol it undergoes Michael reaction to give **3.11**, indicating that the reaction could be used to induce droplet behaviour.

On addition of thiol containing drops to an aqueous solution containing **3.10**, the edges of the drops became less defined, surrounded by aggregates of some floc with the appearance of soap scum (see figure 3. 3. 2. 2. 4). This was assumed to be caused by flocculation of **3.11**, as attempts to sample these aggregates proved challenging because of their small size and lack of integrity. Similar aggregates were observed on addition of a solution of **3.11** to an aqueous with oil drops present on its surface.

The behaviour of thiol containing droplets on an aqueous phase of **3.10** are summarised in table 3. 3. 2. 2. 1. Pleasingly, 1:9 1-hexanethiol/**b** droplets showed division (entry 1), as did 1:9 1-hexanethiol/**e** droplets albeit to a significantly lesser extent (entry 2). The proportion of 1-hexanethiol was increased to attempt to increase the rate and amount of division (entries 3-6). Though a larger amount of floccing was observed with increasing thiol 10-40%, there was no significant difference in division or other behaviour. Above 40% 1-hexanethiol resulted in poorly defined drops with both oil **b** and **e**. Entry 1 was therefore taken forward for further study.



Entry	Droplet composition	Droplet behaviour			
		Droplet definition	Motion	Vibration	Division
1	1:9 1-hexanethiol/**b**	Good	Yes[a]	No	Yes
2	1:9 1-hexanethiol/**e**	Good	Yes[a]	No	Yes[b]
3	2:8 1-hexanethiol/**b**	Good	Yes[a]	No	Yes
4	4:6 1-hexanethiol/**b**	Good	Yes[a]	No	Yes
5	6:4 1-hexanethiol/**b**	Poor	-	-	-
6	1-hexanethiol	Poor	-	-	-
7	**b**	Good	Yes[a]	No	Yes[b]

*Table 3. 3. 2. 2. 1. Behaviour of 1-hexanethiol doped droplets in the presence of **3.10**, formed in situ from **3.9**. See table 3. 3. 2. 1. 4 for the compositions of **b** and **e**. a – a small amount of motion was observed, b – a small amount of division was observed. n = 1.*

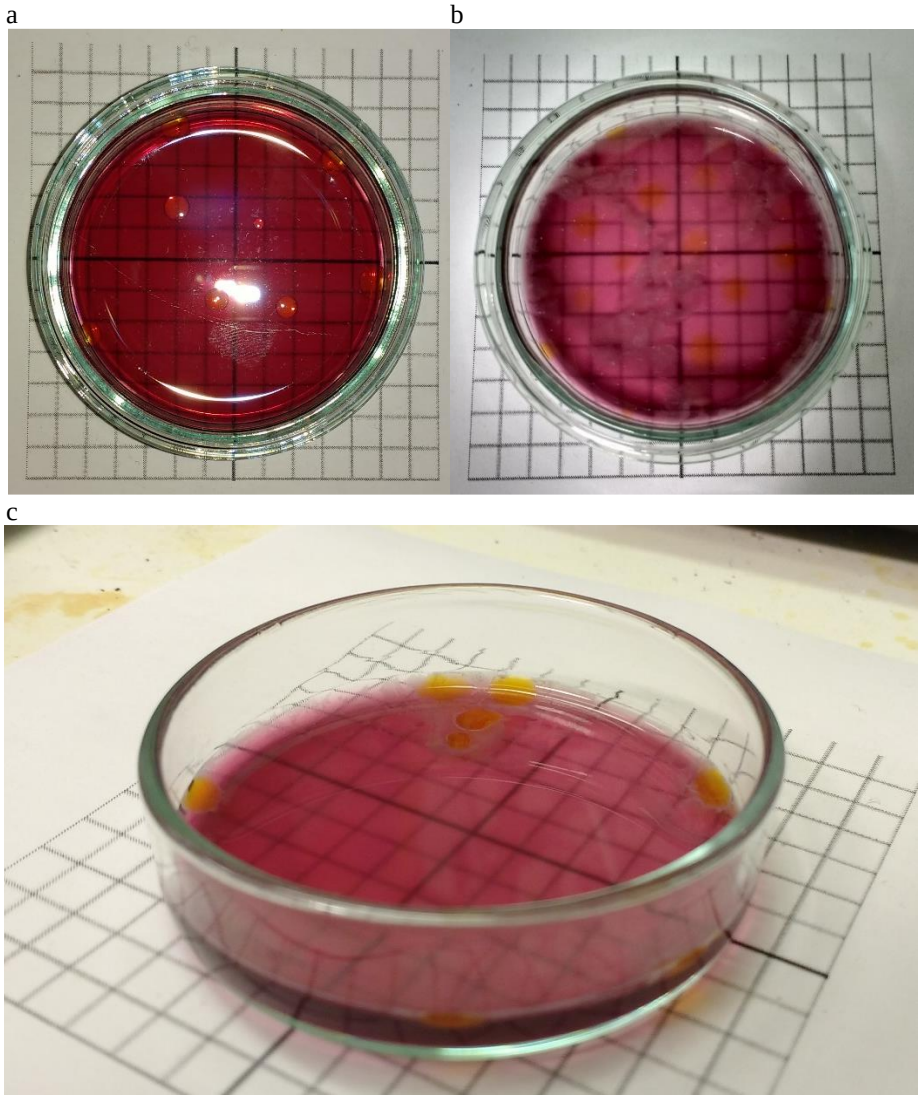


*Figure 3. 3. 2. 2. 4. Appearance of droplets under conditions where reaction between **3.10** and 1-hexanethiol form **3.11**. The dark red colour of the aqueous is due to **3.10**. a – appearance of 1:9 1-hexanethiol/**b** droplets (dyed orange) at the beginning of the reaction. b – appearance of 1:9 1-hexanethiol/**b** droplets after 5 h. Floc aggregates, presumed to be **3.11**, show up as dark purple in this image. Note there is a large size distribution in droplets and they are less well defined than in image a. c – appearance of 1:9 1-hexanethiol/**b** droplets after 1 h, as viewed from the side. Here the beginnings of floc formation can be seen.*

The extent of division in 1:9 1-hexanethiol/**b** droplets is quantified in figure 3. 3. 2. 2. 5. Starting with 8 droplets, division brings the average number to 200 in 1 h. Only a small amount of division is seen in the control experiment where pure **b** is used. Runs using 1:9 1-hexanethiol/**b** droplets with 0.15 equiv. **3.9** added from the start showed low

reproducibility, however the time until the onset of flocs around the droplets was similar to without **3.11**, both around 1 h. Overall, although the division behaviour is promising, it shows broad error bars due to the stochasticity of the process, and counting the droplets by eye or images proved challenging due to the very small size of many of the droplets. In future studies, the most interesting behaviour may be observed with more time points taken between 0.5 h and 1 h, the main period of droplet division.

The mechanism by which division in this system occurs appears to be different from that seen in section 3. 3. 2. 1, which is a rapid process brought about through Marangoni stresses. Here, division is comparatively slow, with individual droplets dividing asymmetrically to form a series of much smaller droplets whilst maintaining a central larger droplet. The mechanism here appears to be caused by flocs of **3.11**. Flocculation begins after about 0.5-1 h, occurring principally around edges the droplets, which seems to cause the edges to become less well defined (as seen in figure 3. 3. 2. 2. 4c). The smaller "daughter" droplets are primarily located within the flocs at early time points.

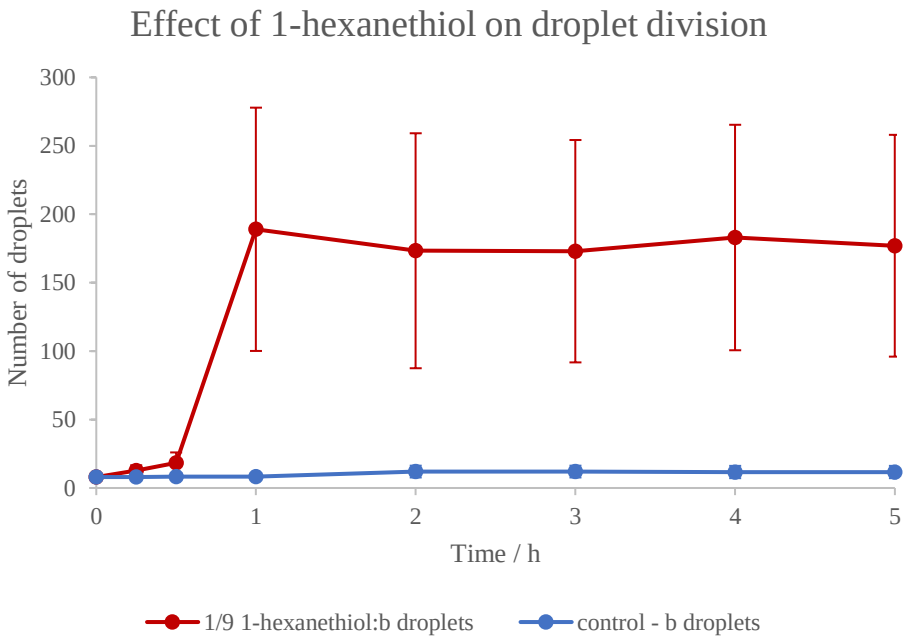


Figure 3. 3. 2. 2. 5. Division in thiol containing drops in a medium containing ***3.10****. Conditions used are as table 3. 3. 2. 2. 1 entry 1 and entry 7. A small amount of droplet division is observed in the control where droplets containing no 1-hexanethiol were used. n = 3, error bars show one standard deviation and are in some cases too small to be visible.*

3. 4 Conclusions and future work

In section 3. 2, we have successfully established a mechanism by which droplet protocells can propel through a heterogeneous medium in which lipid formation occurs. Feedback between protocells and the lipid forming reaction shows an interesting coupling of physical and chemical processes across length scales. One of the strengths of this work is its highly reductionist nature, showing the such seemingly complex function can emerge from parts as simple as a non-biological lipid forming reaction and oil droplets. We also show that a relatively small change in the physical properties of the droplets can lead to a large difference in efficiency of motion when changing composition from octanol to decanol.

This study raises an interesting open question about physical autocatalysis and lipid replicators in general, is self-propelled motion in these systems a universal or common phenomenon. There is no requirement in the proposed mechanism of motion for the oil droplets to be made of any particular material, and it is easily imagined that alkyl thiol droplets could be formed in a slowly stirred aqueous phase. These droplets could act as Marangoni swimmers, moving towards the thiol rich interface, increasing mixing and rate of reaction analogously to as alcohol droplets do in this study. This adds a new possible contribution to the mechanism of physical autocatalysis, which has to our knowledge not previously been considered. Within the system described in this chapter, although rarely, small thiol droplets (around 5 μm) were seen within the emulsion undergoing self-propulsion. In the next chapter this idea is discussed more in section 4. 3. 3. 1.

The study of large drops in section 3. 3 showed good initial results, with a lipid inducing division of the drops, and it being possible to form the lipid *in situ*. Currently this work is limited in scope however because of the difficulty in visualisation and tracking drops

when dividing, making quantification of behaviour difficult. Also, the kinetics of formation of the lipid remain to be established and therefore how lipid formation and drop division are linked is largely unknown. It appears flocculation is somewhat stochastic, and that this is a critical step for droplet division.

In regard to future development, I believe that it would be most interesting to link a second function to motion of the droplet protocells. One such possible function could be catalysis, were it possible for droplet-bound lipid to produce the constituent oil of the protocell, and also lipid induced division, then it may be possible to build droplets which move around in their surroundings, feeding, growing and dividing.

Currently the work in section 3.3 regarding the division of surface droplets is limited by relatively low reproducibility and difficulty of quantifying division. The reproducibility may well be able to be improved by changing the lipid formed to one where flocculation is faster relative to the lipid formation. The quantification of division needs to be improved. It is likely that using a microscope set up and labelling the droplets with a fluorescent dye may give a high enough contrast to allow particle tracking software to be used.

3. 5 Experimental

General synthetic experimental information for this chapter is as found in section 2. 6. 1.

3. 5. 1 Microfluidic preparation of droplets

The oil droplets were prepared using a PDMS microfluidic devices fabricated by soft-lithography in a similar method to Jin et al.[40] Droplet production was by standard flow focussing methods using a Fluigent microfluidic flow control system to control the flow rates of dyed oil (typically octanol dyed with Nile red) and the aqueous phase (milliQ water with 4 mM SDS and 300 mM MPC) in the microfluidic device using the appropriate connectors (Precision tips, Nordson EFD) and tubing (Tygon tubing, Cole-Parmer). Droplets could be stored for a period of weeks to months without coalescence or ripening.

3. 5. 2 CMC measurement

CMC of compound **3.1** was determined using the method of Chattopadhyay and London.[82]

A Nile Red dye, (9-(diethylamino)-2-hydroxy-5*H*-benzo[α]phenoxazin-5-one) was dissolved in DMSO to form a 10 mM solution. For each member of a dilution series, 1.0 µL of dye solution was added to 2.00 mL of lipid **3.1** solution in milliQ water. Each sample was exposed to an excitation wavelength of 552 nm, and emission spectra between 580 nm and 740 nm recorded, using a Perkin Elmer LS 55 fluorescence spectrometer (Figure 3. 4. 2. 1). Plotting maximum emission intensity (λ_{max} ~ 635 nm) against lipid concentration (Figure 3. 4. 2. 2) gave the CMC (20.8 mM).

Aggregation was found to be as micelles as measured by DLS, using a similar approach to as described in section 4. 6. 6.

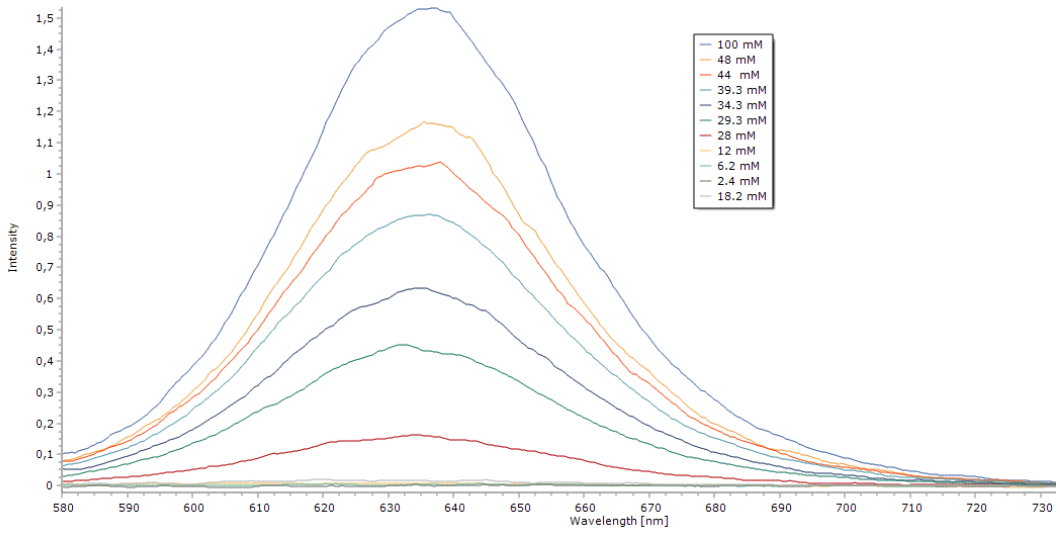


*Figure 3. 5. 2. 1. Emission spectra of containing surfactant **3.1** solutions containing equimolar quantities of Nile red. Intensity is recorded in arbitrary units. n = 1.*

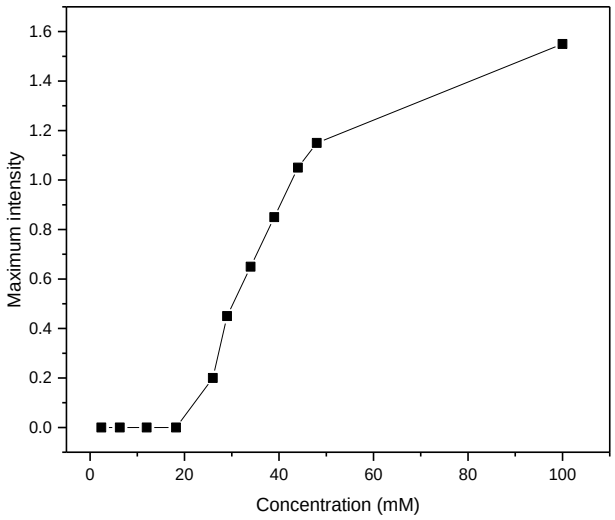


*Figure 3. 5. 2. 2. Plot of maximum emission intensity against lipid **3.1** concentration. n = 1.*

3. 5. 3 Reaction setup for droplet movement and observation

3. 5. 3. 1 Reaction setup

An aqueous solution of 2-methacryloyloxyethyl phosphorylcholine, MPC (100 µL, 0.12 mmol, 1.2 M, 1.1 equiv.) was added to an aqueous solution of caesium carbonate (100 µL, 0.02 mmol, 0.2 M, 0.2 equiv.), followed by 1-hexanethiol (15 µL, 0.11 mmol,

1.0 equiv.) in a 4 mL cylindrical vial. After addition, they were mixed for precisely 3 s at 80 rpm with a 1 cm rod shaped stir bar. A sample of the reaction mixture was transferred as quickly as possible into an observation chamber, formed from 1 mm thick silicone film with a 13 mm diameter circular well attached to a glass slide. Then octanol droplets were added and covered with a glass cover slip.

The lag phase is defined as the time between addition of 1-hexanethiol to MPC solution and the onset of motion of droplets. The onset of motion is defined to be when the droplet leave its lipid aggregate corona for practical reasons, often droplets show a long period of very slow motion.

For experiments involving a thiol reservoir, a functionalised cover slip was prepared by taking a glass slide and adding a trimethoxy(octadecyl)silane solution (50 µL, 1.1 µmol, 22 mM in toluene). After 1 h, the glass slide was washed sequentially with toluene, water and acetone. This formed a cover slide with a 2 mm diameter circular hydrophobic patch. Typical pre-treatments such as plasma discharge were not required. The reaction mixture was prepared and transferred as above without the thiol, then 1-hexanethiol was added to the well and sealed with the functionalised cover slip. The thiol localised only on the functionalised regions of the slip.

3. 5. 3. 2 Observation and tracking

Droplets were observed and videos of their movement were recorded using a Nikon DS Ri2 camera attached to a Nikon Eclipse E200 microscope. Videos were extracted to obtain an image sequence, before being analysed with a homemade MATLAB script. The script was used for object tracking to obtain droplet position within an image and from this velocity was found. “Instantaneous” velocities are the mean over a one second, and average velocities were calculated over the full period of motion of each droplet. Motion

of the droplets was assumed to be constrained to the horizontal plane, which is justified as they are composed of a lighter-than-water oil, typically octanol, which localise on the top aqueous-cover slip surface. Deviation from this location can typically be observed through loss of focus, which was never observed.

3. 5. 4 ^{1}H NMR kinetics study

The rate of lipid **3.1** formation was determined by following concentration of **3.1** by ^{1}H NMR (400 MHz). The reaction mixture was prepared as in section 3. 4. 3. 1, but after stirring left to react in the vial. After stirring, the reaction was left to proceed with no stirring. One reaction was used for each time point, being quenched with a solution of HCl (100 µL, 0.04 mmol, 0.4 M in D_2O, 0.37 eq.) after the required time. Rapidly, the reaction mixture was then extracted with hexanes (3 x 1.0 mL) to remove unreacted thiol. This was performed by addition of hexanes followed by stirring for precisely 20 s at 3000 rpm, then removal of the organic phase with a 1 mL Braun Injekt-F syringe. A solution of acetone (600 µL, 0.04 mmol, 67 mM in D_2O) was added to the aqueous phase and analysed with ^{1}H NMR spectroscopy. Concentrations were calculated from the relative integrals of the lipid peak (2H) at δ 2.57 ppm and the acetone peak (6H) at 2.22 ppm. Where octanol droplets were present, the same method was used, with the aqueous emulsion of droplets (3 µL) being added to the vial immediately after stirring. An average of 15-20 octanol droplets were added by this method.

3. 5. 5 Setup for large drop studies of section 3. 3

The experimental procedure was developed at an early stage to ensure reproducibility of each run, and is closely related to the automated approach described by Gutierrez et al.[79] 3mL of the relevant aqueous solution was prepared and dispensed into a Petri dish, and then oil droplets (4 × 5 µL, unless otherwise stated) were added from a microsyringe,

attempting to lay them onto the surface. Where possible, the placement of the droplets was at the corners of a 2.0 × 2.0 cm square at the centre of the Petri dish, as determined by underlying graph paper. The lid was then replaced, with care taken not to disturb the liquid. The entire process was filmed from above, using a Motorola MOTO G4 XT1622 phone.

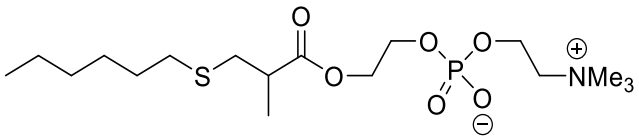
3. 5. 6 Supplementary table for large drop studies of section 3. 3

Entry	Droplet composition	[CTAB] / mM	Droplet behaviour			
			Droplet definition	Motion	Vibration	Division
1	Oct	20	Good	Yes	No	No
2	Oct	0.5	Good	No	No	No
3	2:1 Oct/pent	20	Good	Yes	No	No
4	2:1 Oct/pent	0.5	Good	No	No	No
5	1:2 Oct/pent	20	Good	Yes	Yes	No
6	1:2 Oct/pent	0.5	Good	No	No	No
7	Pent	20	Good	Yes	Yes	No
8	Pent	0.5	Good	No	No	No
9	4:36:18:42 oct a/oct/pent/DEP	20	Good	Yes	Yes	Yes
10	4:36:18:42 oct a/oct/pent/DEP	0.5	Good	No	No	No
11	40:20:40 oct/pent/DEP	20	Good	No	No	No
12	40:20:40 oct/pent/DEP	0.5	Good	Yes	No	No
13	5:20:15:60 oct a/oct/pent/DEP	20	Good	No	No	No
14	5:20:15:60 oct a/oct/pent/DEP	0.5	Good	Yes	No	No
15	5:60:15:20 oct a/oct/pent/DEP	20	Good	No	No	No
16	5:60:15:20 oct a/oct/pent/DEP	0.5	Good	Yes	No	No

Table 3. 5. 6. 1. Behaviour observed in droplets of various oil compositions on an aqueous phase containing 5.0 M NaOH and surfactant. Composition used in entries 9 and 10 is taken from Gutierrez et al. where it is optimised for division under their conditions.[79] *oct a – octanoic acid, oct – octanol, pent – pentanol, DEP – diethyl phthalate. Pairs of entries which show the desired combination behaviours in high and low surfactant concentration are shown in green.*

3. 5. 7 Synthesis and characterization of compounds

(±)-2-((3-(Hexylthio)-2-methylpropanoyl)oxy)ethyl (2-(trimethylammonio)ethyl) phosphate, 3.1

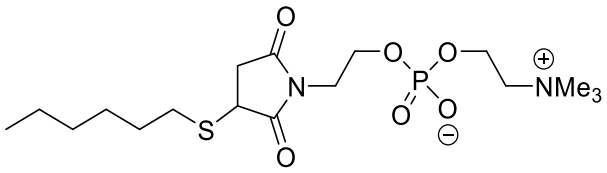


To a stirred solution of 2-methacryloyloxyethyl phosphorylcholine (500.0 mg, 1.69 mmol, 1.0 equiv.) in ethanol (10 mL) was added 1-hexanethiol (264 µL, 1.86 mmol, 1.1 equiv.) followed by diisopropylamine (24 µL, 0.169 mmol, 0.1 equiv.). After 4 h solvent removed *in vacuo,* and the residue washed with hexanes (10 mL). (±)-2 ((3-(Hexylthio)-2-methylpropanoyl)oxy)ethyl (2-(trimethylammonio)ethyl) phosphate was obtained without further purification as a colourless gum (508.0 mg, 1.23 mmol, 73%).

IR (gum, ν_{max} / cm^{-1}) 3285, 2963, 2926, 2858, 1733, 1458, 1377, 1340, 1239, 1166, 1077, 1050; **^{1}H NMR** (400 MHz, D_2O) δ 4.47 – 4.30 (m, 4H, OC*H*$_2$CH$_2$N(CH$_3$)$_3$ + OC*H*$_2$CH$_2$OC=O), 4.15 (dt, *J* = 7.0, 5.0 Hz, 2H, C*H*$_2$OC=O), 3.75 – 3.70 (m, 2H, C*H*$_2$N(CH$_3$)$_3$), 3.28 (s, 9H, N(CH$_3$)$_3$), 2.93 – 2.81 (m, 2H, SC*H*H'CHC=O + CHC=O), 2.79 – 2.67 (m, 1H SCH*H*'CHC=O), 2.62 (t, *J* = 7.5 Hz, 2H, SCH$_2$), 1.63 (p, *J* = 7.5 Hz, 2H, SCH$_2$C*H*$_2$), 1.48 – 1.33 (m, 6H, alk CH$_2$), 1.31 (t, *J* = 6.5 Hz, 3H, CHC*H*$_3$), 0.96 – 0.90 (m, 3H, CH$_2$C*H*$_3$); **^{13}C NMR** (101 MHz, $CDCl_3$) δ 176.9 (C=O), 66.2 – 66.0 (m, *C*H$_2$N(CH$_3$)$_3$), 63.7 (d, *J* = 5.5 Hz O*C*H$_2$CH$_2$OC=O), 59.4 (d, *J* = 5.0 Hz, OCH$_2$CH$_2$N(CH$_3$)$_3$), 57.5 (OCH$_2$*C*H$_2$OC=O), 54.2 – 53.8 (m, N(CH$_3$)$_3$), 40.2 (*C*HC=O), 34.8 (S*C*H$_2$CH), 32.2 (S*C*H$_2$CH$_2$), 31.1 (alk CH$_2$), 29.2 (alk CH$_2$), 28.1 (alk CH$_2$), 22.3 (*C*H$_2$CH$_3$), 16.8 (CH*C*H$_3$), 13.7 (CH$_2$*C*H$_3$); **^{31}P NMR** (162 MHz, D_2O) 0.83; **HRMS** (ES+) calc. for $C_{17}H_{36}O_6NP^{32}S_2Na$ $[M+Na]^+$ 436.1893, found 436.1891.

Data consistent with literature values.[83]

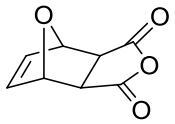
(±)-2-(3-(Hexylthio)-2,5-dioxopyrrolidin-1-yl)ethyl (2-(trimethylammonio)ethyl) phosphate, 3.2



To a stirred solution of 2-(2,5-dioxo-2,5-dihydro-1*H*-pyrrol-1-yl)ethyl (2-(trimethylammonio)ethyl) phosphate, **3.7** (250.0 mg, 0.816 mmol, 1.0 equiv.) in ethanol (5 mL) was added 1-hexanethiol (128 µL, 0.898 mmol, 1.1 equiv.) followed by diisopropylamine (11 µL, 0.082 mmol, 0.1 equiv.). After 2 h solvent removed *in vacuo,* and the residue washed with hexanes (5 mL). (±)-2-(3-(Hexylthio)-2,5-dioxopyrrolidin-1-yl)ethyl (2-(trimethylammonio)ethyl) phosphate was obtained without further purification as a colourless gum (163.0 mg, 0.384 mmol, 47%).

IR (thin film, ν_{max} / cm^{-1}) 3386, 2473, 1697, 1462, 1205, 1085; **^{1}H NMR** (400 MHz, D_2O) δ 4.30 – 4.22 (m, 2H, OC*H*$_2$CH$_2$N(CH$_3$)$_3$), 4.09 – 3.97 (m, 3H, OC*H*$_2$CH$_2$NC=O + SC*H*C=O), 3.85 – 3.74 (m, 2H, C*H*$_2$NC=O), 3.65 (m, 2H, C*H*$_2$N(CH$_3$)$_3$), 3.33 (dd, *J* = 19.0, 9.0 Hz, 1H, C=OC*H*CHS (*cis* to thiol)), 3.21 (s, 9H, N(CH$_3$)$_3$), 2.77 – 2.68 (m, 1H, C=OC*H*CHS (*trans* to thiol)), 1.67 – 1.52 (m, 2H, SCH$_2$), 1.44 – 1.32 (m, 2H, SCH$_2$C*H*$_2$), 1.34 – 1.19 (m, 6H, alk CH$_2$), 0.86 (t, *J* = 7.0 Hz, 3H, CH$_2$C*H*$_3$); **^{13}C NMR** (101 MHz, D_2O) δ 179.7 (C=O), 178.3 (C=O), 66.1 – 65.9 (m, *C*H$_2$N(CH$_3$)$_3$), 61.9 (d, *J* = 5.0 Hz, OCH$_2$CH$_2$NC=O), 59.5 (d, *J* = 5.5 Hz, OCH$_2$CH$_2$N(CH$_3$)$_3$), 54.1 – 53.9 (m, N(CH$_3$)$_3$), 40.2 (S*C*HC=O), 39.6 (d, *J* = 8.0 Hz, OCH$_2$*C*H$_2$NC=O), 36.2 (*C*H$_2$C=O), 36.1 (CH$_2$S), 30.6 (alk CH$_2$), 28.4 (alk CH$_2$), 27.6 (alk CH$_2$), 21.9 (*C*H$_2$CH$_3$), 13.3 (CH$_2$*C*H$_3$); **^{31}P NMR** (162 MHz, D_2O) -0.34; **HRMS** (ES+) calc. for $C_{17}H_{33}N_2NaO_6P^{32}S$ $[M+Na]^+$ 447.1689, found 447.1693.

(3a*R*,4*S*,7*R*)-3a,4,7,7a-Tetrahydro-4,7-epoxyisobenzofuran-1,3-dione, 3.12

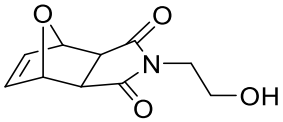


To a stirred suspension of maleic anhydride (50.0 g, 509.9 mmol, 1.00 equiv.) in benzene (250 mL) was added furan (37.5 mL, 516.0 mmol, 1.01 equiv.) portionwise over the course of 20 minutes. After 24 h the reaction mixture filtered and the solids washed with cold benzene (2 x 100 mL). (3a*R*,4*S*,7*R*)-3a,4,7,7a-tetrahydro-4,7-epoxyisobenzofuran-1,3-dione was obtained as an amorphous white solid (50.9 g, 306.4 mmol, 60%). Exclusively the *exo* product was observed by ^{1}H NMR.

IR (solid, ν_{max} / cm^{-1}) 2161, 2034, 1858, 1782, 1568, 1230, 1212, 1145, 1085, 1020; **^{1}H NMR** (400 MHz, DMSO-d_6) δ 6.58 (t, *J* = 1.0 Hz, 2H, C=CH), 5.35 (t, *J* = 1.0 Hz, 2H, OCH), 3.31 (s, 2H, CHC=O); **^{13}C NMR** (101 MHz, $CDCl_3$) δ 171.5 (C=O), 136.9 (C=C), 81.6 (OCH), 49.1 (*C*HC=O); **LRMS** (ES+) calc. for $C_8H_6O_4Na$ $[M+Na]^+$ 189.0, found 189.2, **mp** (benzene) 119.2 °C.

Data consistent with literature values.[84]

(3a*R*,4*S*,7*R*)-2-(2-hydroxyethyl)-3a,4,7,7a-tetrahydro-1H-4,7-epoxyisoindole-1,3(2H)-dione, 3.13



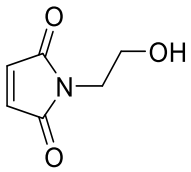
To a stirred suspension of (3a*R*,4*S*,7*R*)-3a,4,7,7a-tetrahydro-4,7-epoxyisobenzofuran-1,3-dione, **3.12** (20.0 g, 120.4 mmol, 1.0 equiv.) in methanol (40 mL) was added ethanolamine (7.27 mL, 120.4 mmol, 1.0 equiv.) portionwise over the course of 5 minutes. After a further 30 minutes, the reaction mixture was heated to reflux overnight, allowed to cooled to room temperature and after 2 h filtered to obtain the first crop of crystals. Around half of the solvent was removed *in vacuo* from the filtrate, and the

remainder cooled to -24 °C overnight. This was then filtered to obtain a second crop of crystals. (3a*R*,4*S*,7*R*)-2-(2-Hydroxyethyl)-3a,4,7,7a-tetrahydro-1H-4,7-epoxyisoindole-1,3(2H)-dione was obtained as a white crystalline solid (13.97 g, 66.8 mmol, 55%). Exclusively the *exo* product was observed by ^{1}H NMR.

IR (solid, ν_{max} / cm^{-1}) 3475, 3260, 3114, 2932, 2161, 2027, 1764, 1691, 1439, 1404, 1388, 1362, 1320, 1157, 1066, 1052; **^{1}H NMR** (400 MHz, $CDCl_3$) δ 6.51 (t, *J* = 1.0 Hz, 2H, C=CH), 5.26 (t, *J* = 1.0 Hz, 2H, OCH), 3.76 – 3.71 (m, 2H, CH_2N), 3.69 – 3.65 (m, 2H, CH_2O), 2.88 (s, 2H, CHC=O), 2.44 (s, 1H, OH); **^{13}C NMR** (101 MHz, $CDCl_3$) δ 176.5 (C=O), 136.4 (C=C), 80.3 (OCH), 57.3 (CH_2O), 47.1 (*C*HC=O), 40.6 (CH_2N); **LRMS** (ES+) calc. for $C_{10}H_{11}O_4NNa$ $[M+Na]^+$ 232.1, found 232.0, **mp** (methanol) 134.5 °C.

Data consistent with literature values.[84]

N-Hydroxyethyl maleimide, 3.14



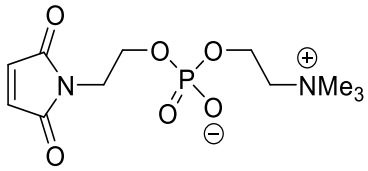
(3a*R*,4*S*,7*R*)-2-(2-hydroxyethyl)-3a,4,7,7a-tetrahydro-1H-4,7-epoxyisoindole-1,3(2H)-dione, **3.13** (18.75 g, 89.6 mmol, 1.0 equiv.) in toluene (150 mL) was heated to reflux for 7 h. The reaction mixture was then allowed to cooled to room temperature and solvent removed *in vacuo.* As the published recrystallisation technique proved unreliable, the crude material was purified by column chromatography (ethyl acetate/ petroleum ether (1:1 to 7:3)) to give N-hydroxyethyl maleimide as a white solid (8.11 g, 57.5 mmol, 64%).

IR (solid, ν_{max} / cm^{-1}) 3258, 3114, 2961, 2161, 2030, 1750, 1708, 1441, 1404, 1387, 1362, 1321, 1158, 1066, 1051; **^{1}H NMR** (400 MHz, $CDCl_3$) δ 6.72 (s, 2H, CH=CH), 3.77

– 3.74 (m, 2H, CH_2N), 3.71 – 3.68 (m, 2H, CH_2O), 2.37 (s, 1H, OH); **^{13}C NMR** (101 MHz, $CDCl_3$) δ 171.1 (C=O), 134.5 (C=C), 57.9 (CH_2O), 43.6 (CH_2N); **LRMS** (ES+) calc. for $C_6H_7O_3NNa$ $[M+Na]^+$ 164.0, found 164.0.

Data consistent with literature values.[84]

2-(2,5-Dioxo-2,5-dihydro-1*H*-pyrrol-1-yl)ethyl (2-(trimethylammonio)ethyl) phosphate, 3.9



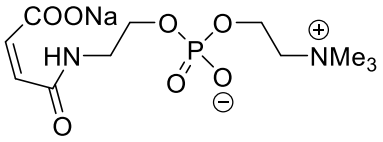
To a stirred solution of N-hydroxyethyl maleimide, **3.14** (4.50 g, 31.9 mmol, 1.0 equiv.) and triethylamine (8.33 mL, 59.8 mmol, 1.5 equiv.) in tetrahydrofuran (200 mL) at 0 °C was added dropwise 2-chloro-1,3,2-dioxaphospholane-2-oxide (4.40 mL, 47.8 mmol, 1.2 equiv.) and allowed to warm to room temperature. After 1.5 h the reaction mixture was filtered through a plug of silica as quickly as possible washed with ethyl acetate (600 mL), and solvent removed *in vacuo.* To a stirred suspension of the solid (7.68 g, 31.1 mmol) in acetonitrile (60 mL) was added trimethylamine solution in (23.3 mL, 2.0 M in tetrahydrofuran, 46.7 mmol, 1.5 equiv.) and the vessel sealed and heated to 70 °C. After 3 days, the reaction mixture was cooled to room temperature and solvent removed *in vacuo.* The crude material was purified by column chromatography (water/ acetonitrile (1:4 to 3:7)) to give 2-(2,5-dioxo-2,5-dihydro-1*H*-pyrrol-1-yl)ethyl (2-(trimethylammonio)ethyl) phosphate as an oil (4.42 g, 14.4 mmol, 45%).

IR (thin film, ν_{max} / cm^{-1}) 3361, 3034, 2956, 1773, 1695, 1481, 1431, 1403, 1361, 1336, 1234, 1051; **^{1}H NMR** (400 MHz, D_2O) δ 6.85 (s, 2H, CH=CH), 4.24 – 4.19 (m, 2H, $OCH_2CH_2N(CH_3)_3$), 3.98 (app q, *J* = 7.0 Hz, 2H, $OCH_2CH_2NC{=}O$), 3.75 (app t, *J* = 6.0 Hz, 2H, $OCH_2CH_2NC{=}O$), 3.64 – 3.59 (m, 2H, $OCH_2CH_2N(CH_3)_3$), 3.18 (s, 9H,

$N(CH_3)_3$); **^{13}C NMR** (101 MHz, D_2O) δ 172.9 (C=O), 134.5 (C=C), 66.1 – 65.9 (m, $CH_2N(CH_3)_3$), 62.8 (d, *J* = 5.0 Hz, $OCH_2CH_2NC{=}O$), 59.5 (d, *J* = 5.0 Hz, $OCH_2CH_2N(CH_3)_3$), 54.1 – 53.9 (m, $OCH_2CH_2NC{=}O$) 38.2 (d, *J* = 7.5 Hz, $N(CH_3)_3$); **^{31}P NMR** (162 MHz, D_2O) -0.31; **HRMS** (ES+) calc. for $C_{11}H_{19}N_2NaO_6P$ $[M+Na]^+$ 329.0873, found 329.0875.

Data consistent with literature values.[71]

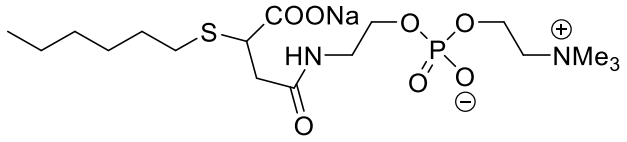
Sodium (*Z*)-4-((2-((oxido(2-(trimethylammonio)ethoxy)phosphoryl)oxy)ethyl)amino) -4-oxobut-2-enoate, 3.10



To a stirred solution of 2-(2,5-dioxo-2,5-dihydro-1*H*-pyrrol-1-yl)ethyl (2-(trimethylammonio)ethyl) phosphate, **3.9** (250.0 mg, 0.816 mmol, 1.0 equiv.) in water (5 mL) was added sodium hydroxide (32.7 mg, 0.816 mmol, 1.0 equiv.). After 2 mins solvent removed *in vacuo.* Sodium (*Z*)-4-((2-((oxido(2-(trimethylammonio)ethoxy)phosphoryl)oxy)ethyl)amino)-4-oxobut-2-enoate was obtained without further purification as a purple-red gum (265.3 mg, 0.767 mmol, 94%). **IR** (thin film, ν_{max} / cm^{-1}) 3393, 2471, 1570, 1476, 1205, 1084; **^{1}H NMR** (400 MHz, D_2O) δ 6.38 (d, *J* = 12.5 Hz, 1H, $CHCHCO_2Na$), 5.96 (d, *J* = 12.5 Hz, 1H, $CHCO_2Na$), 4.45 – 4.25 (m, 2H, $OCH_2CH_2N(CH_3)_3$), 4.09 – 3.86 (m, 2H, $OCH_2CH_2NC{=}O$), 3.80 – 3.64 (m, 2H, $CH_2NC{=}O$), 3.52 (td, *J* = 5.5, 1.0 Hz, 2H, $CH_2N(CH_3)_3$), 3.25 (s, 9H, $N(CH_3)_3$); **^{13}C NMR** (101 MHz, D_2O) δ 174.5 (C=OONa), 167.9 (C=ON), 130.4 ($CH{=}CHCOONa$), 123.9 ($CH{=}CHCOONa$), 66.1 – 65.9 (m, $CH_2N(CH_3)_3$), 64.3 (d, *J* = 5.5 Hz, $OCH_2CH_2NC{=}O$), 59.5 (d, *J* = 5.0 Hz, $OCH_2CH_2N(CH_3)_3$), 54.2 – 53.9 (m,

$N(CH_3)_3$), 39.8 (d, *J* = 7.5 Hz $OCH_2CH_2NC{=}O$); **^{31}P NMR** (162 MHz, D_2O) -0.24; **HRMS** (ES-) calc. for $C_{11}H_{20}O_7N_2P$ $[M\text{-}Na]^-$ 323.1014, found 323.1013.

(±)-Sodium 2-(hexylthio)-4-((2-((oxido(2-(trimethylammonio)ethoxy)phosphoryl)oxy)ethyl)amino)-4-oxobutanoate, 3.11

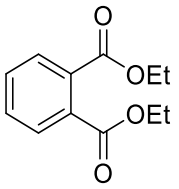


To a stirred solution of 2-(2,5-dioxo-2,5-dihydro-1*H*-pyrrol-1-yl)ethyl (2-(trimethylammonio)ethyl) phosphate, **3.9** (200.0 mg, 0.653 mmol, 1.0 equiv.) in water (5 mL) was added sodium hydroxide (26.1 mg, 0.653 mmol, 1.0 equiv.). After about 5 mins 1-hexanethiol (102 µL, 0.717 mmol, 1.1 equiv.) was added. After 8 h, the reaction mixture was extracted with diethyl ether (3 x 5 mL), the aqueous taken and solvent removed *in vacuo*. (±)-Sodium 2-(hexylthio)-4-((2-((oxido(2-(trimethylammonio)ethoxy)phosphoryl)oxy)ethyl)amino)-4-oxobutanoate was obtained without further purification as a colourless gum (242.6 mg, 0.522 mmol, 80%). Trace hydrolysed maleimide was present in this compound.

IR (thin film, ν_{max} / cm^{-1}) 3402, 2958, 2470, 1571, 1474, 1205, 1084; **^{1}H NMR** (400 MHz, D_2O) δ 4.39 – 4.28 (m, 2H, $OCH_2CH_2N(CH_3)_3$), 4.02 – 3.94 (m, 2H, $OCH_2CH_2NC{=}O$), 3.73 – 3.67 (m, 4H, $CH_2N(CH_3)_3$), 3.61 – 3.57 (m, 1H, SCHCOONa), 3.48 (t, *J* = 5.5 Hz, 2H, $CH_2NC{=}O$), 3.25 (s, 9H, $N(CH_3)_3$), 2.78 (d, *J* = 6.5 Hz, 1H, SCHC*H*H'C=O), 2.70 (t, *J* = 7.0 Hz, 1H, SCHCH*H*'C=O), 2.67 – 2.61 (m, 2H, SCH_2), 1.72 (p, *J* = 7.5 Hz, 2H, SCH_2CH_2), 1.50 – 1.27 (m, 6H, alk CH_2), 0.92 – 0.85 (m, 3H, CH_2CH_3); **^{13}C NMR** (101 MHz, D_2O) δ 178.8 (C=OONa), 173.5 (C=ON), 66.2 – 65.9 (m, $CH_2N(CH_3)_3$), 64.2 (d, *J* = 6.0 Hz, $OCH_2CH_2NC{=}O$), 59.6 – 59.4 (m, $OCH_2CH_2N(CH_3)_3$), 54.2 – 53.8 (m, $N(CH_3)_3$), 46.6 (SCHCOONa), 40.1 – 39.9 (m,

$OCH_2CH_2NC{=}O$), 39.0 ($CH_2C{=}ON$), 31.6 (SCH_2), 29.3 (alk CH_2), 28.6 (alk CH_2), 27.7 (alk CH_2), 21.9 (CH_2CH_3), 14.0 (CH_3); **^{31}P NMR** (162 MHz, D_2O) -0.25; **HRMS** (ES-) calc. for $C_{17}H_{34}O_7N_2P^{32}S$ $[M\text{-}Na]^-$ 441.1830, found 441.1827.

Diethyl phthalate, 3.15

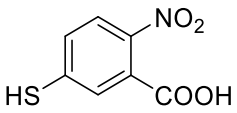


To a solution of phthalic anhydride (1.14 g, 7.70 mmol, 1.0 equiv.) in ethanol (25 mL) and dichloromethane (15 mL) was added concentrated sulfuric acid (1 mL) and heated to reflux overnight. The reaction mixture was allowed to cool to room temperature, water added (30 mL) and extracted with dichloromethane (3 x 30 mL). The combined organics were washed with brine (40 mL), dried ($MgSO_4$) and the solvent removed *in vacuo.* The crude material was purified by column chromatography (ethyl acetate/ petroleum ether (1:9)) to give diethyl phthalate as a colourless oil (706.6 mg, 3.18 mmol, 41%).

IR (oil, ν_{max} / cm^{-1}) 2983, 2939, 1718, 1600, 1579, 1465, 1447, 1391, 1366, 1273, 1173, 1120, 1070, 1039, 1015; **^{1}H NMR** (400 MHz, $CDCl_3$) δ 7.71 (dd, *J* = 5.5, 3.5 Hz, 2H, CHC*H*C(C)COO), 7.52 (dd, *J* = 5.5, 3.5 Hz, 2H, C*H*CHC(C)COO), 4.36 (q, *J* = 7.0 Hz, 4H, OCH_2CH_3), 1.36 (t, *J* = 7.0 Hz, 6H, OCH_2CH_3); **^{13}C NMR** (101 MHz, $CDCl_3$) δ 167.6 (C=O), 132.2 (CC=O), 130.9 ($CHCHCC{=}O$), 128.8 ($CHCC{=}O$), 61.6 (CH_2), 14.1 (CH_3); **LRMS** (ES+) calc. for $C_{12}H_{14}O_4Na$ $[M+Na]^+$ 245.1, found 245.0.

Data consistent with literature values.[85]

5-Mercapto-2-nitrobenzoic acid, 3.7



To a suspension of 5,5'-dithiobis(2-nitrobenzoic acid), **3.5** (2.55 g, 6.43 mmol, 1.0 equiv.) in ethanol (24 mL) and water (6 mL) was added dropwise a suspension of sodium borohydride (2.65 g, 51.44 mmol, 8.0 equiv.) in water (12 mL) over the course of 20 minutes. After 1 h, the reaction mixture was diluted with ethanol (25 mL) and water (25 mL), acidified with 1M HCl solution to pH 1, and extracted with dichloromethane (3 x 50 mL). The combined organics were dried ($NaSO_4$) and the solvent removed *in vacuo*. 5-Mercapto-2-nitrobenzoic acid was obtained without further purification as a yellow amorphous solid (2.428 g, 12.19 mmol, 95%).

IR (solid, ν_{max} / cm^{-1}) 1710, 1643, 1604, 1585, 1572, 1511, 1328, 1039; **^{1}H NMR** (400 MHz, DMSO-d_6) δ 8.05 (d, *J* = 8.5 Hz, 1H, C*H*CHCS), 7.96 (d, *J* = 2.0 Hz, 1H, CSC*H*CCOOH), 7.89 (dd, *J* = 8.5, 2.0 Hz, 1H, CHC*H*CS); **^{13}C NMR** (101 MHz, DMSO-d_6) δ 165.8 (C=O), 147.0 (CN), 142.1 (CS), 129.4 (CH*C*HCS), 129.4 (CS*C*HCCOOH), 127.1 (*C*HCHCS), 125.7 (*C*C=O); **HRMS** (ES-) calc. for $C_{17}H_7O_4NF_{17}{}^{32}S_2$ [M-H]$^-$for $C_7H_4O_4N{}^{32}S$, 197.9867, found 197.9866.

Data consistent with literature values.[72]

3. 6 References

1. Williams, T. C. *Chemotaxis : types, clinical significance, and mathematical models*. (Nova Science Publishers, 2011).
2. Wadhams, G. H. & Armitage, J. P. Making sense of it all: Bacterial chemotaxis. *Nature Reviews Molecular Cell Biology* **5**, 1024–1037 (2004).
3. de Oliveira, S., Rosowski, E. E. & Huttenlocher, A. Neutrophil migration in infection and wound repair: going forward in reverse. *Nat. Rev. Immunol.* **16**, 378–91 (2016).
4. Wolpert, L. (Lewis). *Principles of development*. (Oxford University Press, 2011).
5. Čejková, J. *et al.* Chemotaxis and Chemokinesis of Living and Non-living Objects. In (Adamatzky, A.) *Advances in Unconventional Computing. Emergence, Complexity and Computation* (Springer, Cham, 2016).
6. Agudo-Canalejo, J., Adeleke-Larodo, T., Illien, P. & Golestanian, R. Enhanced Diffusion and Chemotaxis at the Nanoscale. *Acc. Chem. Res.* **51**, 2365–2372 (2018).
7. Bonner, J. T. & Savage, L. J. Evidence for the formation of cell aggregates by chemotaxis in the development of the slime mold Dictyostelium discoideum. *J. Exp. Zool.* **106**, 1–26 (1947).
8. Budrene, E. O. & Berg, H. C. Dynamics of formation of symmetrical patterns by chemotactic bacteria. *Nature* **376**, 49–53 (1995).
9. Kondo, S. & Miura, T. Reaction-diffusion model as a framework for understanding biological pattern formation. *Science* **329**, 1616–1620 (2010).
10. Szurmant, H. & Ordal, G. W. Diversity in Chemotaxis Mechanisms among the Bacteria and Archaea. *Microbiol. Mol. Biol. Rev.* **68**, 301–319 (2004).
11. Richard P. Feynman. There's a Plenty of Room At the bottom. *Eng. Sci.* **23**, 22–36 (1960).
12. Barry, N. P. & Bretscher, M. S. Dictyostelium amoebae and neutrophils can swim. *Proc. Natl. Acad. Sci. USA* **107**, 11376–11380 (2010).
13. Purcell, E. M. Life at low Reynolds number. *Am. J. Phys.* **45**, 3–11 (1977).
14. Kumar, B. V. V. S. P., Patil, A. J. & Mann, S. Enzyme-powered motility in buoyant organoclay/DNA protocells. *Nat. Chem.* **10**, 1154–1163 (2018).
15. Joyce, G. F. & Szostak, J. W. Protocells and RNA self-replication. *Cold Spring Harb. Perspect. Biol.* **10**, a034801 (2018).
16. Schwille, P. How Simple Could Life Be? *Angew. Chemie - Int. Ed.* **56**, 10998–11002 (2017).
17. Szostak, J. W., Bartel, D. P. & Luisi, P. L. Synthesizing life. *Nature* **409**, 387–390 (2001).
18. Tomlinson, C. XLVII. On the motions of camphor on the surface of water. *London, Edinburgh, Dublin Philos. Mag. J. Sci.* **38**, 409–424 (1869).

19. Nakata, S., Pimienta, V., Lagzi, I., Kitahata, H. & Suematsu, N. J. *Theoretical and computational chemistry series : physicochemical design based on nonlinear dynamics. Volume 14, Self-organized Motion*. (RSC, 2018).

20. Heide, A. de. *Anatome mytuli, Belgicè mossel, structuram elegantem ejusque motum mirandum exponens. Subjecta est Centuria observationum medicarum.* (Janssonius van Waesberghe, 1684).

21. Franklin, B. & Franklin, W. T. *Memoirs of the Life and Writings of Benjamin Franklin vol. 4 Correspondence 2*. (H. Colburn, 1818).

22. Golestanian, R., Liverpool, T. B. & Ajdari, A. Propulsion of a Molecular Machine by Asymmetric Distribution of Reaction Products. *Phys. Rev. Lett.* **94**, 220801 (2005).

23. Tu, Y. *et al.* Self-propelled supramolecular nanomotors with temperature-responsive speed regulation. *Nat. Chem.* **9**, 480–486 (2017).

24. Sengupta, S., Ibele, M. E. & Sen, A. Fantastic voyage: Designing self-powered nanorobots. *Angew. Chemie - Int. Ed.* **51**, 8434–8445 (2012).

25. Guix, M., Mayorga-Martinez, C. C. & Merkoçi, A. Nano/Micromotors in (Bio)chemical science applications. *Chemical Reviews* **114**, 6285–6322 (2014).

26. Wang, J. & Gao, W. Nano/microscale motors: Biomedical opportunities and challenges. *ACS Nano* **6**, 5745–5751 (2012).

27. Desai, N., Shaik, V. A. & Ardekani, A. M. Hydrodynamics-mediated trapping of micro-swimmers near drops. *Soft Matter***14**, 264–278 (2018).

28. Ghosh, A. *et al.* Helical Nanomachines as Mobile Viscometers. *Adv. Funct. Mater.* **28**, 1705687 (2018).

29. Paxton, W. F. *et al.* Catalytic nanomotors: Autonomous movement of striped nanorods. *J. Am. Chem. Soc.* **126**, 13424–13431 (2004).

30. Ke, H., Ye, S., Carroll, R. L. & Showalter, K. Motion Analysis of Self-Propelled Pt−Silica Particles in Hydrogen Peroxide Solutions. *J. Phys. Chem. A* **114**, 5462–5467 (2010).

31. Hu, L., Tao, K., Miao, J. & Grüber, G. Hydrogen-peroxide-fuelled platinum-nickel-SU-8 microrocket with steerable propulsion using an eccentric nanoengine. *RSC Adv.* **6**, 102513–102518 (2016).

32. Catchmark, J. M., Subramanian, S. & Sen, A. Directed rotational motion of microscale objects using interfacial tension gradients continually generated via catalytic reactions. *Small* **1**, 202–206 (2005).

33. Paxton, W. F., Sen, A. & Mallouk, T. E. Motility of catalytic nanoparticles through self-generated forces. *Chem. - A Eur. J.* **11**, 6462–6470 (2005).

34. Pavlick, R. A., Sengupta, S., McFadden, T., Zhang, H. & Sen, A. A polymerization-powered motor. *Angew. Chemie - Int. Ed.* **50**, 9374–9377 (2011).

35. Ibele, M., Mallouk, T. E. & Sen, A. Schooling behavior of light-powered autonomous micromotors in water. *Angew. Chemie - Int. Ed.* **48**, 3308–3312 (2009).

36. Buttinoni, I., Volpe, G., Kümmel, F., Volpe, G. & Bechinger, C. Active Brownian motion tunable by light. *J. Phys. Condens. Matter* **24**, 284129 (2012).

37. Dreyfus, R. *et al.* Microscopic artificial swimmers. *Nature* **437**, 862–865 (2005).

38. Lozano, C., ten Hagen, B., Löwen, H. & Bechinger, C. Phototaxis of synthetic microswimmers in optical landscapes. *Nat. Commun.* **7**, 12828 (2016).

39. Anderson, J. L. Colloid Transport by Interfacial Forces. *Annu. Rev. Fluid Mech.* **21**, 61–99 (1989).

40. Jin, C., Krüger, C. & Maass, C. C. Chemotaxis and autochemotaxis of self-propelling droplet swimmers. *Proc. Natl. Acad. Sci. U. S. A.* **114**, 5089–5094 (2017).

41. Čejková, J., Novák, M., Štěpánek, F. & Hanczyc, M. M. Dynamics of Chemotactic Droplets in Salt Concentration Gradients. *Langmuir* **30**, 11937–11944 (2014).

42. Abécassis, B., Cottin-Bizonne, C., Ybert, C., Ajdari, A. & Bocquet, L. Boosting migration of large particles by solute contrasts. *Nat. Mater.* **7**, 785–789 (2008).

43. Hong, Y., Diaz, M., Córdova-Figueroa, U. M. & Sen, A. Light-Driven Titanium-Dioxide-Based Reversible Microfireworks and Micromotor/Micropump Systems. *Adv. Funct. Mater.* **20**, 1568–1576 (2010).

44. Theurkauff, I., Cottin-Bizonne, C., Palacci, J., Ybert, C. & Bocquet, L. Dynamic clustering in active colloidal suspensions with chemical signaling. *Phys. Rev. Lett.* **108**, 268303 (2012).

45. Stenhammar, J., Nardini, C., Nash, R. W., Marenduzzo, D. & Morozov, A. Role of Correlations in the Collective Behavior of Microswimmer Suspensions. *Phys. Rev. Lett.* **119**, 028005 (2017).

46. Pohl, O. & Stark, H. Dynamic clustering and chemotactic collapse of self-phoretic active particles. *Phys. Rev. Lett.* **112**, 238303 (2014).

47. Saha, S., Golestanian, R. & Ramaswamy, S. Clusters, asters, and collective oscillations in chemotactic colloids. *Phys. Rev. E - Stat. Nonlinear, Soft Matter Phys.* **89**, 062316 (2014).

48. Liebchen, B., Marenduzzo, D., Pagonabarraga, I. & Cates, M. E. Clustering and Pattern Formation in Chemorepulsive Active Colloids. *Phys. Rev. Lett.* **115**, 258301 (2015).

49. Banno, T., Miura, S., Kuroha, R. & Toyota, T. Mode changes associated with oil droplet movement in solutions of gemini cationic surfactants. *Langmuir* **29**, 7689–7696 (2013).

50. Hanczyc, M. Droplets: Unconventional Protocell Model with Life-Like Dynamics and Room to Grow. *Life* **4**, 1038–1049 (2014).

51. Horibe, N., Hanczyc, M. M. & Ikegami, T. Mode switching and collective behavior in chemical oil droplets. *Entropy***13**, 709–719 (2011).

52. Thutupalli, S., Seemann, R. & Herminghaus, S. Swarming behavior of simple model squirmers. *New J. Phys.***13**, 073021 (2011).

53. Herminghaus, S. *et al.* Interfacial mechanisms in active emulsions. *Soft Matter* **10**, 7008–7022 (2014).

54. Krüger, C., Bahr, C., Herminghaus, S. & Maass, C. C. Dimensionality matters in the collective behaviour of active emulsions. *Eur. Phys. J. E* **39**, (2016).

55. Hanczyc, M. M., Toyota, T., Ikegami, T., Packard, N. & Sugawara, T. Fatty acid chemistry at the oil-water interface: Self-propelled oil droplets. *J. Am. Chem. Soc.* **129**, 9386–9391 (2007).

56. Walde, P., Wick, R., Fresta, M., Mangone, A. & Luisi, P. L. Autopoietic Self-Reproduction of Fatty Acid Vesicles. *J. Am. Chem. Soc.* **116**, 11649–11654 (1994).

57. Toyota, T., Maru, N., Hanczyc, M. M., Ikegami, T. & Sugawara, T. Self-propelled oil droplets consuming 'Fuel' surfactant. *J. Am. Chem. Soc.* **131**, 5012–5013 (2009).

58. Kaneko, S., Asakura, K. & Banno, T. Phototactic behavior of self-propelled micrometer-sized oil droplets in a surfactant solution. *Chem. Commun.* **53**, 2237–2240 (2017).

59. Suzuki, K. & Sugawara, T. Phototaxis of Oil Droplets Comprising a Caged Fatty Acid Tightly Linked to Internal Convection. *ChemPhysChem* **17**, 2300–2303 (2016).

60. Nagasaka, Y., Tanaka, S., Nehira, T. & Amimoto, T. Spontaneous emulsification and self-propulsion of oil droplets induced by the synthesis of amino acid-based surfactants. *Soft Matter* **13**, 6450–6457 (2017).

61. Banno, T., Tanaka, Y., Asakura, K. & Toyota, T. Self-Propelled Oil Droplets and Their Morphological Change to Giant Vesicles Induced by a Surfactant Solution at Low pH. *Langmuir* **32**, 9591–9597 (2016).

62. Banno, T., Kuroha, R. & Toyota, T. PH-sensitive self-propelled motion of oil droplets in the presence of cationic surfactants containing hydrolyzable ester linkages. *Langmuir* **28**, 1190–1195 (2012).

63. Miura, S. *et al.* pH-induced motion control of self-propelled oil droplets using a hydrolyzable gemini cationic surfactant. *Langmuir* **30**, 7977–7985 (2014).

64. Ban, T., Aoyama, A. & Matsumoto, T. Self-generated Motion of Droplets Induced by Korteweg Force. *Chem. Lett.***39**, 1294–1296 (2010).

65. Lee, S. W. & Laibinis, P. E. Directed movement of liquids on patterned surfaces using noncovalent molecular adsorption. *J. Am. Chem. Soc.* **122**, 5395–5396 (2000).

66. De Gennes, P. G. Wetting: Statics and dynamics. *Rev. Mod. Phys.* **57**, 827–863 (1985).

67. Lach, S., Yoon, S. M. & Grzybowski, B. A. Tactic, reactive, and functional droplets outside of equilibrium. *Chem. Soc. Rev.* **45**, 4766–4796 (2016).

68. Bain, C. D., Burnett-Hall, G. D. & Montgomerie, R. R. Rapid motion of liquid drops. *Nature* **372**, 414–415 (1994).

69. Banno, T. *et al.* Deformable Self-Propelled Micro-Object Comprising Underwater Oil Droplets. *Sci. Rep.***6**, 31292 (2016).

70. Lagzi, I., Soh, S., Wesson, P. J., Browne, K. P. & Grzybowski, B. A. Maze solving by chemotactic droplets. *J. Am. Chem. Soc.* **132**, 1198–1199 (2010).

71. Bissette, A. J., Odell, B. & Fletcher, S. P. Physical autocatalysis driven by a bond-forming thiol–ene reaction. *Nat. Commun.* **5**, 4607 (2014).

72. Morrow, S. M., Colomer, I. & Fletcher, S. P. A chemically fuelled self-replicator. *Nat. Commun.* **10**, 1011 (2019).

73. Ueno, N. *et al.* Self-Propelled Motion of Monodisperse Underwater Oil Droplets Formed by a Microfluidic Device. *Langmuir* **33**, 5393–5397 (2017).

74. Stricker, L. Numerical simulation of artificial microswimmers driven by Marangoni flow. *J. Comput. Phys.* **347**, 467–489 (2017).

75. Schmitt, M. & Stark, H. Marangoni flow at droplet interfaces: Three-dimensional solution and applications. *Phys. Fluids* **28**, 012106 (2016).

76. Maass, C. C., Krüger, C., Herminghaus, S. & Bahr, C. Swimming Droplets. *Annu. Rev. Condens. Matter Phys.* **7**, 171–193 (2015).

77. Seemann, R., Fleury, J. B. & Maass, C. C. Self-propelled droplets. *European Physical Journal: Special Topics* **225**, 2227–2240 (2016).

78. Popescu, M. N., Uspal, W. E. & Dietrich, S. Self-diffusiophoresis of chemically active colloids. *Eur. Phys. J. Spec. Top.* **225**, 2189–2206 (2016).

79. Gutierrez, J. M. P., Hinkley, T., Taylor, J. W., Yanev, K. & Cronin, L. Evolution of oil droplets in a chemorobotic platform. *Nat. Commun.* **5**, 5571 (2014).

80. Banno, T., Kuroha, R., Miura, S. & Toyota, T. Multiple-division of self-propelled oil droplets through acetal formation. *Soft Matter* **11**, 1459–1463 (2015).

81. Nagai, K., Sumino, Y., Kitahata, H. & Yoshikawa, K. Mode selection in the spontaneous motion of an alcohol droplet. *Phys. Rev. E* **71**, 065301 (2005).

82. Chattopadhyay, A. & London, E. Fluorimetric determination of critical micelle concentration avoiding interference from detergent charge. *Anal. Biochem.* **139**, 408–412 (1984).

83. Matsuno, R., Takami, K. & Ishihara, K. Simple synthesis of a library of zwitterionic surfactants via michael-type addition of methacrylate and alkane thiol compounds. *Langmuir* **26**, 13028–13032 (2010).

84. Heath, W. H. *et al.* Degradable cross-linkers and strippable imaging materials for step-and-flash imprint lithography. *Macromolecules* **41**, 719–726 (2008).

85. Kalsi, D., Barsu, N. & Sundararaju, B. CoIII-Catalyzed Isonitrile Insertion/Acyl Group Migration Between C−H and N−H bonds of Arylamides. *Chem. - A Eur. J.* **24**, 2360–2364 (2018).

Chapter 4.

Self-replication and selection away-from-equilibrium

Chapter 4

Self-replication and selection away-from-equilibrium

Work in this chapter was in part undertaken in collaboration with Michael Howlett (MH) and Maria Lebedeva (ML). The iSCAT experiments described in section 4. 3. 3. 2 were designed, performed and analysed by ML, using compounds prepared by RJHS and MH. The experiments in all other sections were designed by RJHS. Experiments in sections 4. 2. 3 and 4. 3. 1-2 were carried out in part by RJHS and in part by MH.

4. 1 Introduction

4. 1. 1 Prior work on competing replicators and replication away-from-equilibrium

4. 1. 1. 1 Competing replicators

The study of how systems of synthetic replicators interact with one another is key to developing theories of how evolution and selection could occur in prebiotic environments. A number of systems have been developed which show the behaviour of multiple mutually compatible replicators, with selection arising from often unexpected factors and a few of these systems are briefly outlined below.

A DNA based replicator system was described in 1998 where two nucleophilic and two electrophilic precursors form four possible template strands (Figure 4. 1. 1. 1. 1).[1] Two products (ApnB and BpnA) are self-complementary and therefore show autocatalytic kinetics. The two other products (ApnA and BpnB) are complementary to one another, therefore each catalyses the formation of the other, forming a set known as a reciprocal replicator. The authors observe that in the absence of any product added the two autocatalytic products are the primary products present after 1 h. There is a large degree

of product inhibition in this system as 6mer duplexes are stable, therefore when one product template of the reciprocal replicator pair is added, only its complement achieves a rate enhancement.

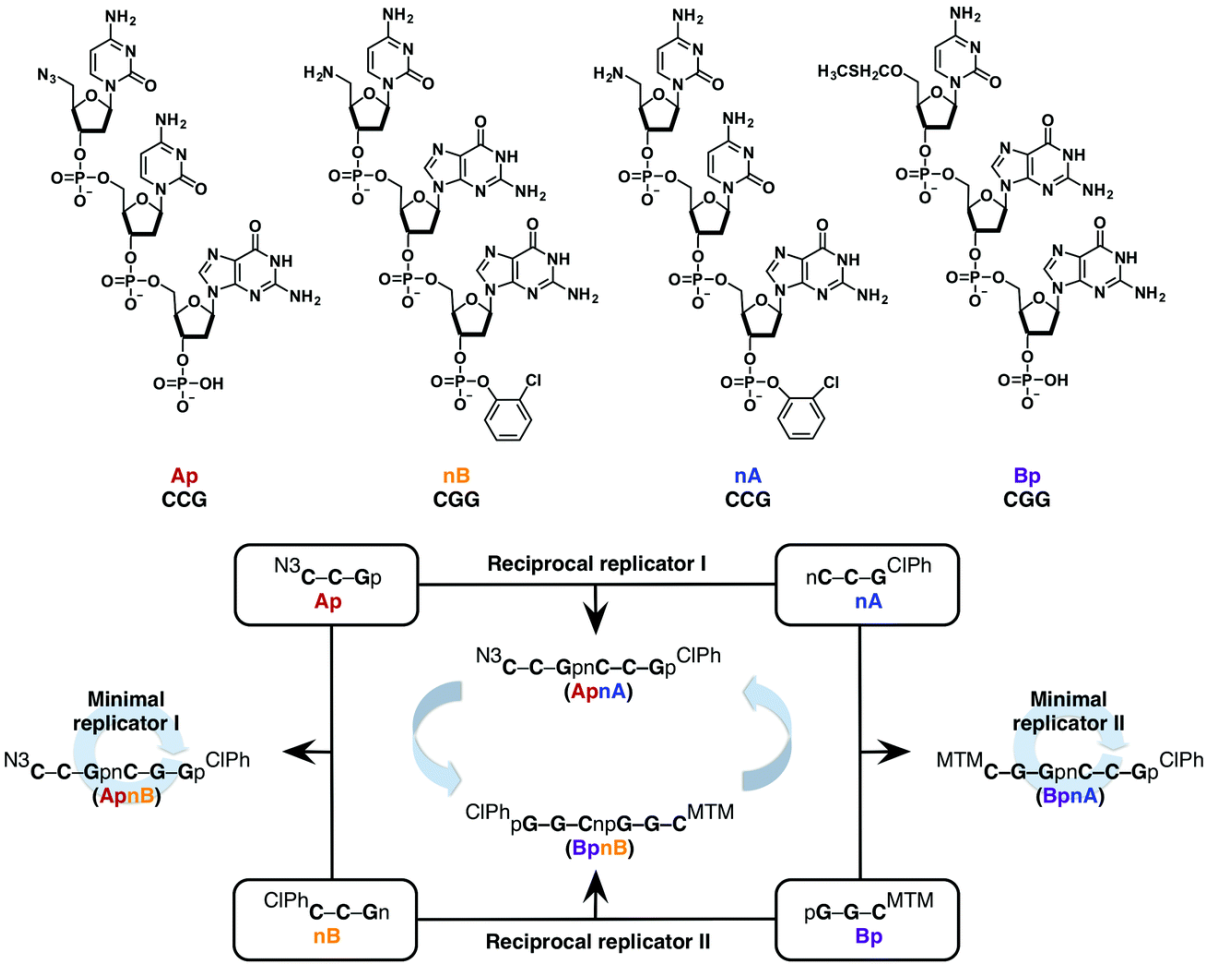


Figure 4. 1. 1. 1. 1. DNA based system of competing templates, showing autocatalysis and cross-catalysis. Reproduced with permission.[2]

Yao et al. reported a system of peptide replicators that showed a similar relationship of two autocatalytic products and a reciprocal replicator.[3] In this work, the authors were able to demonstrate that which synthetic replicator had the highest final concentration could be result from changes to the environment. The ratio of two peptide autocatalysts and two cross-catalytic template products could be dictated by changes to their environment. Under neutral conditions the reciprocal replicator products are slightly more abundant

than the autocatalysts, but at high salt concentration one self-replicator is dominant and the other self-replicator dominant in low pH. This work has been extended to larger networks.[4]

Competition between two small-molecule template replicators was reported by the Philp group in 2017 (Figure 4. 1. 1. 1. 2).[5] This work shows the importance of interactions within replicator populations during competition. When the kinetics of formation of the two replicating species are compared in isolation, replicator T^p is formed faster and shows a greater ability to template its own formation than T^m. Unexpectedly, when the precursors M^p and M^m compete for a limiting amount of N, T^m is dominant, an outcome rationalised by cross-catalysis efficiencies. T^p effectively catalyses T^m production, T^m does not catalyse (or possibly weakly inhibits) T^p formation.

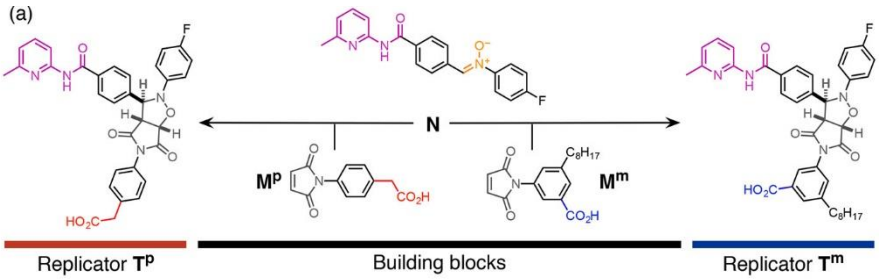


Figure 4. 1. 1. 1. 2. System of two competing replicators based on 1,3-dipolar cycloadditions between a nitrone and maleimides. Reproduced with permission.[5]

Attempts to build adaptive systems that are sensitive to their environment and develop through time based on template replication of this type has been unsuccessful, as shown by a very recent report.[6] The authors show that, regardless of initial conditions similar compositions result, which is in my opinion due to the limited catalytic effects of these replicators, affected by strong product inhibition.

A very impressive example of selection between replicating molecules was developed by the Otto group (Figure 4. 1. 1. 1. 3).[7] Oxidation of an aryl dithiol generates a dynamic

library of disulfides. Some macrocyclic disulfides assemble into fibres under the reaction conditions, growing at the ends.

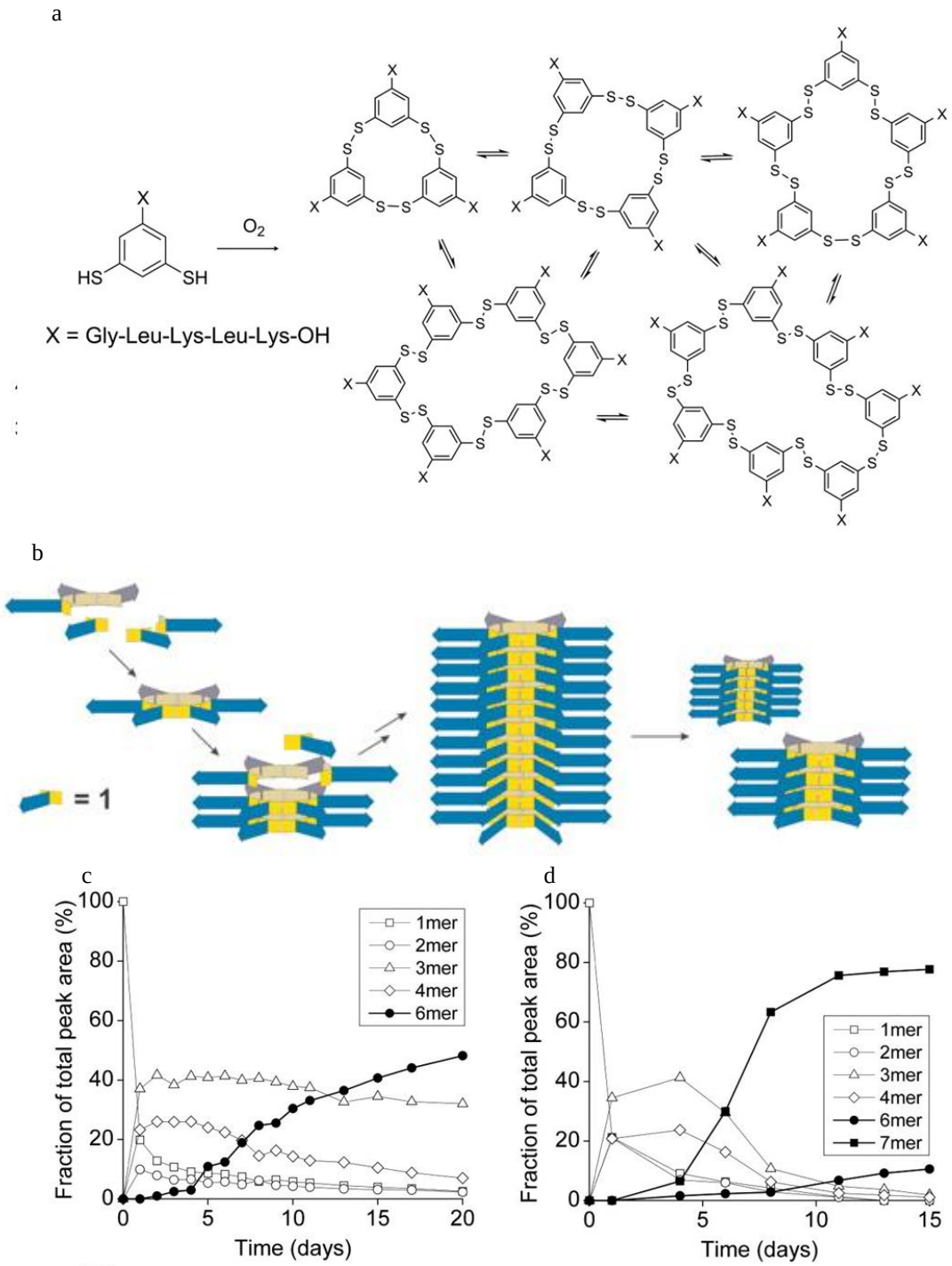


Figure 4. 1. 1. 1. 3. a – Generation of a dynamic library of disulfides through oxidation of an aryl dithiol. b – diagram of the assembly of disulfides into fibres and fibre cleavage. c – Composition of the reaction mixture through time, under shaking (500 rpm) conditions. Peak area is correlated with concentration. d –

Composition of the reaction mixture through time, under stirring (1200 rpm) conditions. Peak area is correlated with concentration. Reproduced with permission.[7]

Agitation-induced fibre breakage increases the total number of ends available and thus system shows exponential kinetics. Several parameters effect the size of the macrocycles that emerge. Interestingly, the nature of agitation provides enough of a difference in environment for a high degree of selection between different fibres to be seen. When shaken, the 6mer predominates after 15 days with no measurable quantity of 7mer present. Whereas when stirred the 7mer is predominant after 7 days, with very little 6mer present. Selection between which macrocycle size predominates can also be controlled by addition of a 2,2,2-trifluoroethanol additive.[8]

When two aryl dithiols are mixed, a greater number of possible replicating species can form through the course of the reaction. In 2016 Sadownik et al. reported such a system, where a 1:1 mixture of two aryl dithiols differing by one amino acid (either phenylalanine or serine) in the peptide chain of the monomer were reacted. Many different macrocycles are grouped for ease of analysis. One group was defined to be cyclic 6mers with more phenylalanine containing monomers, the second group cyclic 6mers with more serine containing monomers. After a week, only 6mers from the more hydrophobic, first group were present. After 12 days the amount of the second group rapidly grew. The second group of replicators the authors describe as being a "descendant" of the first, as the first replicator group removes material from the exchanging solution phase pool of disulfides, thus changing the relative proportions of the two aryl species towards that needed to form the second group of replicators.[9]

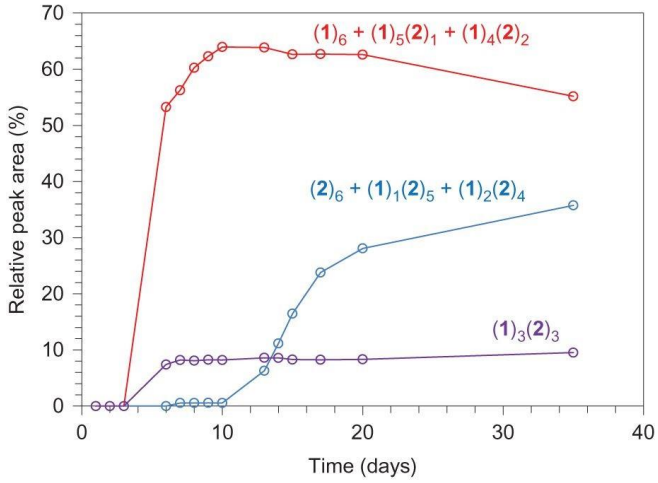


Figure 4. 1. 1. 1. 4. Kinetics of competing replicator system based on two aryl dithiol components. red – cyclic 6mers containing more serine containing monomers, purple – cyclic 6mers containing equal quantities of both monomers, blue – cyclic 6mers containing more phenylalanine containing monomers. Peak area is correlated with concentration. Reproduced with permission.[9]

It is worth noting that the predominant species in these systems does not necessarily arise from the positive feedback of autocatalysis, sometimes the thermodynamic stability of a non-replicating species is enough to override this. In an adenine based system, under a variety of oxidative conditions a 15mer is the primary species present, identified to be a 75-membered ring macrocycle.[10] X-ray crystallography identified this as having a hydrophobic core of five stacks of 3 phenyl rings with offset π-π stacking, capped at both ends by adenine residues. In an ethylene glycol based system, a complex mixture of oligomers is seen, leading to the formation of changing supramolecular aggregates through time, from micelles to vesicles to "sponge phases", without any apparent autocatalysis.[11]

A unifying feature of all prior competing replicator studies is their use of thermodynamically stable replicators, while transient replicators are yet to be studied in competition experiments. This is of high importance if we are to build models of how

simple non-biological replicating species can interact within a population and evolve through time.

4. 1. 1. 2 Replicators away-from-equilibrium

One of the first investigations into replication away from equilibrium was performed by the group of von Kiedrowski.[12] Here, one component containing an amidinium cation reacts with another component containing a carboxylate anion to form an imine product. Through formation of salt bridge interactions, this product can catalyse its own formation (Figure 4. 1. 1. 2. 1). Since this report, a number of systems have been reported which show autocatalysis within a dynamic covalent library, mostly based on imine formation.[13–16] They are of limited scope, however typically involving only one replicator and all reach thermodynamic equilibrium, that is they are not sustained away from equilibrium by fuelling.[2]

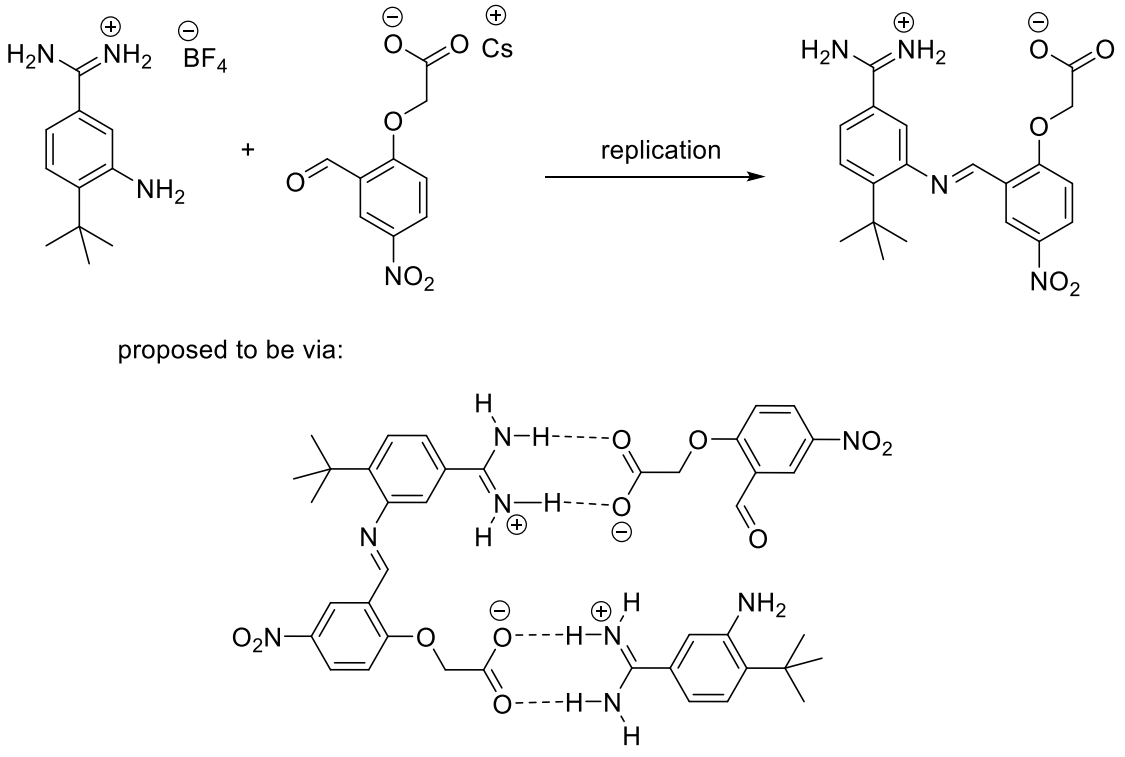


Figure 4. 1. 1. 2. 1. Away-from-equilibrium replication through imine formation described by von Kiedrowski. Adapted with permission.[12]

Away from equilibrium replication has been studied in lipid systems showing physical autocatalysis. Zepik et al. reported in 2001 a system of oleate vesicles being turned over under the reaction conditions.[17] Under the reaction conditions, oleic anhydride is hydrolysed to oleate, forming vesicles. Oleate is also oxidised to a diol which does not form vesicles by potassium ferricyanate in the presence of catalytic osmium tetroxide. Through changing the addition rate of the starting material (oleic anhydride) and oxidising agent (potassium ferricyanide), vesicle concentration can be maintained at a steady state, or made to increase or decrease.

A prominent example of the role of non-equilibrium structures found in life are microtubules.[18] Tubulin dimers are present in the cell as disassembled proteins and polymers. Each dimer has two nucleotide binding domains, with α-tubulin permanently binding GTP and β-tubulin binding GDP or GTP. When the β-tubulin is GTP bound, there is a high affinity for other tubulin molecules, aiding assembly of microtubules at the positive end. Assembly induces a conformational change within β-tubulin, significantly increasing its GTPase activity, hydrolysing GTP to GDP. GDP-tubulin disassembles from the end, but not from internal positions in the tubule. Tubulin therefore acts like a clock at the growing end, in the presence of a high cytosolic concentration of GTP-tubulin microtubules will grow, in low concentrations they rapidly depolymerise. This is often referred to as dynamic instability.

Actin and microtubules are the most ubiquitous elements of the cytoskeleton and both show similar dissipative self-assembly, whilst intermediate filaments found in some animals are thermodynamic structures.[19] The dynamic nature of microtubules is highly useful to the cell providing a scaffold that can be remodelled very rapidly according to need. Microtubules play a central role in many cellular processes, including physical division of the chromosomes in mitosis, aid structural integrity in cilia and flagella and

provide directional information in intracellular transport. They even form the feeding organelles, axopodia, in some diffusion feeders such as Heliozoa.[20]

Artificial systems which operate out of equilibrium are of enormous interest due to the potential to make responsive materials with behaviour impossible at equilibrium. One interesting example which achieves coupling between small molecule chemistry and material properties was reported by Boekhoven et al. (Figure 4. 1. 1. 2. 2).[21] Chemically, a dicarboxylate is monomethylated by dimethyl sulphate to give a gelator. This can assemble into fibres causing gelation. Under the basic reaction conditions, the gelator in the fibre state and in solution undergoes hydrolysis to reform the non-assembling dicarboxylate. Here the lifetime and physical properties of the gel (stiffness) could be tuned by varying pH and initial concentration of dimethyl sulphate. After hydrolysis, a gel could be regenerated with addition of more fuel. Analysis of individual fibres by microscopy showed somewhat similar behaviour to microtubules, with growth and shrinkage occurring at the tips and there was some apparent stochasticity in which occurred.

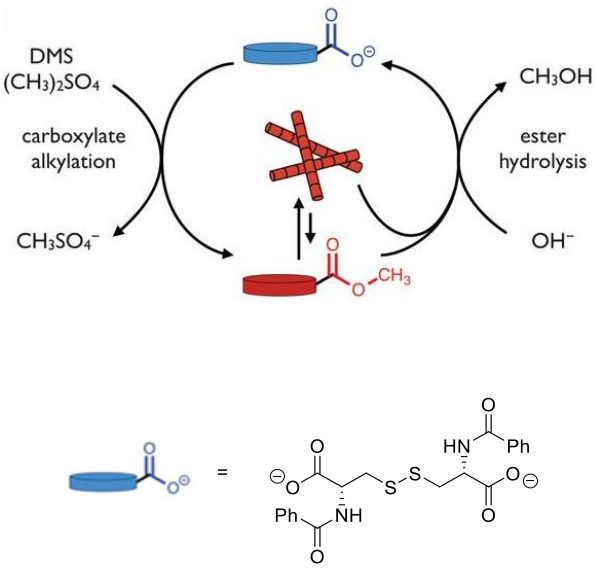


Figure 4. 1. 1. 2. 2. System of dissipative self-assembly of a gel reported by Boekhoven et al. The small molecule dicarboxylate which undergoes gelation when methylated. Adapted with permission.[21]

A general theoretical understanding of composition in away from equilibrium systems is elusive, though there has been much progress since the foundations laid by Prigogine, for which he was awarded the 1977 Nobel Prize in Chemistry.[22] In essence, the dynamic kinetic stability (DKS) put forward by Pross hints at the core principle, that it is insufficient to evaluate merely thermodynamic stabilities or rates of formation when considering which species will be present, dissipative systems operate neither fully under the classical descriptions of kinetic or thermodynamic control.[23–26] The term for this combined property Pross calls persistence. As yet, the framework lacks thorough mathematical treatment.

A model for which supramolecular structures emerge under dissipative conditions has been developed by Jeremy England, which seeks to explain the emergence of energy consuming states.[27–29] The model, based on statistical mechanics approach, predicts the behaviour of mixed systems where a large variety of possible self-assembled structures are accessible and there is a constant energy input. Under such conditions the model predicts a number of possible outcomes. As can be seen intuitively, thermodynamic minima can result, as well as kinetically trapped states. The free energy of these structures does not depend on the energy input, they are what is expected under unworked conditions. There is however a third case, states that are entered because they have a "greater history" of work dissipation than others. The mechanism of this can be understood by thinking about each step which involves dissipation. A single dissipative step forms a supramolecular arrangement which has released free energy in being formed, so may well be kinetically trapped. If so, this state may persist, or a second dissipative step could occur, driving the system toward ever more energy consuming states. The system develops to be much better than average at absorbing energy, it is "resonant" with the energy input, has reached a highly dissipative state. One could imagine this being a

means by which a proto-metabolism could be established, finding a highly dissipative state or states without a Darwinian selection mechanism.

How composition of lipid aggregates varies in time has been modelled by the graded autocatalysis replication domain (GARD) model.[30,31] Here, different lipids incorporate into micelles by exchange with monomers in bulk solution, with rate of incorporation depending on the identity of the monomer and the identity of those within the micelle. Metastable states of composition, referred to as compositional genomes or "composomes", were found under nonequilibrium conditions. To be sustained, these composomes require nonequilibrium conditions. Composomes show homeostasis, with a long lifetime relative to monomer exchange, capacity for self-replication and "mutation-like" rapid changes in composition to other composomes.[32]

An example of a synthetic transient replicator was achieved by the Fletcher group in 2018, based on alkene metathesis (Figure 4. 1. 1. 2. 3). Here an aliphatic internal alkene forms an organic phase, with a glycosylated styrene in the aqueous phase. In the presence of Grubb's 2nd generation catalyst, alkene metathesis occurs to form surfactant products. Under biphasic conditions these products are thermodynamically unstable, forming a stilbene by second metathesis reaction with the hydrophilic starting material.

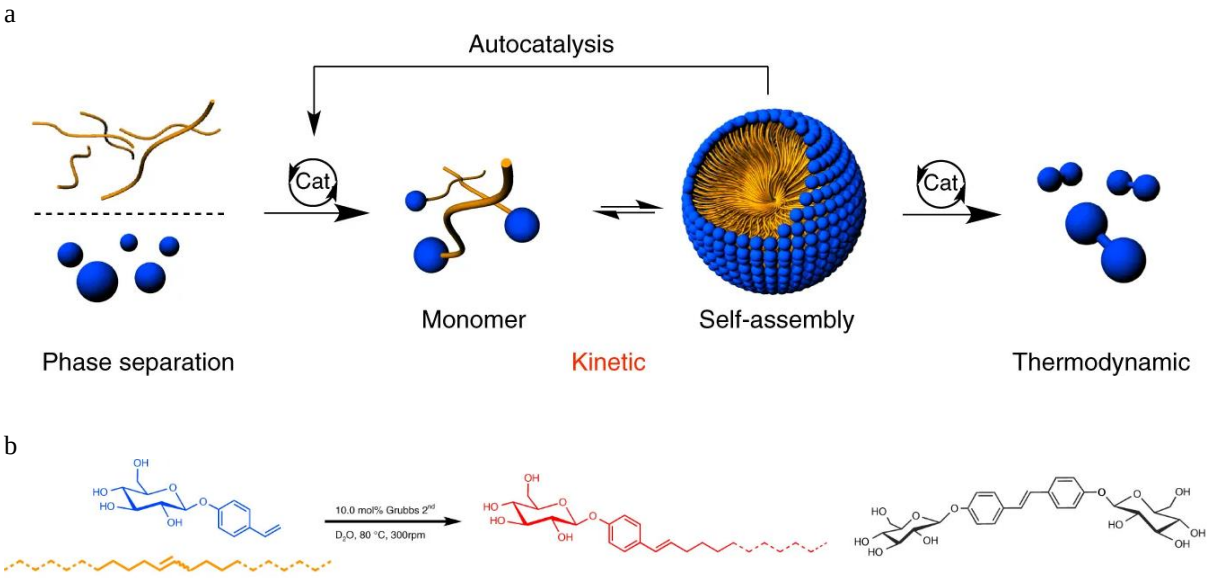
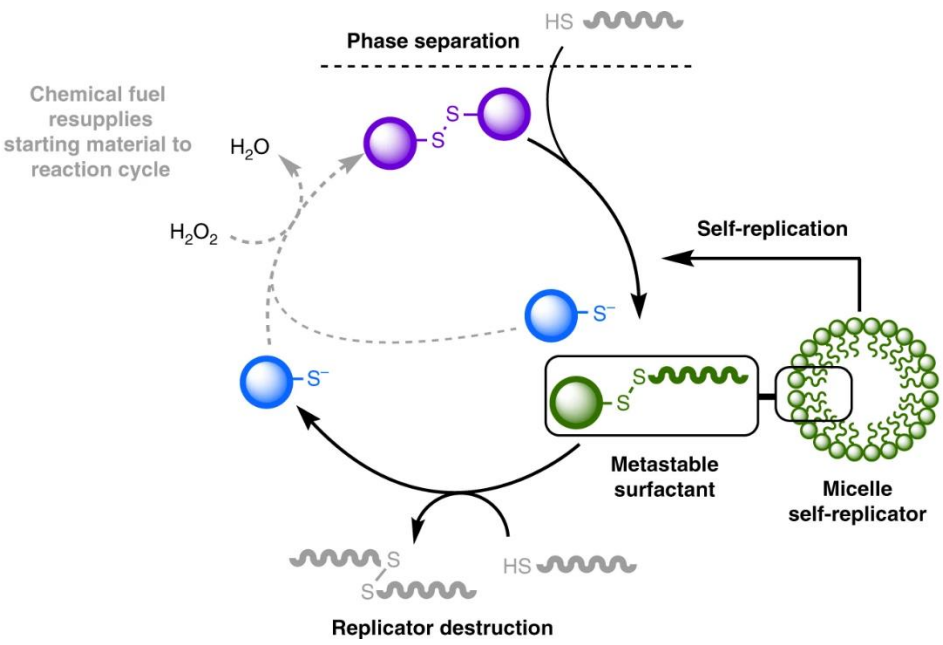


Figure 4. 1. 1. 2. 3. Alkene metathesis based transient replicator formation. a – conceptual diagram showing replicator formation and assembly into micelles, as well as destruction to the thermodynamic composition. b – reaction scheme for this system. Reproduced with permission.[33]

Further to the olefin metathesis based system, a second transient replicator system was reported in 2019, based on thiol-disulfide exchange (Figure 4. 1. 1. 2. 4).[34] The results of this chapter draw inspiration from that work. Here, 1-octanethiol forms the organic phase, with Ellman's reagent (also known as DTNB) dissolved in the aqueous. These react to form a mixed disulfide amphiphile which in the presence of excess alkyl thiol is unstable to the reaction conditions, forming a second equivalent of TNB and alkyl disulfide. Thermodynamically, the reaction can be understood by the S-S bond strength increasing from ArSSAr to RSSAr to RSSR. Excitingly, by selective oxidation of TNB in the aqueous phase by constant addition of hydrogen peroxide, the limiting starting material DTNB can be recycled, allowing for the replicator to be sustained away from equilibrium.

a



b

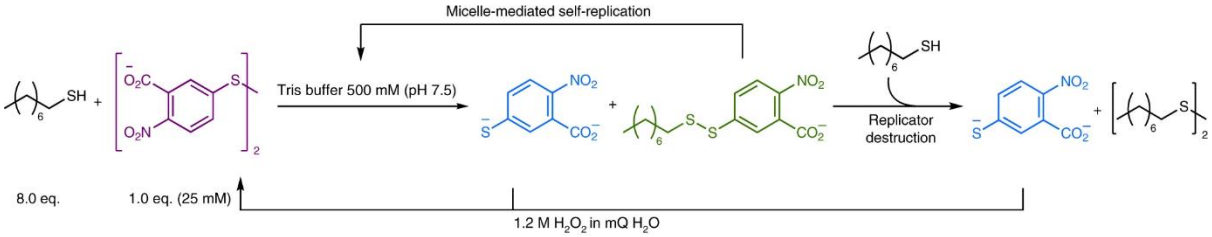


Figure 4. 1. 1. 2. 4. Thiol-disulfide exchange based physical autocatalysis system. Through addition of H_2O_2 fuel the surfactant can be sustained out of equilibrium. a – conceptual diagram showing replicator formation, destruction and the recycling of TNB. b – reaction scheme for this system. Reproduced with permission.[34]

4. 1. 1. 3 Chemical oscillations

Initially, oscillations within chemical systems may seem impossible on thermodynamic grounds. In closed chemical systems, equilibrium is obtained by a monotonic change in composition due to entropy maximisation throughout the reaction. For this not to be the case, then a specific chemical reaction would need to at one time proceed forwards and at another go backwards. As it was put by Gray and Scott: "There are no oscillations, damped or undamped, about chemical equilibrium."[35] Despite this constraint in closed systems, oscillating reactions have in open systems been observed for centuries.

Although the modern study of oscillating chemical systems began with the now pervasive Belousov–Zhabotinsky reaction in the 1950s and 60s,[36] there are far older examples such as Davy's studies on "cold flames" of the 1810s, where the light from a continuous flow of ignited gas rapidly pulsated.[37] Feedback in oscillating chemical systems can be isothermal autocatalysis, eg. The Belousov–Zhabotinsky reaction, or self-heating (non-isothermal), eg. "cold flames".[38]

The theoretical basis for oscillating reaction developed by Lotka in the early twentieth century.[39] Though the Lotka–Volterra equations became famous for their later application by Kolmogorov and many others in ecology as predator-prey relationships, they were initially developed as a model for the as yet unknown isothermal periodic reactions.[40] There is a requirement for nonlinear kinetics for oscillations to occur. Autocatalysis is inherently nonlinear, but theoretically this could be achieved through other feedback mechanisms.[41]

To sustain oscillations, reactions are commonly kept away from equilibrium by the constant addition of starting materials and removal of waste using a continuous stirred-tank reactor (CSTR).[42,43] This is the primary way oscillating reactions are studied today,

although it is not a requirement, for the Belousov–Zhabotinsky reaction a large excess of malonate can be can be seen as the fuel which drives a chemical cycle in which concentrations of Ce(III) and Ce(IV) oscillate. Nonlinear kinetics arise from autocatalytic production of $HBrO_2$ (hypobromous acid), one of the steps within the chemical cycle.[44]

Behaviour in chemical oscillating systems can be extremely complex, and difficult to interpret, as not only can damped and sustained oscillations be present, but also steady state bistabilities (coexistence of multiple stable steady states),[35] "oscillation plus steady state" bistabilities (coexistence of a steady state and an oscillatory state, which may spontaneously interchange or be persistent for some initial conditions)[45,46] and chaos (behaviour characterised by being neither monotonic or periodic).[47] Despite apparent randomness, chaotic systems are deterministic, with small changes in initial conditions leading to very different results.[48]

Today oscillations remain an active area of interest within several fields of chemistry and materials science.[49] Though they are much studied, there are very few different classes of oscillating reaction, typically discovered by chance and there are still many fundamental properties being discovered. How to design an oscillating reaction from scratch, or take an existing reaction with function of interest and make an oscillating variant is essentially unknown.

Oscillating reactions have been applied to construction of functional systems, such as swellable gels for soft robotics and pH clocks.[50–52] One example of how oscillating reactions can achieve motion is the "self-walking" gel of Maeda et al (Figure 4. 1. 1. 3. 1).[53] Here a swellable gel responds to redox potential of the extending fluid it contains, in its Ru(III) state the gel is swollen, forming an etiolated shape, in a Ru(II) state the gel is contracted, forming a more curved shape. On a ratchetted floor, the gel walks in one direction. Oscillations have also been coupled to self-assembly of

nanoparticles through use of a pH clock (Figure 4. 1. 1. 3. 2).[54] Gold nanoparticles were observed to spontaneously assemble and disassemble through time, aggregating at low pH and disassembling at high pH due to deprotonation of mercaptophenol ligands.

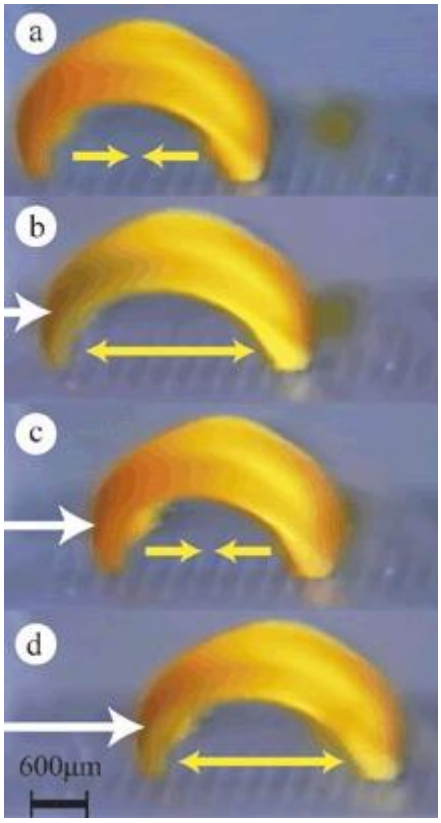


Figure 4. 1. 1. 3. 1. A series of sequential images, a-d, of a self-walking gel, made from a swellable gel containing a Beluosov–Zhabotinskii reaction aqueous on a ratchet surface. The overall time between a and d is 500 seconds. Reproduced with permission.[53]



Figure 4. 1. 1. 3. 2. Diagram of oscillations in Au nanoparticle assembly through coupling to an oscillating chemical reaction which varies in pH. Reproduced with permission.[51]

The work of Cafferty et al. demonstrates how fundamental principles of oscillating reactions are still being discovered.[43] In their system oscillations in total thiol concentration within a reaction network are observed using a CSTR setup. Amplification within the network is achieved through a combination of thiol-disulfide exchange and Kent ligation. Negative feedback is also present, through thio-Michael reactions. Thioesters are supplied as a sulfur source. Some thioesters result in oscillations and others do not. Counterintuitively, oscillations often occur when two thioesters are supplied which do not in isolation result in oscillations. The authors define the maintenance of oscillations through changes to the reaction conditions (pH, space velocity, temperature and others) as robustness. Unexpectedly, the highest robustness is seen in mixtures of thioester, so system heterogeneity can stabilise complex behaviour.

4. 1. 2 Aims

The ultimate aim of this project is to develop an experimental model for prebiotic evolution. It is worthy of note that whilst there has been enormous progress in the understanding of prebiotic synthesis of building blocks, ie. monomers of biomolecules,

and also how they can polymerise in the past six or so decades since the Miller–Urey experiment, the principles of how energy-consuming, living states and how evolvable states can develop from these building blocks are almost completely unknown.[55–58]

Ever since the discovery of the structure of DNA by Crick and Watson in 1953, template based replication has been the dominated discourse on replication in biology and prebiotic chemistry.[59–61] However, it seems likely that different rules for chemical evolution are likely to hold for different classes of replicators, therefore we need to study replicators beyond the case of arguably well understood nucleotide-based systems. It seems likely for lipid replicators compositional inheritance would be highly important, as well as emergence, with certain mixtures having functions not available to the constituent parts in isolation.

Ideally, the architect of synthetic life would mix a few precursors together to form a sustained out-of-equilibrium system of replicating entities, which shows unconstrained chemical evolution through time. This would have sufficient complexity to change through unpredictable and novel states.

The thiol-disulfide exchange system developed in the Fletcher group had a couple of features particularly attractive for use as a chemical evolution model. Firstly, the transient nature of the reported replicator led us to believe that if multiple replicators were present, each may be constantly turned over, and thus replicator populations could change through time. This could lead to a succession or evolution of composition, the course of which would influenced by the environment, be it abundance of food or presence of destructive species. Further, assembly of these replicator mixtures into supramolecular structures is likely to lead to interactions between the different components causing them to act together. The second attractive feature was compartmentalisation. Though in the previously reported system the replicator forms only micelles, it seemed likely structural

modification could give rise to vesicle replicators, an obvious protocell model (Figure 4. 1. 2. 1). In short, we believed that this design could be used form a system of replicating protocells requiring food to be sustained, and that would show evolution sensitive to their environmental conditions.

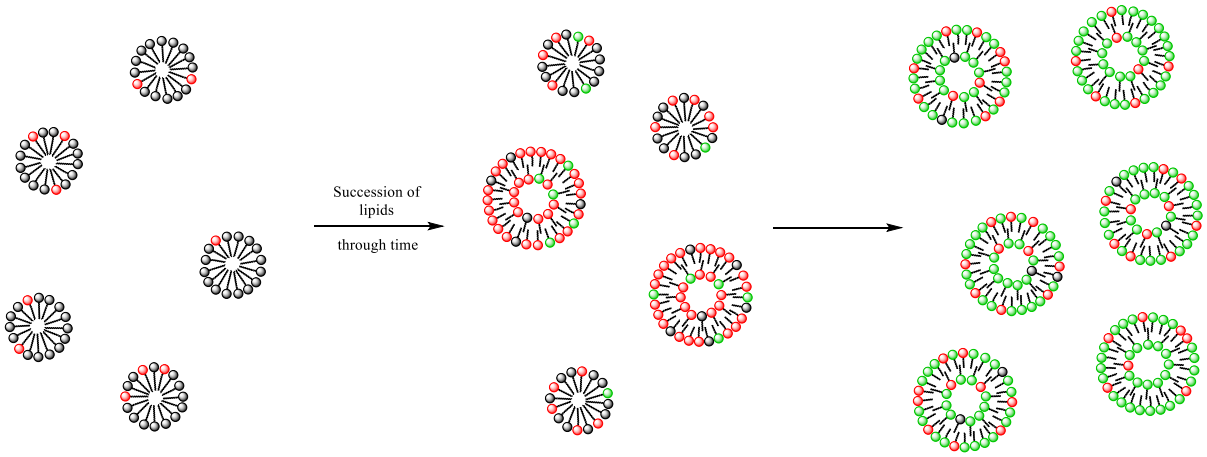


Figure 4. 1. 2. 1. Conceptual figure showing a succession of lipids through time, and associated increase in degree of compartmentalisation from micelles to vesicles. Black red and green balls represent three different lipids, all formed under the reaction conditions.

4. 1. 3 System design

We believed that a system with up to three different alkyl thiols and up to three bis-aryl disulfides could give rise to significant complexity and the desired succession of replicators (Figure 4. 1. 3. 1). Three alkyl thiols (**4.1a**, **4.1b** and **4.1c**) were chosen based on differing steric properties. Three homoaryl disulfides (**4.2, 4.3** and **4.4**) were chosen for their differing electronic properties. It seemed likely that heteroaryl disulfides (**4.5, 4.6** and **4.7**) would also be present in the system, though the effects of these were not obvious at this stage. Thiol disulfide exchange would give rise to three aryl thiols (**4.8, 4.9** and **4.10**) and nine mixed disulfides (**4.11a-c, 4.12a-c** and **4.13a-c**) (Figure 4. 1. 3. 2).

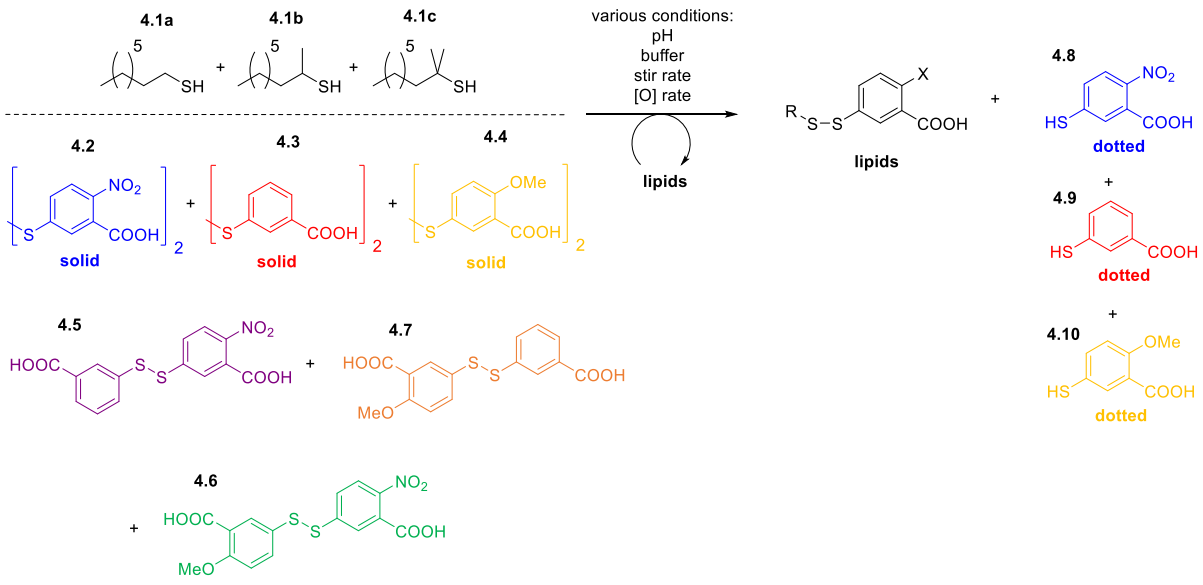


Figure 4. 1. 3. 1. System design of the desired reaction. Lipids are formed by thiol-disulfide exchange reactions. Where descriptors are given in bold below a structure, this refers to the fitting line on kinetics graphs for this molecule in this chapter.

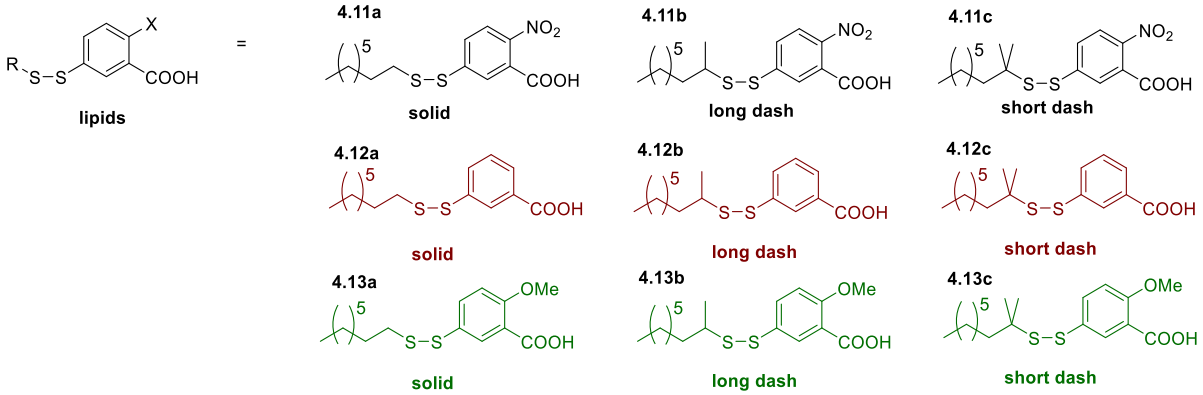


Figure 4. 1. 3. 2. Identity of nine possible lipids formed in figure 4. 1. 3. 1. Where descriptors are given in bold below a structure, this refers to the fitting line on kinetics graphs for this molecule in this chapter.

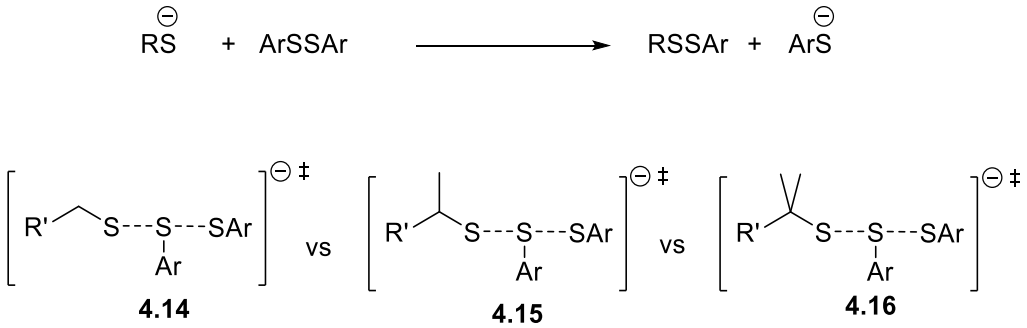
Each mixed disulfide replicator could act autocatalytically, but the nature of physical autocatalysis suggests a network of cross-catalytic relationships would be present. We believed it would be interesting to see if selection and control could emerge under these conditions, when cross-catalysis in prebiotic models is typically associated with “error” and loss of specificity and activity of replicators.

4. 2 System optimisation and mechanistic understanding

4. 2. 1 Initial findings and optimisation of conditions

When the three thiols **4.1a-c** were combined with one aryl disulfide we expected to see a succession in lipid concentration arising from simple steric considerations. We expected that the primary mixed disulfide would form fastest (Figure 4. 2. 1. 1a) but would also be destroyed fastest (Figure 4. 2. 1. 1b) due to having the least steric hinderance in its transition states for formation and destruction.

a



b

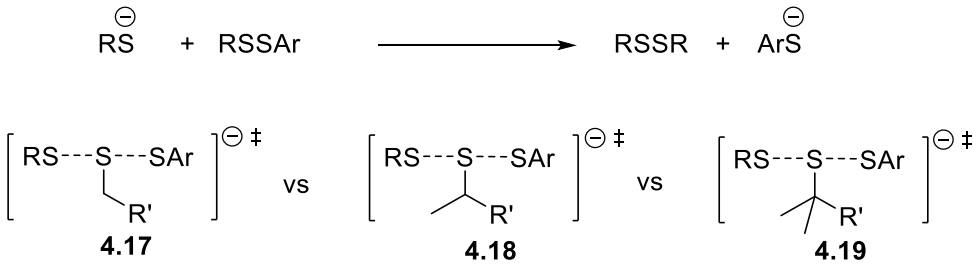
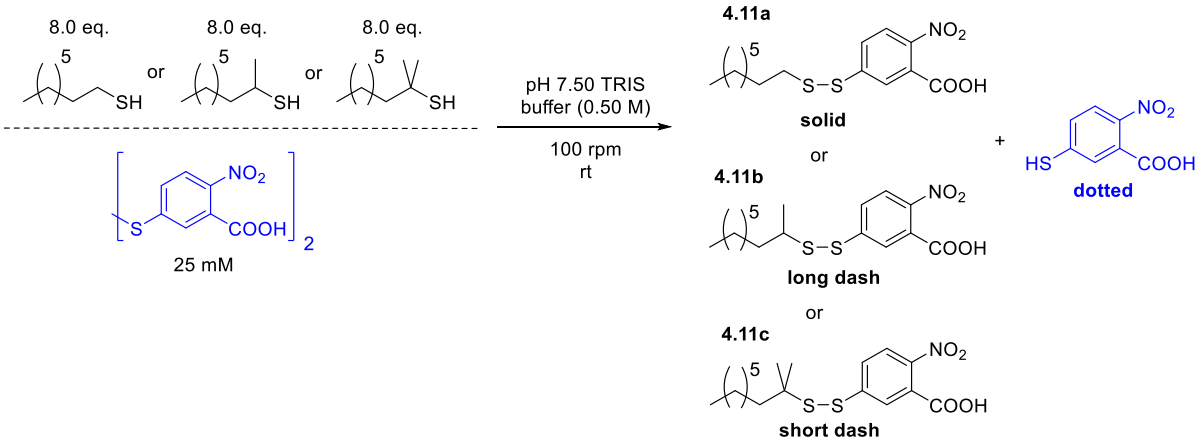


*Figure 4. 2. 1. 1. Comparison between the transition states involving lipids **4.11a-c**. a – formation transition states, where **4.16** is expected to be higher in energy than **4.15**, which is higher in energy than **4.14**, b – destruction transition states, where **4.19** is expected to be higher in energy than **4.18**, which is higher in energy than **4.17**.*

Behaviour of formation of three lipids **4.11a-c** was compared using the conditions previously reported (Figure 4. 2. 1. 2).[34] Here we see that the products formed from less hindered alkyl thiols do form fastest when these reactions are performed in isolation. For **4.11a**, flocculation was often observed under these conditions, hampering quantification. The drop in concentration at t = 5–6 h is an example of this and not destruction by excess

1-octanethiol. We looked for conditions where flocculation did not occur, so conclusions from the system could be made unambiguously.



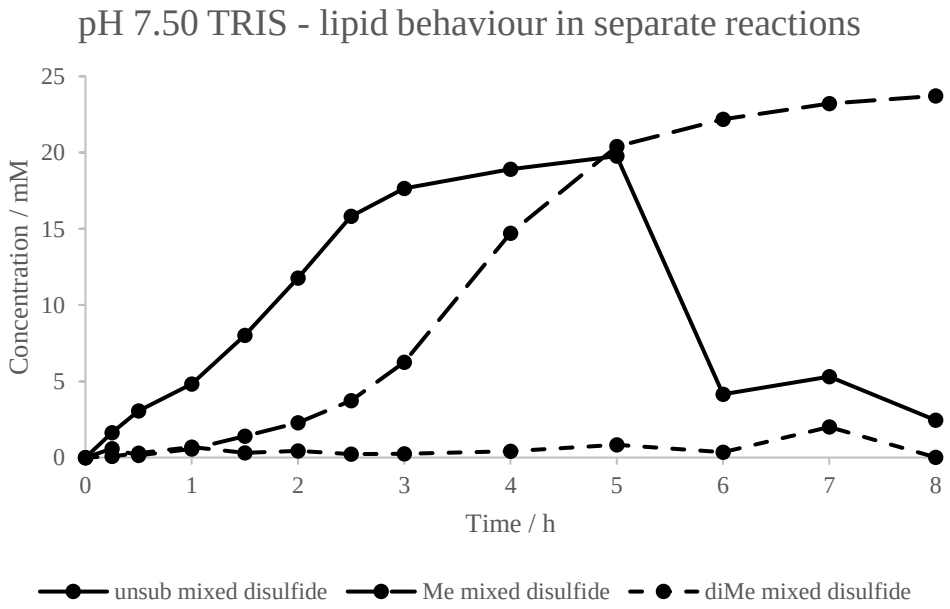
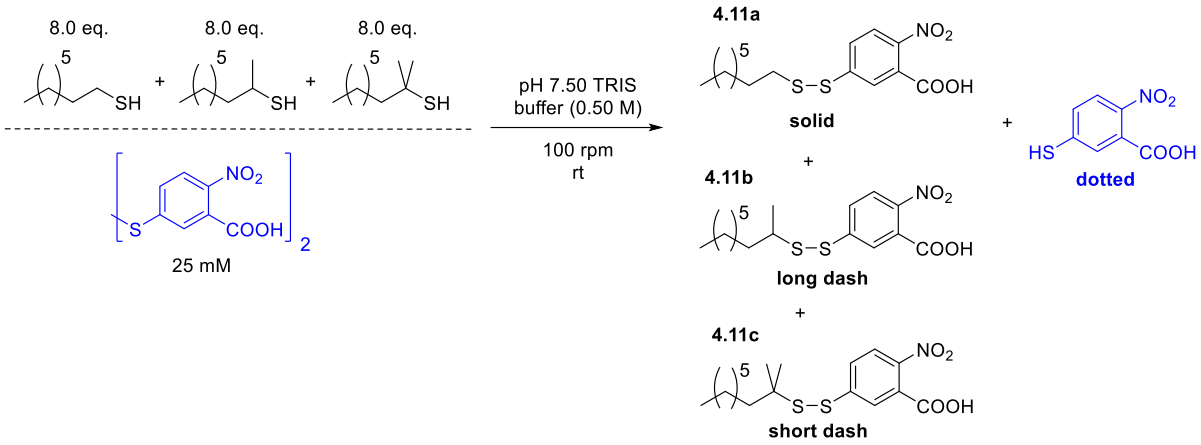


*Figure 4. 2. 1. 2. Comparison between the kinetics of mixed disulfide formation of **4.11a, 4.11b** and **4.11c**. Concentrations of **4.2** and **4.8** are omitted for clarity. n = 1.*

When all three thiols were present, the three lipids **4.11a**, **4.11b** and **4.11c** could form together within one reaction medium, competing for **4.2** (Figure 4. 2. 1. 3). Under the same conditions, flocculation was sometimes observed, and whilst there is a clear selection between the lipids, no succession was observed nor considerable destruction.



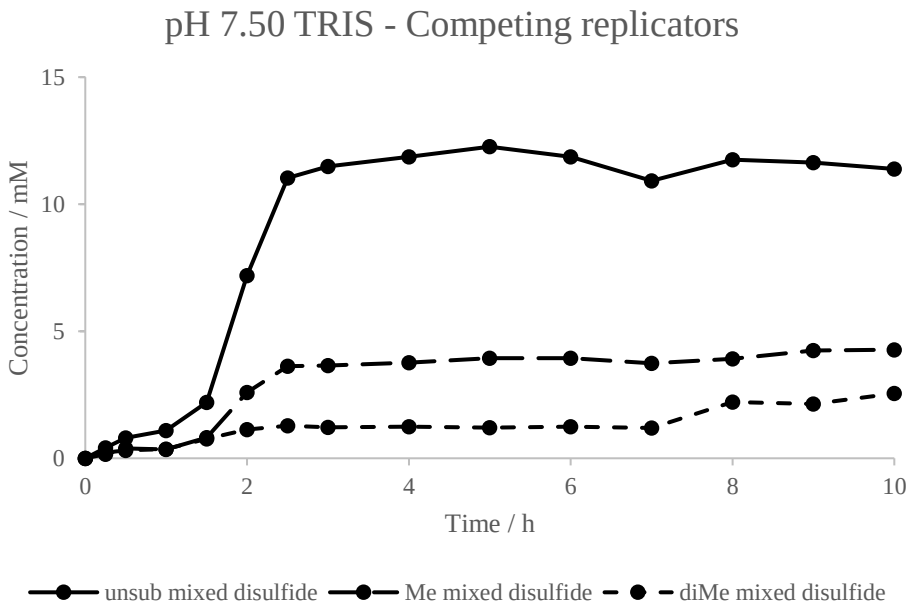


*Figure 4. 2. 1. 3. Kinetics of mixed disulfide formation of **4.11a, 4.11b** and **4.11c** in pH 8.00 HEPES buffer. Concentrations of **4.2** and **4.8** are omitted for clarity. n = 1.*

At higher pH the competing lipid kinetics were more promising, showing a succession in what was the dominant replicator through time (Figure 4. 6. 9. 1. 1). Unfortunately, floccing still sometimes occurred in this medium. In HEPES buffer floccing was not observed and at pH 7.50 the reaction was also too slow (Figure 4. 6. 9. 1. 2), but at pH 8.00 the reaction proceeded as desired within a reasonable timescale (Figure 4. 2. 1. 4), with the succession of lipids being complete within 30 h. Further mechanistic description is given in section 4. 3. 2. 1.

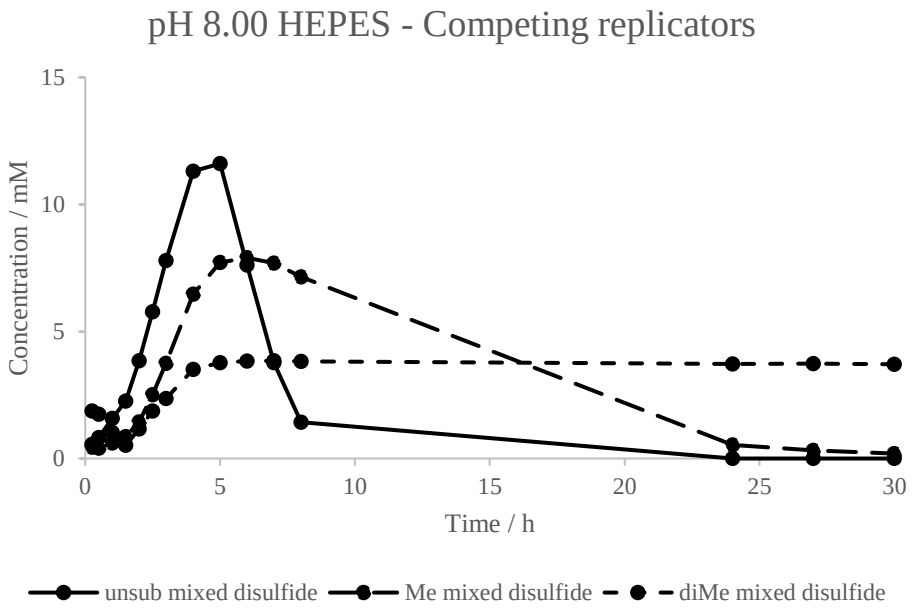
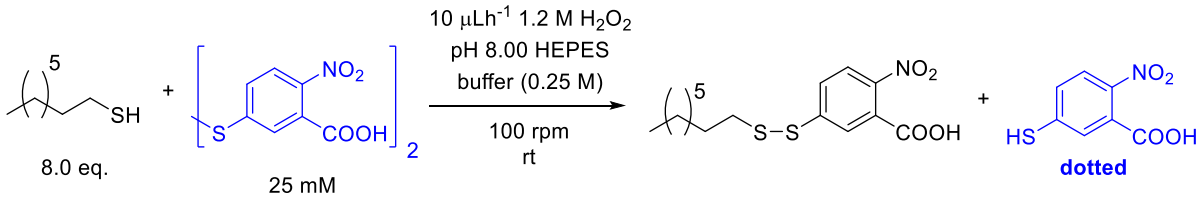


*Figure 4. 2. 1. 4. Kinetics of mixed disulfide formation of **4.11a, 4.11b** and **4.11c** in pH 8.00 HEPES buffer. Reaction setup is otherwise as figure 4. 2. 1. 2. Concentrations of **4.2** and **4.8** are omitted for clarity. n = 1.*

In experiments with surfactant and excess alkyl thiol, complete surfactant destruction was observed for all mixed disulfides suggesting that the thermodynamic product of all these systems was aliphatic disulfide and TNB.

4. 2. 2 Away from equilibrium behaviour and oscillations

Using the new buffer conditions, we tested to see whether the effects of fuelling with hydrogen peroxide would be the same as previously reported for pH 7.50 TRIS buffer, where a sustained steady state of replicator was observed.[34] At pH 8.00 in HEPES buffer, initial results were disappointing, showing only a small sustained population of mixed disulfide (Figure 4. 2. 2. 1). Increasing concentration of the hydrogen peroxide, rather than the expected increase in steady state population of mixed disulfide, more complex behaviour is seen, and as this is an open system there is the possibility that this is an oscillating reaction (Figure 4. 2. 2. 2).



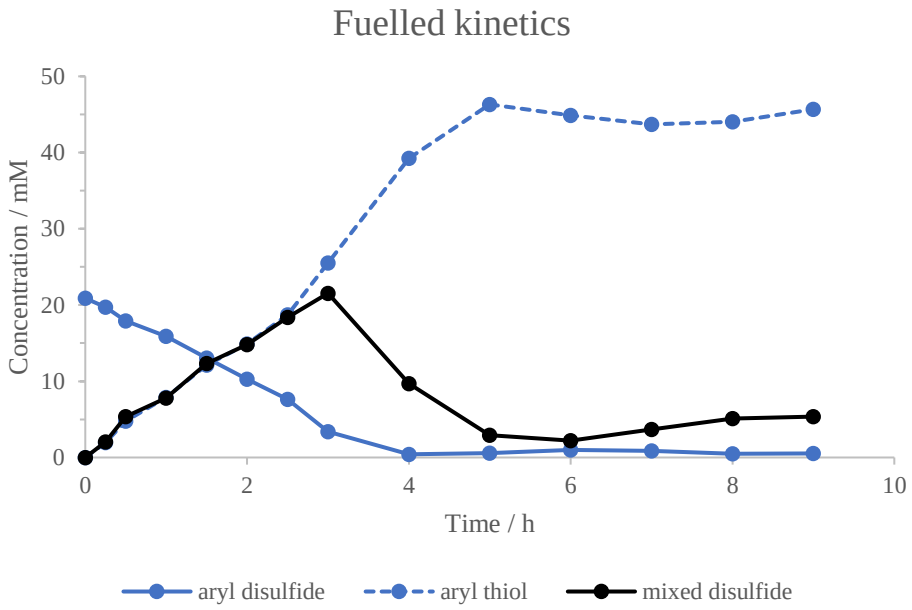


Figure 4. 2. 2. 1. Kinetics of fuelled with hydrogen peroxide. 8.0 equiv. 1-octanethiol, 100 rpm and addition rate of 10 μL h^{-1} of 1.2 M H_2O_2. n = 1.

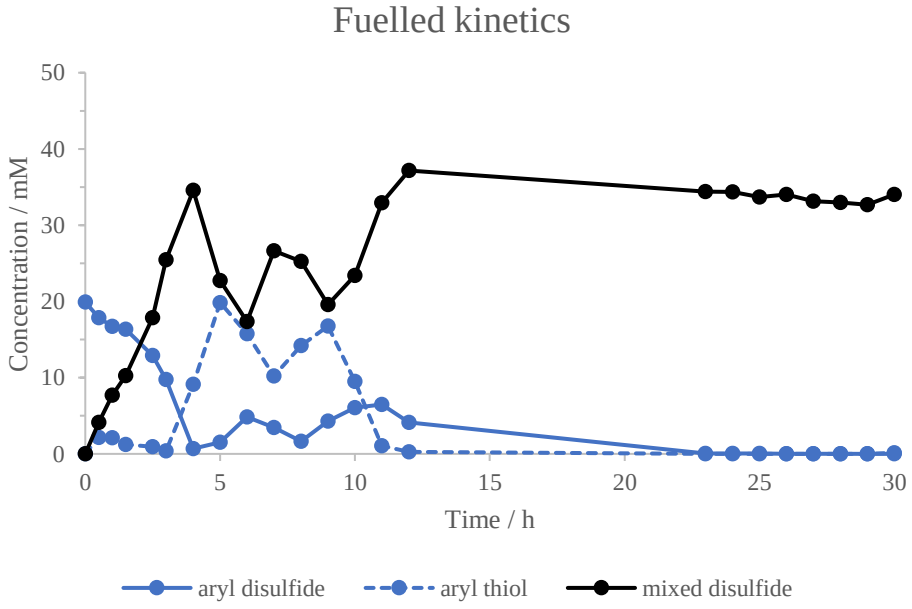


Figure 4. 2. 2. 2. Kinetics of fuelled with hydrogen peroxide. Conditions are as figure 4. 2. 2. 1 but with addition rate of 10 μL h^{-1} of 6.0 M H_2O_2. n = 1.

The oscillations shown in figure 4. 2. 2. 2 can be understood chemically as under-damped oscillations about a steady state composition. At the steady state composition, the three reactions shown in figure 4. 2. 2. 3 are all rate determining, and in the approach towards this state which step is rate determining can change. Initially, the reaction between DTNB and 1-octanethiol produces **4.11a** and TNB which is rapidly oxidised by the fuelling of H_2O_2. Therefore **4.11a** increases, whilst DTNB decreases and TNB stays roughly zero. When **4.11a** overshoots the steady state composition, it begins to be destroyed faster than being formed, thus the concentration of TNB increases, leading to a peak in **4.11a** at 4 h. In turn, when the TNB composition increases above the steady state composition, its higher concentration means oxidation occurs faster and thus DTNB concentration increases, leading to a peak in TNB at 5 h. Finally, with DTNB concentration above the steady state, rate of **4.11a** formation increases, leading to a peak in DTNB at 6 h and the cycle begins again. Under these conditions, the steady state is never reached, 1-octanethiol is fully oxidised sometime between 12 and 24 hours.

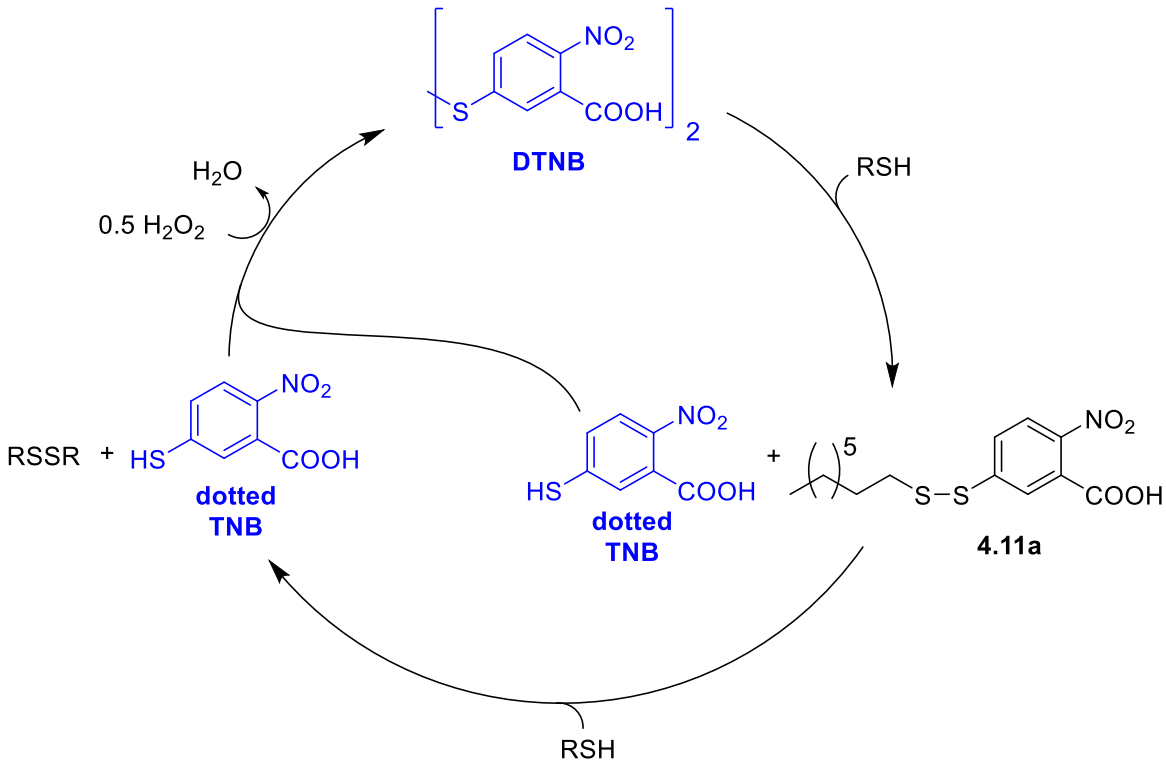


Figure 4. 2. 2. 3. Diagram of the reaction steps within the oscillating reaction. For a steady state to be achieved, all three must be simultaneously rate determining.

Increasing the amount of alkyl thiol in the system to 16.0 equiv. resulted in an increased ratio of TNB:DTNB, but no change to the period of oscillation, around 4 hours (Figure 4. 2. 2. 4). By instead changing the stirring rate, there was a large increase in rate of reaction (Figure 4. 2. 2. 5), with mixed disulfide being formed and fully destroyed within the first 0.5 h of reaction. Intriguingly, between hours 3 and 7, there are apparent rapid oscillations of a period of 1 h, though of reduced amplitude compared with 100 rpm, see also figure 4. 2. 2. 2.

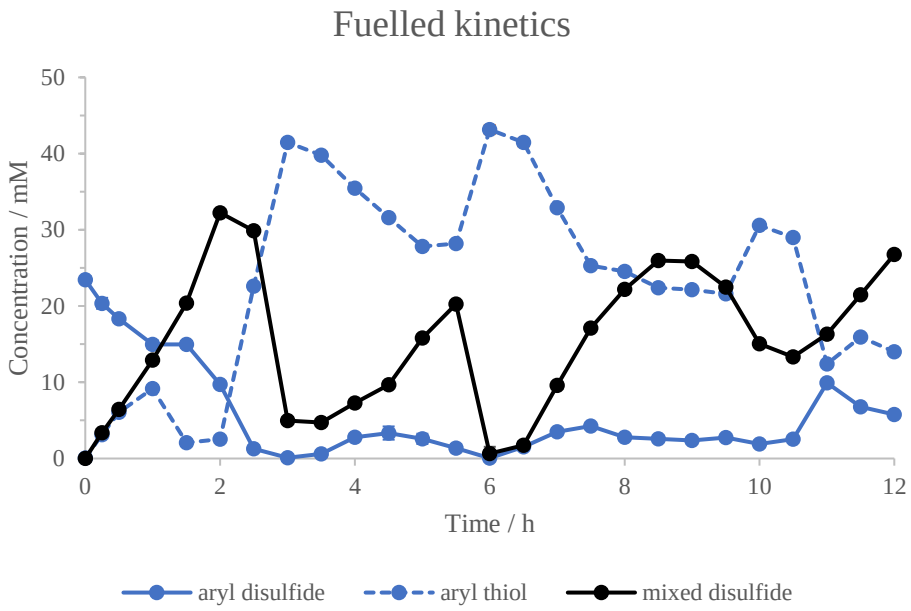


Figure 4. 2. 2. 4. Kinetics of fuelled with hydrogen peroxide. Conditions are as figure 4. 2. 2. 1 but with addition rate of 10 µL h^{-1} of 6.0 M H_2O_2, and 16.0 equiv. 1-octanethiol are used. n = 1.

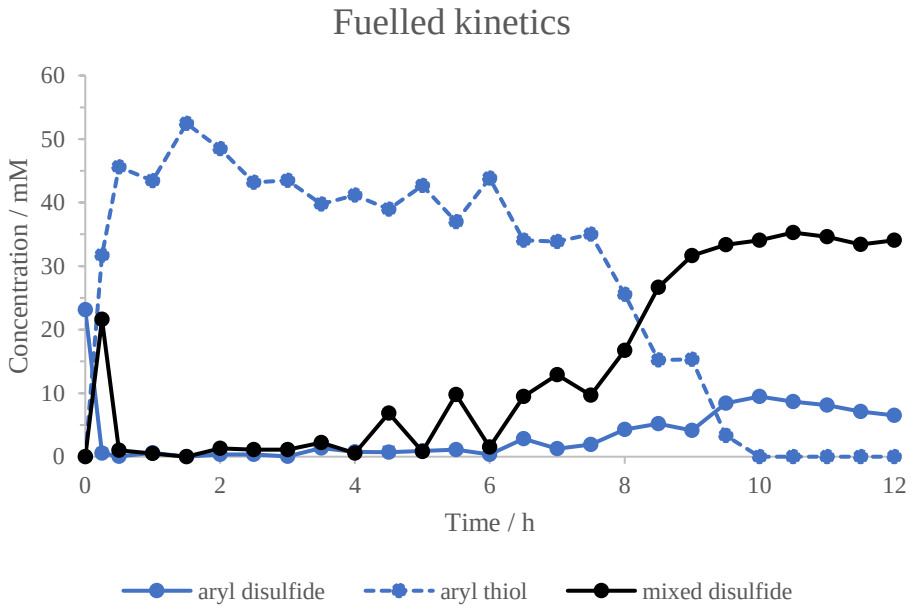


Figure 4. 2. 2. 5. Kinetics of fuelled with hydrogen peroxide. Conditions are as figure 4. 2. 2. 1 but with addition rate of 10 µL h^{-1} of 6.0 M H_2O_2, and a stir rate of 500 rpm is used. n = 1.

Repeating the reaction conditions of those in figure 4. 2. 2. 2 and averaging the results gave broad error bars (Figure 4. 2. 2. 6), presumably because different reactions could be

out of phase with one another, there being no constraint for synchronicity. It is known that far from equilibrium systems that show oscillations can have inherently chaotic behaviour.[47] To investigate this further, more frequent sampling was performed, to establish whether this was a result of poor sampling or inherent variance between reactions (Figure 4. 2. 2. 7). Here the concentrations of all components show smooth and continuous variation in time, suggestive of low random error. Each run shows broadly the same behaviour, following the same succession of peaks. Despite being performed under as rigorously controlled conditions as possible, the exact behaviour of each run is however different, with relative rates being different and the number of oscillations of each component differing.

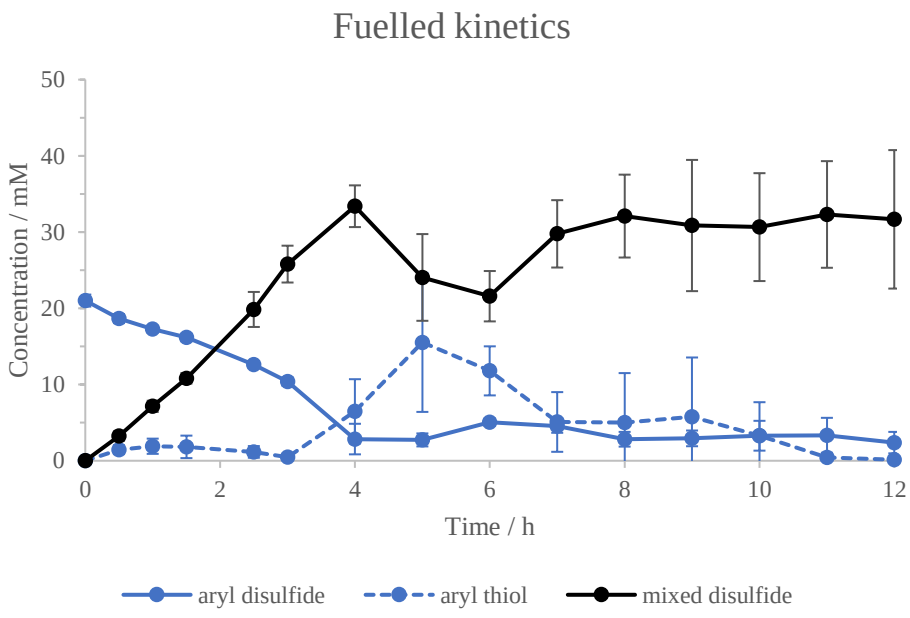


Figure 4. 2. 2. 6. Mean of three runs of the reaction fuelled with hydrogen peroxide. 8.0 equiv. 1-octanethiol, 100 rpm and addition rate of 10 µL h^{-1} of 6.0 M H_2O_2, showing oscillations, but broad error bars. n = 3, error bars show one standard deviation.

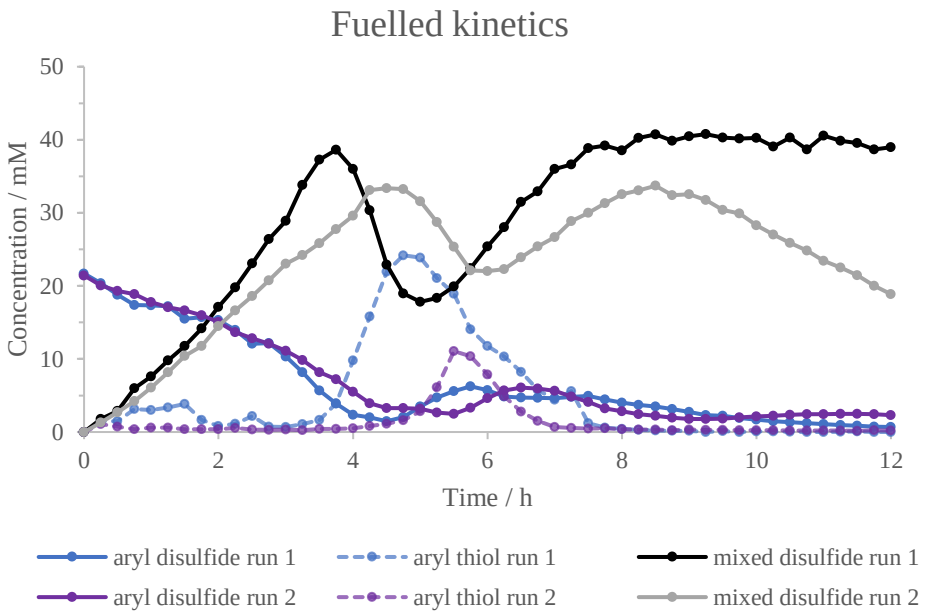


Figure 4. 2. 2. 7. Two runs of the reaction fuelled with hydrogen peroxide. 8.0 equiv. 1-octanethiol, 100 rpm and addition rate of 10 µL h^{-1} of 6.0 M H_2O_2, followed for every 15 minutes over 12 h. n = 2.

The oscillating behaviour proved hard to optimise, likely a fine balance of factors are required to achieve the necessary nonlinear kinetics. Increasing the quantity of thiol by a large amount (to 200 equiv.) resulted in non-oscillating behaviour. No significant difference between HEPES and TRIS buffer were found in oscillation experiments.

4. 2. 3 Characterisation of surfactants

All lipids which could be formed in our system design were synthesised and characterised individually. Critical aggregation constants (CACs) were measured by ring tensiometry (Table 4. 2. 3. 1). Within each headgroup series (**4.11a-c**, **4.12a-c** and **4.13a-c**) the expected trend is followed where the more hydrophobic surfactants aggregate at lower concentrations.[62] The CACs of all these mixed disulfides are far below the typical concentrations present in the reaction (up to 25 mM), thus for the majority of the time where mixed disulfides are present, some supramolecular aggregates are present.

Surfactant	CAC / μM
4.11a	500
4.11b	300
4.11c	80
4.12a	290
4.12b	230
4.12c	190
4.13a	560
4.13b	280
4.13c	160

Table 4. 3. 2. 1. Critical aggregation concentrations of the 9 lipids used in this study. n = 3.

Solutions of the nitro containing series all appeared transparent, typical of micellar solutions, whilst those of the other two series appeared turbid, suggesting the presence of large aggregates such as vesicles. Dynamic light scattering (DLS) measurements were used to measure the size of the mixed disulfide aggregates in solution of pH 8.00 HEPES buffer. Indeed **4.11a-c** were all micelle forming and **4.12a-c** and **4.13a-c** all showed sized distributions consistent with vesicles (Table 4. 3. 2. 2).

Compound	Range of mean size (nm)	Concentration range (mM)
4.11a	5–10	1.56–25.00
4.11b	5–10	1.56–25.00
4.11c	10–15	3.13–25.00
4.12a	80–320	0.19–1.56
4.12b	35–90	0.098–6.25
4.12c	40–100	0.049–25.00
4.13a	20–60	0.19–25.00
4.13b	25–60	0.39–25.00
4.13c	20–40	0.098–25.00

Table 4. 3. 2. 2. Critical aggregation concentrations of the 9 lipids used in this study. Concentration range given is where reproducible data was recorded. n = 3.

As most of the vesicles are very small, 20–60 nm, it appears likely that they are unilamellar, whereas the rare large vesicles 60–320 nm are likely to be multi-lamellar. As the size of the either micelles or vesicles does not vary significantly between different concentrations, it can be inferred that as these compounds are formed, they do not merely make larger and larger aggregates, but instead new aggregates are formed in dynamic processes of monomer binding and division. Such a division of vesicles draws obvious analogy to living systems. There are limitations here however, notably that these measurements are derived from pure compounds and the nature of aggregation in heterogenous reactions may be different.[63] Attempts to measure the size of aggregates through the course of an autocatalytic reaction by DLS were unsuccessful due to poor data quality, which presumably arose from the high polydispersity of the samples.

I propose the difference in aggregation arises due to the relative acidity of the mixed disulfides. Typically supramolecular aggregation of surfactant carboxylic acids can raise their pKa by a few units above those which do not aggregate, which is understood by mutual repulsion of negative charges at the aggregate surface, meaning a higher basicity is required to remove protons. Aggregated carboxylates have a variety of protonation states, from fully protonated to fully deprotonated. When the aggregate is fully deprotonated, the mutual repulsion between headgroups and high solvation leads the headgroup having large effective size. In the case of partial deprotonation, there is less mutual repulsion resulting from the lower average charge and protons form a bridging network through hydrogen-bonding, leading to lower solvation. Taken together this leads to a smaller effective size of the headgroup. This large change in the ratio of headgroup to tail group size can change the preferred interfacial curvature of the surfactant, changing the type of aggregates present.[64] An example of this phenomena is observed with oleic acid, where at high pH (above pH 10.2) it forms micelles, whereas at lower pH (between

pH 4.5–10.2) vesicles are found.[65,66] In this system, those carboxylates bearing nitro substitution are of lower pKa through induction, and therefore are fully deprotonated at pH 8.00, leading to micelles. Those bearing hydrogen or methoxy substitution have a higher pKa, are not fully deprotonated, aggregating into vesicles.

4. 2. 4 Mechanistic points

We envisaged that nucleophilic attack of an alkyl thiol could occur at either end of a mixed disulfide in our system (Figure 4. 2. 4. 1 paths 1 and 2). In the case of a single alkyl component path 2 would be traceless as the product would be the same as the starting material. With different aliphatic components however, such a thiol-disulfide exchange would lead to a different mixed disulfide. The implication is that in the planned system of competing replicators there are two possible distinct paths for formation, and two paths for destruction of the individual replicators.

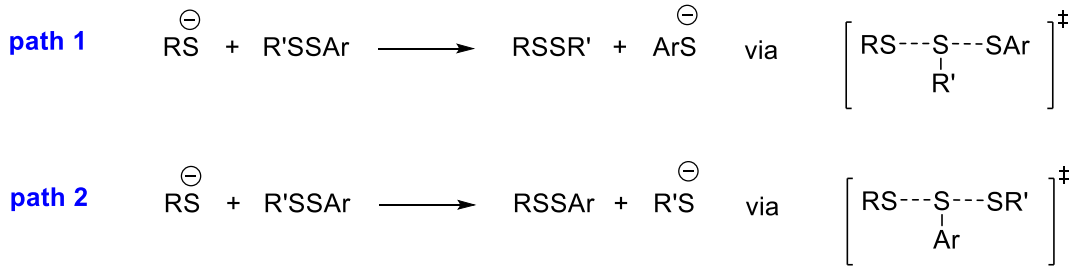
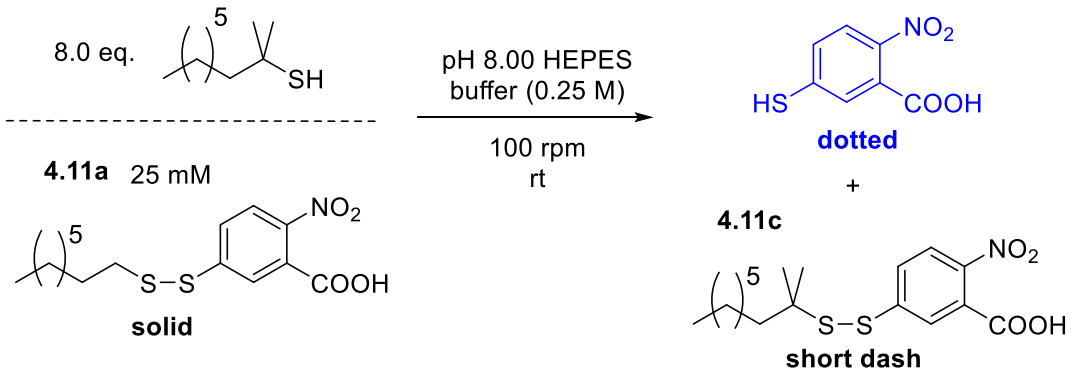


Figure 4. 2. 4. 1. Path 1: thiol-disulfide exchange to form bis-alkyl disulfide and aryl thiol. Path 2: possible thiol-disulfide exchange which could form one lipid at the expense of another.

To test whether both paths do occur, experiments were performed mixing an alkyl thiol with a mixed disulfide derived from a different alkyl thiol (see for example figure 4. 2. 4. 2). Here products of both path 1 and 2 could be followed simultaneously by formation of **4.8** and **4.11c** respectively in this example. These experiments were conducted prior to the optimised conditions being found, so pH 7.50 TRIS buffer was used. Interestingly, the results in figure 4. 2. 4. 2 show that path 2 does occur, but to a

very small extent, with path 1 being favoured approximately 25:1. For the other, less sterically hindered alkyl thiols, no path 2 was observed, only path 1. This is presumable due to path 1 for these thiols being faster, but also possibly because the mixed disulfide formed in these cases are those which are themselves less stable to further thio-disulfide exchange. On the basis of these results, we can assume that the dominant pathway for formation of all mixed disulfides is through reaction with bis-aryl disulfides, and the dominant pathway for destruction is through reaction with an aliphatic thiol.



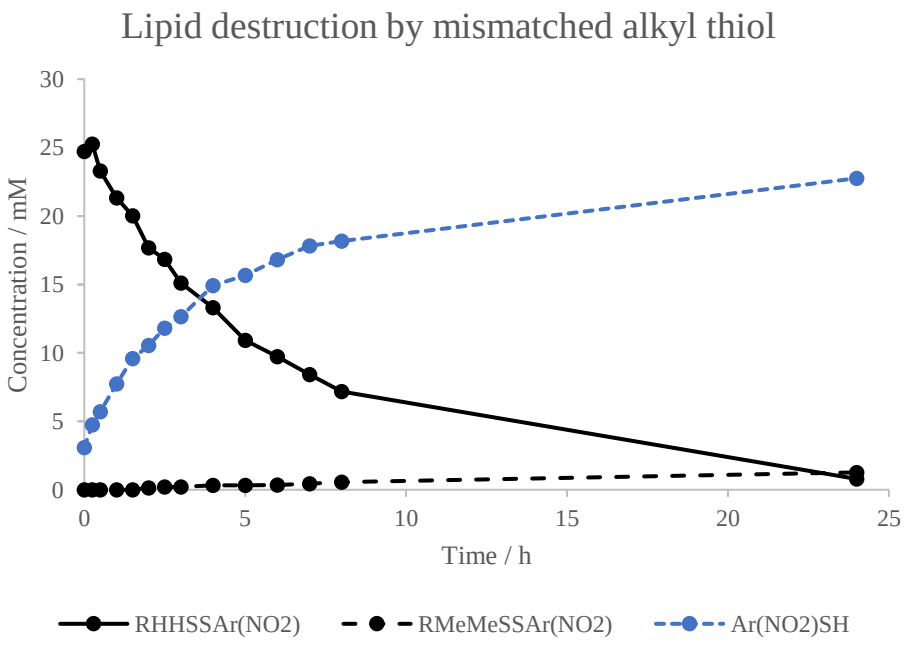


*Figure 4. 2. 4. 2. Destruction kinetics for lipid **4.11a** by thiol **4.1c**, showing both reduction and formation of lipid **4.11c**. Note this experiment was performed in pH 7.50 TRIS buffer. n = 1.*

Exchange in the homoaryl disulfides was observed under the reaction conditions to give heteroaryl disulfides through metathesis (Figure 4. 2. 4. 3 and section 4. 6. 8. 1 for full data). In pH 8.00 HEPES buffer, disulfide metathesis reaches equilibrium over the course of roughly an hour. This is presumably catalysed by aryl thiol, present in small quantities from partial disulfide hydrolysis in the alkaline conditions. No metathesis was observed with samples treated with a maleimide quench, consistent with thiol catalysis. It is assumed that such equilibration between aryl disulfide species is rapid under the reaction conditions, where much larger quantities of aryl thiol is present throughout.

The equilibrium aryl disulfide distribution for each of the pairwise combination is close to the binomial distribution (1:2:1 of ArSSAr:ArSSAr:Ar'SSAr') suggesting all aryl disulfides are of similar energy, and the process is primarily driven entropically rather than enthalpically. Metathesis was observed between all aryl disulfide species, giving rise to six aryl disulfides when three homoaryl disulfides were mixed.

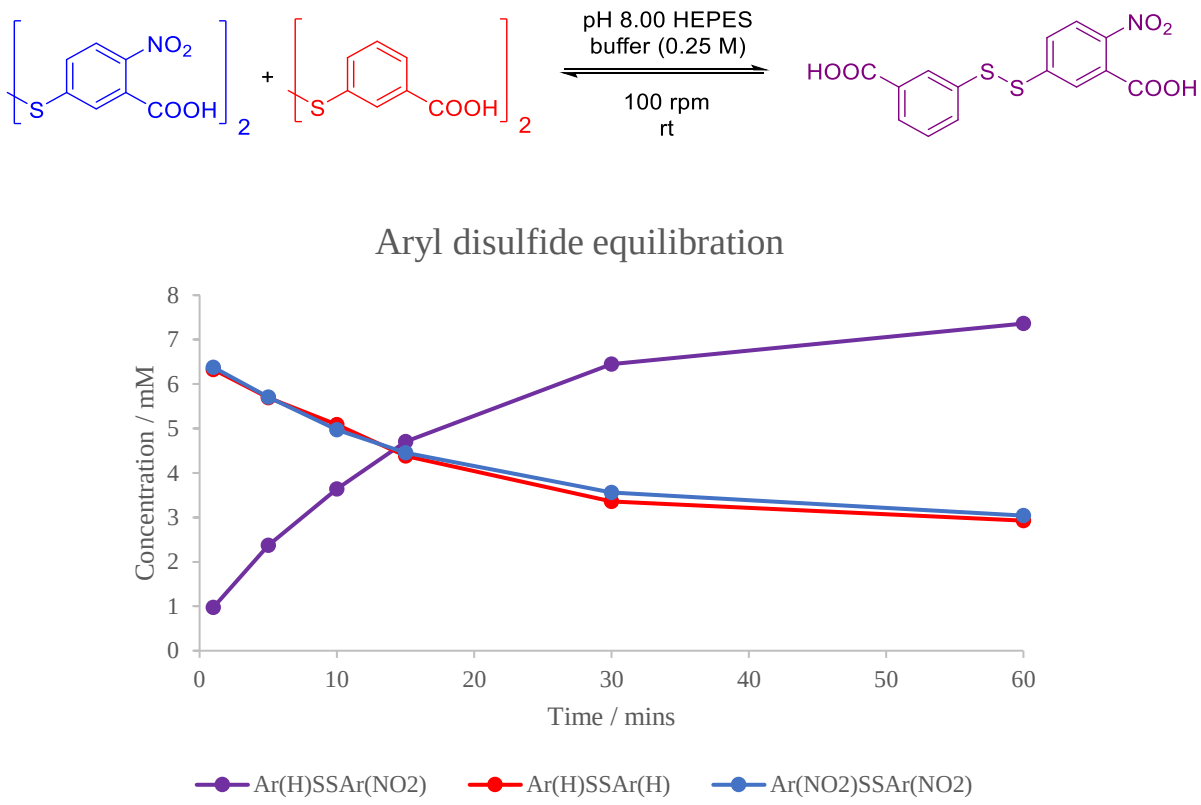
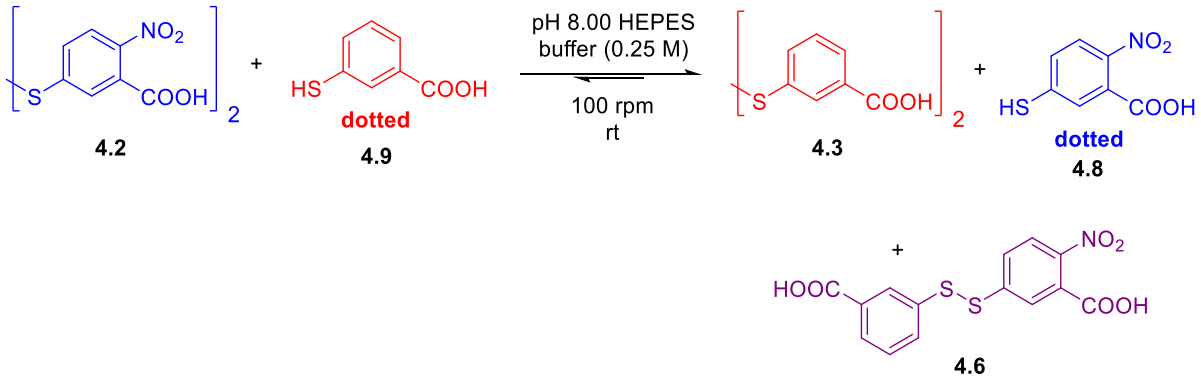


Figure 4. 2. 4. 3. Equilibration via metathesis of two homoaryl disulfides under the reaction conditions, forming a heteroaryl disulfide. n = 1.

Throughout the reactions with multiple aryl substitutions present the equilibration between aryl thiols and bis-aryl disulfides must be considered. This equilibration is rapid relative to lipid formation or destruction, complete in under 5 minutes and by eye appearing to be instantaneous (Figure 4. 2. 4. 4 and section 4. 6. 8. 2 for full data). There is a clear thermodynamic driving force for electron rich aryl species to exist as disulfides in the presence of electron poor aryl thiols, understood through the inductive effect. We therefore expect that as a reaction containing multiple bis-aryl disulfides proceeds, the most electron deficient bis-aryl disulfides to be consumed fastest and the most electron deficient aryl thiols to be form first, regardless of which lipid is being formed. Put simply, there should always be more **4.8** than **4.9**, and more **4.9** than **4.10**.

Another possible pathway for formation and destruction of replicators is via metathesis, analogous to that seen in bis-aryl disulfides. In mixtures of replicators **4.11a** and **4.12c**,

and separately **4.11c** and **4.12a**, no metathesis was observed under the reaction conditions after 24 h (Section 4. 6. 8. 3). Therefore whilst the bis-aryl disulfides undergo metathesis in the system, alkyl-aryl disulfides do not.



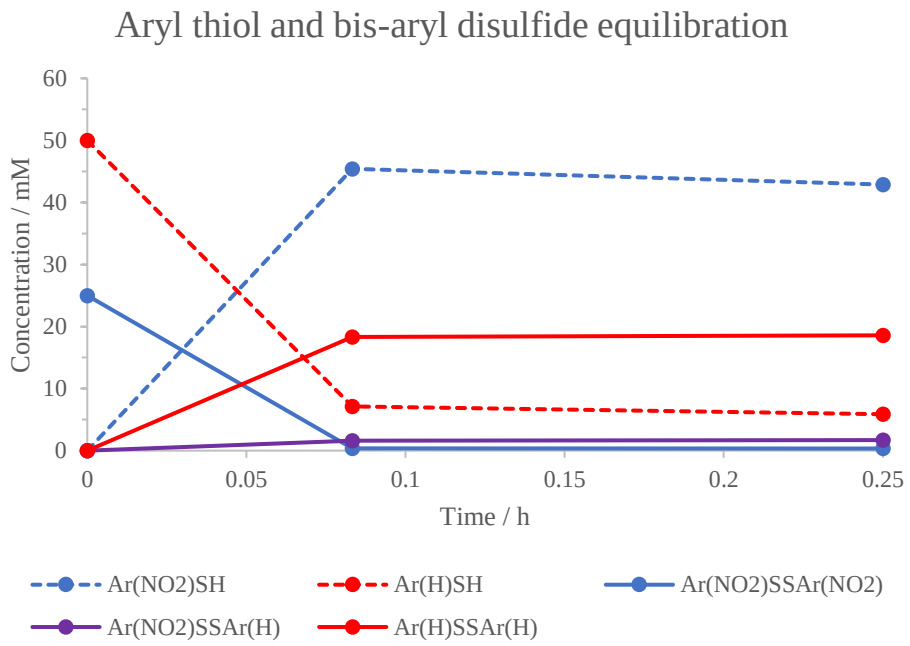


*Figure 4. 2. 4. 4. Equilibration between electron poor disulfide **4.2** and electron rich aryl thiol **4.9**. n = 1.*

4. 3 Reaction kinetics and competition between replicators

4. 3. 1 Comparisons between replicators – kinetics of individual mixed disulfides

4. 3. 1. 1. Formation rates

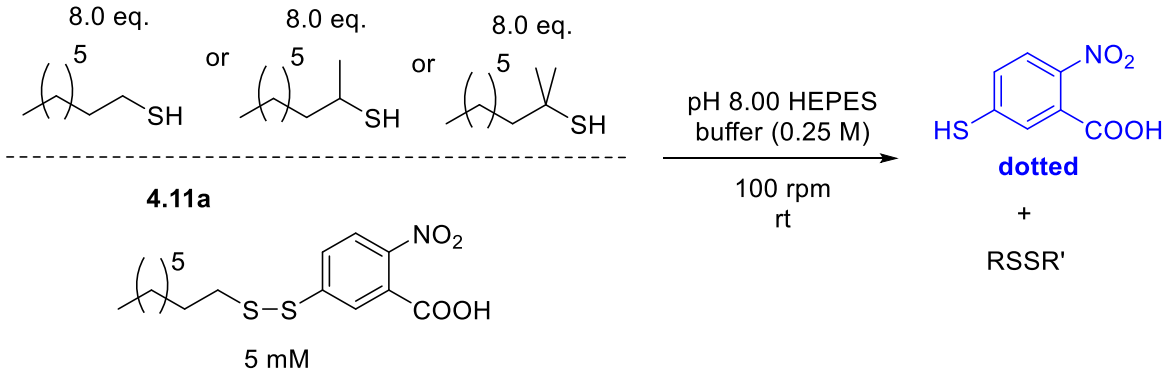
Rates of formation of the replicators was followed over 30 h. **4.11a** is the only mixed disulfide to undergo significant decomposition during this time frame, with the mixed disulfide being fully consumed after 5 h (Figure 4. 6. 9. 2. 1). The other nitro products are also relatively fast, both fully formed within 30 h (Figures 4. 6. 9. 2. 2 and 4. 6. 9. 2. 3). Among the unsubstituted and methoxy substituted mixed disulfides, only those formed from primary 1-octanethiol are formed at appreciable rate (Figures 4. 6. 9. 2. 4 and 4. 6. 9. 2. 7). Note that the low concentration of **4.12a** throughout the time-course is due to low solubility in pure systems and from the concentration of aryl thiol little or no destruction reaction occurs. The solubility of this compound is highly context dependent, and in the presence of other mixed disulfides it was found to be fully soluble. Complete data can be found in section 4. 6. 9. 2.

Taking these data together we get the qualitative understanding that in isolation the rate of lipid formation depends on the steric hinderance of the alkyl thiol, with **4.1a** reacting faster than **4.1b** reacting faster than **4.1c**, and on the electronics of the bis-aryl disulfide, with **4.2** reacting faster than **4.3**, which reacts faster than **4.4** on the basis of leaving group ability.

4. 3. 1. 2. Destruction rates

The rates of a selection of possible destruction reactions were investigated in order to best understand the behaviour of the system as a whole. Firstly, comparing the rates of destruction of **4.11a** (Figure 4. 3. 1. 2. 1) by the three different alkyl thiols we observe

that the less hindered thiol reacts fastest, and so the primary destructive pathway for all mixed disulfides was assumed to be with 1-octanethiol, typically present in large excess (8 equiv.). In the optimised reaction conditions, the trend for destruction rates of sterically differentiated mixed disulfides with 1-octanethiol followed the expected pattern, with the more hindered mixed disulfides being more persistent (Figure 4. 3. 1. 2. 2).



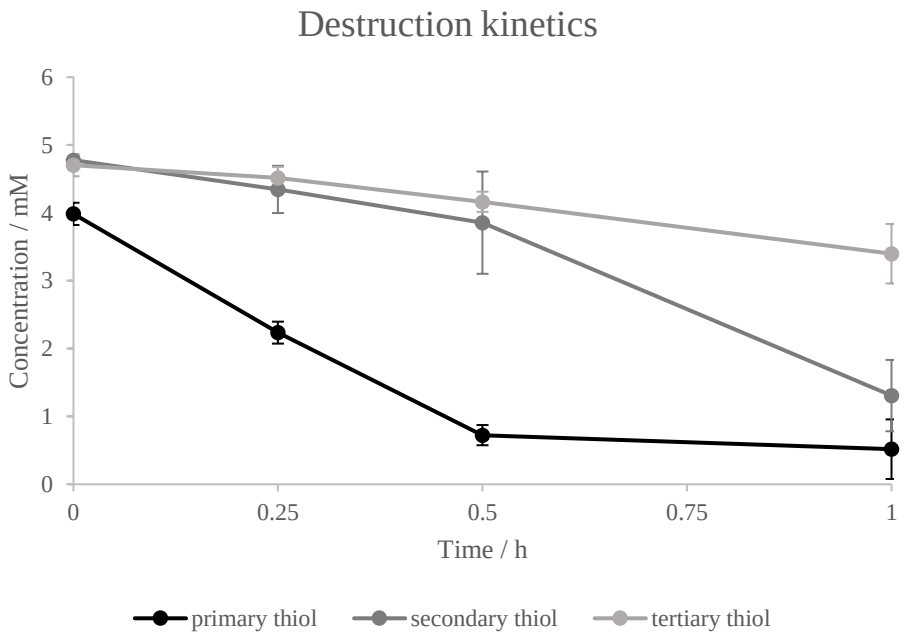


*Figure 4. 3. 1. 2. 1. Comparison between destruction rates of mixed disulfide **4.11a** by the different alkyl thiols, **4.1a-c**. n = 3, error bars show one standard deviation.*

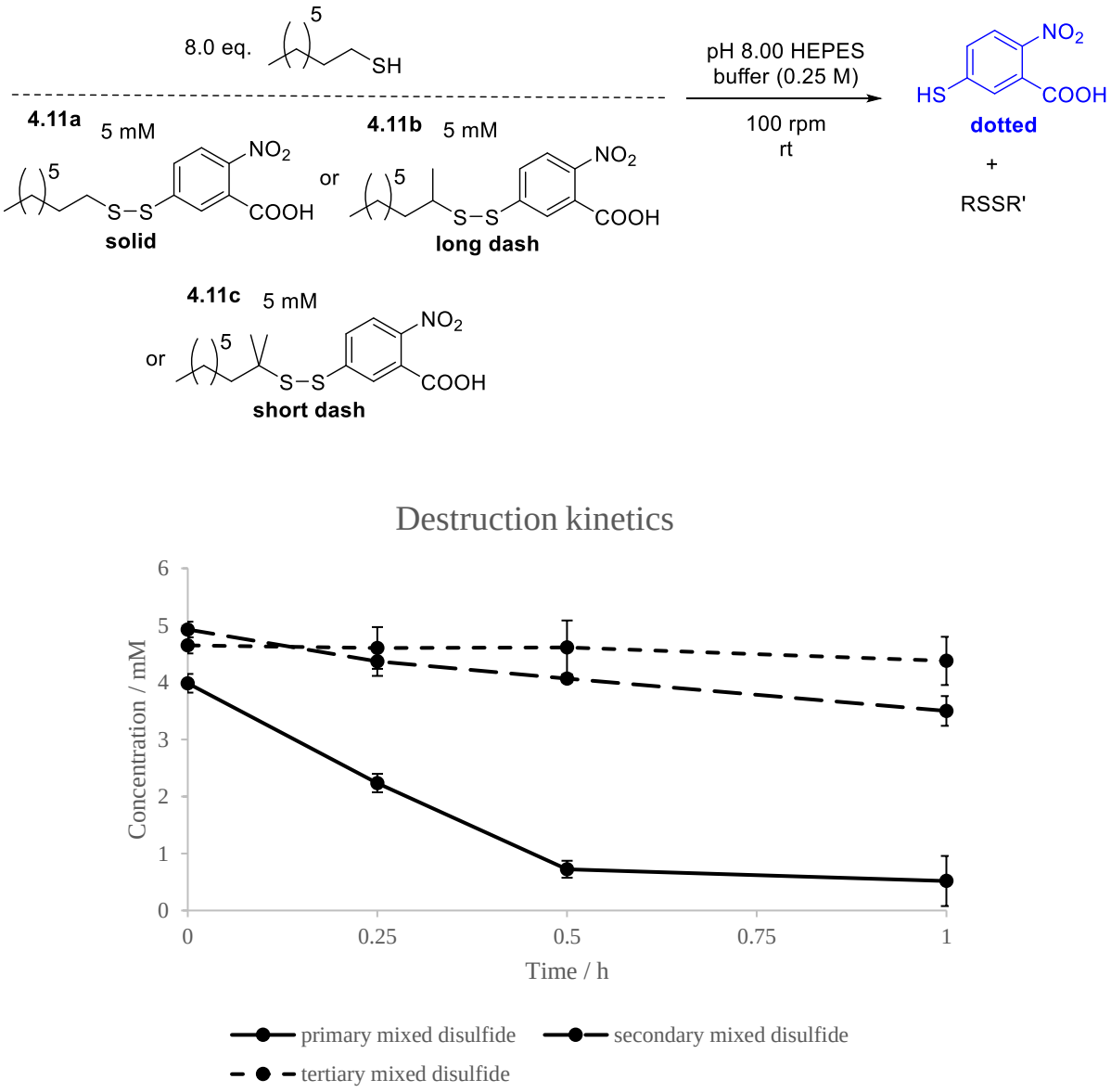


*Figure 4. 3. 1. 2. 2. Comparison between destruction rates of mixed disulfides **4.11a-c** by 1-octanethiol. n = 3, error bars show one standard deviation.*

Comparing the destruction rates of mixed disulfides bearing different aryl substituents we see the trend that more electron deficient substrates are less stable, as they have the best leaving group (Figure 4. 3. 1. 2. 3). The order of stability of the mixed disulfides is therefore Ar(OMe) is most stable, then Ar(H) and Ar(NO_2) the least stable. There were large sampling errors in the vesicle forming mixed disulfide concentration due to sample heterogeneity, similar to that discussed in section 4. 3. 1. 3, and so the rates were compared by measuring the aryl thiol destruction product.

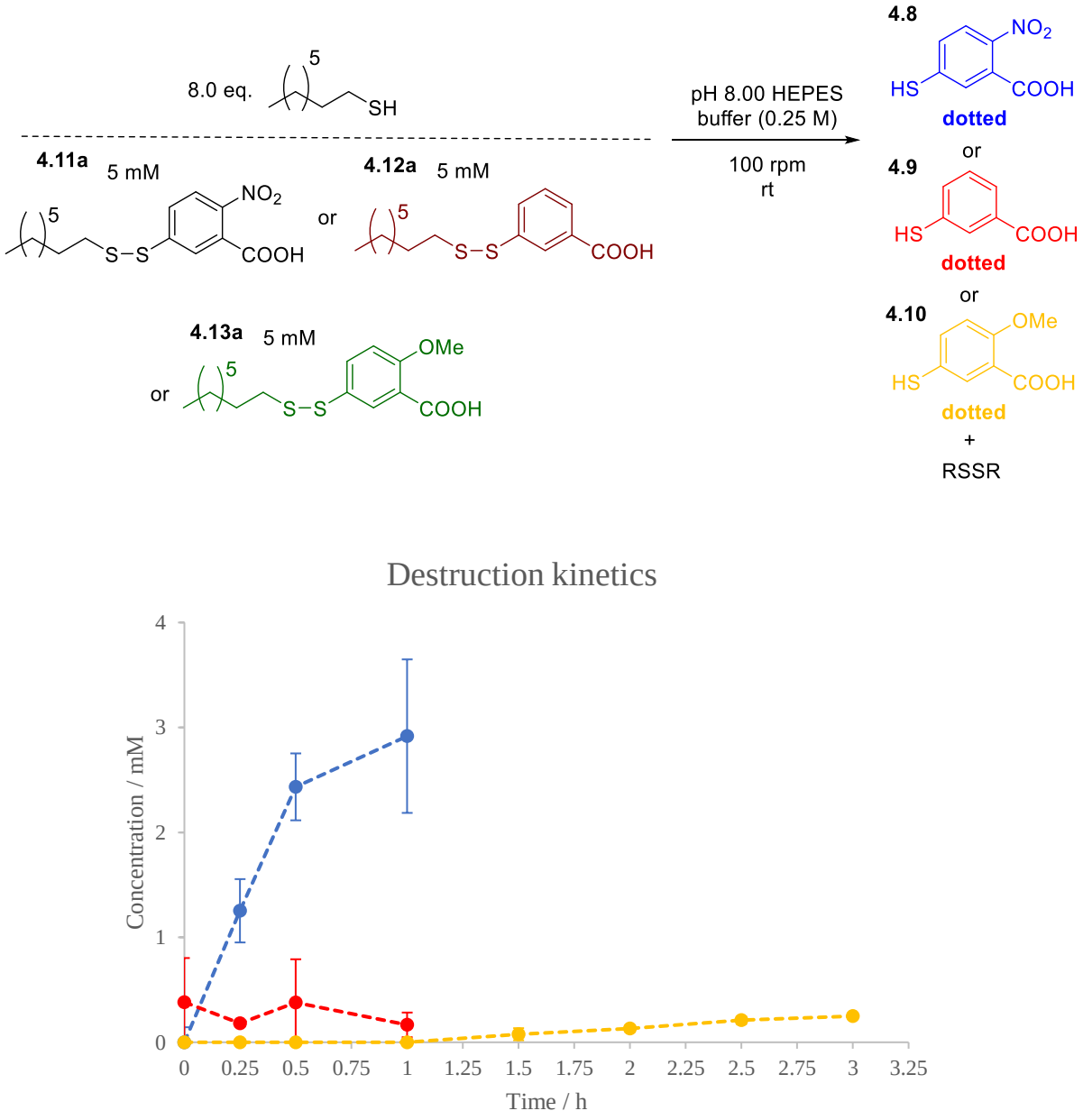


*Figure 4. 3. 1. 2. 3. Comparison between destruction rates of mixed disulfides **4.11a**, **4.12a** and **4.13a** by the different 1-octanethiol. Results are displayed by the formation of aryl thiols **4.8**, **4.9** and **4.10**. n = 3, error bars show one standard deviation.*

4. 3. 1. 3. Seeding experiments

A seeded reaction was performed on the formation of each mixed disulfide, a classical method to establish autocatalysis.[67] Other kinetic phenomena may lead to the characteristic sigmoidal kinetics of autocatalysis, the simplest of which are multistep reactions without a clearly defined rate determining step. This, and the fact that not all

autocatalytic processes show sigmoidity, make sigmoidal kinetics neither necessary nor sufficient to prove autocatalysis. Seeding experiments, where product is added from the start of the reaction, show the effect of product on initial rate. If a rate enhancement is observed, the reaction is autocatalytic.

Our system has two not inconsiderable complications compared with most synthetic replicators. Firstly, in the case of transient replicators, initial rates are difficult to measure in isolation, as the replicating species is being formed and destroyed throughout the reaction. However, if the initial seeded rate exceeds the unseeded rate despite product destruction, the reaction is autocatalytic. Secondly, a mixed disulfide surfactant can be formed from a number of different bis-aryl disulfides, each of which having different reactivities. Therefore it is possible that with some starting materials the mixed disulfide surfactant may be autocatalytic and with others not.

Rates of initial rates of formation for mixed disulfides **4.11a-c** were found to be higher in the presence of 0.2 equiv. product, showing these substrates are autocatalytic (Figure 4. 3. 1. 3. 1 and section 4. 6. 9. 3). For the vesicle forming compounds **4.12a-c** and **4.13a-c** the results are more ambiguous. Some mixed disulfides show a concentration decrease in the seeded runs due to greater rate of destruction than formation, and there are often large fluctuations in concentration from sample to sample, which was due to heterogeneity of the reaction mixtures. What can be seen however is that **4.13a** and **4.13c** are clearly autocatalytic under these conditions (Section 4. 6. 9. 3).

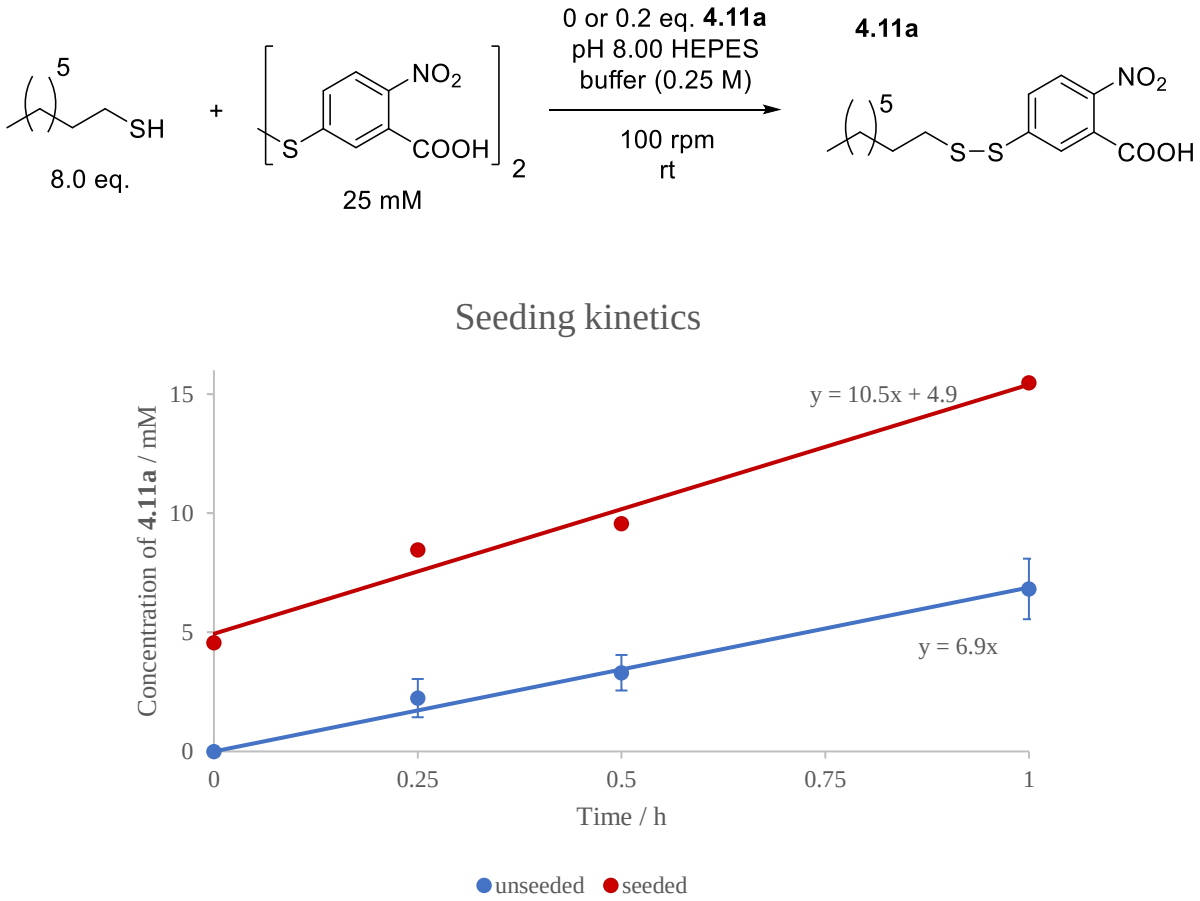


*Figure 4. 3. 1. 3. 1. Comparison between initial rates of mixed disulfide **4.11a** production in the presence (n = 1) and absence (n = 3) of 0.2 equiv. of added product. Error bars show one standard deviation. Initial rate (absence of product) = 6.9 ± 0.8 mMh^{-1}, Initial rate (5 mM product added) = 10.5 ± 1.0 mMh^{-1}.*

Due to the nature of physical autocatalysis we imagined the effects of each replicator to be essentially unspecific, each replicator cross-catalysing the production of others. To investigate this a selection of reactions were seeded with different amphiphilic mixed disulfides (Section 4. 6. 9. 4 for full data). In most cases a rate enhancement was observed, consistent with mutualistic cross-catalysis, however this was not seen in the case of **4.11c** formation seeded with **4.13b**, arising from effects related to high rate of replicator destruction (see figure 4. 1. 3. 2 for lipid identities). These results broadly support there being a high degree of cross-catalysis in our competing replicator systems.

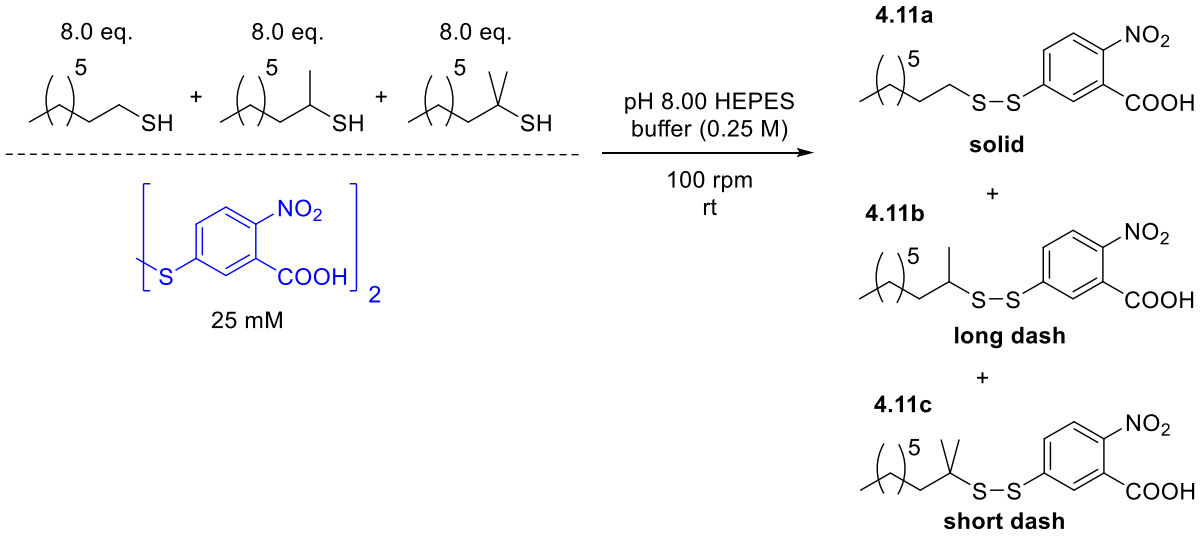
Due to the structural similarity and similar properties as surfactants I believe that all 9 mixed disulfides are replicators under conditions containing a mixture of all bis-aryl

disulfides, as here the relative rate of formation of lipid is fast compared with destruction. Future work should include performing seeding experiments on the lipid formation with multiple bis-aryl disulfides described in section 4. 3. 2. 2.

4. 3. 2 Competing replicators – behaviour of systems with multiple mixed disulfides

4. 3. 2. 1 Succession based on sterically differentiated products

The succession of lipids on steric grounds was shown as a proof of concept in section 4. 2. 1, and figure 4. 3. 2. 1. 1 shows this performed in triplicate. Here, initially the relative abundance of replicator is determined by relative rates of formation, so at first, the dominant lipid is **4.11a**. As the reaction progresses, the lipid destruction becomes a more important factor as DTNB is consumed. As **4.11a** is also fastest to be destroyed, it decreases in concentration faster than the other lipids, leading to a succession of which is dominant. Therefore we see a change in the lipid composition over time, from **4.11a** being dominant, then **4.11b** and finally **4.11c**.



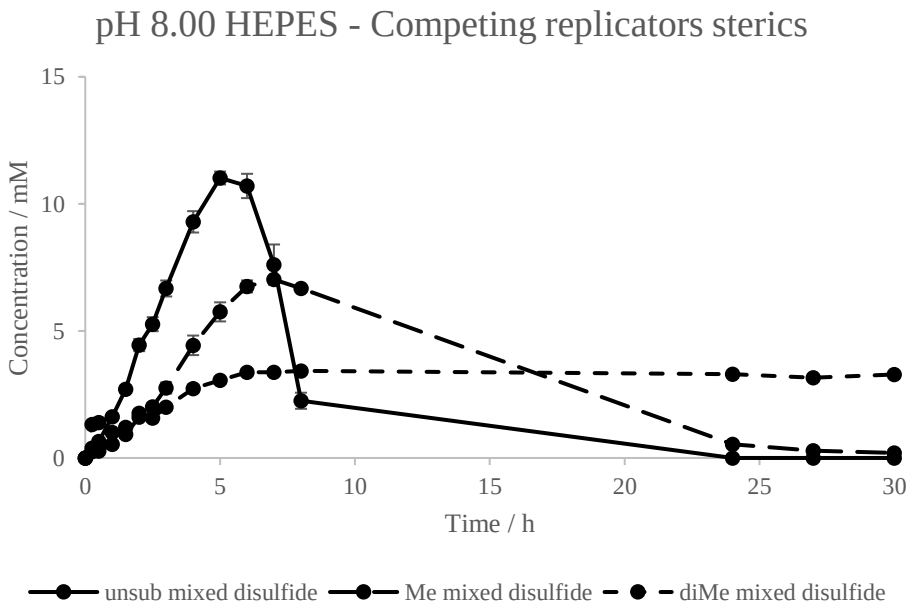
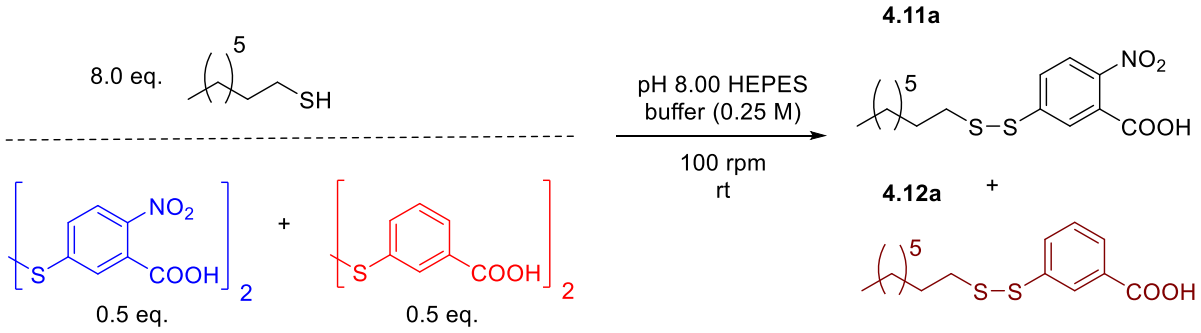


*Figure 4. 3. 2. 1. 1. Reaction kinetics of competition study between lipids **4.11a, 4.11b** and **4.11c**. DNTB and TNB concentrations are omitted for clarity. n = 3, error bars show one standard deviation.*

4. 3. 2. 2 Effects arising from substitution of the aryl disulfides

Studies into the effect of mixtures of aryl disulfides in the aqueous phase began with reactions between 1-octanethiol and pairs of homoaryl disulfides, these reactions giving rise to a competition between two lipids. Like the experiments shown in section 4. 3. 2. 1, the lipids show a succession through time, selectivity changing with extent of reaction, though through a very different means.

Figure 4. 3. 2. 2. 1 shows the competition between lipid **4.11a** and **4.12a**. Here, **4.11a** and **4.12a** are initially formed at approximately the same rate, though by t = 3 h **4.11a** has peaked in composition and **4.11a** continues to increase in concentration until t = 6 h. For most of the reaction, **4.12a** is the most abundant lipid. In effect, **4.12a** gains efficiency as a result of mixing aryl disulfides, and **4.11a** loses efficiency, each compared to their formation in section 4. 6. 9. 2. This arises from a number of effects, see figure 4. 3. 2. 2. 2. Firstly, the aryl-aryl disulfide metathesis generates mixed disulfide **4.5** which reacts primarily to give **4.12a** based on leaving group ability. As described in section 4. 2. 4, the concentration of **4.5** is higher than **4.2**, due to the binomial effect. Also, as described in section 4. 2. 4, as the reaction proceeds the most electron deficient aryl thiol is produced, here **4.8**, and **4.9** is recycled into bis-aryl disulfide. This has the effect of reducing the availability of starting material for **4.12a** production.



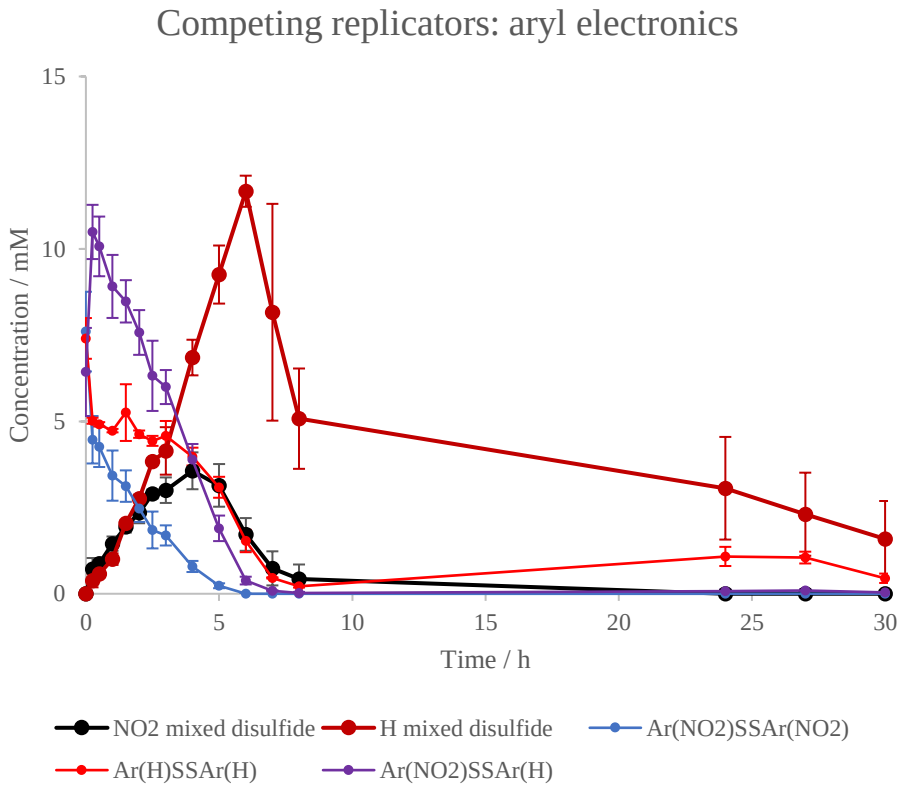


*Figure 4. 3. 2. 2. 1. Reaction kinetics of competition study between mixed lipids **4.11a** and **4.12a**. Aryl thiol concentration was not recorded in these experiments. n = 3, error bars show one standard deviation.*

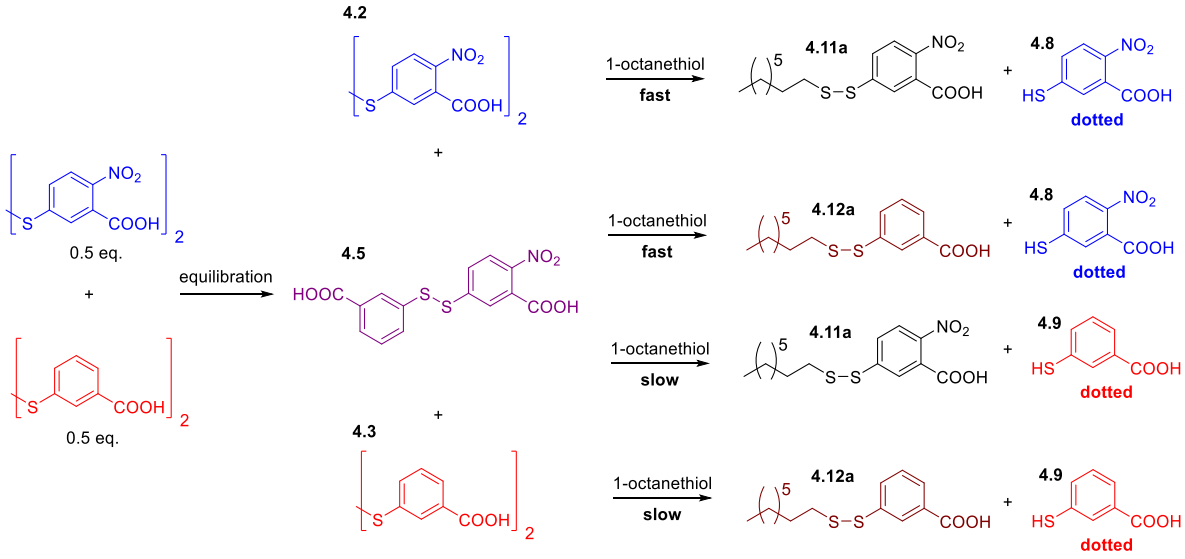


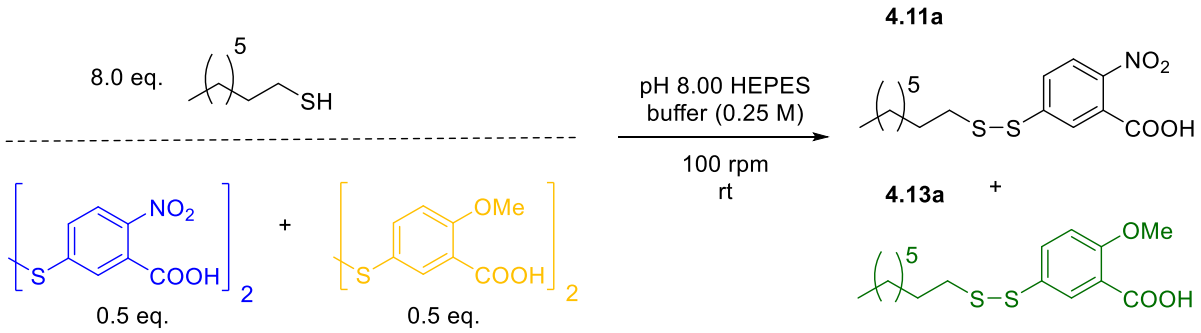
*Figure 4. 3. 2. 2. 2. Reaction pathways occurring in the reaction to form **4.11a** and **4.12a**, seen in figure 4. 3. 2. 2. 1.*

Competition between lipid **4.11a** and **4.13a** shows similar behaviour (Figure 4. 3. 2. 2. 3), with the two lipids initially being formed at similar rates but **4.13a** ultimately predominating. Again this product is seen to be less abundant throughout when these replicators are formed in isolation. In contrast with the **4.11a** and **4.12a** competition in figure 4. 3. 2. 2. 1, the more stable replicator does not significantly decompose over the course of the reaction, it is kinetically trapped on this timescale. See also figures 4. 6. 9. 5. 1 and 4. 6. 9. 5. 2 for full data.

When **4.12a** and **4.13a** are formed under this competition setup (Figure 4. 3. 2. 2. 4) the effects are more subtle. In this case, the rate of formation is initially very similar for both lipids and compositions remain approximately the same throughout, but there is slightly more **4.13a** at long times. See also figures 4. 6. 9. 5. 3 and 4. 6. 9. 5. 4 for full data.

When all three lipids **4.11a**, **4.12a** and **4.13a** compete (Figure 4. 3. 2. 2. 5. See also figures 4. 6. 9. 5. 5-7), the effects appear similar to a combination of the pairwise competition experiments, with initially all three lipids forming at approximately the same

rate. **4.11a** however is unstable, peaking at around 5 hours, at longer reaction times there are similar amounts of **4.12a** and **4.13a** and almost no **4.11a**.



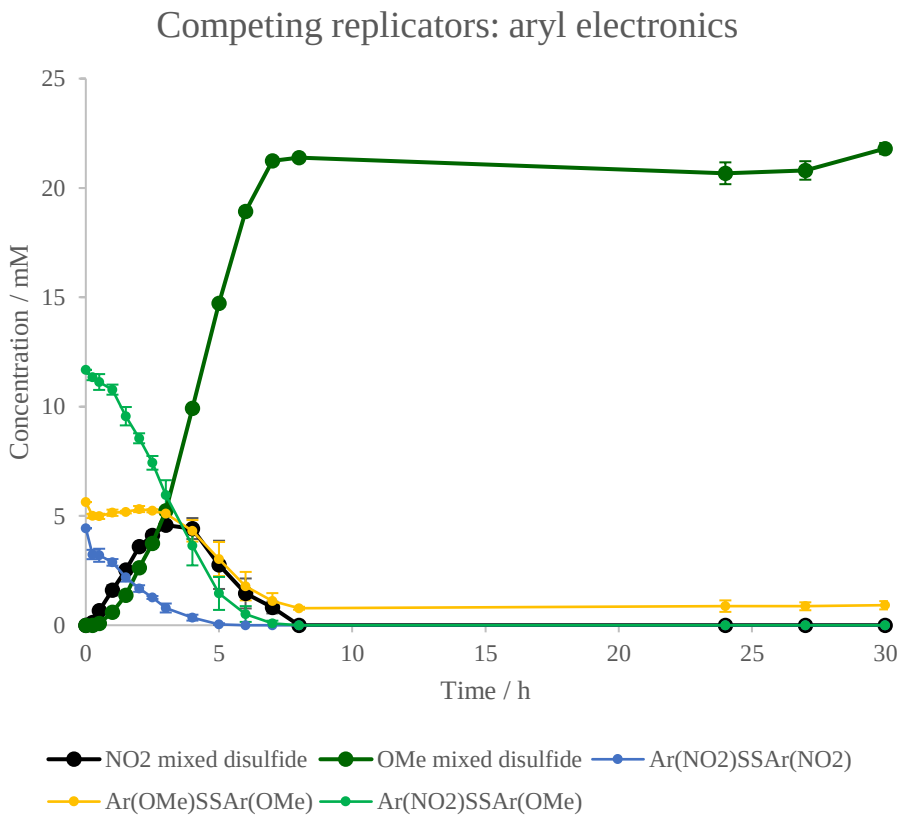


*Figure 4. 3. 2. 2. 3. Reaction kinetics of competition study between mixed lipids **4.11a** and **4.13a**. Aryl thiol concentrations are omitted for clarity. See also figures 4. 6. 9. 5. 1 and 4. 6. 9. 5. 2. n = 3, error bars show one standard deviation.*

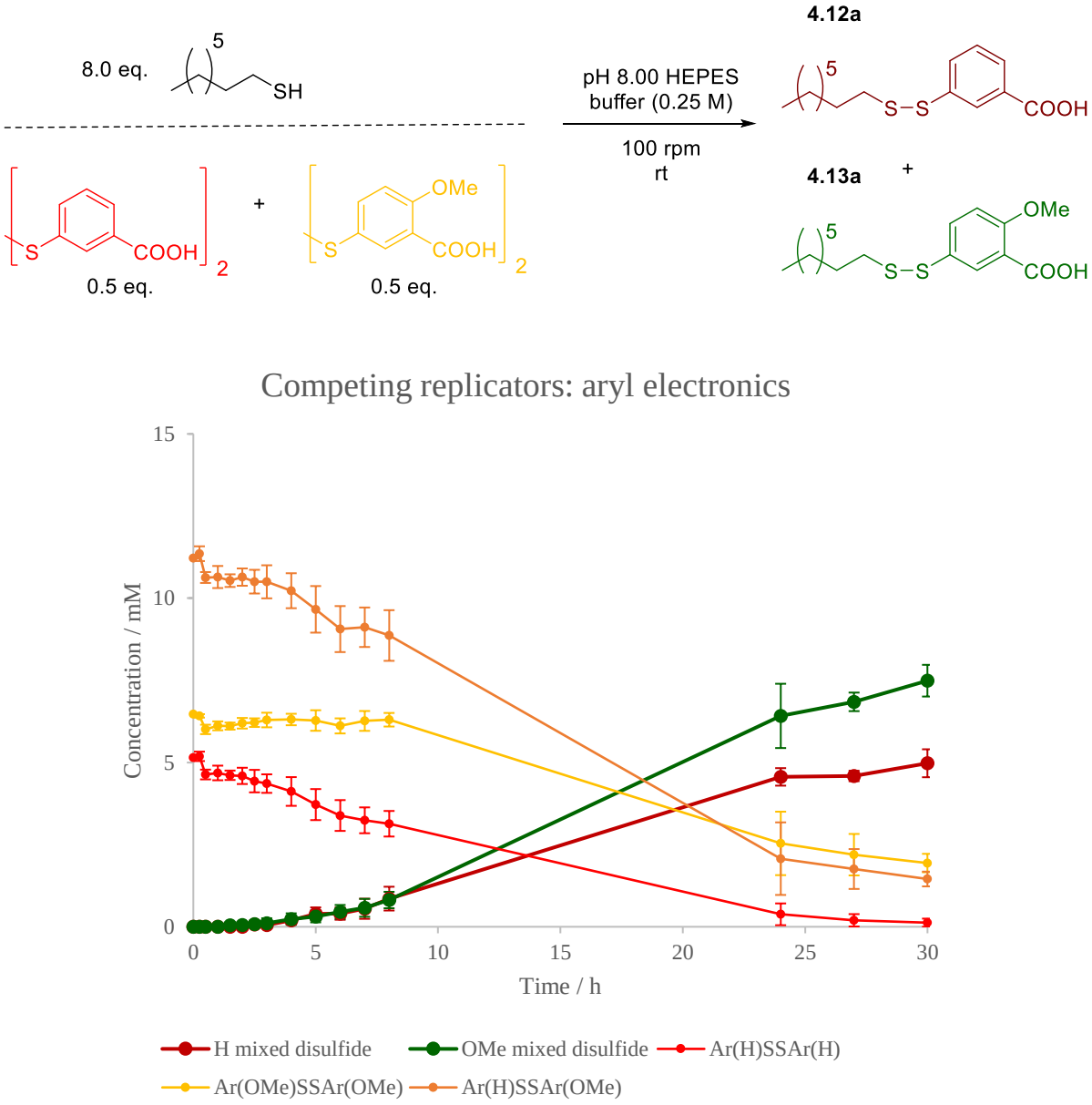


Figure 4. 3. 2. 2. 4. Reaction kinetics of competition study between mixed lipids ***4.12a*** *and* ***4.13a****. Aryl thiol concentrations are omitted for clarity. See also figures 4. 6. 9. 5. 3 and 4. 6. 9. 5. 4. n = 3, error bars show one standard deviation.*

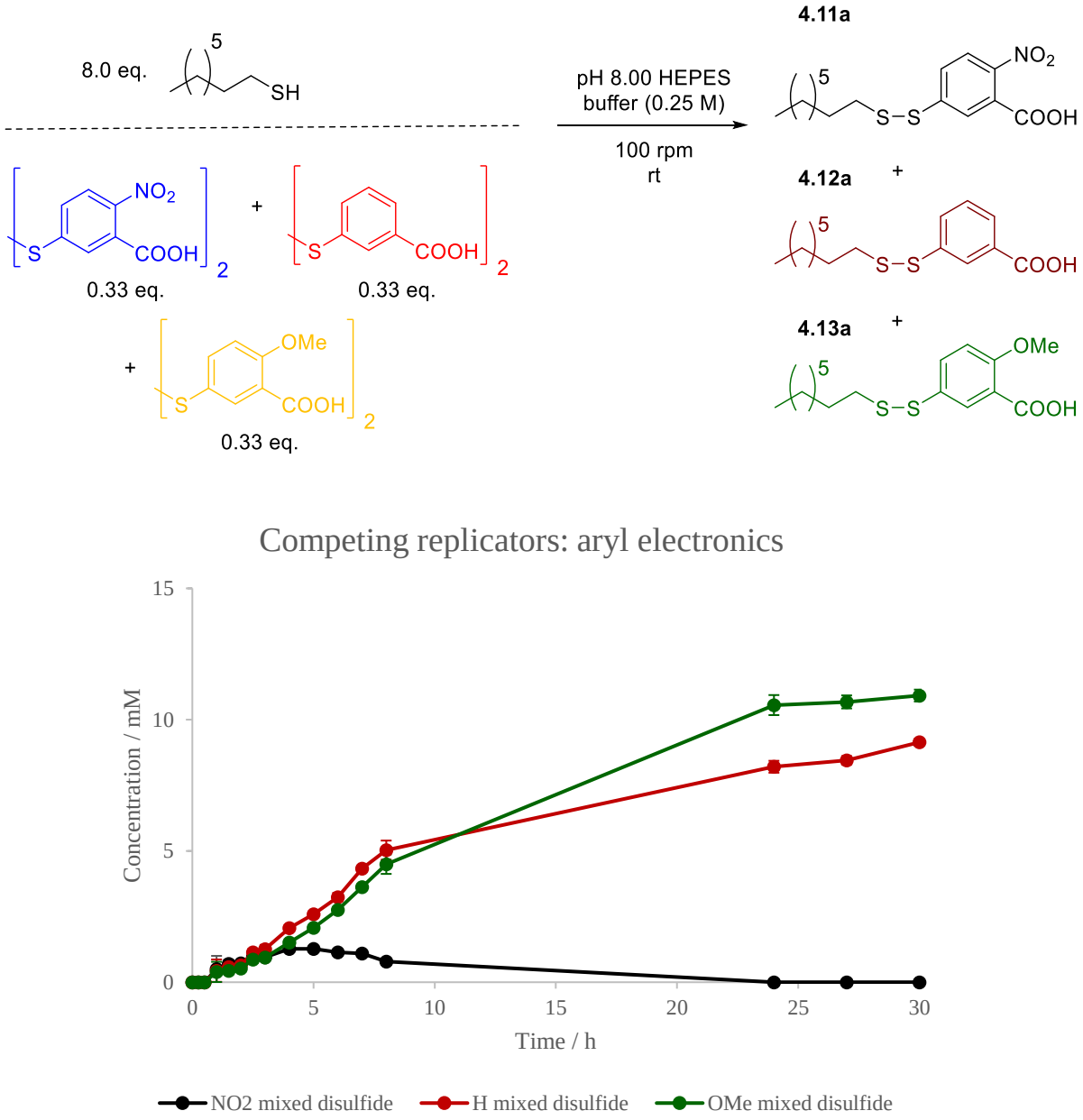


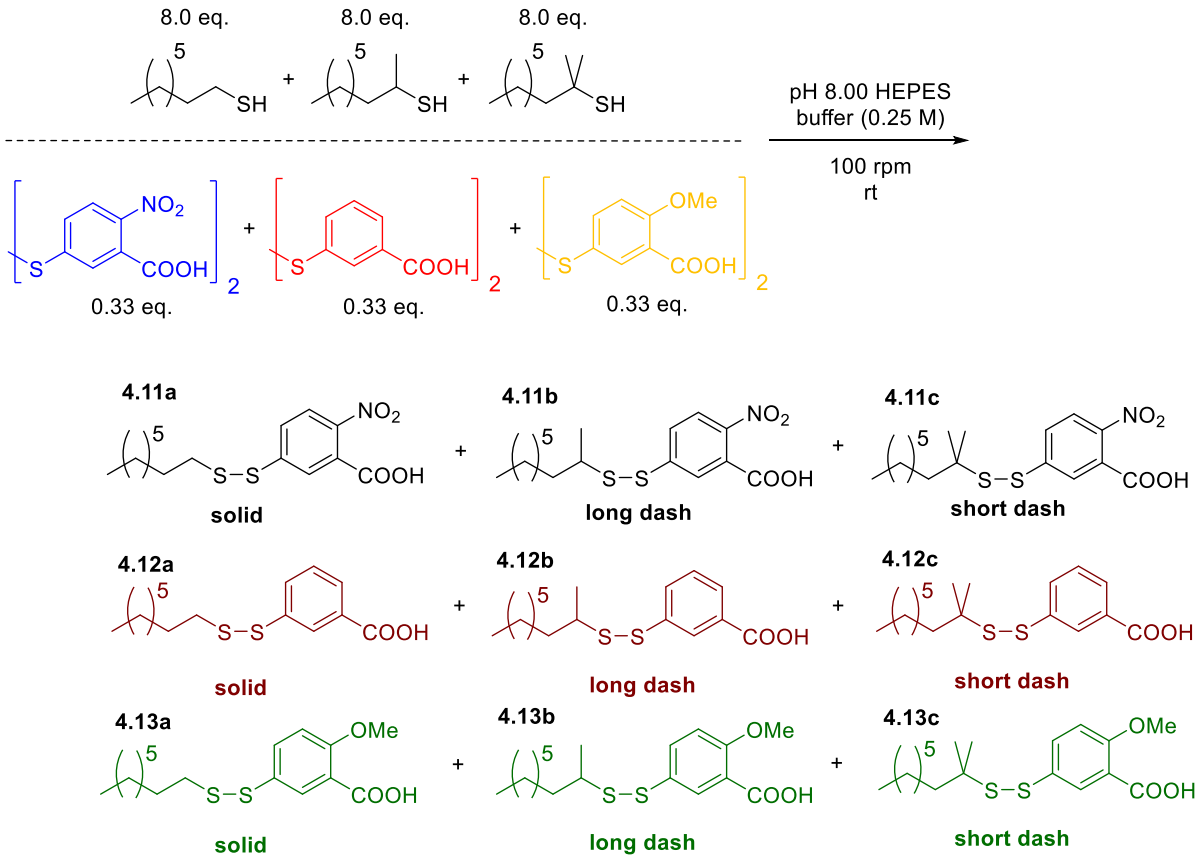
*Figure 4. 3. 2. 2. 5. Reaction kinetics of competition study between mixed lipids **4.11a**, **4.12a** and **4.13a**. Aryl thiol and bis-aryl disulfide concentrations are omitted for clarity. See also figures 4. 6. 9. 5. 5 to 4. 6. 9. 5. 7. n = 3, error bars show one standard deviation.*

4. 3. 2. 3 Behaviour of the 9 lipid system

In combining the methods of the two previous sections (Sections 4. 3. 2. 1 and 4. 3. 2. 2) there was the possibility to create a system of high complexity. By mixing just six different starting materials together, there is the possibility to form a further three bis-aryl disulfides via metathesis, three aryl thiols, nine lipids as well as alkyl disulfides. Other

than merely compositional complexity, the system was also expected to show kinetic and supramolecular complexity, with so many replicating lipids sharing mutual interactions.

The results under the standard conditions of pH 8.00 HEPES buffer are shown in figure 4. 3. 2. 3. 1 and alternative visualisation figure 4. 6. 9. 5. 1. 1. The relative proportions of each mixed disulfide is shown in figure 4. 3. 2. 3. 2, useful in establishing the selectivity of each surfactant through time. Pleasingly clear sigmoidal kinetics are evident, even in such a complex mixture. Initially, the selectivity is fairly low, with little to distinguish each species present, however by around 8 h product **4.11a** is dominant, and remains so over the course of 30 h. This is counter to what may be expected from the results discussed in section 4. 3. 2. 1, where in this timeframe succession to more sterically hindered disulfides was observed, and also counter to what might be expected based on the results in section 4. 3. 2. 2, whereby the more electron-rich aryl disulfides become dominant.



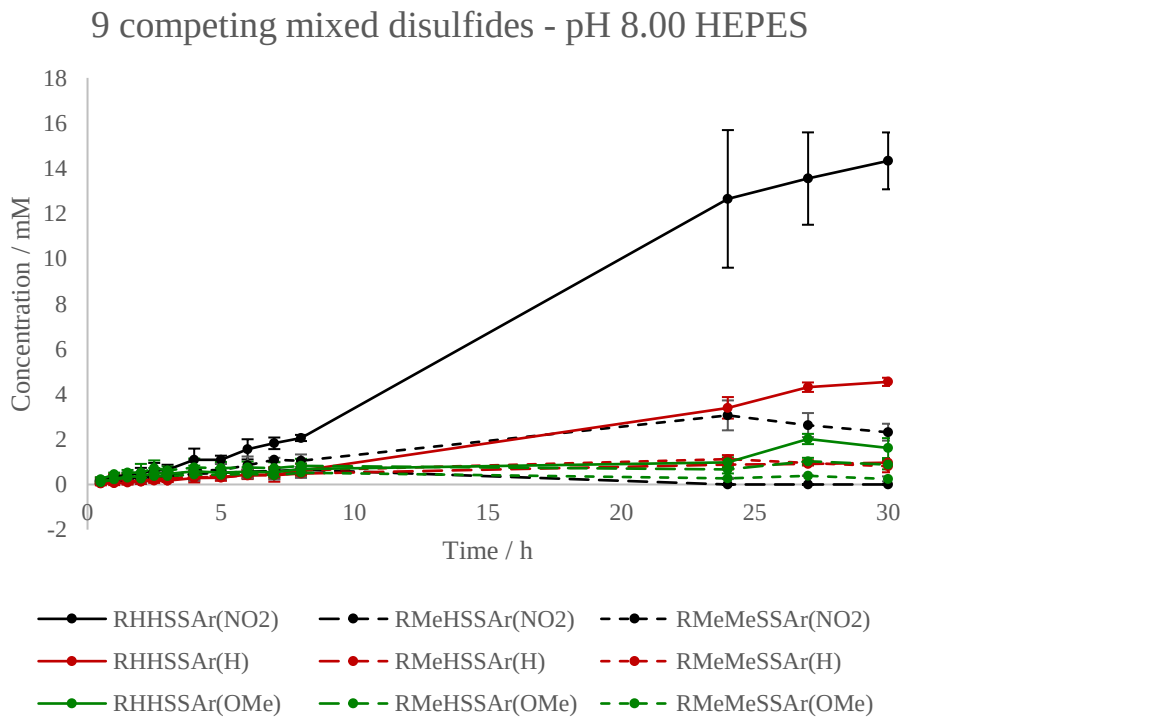


Figure 4. 3. 2. 3. 1. Plot of surfactant kinetics in the 9 lipid system, using pH 8.00 HEPES buffer. n = 3,

error bars show one standard deviation.

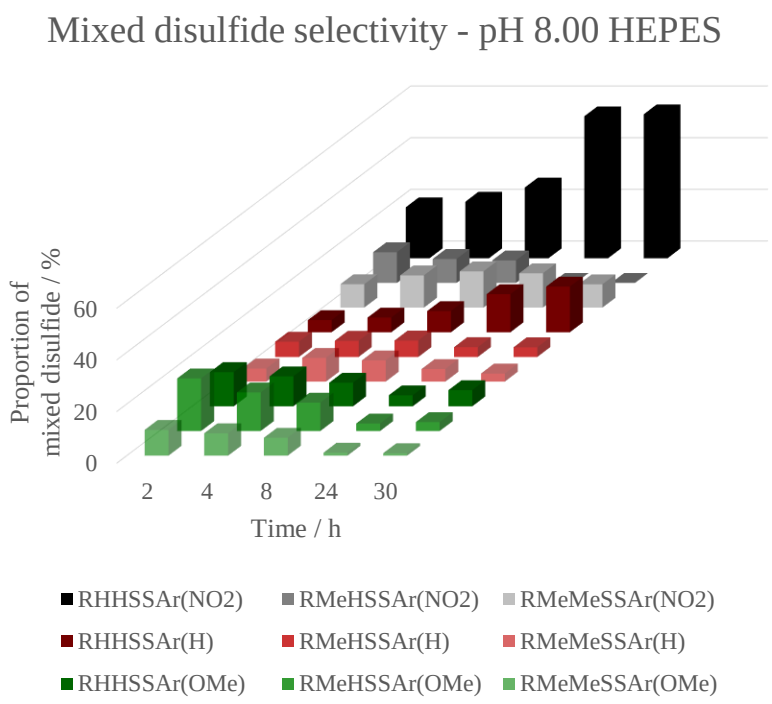
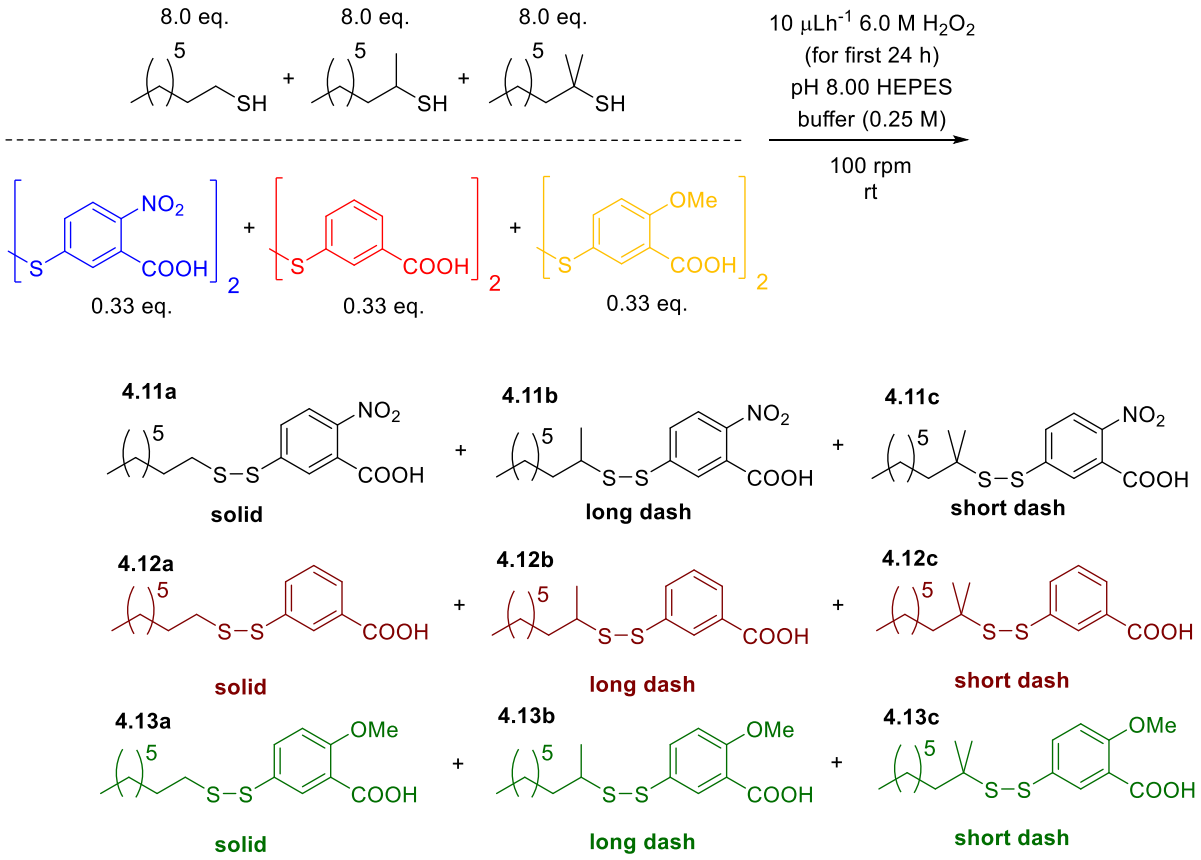


Figure 4. 3. 2. 3. 2. Bar chart of relative surfactant concentrations through time in the 9 lipid system, using pH 8.00 HEPES buffer. n = 3.

Floccing was observed between 4–7 days for all samples under the standard reaction conditions of pH 8.00 HEPES buffer, meaning longer term selectivities could not be followed. Fortunately, under other conditions precipitation occurred less readily, allowing the reaction to be followed over the course of a week, though typically floccing occurred shortly after this.

Under fuelled conditions, the kinetic profile and relative selectivities were essentially indistinguishable during the first 24 h (Figures 4. 3. 2. 3. 3 and 4. 6. 9. 5. 1. 2 for kinetics, figure 4. 6. 9. 5. 2. 1 for selectivity). It proved impractical to fuel these reactions for longer than 24 hours. No floccing was observed in these reactions over one week. After one week, **4.11a** is still predominant, however it has reduced in concentration down from 17 to 11 mM, thus the selectivity shows a broader spread across the surfactants.



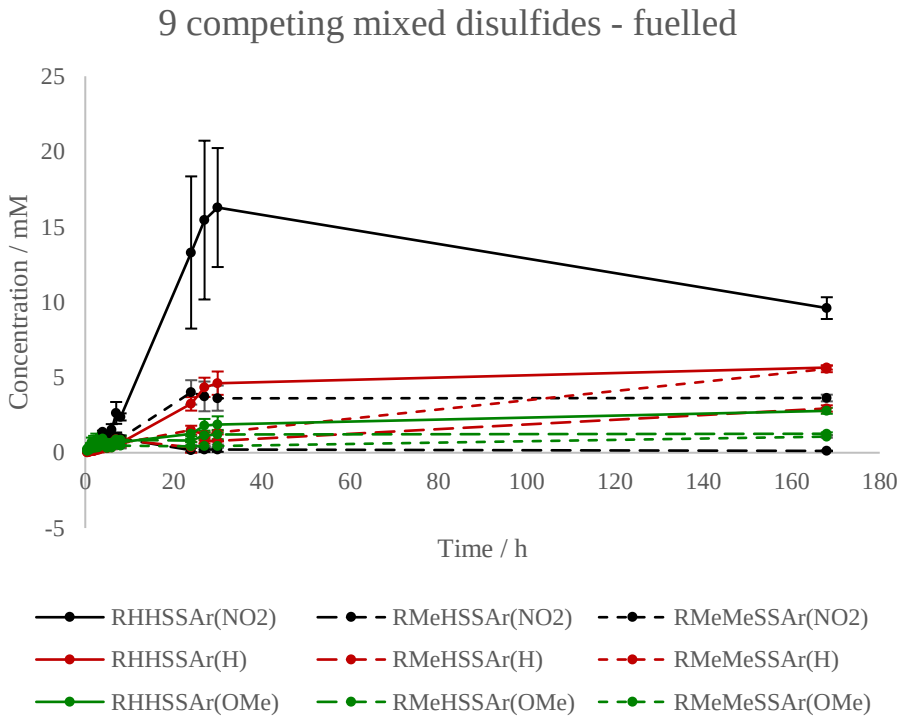
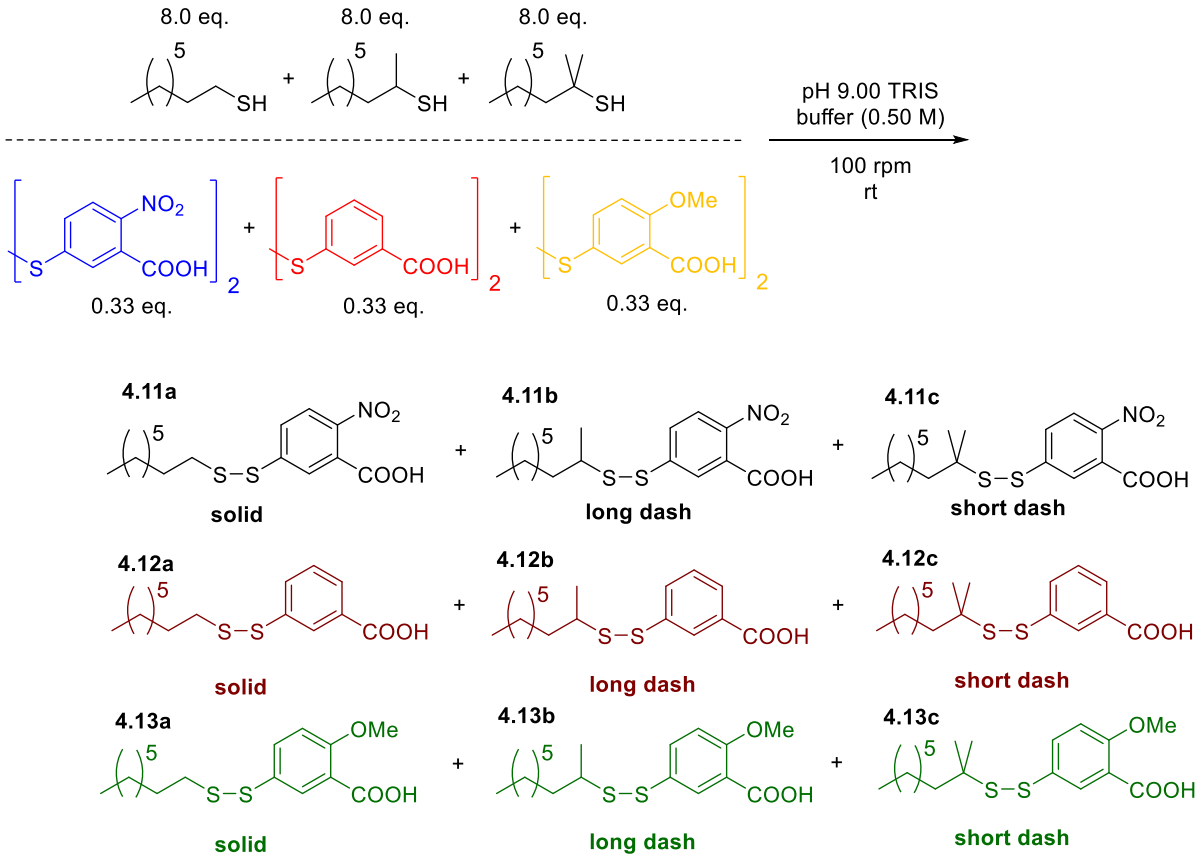


Figure 4. 3. 2. 3. 3. Plot of surfactant kinetics in the 9 lipid system, using pH 8.00 HEPES buffer, fuelled with addition rate of 10 μL h^{-1} of 6.0M H_2O_2 for the first 24 h. n = 3, error bars show one standard deviation.

Pleasingly changing the conditions lead to substantially different behaviour for the lipid mixture and the succession seen through time. In pH 9.00 TRIS buffer, there is a broader distribution across the lipids formed from the beginning (Figure 4. 3. 2. 3. 4). Also **4.11a** peaks far earlier (around t = 4 h rather than after 30 h). Through the course of the reaction there is a general change in selectivity towards the methoxy substituted lipids and away from the nitro substituted ones (Figure 4. 3. 2. 3. 5). Unexpectedly, there is a relatively low abundance throughout of lipids **4.11b**, **4.12b** and **4.13b**. A possible explanation for this is that these lipids are neither the fastest to form, nor the most stable, therefore have no strong selection advantage.



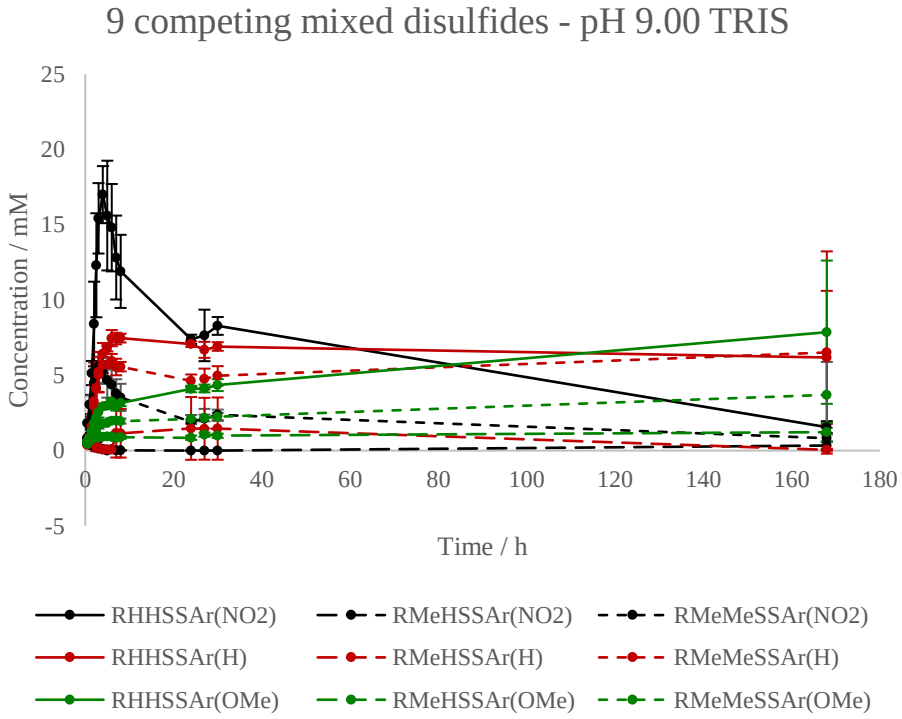


Figure 4. 3. 2. 3. 4. Plot of surfactant kinetics in the 9 lipid system, using pH 9.00 TRIS buffer, over the course of 7 days. A clear succession of replicators can be seen. n = 3, error bars show one standard deviation.

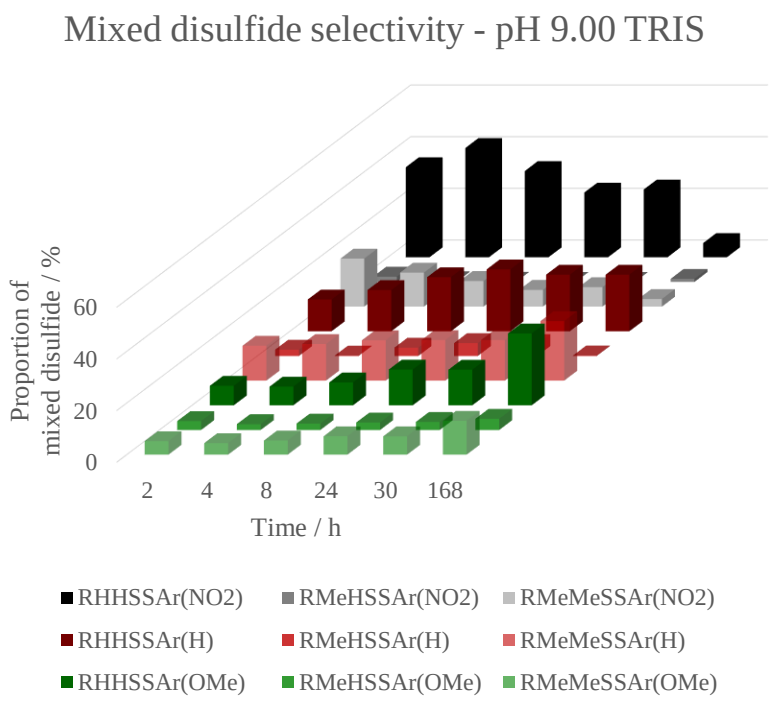
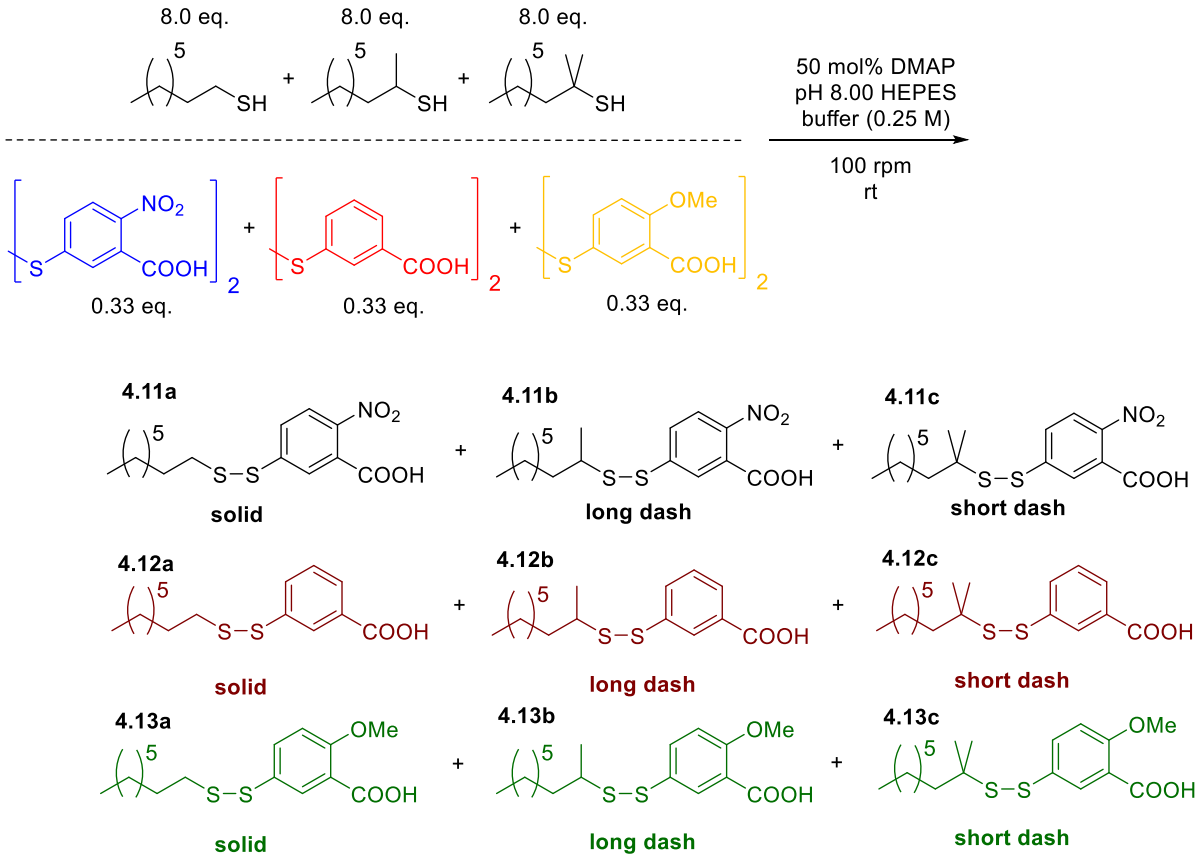


Figure 4. 3. 2. 3. 5. Bar chart of relative surfactant concentrations through time in the 9 lipid system, using pH 9.00 TRIS buffer. n = 3.

In pH 8.00 HEPES buffer with 0.5 equiv. of DMAP as a nucleophilic catalyst, we expected to see a higher rate of formation and destruction and accompanying changes in relative selectivities. What was observed was these conditions did show the greatest change in relative composition of any of the reaction conditions used and also largest variance between runs (Figure 4. 3. 2. 3. 6). As with pH 9.00 TRIS, there is a relatively low abundance of **4.11b**, **4.12b** and **4.13b** derived lipids throughout, again presumably because these lipids are neither the fastest to form, nor the most stable. Relative to the other conditions there is a high abundance of lipids with unsubstituted aryl rings, **4.12a-c**.



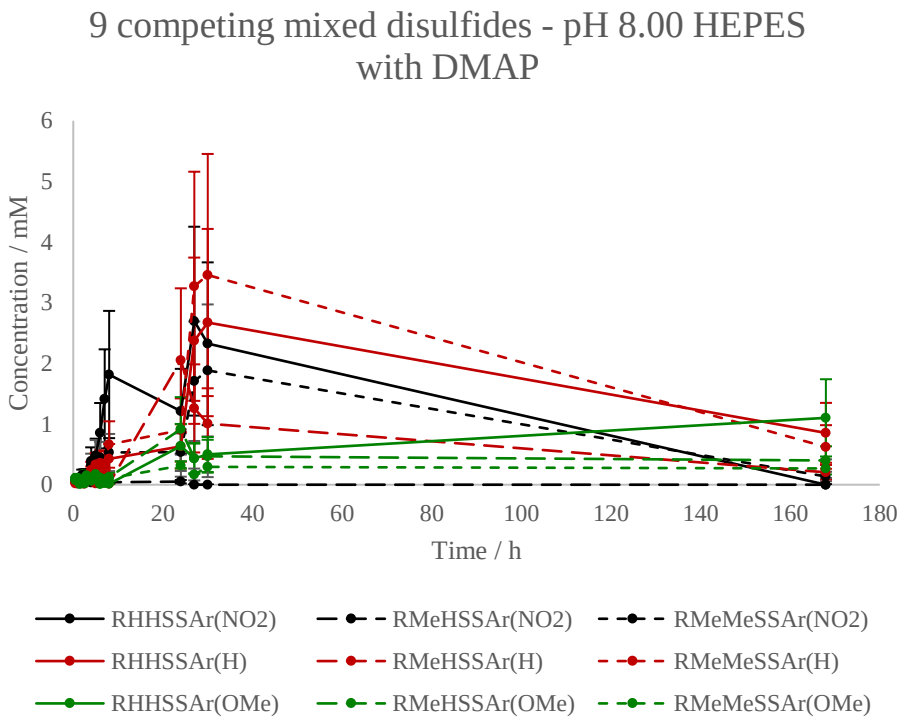


Figure 4. 3. 2. 3. 6. Plot of surfactant kinetics in the 9 lipid system, using pH 8.00 HEPES buffer with 0.5 equiv. DMAP, over the course of 7 days. A clear succession of replicators can be seen. n = 3, error bars

show one standard deviation.

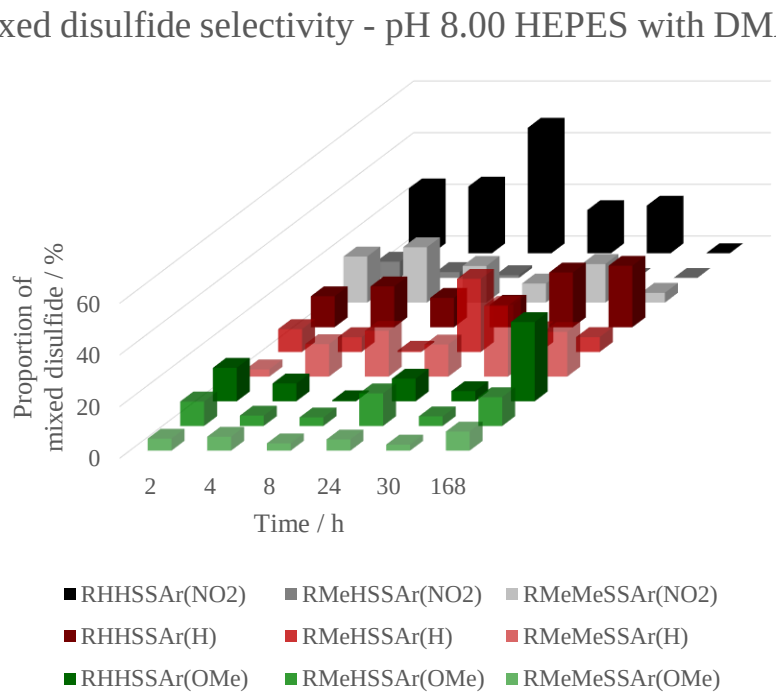


Figure 4. 3. 2. 3. 7. Bar chart of relative surfactant concentrations through time in the 9 lipid system, using pH 8.00 HEPES buffer with 0.5 equiv. DMAP. n = 3.

4. 3. 3 Physical Mechanism

4. 3. 3. 1 Brightfield Microscopy Data

The reaction was followed by microscopy in attempt to understand the physical mechanism by which it proceeds, using alkyl thiol **4.1a** and bis-aryl disulfide **4.2** in pH 8.00 HEPES buffer. Droplets of thiol of size 5-150 μm were observed in the aqueous layer within two minutes. Over the course of the first 2 hours, the droplets appear largely unchanged, although by t = 3 h no droplets larger than 50 μm were present. Around t = 4 h there is a rapid onset of an emulsion throughout the aqueous phase, as can be seen by cloudy aggregates permeated by infrequent small thiol droplets, size 5–10 μm. There was no visible change in the nature of this emulsion through time.

It is worth noting that these droplets forming spontaneously in the reaction are of the same size as those which undergo self-propulsion in the presence of lipid replicators in chapter 3. Care was taken to observe any motion of all droplet sizes we could observe in this setup. No self-propelled motion was seen in our aliquots at any time, though there was motion from coalescence of these drops and apparent thermal effects. We do not know about the possible motion in this system of smaller drops (below around 5 μm), and certainly cannot exclude motion in other similar reactions with physical autocatalysis.

The presence of these thiol droplets could have a large impact on the kinetic studies shown in section 4. 3. 1 and 4. 3. 2, typically during the first 2 hours of reaction. Where large thiol drops were part of the UPLC sample for a particular time point, the thiol would often not be fully quenched, leading to an artificial increase in the conversion of the reaction. Care has taken to exclude these kinetics runs in the previous sections, however an illustrative example has been included (Figure 4. 6. 9. 1. 1) where the t = 0.5 h time point shows enhanced concentration of all three lipids.

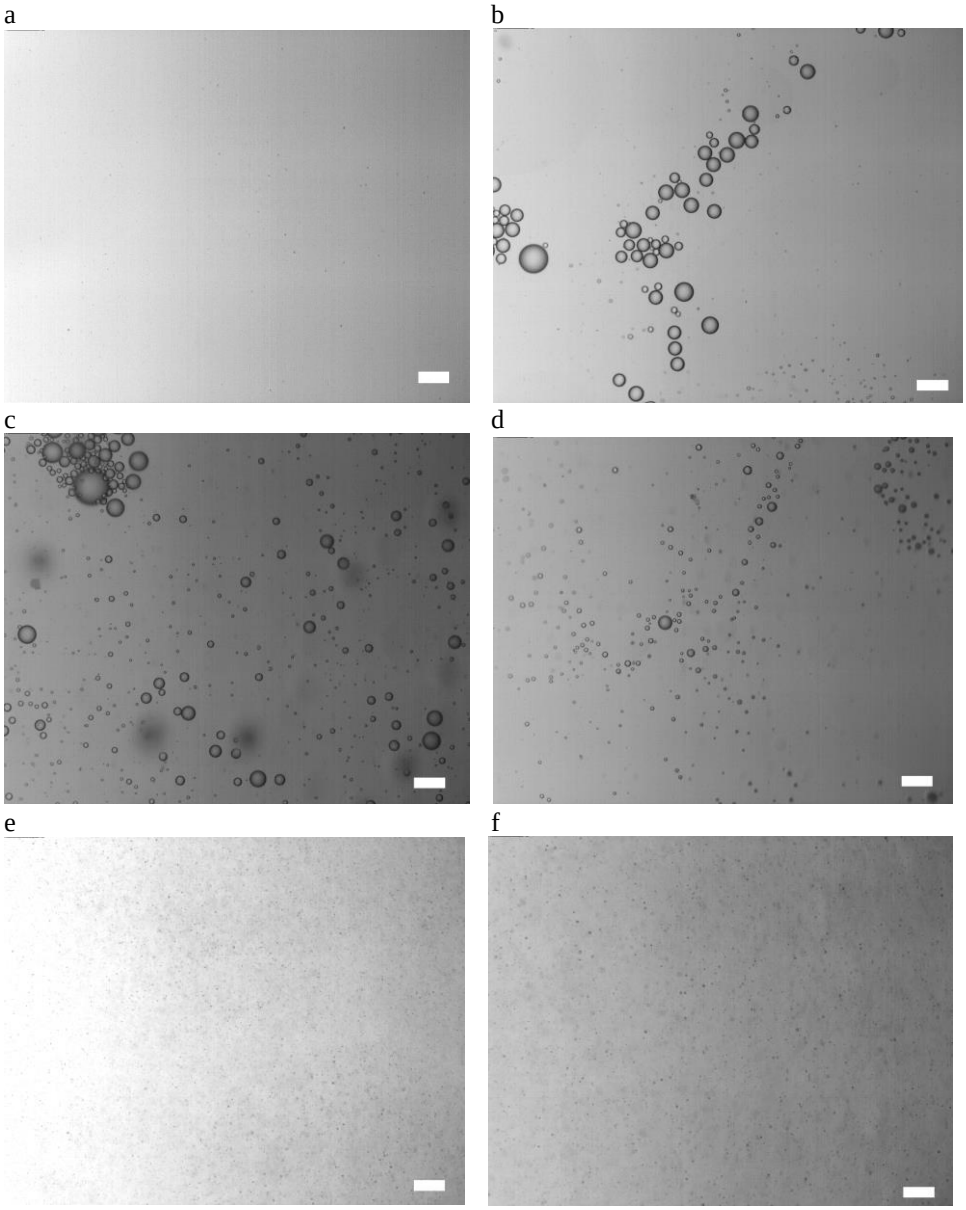


Figure 4. 3. 3. 1. 1. Brightfield microscope images of reaction samples through time. a – t = 0 (prior to addition of thiol), b – t = 2 mins, c – t = 1 h, d – t = 3 h, e – t = 4 h, f – t = 6 h. Scale bar = 100 µm.

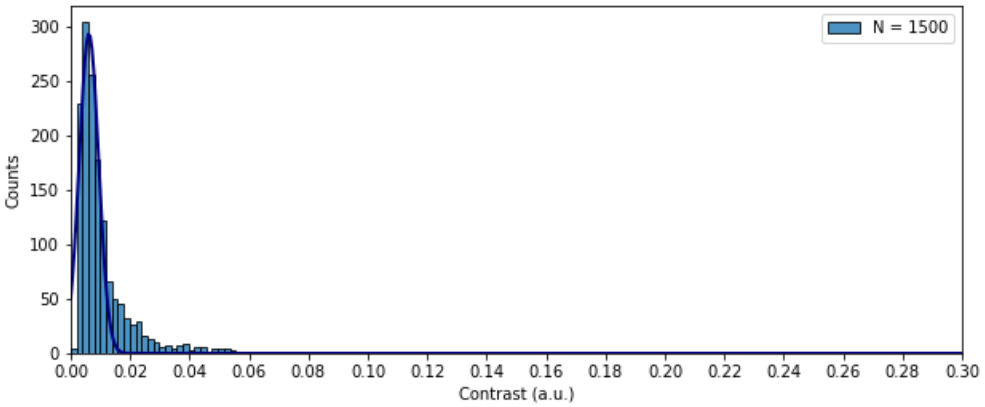
4. 3. 3. 2 iSCAT Data

Interferometric scattering microscopy (iSCAT) has been used to study physical autocatalysis in collaboration between the Fletcher and Kukura groups (both Oxford). This technique allows the real time detection of particles below the diffraction limit of light in their native environment, without the need for perturbations such as labelling with a fluorophore.[68] iSCAT can therefore be used to visualise and count individual micelles and vesicles as well as estimate their size through the course of an autocatalytic reaction.[69,70]

Contrast is a quantitative measure of the intensity of interferomic scattering and is linearly correlated with particle mass.[71] Although there is no exact quantitative conversion between contrast and particle size to date, they are closely related, micelles have low values of contrast 0.01 or below,[69] and vesicles 0.01–0.10. Figures 4. 3. 3. 2. 2 and 4. 3. 3. 2. 5 show typical differential iSCAT images, in which aggregate particles appear as dark circles. Scale bars is given on each image, though the diameter of the diffraction limited spots is typically significantly larger than the particle, and therefore cannot be quantitatively correlated with actual size.

Particle contrast distributions of pre-made solution of **4.12a** show a narrower distribution than those formed in a reaction mixture of similar concentration (Figure 4. 3. 3. 2. 1). This indicates that the supramolecular aggregates formed under the reaction conditions are more diverse than what is found in solutions of pure compound and likely the presence of alkyl thiol influences aggregation in the aqueous phase.

a



b

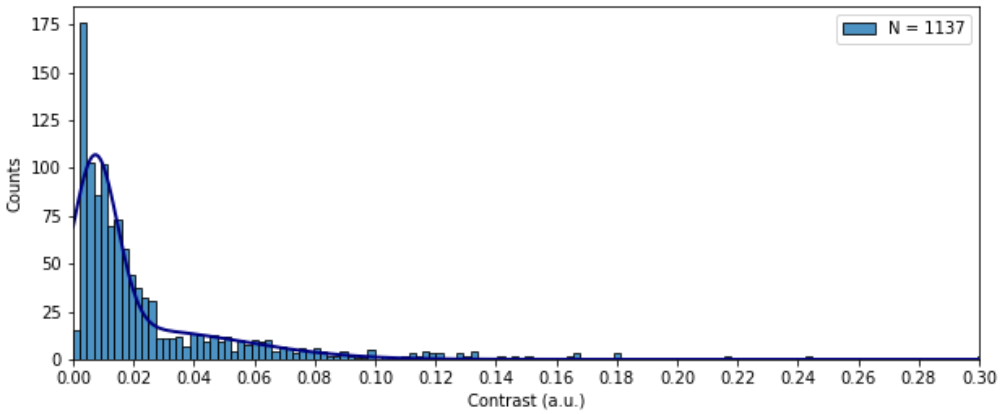


*Figure 4. 3. 3. 2. 1. Two particle contrast distributions for **4.12a**, obtained from iSCAT data. The similar total count number (N) indicates similar concentrations. a – 600 µM solution of **4.12a** in pH 8.00 HEPES buffer. b – reaction mixture from a reaction to form **4.12a**, with 2.5 mM aryl disulfide and 8.0 equiv. alkyl thiol, diluted 10× with pH 8.00 HEPES buffer to avoid saturation of the detector. n = 1.*

Pleasingly snapshots of the vesicle forming reactions appear to show a change in aggregation through time (Figure 4. 3. 3. 2. 2). This is likely a micelle to vesicle transition, as in the early stages of the reaction all particles are of very low contrast, below 0.01, consistent with previous observations of micelles on iSCAT[69] and after around 3 h contrast was much higher, up to 0.05. These data are collected around and below the critical aggregation constants of the surfactants.[72] To avoid saturation of the cover slip and observe each aggregate particle individually, the reactions are run more dilute than the batch conditions used in sections 4. 3. 1 and 4. 3. 2. These data therefore

provide insight into the very early stages of the reactions, key to the onset of autocatalytic effects.

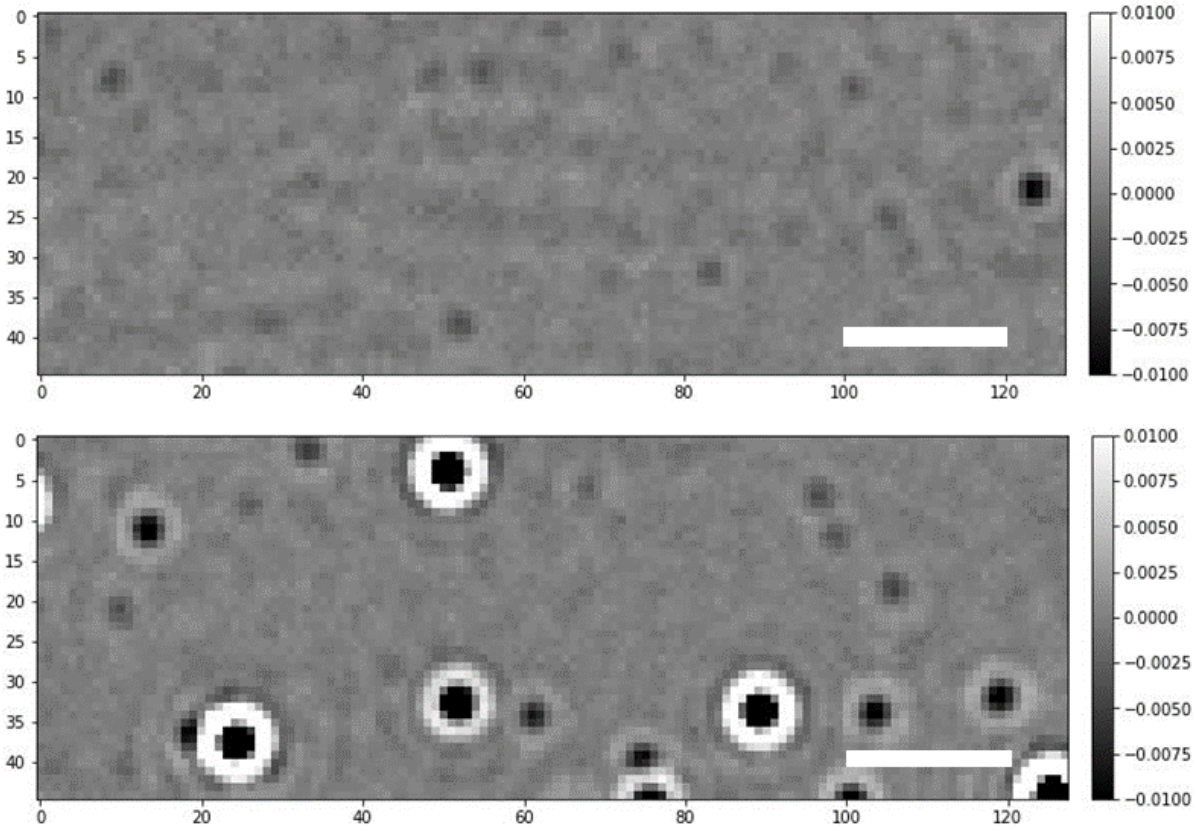
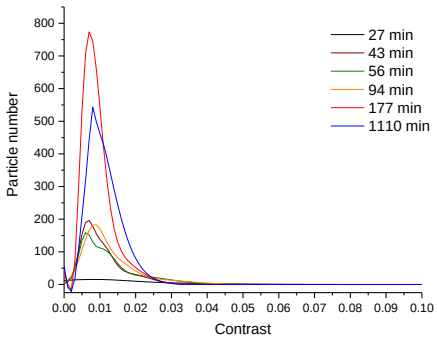


*Figure 4. 3. 3. 2. 2. Two differential iSCAT images from a reaction forming **4.12a**, with 2.5 mM aryl disulfide and 8.0 equiv. alkyl thiol. Top – t = 113 mins. Only small particles are present, indicative of micelles. Bottom – t = 167 mins. Large particles are present, indicative of vesicles. Scale bar = 2 µm.*

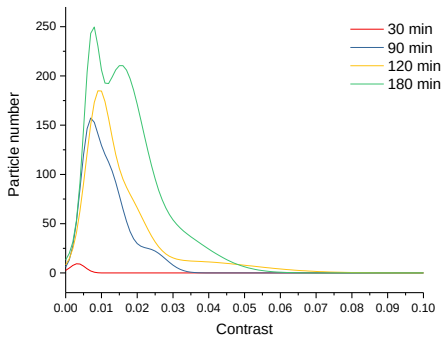
To investigate this further, the contrast distributions through time were compared for reactions forming **4.11a**, **4.12a** and **4.13a** (Figure 4. 3. 3. 2. 3). Compound **4.11a**, as with all the nitro bearing surfactants, was found to form micelles by DLS, and through the course of the reaction no significant change in contrast of the particles was observed by iSCAT, suggestive of micelles being the exclusive supramolecular aggregate throughout the reaction. For both **4.12a** and **4.13a**, found to be vesicle forming by DLS, at early time points only small aggregates are found, indicative of micelles, and at later time points the contrast distributions shift towards higher contrasts, indicating the presence of larger

aggregates such as vesicles. Such a change in aggregation may be explained through entropic arguments, at low concentrations micelles may be favoured over vesicles entropically, requiring fewer molecules to come together, whereas at higher concentrations, vesicles predominate as they are enthalpically more stable for these surfactants.

a



b



c

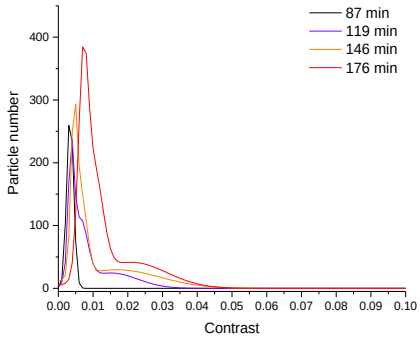


Figure 4. 3. 3. 2. 3. Contrast distributions for three different reactions through time. In all cases 2.5 mM aryl disulfide was used, and 8.0 equiv. of 1-octanethiol. a – reaction forming ***4.11a****, b – reaction forming* ***4.12a****, c – reaction forming* ***4.13a****. n = 1.*

Following the kinetics of the reactions on the single particle level by iSCAT was possible for **4.11a**, **4.12a** and **4.13a** by counting the number of particles detected in a 30 second iSCAT video of a sample aliquot taken at given times. Kinetic plots show a clear lag phase prior to a rate enhancement (Figure 4. 3. 3. 2. 4 shows representative data for **4.13a**). In the early times of the reactions, before surfactant formation is detected, a small

number of large particles are seen (Figure 4. 3. 3. 2. 5), believed to be alkyl thiol droplets analogous to those discussed in section 4. 3. 3. 1.

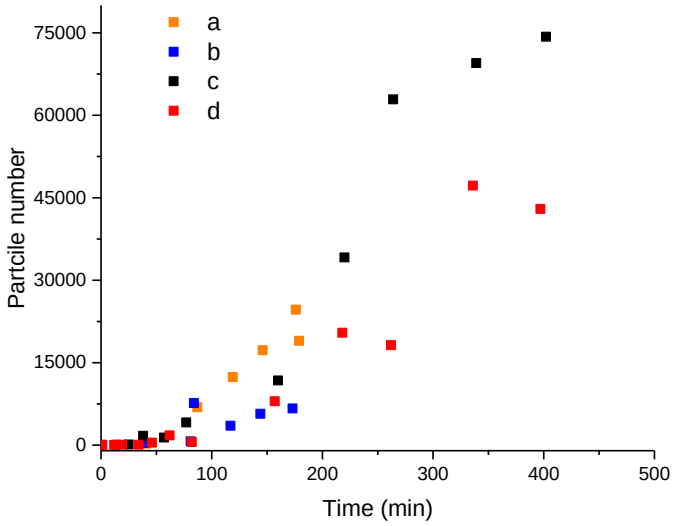


Figure 4. 3. 3. 2. 4. Kinetics by iSCAT. Plot of total particle count against time for reactions to form ***4.13a****. In all cases the initial aryl disulfide concentration was 2.5 mM in pH 8.00 HEPES. a and c – 8.0 equiv. 1-octanethiol. b and d – 1.0 equiv. 1-octanethiol. n = 2.*

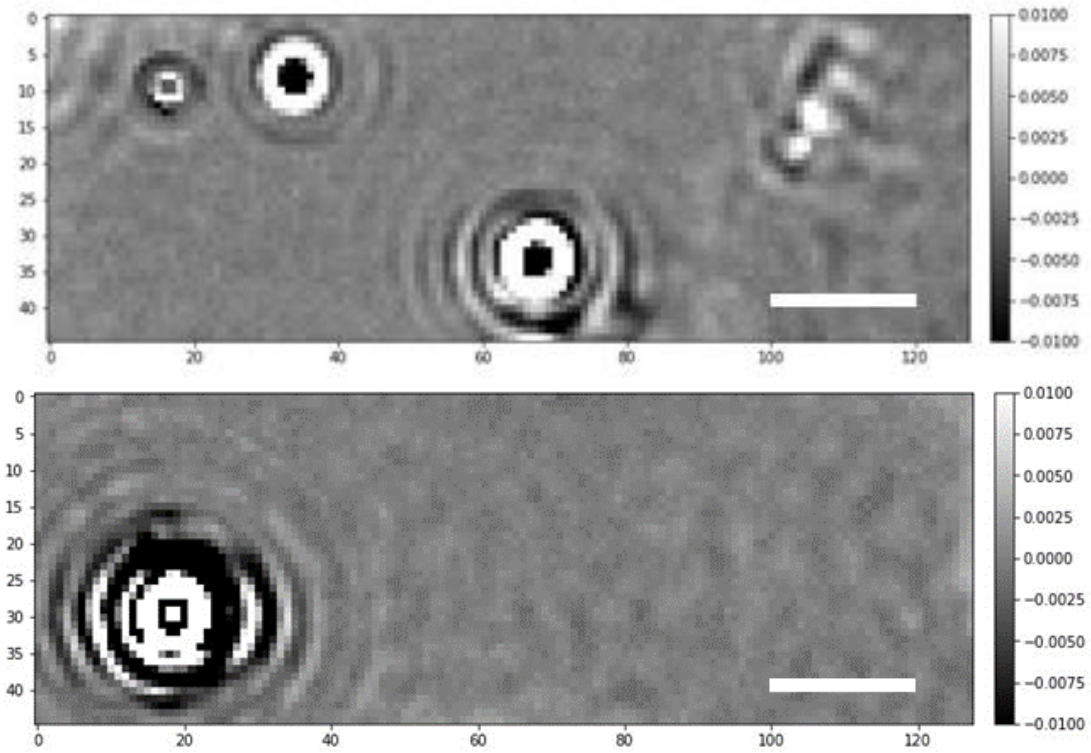


Figure 4. 3. 3. 2. 5. Two snapshots showing very large particles from the early stages of a reaction. They were often seen during the first hour of reactions. These are believed to be thiol droplets. Scale bar = 2 µm.

4. 4 Other thiol-disulfide exchange systems

4. 4. 1 Surfactants for acidic conditions

The aim of this section was to develop a version of the autocatalytic thiol-disulfide exchange reaction which proceeds under acidic conditions (Figure 4. 4. 1. 1). This could show interesting behaviour when under competition conditions, whereby which replicating lipid predominates might be switched by changing the between acidic and alkaline conditions. A candidate reaction was designed to form a pyridine mixed disulfide **4.14** from **4.15** and 1-octanethiol (Figure 4. 4. 1. 1c).

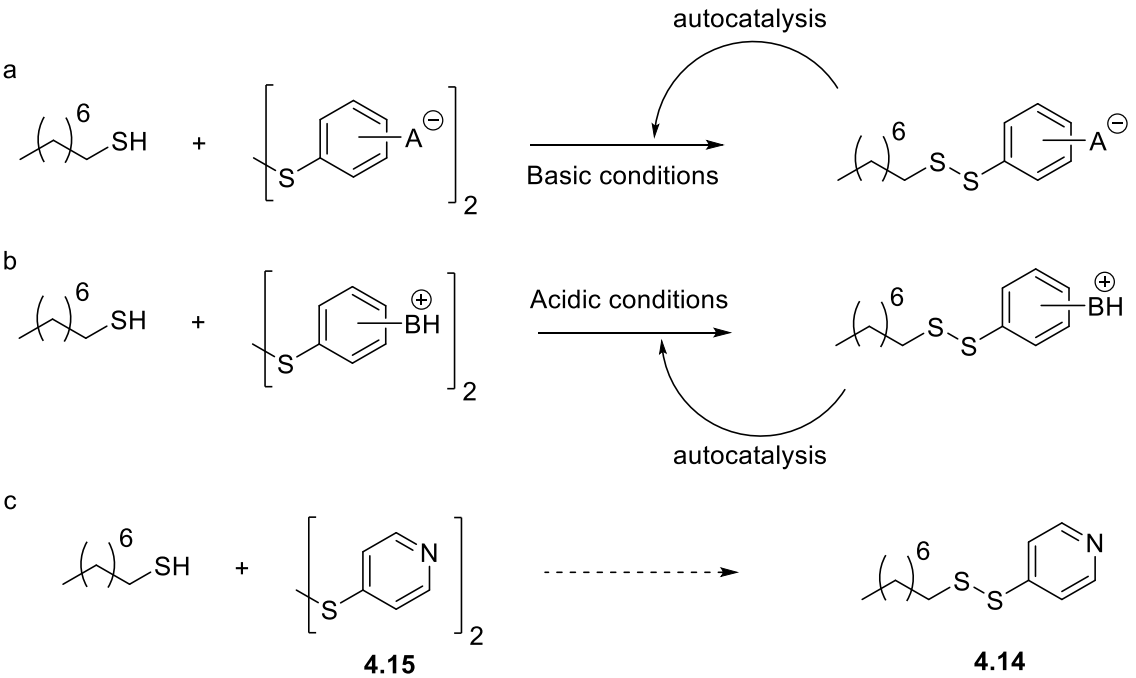
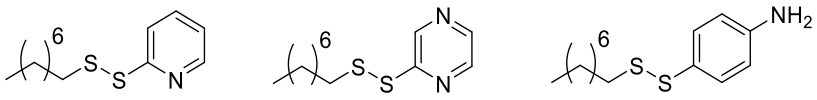


Figure 4. 4. 1. 1. Conceptual diagram for different mixed disulfide replicators at differing pH. a – bis-aryl disulfide starting material contains an acidic functional group, AH. Physical autocatalysis occurs with aggregates of the mixed disulfide product under basic conditions. The work in section 4.2 and 4.3 operates like this. b – an analogous design to a, whereby the bis-aryl disulfide contains a basic functional group, B. We expect water soluble aggregates of the mixed disulfide product to form under acidic conditions. c – reaction design which may perform as b, based on the basicity of pyridine.

Table 4. 4. 1. 1 shows the solubility of **4.14** under a range of acidic conditions. Unfortunately the solubilities were generally low, however under two conditions they were high enough that they could be used for the reaction, pH 1.50 phosphate buffer with added NaCl and 1 M hydrochloric acid (Table 4. 4. 1. 1 entries 6 and 7). Other mixed disulfides containing basic nitrogen sites (**4.16**-**4.18**) were synthesised and their solubilities tested, although all were found to be less soluble than **4.14** in 1 M hydrochloric acid and were essentially insoluble in pH 1.50 phosphate buffer.

Entry	Acid	Solubility / mM
1	pH 4.00 citrate buffer (0.25 M)	< 2
2	pH 3.50 sodium acetate buffer (0.25 M)	< 2
3	pH 3.00 phosphate buffer (0.25 M)	5
4	pH 2.00 phosphate buffer (0.25 M)	4
5	pH 1.50 phosphate buffer (0.25 M)	< 2
6	pH 1.50 phosphate buffer with added NaCl (both 0.25 M)	30
7	1 M hydrochloric acid	210

*Table 4. 4. 1. 1. Solubility of substrate **4.14** in a range of acidic conditions. n = 1.*



4.16 **4.17** **4.18**

*Figure 4. 4. 1. 2. Other mixed disulfides whose solubility was tested. All showed lower solubility than **4.14** in 1 M hydrochloric acid and also very low solubility in pH 1.50 phosphate buffer (0.25 M).*

No **4.14** was formed under biphasic conditions over 24 h in using either of the acidic conditions identified in table 4. 4. 1. 1 (see figure 4. 4. 1. 3). Using shorter chain thiols (1-hexanethiol, 1-butanethiol and ethanethiol), mixed disulfide products were formed, though the kinetics did not show any sigmoidity and no rate enhancement was observed on addition of 0.2 equivalents of product. Therefore under these conditions, it appears that these reactions are not autocatalytic.

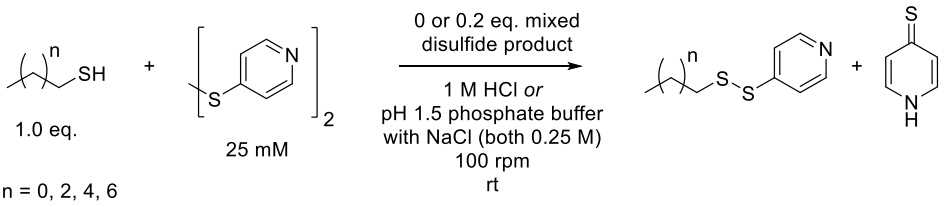


Figure 4. 4. 1. 3. Reaction between alkyl thiols and bis-pyridine disulfide to form amphiphilic mixed disulfide. Kinetics of these reactions were followed, however there were no indications of autocatalysis in any case.

4. 4. 2 Designs for triphasic systems for non-mutualistic competing replicators

The systems of competing replicators in sections 4.2 and 4.3 of this chapter seem to be mutualistic, that is there is significant cross-catalysis, with each lipid product catalysing reactions through the transfer of material across a common phase boundary. How non-mutualistic (i.e. selfish) replicators can be made using lipid replication is not obvious. The design for a proposed triphasic system is shown in figure 4. 4. 2. 1. Here, one alkyl thiol (A) is hydrogenated, localised in the hydrocarbon phase, whilst a second (B) is fluorinated, localised in the fluorous phase. These can both react with a common aqueous bis-aryl disulfide (C) to form two distinct products (D and E), with a common biproduct (F). As the reactions between the thiols and bis-aryl disulfide occur across different phase boundaries, it seemed possible there may be non-mutualistic replication in such a system.

Perfluorinated and partially fluorinated materials can adopt more complex supramolecular morphologies than those formed only from alkyl surfactants.[73] The relative importance of the factors influencing the differences in aggregation between fluorinated and hydrogenated chains are an emerging field of research, but at present it is clear the larger size, different conformational preferences and rigidity, reduced van der Waals interactions and dipole moments all play a role.

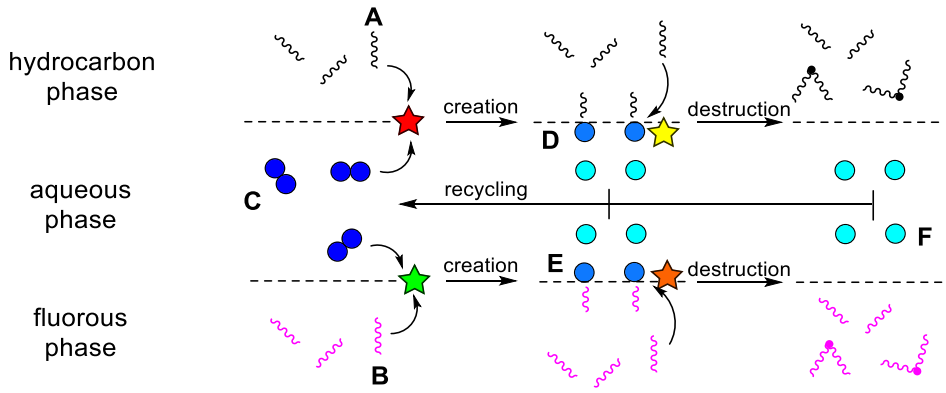


Figure 4. 4. 2. 1. Conceptual diagram of competing replicators design, based on a triphasic system. The fluorous phase is most dense, followed by the aqueous phase, with the hydrocarbon phase being the least dense. The two alkyl thiols A and B are present in the system, and both react with C in the aqueous to form mixed disulfides, D and E respectively. D and E are likely to be present at the phase boundaries and throughout the aqueous phase. Both D and E can undergo a second thiol-disulfide exchange as destruction steps, and biproduct F may be recycled to starting material C by oxidation.

Reactions between fluorous thiols **4.19** and **4.20**, and Ellman's reagent were challenging to monitor and showed poor reproducibility due to the low solubility of products **4.21** and **4.22** in HEPES and TRIS buffers (Figure 4. 4. 2. 2). In order to achieve the system design, clearly more polar bis-aryl disulfides would be required, so that fluorous mixed disulfides would be soluble.

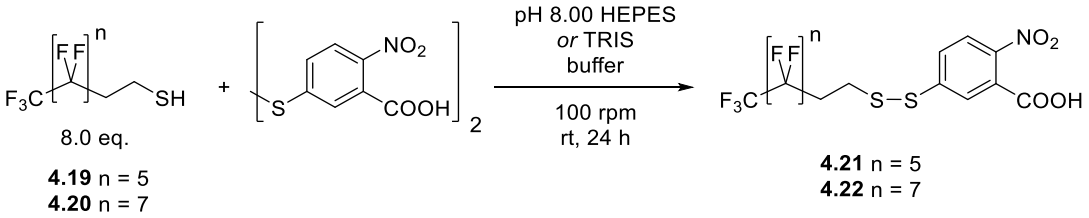


Figure 4. 4. 2. 2. Reaction between fluorous thiols and Ellman's reagent to form mixed disulfide amphiphiles.

The synthesis of polar bis-aryl disulfides proved challenging, due in large part to problems of purification (Figure 4. 4. 2. 3). Commonly compounds such as **4.23** were gave baseline spots in normal phase chromatography, even in the most polar solvent systems (AcOH: H_2O: MeOH: DCM, H_2O: MeOH: $CHCl_3$ or H_2O: MeCN mixtures).

Reverse phase chromatography could be used for the purification of compound **4.23**, however was found to be impractical for starting material synthesis, as a maximum of 50 mg could be prepared in each round of chromatography when performed manually. **4.26** showed very low solubility in basic solutions, below 10 mM in several buffers up to pH 10 and above pH 10 decomposition occurred.

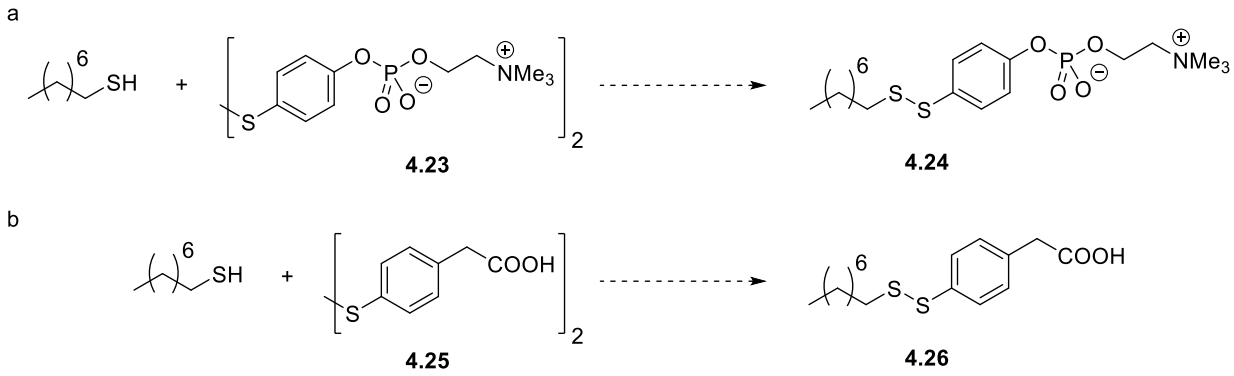
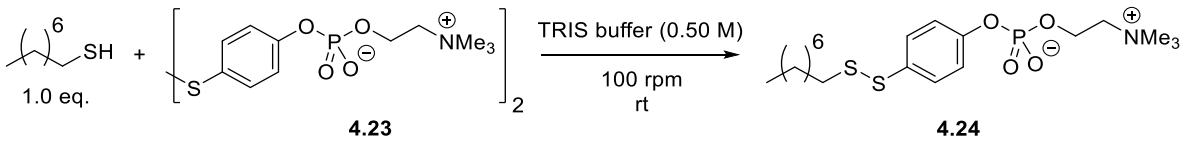


*Figure 4. 4. 2. 3. Other proposed thiol-disulfide systems, developed with the aim of higher solubility. a – phosphocholine based system based on bis-aryl disulfide **4.23** which may form **4.24**. b – Reaction between 1-octanethiol and **4.25** to form **4.26.***

Using the small amount of **4.23** that could be purified, initial kinetics runs were performed (Figure 4. 4. 2. 4). These results are promising, showing a small degree of sigmoidal character, indicative of possible autocatalysis.



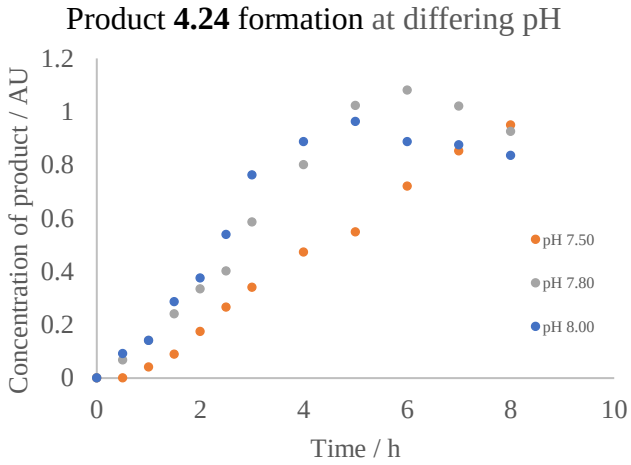


*Figure 4. 4. 2. 4. Reaction kinetics of **4.24** formation from 1-octanethiol and **4.23**. Insufficient amounts of **4.23** and **4.24** were synthesised for calibration of concentration. n = 1.*

4. 5 Conclusions and future work

4. 5. 1 Conclusions

Through this work we have successfully developed a system of competing lipid replicators, which under several conditions show a succession of lipid composition through time. The system is built from a dynamic pool of hydrophobic bis-aryl disulfides, which undergo metathesis under the reaction conditions. Mixtures of alkyl thiols form an organic phase which react via thiol-disulfide exchange to give lipid replicators.

The modular nature of the system allowed analysis of different factors which contribute to overall behaviour. Many of these 2 or 3 lipid systems show interesting behaviour in their own right, such as where the dominant lipid in a competition setup is the one which would be formed slower in isolation. We have also shown that it is possible to achieve dramatic oscillations in a replicating lipid system.

Unfortunately, whilst all lipids were unstable to the reaction conditions, in practice some lipids are kinetically trapped in this system, having a half-life of months. This precluded the study of effect of different fuelling rates on lipid succession.

The 9 lipid system was a significant analytical challenge, requiring around 2 months of method optimisation. It would appear that these results are the realisation of as complex a system of this type that can be analysed by this method, and any further bis-aryl disulfides or alkyl thiols would have to be highly chemically distinct for analysis to be tractable.

4. 5. 2 Future work

The work on oscillations in section 4. 2. 2 is very promising but was limited by the low throughput means of analysis (UPLC). Whilst the results of this method are valuable in showing the absolute concentrations of three species key to the reaction cycle, it puts extreme limitation on screening and optimisation. It would be desirable to develop the

reaction towards having a significantly shorter period of oscillation, but maintaining as much as possible the amplitudes seen in these initial results. TNB can be readily detected by UV-Vis spectroscopy, so using this as an in-line reaction monitoring approach seems ideal to screen conditions, possibly following up results of interest by UPLC analysis.

Further developments of this chemistry should focus on the effect of replicator identity on oscillations, and on how mixtures of replicators effect the dynamic behaviour. The work of Cafferty et al. shows how mixtures can sustain oscillations, but what may be more interesting to a prebiotic context is the influence on mixtures of replicators *away* from oscillation towards steady states.[43] A single replicator, such as is shown in section 4. 2. 2, can be seen as inefficient feeder, unable to form a stable population with a particular fuelling rate. Mixtures of replicators are likely to show damped oscillations, reaching steady state compositions quicker. This would be a form of mutualism, whereby each replicator alone is unstable, but together can coexist as part of a stable mixed population.

Further work is required on the development of more bis-aryl disulfide electrophiles, so that more diverse systems can be developed using this chemistry. Among these possibilities are lipids which replicate under acidic conditions, and triphasic systems using fluorous and hydrogenated alkyl thiols as described in section 4. 4. 2.

4. 6 Experimental

General synthetic experimental information for this chapter is as found in section 2. 6. 1.

4. 6. 1 Buffer preparation

TRIS buffer solutions were prepared by dissolving the required mass of tris(hydroxymethyl)aminomethane in around 90% of the final volume MilliQ water. The pH and volume was adjusted by addition of concentrated hydrochloric acid (12 M) and MilliQ water, as measured with a Jenway 3510 benchtop pH meter. Final pH of the buffer was measured with rapid stirring, at room temperature and after an equilibration time of at least 30 seconds, and to an accuracy of ± 0.01 pH units. HEPES buffers were prepared analogously to those of TRIS, using 4-(2-hydroxyethyl)-1-piperazineethanesulfonic acid. The required pH was achieved by addition of a saturated aqueous solution of potassium hydroxide. Buffer solutions were stored at 4 °C in the dark prior to use and allowed to warm to room temperature prior to reactions.

4. 6. 2 Reaction setup for kinetics runs

Reactions were performed in 10 mL round bottom flasks using Fisherbrand oval 20 x 10 mm PTFE stir bars. Reactions were stirred using IKA RCT basic stir plates, without external calibration of stir rate. Aqueous reagents were dissolved by either rapid stirring followed by reduction to the reaction stir rate, or by sonication. Once all aqueous components were dissolved, the alkyl thiol was added using a layering technique, whereby the dispensing needle of either the Hamilton microsyringe or Braun Injekt-F syringe were placed just above the aqueous surface and the thiol carefully dispensed onto the aqueous, making care not to agitate the solution. In the case of reactions involving multiple aryl disulfides, the aqueous was left for at least 30 minutes prior to the addition of alkyl thiol to allow for equilibration via metathesis.

4. 6. 3 Reaction Sampling

4. 6. 3. 1 Preparation of quench-standard solution

The quench-standard solution was prepared by dissolving maleimide (120.0 mg) in dissolving into the external standard solution (20.0 mL). Quench-standard solutions were used within one day. The external standard solution was prepared by first dissolving 2-methyl-3-nitrobenzoic acid (50.0 mg) in dimethyl sulfoxide (5.00 mL) in a volumetric flask. Then some of this solution (1.50 mL) was diluted with milliQ water to a final volume of 500.0 mL in a volumetric flask to give the external standard.

4. 6. 3. 2 Preparation of reaction samples

Reactions were sampled by withdrawing 25 μL of the aqueous phase of the reaction mixture using a Hamilton 25 μL 80200 1702N Gastight microsyringe, ensuring no large drops of thiol were sampled, a problem prevalent during the first hour of many reactions. Practically this was achieved by withdrawing greater than the desired volume (typically 27-30 μL), removing the microsyringe, dispensing the excess and wiping the needle. The aliquot was then placed into an MS vial, before addition of 1.00 mL of external standard solution containing maleimide quench and mixed using the syringe. Samples were allowed to quench for at least 5 minutes prior to UPLC injection. Typically the quenching reaction of TNB with maleimide could be seen visually (orange to colourless), taking around 30-60 s to complete.

Chromatograms were recorded for each sample, typically using 1.0 μL injections and the gradients in the tables of section 4. 6. 4. Peak areas were integrated manually at a wavelength of 240.0 nm, with peak identity being confirmed by both retention time and UV spectra for every chromatogram (typically one per time point). The areas of the peaks were recorded in arbitrary units, with the area of the external standard peak being

monitored to ensure accuracy in the sampling procedure. Concentrations were quantified using the calibrations in section 4. 6. 10. Heteroaryl disulfides were calibrated by taking the mean of the absorbances of the homoaryl disulfides of each of their aryl rings for a particular gradient.

4. 6. 4 UPLC analysis of reaction samples

Kinetic analysis of reactions was made using a Waters Acquity ultra performance liquid chromatography (UPLC) H-Class system with photodiode array (PDA) detector. For all samples an ACQUITY UPLC BEH C18 column (130 Å, 1.7 µm, 2.1 mm × 50 mm) was used. Empower software was used data processing. The gradient used depended on the composition of the reaction mixture, with some systems requiring multiple injections to separate all UV-active components. The solvent gradients used are shown in the following tables of this section, as are the retention times of species relevant to that gradient.

4. 6. 4. 1 Gradient 1

Time (mins)	Flow rate ($mLmin^{-1}$)	MilliQ H_2O (%)	MeCN (%)	5% TFA in MilliQ H_2O (%)	Curve
0.00	0.600	93.0	2.0	5.0	Initial
0.25	0.600	93.0	2.0	5.0	6
4.00	0.600	2.0	93.0	5.0	6
4.40	0.600	2.0	93.0	5.0	6
4.50	0.600	93.0	2.0	5.0	10

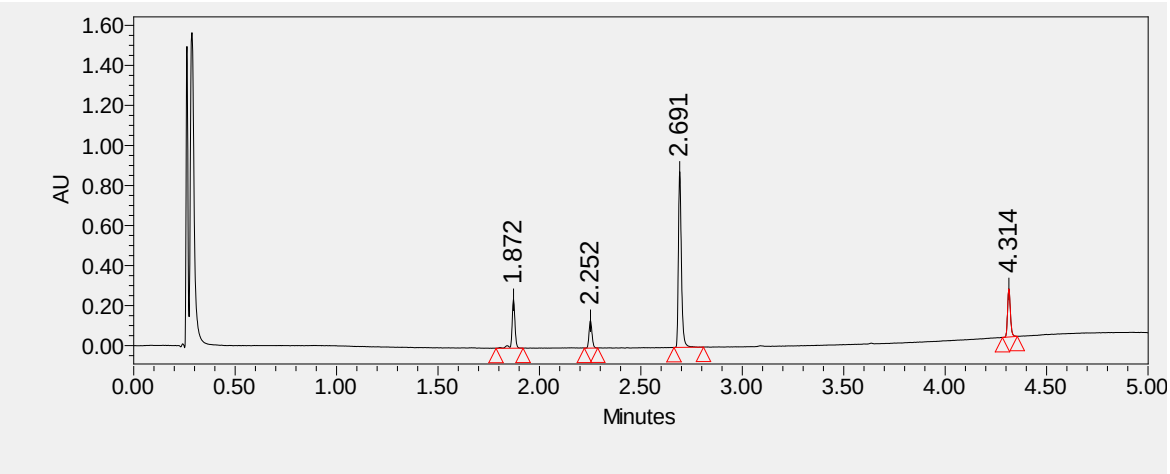
5.00	0.600	93.0	2.0	5.0	10

This general-purpose gradient was used to monitor reactions containing one aryl-disulfide and one alkyl thiol.

Retention times of relevant peaks:

Compound	Retention time (mins)
Standard	2.24
Aryl disulfides	2.63-2.74
Alkyl-aryl mixed disulfides	4.01-4.39
Aryl thiols	1.84-1.90

Typical chromatogram of a reaction containing a single aryl disulfide and a single alkyl thiol, forming a single mixed disulfide product:



4. 6. 4. 1 Gradient 2

Time (mins)	Flow rate	MilliQ H_2O	MeCN (%)	5% TFA in	Curve

	($mLmin^{-1}$)	(%)		MilliQ H_2O (%)	
0.00	0.250	88.0	2.0	10.0	Initial
0.25	0.250	88.0	2.0	10.0	6
0.75	0.250	58.0	32.0	10.0	6
8.50	0.250	58.0	32.0	10.0	6
8.60	0.250	2.0	93.0	5.0	6
9.90	0.250	2.0	93.0	5.0	6
10.00	0.250	88.0	2.0	10.0	10
10.50	0.250	88.0	2.0	10.0	10

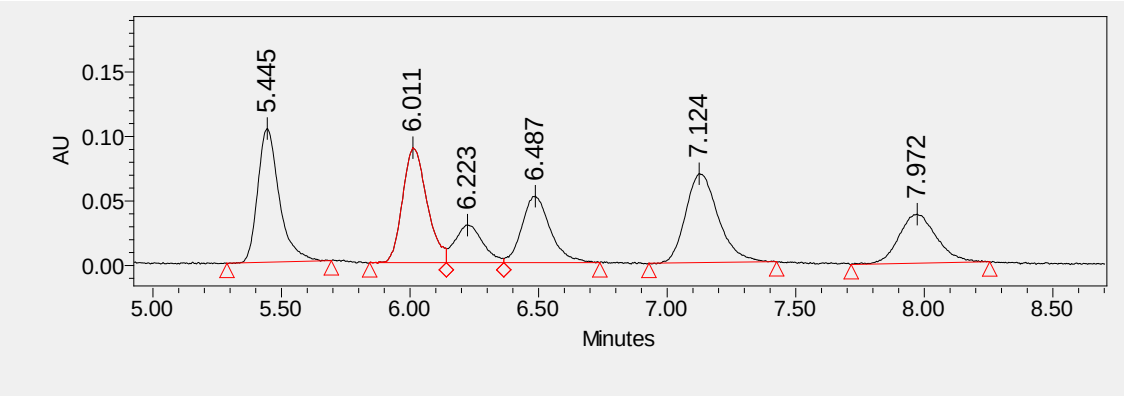
This gradient was used to monitor mixtures of aryl-disulfides, with all possible aryl-aryl disulfides giving a distinct retention time.

Retention times of relevant peaks:

Compound	Retention time (mins)
4.2	5.45
4.5	6.01
4.3	6.22
4.6	6.48
4.7	7.12

4.4	7.97

Chromatogram of a mixture containing all six bis-aryl disulfides.



4. 6. 4. 3 Gradient 3

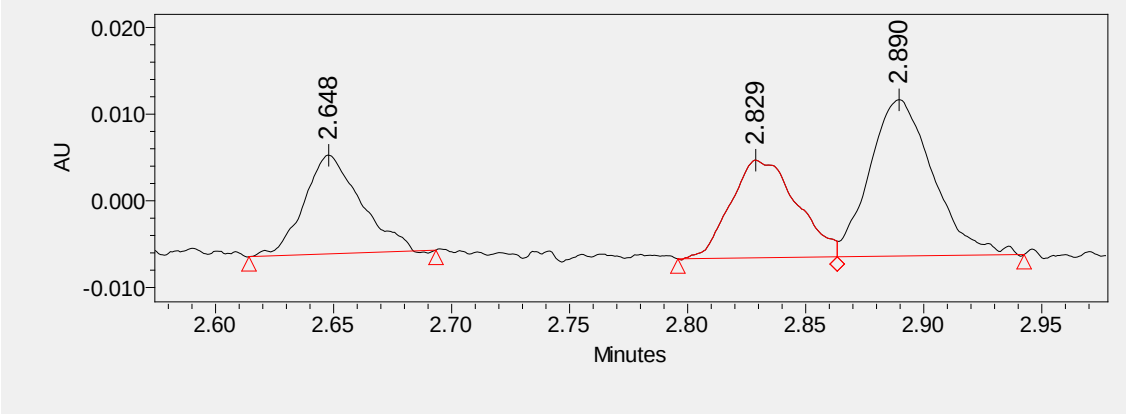
Time (mins)	Flow rate ($mLmin^{-1}$)	MilliQ H_2O (%)	MeCN (%)	5% TFA in MilliQ H_2O (%)	Curve
0.00	0.600	93.0	2.0	5.0	Initial
0.25	0.600	93.0	2.0	5.0	6
0.50	0.600	90.0	5.0	5.0	6
3.75	0.600	68.0	27.0	5.0	6
4.00	0.600	2.0	93.0	5.0	6
4.40	0.600	2.0	93.0	5.0	6
4.50	0.600	93.0	2.0	5.0	11
5.00	0.600	93.0	2.0	5.0	11

This gradient was used to monitor mixtures of aryl thiols, with all three thiols giving a distinct retention time.

Retention times of relevant peaks:

Compound	Retention time (mins)
Ar(NO_2)SH	2.64
Ar(H)SH	2.82
Ar(OMe)SH	2.89

Chromatogram of a mixture of all three aryl thiols:



4. 6. 4. 4 Gradient 4

Time (mins)	Flow rate ($mLmin^{-1}$)	MilliQ H_2O (%)	MeCN (%)	5% TFA in MilliQ H_2O (%)	Curve
0.00	0.450	93.0	2.0	5.0	Initial
0.25	0.450	93.0	2.0	5.0	6

0.50	0.450	90.0	5.0	5.0	6
3.75	0.450	72.0	23.0	5.0	6
4.00	0.450	2.0	93.0	5.0	6
4.40	0.450	2.0	93.0	5.0	6
4.50	0.450	93.0	2.0	5.0	11
5.00	0.450	93.0	2.0	5.0	11

This gradient was used as an alternative to gradient 3.

4. 6. 4. 5 Gradient 5

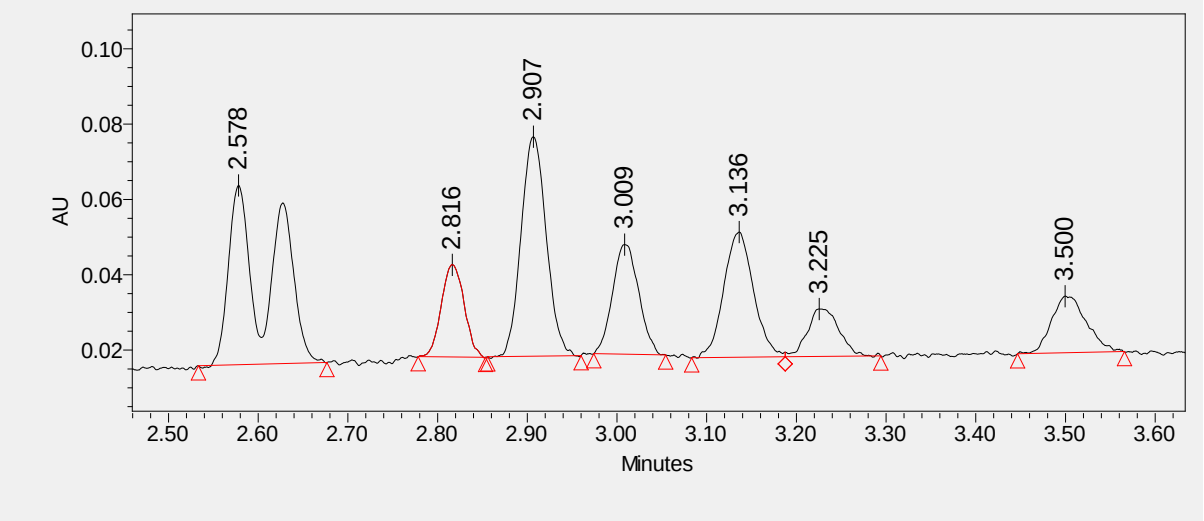
Time (mins)	Flow rate ($mLmin^{-1}$)	MilliQ H_2O (%)	MeCN (%)	MeOH (%)	5% TFA in MilliQ H_2O (%)	Curve
0.00	0.600	78.0	2.0	15.0	5.0	Initial
0.25	0.600	78.0	2.0	15.0	5.0	6
0.75	0.600	23.0	57.0	15.0	5.0	6
3.50	0.600	19.0	61.0	15.0	5.0	5
4.00	0.600	19.0	61.0	15.0	5.0	6
4.10	0.600	1.0	93.0	1.0	5.0	6
4.80	0.600	78.0	2.0	15.0	5.0	11
5.00	0.600	78.0	2.0	15.0	5.0	10

This gradient was used to monitor mixtures of surfactant disulfides. Not all disulfides give distinct retention times, therefore it was used in combination with gradient 6.

Retention times of relevant peaks:

Compound	Retention time (mins)
4.11a	2.36
4.11b	2.39
4.11c	2.63
4.12a	2.56
4.12b	2.63
4.12c	2.90
4.13a	2.71
4.13b	2.80
4.13c	3.12

Chromatogram of a mixture containing all 9 aryl-alkyl mixed disulfides, giving 7 separate peaks. Note the first peak sometimes appears as two almost distinct peaks, sometimes as a single indistinguishable peaks.



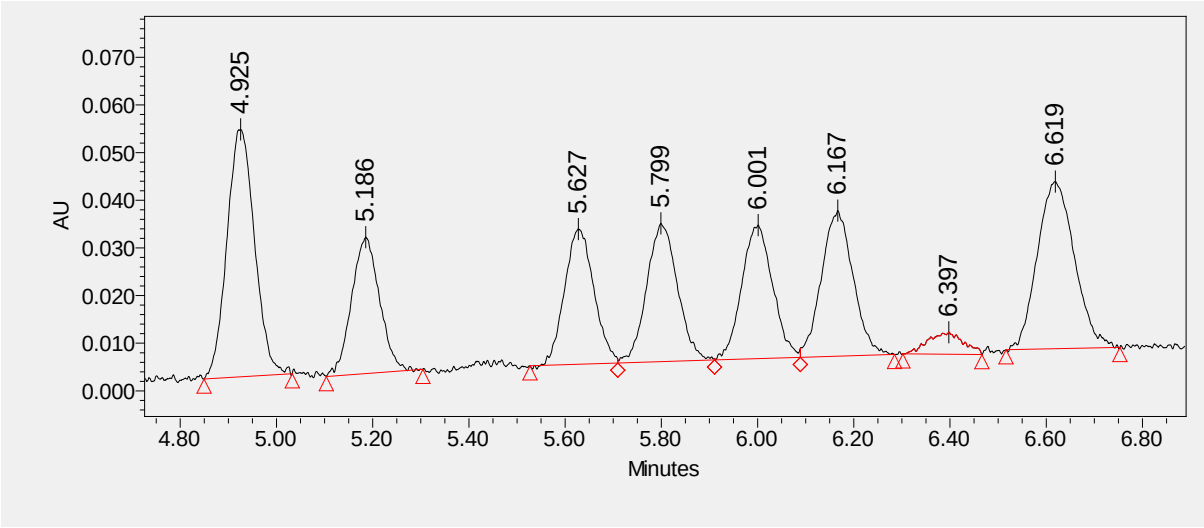
4. 6. 4. 6 Gradient 6

Time (mins)	Flow rate ($mLmin^{-1}$)	MilliQ H_2O (%)	MeCN (%)	MeOH (%)	5% TFA in MilliQ H_2O (%)	Curve
0.00	0.450	83.0	2.0	10.0	5.0	Initial
0.25	0.450	83.0	2.0	10.0	5.0	6
0.75	0.450	34.0	51.0	10.0	5.0	6
3.50	0.450	30.0	55.0	10.0	5.0	5
6.40	0.450	24.0	61.0	10.0	5.0	6
6.50	0.450	1.0	93.0	1.0	5.0	6
7.20	0.450	83.0	2.0	10.0	5.0	11
7.50	0.450	83.0	2.0	10.0	5.0	10

This gradient was used to monitor mixtures of surfactant disulfides. Not all disulfides give distinct retention times, therefore it was used in combination with gradient 5.

Compound	Retention time (mins)
4.11a	4.45
4.11b	4.66
4.11c	5.26
4.12a	5.08
4.12b	5.39
4.12c	6.02
4.13a	5.57
4.13b	6.04
4.13c	6.63

Chromatogram of a mixture containing all 9 aryl-alkyl mixed disulfides, giving 8 peaks.



4. 6. 5 CAC determination

Attempts to measure the CAC of these substrates using fluorimetry by the London method was unsuccessful, presumably due to the surfactants quenching the fluorescence of 1,6-diphenyl-1,3,5-hexatriene.[74]

The critical aggregation concentrations of surfactants were determined using the du Noüy method with a Krus K10ST tensiometer.[75] Measurements and calibration were performed at 25 °C. Surface tensions were measured the of dilution series of each surfactant in HEPES buffer (0.25 M, pH 8.00), typically in a concentration range of 0.024-12.5 mM, using a volume of 3.0 mL per sample. Measurements within a data set done in order of increasing concentration and on the same day. Each measurement was performed in triplicate. Critical aggregation concentrations are the point at which there is a change of linear regime between surface tension and natural logarithm of surfactant concentration.

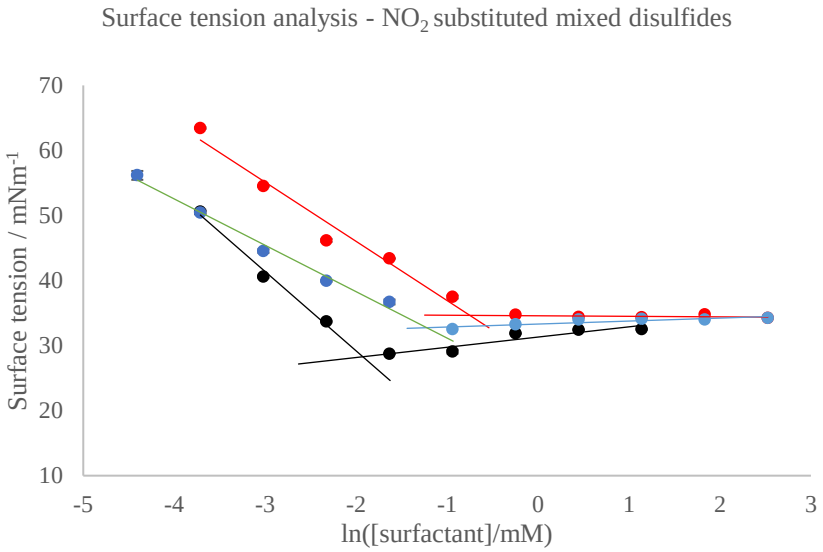


Figure 4. 6. 5. 1. Plot of surface tension of surfactant solutions against the natural logarithm of surfactant concentration. This graph shows the data for all nitro substituted surfactants, red: ***4.11a****, blue =* ***4.11b*** *and black =* ***4.11c****. n = 3, error bars show one standard deviation and are typically too small to be visible.*

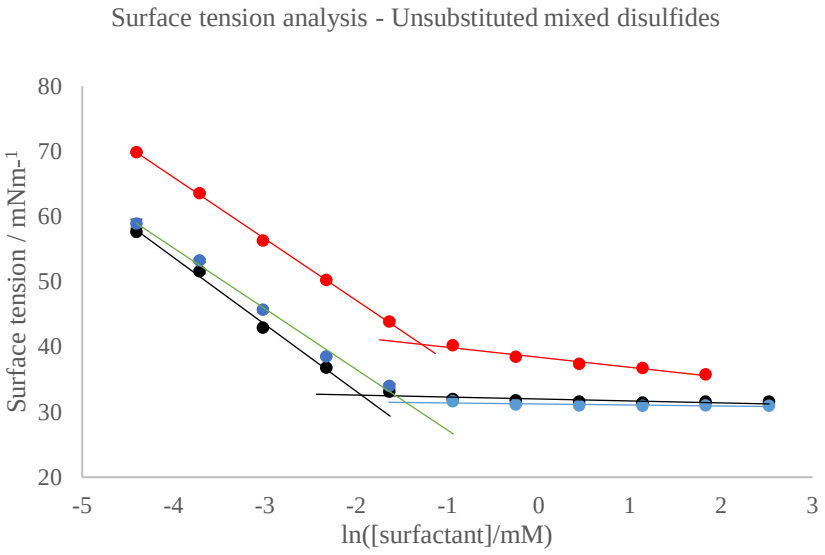


Figure 4. 6. 5. 2. Plot of surface tension of surfactant solutions against the natural logarithm of surfactant concentration. This graph shows the data for all unsubstituted surfactants, red: ***4.12a****, blue =* ***4.12b*** *and black =* ***4.12c****. n = 3, error bars show one standard deviation and are typically too small to be visible.*

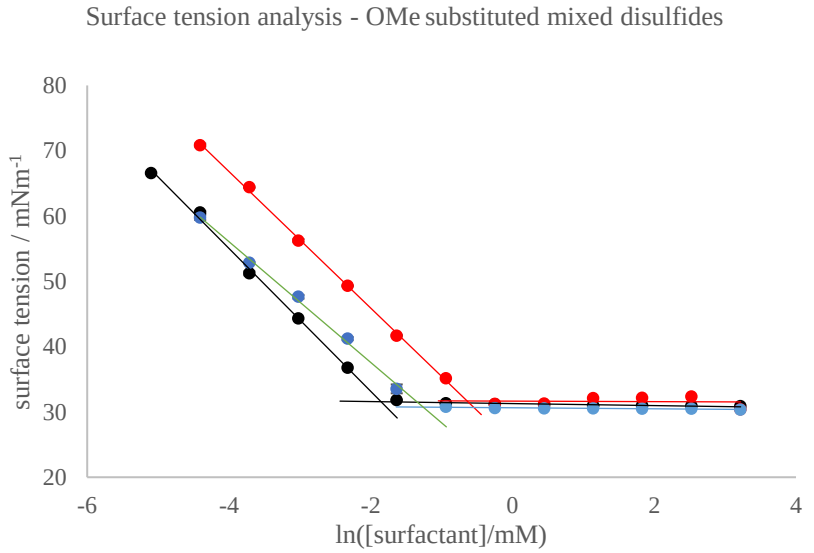


Figure 4. 6. 5. 3. Plot of surface tension of surfactant solutions against the natural logarithm of surfactant concentration. This graph shows the data for all methoxy substituted surfactants, red: ***4.13a****, blue =* ***4.13b*** *and black =* ***4.13c****. n = 3, error bars show one standard deviation and are typically too small to be visible.*

4. 6. 6 Dynamic Light Scattering measurements

DLS measurements were recorded using a Malvern Zetasizer Nano ZEN5600 machine recording particle size. Zetasizer software was used for data processing. Samples were

prepared as a serial dilution from 25.0 mM to 0.049 mM was prepared analogously to as described for CAC determination (see section 4. 6. 5). Three measurements were taken for each sample. Refractive index of 1.371 and viscosity of 1.0780 mPas were used in data processing.

For some samples, at high concentrations multiple scattering events were observed leading to additional peaks. Further, rare large aggregates, dust or other contamination of high diffracting power lead to multimodal distributions, not suited to the processing software. Quality reports and average distributions were therefore not representative.

Below the lower bound of concentration there was low quality data due to noise. This typically arises due to sample imperfections.

4. 6. 6. 1 Representative DLS spectra

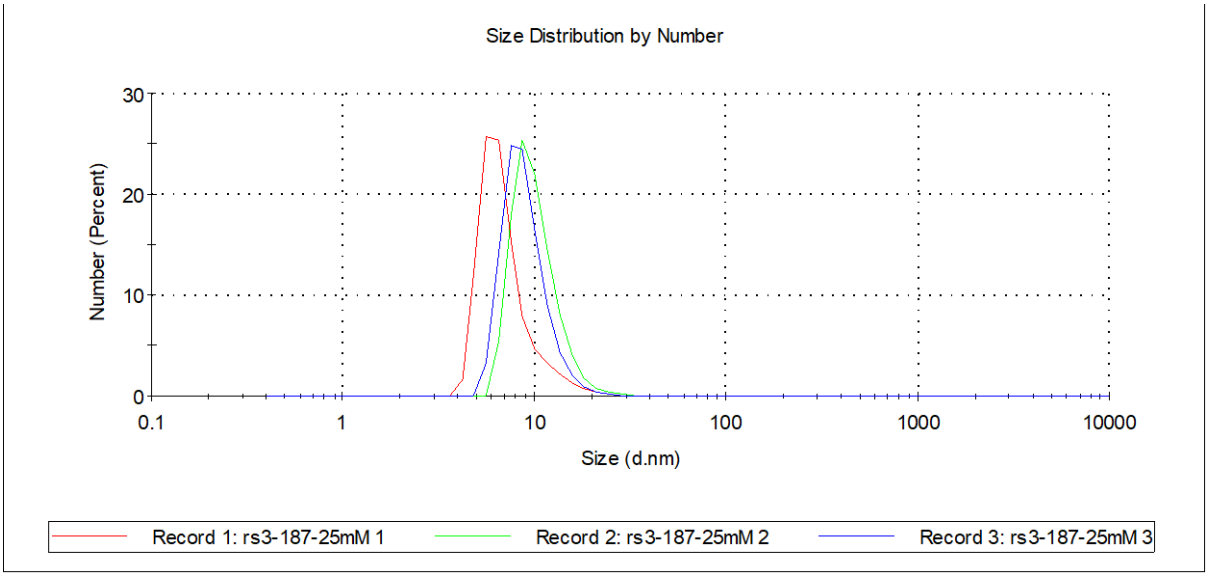


Figure 4. 6. 6. 1. 1. DLS data for a micelle forming compound plotted by number of counts, showing the aggregates of a low polydispersity. n = 3.

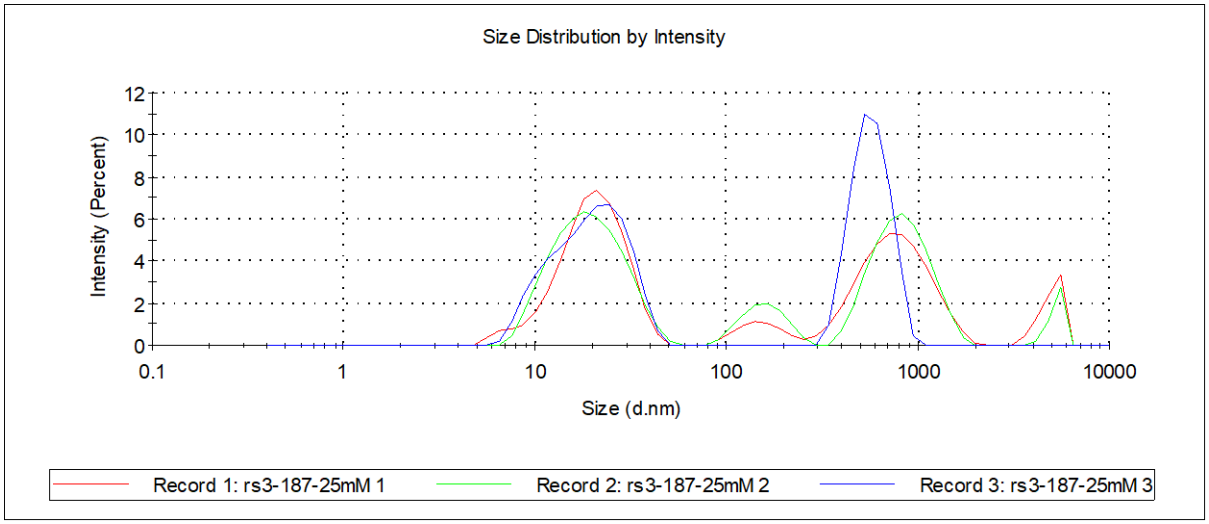


Figure 4. 6. 6. 1. 2. The same DLS data as figure 4. 6. 6. 1, plotted by intensity, showing the presence of a small number of large (up to µm) particles. n = 3.

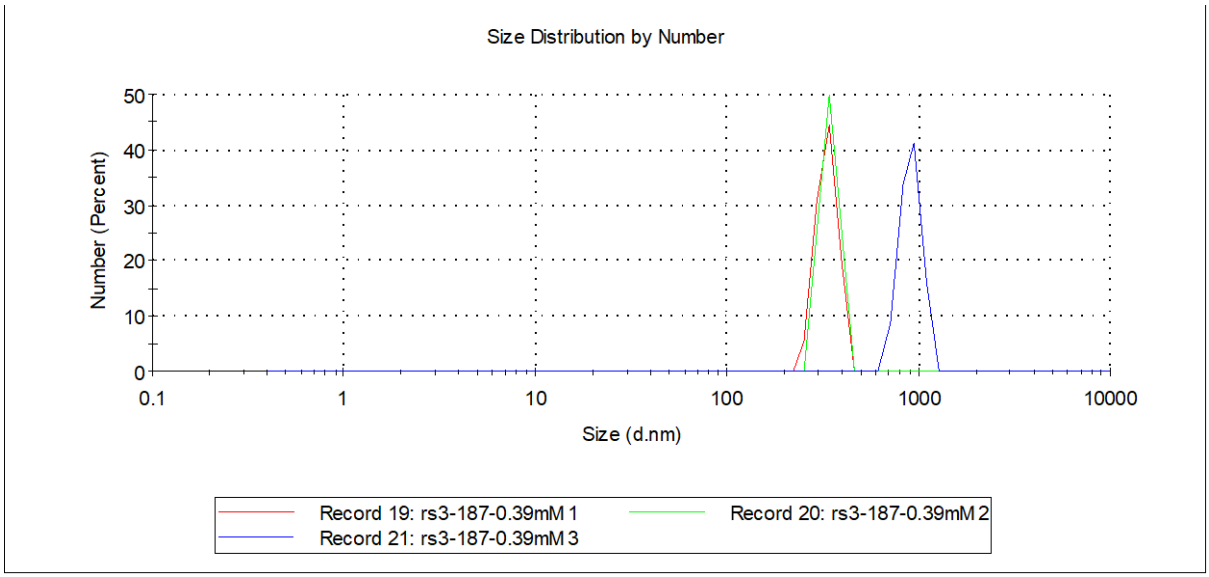


Figure 4. 6. 5. 1. 3. Typical spectrum for a sample taken below the noise threshold, where count number is low (below 1000) and peaks are inconsistent between runs. n = 3.

4. 6. 6. 2 Example DLS spectra for each surfactant

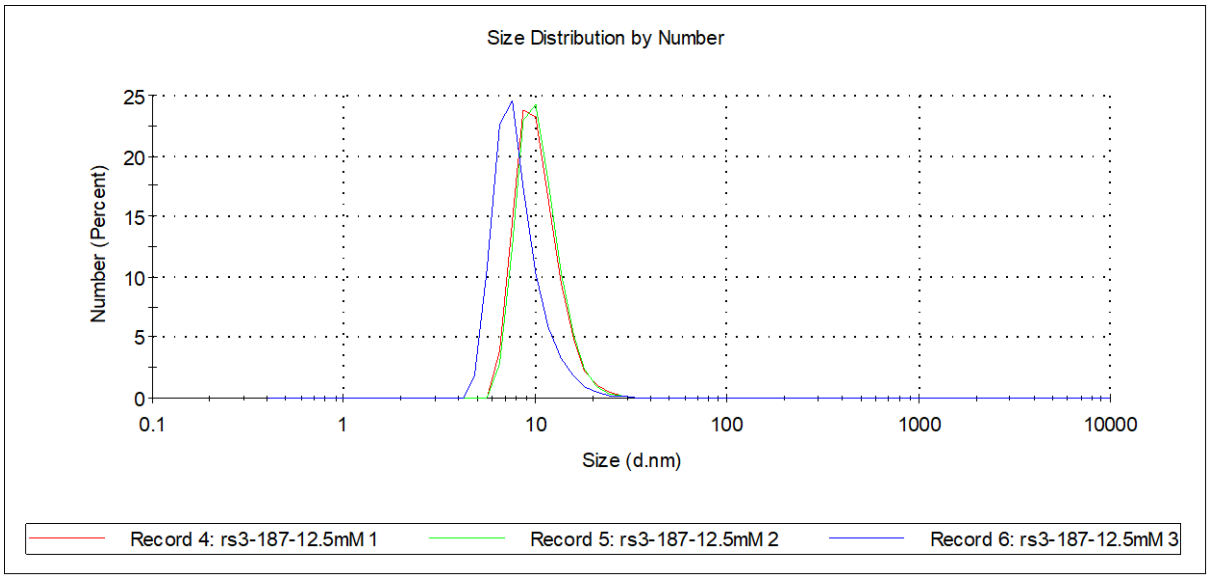


*Figure 4. 6. 6. 2. 1. DLS spectrum for **4.11a**. n = 3.*

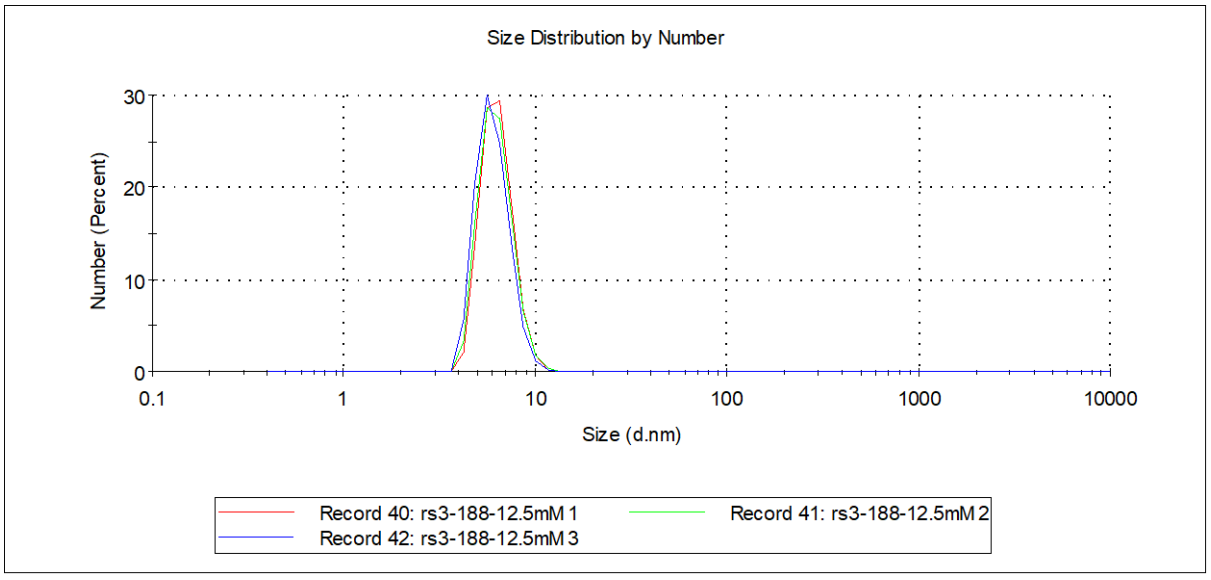


*Figure 4. 6. 6. 2. 2. DLS spectrum for **4.11b**. n = 3.*

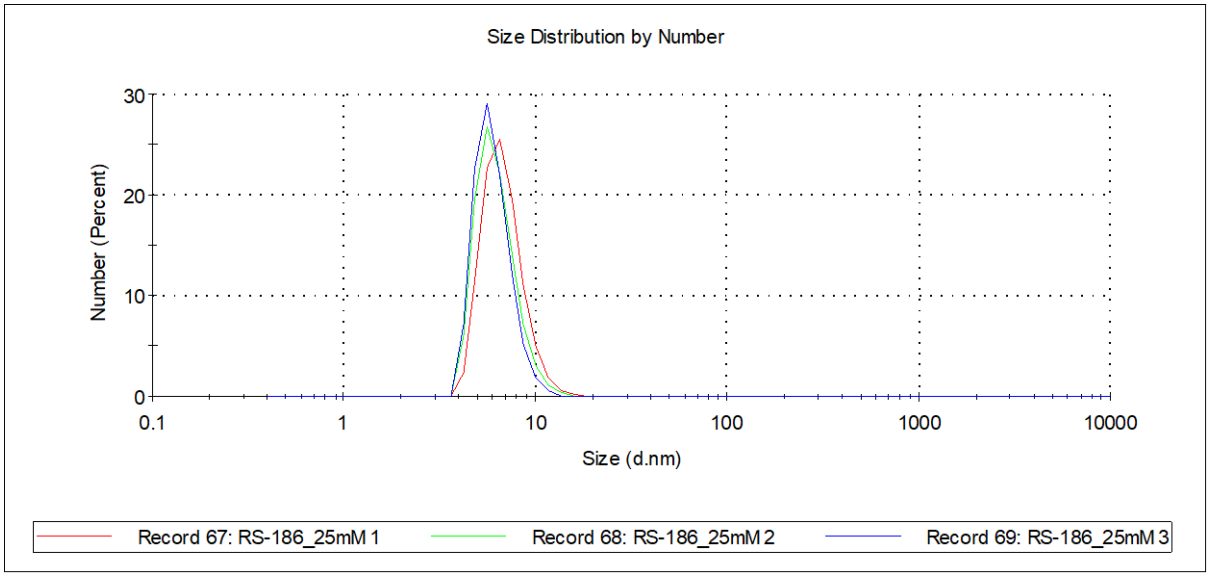


Figure 4. 6. 6. 2. 3. DLS spectrum for ***4.11c****. n = 3.*

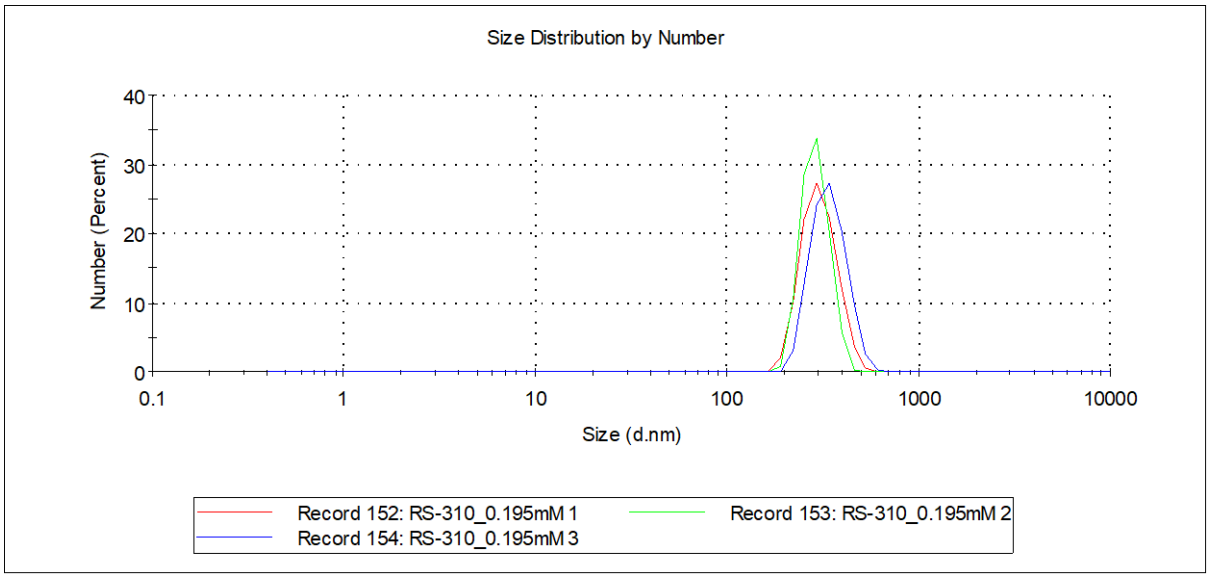


Figure 4. 6. 6. 2. 4. DLS spectrum for ***4.12a****. n = 3.*

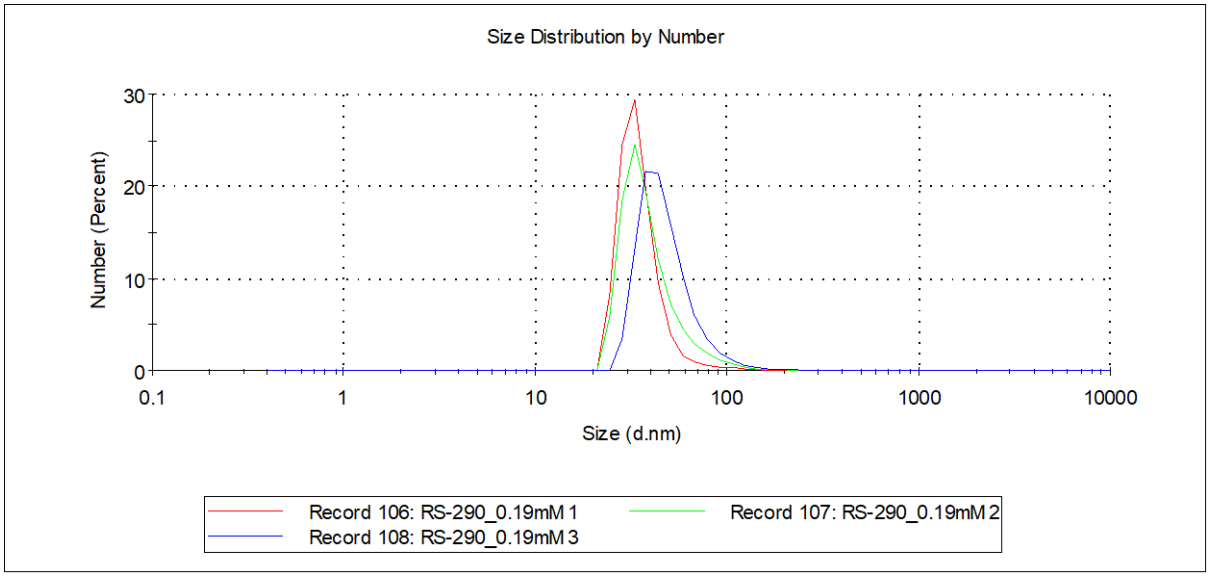


Figure 4. 6. 6. 2. 5. DLS spectrum for ***4.12b****. n = 3.*

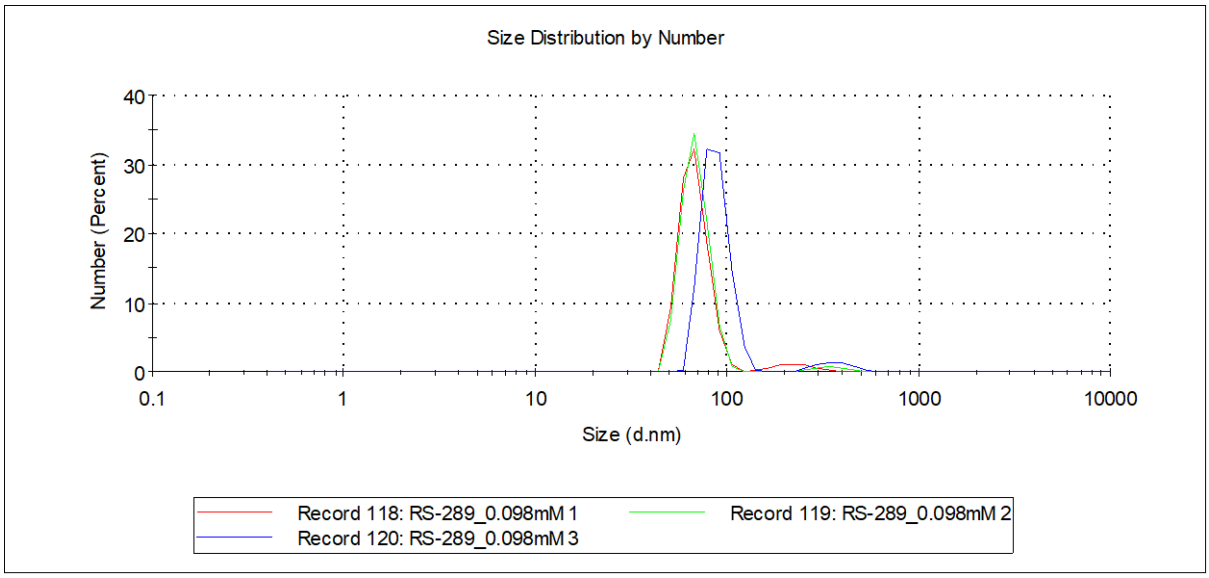


Figure 4. 6. 6. 2. 6. DLS spectrum for ***4.12c.*** *n = 3.*

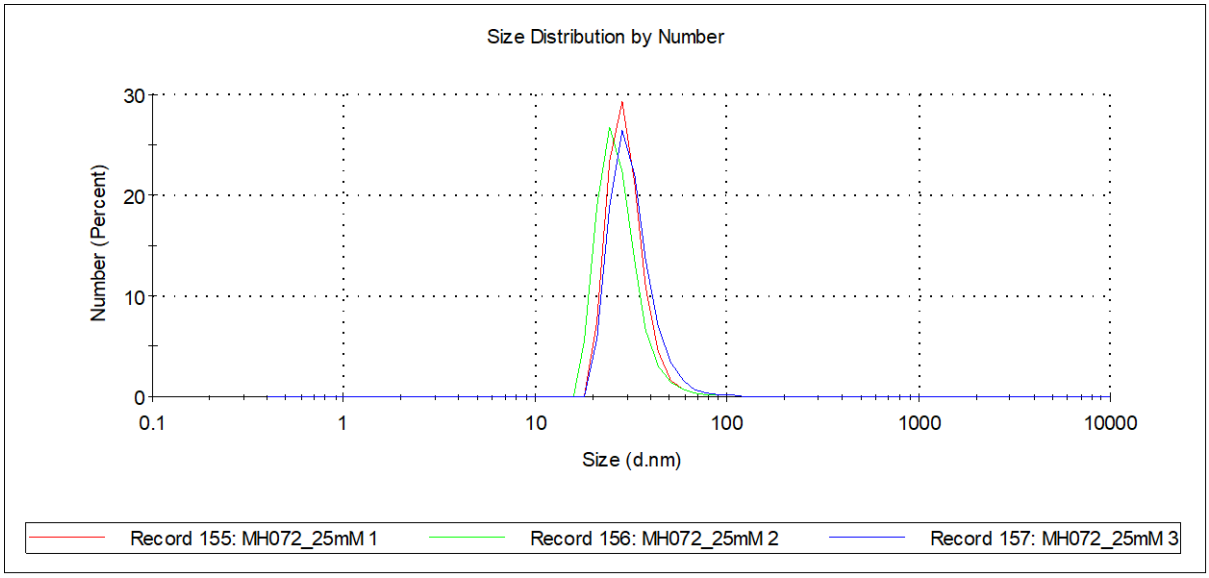


Figure 4. 6. 6. 2. 7. DLS spectrum for ***4.13a****. n = 3.*

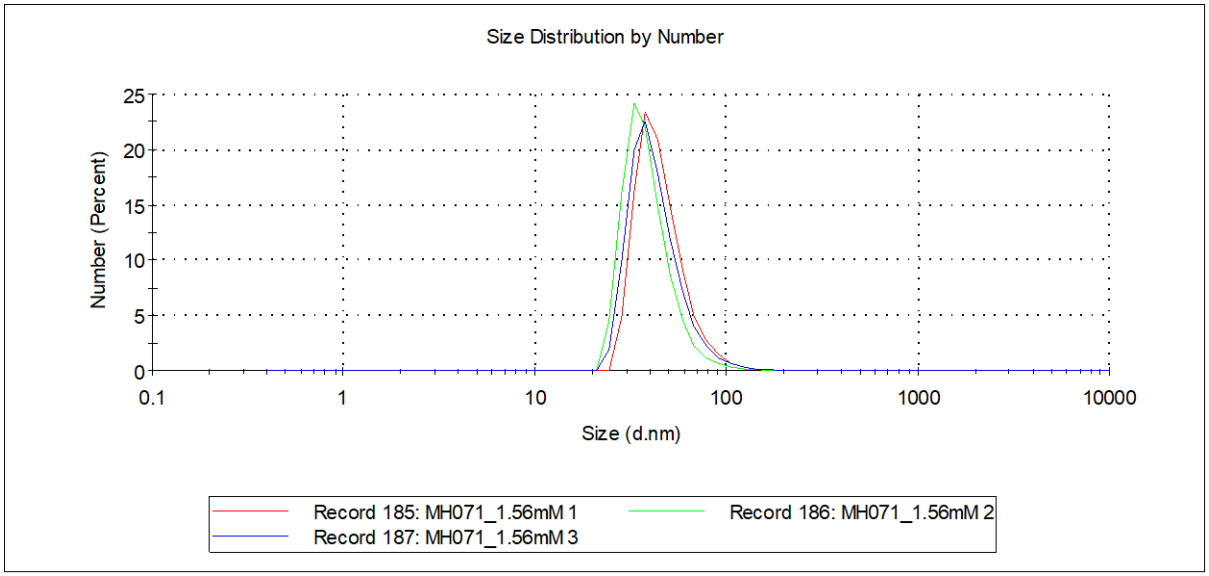


Figure 4. 6. 6. 2. 8. DLS spectrum for ***4.13b****. n = 3.*

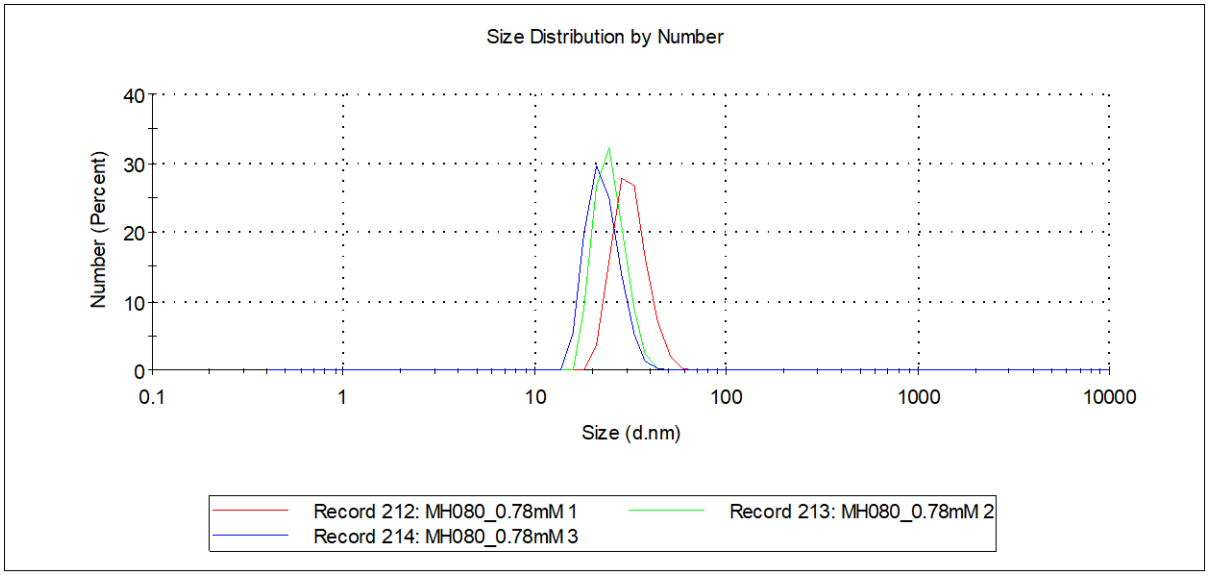


*Figure 4. 6. 6. 2. 9. DLS spectrum for **4.13c**. n = 3.*

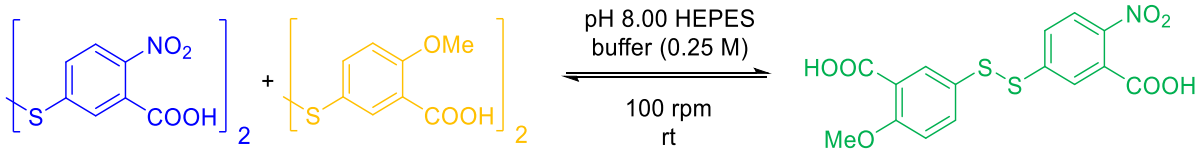
4. 6. 7 Microscopy

For bright-field optical microscopy, biphasic reaction of Ellman's reagent with -1octanethiol were monitored with the under the typical reaction conditions. The aqueous phase was sampled in the usual manner, withdrawing 25 µL with a Hamilton microsyringe and dispensed onto a Petri dish. These were observed using a Zeiss Axio Vert. A1 microscope set to bright-field contrast. Images were recorded with an Axiocam ERc 5s camera. The samples remained unquenched to provide as little disruption as possible, and thus analysed as rapidly, within two minutes. Morphology and colour of the samples was observed to change over a period of roughly 15 minutes due to lamp heating.

For iSCAT microscopy the reaction conditions are described in the text and are more diluted than those of kinetics runs, typically 2.5 mM. The microscope was set up as described by Ortega-Arroyo, using a Photonfocus MV-D1024-160-CL-8 camera and 445 nm diode laser source.[76] Data analysis was performed using National Instruments LabVIEW 2011 and imageJ using methods as described by Spillane for particle counting and Andrecka for noise reduction.[77,78]

4. 6. 8 Equilibration experiments

4. 6. 8. 1 Bis-aryl disulfide equilibration



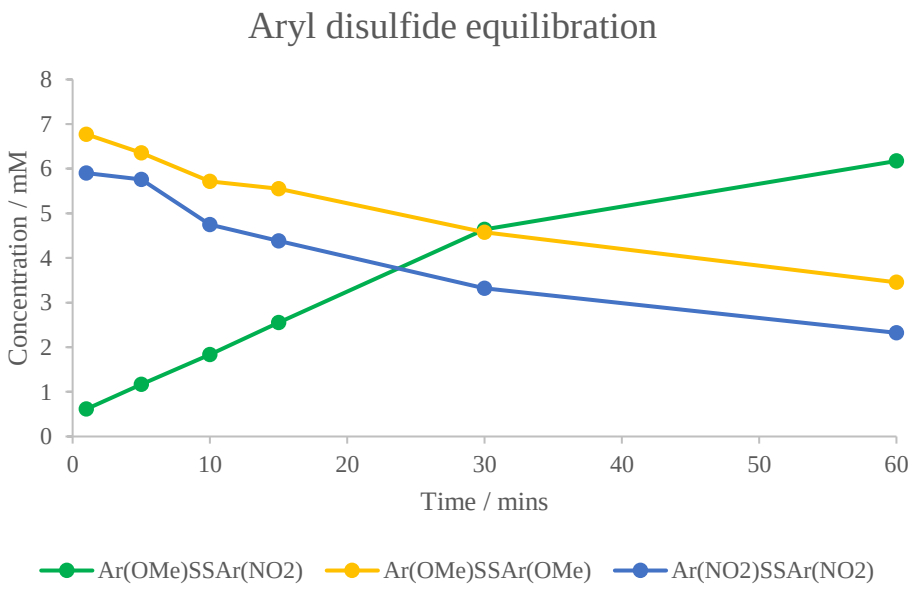
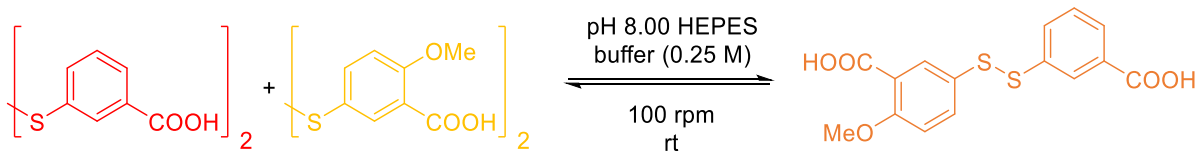


*Figure 4. 6. 8. 1. 1. Plot showing disulfide metathesis between **4.2** and **4.4**. n = 1.*



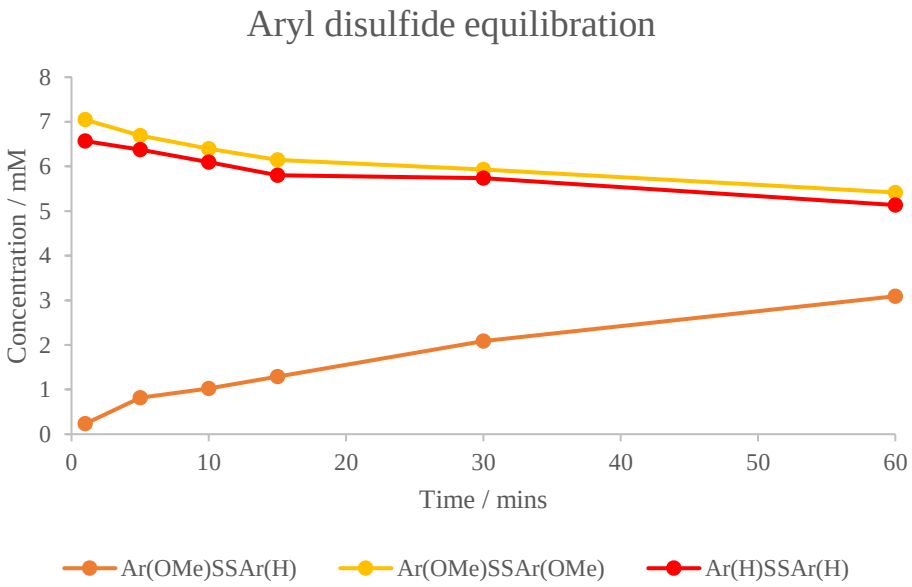
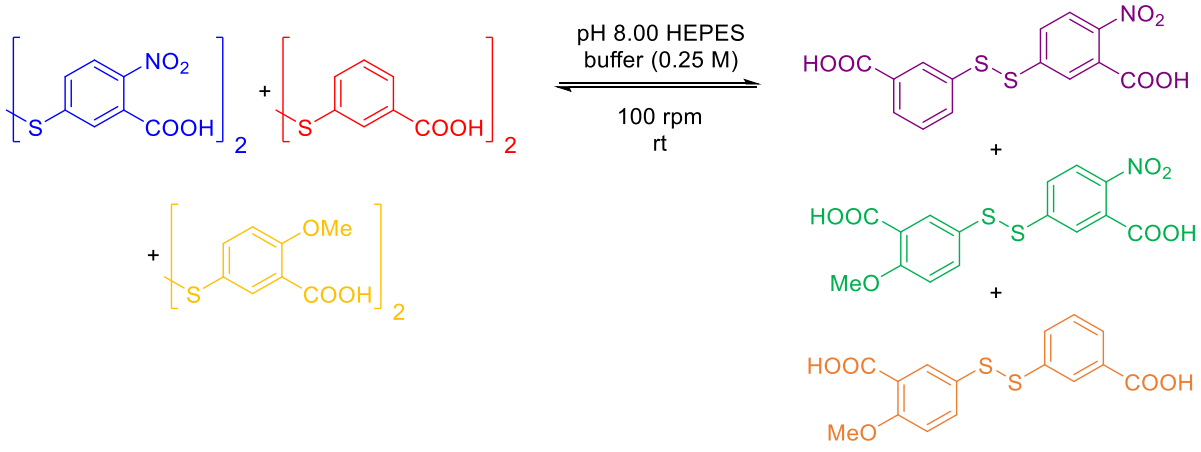


Figure 4. 6. 8. 1. 2. Plot showing disulfide metathesis between ***4.3*** *and* ***4.4****. n = 1.*



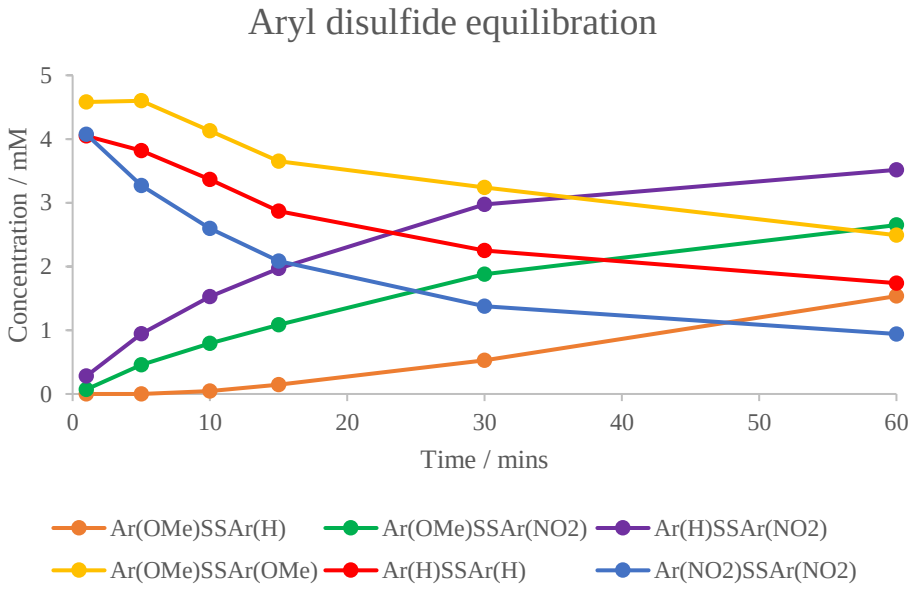
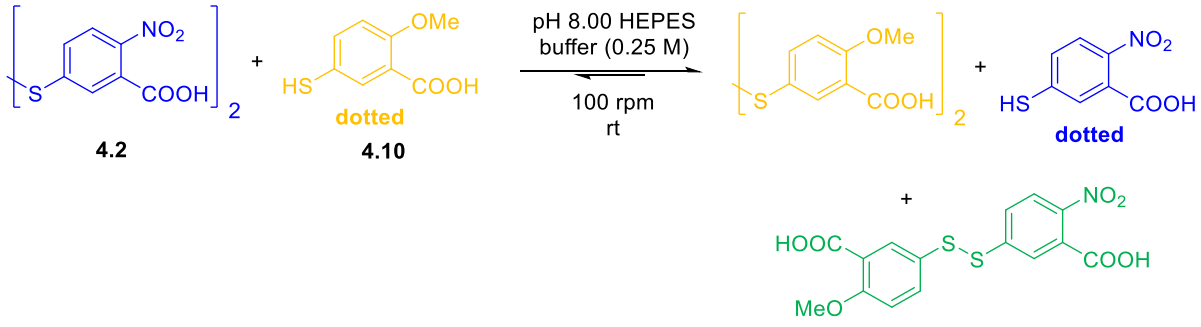


Figure 4. 6. 8. 1. 3. Plot showing disulfide metathesis between ***4.2, 4.3*** *and* ***4.4****. n = 1.*

4. 6. 8. 2 Bis-aryl disulfide and aryl thiol equilibration



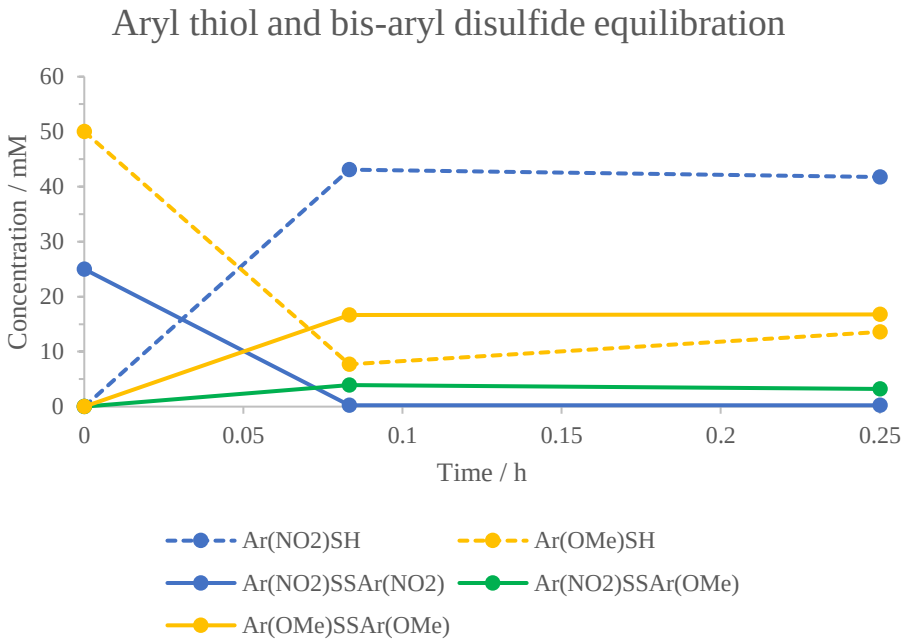
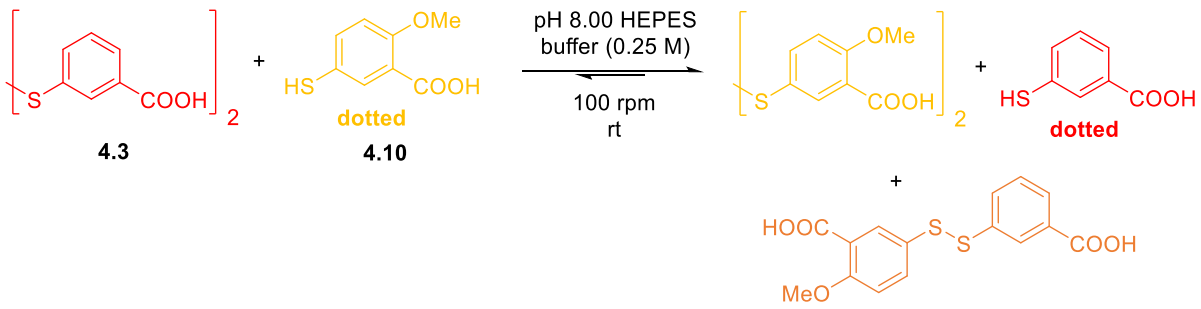


*Figure 4. 6. 8. 2. 1. Plot showing aryl thiol and bis-aryl disulfide equilibration by mixing **4.2** and **4.10.***

n = 1.



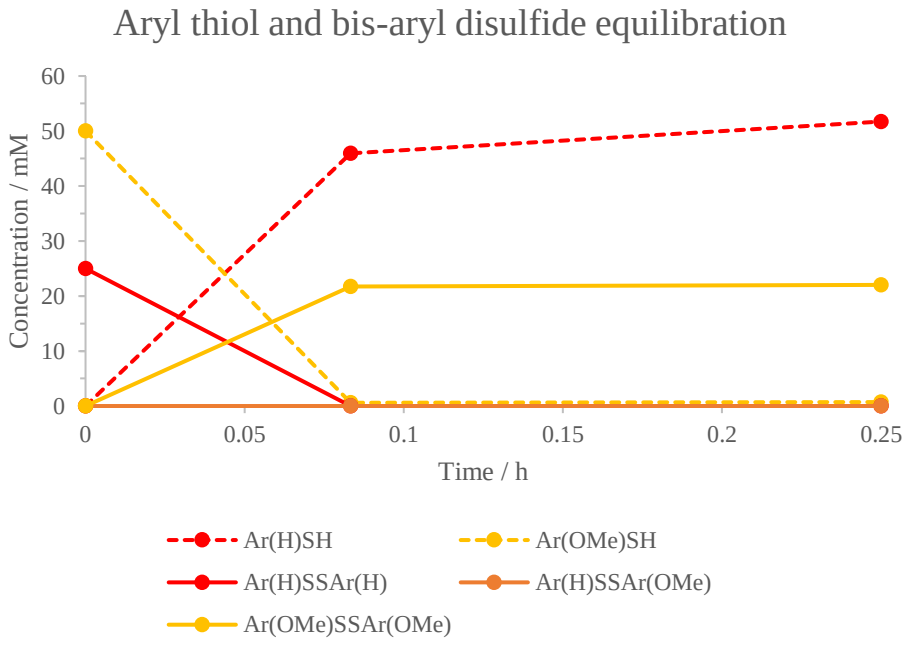


Figure 4. 6. 8. 2. 2. Plot showing aryl thiol and bis-aryl disulfide equilibration by mixing ***4.3*** *and* ***4.10.***

n = 1.

4. 6. 8. 3 Lipid Metathesis

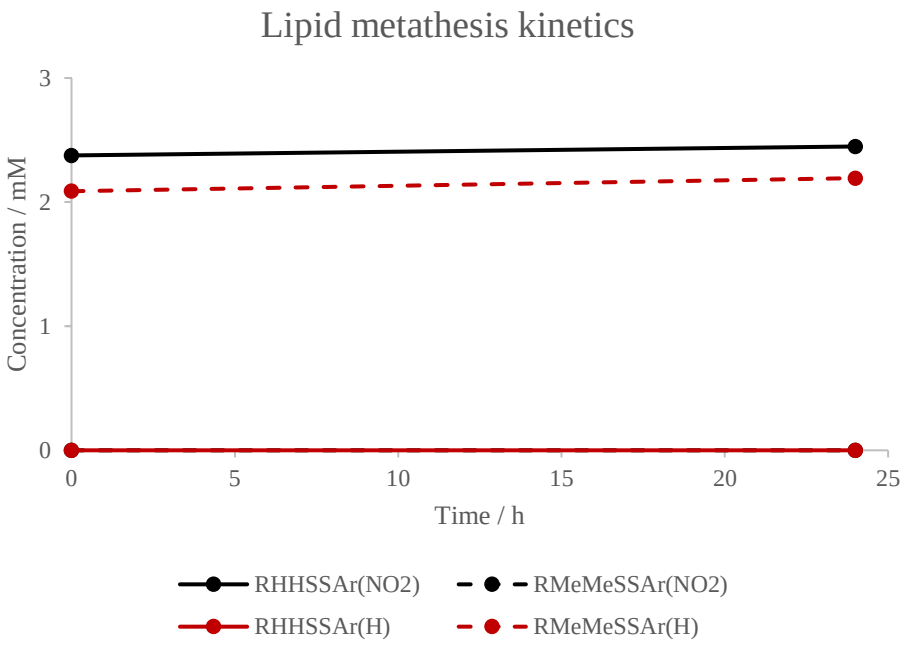


*Figure 4. 6. 8. 3. 1. Plot of lipid metathesis experiment, mixing **4.11a** and **4.12c.** No **4.11c** or **4.12a** is formed in 24 h. n = 1.*

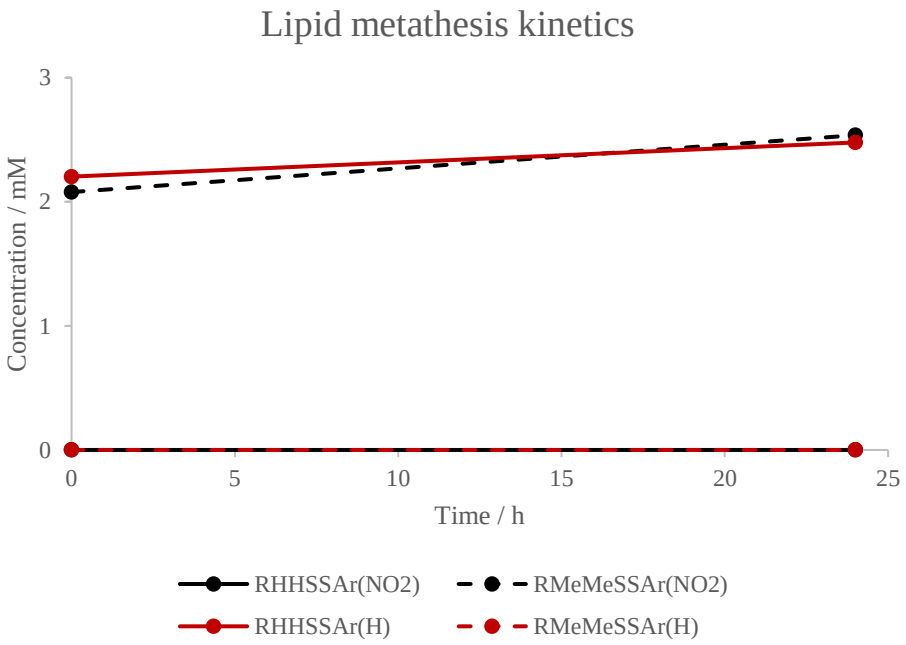


*Figure 4. 6. 8. 3. 2. Plot of lipid metathesis experiment, mixing **4.11c** and **4.12a.** No **4.11a** or **4.12c** is formed in 24 h. n = 1.*

4. 6. 9 Reaction kinetics graphs

4. 6. 9. 1 Kinetics from initial results and optimisation

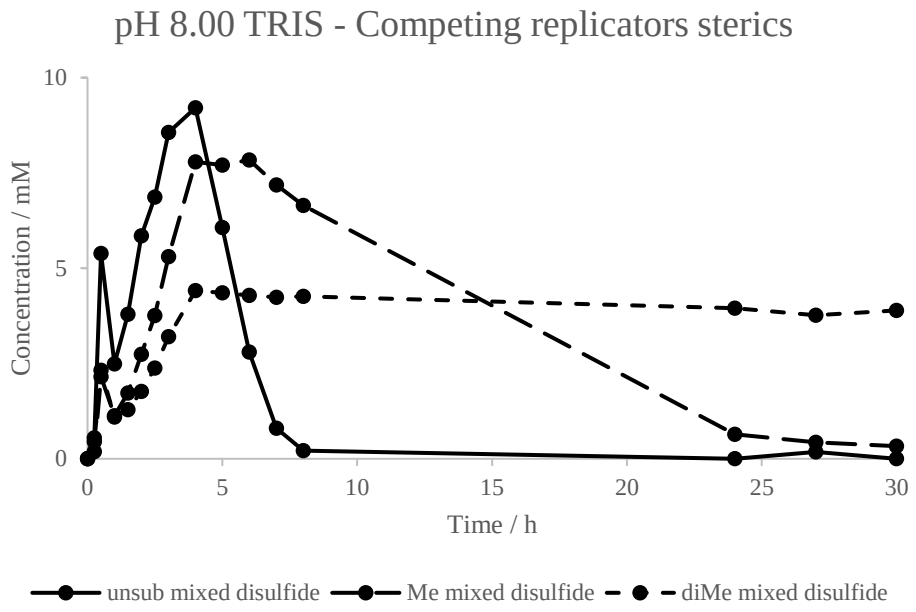


*Figure 4. 6. 9. 1. 1. Kinetics of mixed disulfide formation of **4.11a, 4.11b** and **4.11c** in pH 8.00 TRIS buffer. Concentrations of DTNB and TNB are omitted for clarity. n = 1.*

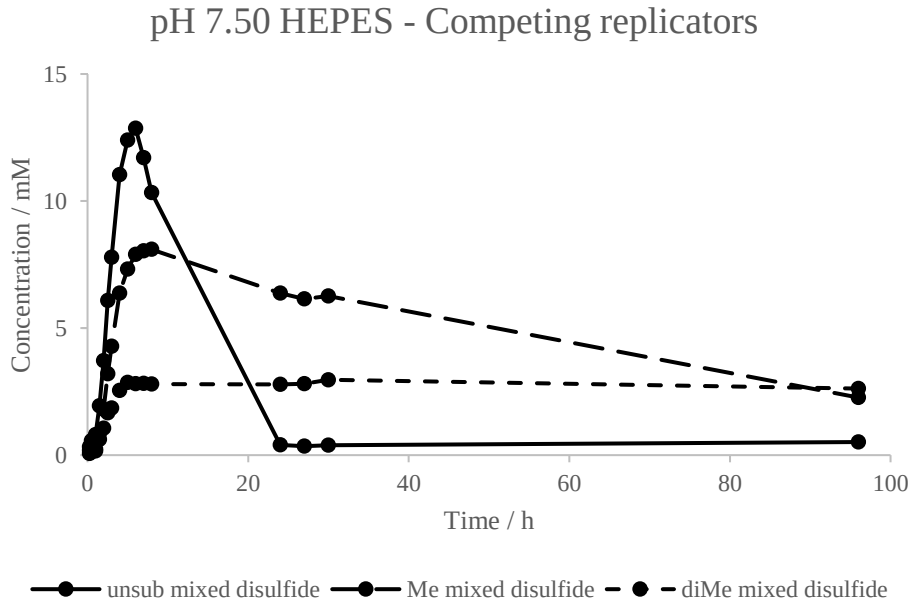
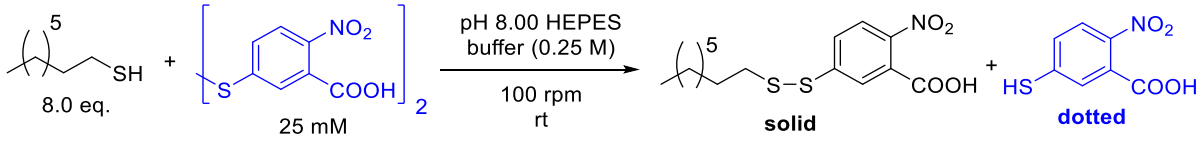


*Figure 4. 6. 9. 1. 2. Kinetics of mixed disulfide formation of **4.11a, 4.11b** and **4.11c** in pH 7.50 HEPES buffer. Concentrations of DTNB and TNB are omitted for clarity. n = 1.*

4. 6. 9. 2 Mixed disulfide formation experiments



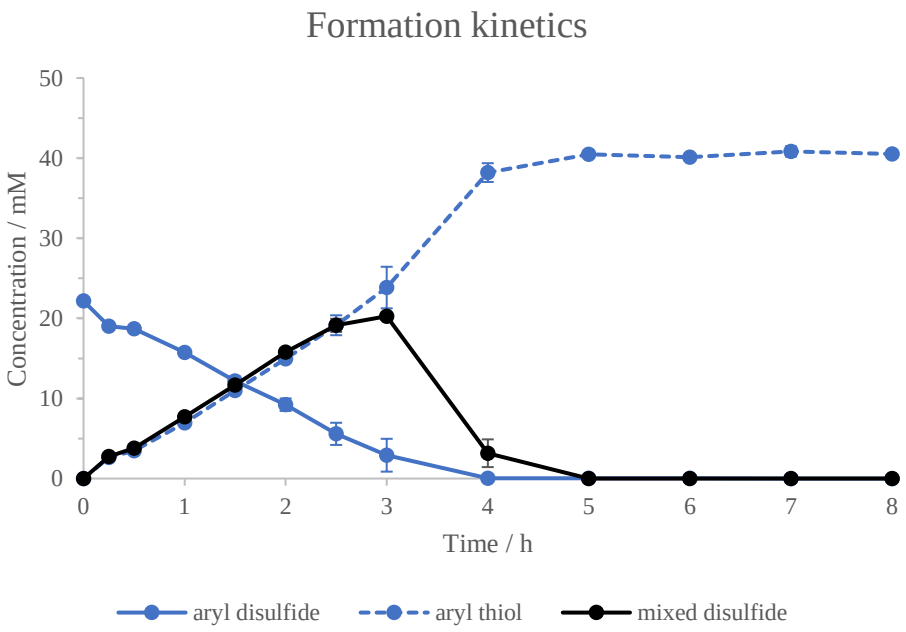


*Figure 4. 6. 9. 2. 1. Formation kinetics of surfactant **4.11a**. n = 3, error bars show one standard deviation and are typically too small to be visible.*

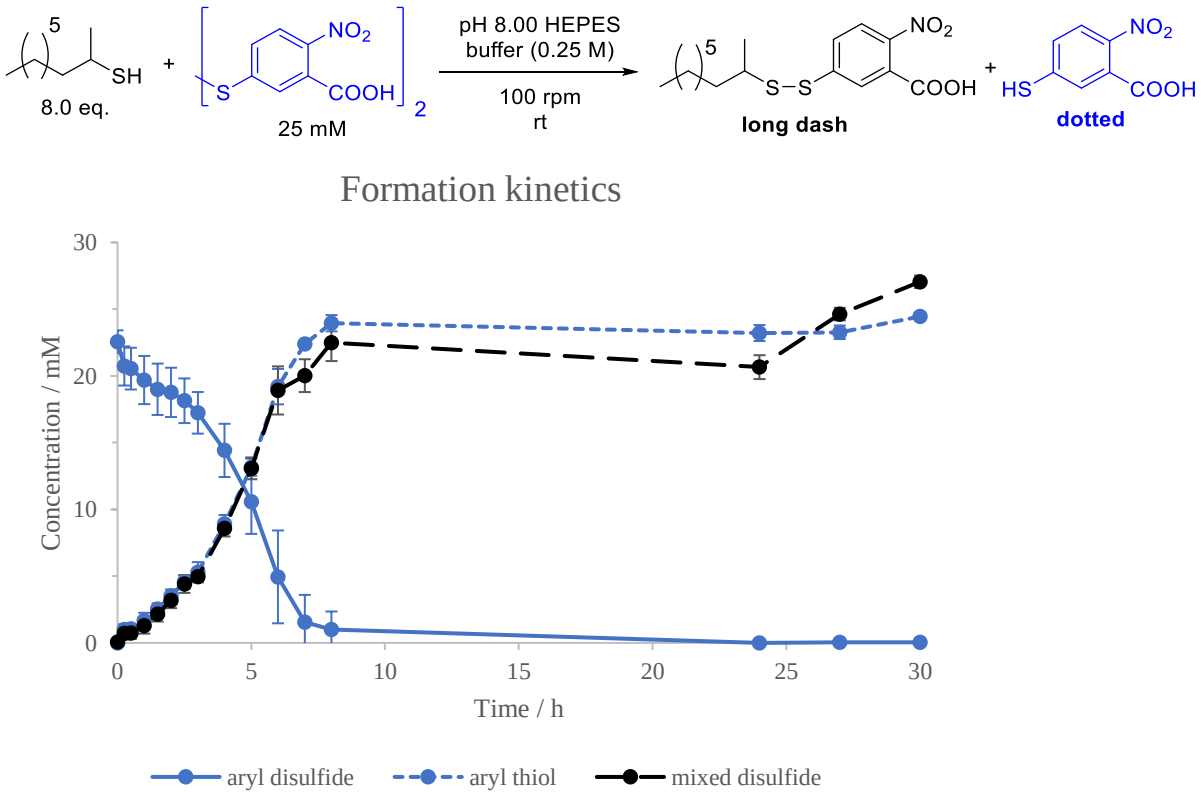


*Figure 4. 6. 9. 2. 2. Formation kinetics of surfactant **4.11b**. n = 3, error bars show one standard deviation.*

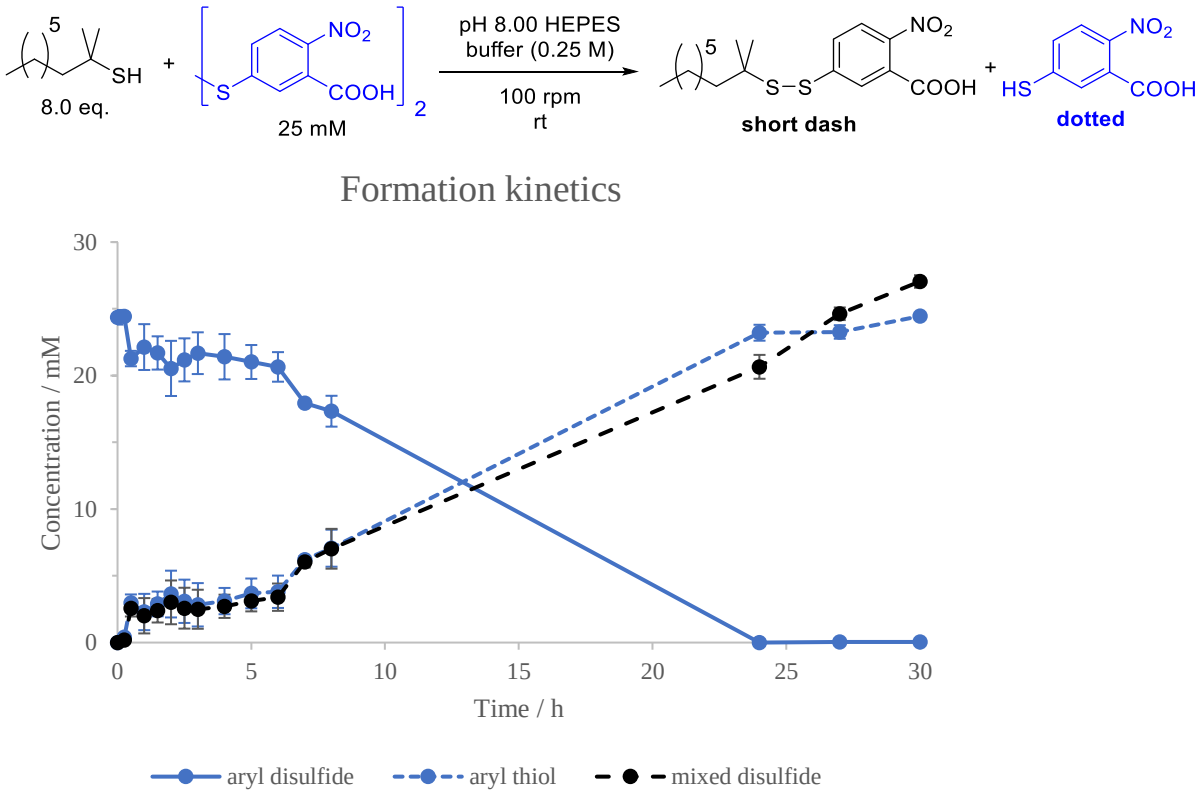


*Figure 4. 6. 9. 2. 3. Formation kinetics of surfactant **4.11c**. n = 3, error bars show one standard deviation.*

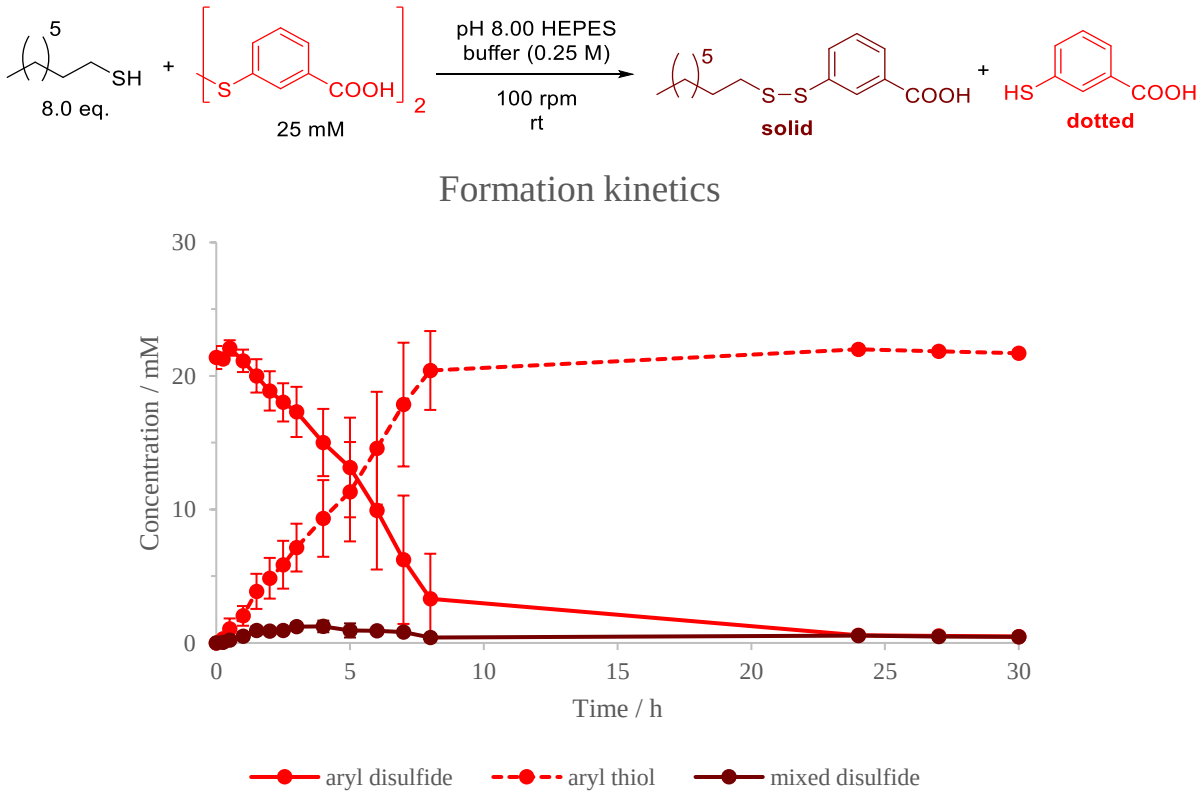


*Figure 4. 6. 9. 2. 4. Formation kinetics of surfactant **4.12a**. n = 3, error bars show one standard deviation.*

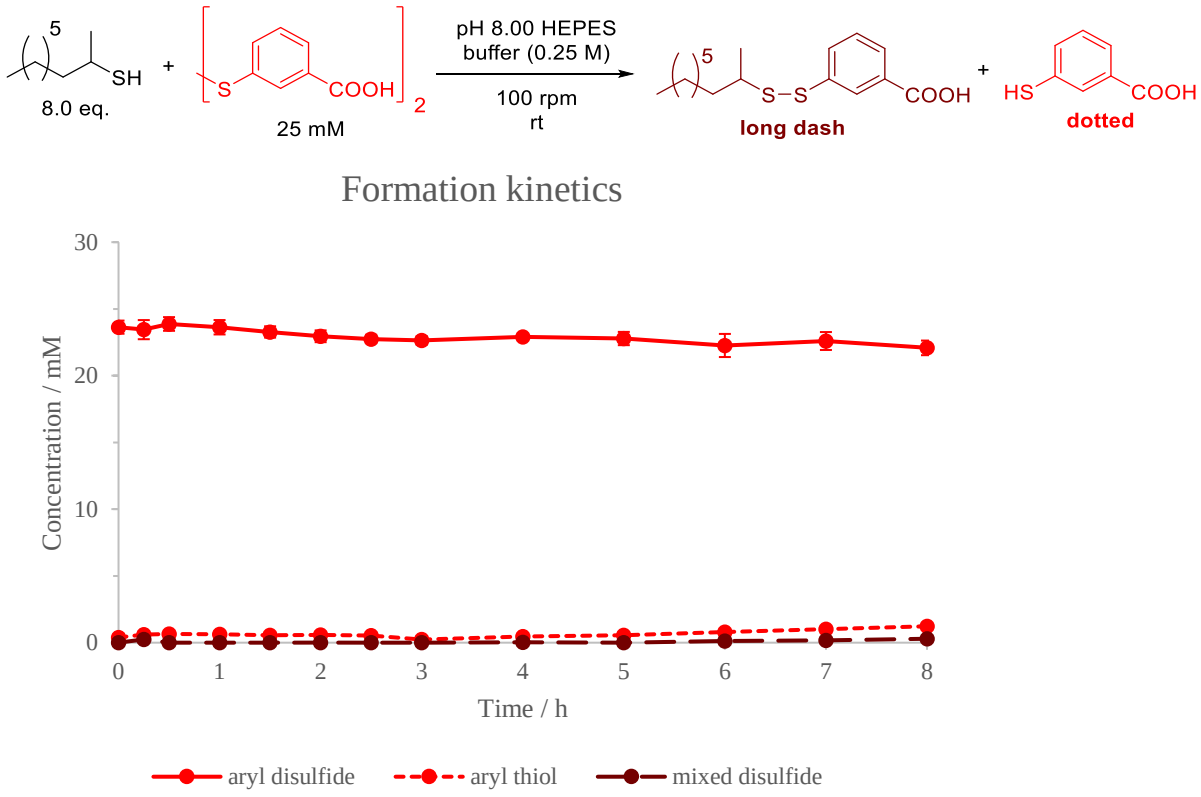


*Figure 4. 6. 9. 2. 5. Formation kinetics of surfactant **4.12b**. n = 3, error bars show one standard deviation.*

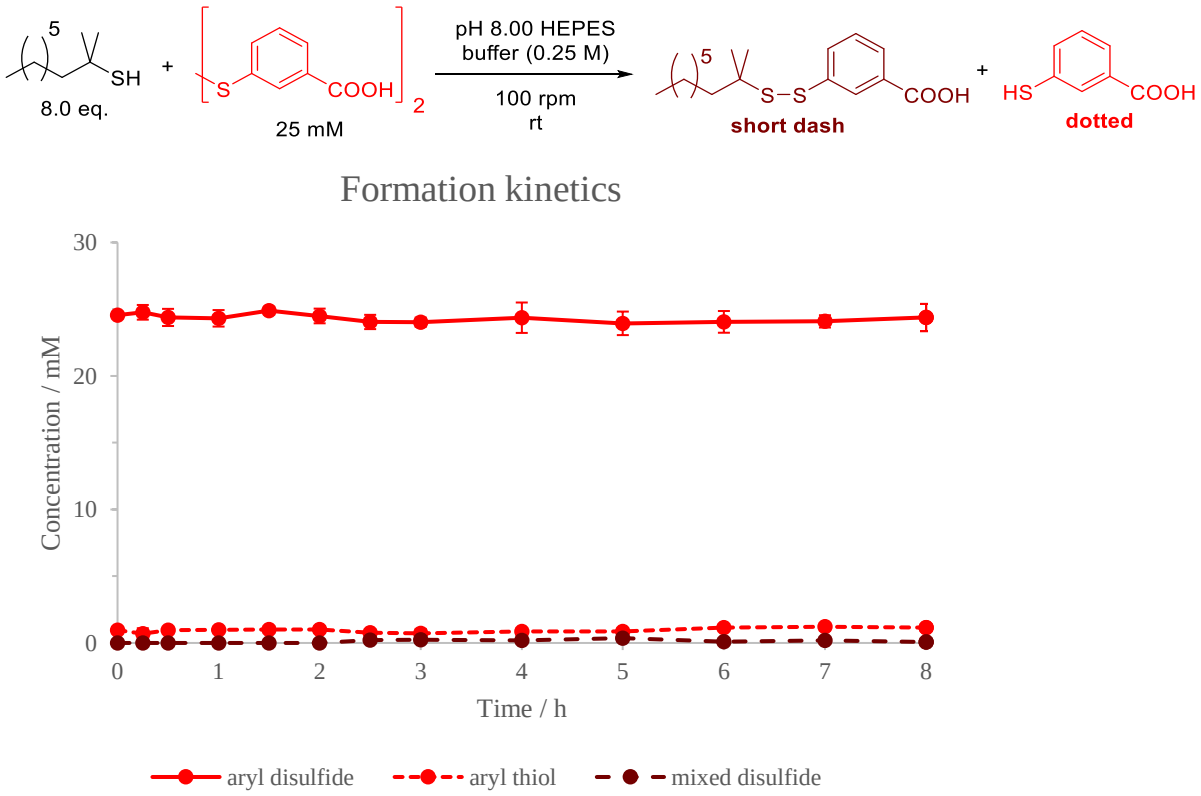


*Figure 4. 6. 9. 2. 6. Formation kinetics of surfactant **4.12c**. n = 3, error bars show one standard deviation.*

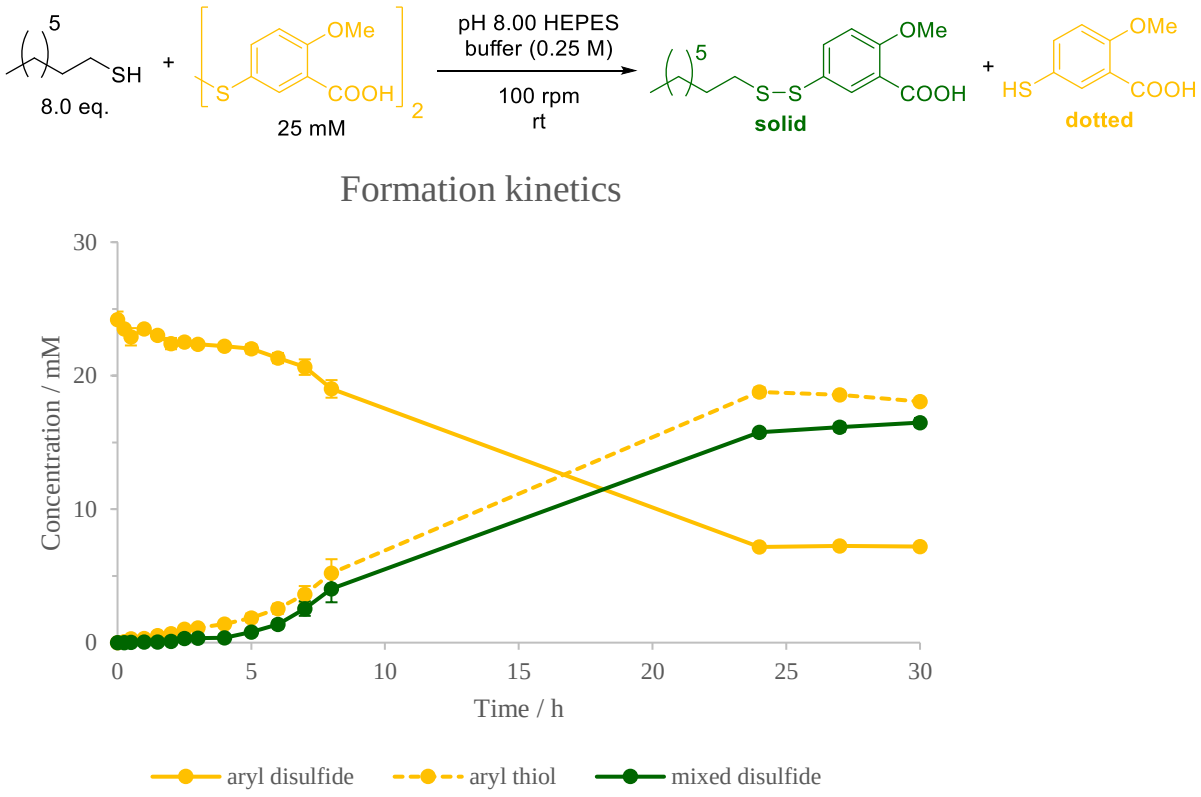


*Figure 4. 6. 9. 2. 7. Formation kinetics of surfactant **4.13a**. n = 3, error bars show one standard deviation.*

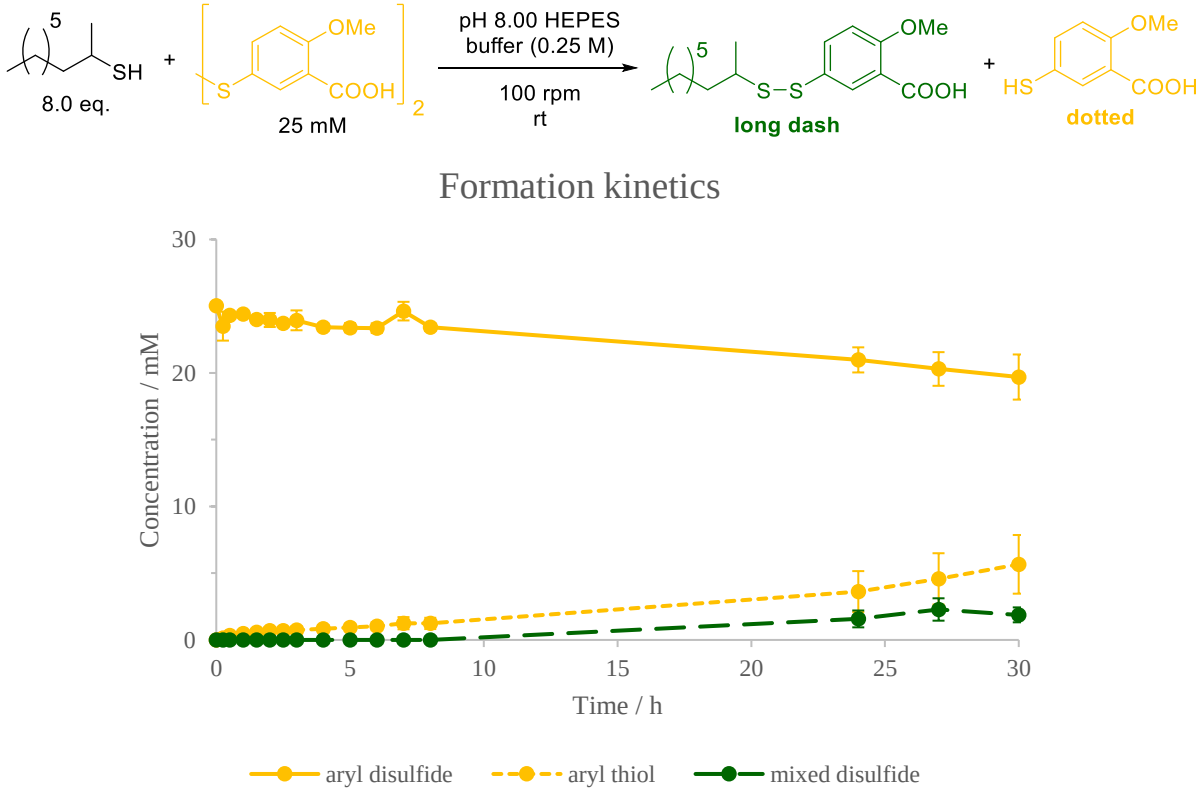


*Figure 4. 6. 9. 2. 8. Formation kinetics of surfactant **4.13b**. n = 3, error bars show one standard deviation.*

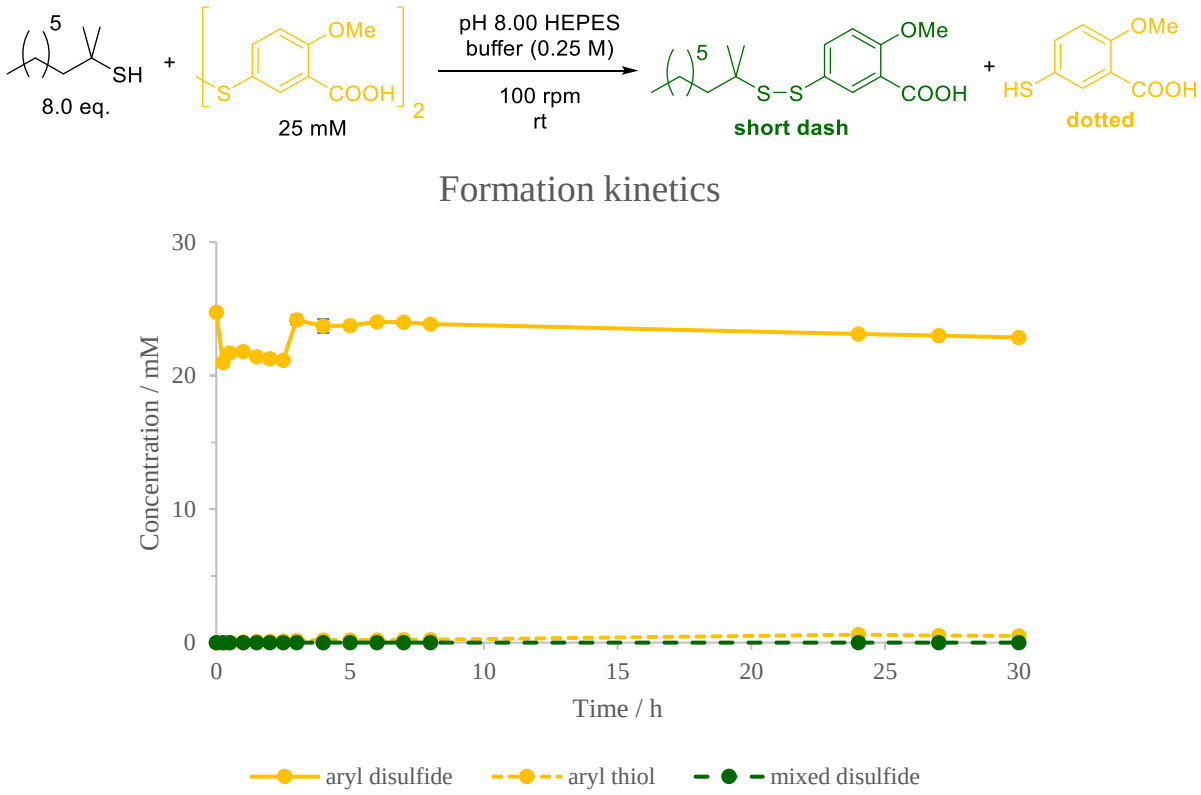


*Figure 4. 6. 9. 2. 9. Formation kinetics of surfactant **4.13c**. n = 3, error bars show one standard deviation.*

4. 6. 9. 3 Self-seeding experiments

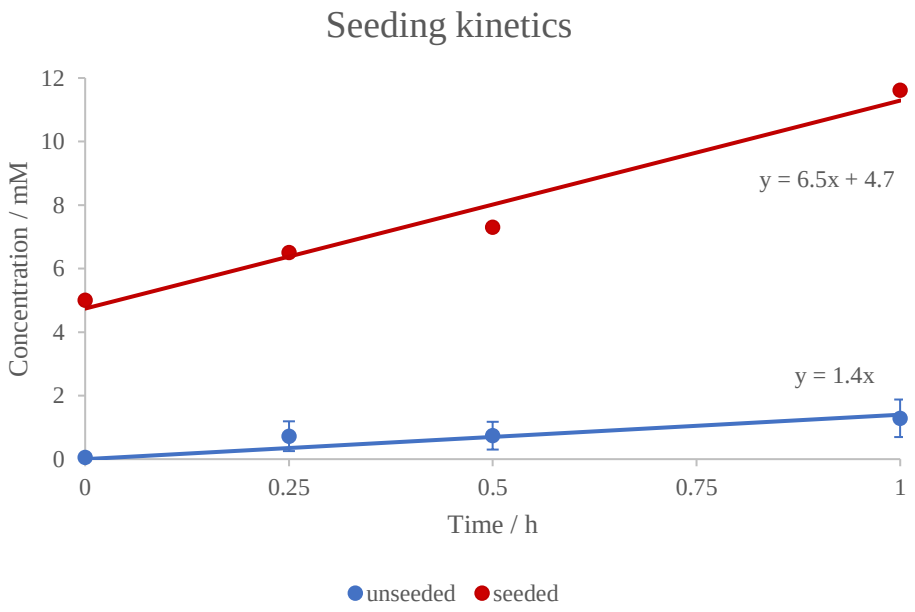


*Figure 4. 6. 9. 3. 1. Plot of surfactant **4.11b** concentration against time. Red – seeded with 0.2 equiv. of **4.11b**, n = 1, blue – unseeded, n = 3, error bars show one standard deviation. Initial rate (absence of product) = 1.4 ± 0.4 mMh^{-1}, Initial rate (5 mM product added) = 6.5 ± 0.9 mMh^{-1}.*

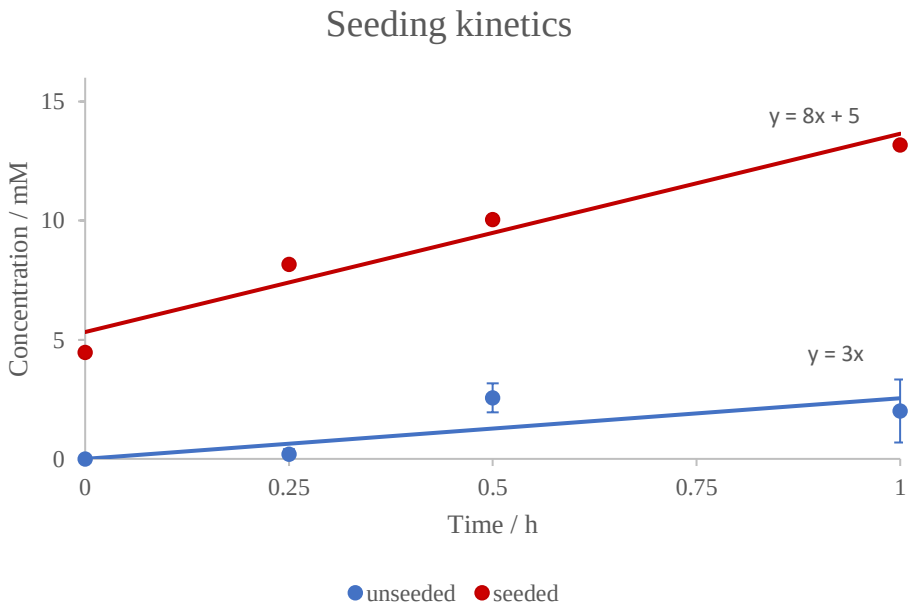


*Figure 4. 6. 9. 3. 2. Plot of surfactant **4.11c** concentration against time. Red – seeded with 0.2 equiv. of **4.11c**, n = 1, blue – unseeded, n = 3, error bars show one standard deviation. Initial rate (absence of product) = 8 ± 2 mMh^{-1}, Initial rate (5 mM product added) = 3 ± 2 mMh^{-1}.*

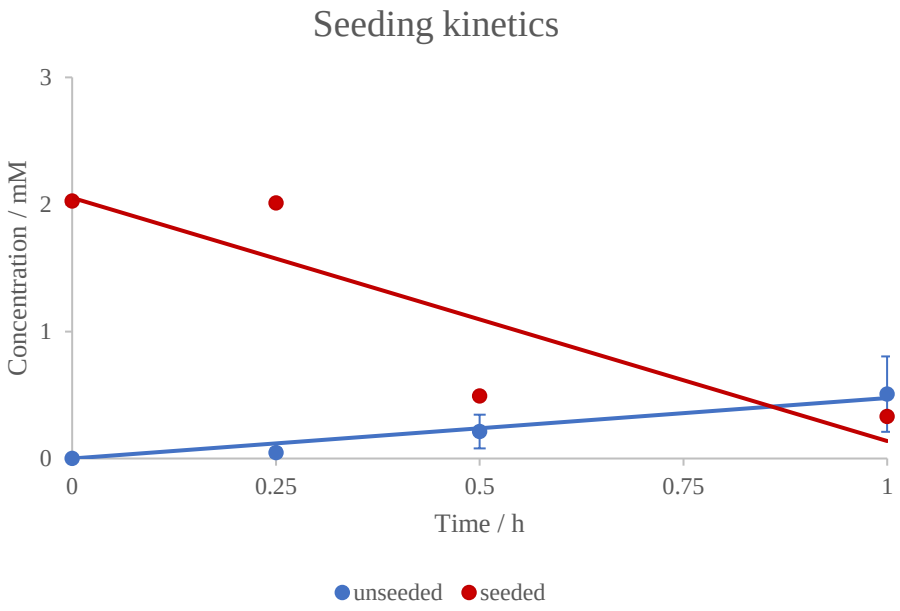


*Figure 4. 6. 9. 3. 3. Plot of surfactant **4.12a** concentration against time. Red – seeded with 0.2 equiv. of **4.12a**, n = 1, blue – unseeded, n = 3, error bars show one standard deviation. Meaningful initial rates could not be obtained.*

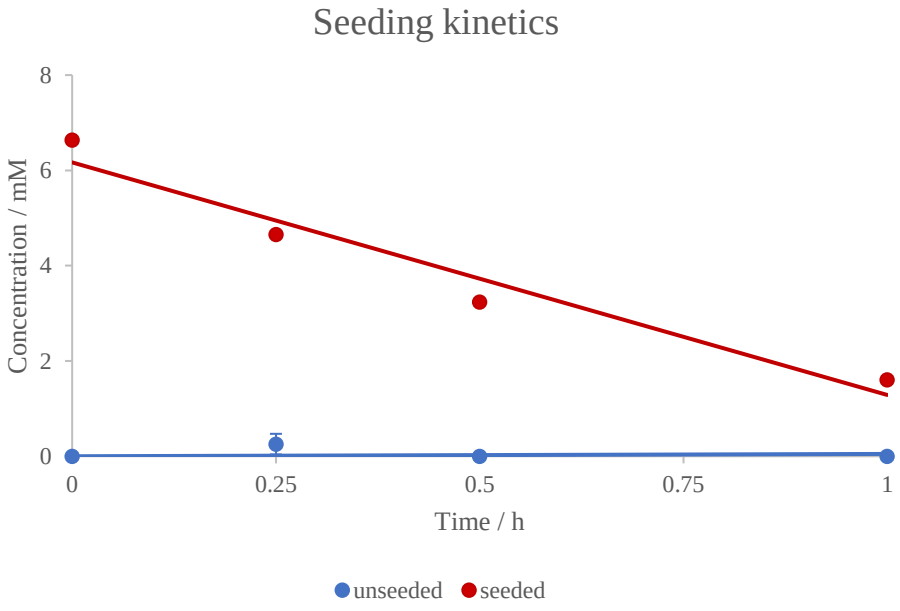


*Figure 4. 6. 9. 3. 4. Plot of surfactant **4.12b** concentration against time. Red – seeded with 0.2 equiv. of **4.12b**, n = 1, blue – unseeded, n = 3, error bars show one standard deviation and are typically too small to be visible. Meaningful initial rates could not be obtained.*

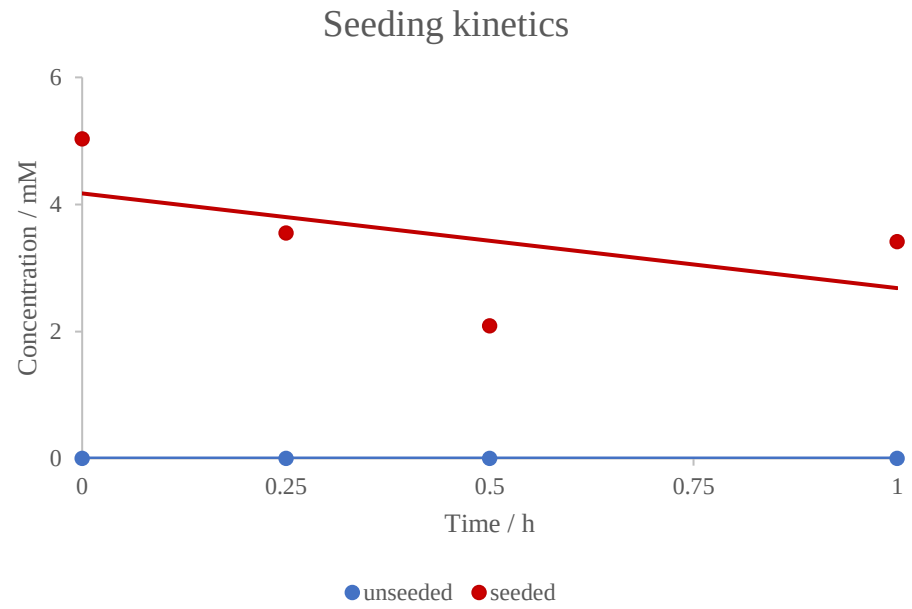


*Figure 4. 6. 9. 3. 5. Plot of surfactant **4.12c** concentration against time. Red – seeded with 0.2 equiv. of **4.12c**, n = 1, blue – unseeded, n = 3, error bars show one standard deviation and are too small to be visible. Meaningful initial rates could not be obtained.*

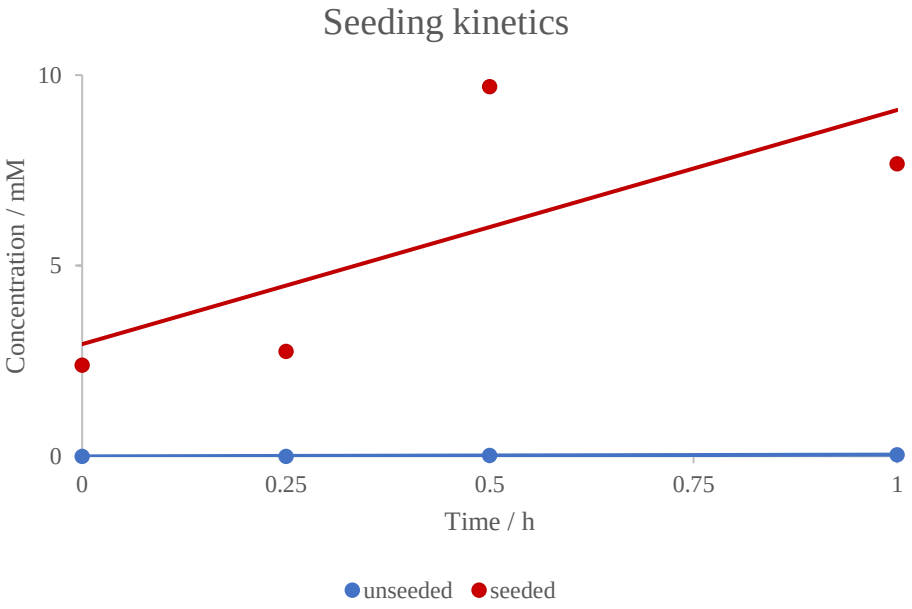


*Figure 4. 6. 9. 3. 6. Plot of surfactant **4.13a** concentration against time. Red – seeded with 0.2 equiv. of **4.13a**, n = 1, blue – unseeded, n = 3, error bars show one standard deviation and are too small to be visible. Meaningful initial rates could not be obtained.*

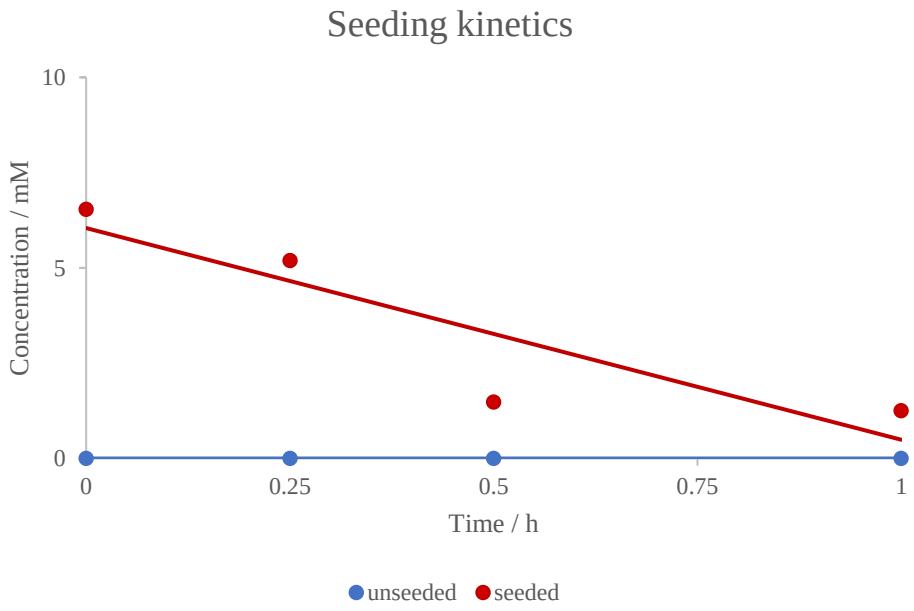


*Figure 4. 6. 9. 3. 7. Plot of surfactant **4.13b** concentration against time. Red – seeded with 0.2 equiv. of **4.13b**, n = 1, blue – unseeded, n = 3, error bars show one standard deviation and are too small to be visible. Meaningful initial rates could not be obtained.*

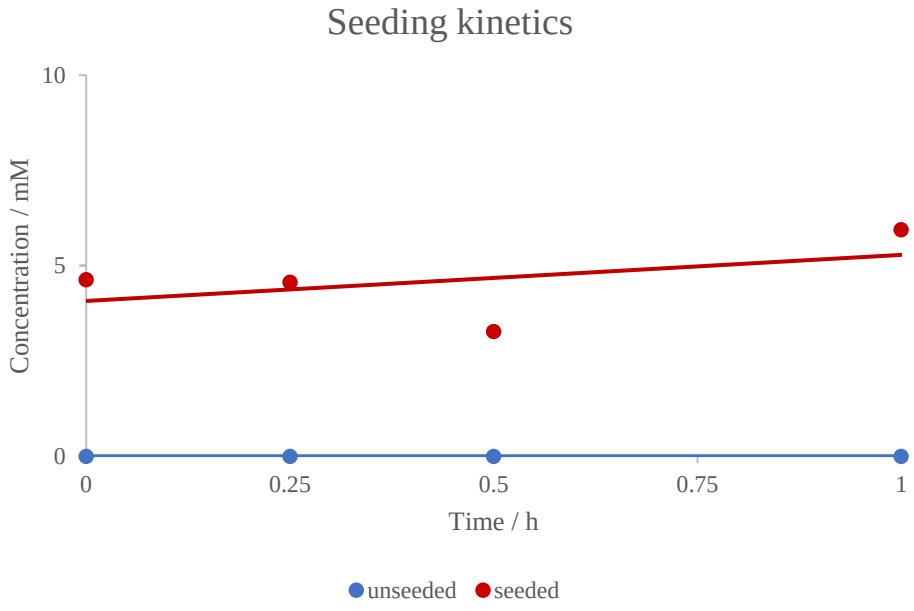


*Figure 4. 6. 9. 3. 8. Plot of surfactant **4.13c** concentration against time. Red – seeded with 0.2 equiv. of **4.13c**, n = 1, blue – unseeded. n = 3, error bars show one standard deviation and are too small to be visible. Meaningful initial rates could not be obtained.*

4. 6. 9. 4 Hetero-seeding experiments

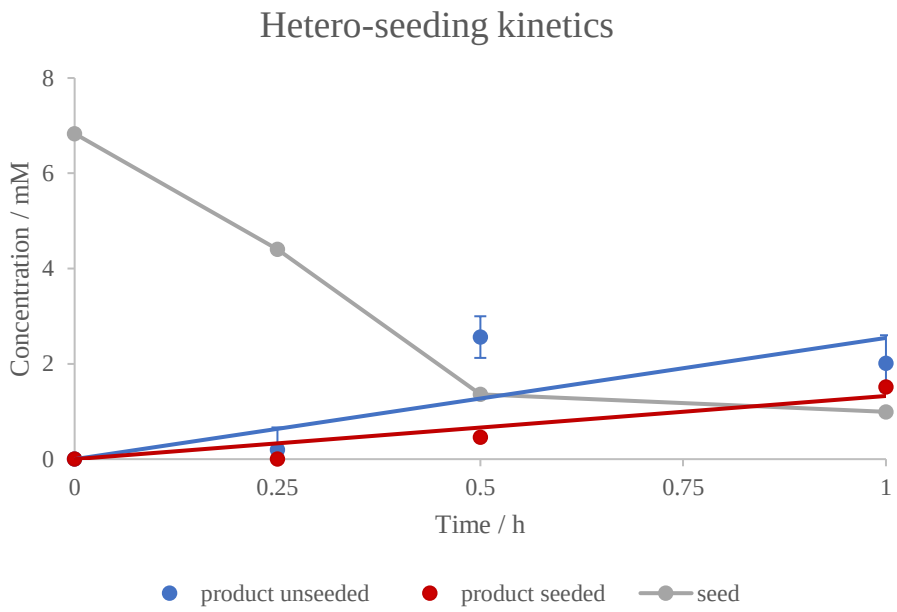


*Figure 4. 6. 9. 4. 1. Plot of surfactant concentrations in hetero-seeding experiments. Red – **4.11c** concentration in reaction seeded with 0.2 equiv. of **4.13b**, n = 1, blue – **4.11c** concentration in unseeded reaction, n = 3, error bars show one standard deviation, grey – **4.13b** concentration during the seeding experiment, n = 1. Meaningful initial rates could not be obtained.*

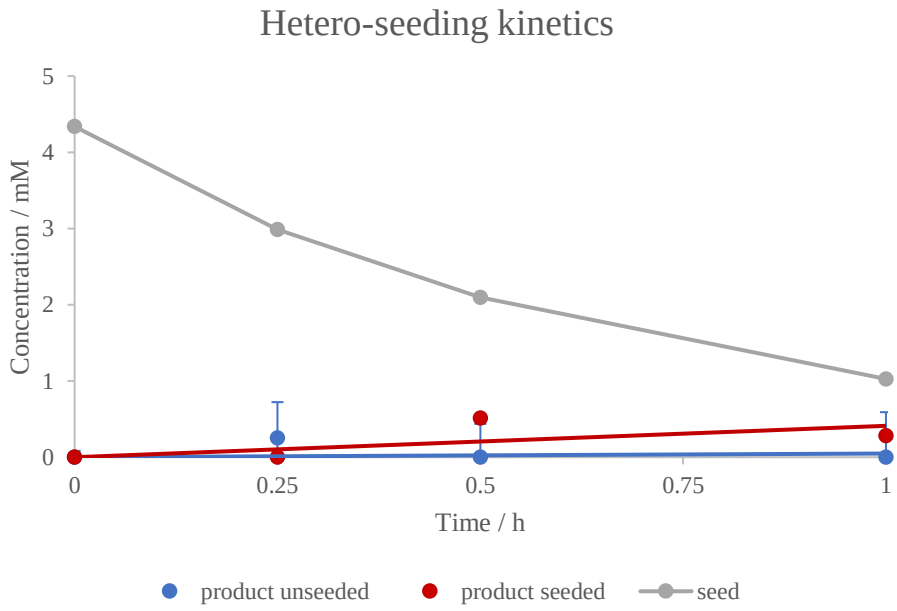


*Figure 4. 6. 9. 4. 2. Plot of surfactant concentrations in hetero-seeding experiments. Red – **4.12b** concentration in reaction seeded with 0.2 equiv. of **4.11a**, n = 1, blue – **4.12b** concentration in unseeded*

*reaction, n = 3, error bars show one standard deviation, grey – **4.11a** concentration during the seeding experiment, n = 1. Meaningful initial rates could not be obtained.*

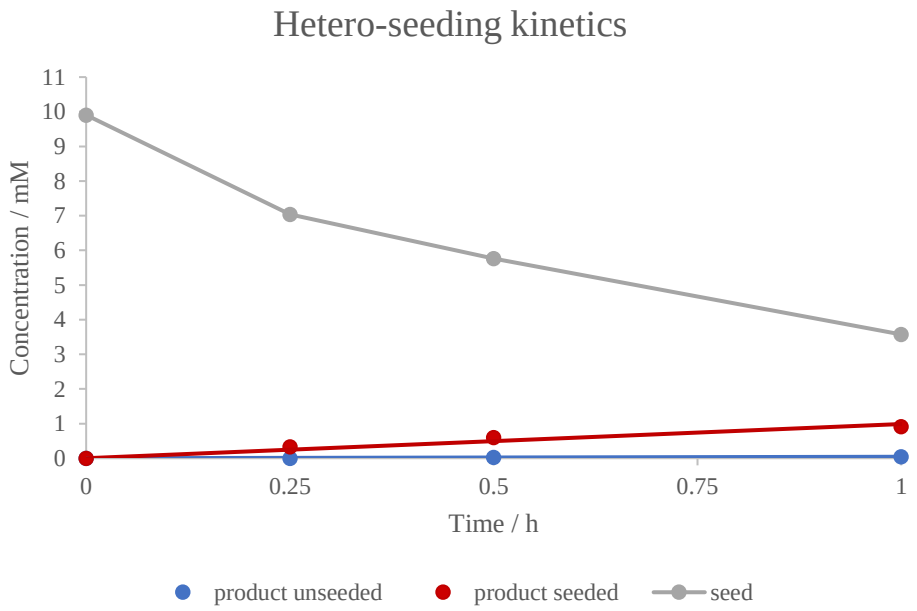


*Figure 4. 6. 9. 4. 3. Plot of surfactant concentrations in hetero-seeding experiments. Red – **4.13a** concentration in reaction seeded with 0.2 equiv. of **4.12c**, n = 1, blue – **4.13a** concentration in unseeded reaction, n = 3, error bars show one standard deviation, grey – **4.12c** concentration during the seeding experiment, n = 1. Meaningful initial rates could not be obtained.*

4. 6. 9. 5 Competing lipids with varying aryl substitution

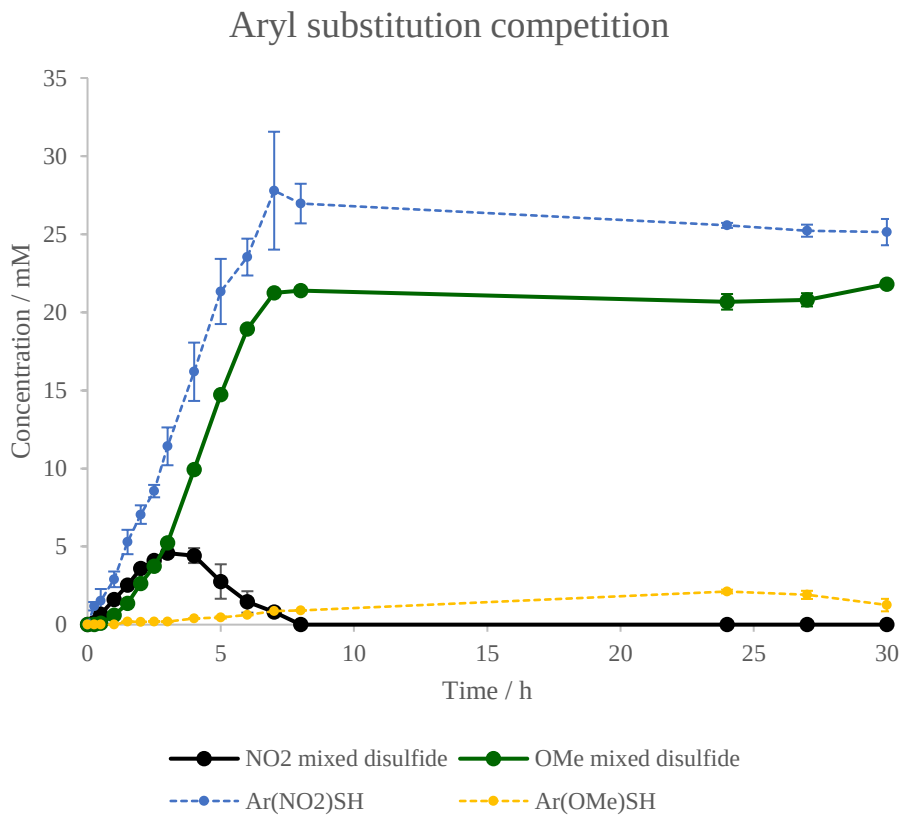


*Figure 4. 6. 9. 5. 1. Reaction kinetics of competition study between mixed lipids **4.11a** and **4.13a**. Bis-aryl disulfide concentrations are omitted for clarity. n = 3, error bars show one standard deviation.*

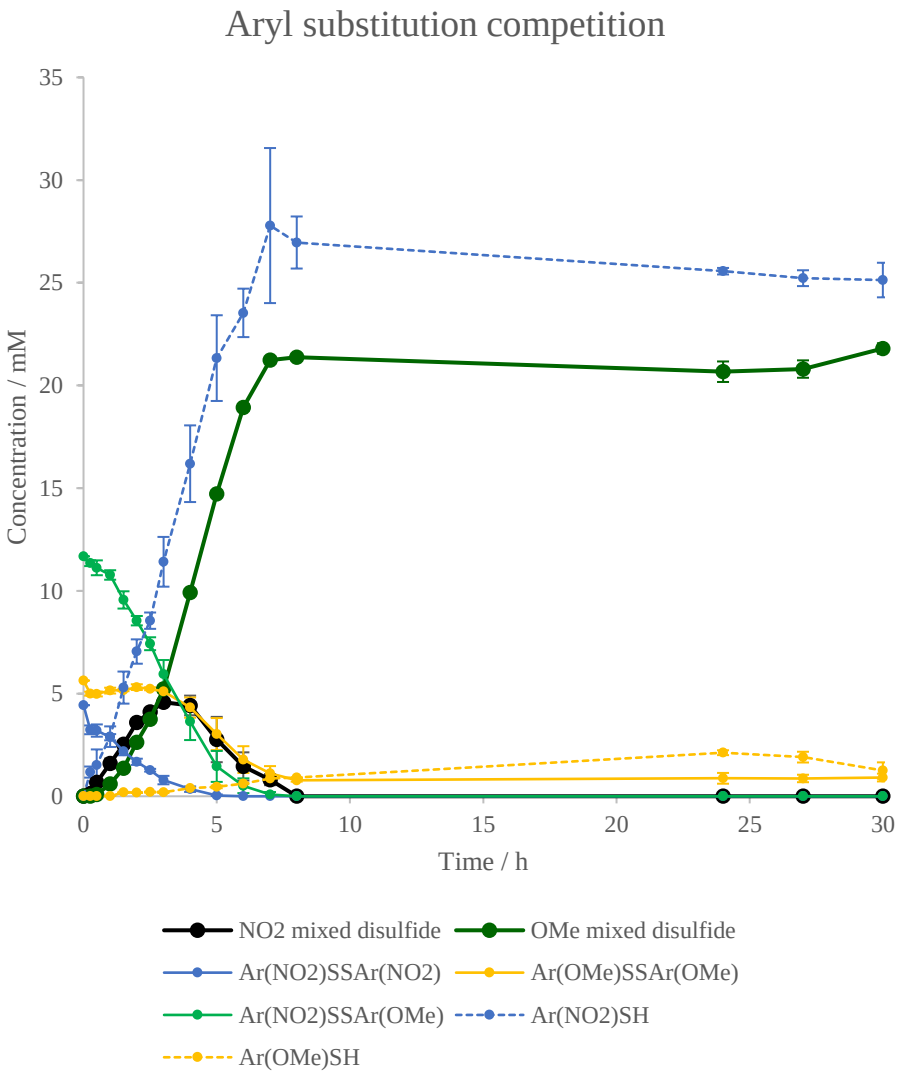


Figure 4. 6. 9. 5. 2. Reaction kinetics of competition study between mixed lipids ***4.11a*** *and* ***4.13a****, showing all UV active components. n = 3, error bars show one standard deviation.*

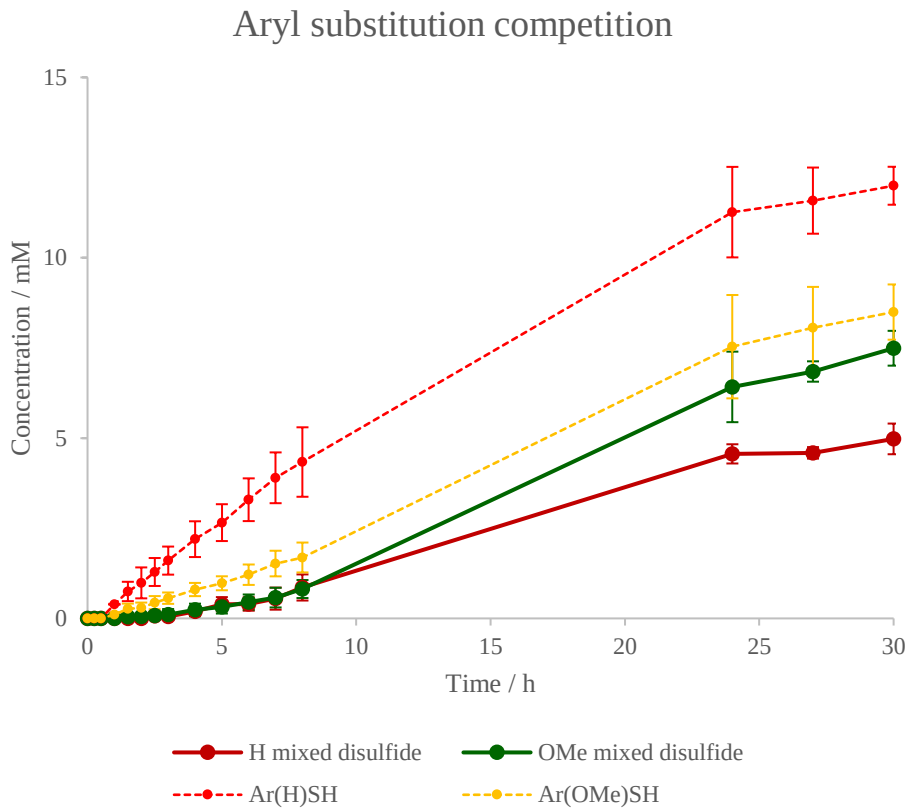


*Figure 4. 6. 9. 5. 3. Reaction kinetics of competition study between mixed lipids **4.12a** and **4.13a**. Bis-aryl disulfide concentrations are omitted for clarity. n = 3, error bars show one standard deviation.*

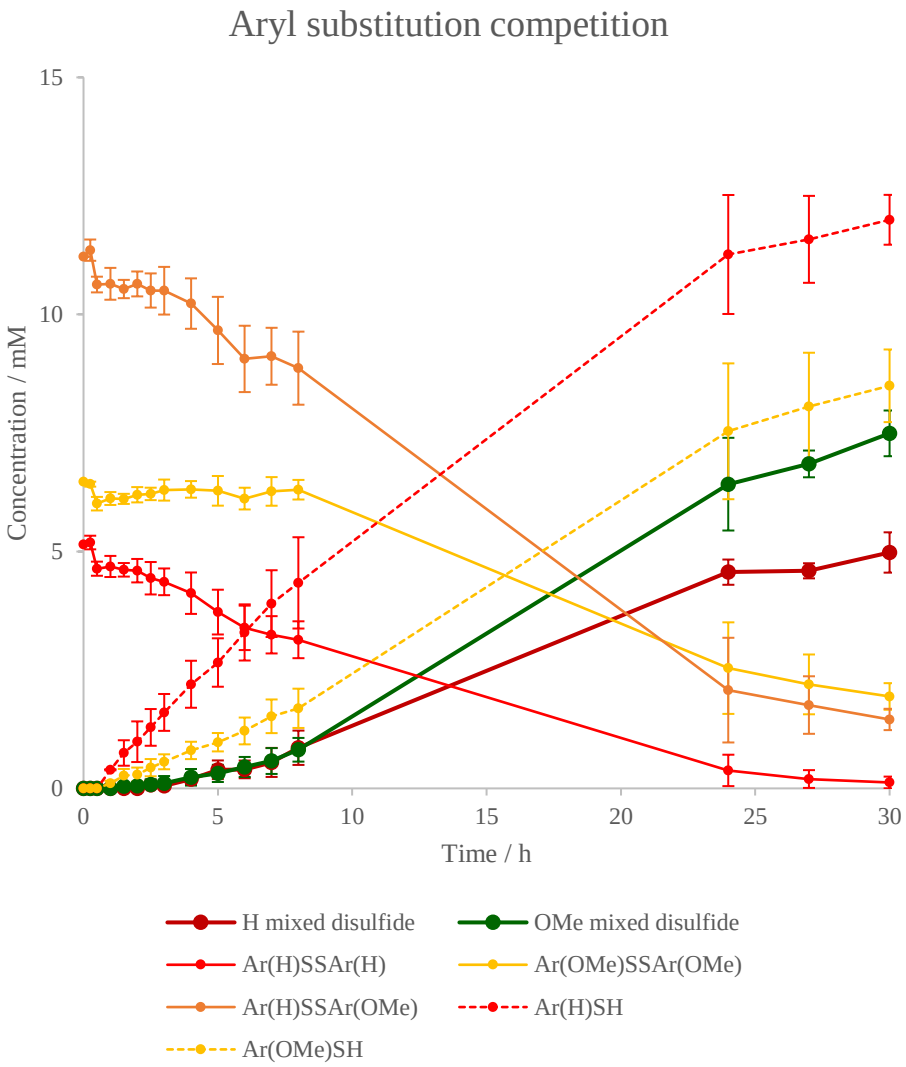


*Figure 4. 6. 9. 5. 4. Reaction kinetics of competition study between mixed lipids **4.12a** and **4.13a**, showing all UV active components. n = 3, error bars show one standard deviation.*

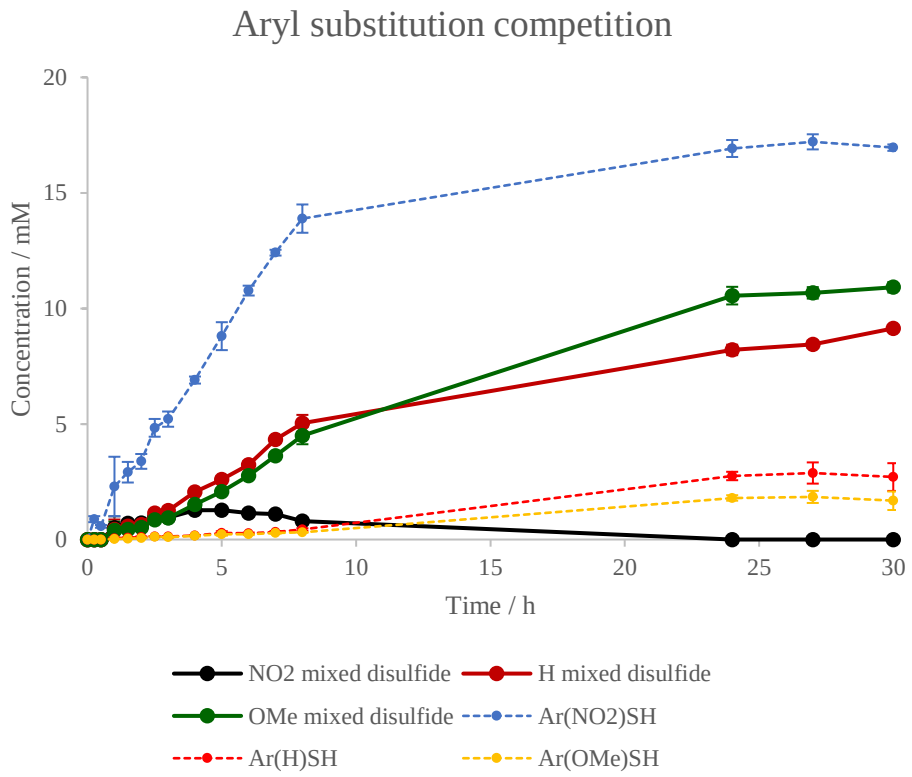


*Figure 4. 6. 9. 5. 5. Reaction kinetics of competition study between mixed lipids **4.11a**, **4.12a** and **4.13a**.*

Bis-aryl disulfide concentrations are omitted for clarity. n = 3, error bars show one standard deviation.

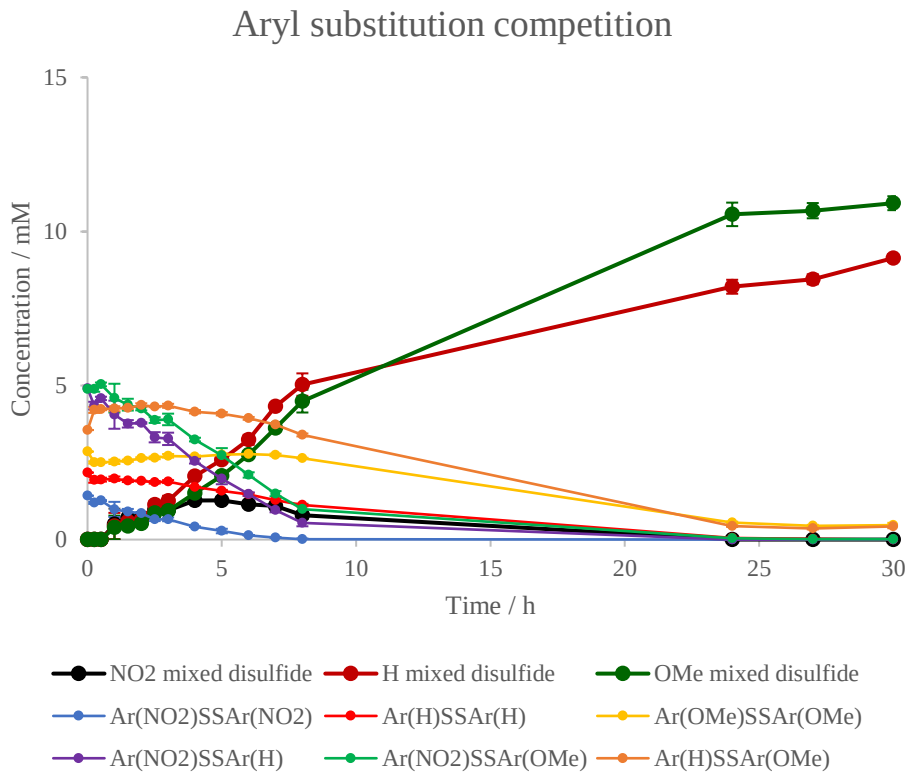


*Figure 4. 6. 9. 5. 6. Reaction kinetics of competition study between mixed lipids **4.11a**, **4.12a** and **4.13a**.*

Aryl thiol concentrations are omitted for clarity. n = 3, error bars show one standard deviation.

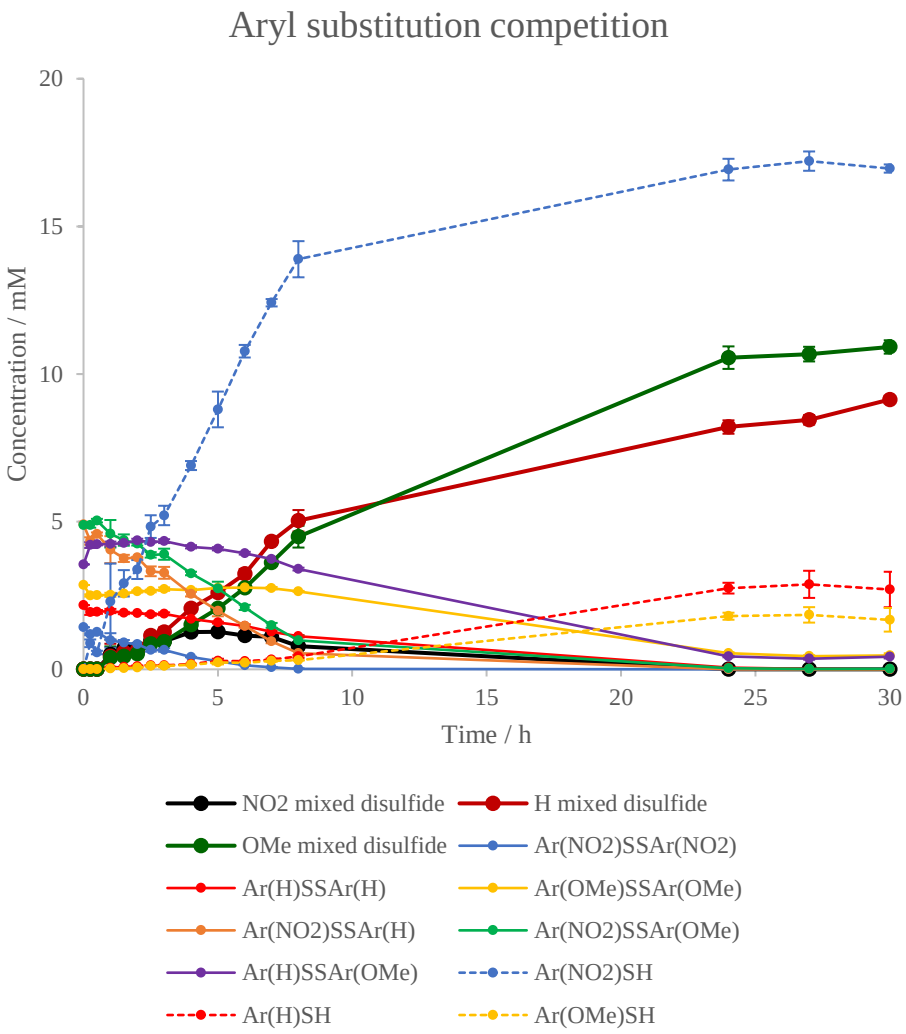


*Figure 4. 6. 9. 5. 7. Reaction kinetics of competition study between mixed lipids **4.11a**, **4.12a** and **4.13a**, showing all UV active components. n = 3, error bars show one standard deviation.*

4. 6. 9. 6 Kinetics of the 9 lipid system

4. 6. 9. 6. 1 Bar chart visualisation of surfactant concentration

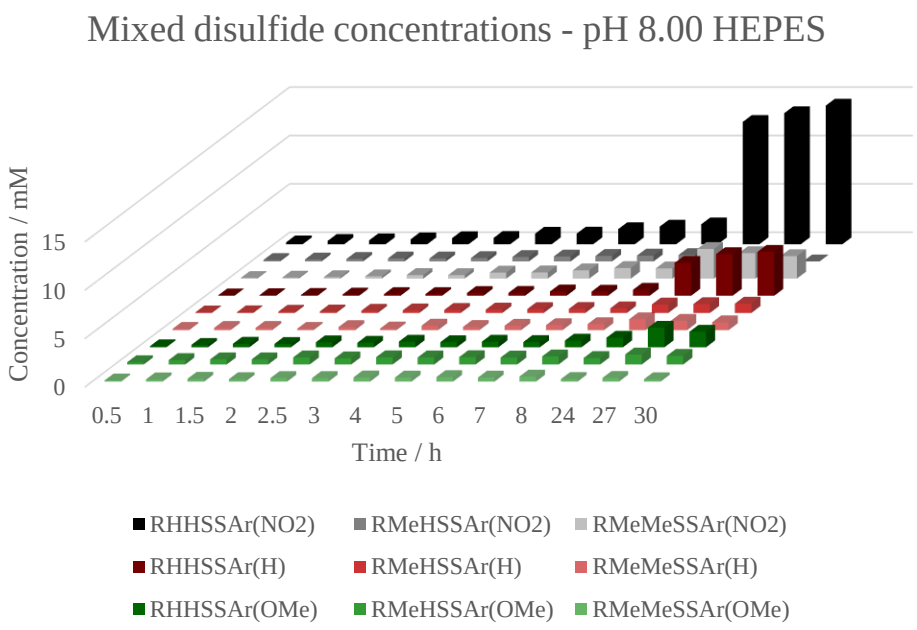


Figure 4. 6. 9. 6. 1. 1. Bar chart visualisation of surfactant kinetics in the 9 lipid system, using pH 8.00 HEPES buffer. n = 3.

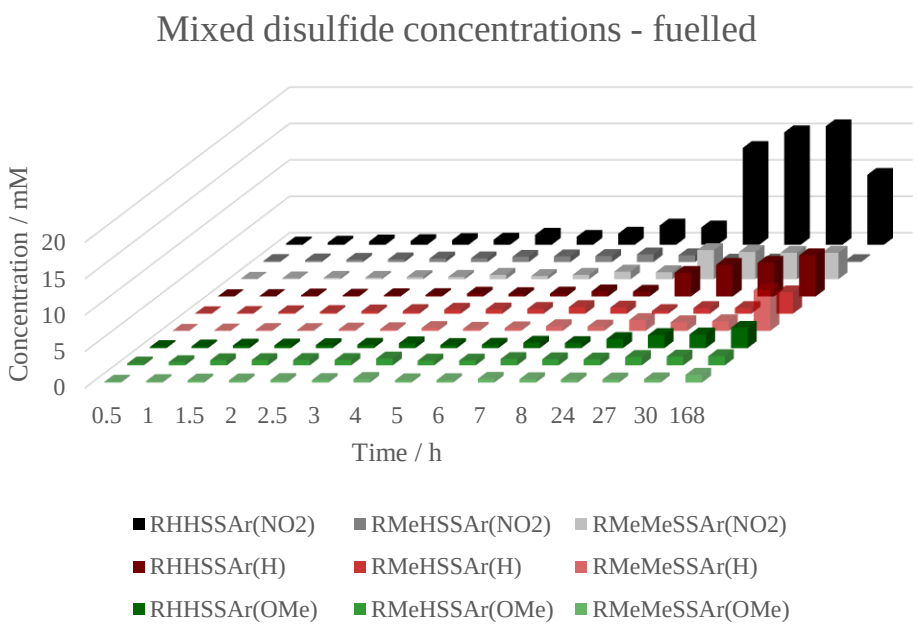


Figure 4. 6. 9. 6. 1. 2. Bar chart visualisation of surfactant kinetics in the 9 lipid system, using pH 8.00 HEPES buffer, fuelled with addition rate of 10 µL h^{-1} of 6.0 M H_2O_2 for the first 24 h. n = 3.

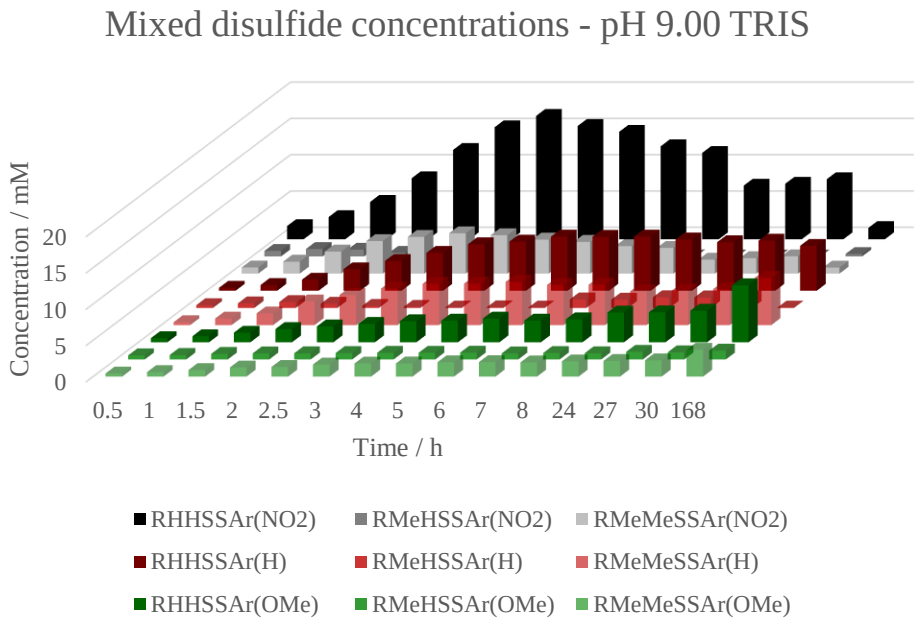


Figure 4. 6. 9. 6. 1. 3. Bar chart visualisation of surfactant kinetics in the 9 lipid system, using pH 9.00 TRIS buffer. n = 3.

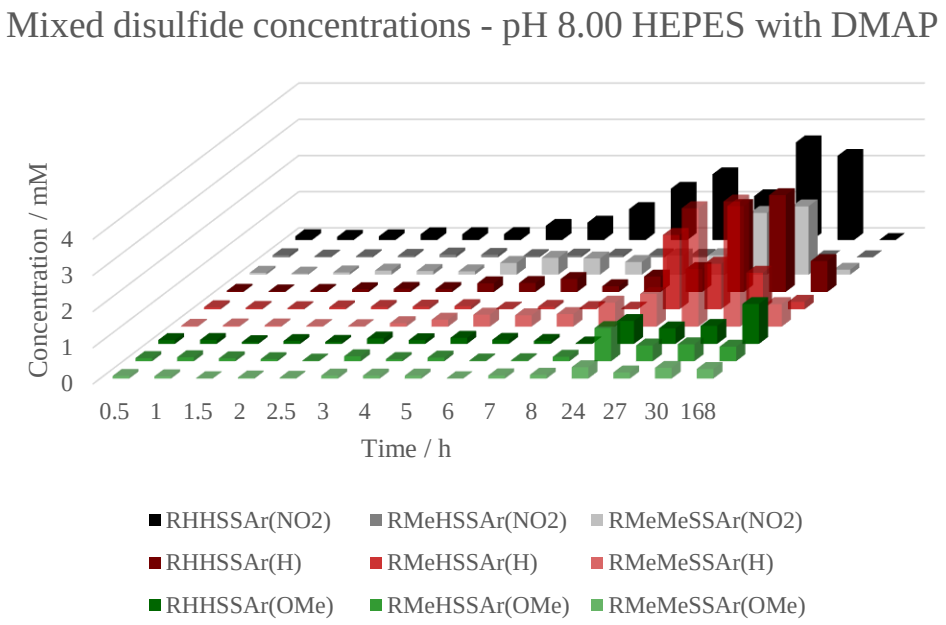


Figure 4. 6. 9. 6. 1. 4. Bar chart visualisation of surfactant kinetics in the 9 lipid system, pH 8.00 HEPES buffer, and 0.5 equiv. DMAP. n = 3.

4. 6. 9. 6. 2 Relative surfactant concentrations

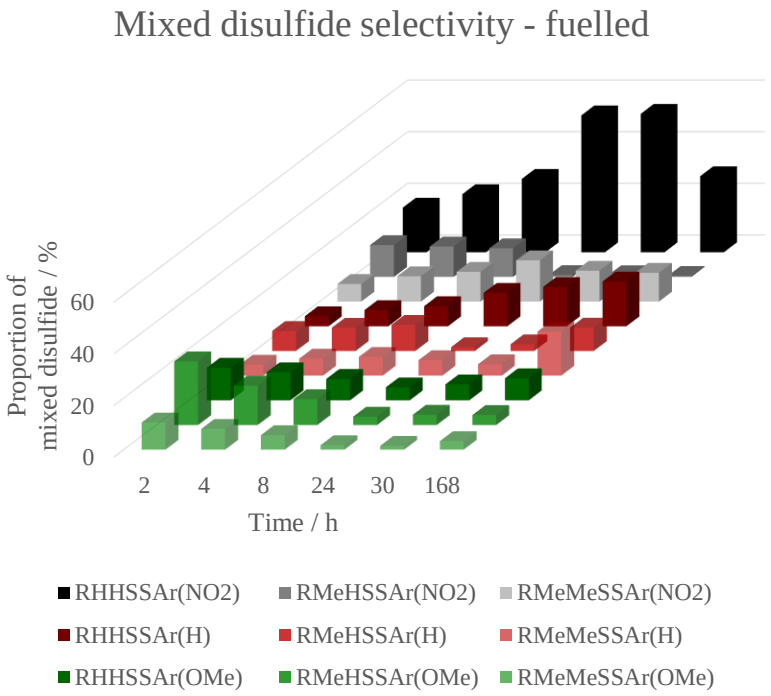


Figure 4. 6. 9. 6. 2. 1. Bar chart of relative surfactant concentrations through time in the 9 lipid system, using pH 8.00 HEPES buffer, fuelled with addition rate of 10 µL h^{-1} of 6.0 M H_2O_2 for the first 24 h. n = 3.

4. 6. 9. 6. 3 Additional scatter plots of surfactant concentration

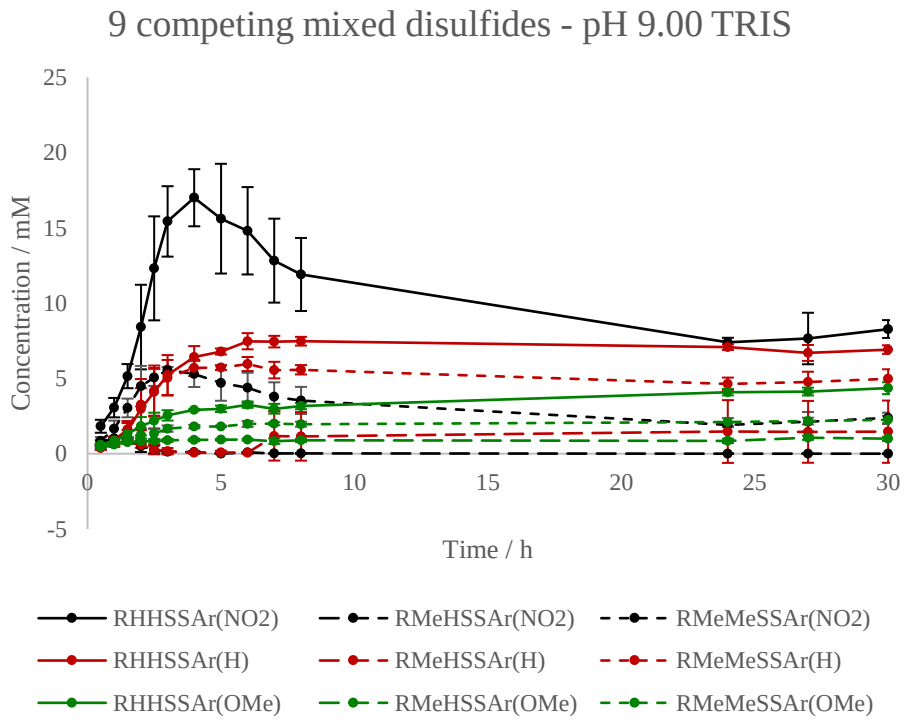


Figure 4. 6. 9. 6. 3. 1. Scatter plot of surfactant concentrations through time in the 9 lipid system, using pH 9.00 TRIS buffer, showing the first 30 h of reaction. n = 3, error bars show one standard deviation.

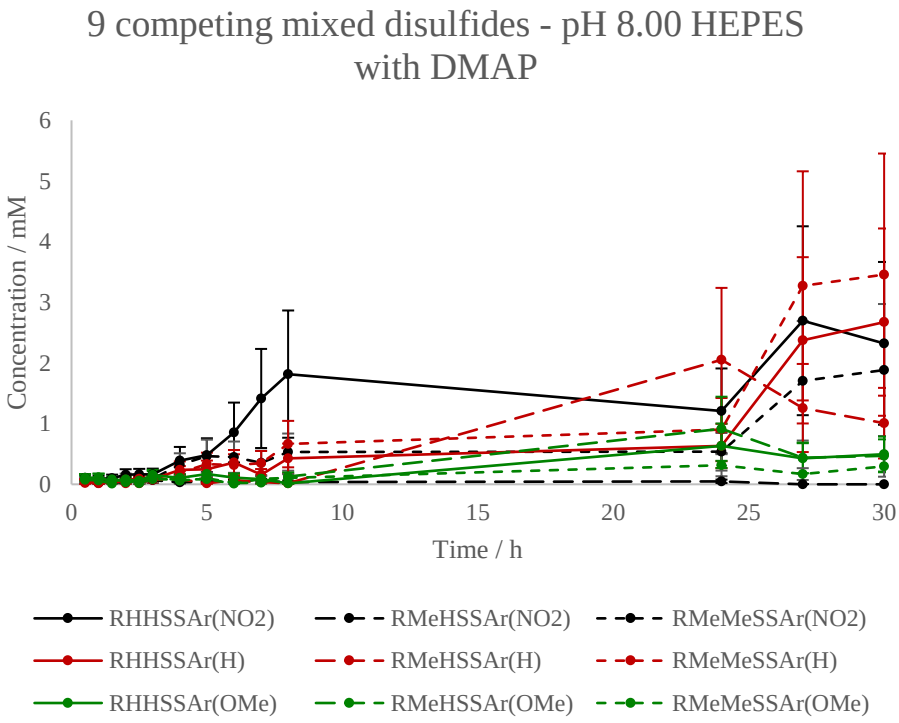


Figure 4. 6. 9. 6. 3. 2. Scatter plot of surfactant concentrations through time in the 9 lipid system, using pH 8.00 HEPES buffer with 0.5 equiv. DMAP, showing the first 30 h of reaction. n = 3, error bars show one standard deviation.

4. 6. 10 UPLC calibration graphs

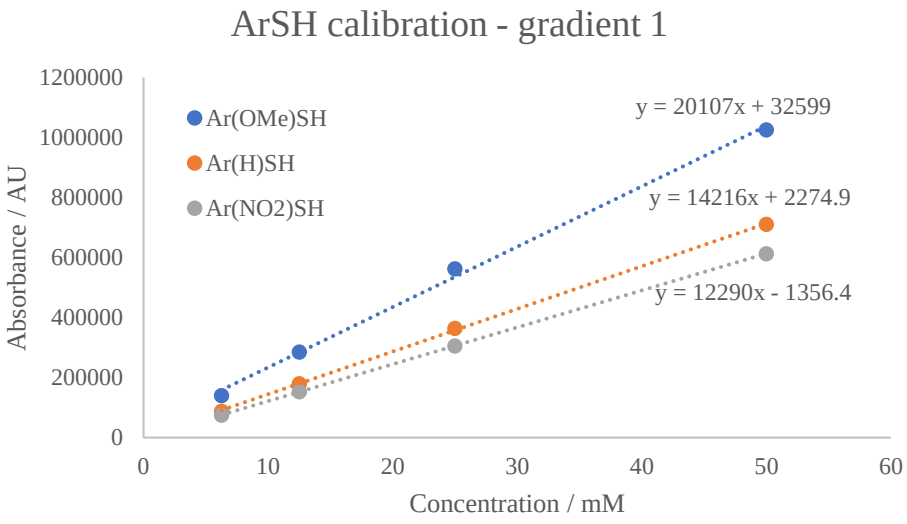


Figure 4. 6. 10. 1. Calibration graph for aryl thiols using gradient 1. n = 3, error bars show one standard deviation and are too small to be visible.

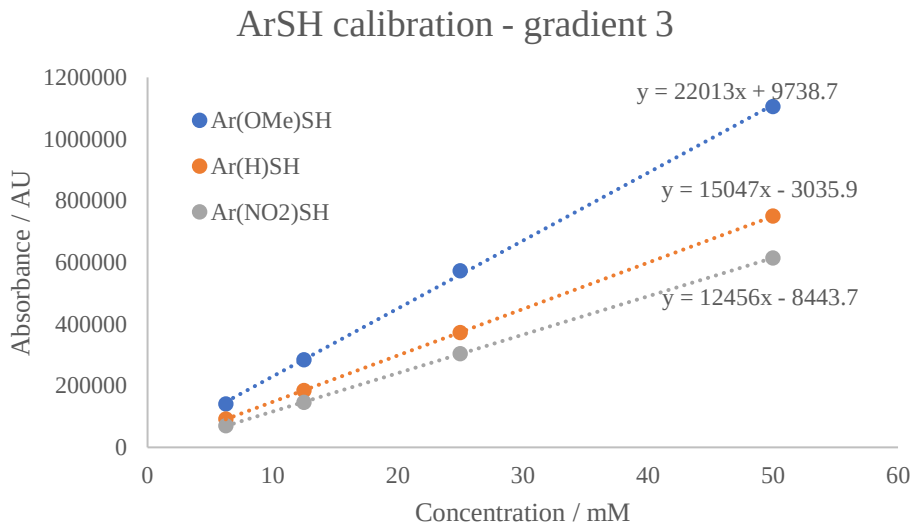


Figure 4. 6. 10. 2. Calibration graph for aryl thiols using gradient 3. n = 3, error bars show one standard deviation and are too small to be visible.

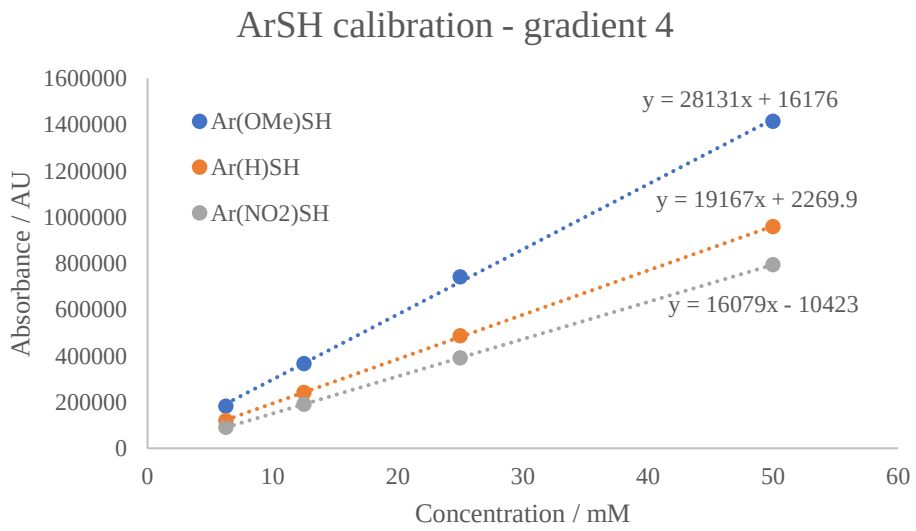


Figure 4. 6. 10. 3. Calibration graph for aryl thiols using gradient 4. n = 3, error bars show one standard deviation and are too small to be visible.

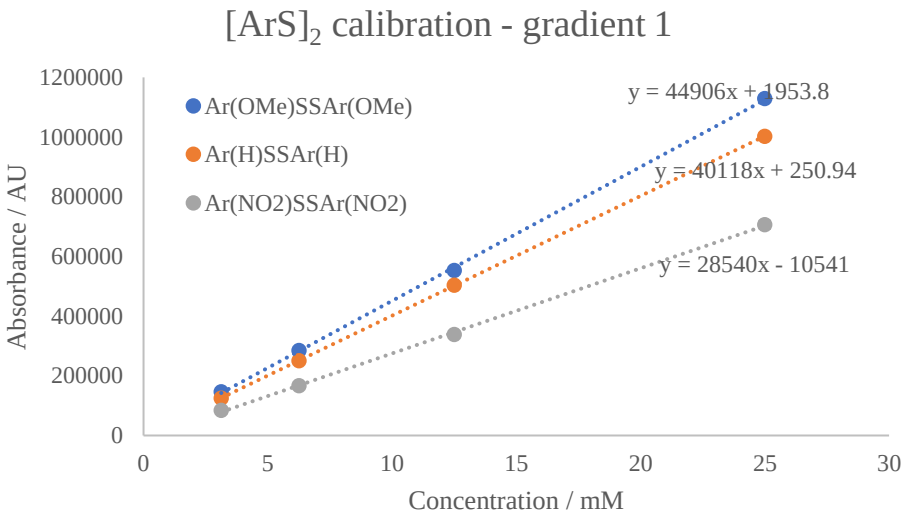


Figure 4. 6. 10. 4. Calibration graph for aryl disulfides using gradient 1. n = 3, error bars show one standard deviation and are too small to be visible.

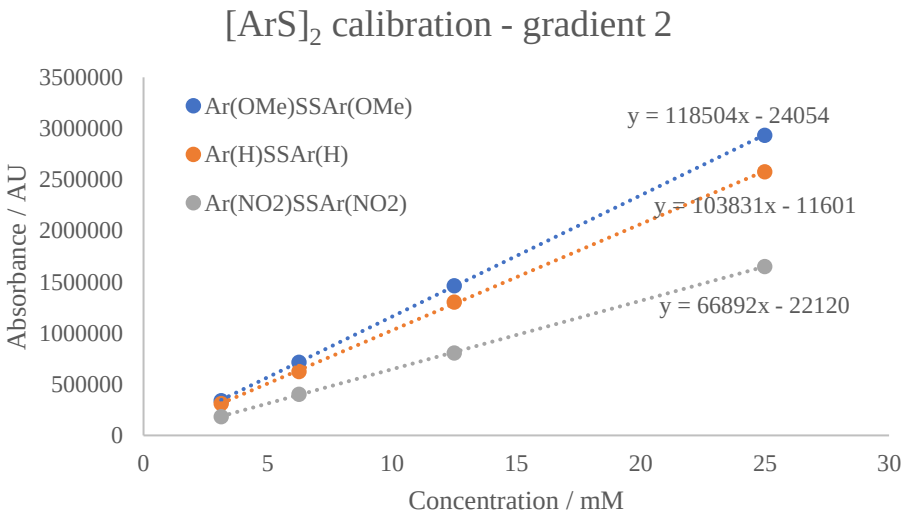


Figure 4. 6. 10. 5. Calibration graph for aryl disulfides using gradient 2. n = 3, error bars show one standard deviation and are too small to be visible.

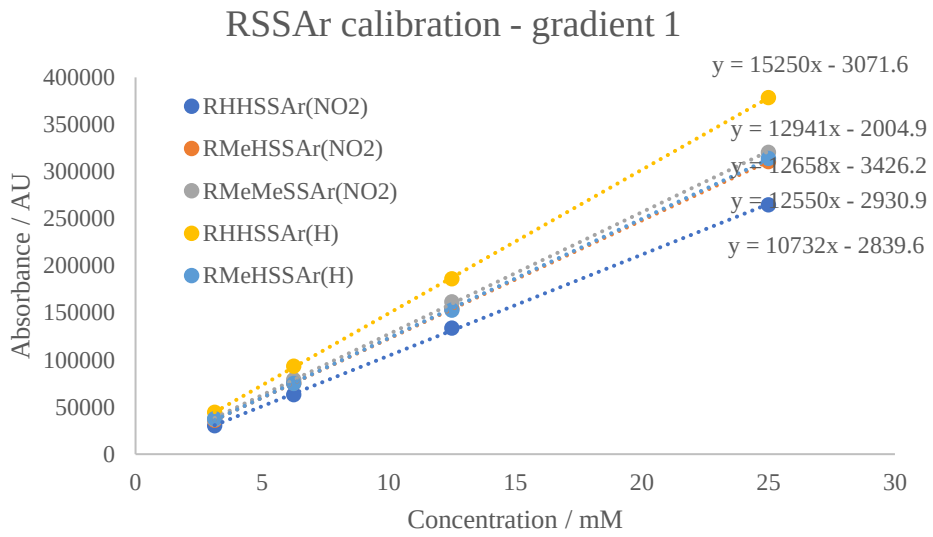


Figure 4. 6. 10. 6. Calibration graph for alkyl-aryl mixed disulfides using gradient 1. n = 3, error bars show one standard deviation and are too small to be visible.

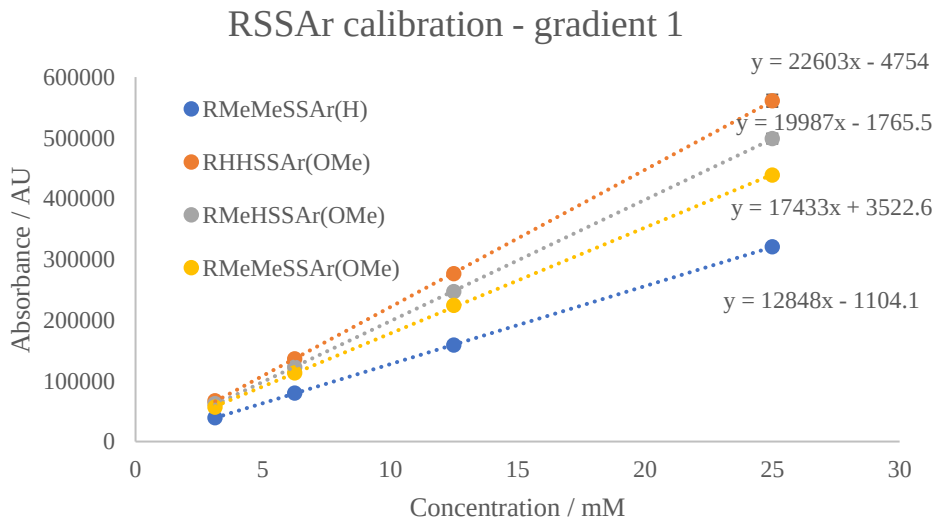


Figure 4. 6. 10. 7. Calibration graph for alkyl-aryl mixed disulfides using gradient 1. n = 3, error bars show one standard deviation and are too small to be visible.

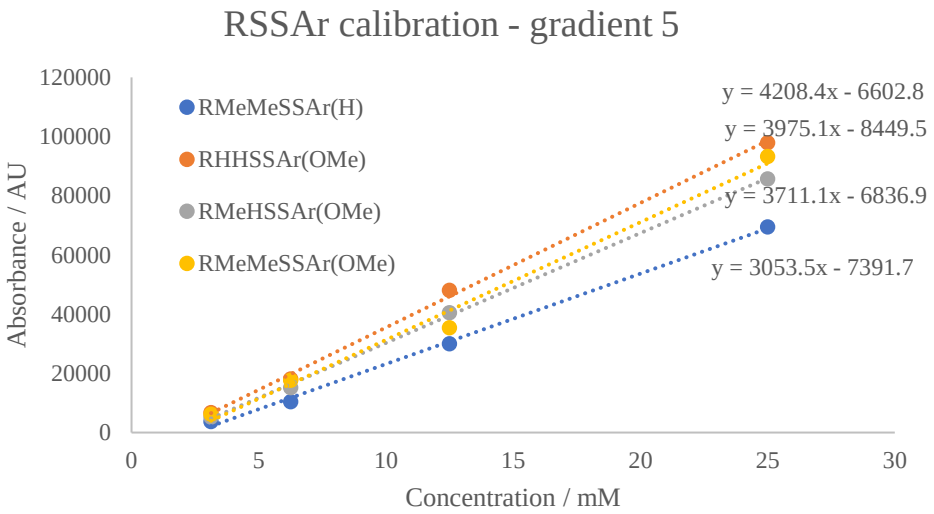


Figure 4. 6. 10. 8. Calibration graph for alkyl-aryl mixed disulfides using gradient 5. n = 3, error bars show one standard deviation and are too small to be visible.

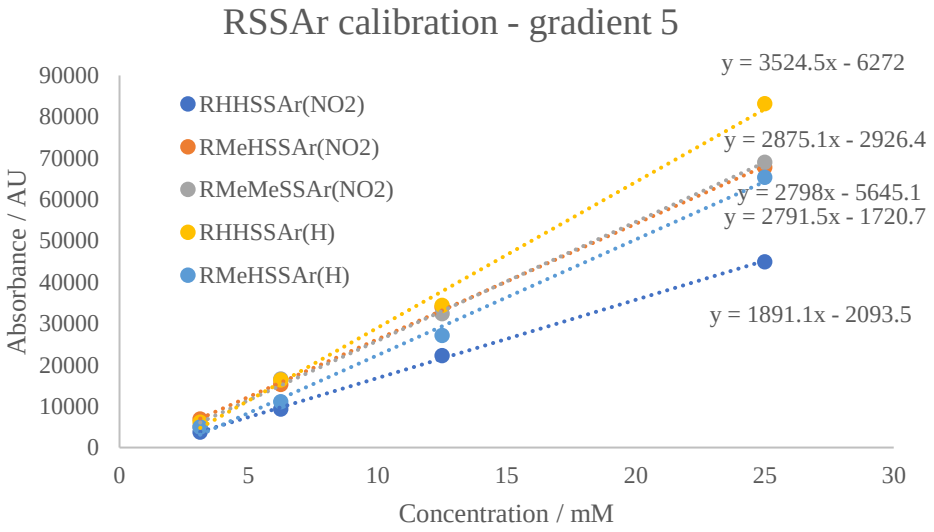


Figure 4. 6. 10. 9. Calibration graph for alkyl-aryl mixed disulfides using gradient 5. n = 3, error bars show one standard deviation and are too small to be visible.

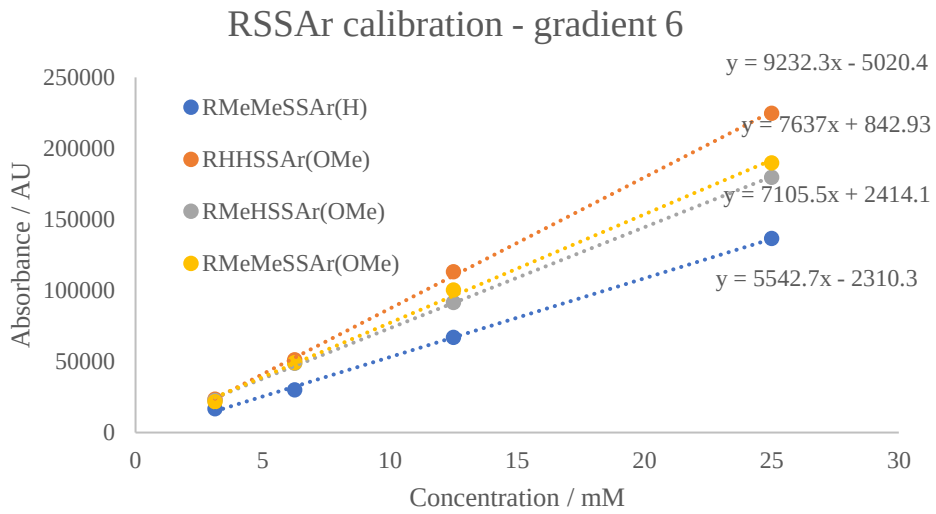


Figure 4. 6. 10. 10. Calibration graph for alkyl-aryl mixed disulfides using gradient 6. n = 3, error bars show one standard deviation and are too small to be visible.

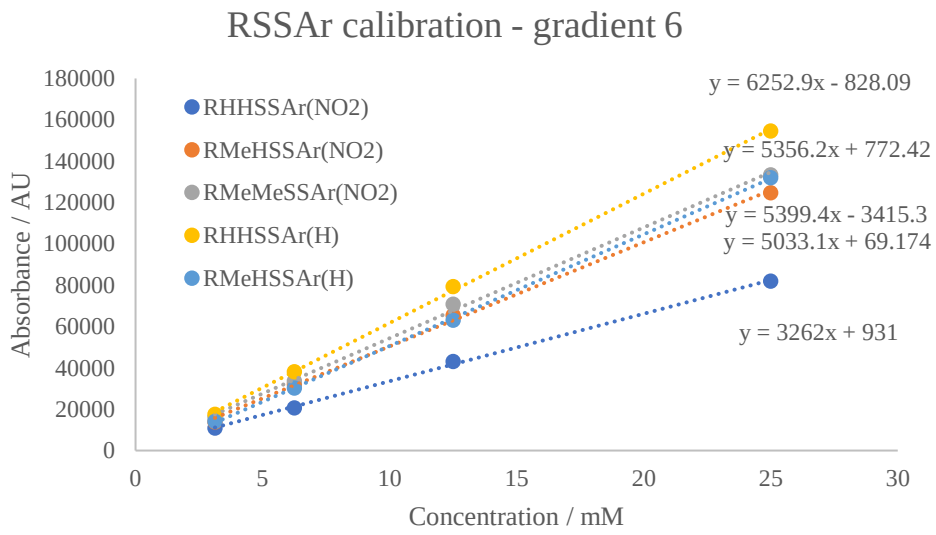
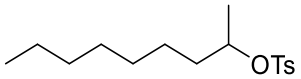


Figure 4. 6. 10. 11. Calibration graph for alkyl-aryl mixed disulfides using gradient 6. n = 3, error bars show one standard deviation and are too small to be visible.

4. 6. 10 Synthesis and characterization of compounds

Synthesis and characterisation of **4.8** are described in chapter 3, labelled **3.7**.

(±)-Nonan-2-yl 4-methylbenzenesulfonate, 4.27

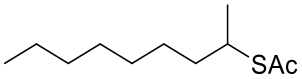


To a stirred solution of 2-nonanol (5.23 mL, 30.0 mmol, 1.0 equiv.) in pyridine (20 mL) was added *p*-toluenesulfonyl chloride (6.29 mL, 33.0 mmol, 1.1 equiv.) portionwise at 0 °C. After addition was complete the reaction mixture was allowed to warm to room temperature, and stirred for a further 16 h. The reaction mixture was diluted with hexanes (50 mL), filtered and the solids washed with hexanes (50 mL). The combined organics were washed with 5 M hydrochloric acid solution (3 x 40 mL), dried ($NaSO_4$) and the solvent removed *in vacuo*. The crude material was purified by column chromatography (ethyl acetate/ petroleum ether (1:19 to 1:9)) to give (±)-nonan-2-yl 4-methylbenzenesulfonate as a colourless oil (7.583 g, 25.4 mmol, 85%).

IR (thin film, ν_{max} / cm^{-1}) 2927, 2856, 1598, 1495, 1459, 1360, 1306, 1291, 1210, 1187, 1174, 1119, 1096, 1038, 1019; **^{1}H NMR** (400 MHz, $CDCl_3$) δ 7.81 – 7.77 (m, 2H, $CHCSO_3$), 7.35 – 7.30 (m, 2H, C*H*CCH_3), 4.60 (hept, *J* = 6.5 Hz, 1H, CHO), 2.44 (s, 3H, ArCH_3), 1.29 – 1.24 (m, 5H, alk CH_2 + OCHC*H*$_3$), 1.21 – 1.10 (m, 10H, alk CH_2), 0.86 (t, *J* = 7.0 Hz, 3H, CH_2CH_3); **^{13}C NMR** (101 MHz, $CDCl_3$) δ 144.3 (C=*C*O), 134.6 (C(*C*=C)C), 129.6 (*C*HCHCO), 127.7 (*C*HCO), 80.7 (CHO), 36.5 (alk CH_2), 31.6 (alk CH_2), 29.1 (alk CH_2), 29.0 (alk CH_2), 24.8 (alk CH_2), 22.6 (CH*C*H_3), 21.6 (Ar*C*H_3), 20.8 (*C*H_2CH_3), 14.0 (CH_2*C*H_3); **LRMS** (ES+) calc. for $C_{16}H_{26}O_3Na^{32}S$ $[M-H]^-$ 321.1, found 321.0.

Data consistent with literature values.[79]

(±)-S-(Nonan-2-yl) ethanethioate, 4.28

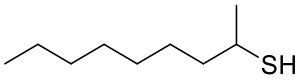


To a stirred solution of potassium thioacetate (5.71 g, 50.0 mmol, 2.5 equiv.) in dimethylformamide (20 mL) was added (±)-nonan-2-yl 4-methylbenzenesulfonate, **4.27** (5.97 g, 20.0 mmol, 1.0 equiv.) and heated to 80 °C for 2 h. The reaction mixture was allowed to cool to room temperature, brine (100 mL) added and extracted with diethyl ether (3 x 100 mL). The combined organics were washed with brine (5 x 50 mL), dried ($NaSO_4$) and the solvent removed *in vacuo*. The crude material was purified by column chromatography (diethyl ether/ pentane (1:99)) to give (±)-S-(nonan-2-yl) ethanethioate as a red oil (3.36 g, 16.6 mmol, 83%).

IR (oil, ν_{max} / cm^{-1}) 2957, 2925, 2855, 2360, 1690, 1456, 1377, 1352, 1272, 1113, 1019; **^{1}H NMR** (400 MHz, $CDCl_3$) δ 3.53 (hept, *J* = 7.0 Hz, 1H, SCH), 2.29 (s, 3H, C=OCH_3), 1.63 – 1.46 (m, 2H, CHSCH_2), 1.38 – 1.18 (m, 13H, alk CH_2 + CHCH_3), 0.93 – 0.80 (m, 3H, CH_2CH_3); **^{13}C NMR** (101 MHz, $CDCl_3$) δ 196.0 (C=O), 39.6 (CHS), 36.4 (alk CH_2), 31.8 (alk CH_2), 29.3 (alk CH_2), 29.2 (alk CH_2), 27.0 (alk CH_2), 22.6 (CSCH_3), 21.3 (CH_2CH_3), 14.1 (CH_2CH_3); **LRMS** (ES+) calc. for $C_{11}H_{22}ONa^{32}S$ $[M+Na]^+$ 255.1, found 225.2.

Data consistent with literature values.[79]

(±)-Nonane-2-thiol, 4.1b



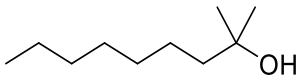
To a stirred solution of (±)-S-(nonan-2-yl) ethanethioate, **4.28** (1.914 g, 9.46 mmol, 1.0 equiv.) in diethyl ether (40 mL) was added dropwise lithium aluminium hydride solution (4.73 mL, 4.0 M in diethyl ether, 18.92 mmol, 2.0 equiv.) at 0 °C and allowed to

warm to room temperature. After 2 h, the reaction mixture was cooled to 0 °C, saturated aqueous ammonium chloride solution (20 mL) added dropwise, followed by 1 M hydrochloric acid (50 mL). The layers were separated and the aqueous extracted with diethyl ether (3 x 70 mL). The combined organics were washed sequentially with saturated aqueous sodium bicarbonate solution (50 mL) and water (50 mL), dried ($NaSO_4$) and the solvent removed *in vacuo*. The crude material was purified by column chromatography (pentane) to give (±)-nonane-2-thiol as a colourless oil (1.106 g, 6.90 mmol, 73%).

IR (thin film, ν_{max} / cm^{-1}) 2956, 2924, 2855, 2360, 2341, 2272, 1457, 1376, 1266, 1103; **^{1}H NMR** (400 MHz, $CDCl_3$) δ 2.93 (hept, *J* = 7.0 Hz, 1H, SCH), 1.60 – 1.45 (m, 3H, C*H*$_2$CHS + SH), 1.32 (d, *J* = 7.0 Hz, 3H, CHC*H*$_3$), 1.31 – 1.22 (m, 10H, alk CH_2), 0.91 – 0.85 (m, 3H, CH_2C*H*$_3$); **^{13}C NMR** (101 MHz, $CDCl_3$) δ 41.0 (CS), 35.6 (alk CH_2), 31.8 (alk CH_2), 29.3 (alk CH_2), 29.2 (alk CH_2), 27.5 (alk CH_2), 25.6 (CS*C*H_3), 22.6 (*C*H_2CH_3), 14.1 (CH_2*C*H_3); **LRMS** (ES-) calc. for $C_9H_{19}{}^{32}S$ $[M-H]^-$ 159.1, found 158.9.

Data consistent with literature values.[79]

2-Methylnonan-2-ol, 4.29

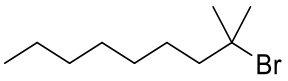


To a stirred solution of 2-nonanone (6.94 mL, 40.0 mmol, 1.0 equiv.) in diethyl ether (100 mL) was added methylmagnesium bromide (19.0 mL, 56.0 mmol, 1.4 equiv., 3.0 M in diethyl ether) slowly at room temperature and then heated to reflux. After 2 h the reaction mixture was allowed to cool to room temperature, water (50 mL) added dropwise followed by saturated ammonium chloride solution (40 mL). The phases were separated and the aqueous extracted with diethyl ether (3 x 50 mL). The combined organics were washed with sequentially with saturated sodium bicarbonate solution (50 mL) and water

(50 mL), dried ($NaSO_4$) and the solvent removed *in vacuo*. 2-Methylnonan-2-ol was obtained without further purification as a colourless oil (5.82 g, 36.8 mmol, 92%).

IR (thin film, ν_{max} / cm^{-1}) 3362, 2960, 2927, 2855, 1467, 1377, 1364, 1300, 1196, 1152, 1109, 1033; **^{1}H NMR** (400 MHz, $CDCl_3$) δ 1.74 (s, 1H, OH), 1.53 – 1.40 (m, 2H, C*H*$_2$C(CH_3)$_2$), 1.35 – 1.25 (m, 10H, alk CH_2), 1.21 (s, 6H, C(CH_3)$_2$), 0.96 – 0.82 (t, *J* = 7.0 Hz, 3H, CH_2CH_3); **^{13}C NMR** 101 MHz, $CDCl_3$) δ 71.0 (CO), 44.0 (*C*H_2C(CH_3)$_2$), 31.8 (alk CH_2), 30.1 (alk CH_2), 29.3 (alk CH_2), 29.1 (C(*C*H_3)$_2$), 24.3 (alk CH_2), 22.6 (*C*H_2CH_3), 14.0 (CH_2*C*H_3); **LRMS** (ES-) calc. for $C_{10}H_{21}O$ $[M-H]^-$ 151.2, found 151.2. Data consistent with literature values.[79]

2-Bromo-2-methylnonane, 4.30

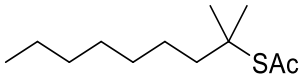


Lithium bromide (3.90 g, 45.0 mmol, 1.5 equiv.) was suspended in 2-methylnonan-2-ol, **4.29** (4.75 g, 30.0 mmol, 1.0 equiv.) and to this was added hydrobromic acid (6.74 mL, 60.0 mmol, 2.0 equiv., 48% in water) over 5 minutes. After a further 15 minutes the phases were separated, the organic diluted with diethyl ether (10 mL), extracted with ethylene glycol (3 x 50 mL) and the solvent was removed from the organic phase *in vacuo.* 2-Bromo-2-methylnonane was obtained without further purification as a colourless oil (4.31 g, 19.5 mmol, 65%).

IR (oil, ν_{max} / cm^{-1}) 3284, 2930, 1687, 1454, 1368, 1200, 1078, 1030; **^{1}H NMR** (400 MHz, $CDCl_3$) δ 1.75 (s, 6H, C(CH_3)$_2$), 1.56 – 1.43 (m, 2H, C*H*$_2$C(CH_3)$_2$), 1.33 – 1.25 (m, 10H, alk CH_2), 0.92 – 0.84 (t, *J* = 7.0 Hz, 3H, CH_2CH_3); **^{13}C NMR** (101 MHz, $CDCl_3$) δ 47.6, (*C*H_2C(CH_3)$_2$), 44.0 (*C*(CH_3)$_2$), 34.2 (C(*C*H_3)$_2$), 31.8 (alk CH_2), 29.6 (alk CH_2), 29.2 (alk CH_2), 26.3 (alk CH_2), 22.6 (alk CH_2), 14.1 (CH_2*C*H_3); **LRMS** (ES-) calc. for $C_{10}H_{21}BrCl$ $[M+Cl]^-$ 255.1, found 255.5.

Data consistent with literature values.[79]

S-(2-Methylnonan-2-yl) ethanethioate, 4.31

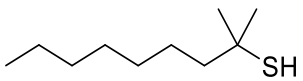


To a stirred solution of diethylzinc (20.0 mL, 20.0 mmol, 1.1 equiv., 1.0 M in hexanes) in dichloromethane (40 mL) was added dropwise thioacetic acid (3.53 mL, 40.0 mmol, 2.2 equiv.) at room temperature. After 2 h, 2-bromo-2-methylnonane, **4.30** (4.05 g, 18.3 mmol, 1.0 equiv.) was added and left for 16 h. The reaction mixture was filtered and the solids washed with dichloromethane (50 mL). The filtrate was washed sequentially with 2 M hydrochloric acid solution (30 mL) and saturated sodium bicarbonate (30 mL), then dried ($NaSO_4$) and the solvent removed *in vacuo.* The crude material was purified by column chromatography (diethyl ether/ pentane (1:99)) to give S-(2-methylnonan-2-yl) ethanethioate as a light pink oil (3.36 g, 15.5 mmol, 78%).

IR (thin film, ν_{max} / cm^{-1}) 2957, 2926, 2856, 1686, 1467, 1382, 1363, 1350, 1194, 1112, 1001; **^{1}H NMR** (400 MHz, $CDCl_3$) δ 2.22 (s, 3H, C=OCH_3), 1.71 – 1.67 (m, 2H, CH_2C$(CH_3)_2$), 1.42 (s, 6H, C$(CH_3)_2$), 1.34 – 1.22 (m, 10H, alk CH_2), 0.88 (t, *J* = 7.0 Hz, 3H, CH_2CH_3); **^{13}C NMR** (101 MHz, $CDCl_3$) δ 196.8 (C=O), 41.6 ($CH_2C(CH_3)_2$), 31.8 (alk CH_2), 31.5 ($C(CH_3)_2$), 29.9 alk CH_2), 29.2 (alk CH_2), 27.5 ($CSCH_3$), 24.7 (alk CH_2), 22.6 (CH_2CH_3), 14.1 (CH_2CH_3); **LRMS** (ES+) calc. for $C_{12}H_{24}ONa^{32}S$ $[M+Na]^+$ 239.1, found 239.4.

Data consistent with literature values.[79]

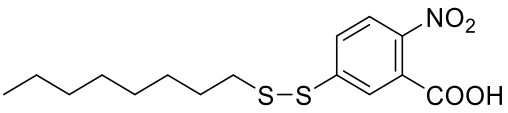
2-Methylnonane-2-thiol, 4.1c



To a stirred solution of S-(nonan-2-yl) ethanethioate, **4.31** (3.044 g, 14.07 mmol, 1.0 equiv.) in diethyl ether (100 mL) was added dropwise lithium aluminium hydride solution (7.04 mL, 4.0 M in diethyl ether, 28.14 mmol, 2.0 equiv.) at 0 °C and allowed to warm to room temperature. After 2 h, the reaction mixture was cooled to 0 °C, saturated aqueous ammonium chloride solution (40 mL) added dropwise, followed by 1 M hydrochloric acid (100 mL). The layers were separated and the aqueous extracted with diethyl ether (3 x 150 mL). The combined organics were washed sequentially with saturated aqueous sodium bicarbonate solution (100 mL) and water (100 mL), dried ($NaSO_4$) and the solvent removed *in vacuo*. The crude material was purified by column chromatography (pentane) to give 2-methylnonane-2-thiol as a colourless oil (2.218 g, 12.72 mmol, 90%).

IR (thin film, ν_{max} / cm^{-1}) 2957, 2927, 2855, 2360, 2341, 1465, 1384, 1365, 1267, 1196, 1138; **^{1}H NMR** (400 MHz, $CDCl_3$) δ 1.67 (s, 1H, SH), 1.58 – 1.52 (m, 2H, C*H*$_2$C$(CH_3)_2$), 1.46 – 1.39 (m, 2H, alk CH_2), 1.37 (s, 6H, C$(CH_3)_2$), 1.33 – 1.23 (m, 8H, alk CH_2), 0.89 (t, *J* = 7.0 Hz, 3H, CH_2CH_3); **^{13}C NMR** (101 MHz, $CDCl_3$) δ 44.6 (*C*H_2CS), 44.8 (CS), 32.8 (CS*C*H_3), 31.8 (alk CH_2), 30.0 (alk CH_2), 29.3 (alk CH_2), 25.4 (alk CH_2), 24.7 (*C*H_2CH_3), 14.1 (CH_2*C*H_3); **LRMS** (ES-) calc. for $C_{10}H_{21}{}^{32}S$ $[M-H]^-$ 173.1, found 172.9. Data consistent with literature values.[79]

2-Nitro-5-(octyldisulfaneyl)benzoic acid, 4.11a

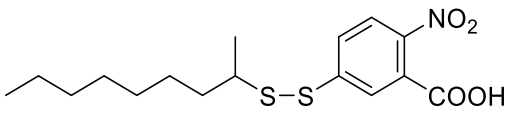


Triethylamine (702 μL, 5.04 mmol, 2.0 equiv.) was added to a suspension of 5,5′-dithiobis(2-nitrobenzoic acid), **4.2** (1.00 g, 2.52 mmol, 1.0 equiv.) in dichloromethane (10 mL) and stirred for 5 minutes. Triethylamine (351 μL, 2.52 mmol,

1.0 equiv.) was added to 1-octanethiol (437 μL, 2.52 mmol, 1.0 equiv.) in dichloromethane (10 mL) and also stirred for 5 minutes. The thiol solution was added dropwise to the disulfide solution and stirred for 1 h. 1 M Hydrochloric acid (10 mL) was added to the reaction mixture, the phases were separated and the aqueous extracted with dichloromethane (3 x 20 mL). The combined organics were dried ($NaSO_4$) and the solvent removed *in vacuo*. The crude material was purified by column chromatography (methanol/ chloroform (1:99)) to give 2-nitro-5-(octyldisulfaneyl)benzoic acid as a colourless oil (766.2 mg, 2.23 mmol, 88%).

IR (oil, ν_{max} / cm^{-1}) 2923, 2852, 1706, 1603, 1567, 1520, 1420, 1344, 1291, 1148; **^{1}H NMR** (400 MHz, DMSO-d_6) δ 7.92 (d, *J* = 8.5 Hz, 1H, $CHCNO_2$), 7.83 (d, *J* = 2.0 Hz, 1H, C*H*CCOOH), 7.77 (dd, *J* = 8.5, 2.0 Hz, 1H, C*H*$CHCNO_2$), 2.82 (t, *J* = 7.0 Hz, 2H, SCH_2CH_2), 1.59 (p, *J* = 7.0 Hz, 2H, SCH_2CH_2), 1.37 – 1.27 (m, 2H, alk CH_2), 1.27 – 1.12 (m, 8H, alk CH_2), 0.83 (t, *J* = 7.0 Hz, 3H, CH_3); **^{13}C NMR** (101 MHz, DMSO-d_6) δ 165.9 (COOH), 145.9 (CN), 143.5 (CS), 127.1 (SC*C*HCH), 125.9 (*C*HCCOOH), 124.4 (SCCH*C*H), 120.8 (*C*COOH), 38.1 (CH_2S), 31.1(alk CH_2), 28.4 (alk CH_2), 28.2 (alk CH_2), 27.6 (alk CH_2), 22.0 (CH_2CH_3), 13.9 (CH_2CH_3); **HRMS** (ES-) calc. for $C_{15}H_{20}O_4N^{32}S_2$ $[M-H]^-$ 342.0828, found 342.0834.
Data consistent with literature values.[34]

(±)-2-Nitro-5-(nonan-2-yldisulfaneyl)benzoic acid, 4.11b

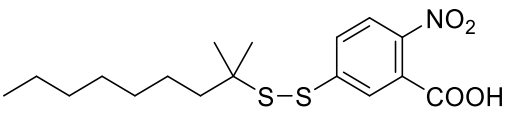


Triethylamine (348 μL, 2.50 mmol, 2.0 equiv.) was added to a suspension of 5,5′-dithiobis(2-nitrobenzoic acid), **4.2** (494.6 mg, 1.25 mmol, 1.0 equiv.) in

dichloromethane (5 mL) and stirred for 5 minutes. Triethylamine (174 μL, 1.25 mmol, 1.0 equiv.) was added to (±)-nonane-2-thiol **4.1b** (200.0 mg, 1.25 mmol, 1.0 equiv.) in dichloromethane (5 mL) and also stirred for 5 minutes. The thiol solution was added dropwise to the disulfide solution and stirred for 1 h. 1 M Hydrochloric acid (10 mL) was added to the reaction mixture, the phases were separated and the aqueous extracted with dichloromethane (3 x 10 mL). The combined organics were dried ($NaSO_4$) and the solvent removed *in vacuo*. The crude material was purified by column chromatography (acetic acid/ methanol/ dichloromethane (1:1:98 to 1:5:94)) to give (±)-2-nitro-5-(nonan-2-yldisulfaneyl)benzoic acid as a colourless oil (408.5 mg, 1.14 mmol, 91%).

IR (oil, ν_{max} / cm^{-1}) 2924, 1709, 1567, 1526, 1417, 1339, 1282, 1144; **^{1}H NMR** (400 MHz, DMSO-d_6) δ 8.02 (d, J = 8.5 Hz, 1H, $CHCNO_2$), 7.93 (d, J = 2.0 Hz, 1H, C*H*CCOOH), 7.90 (dd, J = 8.5, 2.0 Hz, 1H, C*H*CHCNO$_2$), 3.05 (hept, J = 6.5 Hz, 1H, CHS), 1.61 – 1.40 (m, 2H, C*H*$_2$CHS), 1.33 (p, J = 7.5 Hz, 2H, alk CH_2), 1.24 (d, J = 6.5 Hz, 3H, SCHC*H*$_3$), 1.22 – 1.08 (m, 8H, alk CH_2), 0.83 (t, J = 7.0 Hz, 3H, CH_2C*H*$_3$); **^{13}C NMR** (101 MHz, DMSO-d_6) δ 165.6 (COOH), 145.6 (CN), 145.0 (CS), 128.8 (*C*COOH), 128.3 (SC*C*HCH), 125.9 (*C*HCCOOH), 124.7 (SCCH*C*H), 46.8 (SCH_2), 35.2 (alk CH_2), 31.1 (alk CH_2), 28.7 (alk CH_2), 28.4 (alk CH_2), 26.3 (alk CH_2), 22.0 (*C*H_2CH$_3$), 20.3 (CS*C*H$_3$), 13.9 (CH_2*C*H$_3$); **HRMS** (ES-) calc. for $C_{16}H_{22}O_4N^{32}S_2$ $[M-H]^-$ 356.0996, found 356.0993.

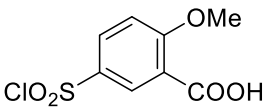
5-((2-Methylnonan-2-yl)disulfaneyl)-2-nitrobenzoic acid, 4.11c



Triethylamine (320 μL, 2.30 mmol, 2.0 equiv.) was added to a suspension of 5,5′-dithiobis(2-nitrobenzoic acid), **4.2** (454.6 mg, 1.15 mmol, 1.0 equiv.) in dichloromethane (5 mL) and stirred for 5 minutes. Triethylamine (160 μL, 1.15 mmol, 1.0 equiv.) was added to 2-methylnonane-2-thiol **4.1c** (200.0 mg, 1.15 mmol, 1.0 equiv.) in dichloromethane (5 mL) and also stirred for 5 minutes. The thiol solution was added dropwise to the disulfide solution and stirred for 1 h. 1 M Hydrochloric acid (10 mL) was added to the reaction mixture, the phases were separated and the aqueous extracted with dichloromethane (3 x 10 mL). The combined organics were dried ($NaSO_4$) and the solvent removed *in vacuo*. The crude material was purified by column chromatography (acetic acid/ methanol/ dichloromethane (1:1:98 to 1:5:94)) to give 5-((2-methylnonan-2-yl)disulfaneyl)-2-nitrobenzoic acid as a colourless oil (291.1 mg, 0.784 mmol, 68%).

IR (thin film, ν_{max} / cm^{-1}) 2957, 2928, 2855, 2651, 2360, 2341, 1712, 1602, 1567, 1528, 1465, 1418, 1364, 1341, 1284, 1144, 1131, 1103, 1054; **^{1}H NMR** (400 MHz, DMSO-d_6) δ 13.98 (s, 1H, COOH), 8.00 (d, J = 8.5 Hz, 1H, $CHCNO_2$), 7.94 (d, J = 2.0 Hz, 1H, C*H*CCOOH), 7.92 (dd, J = 8.5, 2.0 Hz, 1H, C*H*$CHCNO_2$), 1.52 – 1.45 (m, 2H, $C(CH_3)_2CH_2$), 1.29 – 1.12 (m, 14H, alk CH_2 + $C(CH_3)_2$), 1.10 – 1.01 (m, 2H, alk CH_2), 0.83 (t, J = 7.0 Hz, 3H, CH_2CH_3); **^{13}C NMR** (101 MHz, DMSO-d_6) δ 165.6 (COOH), 145.7 (CN), 145.2 (ArS), 128.7 (SC*C*HCH), 126.2 (*C*HCCOOH), 124.6 (SCCH*C*H), 120.4 (*C*COOH), 53.7 (CH_2CS), 40.5 (alk CS), 31.2 ($CSCH_3$), 29.3 (alk CH_2), 28.5 (alk CH_2), 27.1 (alk CH_2), 24.2 (alk CH_2), 22.0 (CH_2CH_3), 13.9 (CH_2CH_3); **HRMS** (ES-) calc. for $C_{17}H_{24}O_4N^{32}S_2$ $[M-H]^-$ 370.1152, found 370.1149.

5-(Chlorosulfonyl)-2-methoxybenzoic acid, 4.32

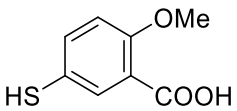


2-Methoxybenzoic acid (2.50 g, 16.4 mmol, 1.0 equiv.) was added to chlorosulfonic acid (4.92 mL, 73.8 mmol, 4.5 equiv.) portionwise over 10 minutes at 0 °C and stirred for a further 30 minutes. Then thionyl chloride (1.19 mL, 16.4 mmol, 1.0 equiv.) was added dropwise and the mixture allowed to warm to room temperature. After 3 hours the reaction mixture was poured onto ice (around 100 g) and the precipitate collected by vacuum filtration with cold 1 M hydrochloric acid washings (2 x 20 mL). Solvent was removed *in vacuo* to give 5-(chlorosulfonyl)-2-methoxybenzoic acid as a white solid (3.93 g, 15.7 mmol, 96%).

IR (solid, ν_{max} / cm^{-1}) 1710, 1670, 1373, 1170; **^{1}H NMR** (400 MHz, $CDCl_3$): δ 8.77 (m, 1H, C*H*CCOOH), 8.22 (dd, *J* = 9.0, 2.5 Hz, 1H, SCC*H*CH), 7.25 (d, *J* = 9.0 Hz, 1H, SCCHC*H*), 4.17 (s, 3H, OCH_3); **^{13}C NMR** (101 MHz, $CDCl_3$): δ 173.2 (COOH), 163.2 (ArO), 137.4 (SC*C*HCH), 133.7 (*C*HCCOOH), 133.4 (CS), 119.4 (CCOOH), 113.1 (SCCH*C*H), 57.7 (CH_3); **HRMS** (ES-) calc. for $C_8H_6O_5Cl^{32}S$ $[M-H]^-$ 248.9630, found 248.9629; **mp** (water) 147.7 °C.

Data consistent with literature values.[80]

5-Mercapto-2-methoxybenzoic acid, 4.10



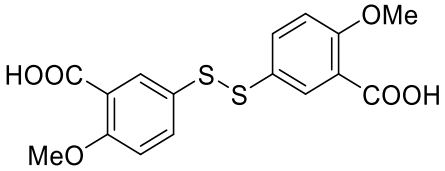
To a suspension of 5-(chlorosulfonyl)-2-methoxybenzoic acid, **4.32** (10.05 g, 40.1 mmol, 1.0 equiv.) in acetic acid (120 mL) was added a suspension of tin dichloride (54.30 g, 240.6 mol, 6.0 equiv.) in conc. hydrochloric acid (60 mL) at room temperature. The

reaction mixture was heated to 80 °C for 16 hours, allowed to cool to room temperature and solution was then poured onto ice (around 20 g) and extracted with methanol/ chloroform (1:9, 5 x 50 mL). The combined organics were washed with acidified brine (100 mL) and dried ($MgSO_4$). Solvent was removed *in vacuo* to give 5-mercapto-2-methoxybenzoic acid (6.65 g, 36.1 mmol, 91%) as a pale yellow powder without further purification.

IR (thin film, ν_{max} / cm^{-1}) 3222, 1713, 1594, 1350, 1007; **^{1}H NMR** (400 MHz, $CO(CD_3)_2$) δ 12.71, (s, 1H, COOH), 7.56 (d, *J* = 2.5 Hz, 1H, C*H*CCOOH), 7.41 (dd, *J* = 8.5, 2.5 Hz, 1H, SCC*H*CH), 7.04 (d, *J* = 9.0 Hz, 1H, SCCHC*H*), 3.77 (s, 3H, OCH_3); **^{13}C NMR** (101 MHz, $CO(CD_3)_2$): δ 165.9 (COOH), 158.0 (ArO), 136.1(SC*C*HCH), 133.9 (*C*HCCOOH), 123.2 (CS), 121.3 (CCOOH), 114.4 (SCCH*C*H), 56.9 (CH_3); **HRMS** (ES-) calc. for $C_8H_7O_3{}^{32}S$ $[M-H]^-$ 183.0121, found 183.0120.

Data consistent with literature values.[81]

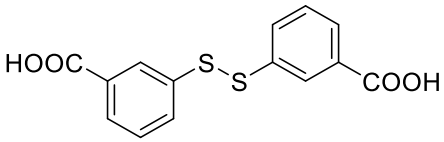
5,5'-Disulfanediylbis(2-methoxybenzoic acid), 4.4



5-Mercapto-2-methoxybenzoic acid, **4.10** (6.615 g, 35.9 mmol, 1.0 equiv.) was dissolved in DMSO (130 mL) stirring at room temperature for 18 hours. The solution was then slowly acidified with 1 M hydrochloric acid (700.0 mL) forming a white precipitate. This was filtered and washed with 1 M hydrochloric acid (2 x 20 mL). Solvent was removed *in vacuo,* then the solid was dissolved in methanol/ chloroform (1:1) at 40 °C and separation of inorganics was achieved by passing through a celite plug. Solvent was removed from the filtrate *in vacuo* to give 5,5'-disulfanediylbis(2-methoxybenzoic acid) as a white powder (6.469 g, 17.7 mmol, 98%).

IR (thin film, ν_{max} / cm^{-1}) 2829, 1688, 1590, 1277, 1248; **^{1}H NMR** (400 MHz, DMSO-d_6) δ 12.84 (s, 2H, COOH), 7.72 (d, *J* = 2.5 Hz, 2H, C*HC*COOH), 7.60 (dd, *J* = 8.5, 2.5 Hz, 1H, SCC*H*CH), 7.16 (d, *J* = 9.0 Hz, 2H, SCCHC*H*), 3.83 (s, 6H, OCH_3); **^{13}C NMR** (101 MHz, DMSO-d_6): δ 166.3 (COOH), 158.4 (ArO), 134.7 (SC*C*HCH), 132.3 (*C*HCCOOH), 126.3 (CS), 122.3 (CCOOH), 113.8 (SCCH*C*H), 56.1 (CH_3); **HRMS** (ES-) calc. for $C_{16}H_{13}O_6{}^{32}S_2$ $[M-H]^-$ 365.0159, found 365.0158.

3,3'-Disulfanediyldibenzoic acid, 4.3

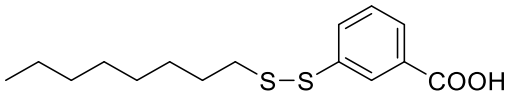


To a stirred solution of 3-mercaptobenzoic acid, **4.9** (500 mg, 3.24 mmol, 1.0 equiv.) in methanol (10 mL) was added anhydrous iron(III) chloride (788 mg, 4.86 mmol, 1.5 equiv.) slowly at room temperature. After 2 hours, the reaction mixture was poured into 1 M hydrochloric acid (30 mL) and extracted with ethyl acetate (3 x 50 mL). The combined organics were washed with 1 M hydrochloric acid (4x 50 mL), dried ($NaSO_4$) and the solvent removed *in vacuo*. 3,3'-Disulfanediyldibenzoic acid was obtained as a white solid (396.8 mg, 1.30 mmol, 80 %).

IR (solid, ν_{max} / cm^{-1}) 2924, 2545, 2161, 1977, 1679, 1569, 1437, 1409, 1292, 1259; **^{1}H NMR** (400 MHz, DMSO-d_6) δ 13.19 (s, 2H, COOH), 8.06 (t, *J* = 2.0 Hz, 2H, SCC*H*CCOOH), 7.85 (dt, *J* = 7.5, 1.5 Hz, 2H, CHC*H*CCOOH), 7.78 (ddd, *J* = 8.0, 2.0, 1.0 Hz, 2H, SCC*H*CH), 7.53 (t, *J* = 8.0 Hz, 2H, CHC*H*CH); **^{13}C NMR** (101 MHz, DMSO-d_6) δ 167.2 (C=O), 136.5 (CS), 133.4 (*quat* C), 131.3 (SCC*H*CH), 130.1 (CHC*H*CH), 128.9 (SC*C*HCCOOH), 127.9 (CH*C*HCCOOH); **LRMS** (ES-) calc. for $C_{14}H_9O_4{}^{32}S_2$ $[M-H]^-$ 305.0, found 305.4.

Data consistent with literature values.[82]

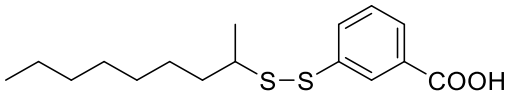
3-(Octyldisulfaneyl)benzoic acid, 4.12a



Triethylamine (90.9 μL, 0.652 mmol, 2.0 equiv.) was added to a suspension of 3,3'-disulfanediyldibenzoic acid, **4.3** (100.0 mg, 0.326 mmol, 1.0 equiv.) in dichloromethane (2 mL) and stirred for 5 minutes. Triethylamine (45.4 μL, 0.326 mmol, 1.0 equiv.) was added to 1-octanethiol (56.5 μL, 0.326 mmol, 1.0 equiv.) in dichloromethane (1 mL) and also stirred for 5 minutes. The thiol solution was added dropwise to the disulfide solution and stirred for 1 h. 1 M Hydrochloric acid (5 mL) was added to the reaction mixture, the phases were separated and the aqueous extracted with dichloromethane (3 x 10 mL). The combined organics were dried ($NaSO_4$) and the solvent removed *in vacuo*. The crude material was purified by column chromatography (methanol/ chloroform (1:99)) to give 3-(octyldisulfaneyl)benzoic acid as a colourless oil (68.0 mg, 0.228 mmol, 70%).

IR (oil, ν_{max} / cm^{-1}) 2920, 2849, 1683, 1572, 1434, 1312, 1262, 1140; **^{1}H NMR** (400 MHz, DMSO-d_6) δ 13.17 (s, 1H, COOH), 8.10 (t, *J* = 2.0 Hz, 1H, SCC*H*CCOOH), 7.82 (dt, *J* = 7.5, 1.5 Hz, 1H, CHC*H*CCOOH), 7.76 (ddd, *J* = 8.0, 2.0, 1.0 Hz, 1H, SCC*H*CH), 7.51 (t, *J* = 8.0 Hz, 1H, CHC*H*CH), 2.80 (t, *J* = 7.0 Hz, 2H, CH_2S), 1.58 (p, *J* = 7.0 Hz, 2H, C*H*$_2$$CH_2S$), 1.36 – 1.12 (m, 10H, alk CH_2), 0.83 (t, *J* = 7.0 Hz, 3H, CH_3); **^{13}C NMR** (101 MHz, DMSO-d_6) δ 166.6 (C=O), 137.6 (CS), 131.9 (*quat* C), 131.0 (SCC*H*CH), 129.5 (CHC*H*CH), 127.7 (SC*C*HCCOOH), 127.1 (CH*C*HCCOOH), 38.3 (CH_2S), 31.1 (alk CH_2), 28.4 (alk CH_2), 28.4 (alk CH_2), 28.1 (alk CH_2), 27.5 (alk CH_2), 22.0 (*C*H_2CH_3), 13.9 (CH_2*C*H_3); **HRMS** (ES-) calc. for $C_{15}H_{21}O_2{}^{32}S_2$ $[M-H]^-$ 297.0988, found 297.0985.

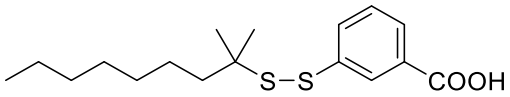
(±)-3-(Nonan-2-yldisulfaneyl)benzoic acid, 4.12b



Triethylamine (90.9 μL, 0.652 mmol, 2.0 equiv.) was added to a suspension of 3,3'-disulfanediyldibenzoic acid, **4.3** (100.0 mg, 0.326 mmol, 1.0 equiv.) in dichloromethane (2 mL) and stirred for 5 minutes. Triethylamine (45.4 μL, 0.326 mmol, 1.0 equiv.) was added to (±)-nonane-2-thiol, **4.1b** (52.3 mg, 0.326 mmol, 1.0 equiv.) in dichloromethane (1 mL) and also stirred for 5 minutes. The thiol solution was added dropwise to the disulfide solution and stirred for 1 h. 1 M Hydrochloric acid (5 mL) was added to the reaction mixture, the phases were separated and the aqueous extracted with dichloromethane (3 x 10 mL). The combined organics were dried ($NaSO_4$) and the solvent removed *in vacuo*. The crude material was purified by column chromatography (methanol/ chloroform (1:99)) to give (±)-3-(nonan-2-yldisulfaneyl)benzoic acid as a colourless oil (56.9 mg, 0.183 mmol, 56%).

IR (oil, ν_{max} / cm^{-1}) 2924, 2854, 1692, 1591, 1572, 1431, 1407, 1375, 1285, 1261, 1138, 1071; **^{1}H NMR** (400 MHz, DMSO-d_6) δ 13.14 (s, 1H, COOH), 8.12 (t, *J* = 2.0 Hz, 1H, SCC*H*CCOOH), 7.80 (dt, *J* = 7.5, 1.5 Hz, 1H, CHC*H*CCOOH), 7.76 (ddd, *J* = 8.0, 2.0, 1.0 Hz, 1H, SCC*H*CH), 7.49 (t, *J* = 8.0 Hz, 1H, CHC*H*CH), 2.97 (hept, *J* = 6.5 Hz, 1H, CHS), 1.59 – 1.44 (m, 1H, CH*H*CHS), 1.43 – 1.38 (m, 1H, C*H*HCHS), 1.33 – 1.04 (m, 13H, alk CH_2 + SCHCH_3), 0.83 (t, *J* = 7.0 Hz, 3H, CH_2CH_3); **^{13}C NMR** (101 MHz, DMSO-d_6) δ 166.6 (C=O), 138.1 (ArS), 131.8 (*quat* C), 131.0 (SCC*H*CH), 129.4 (CHC*H*CH), 127.6 (SC*C*HCCOOH), 127.2 (CH*C*HCCOOH), 46.6 (alk CS), 35.1 (alk CH_2), 31.1 (alk CH_2), 28.7 (alk CH_2), 28.4 (alk CH_2), 26.2 (alk CH_2), 22.0 (CH_2CH_3), 20.4 (CSCH_3), 13.9 (CH_2CH_3); **HRMS** (ES-) calc. for $C_{16}H_{23}O_2{}^{32}S_2$ $[M-H]^-$ 311.1145, found 311.1142.

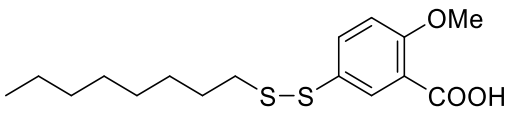
3-((2-Methylnonan-2-yl)disulfaneyl)benzoic acid, 4.12c



Triethylamine (90.9 μL, 0.652 mmol, 2.0 equiv.) was added to a suspension of 3,3'-disulfanediyldibenzoic acid, **4.3** (100.0 mg, 0.326 mmol, 1.0 equiv.) in dichloromethane (2 mL) and stirred for 5 minutes. Triethylamine (45.4 μL, 0.326 mmol, 1.0 equiv.) was added to 2-methylnonane-2-thiol, **4.1c** (56.8 mg, 0.326 mmol, 1.0 equiv.) in dichloromethane (1 mL) and also stirred for 5 minutes. The thiol solution was added dropwise to the disulfide solution and stirred for 1 h. 1 M hydrochloric acid (5 mL) was added to the reaction mixture, the phases were separated and the aqueous extracted with dichloromethane (3 x 10 mL). The combined organics were dried ($NaSO_4$) and the solvent removed *in vacuo*. The crude material was purified by column chromatography (methanol/ chloroform (1:99)) to give 3-((2-methylnonan-2-yl)disulfaneyl)benzoic acid as a colourless oil (24.8 mg, 0.076 mmol, 23%).

IR (oil, ν_{max} / cm^{-1}) 2956, 2927, 2855, 1692, 1591, 1465, 1430, 1407, 1382, 1363, 1285, 1261, 1135, 1104, 1071; **^{1}H NMR** (400 MHz, DMSO-d_6) δ 13.15 (s, 1H, COOH), 8.13 (t, *J* = 2.0 Hz, 1H, SCC*H*CCOOH), 7.82 – 7.76 (m, 2H, CHC*H*CCOOH + SCC*H*CH), 7.48 (t, *J* = 8.0 Hz, 1H, CHC*H*CH), 1.47 – 1.39 (m, 2H, $C(CH_3)_2CH_2$), 1.29 – 1.04 (m, 14H, alk CH_2 + $C(CH_3)_2$), 1.00 – 0.89 (m, 2H, alk CH_2), 0.82 (t, *J* = 7.0 Hz, 3H, CH_2CH_3); **^{13}C NMR** (101 MHz, DMSO-d_6) δ 166.6 (C=O), 138.4 (ArS), 131.7 (Ar *quat* C), 131.2 (SCC*H*CH), 129.2 (CHC*H*CH), 127.6 (CH*C*HCCOOH or SC*C*HCCOOH), 127.6 (CH*C*HCCOOH or SC*C*HCCOOH), 52.9 (CH_2CS), 40.5 (alk CS), 31.2 (CSCH_3), 29.2 (alk CH_2), 28.5 (alk CH_2), 27.2 (alk CH_2), 24.2 (alk CH_2), 22.0 (CH_2CH_3), 13.9 (CH_2CH_3); **HRMS** (ES-) calc. for $C_{17}H_{25}O_2{}^{32}S_2$ $[M-H]^-$ 325.1290, found 325.1299.

2-Methoxy-5-(octyldisulfaneyl)benzoic acid, 4.13a

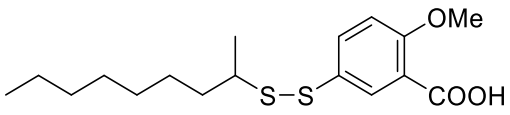


1-Octanethiol (1.38 mL, 8.00 mmol, 8.0 equiv.) was layered onto a solution of 5,5'-disulfanediylbis(2-methoxybenzoic acid), **4.4** (366.4 mg, 1.00 mmol, 1.0 equiv.) in HEPES buffer (40.0 mL, pH 8.00, 0.25 M) stirred at 100 rpm. After 22 hours, the reaction mixture was acidified with 1 M hydrochloric acid (20.0 mL) and extracted with methanol/ chloroform (1:9, 5 x 50 mL), the combined organics washed with acidified brine (100 mL) and dried ($MgSO_4$). Solvent was removed *in vacuo* to give a crude yellow oil. The crude material was purified by column chromatography (methanol/ chloroform (0:100 to 3:97)) to yield a small crop of pure 2-methoxy-5-(octyldisulfaneyl)benzoic acid (37.5 mg). Combined impure fractions were dried before dissolution in DMSO (2.0 mL) and stired for 4 hours. This solution was then acidified with 1M hydrochloric acid (5 mL), extracted with chloroform (3 x 10 mL) and the combined organics washed with 1M hydrochloric acid (5 mL), dried ($MgSO_4$) and filtered through celite. Solvent was removed *in vacuo* and the resultant oil purified by preparative TLC (methanol/ chloroform (3:97)). The two crops were combined to give 2-methoxy-5-(octyldisulfaneyl)benzoic acid a clear yellow oil (188.1 mg, 0.69 mmol, 69%). Yield assumes no reoxidation of 5-mercapto-2-methoxybenzoic acid to starting material.

IR (oil, ν_{max} / cm^{-1}) 2924, 1735, 1694, 1405, 1273; **^{1}H NMR** (400 MHz, DMSO-d_6): δ 7.77 (d, *J* = 2.5 Hz, 1H, SCC*H*CCOOH), 7.65 (dd, *J* = 8.5, 2.5 Hz, 1H, CHC*H*CCOOH), 7.15 (d, *J* = 8.5 Hz, 1H, SCC*H*CH), 3.82 (s, 3H, OCH_3), 2.76 (t, *J* = 7.0 Hz, 2H, CH_2S), 1.59 (p, *J* = 7.0 Hz, 2H, C*H*$_2$$CH_2S$), 1.36 – 1.12 (m, 10H, alk CH_2), 0.84 (t, *J* = 7.0 Hz, 3H, CH_2CH_3); **^{13}C NMR** (101 MHz, DMSO-d_6): δ 166.6 (COOH), 157.9 (ArO), 134.1

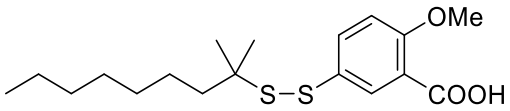
(SC*C*HCH), 131.6 (*C*HCCOOH), 127.2 (ArS), 122.4 (*C*COOH), 113.6 (SCCH*C*H), 56.0 (OCH_3), 38.1 (CH_2S), 31.2 (alk CH_2), 28.5 (alk CH_2), 28.5 (alk CH_2), 28.1 (alk CH_2), 27.6 (alk CH_2), 22.1 (*C*H_2CH_3), 14.0 (CH_2*C*H_3); **HRMS** (ES-) calc. for $C_{16}H_{23}O_3{}^{32}S_2$ $[M-H]^-$ 327.1094, found 327.1097.

(±)-2-Methoxy-5-(nonan-2-yldisulfaneyl)benzoic acid, 4.13b



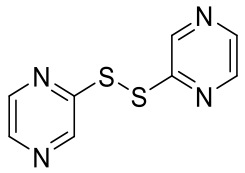
This was prepared analogously to 2-methoxy-5-(octyldisulfaneyl)benzoic acid, **4.13a**, using (±)-nonane-2-thiol, **4.1b** (0.38 mL, 2.00 mmol, 2.0 equiv.) and 5,5'-disulfanediylbis(2-methoxybenzoic acid), **4.4** (366.4 mg, 1.00 mmol, 1.0 equiv.), with a reaction time of 52 hours and stir rate of 500 rpm. The crude material was purified by preparative TLC (methanol/ chloroform (1:24)). (±)-2-Methoxy-5-(nonan-2-yldisulfaneyl)benzoic acid was obtained as a yellow oil (340.8 mg, 0.99 mmol, 99%). Yield assumes no reoxidation of 5-mercapto-2-methoxybenzoic acid to starting material. **IR** (oil, ν_{max} / cm^{-1}) 2925, 1736, 1693, 1406, 1274, 1241; **^{1}H NMR** (400 MHz, DMSO-d_6): δ 7.80 (d, *J* = 2.5 Hz, 1H, C*HC*COOH), 7.67 (dd, *J* = 8.5, 2.5 Hz, 1H, SCC*H*CH), 7.14 (d, *J* = 9.0 Hz, 1H, SCCHC*H*), 3.81 (s, 3H, OCH_3), 2.92 (hept, *J* = 6.5 Hz, 1H, CHS), 1.61 – 1.35 (m, 2H, C*H*$_2$CHS), 1.32 – 1.03 (m, 13H, alk CH_2 + SCHC*H*$_3$), 0.83 (t, *J* = 7.0 Hz, 3H, CH_2C*H*$_3$); **^{13}C NMR** (101 MHz, DMSO-d_6): δ 166.5 (COOH), 157.8 (ArO), 133.8 (SC*C*HCH), 131.4 (*C*HCCOOH), 127.7 (ArS), 122.0 (*C*COOH), 113.5 (SCCH*C*H), 56.0 (OCH_3), 46.4 (HCS), 35.1 (alk CH_2), 31.2 (alk CH_2), 28.7 (alk CH_2), 28.5 (alk CH_2), 26.3 (alk CH_2), 22.0 (CS*C*H_3), 20.5 (*C*H_2CH_3), 13.9 (CH_2*C*H_3); **HRMS** (ES+) calc. for $C_{17}H_{27}O_3{}^{32}S_2$ $[M+H]^+$ 343.1396, found 343.1397.

2-Methoxy-5-((2-methylnonan-2-yl)disulfaneyl)benzoic acid , 4.13c



This was prepared analogously to 2-methoxy-5-(octyldisulfaneyl)benzoic acid, **4.13a**, using 2-methylnonane-2-thiol, **4.1c** (0.38 mL, 2.00 mmol, 2.0 equiv.) and 5,5'-disulfanediylbis(2-methoxybenzoic acid), **4.4** (366.4 mg, 1.00 mmol, 1.0 equiv.), with a reaction time of 71 hours and stir rate of 500 rpm. The crude material was purified by preparative TLC (methanol/ chloroform (1:24)). 2-Methoxy-5-((2-methylnonan-2-yl)disulfaneyl)benzoic acid was obtained as a yellow oil (251.1 mg, 0.70 mmol, 70%). Yield assumes no reoxidation of 5-mercapto-2-methoxybenzoic acid to starting material. **IR** (oil, ν_{max} / cm^{-1}) 2928, 1737, 1693, 1274, 1241; **^{1}H NMR** (400 MHz, DMSO-d_6): δ 7.81 (d, *J* = 2.5 Hz, 1H, C*H*CCOOH), 7.68 (dd, *J* = 9.0, 2.5 Hz, 1H, SCC*H*CH), 7.13 (d, *J* = 9.0 Hz, 1H, SCCHC*H*), 3.81 (s, 3H, OCH_3), 1.47 – 1.38 (m, 2H, $C(CH_3)_2CH_2$), 1.26 – 0.91 (m, 16H, alk CH_2 + $C(CH_3)_2$), 0.83 (t, *J* = 7.0, 3H, CH_2CH_3); **^{13}C NMR** (101 MHz, DMSO-d_6): δ 166.4 (COOH), 157.8 (ArO), 133.8 (SC*C*HCH), 131.4 (*C*HCCOOH), 128.0 (ArS), 121.8 (*C*COOH), 113.4 (SCCH*C*H),); 56.0 (OCH_3), 52.6 (CH_2CS), 40.5 (CH_2*C*S), 31.2 (CS*C*H_3), 29.3 (alk CH_2), 28.6 (alk CH_2), 27.4 (alk CH_2), 24.3 (alk CH_2), 22.0 (*C*H_2CH_3), 13.9 (CH_2*C*H_3); **HRMS** (ES+) calc. for $C_{18}H_{29}O_3{}^{32}S_2$ $[M+H]^+$ 357.1553, found 357.1554.

1,2-Di(pyrazin-2-yl)disulfane, 4.33

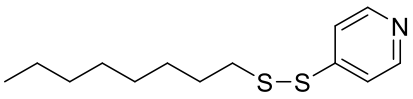


To a solution of iodine (1.30 g, 5.12 mmol, 1.2 equiv.) and potassium iodide (2.50 g, 15.05 mmol, 3.6 equiv.) in water (10 mL) was added dropwise to a solution of 2-mercaptopyrazine (527.0 mg, 4.21 mmol, 1.0 equiv.) in 2 M sodium hydroxide solution (5 mL), then cooled to 4 °C for 2 h. The precipitate was filtered and washed with cold water (2 x 10 mL). 1,2-Di(pyrazin-2-yl)disulfane was obtained as a white amorphous solid (156.6 mg, 0.705 mmol, 17%).

IR (solid, ν_{max} / cm^{-1}) 1505, 1455, 1389, 1290, 1116, 1043, 1005; **^{1}H NMR** (400 MHz, DMSO-d_6) δ 8.91 (d, J = 1.5 Hz, 2H, CHCS), 8.57 – 8.50 (m, 4H, SCNCHCH + SCNCHCH); **^{13}C NMR** (101 MHz, DMSO-d_6) δ 154.6 (CS), 144.9 (CHCS), 143.0 (SCNCHCH or SCNCHCH), 142.9 (SCNCHCH or SCNCHCH); **LRMS** (ES+) calc. for $C_8H_6N_4Na^{32}S_2$ $[M+Na]^+$ 245.0, found 245.7, **mp** (water) 57.3 °C.

Data consistent with literature values.[83]

4-(Octyldisulfaneyl)pyridine, 4.14

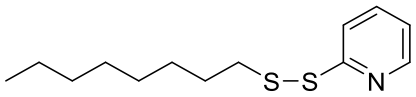


To a stirred solution of 4,4′-dipyridyl disulfide, **4.15** (200.0 mg, 0.908 mmol, 1.0 equiv.) in methanol (5 mL) was added 1-octanethiol (157.6 µL, 0.908 mmol, 1.0 equiv.). After 2 h the solvent removed *in vacuo*, and the crude material was purified by column chromatography (ethyl acetate/ petroleum ether (1:9)) to give 4-(octyldisulfaneyl)pyridine as a colourless oil (128.8 mg, 0.504 mmol, 56%).

IR (oil, ν_{max} / cm^{-1}) 1567, 1478, 1454, 1396, 1348, 1327, 1221, 1038; **^{1}H NMR** (400 MHz, $CDCl_3$) δ 8.49 – 8.43 (m, 2H, CHN), 7.46 – 7.41 (m, 2H, C*H*CHN), 2.73 (t, J = 7.5 Hz, 2H, CH_2S), 1.72 – 1.58 (m, 2H, CH_2CH_2S), 1.45 – 1.33 (m, 2H, C$H_2CH_2CH_2S$), 1.32 – 1.17 (m, 8H, alkyl CH_2), 0.93 – 0.78 (m, 3H, CH_2CH_3); **^{13}C NMR**

(101 MHz, $CDCl_3$) δ 149.4 (CHN), 148.9 (ArS), 119.8 (*C*HCHN), 38.5 (CH_2S), 30.9 (alk CH_2), 29.1 (alk CH_2), 29.0 (alk CH_2), 28.9 (alk CH_2), 27.4 (alk CH_2), 21.9 (*C*H_2CH_3), 14.2 (CH_3); **HRMS** (ES+) calc. for $C_{13}H_{22}N^{32}S_2$ $[M+H]^+$ 256.1188, found 256.1190.

2-(Octyldisulfaneyl)pyridine, 4.16

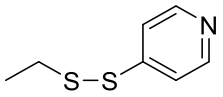


To a stirred solution of 2,2′-dipyridyl disulfide (200.0 mg, 0.908 mmol, 1.0 equiv.) in methanol (5 mL) was added 1-octanethiol (157.6 µL, 0.908 mmol, 1.0 equiv.). After 2 h the solvent removed *in vacuo*, and the crude material was purified by column chromatography (ethyl acetate/ petroleum ether (1:19)) to give 2-(octyldisulfaneyl)pyridine as a colourless oil (153.3 mg, 0.600 mmol, 66%).

IR (oil, ν_{max} / cm^{-1}) 2924, 2853, 1573, 1445, 1416, 1117, 1082, 1043; **^{1}H NMR** (400 MHz, $CDCl_3$) δ 8.45 (ddd, *J* = 5.0, 2.0, 1.0 Hz, 1H, CHCHCHC*H*N), 7.73 (dt, *J* = 8.0, 1.0 Hz, 1H, C*H*CHCHCHN), 7.66 – 7.60 (m, 1H, CHC*H*CHCHN), 7.07 (ddd, *J* = 7.5, 5.0, 1.0 Hz, 1H, CHCHC*H*CHN), 2.80 (t, *J* = 7.0 Hz, 2H, CH_2S), 1.74 – 1.61 (m, 2H, C*H*$_2$$CH_2S$), 1.45 – 1.33 (m, 2H, C*H*$_2$$CH_2CH_2S$), 1.32 – 1.18 (m, 8H, alk CH_2), 0.88 (t, *J* = 7.0 Hz, 3H, CH_3); **^{13}C NMR** (101 MHz, $CDCl_3$) δ 160.7 (CNS), 149.5 (CHN), 136.9 (*C*HCHCNS), 120.4 (*C*HCNS or *C*HCHN), 119.5 (*C*HCNS or *C*HCHN), 39.0 (CH_2S), 31.7 (alk CH_2), 29.1 (alk CH_2 + alk CH_2), 28.9 (alk CH_2), 28.5 (alk CH_2), 22.6 (*C*H_2CH_3), 14.0 (CH_3); **LRMS** (ES+) calc. for $C_{13}H_{21}NNa^{32}S_2$ $[M+Na]^+$ 278.1, found 278.0.

Data consistent with literature values.[84]

4-(Ethyldisulfaneyl)pyridine, 4.34

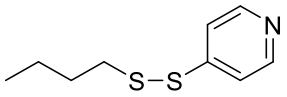


To a stirred solution of 4,4′-dipyridyl disulfide, **4.15** (200.0 mg, 0.908 mmol, 1.0 equiv.) in methanol (5 mL) was added ethanethiol (67.2 µL, 0.908 mmol, 1.0 equiv.). After 2 h the solvent removed *in vacuo*, and the crude material was purified by column chromatography (ethyl acetate/ petroleum ether (3:7)) to give 4-(ethyldisulfaneyl)pyridine as a colourless oil (64.4 mg, 0.376 mmol, 41%).

IR (thin film, ν_{max} / cm^{-1}) 3030, 2974, 2926, 1568, 1543, 1477, 1448, 1403, 1374, 1314, 1253, 1213, 1092, 1062; **^{1}H NMR** (400 MHz, $CDCl_3$) δ 8.47 – 8.43 (m, 2H, CHN), 7.48 – 7.41 (m, 2H, C*H*CHN), 2.75 (q, *J* = 7.5 Hz, 2H, C*H*$_2$CH$_3$), 1.30 (t, *J* = 7.5 Hz, 3H, CH_3); **^{13}C NMR** (101 MHz, $CDCl_3$) δ 149.5 (CHN), 149.2 (ArCS), 120.0 (*C*HCHN), 32.7 (CH_2S), 14.2 (CH_3); **HRMS** (ES+) calc. for $C_7H_{10}N^{32}S_2$ $[M+H]^+$ 172.0249, found 172.0252.

Compound previously reported without characterization data.[85]

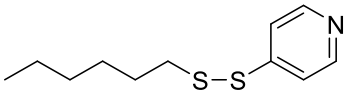
4-(Butyldisulfaneyl)pyridine, 4.35



To a stirred solution of 4,4′-dipyridyl disulfide, **4.15** (200.0 mg, 0.908 mmol, 1.0 equiv.) in methanol (5 mL) was added 1-butanethiol (97.0 µL, 0.908 mmol, 1.0 equiv.). After 2 h the solvent removed *in vacuo*, and the crude material was purified by column chromatography (ethyl acetate/ petroleum ether (1:4)) to give 4-(butyldisulfaneyl)pyridine as a colourless oil (42.4 mg, 0.213 mmol, 23%).

IR (thin film, ν_{max} / cm^{-1}) 2956, 2928, 2870, 1568, 1543, 1476, 1463, 1403, 1314, 1273, 1215, 1091, 1063; **^{1}H NMR** (400 MHz, $CDCl_3$) δ 8.50 – 8.43 (br s, 2H, CHN), 7.46 – 7.41 (m, 2H, C*H*CHN), 2.73 (t, *J* = 7.5 Hz, 2H, CH_2S), 1.63 (p, *J* = 7.5 Hz, 2H, CH_2CH_2S), 1.40 (sext, *J* = 7.5 Hz, 2H, CH_2CH_3), 0.88 (t, *J* = 7.5 Hz, 3H, CH_3); **^{13}C NMR** (101 MHz, $CDCl_3$) δ 149.7 (CHN), 149.3 (ArCS), 120.0 (*C*HCHN), 38.9 (CH_2S), 31.0 (*C*H_2CH_2S), 21.6 (*C*H_2CH_3), 13.6 (CH_3); **HRMS** (ES+) calc. for $C_9H_{14}N^{32}S_2$ $[M+H]^+$ 200.0562, found 200.0565.

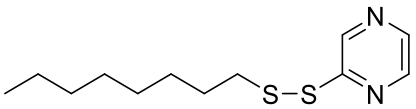
4-(Hexyldisulfaneyl)pyridine, 4.36



To a stirred solution of 4,4′-dipyridyl disulfide, **4.15** (200.0 mg, 0.908 mmol, 1.0 equiv.) in methanol (5 mL) was added 1-hexanethiol (129 µL, 0.908 mmol, 1.0 equiv.). After 2 h the solvent removed *in vacuo*, and the crude material was purified by column chromatography (ethyl acetate/ petroleum ether (1:4)) to give 4-(hexyldisulfaneyl)pyridine as a colourless oil (91.3 mg, 0.402 mmol, 44%).

IR (thin film, ν_{max} / cm^{-1}) 2960, 2925, 1565, 1544, 1482, 1455, 1400, 1354, 1327, 1221, 1058; **^{1}H NMR** (400 MHz, $CDCl_3$) δ 8.46 (d, *J* = 5.5 Hz, 2H, CHN), 7.45 – 7.41 (m, 2H, C*H*CHN), 2.73 (t, *J* = 7.5 Hz, 2H, CH_2S), 1.65 (p, *J* = 7.5 Hz, 2H, CH_2CH_2S), 1.43 – 1.33 (m, 2H, alk CH_2), 1.32 – 1.19 (m, 4H, alkyl CH_2), 0.87 (t, *J* = 7.0 Hz, 3H, CH_3); **^{13}C NMR** (101 MHz, $CDCl_3$) δ 149.4 (CHN), 149.2 (ArCS), 119.9 (*C*HCHN), 38.9 (CH_2S), 31.3 (*C*H_2CH_2S), 28.9 (alk CH_2), 28.1 (alk CH_2), 22.4 (*C*H_2CH_3), 13.9 (CH_3); **HRMS** (ES+) calc. for $C_{11}H_{18}N^{32}S_2$ $[M+H]^+$ 228.0875, found 228.0881.

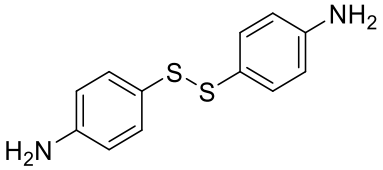
2-(Octyldisulfaneyl)pyrazine, 4.17



To a stirred solution of 1,2-di(pyrazin-2-yl)disulfane, **4.33** (100.0 mg, 0.450 mmol, 1.0 equiv.) in methanol (5 mL) was added 1-octanethiol (78.0 µL, 0.450 mmol, 1.0 equiv.). After 16 h the solvent removed *in vacuo*, and the crude material was purified by column chromatography (pure dichloromethane) to give 2-(octyldisulfaneyl)pyrazine as a colourless oil (82.5 mg, 0.322 mmol, 72%).

IR (thin film, ν_{max} / cm^{-1}) 1557, 1543, 1520, 1479, 1449, 1333, 1267, 1211, 1054; **^{1}H NMR** (400 MHz, $CDCl_3$) δ 8.89 (d, *J* = 1.5 Hz, 1H, SCCHN), 8.42 (dd, *J* = 2.5, 1.5 Hz, 1H, C*H*CHNCS), 8.35 (d, *J* = 2.5 Hz, 1H, CHC*H*NCS), 2.85 (t, *J* = 7.5 Hz, 2H, CH_2S), 1.44 – 1.34 (m, 2H, C*H*$_2$$CH_2S$), 1.31 – 1.21 (m, 10H, alkyl CH_2), 0.93 – 0.83 (m, 3H, CH_3); **^{13}C NMR** (101 MHz, $CDCl_3$) δ 154.2 (CS), 143.6 (CHCS), 143.0 (SCNCHCH or SCNCHCH), 142.8 (SCNCHCH or SCNCHCH), 39.2 (CH_2S), 31.5 (alk CH_2), 29.2 (alk CH_2), 28.9 (alk CH_2), 28.9 (alk CH_2), 28.3 (alk CH_2), 22.7 (*C*H_2CH_3), 13.9 (CH_3); **HRMS** (ES+) calc. for $C_{12}H_{21}N_2{}^{32}S_2$ $[M+H]^+$ 257.1141, found 257.1147.

4,4'-Disulfanediyldianiline, 4.37



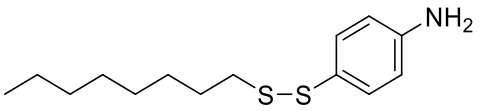
To a stirred solution of 4-aminothiophenol (1.837 g, 14.7 mmol, 1.0 equiv.) in a tetrahydrofuran (25 mL) and water (25 mL) was added hydrogen peroxide (832 µL, 50% aqueous solution, 14.7 mmol, 1.0 equiv.) dropwise at room temperature. After a further 3 hours, the reaction mixture was extracted with diethyl ether (3 x 50 mL), the combined organics washed with brine (50 mL), dried ($NaSO_4$) and solvent removed *in vacuo.* The

crude material was purified by column chromatography (methanol / dichloromethane (0:100 to 1:49)) to give 4,4'-disulfanediyldianiline as a yellow solid (638.1 mg, 2.60 mmol, 35%).

IR (solid, ν_{max} / cm^{-1}) 3441, 3357, 1657, 1632, 1602, 1553, 1528, 1119, 1039; **^{1}H NMR** (400 MHz, $CDCl_3$) δ 7.23 (d, 4H, *J* = 8.0 Hz, CHCS), 6.55 (d, 4H, *J* = 8.0 Hz, CHCN), 3.66 (s, 4H, NH_2); **^{13}C NMR** (101 MHz, $CDCl_3$) δ 147.7 (CN), 134.2 (CS), 124.6 (*C*HCS), 115.3 (*C*HCN); **LRMS** (ES+) calc. for $C_{12}H_{13}N_2{}^{32}S_2$ $[M+H]^+$ 249.1, found 249.3.

Data consistent with literature values.[86]

4-(Octyldisulfaneyl)aniline, 4.18

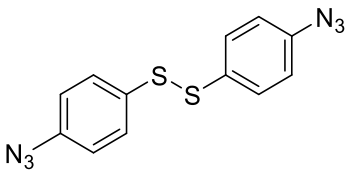


To a stirred solution of triethylamine (112 μL, 0.805 mmol, 1.0 equiv.) was added to 1-octanethiol (139.7 μL, 0.805 mmol, 1.0 equiv.) in dichloromethane (5 mL) was added 4,4'-disulfanediyldianilin**e**, **4.37** (200 mg, 0.805 mmol, 1.0 equiv.) at room temperature. After 16 hours, the solvent removed *in vacuo.* The crude material was purified by column chromatography (pure dichloromethane) to give 4-(octyldisulfaneyl)aniline as a colourless oil (147.6 mg, 0.547 mmol, 68%).

IR (thin film, ν_{max} / cm^{-1}) 3360, 2933, 1662, 1629, 1604, 1527, 1378, 1157, 1038; **^{1}H NMR** (400 MHz, $CDCl_3$) δ 7.21 (d, 2H, *J* = 8.0 Hz, CHCS), 6.50 (d, 2H, *J* = 8.0 Hz, CHCN), 3.92 (s, 2H, NH_2), 2.64 (t, *J* = 7.5 Hz, 2H, CH_2S), 1.47 – 1.38 (m, 2H, C*H*$_2$$CH_2S$), 1.29 – 1.19 (m, 10H, alkyl CH_2), 0.89 (t, *J* = 7.0 Hz, 3H, CH_3); **^{13}C NMR** (101 MHz, $CDCl_3$) δ 151.2 (CN), 134.7 (CS), 127.5 (*C*HCS), 116.2 (*C*HCN), 38.0 (CH_2S), 31.4 (alk CH_2), 28.7 (alk CH_2), 28.5 (alk CH_2), 28.0 (alk CH_2), 27.7 (alk CH_2),

22.1 (CH_2CH_3), 13.9 (CH_2CH_3); **HRMS** (ES+) calc. for $C_{14}H_{24}N^{32}S_2$ $[M+H]^+$ 270.1345, found 270.1353.

1,2-Bis(4-azidophenyl)disulfane, 4.38

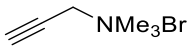


To a stirred solution of 4-aminothiophenol (2.25 g, 18.0 mmol, 1.0 equiv.) in acetonitrile (30 mL) at 0 °C was added concentrated hydrochloric acid (6.9 mL, 126 mmol, 13 equiv.) was added a solution of sodium nitrite (2.11 g, 30.55 mmol, 1.7 equiv.) in water (30 mL) dropwise, over a period of around 15 minutes. After a further 15 minutes, a solution of sodium azide (4.67 g, 71.9 mmol, 4.0 equiv.) in water (40 mL) was added, allowed to warm to room temperature. After 4 hours, the reaction mixture was diluted with water (50 mL) and extracted with ethyl acetate (3 x 50 mL), the combined organics dried ($NaSO_4$) and solvent removed *in vacuo.* The crude material was purified by column chromatography (pure hexanes) to give 1,2-bis(4-azidophenyl)disulfane as a brown oil (2.09 g, 6.95 mmol, 77%).

IR (thin film, ν_{max} / cm^{-1}) 2416, 2360, 2341, 2257, 2122 (N_3), 2085, 1886, 1636, 1586, 1567, 1482, 1402, 1289, 1270, 1177, 1129, 1115, 1076, 1010; **^{1}H NMR** (400 MHz, $CDCl_3$) δ 7.49 – 7.44 (m, 4H, CHCS), 7.00 – 6.95 (m, 4H, CHCN); **^{13}C NMR** (101 MHz, $CDCl_3$) δ 139.9 (CN), 133.1 (CS), 130.6 (*C*HCN), 119.7 (*C*HCS), **LRMS** (ES+) calc. for $C_{12}H_9N_4{}^{32}S_2$ $[M-N_2+H]^+$ 273.0, found 273.0.

Data consistent with literature values.[87]

N,N,N-Trimethylaminiopropyne bromide, 4.39

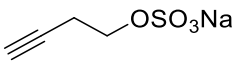


To a stirred solution of propargyl bromide (0.80 mL, 7.2 mmol, 80% in toluene, 1.0 equiv.) in diethyl ether (8 mL) was added trimethylamine (7.2 mL, 14.4 mmol, 2 M in tetrahydrofuran, 2.0 equiv.) at room temperature. After 1 hour the reaction mixture was filtered and the precipitate washed with diethyl ether (3 x 15 mL) to give N,N,N-trimethylaminiopropyne bromide as a yellow-white solid (1.26 g, 7.1 mmol, 98%).

IR (solid, ν_{max} / cm^{-1}) 1434, 1276, 1167, 1144, 1007; **^{1}H NMR** (400 MHz, D_2O) δ 4.27 (d, *J* = 2.5 Hz, 2H, CH_2), 3.27 (t, *J* = 2.5 Hz, 1H, CH), 3.23 (s, 9H, NCH_3); **^{13}C NMR** (101 MHz, D_2O) δ 81.8 (*quat* C), 71.3 (CH), 56.4 (t, *J* = 4.0 Hz, CH_2), 53.0 (t, *J* = 4.0 Hz, CH_3); **mp** (Et_2O) 176.0 °C.

Data consistent with literature values.[88]

But-3-yn-1-yl sulfate, 4.40

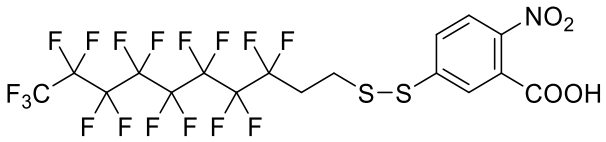


Chlorosulfonic acid (0.94 mL, 14.3 mmol, 1.0 equiv.) was added dropwise to a stirred solution of pyridine (2.54 mL, 31.4 mmol, 2.2 equiv.) in carbon tetrachloride (13 mL) at 0 °C. After 15 minutes 3-butyn-1-ol (0.94 mL, 14.3 mmol, 1.0 equiv.) was added, stirred for a further 4 hours, allowed to warm to room temperature and stirred for a further 12 hours. The reaction mixture was diluted with dichloromethane (15 mL) and extracted with water (3 x 30 mL). Saturated sodium carbonate solution was added to the aqueous until bubbling ceased, and then dried *in vacuo.* The crude material was purified by trituration from boiling ethanol (160 mL), hot filtered and the filtrate evaporated *in vacuo* to give but-3-yn-1-yl sulfate as a white solid (2.192 g, 12.73 mmol, 89%).

IR (thin film, ν_{max} / cm^{-1}) 3328, 2921, 1468, 1439, 1384, 1212, 1114; **^{1}H NMR** (400 MHz, D_2O) δ 4.12 (t, *J* = 6.5 Hz, 2H, CH_2O), 2.61 (td, *J* = 6.5, 2.5 Hz, 2H, CH_2CH_2O), 2.38 (t, *J* = 2.5 Hz, 1H, CH); **^{13}C NMR** (101 MHz, D_2O) δ 81.0 (*C*CH), 70.5 (CH), 66.5 (CH_2O), 18.6 (CH_2CH_2O); **LRMS** (ES-) calc. for $C_4H_5O_4{}^{32}S$ $[M\text{-}Na]^-$ 149.0, found 149.0.

Data consistent with literature values.[89]

5-((1*H*,1*H*,2*H*,2*H*-Perfluorodecanyl)disulfaneyl)-2-nitrobenzoic acid, 4.22



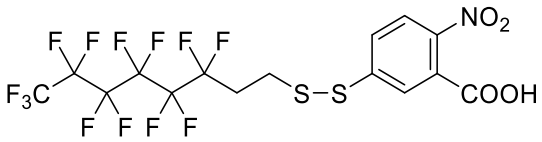
To a stirred solution of 1*H*,1*H*,2*H*,2*H*-perfluorodecane-1-thiol, **4.20** (150.0 mg, 0.312 mmol, 1.0 equiv.) and triethylamine (43.5 μL, 0.312 mmol, 1.0 equiv.) in dichloromethane (4 mL) was added 5,5'-dithiobis(2-nitrobenzoic acid), **4.2** (123.6 mg, 0.312 mmol, 1.0 equiv.) at room temperature. After 2 hours the reaction mixture was diluted with dichloromethane (20 mL), washed with 1M hydrochloric acid (10 mL) and the phases separated. The aqueous extracted with dichloromethane (3 × 10 mL). The combined organics were dried ($MgSO_4$) and the solvent removed *in vacuo*. The residue was purified column chromatography (acetic acid / methanol / dichloromethane (1:10:89)) to give 5-((1*H*,1*H*,2*H*,2*H*-perfluorodecanyl)disulfaneyl)-2-nitrobenzoic acid as a white solid (152.2 mg, 0.225 mmol, 72%).

IR (thin film, ν_{max} / cm^{-1}) 3375, 2361, 2341, 1638, 1568, 1527, 1344, 1200, 1146, 1115, 1083; **^{1}H NMR** (400 MHz, acetone-d_6) δ 8.04 – 7.96 (m, 3H, ArH), 3.24 – 3.16 (m, 2H, CH_2S), 2.82 – 2.66 (m, 2H, CH_2CF); **^{13}C NMR** (101 MHz, acetone-d_6) δ 166.9 (COOH), 145.7 (CN), 145.2 (ArCS), 128.8 (*C*COOH), 128.2 (SC*C*HCH), 125.5 (*C*HCCOOH), 124.8 (SCCH*C*H), 36.0 (t, *J* = 22.0 Hz, *C*H_2CF_2), 15.6 (t, *J* = 5.0 Hz, SCH_2); **^{19}F NMR**

(376 MHz, acetone-d_6) δ -82.57 (tt, J = 10.0, 2.5 Hz, CF_3), -114.28 – -114.63 (m, CH_2CF_2), -121.65 – -121.99 (m, CF_2), -122.07 – -122.21 (m, CF_2), -122.65 – -122.83 (m, CF_2), -123.30 – -123.84 (m, CF_2 + CF_2), -126.18 – -126.47 (m, CF_2); **HRMS** (ES-) calc. for $C_{17}H_7O_4NF_{17}{}^{32}S_2$ $[M-H]^-$ 675.9551, found 675.9547.

Some carbon peaks show high degree of coupling to ^{19}F and thus are not reported.

5-((1*H*,1*H*,2*H*,2*H*-Perfluorooctanyl)disulfaneyl)-2-nitrobenzoic acid, 4.21



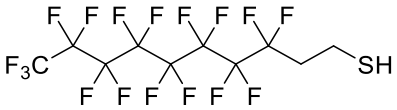
To a stirred solution of 1*H*,1*H*,2*H*,2*H*-perfluorooctane-1-thiol, **4.19** (100.0 mg, 0.263 mmol, 1.0 equiv.) and triethylamine (36.7 μL, 0.263 mmol, 1.0 equiv.) in dichloromethane (5 mL) was added 5,5'-dithiobis(2-nitrobenzoic acid), **4.2** (104.2 mg, 0.263 mmol, 1.0 equiv.) at room temperature. After 2 hours the reaction mixture was diluted with dichloromethane (20 mL), washed with 1M hydrochloric acid (10 mL) and the phases separated. The aqueous extracted with dichloromethane (3 × 10 mL). The combined organics were dried ($MgSO_4$) and the solvent removed *in vacuo*. The residue was purified column chromatography (acetic acid / methanol / dichloromethane (1:1:98)) to give 5-((1*H*,1*H*,2*H*,2*H*-perfluorooctanyl)disulfaneyl)-2-nitrobenzoic acid as a white solid (31.8 mg, 0.055 mmol, 21%).

IR (thin film, ν_{max} / cm^{-1}) 3373, 2357, 2343, 1642, 1568, 1515, 1355, 1332, 1200, 1157, 1140, 1121, 1082, 1054; **^{1}H NMR** (400 MHz, acetone-d_6) δ 8.06 – 7.98 (m, 2H, ArH), 3.24 – 3.17 (m, 2H, CH_2S), 2.82 – 2.65 (m, 2H, CH_2F); **^{13}C NMR** (101 MHz, acetone-d_6) δ 166.2 (COOH), 145.6 (CN), 144.6 (ArCS), 128.9 (*C*COOH), 128.4 (SC*C*HCH), 126.3 (*C*HCCOOH), 124.6 (SCCH*C*H), 36.1 (t, J = 22.0 Hz, CH_2CF_2), 15.6 (t, J = 5.0 Hz, SCH_2); **^{19}F NMR** (376 MHz, acetone-d_6) δ -81.73 (tt, J = 10.0, 2.5 Hz, CF_3), -114.32 –

-114.60 (m, CH_2CF_2), -121.88 – -122.17 (m, CF_2), -122.82 – -123.05 (m, CF_2), -123.64 – -123.83 (m, CF_2), -126.19 – -126.52 (m, CF_2); **HRMS** (ES-) calc. for $C_{15}H_7O_4NF_{13}{}^{32}S_2$ $[M-H]^-$ 575.9609, found 575.9607.

Some carbon peaks show high degree of coupling to ^{19}F and thus are not reported.

1*H*,1*H*,2*H*,2*H*-perfluorodecane-1-thiol, 4.20



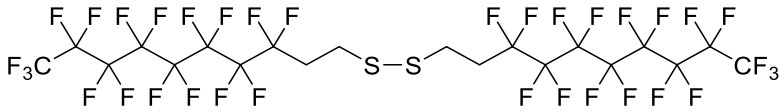
A solution of 1*H*,1*H*,2*H*,2*H*-perfluorodecyl iodide (5.00 g, 8.71 mmol, 1.00 equiv.) and thiourea (696.0 mg, 9.15 mmol, 1.05 equiv.) in ethanol (40 mL) was heated to reflux for 18 h. The reaction mixture was allowed to cool to room temperature and the solvent removed *in vacuo.* The solid was added to a suspension of potassium carbonate (12.0 g, 87 mmol, 10 equiv.) in methanol (500 mL) was heated to reflux for 30 minutes. The reaction mixture was allowed to cool to room temperature and most the solvent removed *in vacuo*. Water (100 mL) was added and extracted with dichloromethane (4 × 100 mL). The combined organics were dried ($MgSO_4$) and the solvent removed *in vacuo*. *1H,1H,2H,2H*-Perfluorodecane-1-thiol was obtained without further purification as an oil (2.92 g, 6.07 mmol, 70%). This compound was found to have a melting point close to room temperature.

IR (thin film, ν_{max} / cm^{-1}) 1365, 1198, 1145, 1114; **^{1}H NMR** (400 MHz, $CDCl_3$) δ 2.82 – 2.73 (m, 2H, SCH_2), 2.51 – 2.34 (m, 2H, CH_2CF_2); **^{13}C NMR** (101 MHz, $CDCl_3$) δ 36.0 (t, *J* = 22.0 Hz, *C*H_2CF_2), 15.6 (t, *J* = 5.0 Hz, SCH_2); **^{19}F NMR** (376 MHz, $CDCl_3$) δ -81.04 (tt, *J* = 10.5, 2.5 Hz, CF_3), -114.34 – -114.64 (m, CH_2CF_2), -121.61 – -121.90 (m, CF_2), -121.97 – -122.14 (m, CF_2), -122.78 – -122.99 (m, CF_2), -123.47 – -123.82 (m, CF_2 + CF_2), -126.20 – -126.44 (m, CF_2); **LRMS** (ES-) calc. for $C_{10}H_4O_4F_{17}{}^{32}S$ $[M-H]^-$ 479.0, found 479.0.

Some carbon peaks show high degree of coupling to ^{19}F and thus are not reported.

Data consistent with literature values.[90]

1,2-Bis(1*H*,1*H*,2*H*,2*H*-perfluorodecanyl)disulfane, 4.41



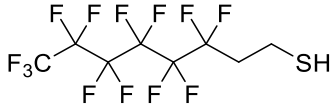
To a stirred solution of 1*H*,1*H*,2*H*,2*H*-perfluorodecane-1-thiol, **4.20** (100.0 mg, 0.208 mmol, 1.0 equiv.) in dichloromethane (10 mL) was added iodine (58.1 mg, 0.229 mmol, 1.1 equiv.) at room temperature. After 1 hour the reaction mixture was diluted with dichloromethane (50 mL), washed with 5% sodium thiosulfate (5 mL) then water (5 mL), dried ($MgSO_4$) and the solvent removed *in vacuo*. 1,2-Bis(1*H*,1*H*,2*H*,2*H*-perfluorodecanyl)disulfane was obtained without further purification as a white solid (93.9 mg, 0.098 mmol, 94%).

IR (thin film, ν_{max} / cm^{-1}) 3733, 3628, 2360, 2341, 1200, 1147; **^{1}H NMR** (400 MHz, $CDCl_3$) δ 2.91 – 2.85 (m, 4H, SCH_2), 2.51 – 2.34 (m, 4H, CH_2CF_2); **^{13}C NMR** (101 MHz, $CDCl_3$) δ 36.0 (t, *J* = 22.0 Hz, *C*H_2CF_2), 22.9 – 22.8 (m, SCH_2); **^{19}F NMR** (376 MHz, $CDCl_3$) δ -81.04 (tt, *J* = 10.5, 2.5 Hz, CF_3), -113.80 – -114.09 (m, CH_2CF_2), -121.67 – -121.99 (m, CF_2), -122.34 – -122.46 (m, CF_2), -122.85 – -123.37 (m, CF_2), -123.56 – -124.05 (m, CF_2 + CF_2), -126.17 – -126.49 (m, CF_2); **mass** not found.

Some carbon peaks show high degree of coupling to ^{19}F and thus are not reported.

Data consistent with literature values.[91]

1*H*,1*H*,2*H*,2*H*-perfluorooctane-1-thiol, 4.19



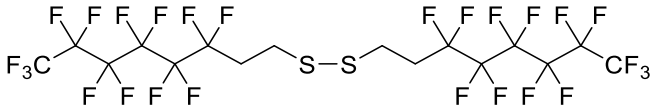
A solution of 1*H*,1*H*,2*H*,2*H*-perfluorooctyl iodide (2.00 g, 4.22 mmol, 1.00 equiv.) and thiourea (337.2 mg, 4.43 mmol, 1.05 equiv.) in ethanol (20 mL) was heated to reflux for 18 h. The reaction mixture was allowed to cool to room temperature and the solvent removed *in vacuo.* The solid was added to a suspension of potassium carbonate (5.8 g, 42 mmol, 10 equiv.) in methanol (250 mL) was heated to reflux for 30 minutes. The reaction mixture was allowed to cool to room temperature and most the solvent removed *in vacuo*. Water (40 mL) was added and extracted with dichloromethane (4 × 30 mL). The combined organics were dried ($MgSO_4$) and the solvent removed *in vacuo*. *1H,1H,2H,2H*-Perfluorodecane-1-thiol was obtained without further purification as an oil (1.36 g, 3.59 mmol, 85%).

IR (thin film, ν_{max} / cm^{-1}) 1443, 1363, 1186, 1142, 1121, 1072; **^{1}H NMR** (400 MHz, $CDCl_3$) δ 2.83 – 2.72 (m, 2H, SCH_2), 2.51 – 2.35 (m, 2H, CH_2CF_2); **^{13}C NMR** (101 MHz, $CDCl_3$) δ 36.0 (t, *J* = 22.0 Hz, *C*H_2CF_2), 15.6 (t, *J* = 5.0 Hz, SCH_2); **^{19}F NMR** (376 MHz, $CDCl_3$) δ -80.95 (tt, *J* = 10.0, 2.5 Hz, CF_3), -114.34 – -114.57 (m, CH_2CF_2), -121.87 – -122.07 (m, CF_2), -122.85 – -123.06 (m, CF_2), -123.57 – -123.72 (m, CF_2), -126.18 – -126.31 (m, CF_2); **LRMS** (ES-) calc. for $C_8H_4F_{13}{}^{32}S$ $[M-H]^-$ 379.0, found 378.8.

Some carbon peaks show high degree of coupling to ^{19}F and thus are not reported.

Data consistent with literature values.[92]

1,2-Bis(1*H*,1*H*,2*H*,2*H*-perfluorooctanyl)disulfane, 4.42



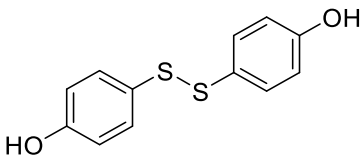
To a stirred solution of 1*H*,1*H*,2*H*,2*H*-perfluorooctane-1-thiol, **4.19** (100.0 mg, 0.263 mmol, 1.0 equiv.) in dichloromethane (10 mL) was added iodine (73.4 mg, 0.289 mmol, 1.1 equiv.) at room temperature. After 1 hour the reaction mixture was diluted with dichloromethane (50 mL), washed with 5% sodium thiosulfate (5 mL) then

water (5 mL), dried ($MgSO_4$) and the solvent removed *in vacuo*. 1,2-Bis(1*H*,1*H*,2*H*,2*H*-perfluorooctanyl)disulfane was obtained without further purification as a white solid (91.4 mg, 0.121 mmol, 92%).

IR (thin film, ν_{max} / cm^{-1}) 1230, 1184, 1152, 1127, 1119, 1073, 1042; **^{1}H NMR** (400 MHz, $CDCl_3$) δ 2.91 – 2.86 (m, 4H, SCH_2), 2.51 – 2.35 (m, 4H, CH_2CF_2); **^{13}C NMR** (101 MHz, $CDCl_3$) δ 36.0 (t, *J* = 22.0 Hz, *C*H_2CF_2), 22.9 – 22.8 (m, SCH_2); **^{19}F NMR** (376 MHz, $CDCl_3$) δ -80.99 (tt, *J* = 10.0, 2.5 Hz, CF_3), -113.72 – -113.92 (m, CH_2CF_2), -121.93 – -122.10 (m, CF_2), -122.89 – -123.05 (m, CF_2), -123.55 – -123.72 (m, CF_2), -126.16 – -126.33 (m, CF_2); **mass** not found.

Some carbon peaks show high degree of coupling to ^{19}F and thus are not reported.

4,4'-Disulfanediyldiphenol, 4.43



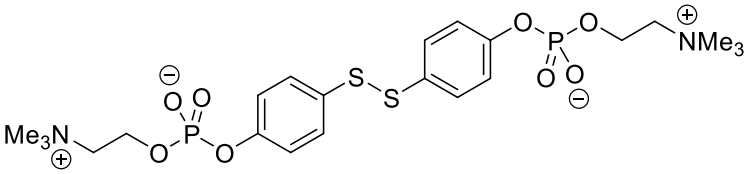
Alumina (5 g) was stirred with water (1 mL) until no large clumps were observed. This was added to a suspension of 4-mecaptophenol (1.32 g, 10.5 mmol, 1.0 equiv.) and sodium iodate (4.14g, 20.9 mmol, 2.0 equiv.) in hexanes (25mL) and vigorously stirred for 1.5 h. The reaction mixture was filtered, with the solid residue being washed with hexanes (3 × 15 mL). The filtrate was taken and the solvent removed *in vacuo*. 4,4'-Disulfanediyldiphenol was obtained without further purification as an off-white solid (1.306 g, 5.22 mmol, 99%).

IR (thin film, ν_{max} / cm^{-1}) 3314, 2480, 2161, 2034, 1877, 1598, 1583, 1491, 1432, 1358, 1286, 1255, 1217, 1181, 1163, 1097, 1010; **^{1}H NMR** (400 MHz, DMSO-d_6) δ 9.84 (s, 2H, OH), 7.29 – 7.25 (m, 4H, CHCS), 6.79 – 6.73 (m, 4H, CHCO); **^{13}C NMR** (101 MHz,

DMSO-d_6) δ 158.3 (CO), 133.0 (*C*CS), 125.1 (CS), 116.3 (*C*CO); **LRMS** (ES-) calc. for $C_{12}H_9O_2{}^{32}S_2$ $[M-H]^-$ 249.0, found 249.0; **mp** (hexanes) 151.3 °C.

Data consistent with literature values.[93]

1,2-Bis(4-phenyl (2-(trimethylammonio)ethyl) phosphate)disulfane, 4.23

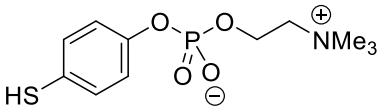


Crude material: A stirred solution of 4,4'-disulfanediyldiphenol, **4.43** (400 mg, 1.60 mmol, 1.0 equiv.) in tetrahydrofuran (25 mL) was cooled to 0 °C, triethylamine (0.675 mL, 3.52 mmol, 2.2 equiv.) added, followed by 2-chloro-1,3,2-dioxaphospholane 2-oxide (0.323 mL, 4.80 mmol, 3.0 equiv.). The reaction mixture was then allowed to warm to room temperature. After 2 hours, the reaction mixture was filtered as quickly as possible through a short silica plug, washing with ethyl acetate (5 × 80 mL) and the solvent removed *in vacuo.* The residue was dissolved in acetonitrile (10 mL) and to this was added trimethylamine solution (2.00 mL, 4.00 mmol, 2.0 M in tetrahydrofuran, 2.5 equiv.) the vessel sealed with a glass stopper and heated to 70 °C. After 72 hours, the vessel was allowed to cool to room temperature before being carefully opened, and the solvent removed *in vacuo*.

Pure material: 4-Mercaptophenyl (2-(trimethylammonio)ethyl) phosphate, **4.44** (200 mg, 0.687 mmol, 1.0 equiv.) was dissolved in water (12 mL) and oxygen bubbled through. After 30 minutes the reaction mixture was heated to 50 °C, with continued bubbling. After a further 18 hours, the solvent removed *in vacuo* to give 1,2-bis(4-phenyl (2-(trimethylammonio)ethyl) phosphate)disulfane as a pink oil (175.8 mg, 0.302 mmol, 88%) without further purification.

IR (oil, ν_{max} / cm^{-1}) 3029, 1588, 1483, 1263, 1233, 1165, 1091, 1052, 1010; **^{1}H NMR** (400 MHz, D_2O) δ 7.54 – 7.48 (m, 4H, CHCS), 7.20 – 7.14 (m, 4H, CHCO), 4.32 (br s, 4H, CH_2O), 3.59 – 3.53 (m, 4H, CH_2N), 3.07 (s, 18H, $N(CH_3)_3$); **^{13}C NMR** (101 MHz, D_2O) δ 150.8 (d, *J* = 7.0 Hz, Ar CO), 130.8 (CHCS), 129.5 (CS), 120.2 (d, *J* = 4.5 Hz, CHCO), 64.9 (d, *J* = 8.0 Hz, CH_2N), 58.9 (d, *J* = 5.0 Hz, CH_2O), 52.9 (CH_3); **^{31}P NMR** (162 MHz, D_2O) -4.92; **HRMS** (ES+) calc. for $C_{22}H_{34}O_8N_2NaP_2{}^{32}S_2$ $[M+Na]^+$ 603.1124, found 603.1127.

4-Mercaptophenyl (2-(trimethylammonio)ethyl) phosphate, 4.44



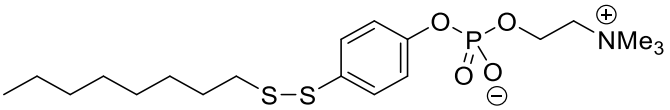
1-Octanethiol (2.08 mL, 12.0 mmol, approx. 3.5 equiv.) was added to a stirred solution of potassium methoxide (720.9 mg, 10.3 mmol, approx. 3 equiv.) in water (15 mL) and tetrahydrofuran (30 mL). After 15 minutes, this was added to a stirred solution of crude 1,2-bis(4-phenyl (2-(trimethylammonio)ethyl) phosphate)disulfane, **4.23** (1.99 g, 3.43 mmol, approx. 1.0 equiv.) in water (15 mL) and heated to 60 °C. After 4 hours, the reaction mixture was allowed to cool to room temperature, then neutralized with 1 M hydrochloric acid, extracted with isopropanol/ chloroform (1:3, 3 × 30 mL). The solvent removed from the aqueous *in vacuo* to give 4-mercaptophenyl (2-(trimethylammonio)ethyl) phosphate as a pink oil (359.7 mg, 1.23 mmol, 18%).

Note: On smaller scales no heating of the reaction was required.

IR (oil, ν_{max} / cm^{-1}) 3022, 2997, 1590, 1484, 1456, 1263, 1164, 1086, 1052; **^{1}H NMR** (400 MHz, D_2O) δ 7.33 (d, *J* = 8.0 Hz, 2H, CHCS), 6.94 (d, *J* = 8.5 Hz, 2H, CHCO), 4.41 – 4.33 (m, 2H, CH_2O), 3.66 – 3.59 (m, 2H, CH_2N), 3.15 (s, 9H, $N(CH_3)_3$); **^{13}C NMR** (101 MHz, D_2O) δ 149.5 (d, *J* = 7.0 Hz, Ar CO), 130.7 (CHCS), 128.8 (CS), 119.8 (d, *J* = 4.0 Hz, CHCO), 64.8 – 64.6 (m, CH_2N), 59.3 – 59.1 (d, *J* = 5.0 Hz, CH_2O), 52.9 – 52.8

(m, CH_3); **^{31}P NMR** (162 MHz, D_2O) -3.73; **HRMS** (ES+) calc. for $C_{11}H_{18}O_4NNaP^{32}S$ $[M+Na]^+$ 314.0586, found 314.0591.

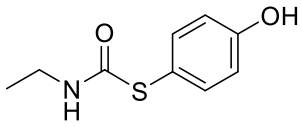
4-(Octyldisulfaneyl)phenyl (2-(trimethylammonio)ethyl) phosphate, 4.24



To a stirred solution of 1-octanethiol (10.7 μL, 61.7 μmol, 1.0 equiv.) in acetonitrile (2 mL) was added triethylamine (8.6 μL, 61.7 μmol, 1.0 equiv.) at room temperature. After 15 minutes 1,2-bis(4-phenyl (2-(trimethylammonio)ethyl) phosphate)disulfane, **4.23** (35.8 mg, 61.7 mmol, 1.0 equiv.) was added, and the reaction mixture stirred for 2 h. The solvent removed *in vacuo* and the crude material was purified by column chromatography (water/ methanol/ dichloromethane (1:9:10 to 4:21:25)) to give 4-(octyldisulfaneyl)phenyl (2-(trimethylammonio)ethyl) phosphate as an oil (3.5 mg, 8.0 mmol, 13%).

IR (thin film, ν_{max} / cm^{-1}) 2335, 1620, 1579, 1515, 1347, 1157, 1104, 1062; **^{1}H NMR** (400 MHz, D_2O) δ 7.38 (d, *J* = 8.5 Hz, 2H, CHCS), 7.15 (d, *J* = 9.0 Hz, 2H, CHCO), 4.21 (br s, 2H, CH_2O), 3.45 (br s, 2H, CH_2N), 3.01 (s, 9H, $N(CH_3)_3$), 2.67 (t, *J* = 7.0 Hz, 2H, CH_2S), 1.66 (s, 2H, CH_2CH_2S), 1.28 – 1.18 (m, 10H, alk CH_2), 0.89 (t, *J* = 6.4 Hz, 3H, CH_2CH_3); **^{13}C NMR** (101 MHz, D_2O) δ 150.8 (d, *J* = 7.0 Hz, Ar CO), 131.0 (CHCS), 129.6 (CS), 120.1 (d, *J* = 4.0 Hz, CHCO), 64.7 – 64.5 (m, CH_2N), 59.0 – 58.9 (m, CH_2O), 53.1 – 52.9 (m, $N(CH_3)_3$), 39.1 (CH_2S), 30.7 (alk CH_2), 29.2 (alk CH_2), 29.1 (alk CH_2), 28.9 (alk CH_2), 27.5 (alk CH_2), 22.0 (CH_2CH_3), 13.9 (CH_2CH_3); **^{31}P NMR** (162 MHz, D_2O) -4.70; **HRMS** (ES+) calc. for $C_{19}H_{34}O_4NNaP^{32}S_2$ $[M+Na]^+$ 458.1559, found 458.1564.

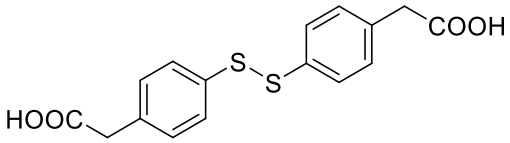
S-(4-Hydroxyphenyl) ethylcarbamothioate, 4.45



To a stirred solution of 4-mercaptophenol (2.30 g, 18.2 mmol, 1.0 equiv.) in toluene (50 mL) was added trimethylamine (126 μL, 0.91 mmol, 0.05 equiv.) followed by ethyl isocyanate (1.44 mL, 18.2 mmol, 1.0 equiv.) at room temperature. After 2 hours the solvent removed *in vacuo*. The crude material was purified by column chromatography (ethyl acetate / petroleum ether (2:3)) to give S-(4-hydroxyphenyl) ethylcarbamothioate as a white solid (3.06 g, 15.5 mmol, 85%).

IR (solid, ν_{max} / cm^{-1}) 3425, 3302, 1674, 1660, 1639, 1552, 1523, 1339, 1215, 1119, 1081; **^{1}H NMR** (400 MHz, $CDCl_3$) δ 7.36 – 7.31 (d, *J* = 8.5 Hz, 2H), 6.75 – 6.70 (d, *J* = 8.5 Hz, 2H), 5.49 (s, 1H, NH), 3.32 (qd, *J* = 7.0, 5.5 Hz, 2H, CH_2), 1.13 (t, J = 7.5 Hz, 3H, CH_3); **^{13}C NMR** (101 MHz, $CDCl_3$) δ 169.4 (C=O), 155.3 (COH), 133.6 (*C*CS), 124.0 (CS), 118.2 (*C*COH), 37.2 (CH_2), 16.4 (CH_3); **HRMS** (ES-) calc. for $C_9H_{10}O_2N^{32}S$ $[M-H]^-$ 196.0438, found 196.0440.

2,2'-(Disulfanediylbis(4,1-phenylene))diacetic acid, 4.25



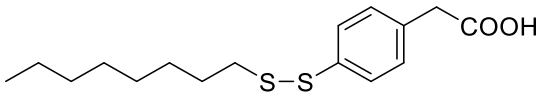
To a stirred solution of 4-mercaptophenylacetic acid (1.00 g, 5.94 mmol, 1.0 equiv.) in ethanol (25 mL) was added iodine (2.26 g, 8.91 mmol, 1.5 equiv.). After 2 h, 10% aqueous sodium thiosulfate solution (10 mL) was added and the reaction mixture acidified to pH 1 with concentrated hydrochloric acid and extracted with dichloromethane (3 × 30 mL). The combined organics were dried ($NaSO_4$) and the solvent removed

in vacuo. 2,2'-(Disulfanediylbis(4,1-phenylene))diacetic acid was obtained as a yellow oil (577.7 mg, 1.73 mmol, 58%).

IR (thin film, ν_{max} / cm^{-1}) 2980, 2961, 2935, 1723, 1669, 1644, 1600, 1416, 1295, 1079; **^{1}H NMR** (400 MHz, DMSO-d_6) δ 7.51 – 7.43 (m, 4H, CHCS), 7.32 – 7.24 (m, 4H, C*H*CHCS), 3.65 (s, 4H, CH_2); **^{13}C NMR** (101 MHz, DMSO-d_6) δ 173.5 (C=O), 136.9 (*quat* C or Ar CS), 135.6 (*quat* C or Ar CS), 131.3 (*C*HCS), 129.2 (*C*HCHCS), 43.0 (CH_2); **LRMS** (ES-) calc. for $C_{16}H_{13}O_4{}^{32}S_2$ $[M-H]^-$ 333.0, found 332.7.

Data consistent with literature values.[94]

2-(4-(Octyldisulfaneyl)phenyl)acetic acid, 4.26



To a stirred solution of 2,2'-(disulfanediylbis(4,1-phenylene))diacetic acid (50.0 mg, 0.150 mmol, 1.0 equiv.) and triethylamine (20.9 µL, 0.150 mmol, 1.0 equiv.) in dichloromethane (3 mL) was added 1-octanethiol (26.8 µL, 0.150 mmol, 1.0 equiv.). After 18 h, 1 M hydrochloric acid was added (2 mL), the phases separated and the aqueous extracted with dichloromethane (3 × 3 mL). The combined organics were dried ($NaSO_4$) and the solvent removed *in vacuo*. The residue was purified column chromatography (acetic acid / methanol / dichloromethane (1:1:98)) to give 2-(4-(octyldisulfaneyl)phenyl)acetic acid as a tan oil (35.1 mg, 0.113 mmol, 75%).

IR (thin film, ν_{max} / cm^{-1}) 2985, 2971, 2966, 1721, 1666, 1642, 1480, 1291, 1195, 1042; **^{1}H NMR** (400 MHz, DMSO-d_6) δ 7.77 – 7.68 (m, 2H, CHCS), 7.33 – 7.26 (m, 2H, C*H*CHCS), 3.67 (s, 2H, CH_2), 2.65 (t, J = 7.5 Hz, 2H, CH_2S), 1.51 – 1.43 (m, 2H, CH_2CH_2S), 1.30 – 1.15 (m, 10H, alkyl CH_2), 0.89 (t, J = 7.0 Hz, 3H, CH_3); **^{13}C NMR** (101 MHz, DMSO-d_6) δ 174.2 (C=O), 136.6 (*quat* C or Ar CS), 135.8 (*quat* C or Ar CS), 131.1 (*C*HCS), 129.5 (*C*HCHCS), 43.2 (CH_2C=O), 38.2 (CH_2S), 31.2 (alk CH_2), 29.2

(alk CH_2), 29.0 (alk CH_2), 28.9 (alk CH_2), 27.2 (alk CH_2), 21.8 (CH_2CH_3), 14.0 (CH_3);

HRMS (ES+) calc. for $C_{16}H_{22}{}^{32}S_2$ $[M-H]^-$ 311.1145, found 311.1140.

4. 7 References

1. Sievers, D. & Von Kiedrowski, G. Self-replication of hexadeoxynucleotide analogues: Autocatalysis versus cross-catalysis. *Chem. - A Eur. J.* **4**, 629–641 (1998).
2. Kosikova, T. & Philp, D. Exploring the emergence of complexity using synthetic replicators. *Chemical Society Reviews* **46**, 7274–7305 (2017).
3. Yao, S., Ghosh, I., Zutshi, R. & Chmielewski, J. Selective amplification by auto- and cross-catalysis in a replicating peptide system. *Nature* **396**, 447–450 (1998).
4. Ashkenasy, G., Jagasia, R., Yadav, M. & Ghadiri, M. R. Design of directed molecular networks. *Proc. Natl. Acad. Sci. U. S. A.* **101**, 10872–10877 (2004).
5. Kosikova, T. & Philp, D. A Critical Cross-Catalytic Relationship Determines the Outcome of Competition in a Replicator Network. *J. Am. Chem. Soc.* **139**, 12579–12590 (2017).
6. Huck, J., Kosikova, T. & Philp, D. Compositional persistence in a multicyclic network of synthetic replicators. *J. Am. Chem. Soc.* **141**, 13905–13913 (2019).
7. Carnall, J. M. A. *et al.* Mechanosensitive self-replication driven by self-organization. *Science* **327**, 1502–1506 (2010).
8. Leonetti, G. & Otto, S. Solvent composition dictates emergence in dynamic molecular networks containing competing replicators. *J. Am. Chem. Soc.* **137**, 2067–2072 (2015).
9. Sadownik, J. W., Mattia, E., Nowak, P. & Otto, S. Diversification of self-replicating molecules. *Nat. Chem.* **8**, 264–269 (2016).
10. Liu, B. *et al.* Complex Molecules That Fold Like Proteins Can Emerge Spontaneously. *J. Am. Chem. Soc.* **141**, 1685–1689 (2019).
11. Bartolec, B. *et al.* Emergence of Compartments Formed from Unconventional Surfactants in Dynamic Combinatorial Libraries. *Langmuir* **35**, 5787–5792 (2019).
12. Terfort, A. & von Kiedrowski, G. Self-Replication by Condensation of 3-Aminobenzamidines and 2-Formylphenoxyacetic Acids. *Angew. Chemie - Int. Ed. Eng.* **31**, 654–656 (1992).
13. Xu, S. & Giuseppone, N. Self-duplicating amplification in a dynamic combinatorial library. *J. Am. Chem. Soc.* **130**, 1826–1827 (2008).
14. Del Amo, V., Slawin, A. M. Z. & Philp, D. Manipulating replication processes within a dynamic covalent framework. *Org. Lett.* **10**, 4589–4592 (2008).
15. Kosikova, T., MacKenzie, H. & Philp, D. Probing the Limits of Selectivity in a Recognition-Mediated Reaction Network Embedded within a Dynamic Covalent Library. *Chem. - A Eur. J.* **22**, 1831–1839 (2016).
16. Sadownik, J. W. & Philp, D. A simple synthetic replicator amplifies itself from a dynamic reagent pool. *Angew. Chemie - Int. Ed.* **47**, 9965–9970 (2008).
17. Zepik, H. H., Blöchliger, E. & Luisi, P. L. A chemical model of homeostasis. *Angew. Chemie - Int. Ed.* **40**, 199–202 (2001).

18. Mitchison, T. & Kirschner, M. Dynamic instability of microtubule growth. *Nature* **312**, 237–242 (1984).

19. Herrmann, H., Bär, H., Kreplak, L., Strelkov, S. V. & Aebi, U. Intermediate filaments: From cell architecture to nanomechanics. *Nature Reviews Molecular Cell Biology* **8**, 562–573 (2007).

20. Cavalier-Smith, T. & von der Heyden, S. Molecular phylogeny, scale evolution and taxonomy of centrohelid heliozoa. *Mol. Phylogenet. Evol.* **44**, 1186–1203 (2007).

21. Boekhoven, J., Hendriksen, W. E., Koper, G. J. M., Eelkema, R. & Van Esch, J. H. Transient assembly of active materials fueled by a chemical reaction. *Science* **349**, 1075–1079 (2015).

22. Prigogine, I. & Rice, S. A. *Advances in chemical physics. Volume 81*. (Wiley, 1992).

23. Pascal, R., Pross, A. & Sutherland, J. D. Towards an evolutionary theory of the origin of life based on kinetics and thermodynamics. *Open Biol.* **3**, 130156 (2013).

24. Pascal, R. & Pross, A. Stability and its manifestation in the chemical and biological worlds. *Chem. Commun.* **51**, 16160–16165 (2015).

25. Pross, A. *What is life? : how chemistry becomes biology*. (Oxford University Press, 2012).

26. Pross, A. & Pascal, R. How and why kinetics, thermodynamics, and chemistry induce the logic of biological evolution. *Beilstein J. Org. Chem.* **13**, 665–674 (2017).

27. England, J. L. Dissipative adaptation in driven self-assembly. *Nature Nanotechnology* **10**, 919–923 (2015).

28. Horowitz, J. M. & England, J. L. Spontaneous fine-tuning to environment in many-species chemical reaction networks. *Proc. Natl. Acad. Sci. U. S. A.* **114**, 7565–7570 (2017).

29. Kachman, T., Owen, J. A. & England, J. L. Self-Organized Resonance during Search of a Diverse Chemical Space. *Phys. Rev. Lett.* **119**, (2017).

30. Segré, D. & Lancet, D. A statistical chemistry approach to the origin of life. *Chemtracts***12**, 382–397 (1999).

31. Segré, D. & Lancet, D. Composing life. *EMBO Rep.* **1**, 217–222 (2000).

32. Segré, D., Ben-Eli, D. & Lancet, D. Compositional genomes: Prebiotic information transfer in mutually catalytic noncovalent assemblies. *Proc. Natl. Acad. Sci. U. S. A.* **97**, 4112–4117 (2000).

33. Colomer, I., Morrow, S. M. & Fletcher, S. P. A transient self-assembling self-replicator. *Nat. Commun.* **9**, 2239 (2018).

34. Morrow, S. M., Colomer, I. & Fletcher, S. P. A chemically fuelled self-replicator. *Nat. Commun.* **10**, 1011 (2019).

35. Gray, P. & Scott, S. K. *Chemical oscillations and instabilities : non-linear chemical kinetics*. (Clarendon Press, 1990).

36. Hudson, J. L. & Mankin, J. C. Chaos in the Belousov–Zhabotinskii reaction. *J. Chem. Phys.* **74**, 6171–6177 (1981).

37. Davy, H. Some New Experiments and Observations on the Combustion of Gaseous Mixtures; with an Account of a Method of Preserving a Continued Light in Mixtures of Inflammable Gases and Air without Flame. *Proc. R. Soc. London* **2**, 61–62 (1815).

38. Griffiths, J. F. & Inomata, T. Oscillatory cool flames in the combustion of diethyl ether. *J. Chem. Soc. Faraday Trans.* **88**, 3153–3158 (1992).

39. Lotka, A. J. Contribution to the Theory of Periodic Reactions. *J. Phys. Chem.* **14**, 271–274 (1909).

40. Freedman, H. I. *Deterministic mathematical models in population ecology*. (M. Dekker, 1980).

41. Armao, J. J. & Lehn, J. M. Nonlinear Kinetic Behavior in Constitutional Dynamic Reaction Networks. *J. Am. Chem. Soc.* **138**, 16809–16814 (2016).

42. Semenov, S. N. *et al.* Autocatalytic, bistable, oscillatory networks of biologically relevant organic reactions. *Nature* **537**, 656–660 (2016).

43. Cafferty, B. J. *et al.* Robustness, Entrainment, and Hybridization in Dissipative Molecular Networks, and the Origin of Life. *J. Am. Chem. Soc.* **141**, 8289–8295 (2019).

44. Field, R. J. & Foersterling, H. D. On the oxybromine chemistry rate constants with cerium ions in the Field-Koeroes-Noyes mechanism of the Belousov-Zhabotinskii reaction: the equilibrium $HBrO_2 + BrO3^- + H^+ \rightarrow 2BrO_2^{\cdot} + H_2O$. *J. Phys. Chem.* **90**, 5400–5407 (1986).

45. Aguda, B. D., Hofmann Frisch, L. L. & Olsen, L. F. Experimental Evidence for the Coexistence of Oscillatory and Steady States in the Peroxidase-Oxidase Reaction. *J. Am. Chem. Soc.* **112**, 6652–6656 (1990).

46. Larter, R., Bush, C. L., Lonis, T. R. & Aguda, B. D. Multiple steady states, complex oscillations, and the devil's staircase in the peroxidase-oxidase reaction. *J. Chem. Phys.* **87**, 5765–5771 (1987).

47. May, R. M. Simple mathematical models with very complicated dynamics. *Nature* **261**, 459–467 (1976).

48. Olsen, L. F. & Degn, H. Chaos in an enzyme reaction. *Nature* **267**, 177–178 (1977).

49. Wagner, N. & Ashkenasy, G. Rhythm before life. *Nat. Chem.* **11**, 681–683 (2019).

50. Yoshida, R. Self-oscillating gels driven by the belousov-zhabotinsky reaction as novel smart materials. *Adv. Mater.* **22**, 3463–3483 (2010).

51. Grzybowski, B. A. & Huck, W. T. S. The nanotechnology of life-inspired systems. *Nat. Nanotechnol.* **11**, 585–592 (2016).

52. Hu, G., Bounds, C., Pojman, J. A. & Taylor, A. F. Time-lapse thiol-acrylate polymerization using a pH clock reaction. *J. Polym. Sci. Part A Polym. Chem.* **48**, 2955–2959 (2010).

53. Maeda, S., Hara, Y., Sakai, T., Yoshida, R. & Hashimoto, S. Self-walking gel. *Adv. Mater.* **19**, 3480–3484 (2007).

54. Lagzi, I., Kowalczyk, B., Wang, D. & Grzybowski, B. A. Nanoparticle oscillations and fronts. *Angew. Chemie - Int. Ed.* **49**, 8616–8619 (2010).

55. Miller, S. L. A production of amino acids under possible primitive earth conditions. *Science* **117**, 528–529 (1953).

56. Parker, E. T. *et al.* Primordial synthesis of amines and amino acids in a 1958 Miller H_2S-rich spark discharge experiment. *Proc. Natl. Acad. Sci. U. S. A.* **108**, 5526–5531 (2011).

57. Powner, M. W., Gerland, B. & Sutherland, J. D. Synthesis of activated pyrimidine ribonucleotides in prebiotically plausible conditions. *Nature* **459**, 239–242 (2009).

58. Bonfio, C. *et al.* Length-Selective Synthesis of Acylglycerol-Phosphates through Energy-Dissipative Cycling. *J. Am. Chem. Soc.* **141**, 3934–3939 (2019).

59. Watson, J. D. & Crick. F. H. C. Molecular Structures of Nucleic Acids. *Nature* **171**, 737–738 (1953).

60. Vidonne, A. & Philp, D. Making Molecules Make Themselves - the Chemistry of Artificial Replicators. *European J. Org. Chem.* **2009**, 593–610 (2009).

61. Le Vay, K., Weise, L. I., Libicher, K., Mascarenhas, J. & Mutschler, H. Templated Self-Replication in Biomimetic Systems. *Advanced Biosystems* **3**, 1800313 (2019).

62. Phillips, J. N. The energetics of micelle formation. *Trans. Faraday Soc.* **51**, 561–569 (1955).

63. Garavito, R. M. & Ferguson-Miller, S. Detergents as tools in membrane biochemistry. *J. Biol. Chem.* **276**, 32403–6 (2001).

64. Okur, H. I., Tarun, O. B. & Roke, S. Chemistry of Lipid Membranes from Models to Living Systems: A Perspective of Hydration, Surface Potential, Curvature, Confinement and Heterogeneity. *J. Am. Chem. Soc.* **141**, 12168–12181 (2019).

65. Peterlin, P., Arrigler, V., Kogej, K., Svetina, S. & Walde, P. Growth and shape transformations of giant phospholipid vesicles upon interaction with an aqueous oleic acid suspension. *Chem. Phys. Lipids* **159**, 67–76 (2009).

66. Blain, J. C. & Szostak, J. W. Progress Toward Synthetic Cells. *Annu. Rev. Biochem.***83**, 615–640 (2014).

67. Bissette, A. J. & Fletcher, S. P. Mechanisms of Autocatalysis. *Angew. Chemie - Int. Ed.* **52**, 12800–12826 (2013).

68. Young, G. & Kukura, P. Interferometric Scattering Microscopy. *Annu. Rev. Phys. Chem.***70**, 301–322 (2019).

69. Ortega-Arroyo, J., Bissette, A. J., Kukura, P. & Fletcher, S. P. Visualization of the spontaneous emergence of a complex, dynamic, and autocatalytic system. *Proc. Natl. Acad. Sci. U. S. A.* **113**, 11122–11126 (2016).

70. Morrow, S. M., Bissette, A. J. & Fletcher, S. P. Potential for minimal self-replicating systems in a dynamic combinatorial library of equilibrating imines. *Tetrahedron***73**, 5005–5010 (2017).

71. Young, G. *et al.* Quantitative mass imaging of single biological macromolecules. *Science* **360**, 423–427 (2018).

72. Al-Soufi, W., Piñeiro, L. & Novo, M. A model for monomer and micellar concentrations in surfactant solutions: Application to conductivity, NMR, diffusion, and surface tension data. *J. Colloid Interface Sci.* **370**, 102–110 (2012).

73. Silva, G. M. C., Morgado, P., Lourenço, P., Goldmann, M. & Filipe, E. J. M. Spontaneous self-assembly and structure of perfluoroalkylalkane surfactant hemimicelles by molecular dynamics simulations. *Proc. Natl. Acad. Sci. U. S. A.* **116**, 14868–14873 (2019).

74. Chattopadhyay, A. & London, E. Fluorimetric determination of critical micelle concentration avoiding interference from detergent charge. *Anal. Biochem.***139**, 408–412 (1984).

75. Butt, H.-J., Graf, K. & Kappl, M. *Physics and chemistry of interfaces*. (Wiley, 2003).

76. Ortega Arroyo, J. *et al.* Label-Free, All-Optical Detection, Imaging, and Tracking of a Single Protein. *Nano Lett.* **14**, 2065–2070 (2014).

77. Spillane, K. M. *et al.* High-Speed Single-Particle Tracking of GM1 in Model Membranes Reveals Anomalous Diffusion due to Interleaflet Coupling and Molecular Pinning. *Nano Lett.* **14**, 5390–5397 (2014).

78. Andrecka, J. *et al.* Structural dynamics of myosin 5 during processive motion revealed by interferometric scattering microscopy. *Elife* **4**, (2015).

79. Polster, J. & Schieberle, P. Structure–Odor Correlations in Homologous Series of Alkanethiols and Attempts To Predict Odor Thresholds by 3D-QSAR Studies. *J. Agric. Food Chem.* **63**, 1419–1432 (2015).

80. Shin, J. M., Sachs, G., Cho, Y. M. & Garst, M. 1-arylsulfonyl-2-(Pyridylmethylsulfinyl) benzimidazoles as new proton pump inhibitor prodrugs. *Molecules* **14**, 5247–5280 (2009).

81. Hudson, R., Beausoleil, A.-M., Miller, R. A. & Verner, E. Compounds and methods for modulating Bruton's Tyrosine Kinase. (2017).

82. Evans, B. J., Takahashi Doi, J. & Kenneth Musker, W. The aqueous periodate oxidation of aromatic and aliphatic carboxylic acid disulfides. *Phosphorus. Sulfur. Silicon Relat. Elem.* **73**, 5–13 (1992).

83. Lim, S. *et al.* Inhibition of lipopolysaccharide-induced inducible nitric oxide synthase expression by a novel compound, mercaptopyrazine, through suppression of nuclear factor-kappaB binding to DNA. *Biochem. Pharmacol.* **68**, 719–728 (2004).

84. Huang, P., Wang, P., Tang, S., Fu, Z. & Lei, A. Electro-Oxidative S−H/S−H Cross-Coupling with Hydrogen Evolution: Facile Access to Unsymmetrical Disulfides. *Angew. Chemie - Int. Ed.* **57**, 8115–8119 (2018).

85. Bell, C. M., Arendt, M. F., Gomez, L., Schmehl, R. H. & Mallouk, T. E. Growth of lamellar Hofmann clathrate films by sequential ligand exchange reactions: assembling a coordination solid one layer at a time. *J. Am. Chem. Soc.* **116**, 8374–8375 (1994).

86. Li, X. B. *et al.* Mechanistic insights into the interface-directed transformation of thiols into disulfides and molecular hydrogen by visible-light irradiation of quantum dots. *Angew. Chemie - Int. Ed.* **53**, 2085–2089 (2014).

87. Nalbandian, C. J., Miller, E. M., Toenjes, S. T. & Gustafson, J. L. A conjugate Lewis base-Brønsted acid catalyst for the sulfenylation of nitrogen containing heterocycles under mild conditions. *Chem. Commun.* **53**, 1494–1497 (2017).

88. Ryu, E. H. & Zhao, Y. Efficient synthesis of water-soluble calixarenes using click chemistry. *Org. Lett.* **7**, 1035–1037 (2005).

89. Sousa-Herves, A., Fernandez-Megia, E. & Riguera, R. Synthesis and supramolecular assembly of clicked anionic dendritic polymers into polyion complex micelles. *Chem. Commun.* **2008**, 3136–3138 (2008).

90. Moisan, S., Marty, J. D., Cansell, F. & Aymonier, C. Preparation of functional hybrid palladium nanoparticles using supercritical fluids: A novel approach to detach the growth and functionalization steps. *Chem. Commun.* **2008**, 1428–1430 (2008).

91. Levick, M. T. *et al.* A Sm(II)-mediated cascade approach to dibenzoindolo[3,2- b]carbazoles: Synthesis and evaluation. *Org. Lett.* **16**, 2292–2295 (2014).

92. Menczinger, B., Nemes, A., Szíjjártó, C. & Rábai, J. Preparation of (perfluoroalkyl)alkane thiols via Zemplén deacylation of fluorous (perfluoroalkyl)alkyl thioacetates. *J. Fluor. Chem.* **210**, 70–77 (2018).

93. Dou, Y. *et al.* Reusable cobalt-phthalocyanine in water: Efficient catalytic aerobic oxidative coupling of thiols to construct S-N/S-S bonds. *Green Chem.* **19**, 2491–2495 (2017).

94. Gough, J. D., Williams, R. H., Donofrio, A. E. & Lees, W. J. Folding disulfide-containing proteins faster with an aromatic thiol. *J. Am. Chem. Soc.* **124**, 3885–3892 (2002).

Chapter 5

Conclusions and future work

Chapter 5

Conclusions and future work

5. 1 Asymmetric autocatalysis

Considering the enormous advances that have been made in asymmetric catalysis since 1995, it seems almost inconceivable that the Soai reaction should still stand alone in asymmetric autocatalysis, a fact those engaging in the endeavour should carefully consider.

Chapter 2 described synthetic efforts towards novel asymmetric autocatalytic reactions, all based around hydrogen bonding catalysis. Lack of desired reactivity ultimately drove coach and horses through our designs. The majority of substrates were either unstable, displayed undesired reactivity with nucleophiles or most commonly were unreactive. We were able to identify a single example of the desired reactivity, involving the addition of benzenethiols to aziridine urea electrophiles. This reaction was limited in scope but allowed products to be formed with varying substitution patterns on two aryl rings.

Though in some cases chiral hydrogen bond donors did catalyse the addition of nucleophiles to our aziridine urea substrates, inducing asymmetry in these reactions proved challenging. We did not observe any autocatalysis in the reactions of chapter 2. While studying possible autocatalysis using hydrogen bonding catalysis we were able find strong positive nonlinear effects in thiourea organocatalysis.

It seems highly likely to me that the next asymmetric autocatalytic reaction to show amplification of chirality will heavily involve phase transfer processes, likely between a solid and solution phase. Though the restrictions of the Frank model, enantioselective autocatalysis and cross-inhibition of enantiomers may seem small at first, they are very

challenging to achieve together. Both of these properties could well be achieved using phase transfer processes however, as phase changes such as crystallisation are often show autocatalytic behaviour, and the close, regular packing of crystalline solids often leads to a difference in physical properties of enantiopure and racemic solids.[1,2]

5. 2 Lipids and protocell behaviour

The beginning of chapter 3 described the motion of droplet protocells induced by a lipid replicator. I believe this work's strength is its simplicity, providing an extreme reductionist prebiotic model for directed motion of protocells. Here, a lipid forming reaction can drive the motion of droplet protocells toward precursor rich regions, aiding lipid formation through mixing. As such this is a minimal model for feedback between physical and chemical processes across length scales.

Motion in this system is a complex phenomenon, beginning with the formation of a corona of material surrounding a droplet, during which time the droplets are stationary, the so-called lag period. This is followed by rapid acceleration to an average speed of around 50 μms^{-1}, maintained for several minutes before the droplets cease moving. The findings are consistent with a mechanism of motion caused by the Marangoni effect.

Extrapolating the lessons learned in developing this system to larger length scales proved challenging. In the second half of chapter 3 we were interested in inducing behaviour, particularly division, in larger droplets using autocatalytic lipid formation. The first challenge associated with this study was that the conditions for the autocatalytic lipid formation developed by the Fletcher group were not suitable for the study of microliter size droplets, where they typically lost definition, becoming oil slicks. For stable, well defined drops sodium hydroxide solutions were required and it turned out several of the previously developed lipid forming reactions were not compatible with these conditions.

Though it was possible to screen behaviour of a fairly large number of oil compositions on various aqueous phases, the sensitivity of behaviour to oil composition was far more than expected. It proved challenging to develop thiol containing oil droplets which were both: a) stationary in the absence of surfactant, and b) showed behaviour in the presence of surfactant. Despite these difficulties, it was possible to find a combination of oil composition and aqueous phase where droplets divided in the in the presence of a lipid forming reaction.

Maybe one of the most interesting future developments from the Marangoni microswimmer section of chapter 3 would be to study systems where the hydrophobic lipid precursor is found within the motile droplets. This could provide an interesting combination of physical effects, changing in significance through time like an autoinductive pathway. One can imagine autocatalysis arising from a number of factors, initially through micellar catalysis around the CMC of the lipid, followed by rate increase due to motion around the CPC of the droplets, followed by a further increase in rate around the lipid concentration where the two phases become an emulsion (like the emulsion seen in section 4. 3. 3. 1).

Further work on the surface droplets system should try to overcome the problems of reproducibility, which appears to be caused by two key factors. Firstly, lipid floccing has a large degree of stochasticity, with the visible onset of flocculation occurring at different times in otherwise identical reactions. This is likely due to some combination of physical properties of the lipid in question, **3.11**. The structure of the lipid should be varied to give more controllable and predictable behaviour, with the easiest modification being changing the cation for other metals, simply by using other hydroxides than NaOH. Secondly there is the problem of quantification, which was done by eye in our study. It

proved hard to see the smallest of the "daughter" droplets, I propose image-processing software should be used for consistency.

5. 3 Self-replication and selection

In chapter 4 we sought to study competition between replicating molecules. This work build upon the report of a lipid replicator which was unstable to the reaction conditions, but could be maintained away from equilibrium by fuelling.[3] Initially during optimisation it was found that oscillations in lipid concentration could result from fuelling, as well as the stable concentrations previously reported.

Currently studies of competing synthetic replicators are very limited, with our work being distinguished by the number of replicating species present (up to 9 chemically distinct lipids were monitiored), the use of transient replicators and the structural diversity of the aggregates present. Perhaps more fundamentally, competition studies typically use elaborate molecules, replicating through templating effects which may well be less efficient in heterogenous environments and/or away from their optimised conditions. For that reason I believe that our model system is unusual in showing the types of selection effects between replicating species which may be operative in a prebiotic environment.

Using a variety of precursor combinations it was possible to observe succession in lipid composition through time, with there often being changes in which replicator was dominant. Selection between lipids in this system occurs through both formation and destruction, the relative rates of which may be understood on the basis of steric and electronic effects.

During this study iSCAT microscopy was used to characterise the micelles and vesicles formed in these reactions on the single particle level. The technique gives radically greater resolution than DLS which is typically used to analyse particles of this size range.

During the reactions of micelle forming compounds, the aggregates present remained of fairly uniform size throughout. Interestingly, in vesicle forming reactions, the average size of lipid aggregates increased through time, suggestive that in reactions containing vesicle forming lipids the size of the vesicles grows through time. Until recently it would not have been possible to measure the *in situ* behaviour of individual lipid aggregates at the nanometre scale, and this hold the possibility for new levels of understanding in the dynamics of physical autocatalysis and also lipid aggregate protocell models more generally.

Discovery of oscillations in reactions fuelled with hydrogen peroxide was unexpected. Studying this system was challenging by UPLC due to low throughput. Future work should focus on developing an in-line technique so that conditions can be screened quicker. A number of possible techniques could be used, for example UV-vis spectroscopy. “Optimisation” of oscillating reactions lacks a good definition owing to the number of related parameters, for example, amplitude of oscillation, wave shape, period of oscillation and duration of oscillatory period before the system is exhausted. That being said it would be desirable to make the reaction oscillate faster with a longer duration of oscillations before complete oxidation is observed.

Further studies on the systems described in chapter 4 should include following the kinetics of some reactions containing multiple competing lipids by iSCAT microscopy. This would be informative because in some cases (where two different aryl substitutions are present, for example that shown in figure 4. 3. 2. 2. 1) the different lipids in isolation form different aggregates. It seems likely that through time the size and nature of the aggregates change, and as the vesicle forming compounds tend to be more stable, we could observe replicating lipid aggregates which firstly form micelles which transform into vesicles at some time during the reaction.

We were not able to achieve one of the initial aims of the study, which was to build a system of competing lipids which showed succession through time and also required fuelling to maintain lipid population. The shortcoming arose because despite all lipids in this chapter being unstable to the reaction conditions, the rates of destruction for some replicators was too slow to fully decay under the reaction conditions, with some of the more electron rich and sterically hindered mixed disulfides having a half-life of months. As such, during the period of study, these lipids are kinetically trapped. Though this problem was ameliorated by the addition of DMAP as a nucleophilic catalyst, with a significant reduction in final lipid concentration after 7 days, there was not time to fully optimise these conditions. Future work should focus on gaining reproducible data with more time points during the first 30 h of reaction, so that clearer succession patterns can be seen. It is worth noting that although the utmost care was taken, the results with DMAP show broad error bars (see figure 4. 3. 2. 3. 6 and figure 4. 6. 9. 6. 3. 2). Were this to be consistently observed, other nucleophilic catalysts could be used, or more basic conditions without a nucleophilic catalyst.

5. 4 Final remarks

Since time immemorial humans have made tools and machinery built on scales similar to our bodies. A recent review from the Leigh group pointed out that at this macroscopic scale, the six “simple machines” used to change the direction and/or magnitude of a force have been known since the middle ages.[4] These include the lever and the inclined plane, forming the basis set of rigid components which are used in combination within mechanical devices to achieve complex functions, from scissors to clocks. As noted by Leigh and many others, many of these however are not useful at the atomic scale, an inclined plane is unlikely to provide mechanical advantage in a regime where gravitational effects are negligible.[5,6]

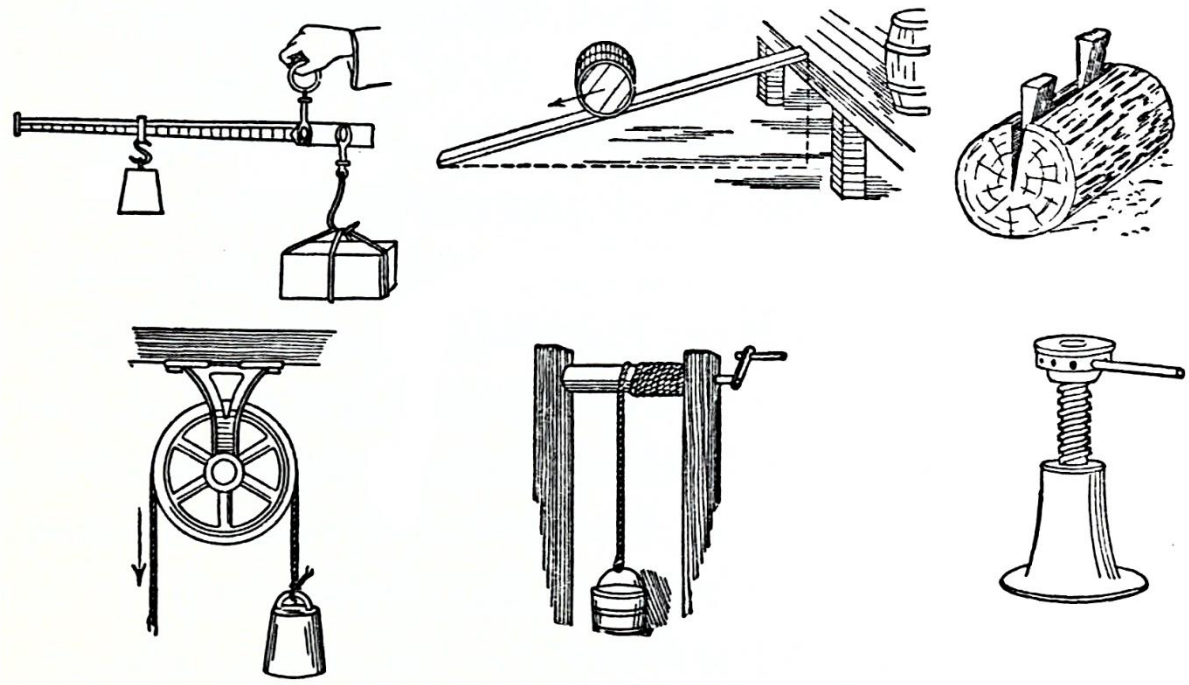


Figure 5. 4. 1. The six "simple machines" known since the middle ages as means of gaining mechanical advantage. Left to right, top to bottom they are: the lever, the inclined plane, the wedge, the pulley, wheel and axle, and the screw. Image is reproduced from book in the public domain.[7]

Some of the macroscopic simple machines certainly can inform the construction of synthetic molecular machines, for example Feringa's unidirectional motors can be seen as molecular analogues of the wheel and axle, converting chemical energy[8] or energy from light[9] into rotary motion. Currently, no definitive list exists of the simple machines which may be theoretically available to the synthetic organic chemist and it remains to be seen how they may be combined to build complex functional systems.

Without the knowledge and technology of how to transform energy between desired forms at the molecular scale, we cannot currently take "off the shelf" components and combine them to build machines of arbitrary function and complexity. Perhaps given this state of the field it is best to take a systems chemistry approach, whereby some chemical intuition is used in the design, but also there is room for complexity arising from the unknown interaction of many different parts.

Projects in this thesis all represent a kind of "middle way" approach to design, some combination of deterministic design and emergence from complexity. Our designs for amplification of enantiomeric enrichment via asymmetric autocatalysis were based on established principles of reactivity, nucleophilic aziridine ring opening and hydrogen bonding catalysis. How exactly nonlinear effects would arise in these reactions was unknown and would derive from experiment. In chapter 3, the induction of motion by surfactant products on droplets was designed on the basis of prior work with Marangoni microswimmers, however, the effects of chemotaxis on lipid formation were not known in the beginning. Finally, in chapter 4 the effects of different degrees of steric bulk on the rates of replicator formation and destruction, and resulting succession of composition could be designed on the basis of chemical intuition, however the effects of differing aryl substitutions, which disulfide metatheses occur spontaneously, and the effect of structure on supramolecular aggregation were all open factors prior to experiment.

Finally, I think it is all too easy for prebiotic models to be misconstrued as dogma rather than conjecture, and therefore I believe it is important for people to study models which are highly different to the accepted ideas and "received wisdom". This approach is more likely to uncover unknown reactivity may have a higher chance of providing genuinely new understanding of molecular evolution. Darwin has taught us so much but doesn't explain the transition from non-living to living systems and it is erroneous to apply the lessons from Darwinism too strictly in prebiotic models. A series of charismatic communicators of science from Darwin to Dawkins have ensured the legacy of natural selection as a central way of looking at the biological world.[10–13] This has trickled down into the popular imagination, but has lead to perhaps false perspectives on what are the important factors to making life in the first place. In the absence of highly evolved structures of life, it seems unlikely that the first replicators that emerge would be effective

enough for their prevalence to be dictated by the factors of contemporary evolution, with cooperative effects likely to be more important.

Chapters 3 and 4 focus on the physical replication of lipid aggregates and what life-like properties can be found in these systems in mixed environments. These systems are minimal models for the emergence of replicating compartments in life, showing close analogy to simple membranes. What these chapters show is that the "success" of a replicator is not based merely on its physical properties, or just its environment, but also on the availability of similar precursors and presence of other competing replicators. Understanding these systems requires a holistic approach, whereby the concentration of a particular lipid is influenced by numerous factors, many of which are not related to properties of the lipid itself, for instance the presence or absence of motile droplets.

5. 5 References

1. Garbarczyk, J. B. & Jones, D. W. (Derry W.) *Organic crystal chemistry*. (International Union of Crystallography, 1991).
2. Viedma, C. Chiral symmetry breaking during crystallization: Complete chiral purity induced by nonlinear autocatalysis and recycling. *Phys. Rev. Lett.* **94**, 065504 (2005).
3. Morrow, S. M., Colomer, I. & Fletcher, S. P. A chemically fuelled self-replicator. *Nat. Commun.* **10**, 1011 (2019).
4. Zhang, L., Marcos, V. & Leigh, D. A. Molecular machines with bio-inspired mechanisms. *Proc. Natl. Acad. Sci. U. S. A.* **115**, 9397–9404 (2018).
5. Richard P. Feynman. There's a Plenty of Room At the bottom. *Eng. Sci.* **23**, 22–36 (1960).
6. Siegel, J. Inventing the nanomolecular wheel. *Science* **310**, 63–64 (2005).
7. Mills, J. *The Realities of Modern Science: An Introduction for the General Reader*. (The Macmillan Co., 1919).
8. Fletcher, S. P., Dumur, F., Pollard, M. M. & Feringa, B. L. Chemistry: A reversible, unidirectional molecular rotary motor driven by chemical energy. *Science* **310**, 80–82 (2005).
9. Koumura, N., Zijistra, R. W. J., Van Delden, R. A., Harada, N. & Feringa, B. L. Light-driven monodirectional molecular rotor. *Nature* **401**, 152–155 (1999).
10. Darwin, C. *On the origin of species by means of natural selection, or the preservation of favoured races in the struggle for life.* (John Murray, 1859).
11. Gould, S. J. *Hen's teeth and horse's toes*. (Norton, 1983).
12. Dawkins, R. *The selfish gene. The Selfish Gene* (Oxford University Press, 1976).
13. Dawkins, R. *Climbing Mount Improbable*. (Viking, 1996).

Description of Electronic Supporting Information

ESI Video 1: “Whirling droplets” observed when octanol droplets are in an aqueous phase containing **3.2**.

ESI Video 2: Moving octanol droplets observed when 3.1 is formed in situ.

ESI Video 3: Onset of motion in a single 50 μm octanol droplet, after a lag phase. Corona of material can be seen around the droplet

ESI Video 4: Chemotaxis seen in octanol droplets of mixed sizes, using a 1-hexanethiol reservoir setup.

ESI Video 5: Competition in chemotaxis between octanol (dyed red) and decanol (dyed yellow) droplets in a 1-hexanethiol reservoir setup.

ESI Video 6: Surface droplet behaviour of 2:1 octanol/pentanol mixture in 0.2 M NaOH containing 20 mM CTAB. Motion, vibration, and division are observed. This corresponds to table 3. 3. 2. 1. 2 entry 3.

ESI Video 7: Surface droplet behaviour of pentanol in 0.2 M NaOH containing 20 mM CTAB. Motion, vibration, and division are observed. This corresponds to table 3. 3. 2. 1. 2 entry 7.

ESI Video 8: Surface droplet behaviour of 1-hexanethiol containing droplets in 0.2 M NaOH containing 20 mM CTAB. Motion, vibration, and division are observed. This corresponds to table 3. 3. 2. 1. 5 entry 9.

ESI Video 9: Surface droplet behaviour of 1-hexanethiol containing droplets in 0.2 M NaOH containing 0.5 mM CTAB. No significant behaviour is observed. This corresponds to table 3. 3. 2. 1. 5 entry 10, and is a control experiment for ESI video 8.